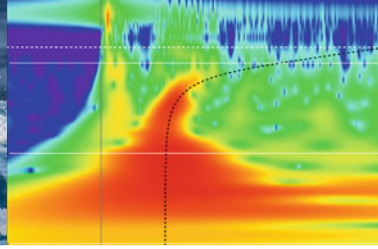


Boris W. Levin · Mikhail A. Nosov



Physics of Tsunamis

Second Edition

 Springer

Physics of Tsunamis

Boris W. Levin · Mikhail A. Nosov

Physics of Tsunamis

Second Edition

 Springer

Boris W. Levin
Russian Academy of Sciences
Yuzhno-Sakhalinsk
Russia

Mikhail A. Nosov
Faculty of Physics
M.V. Lomonosov Moscow State University
Moscow
Russia

ISBN 978-3-319-24035-0 ISBN 978-3-319-24037-4 (eBook)
DOI 10.1007/978-3-319-24037-4

Library of Congress Control Number: 2015949315

Springer Cham Heidelberg New York Dordrecht London
© Springer International Publishing Switzerland 2009, 2016

This work is subject to copyright. All rights are reserved by the Publisher, whether the whole or part of the material is concerned, specifically the rights of translation, reprinting, reuse of illustrations, recitation, broadcasting, reproduction on microfilms or in any other physical way, and transmission or information storage and retrieval, electronic adaptation, computer software, or by similar or dissimilar methodology now known or hereafter developed.

The use of general descriptive names, registered names, trademarks, service marks, etc. in this publication does not imply, even in the absence of a specific statement, that such names are exempt from the relevant protective laws and regulations and therefore free for general use.

The publisher, the authors and the editors are safe to assume that the advice and information in this book are believed to be true and accurate at the date of publication. Neither the publisher nor the authors or the editors give a warranty, express or implied, with respect to the material contained herein or for any errors or omissions that may have been made.

Printed on acid-free paper

Springer International Publishing AG Switzerland is part of Springer Science+Business Media
(www.springer.com)

Preface to the Second Edition

In the first edition, we paid attention not only to tsunami waves, but to related phenomena, namely, seaquakes, as well, which to a significant extent reflected the interests of the authors at the time. The second edition is more “tsunami-oriented”: the chapter dedicated to seaquakes and the information on killer waves have been dropped.

A new chapter on the fundamental properties of coseismic bottom deformations at the tsunami source has been added in the second edition. The theoretical material expounded in the first edition has been supplemented with information on the hydrodynamic formulation of the problem both in the case of an incompressible ocean and when the compressibility of seawater is taken into account. The concrete problems concerning wave generation by dynamic deformations, dealt with within the framework of the theory of an incompressible liquid, are supplemented with two static problems: on calculation of the initial elevation at a tsunami source and on residual hydrodynamic fields that accompany tsunami generation by an earthquake in a rotating ocean. The chapter on hydroacoustic and nonlinear effects is supplemented with an analysis of new information on the manifestations of tsunamigenic earthquakes based on the data from deep-water stations. The chapter on the Propagation of a Tsunami in the Ocean and its Interaction with the Coast has also undergone essential revision: amendments mainly concern the section on numerical tsunami simulation, in which much new important information is added. The chapter on methods for tsunami registration is supplemented with a paragraph devoted to ionospheric manifestations of tsunamis. Besides the aforementioned amendments, numerous corrections were made in order to render the sounding of the text more modern; new important information was added together with references to new publications.

The tsunami problem is an outstanding example of an interdisciplinary problem. Researchers, who are specialists in different fields, work for implementing its resolution: oceanologists and seismologists, geophysicists and geologists, geographers and geomorphologists, hydroacousticicians and engineers, computer scientists and mathematicians, marine biologists, and soil scientists and even sociologists.

Evidently, only joint efforts of the representatives of many scientific professions can result in essential progress toward resolving the problem, which we understand to involve lowering risks, the reduction of material damage, and, finally, most important, the elimination or reduction to a minimum of human casualties.

Although the authors acknowledge that the tsunami problem is an interdisciplinary problem, we do not claim to have created a comprehensive monograph reflecting all the achievements of modern “tsunami science”. The main scope of this edition—in accordance with its title—consists in reflection of the principal physical aspects of the tsunami problem. Nevertheless, the authors sincerely hope the book turns out to be useful to researchers and experts in any other professions having any whatever relationship to studying the tsunami phenomenon.

The authors are especially grateful to Dr. Tatiana Pinegina, who assumed the responsibility of totally revising Sect. 7.2, Dr. Ira Didenkulova for editing Sect. 6.3, Dr. Tatiana Ivelskaya for help in editing Sect. 1.4, Dr. Alexander Rozhnoi, Dr. Maria Solovieva, Prof. Vyacheslav Kunitsyn, and Dr. Artem Vorontsov for help in editing Sect. 7.4, Dr. Elena Sasorova for participating in the creation of Sect. 2.5 and Dr. Anna Bolshakova for preparing the illustrations to Sect. 2.3.

Boris W. Levin
Mikhail A. Nosov

Preface to the First Edition

Till the very end of the twentieth century tsunami waves (or “waves in a harbour”, translated from Japanese) were considered an extremely rare and exotic natural phenomenon, originating in the ocean and unexpectedly falling upon the seaside as gigantic waves. The 26th of December 2004, when tsunami waves wiped out, in a single day, more than 250 thousand human lives, mourned in many countries, turned out to be a tragic date for all mankind.

The authors of this book, who have studied tsunami waves for many years, intended it to be a systematic exposition of modern ideas concerning

- the mechanisms of tsunami wave generation,
- the peculiarities of tsunami wave propagation in the open ocean and of how waves runup beaches,
- the methods for tsunami wave registration and the operation of a tsunami warning system,
- the mechanisms of other catastrophic processes in the ocean related to the seismic activity of our planet.

The authors considered their main goal to be the creation of book presenting modern knowledge of tsunami waves and of other catastrophes in the ocean to scientific researchers and specialists in geophysics, oceanography, seismology, hydroacoustics, geology, geomorphology, civil and seaside engineering, post-graduate students and students of relevant professions. At present, in 2005, it has become clear that the demand for the information and scientific results presented in the book may be significantly broader and that they may be of interest to a large part of the population. Politicians, administrators, mass media, insurance companies, owners of seaside resorts and hotels, the civil fleet and the navy, oil-extracting companies, security services, space agencies, publishing houses, public education systems, such is a short list of possible users interested today in assimilating and spreading knowledge of the nature and manifestations of tsunami waves.

Waves, that regularly devastate the coasts of oceanic islands and are called tsunami in Japan, have been known for several centuries. The European civilization first encountered such catastrophic waves in 1755, when an exceptionally strong earthquake took place in the Atlantic ocean near the coast of Portugal and gave rise to a tsunami wave that immediately killed over 50 thousand people in the blooming city of Lisbon, which was about a quarter of the city's population. In the USSR, the Kamchatka tsunami of 1952 (2336 victims) resulted in creation of a State tsunami warning system. During the past 10 years (not counting the tragedy caused by the Indonesian tsunami in 2004) tsunami waves in the Pacific ocean took the lives of more than 10 thousand people.

According to UNESCO information, by the year 2010 residents of the coasts of oceans and seas will represent about 70 % of the total population of our planet. One should add persons visiting numerous seaside resorts, those who like to celebrate the New Year on exotic oceanic islands and, also, individuals seeking maritime adventures. All these people may happen to be within reach of one of the oceanic catastrophes, of which tsunami waves are the most dangerous.

Today, many states of the Pacific region,—Russia, Japan, the USA, Chile operate tsunami warning systems. The Russian system includes two tsunami Centers, situated in Yuzhno-Sakhalinsk and Petropavlovsk-Kamchatskii that are managed by the respective Board of the State Committee (Goskomitet) for hydrometeorology of Russia. The tsunami centers receive on-line information from seismic stations that carry out round-the-clock observation within the framework of the Geophysical Service of the Russian Academy of Sciences (RAS). In former times there were six such specialized seismic stations functioning along the Far-East coast of the USSR. At present only 3 stations (Yuzhno-Sakhalinsk, Petropavlovsk-Kamchatskii, SeveroKurul'sk) are in operation, and they all long need to be modernized and re-equipped.

The International Tsunami Information Center, the Pacific Tsunami Warning Center, the Alaska Tsunami Warning Center function successfully within the framework of the USA National Oceanic and Atmospheric Administration with participation of the UNESCO Intergovernmental Oceanic Commission (IOC/UNESCO). In Japan the duties of tsunami warning are performed by several hundred seismic and sea level stations united in a common information system managed by national agencies (JMA, JAMSTEC).

All national Tsunami warning services exchange on-line information via Internet, electronic mail and the specialized Tsunami Board Bulletin. Scientific studies of tsunami waves are coordinated by the International Tsunami Commission within the International Union for Geodesy and Geophysics (IUGG). During the period between 1977 and 1979 this commission was led by Academician S. L. Soloviev, who founded the Soviet Tsunami School. Another Russian scientist, Dr. V. K. Gusakov (Novosibirsk) occupied this position from 1995 up to 2003. In 2003, Professor K. Satake (Japan) was elected Chairman of the Commission. The Tsunami Commission and the International Group of the UNESCO Intergovernmental Oceanographic Commission (IOC/UNESCO) organize regular international scientific and practical conferences, devoted to the problem of tsunami

waves, in-situ inspections of coasts that were victims of tsunami waves, they publish reviews, information bulletins, national reports, general-education literature, and support the creation of databases.

In 1996, The European Geophysical Society (EGS) established the Sergei Soloviev medal to mark the recognition of S. L. Soloviev's scientific achievements. This medal is presented to scientists who have made essential contributions to the investigation of natural catastrophes.

The Russian school of tsunami researchers organized and led for many years by Academician S. L. Soloviev, is still considered a leading team in this scientific sector. A large contribution to the development of tsunami studies has been made by RAS Corresponding members S. S. Lappo and L. N. Rykunov; the Doctors of Sciences, who grew up in the Russian Tsunami School, A. V. Nekrasov, A. A. Dorfman (Leningrad), B. W. Levin, M. A. Nosov, A. B. Rabinovich, E. A. Kulikov, L. I. Lobkovsky (Moscow), E. N. Pelinovsky, V. E. Friedman, T. K. Talipova (Nizhny Novgorod), V. K. Gussyakov, L. B. Chubarov, An. G. Marchuk (Novosibirsk), P. D. Kovalev, V. V. Ivanov (Yuzhno-Sakhalinsk), and their pupils have done much for successful development of the science of tsunami waves. Specialized tsunami laboratories and several scientific groups work in the M. V. Lomonosov Moscow State University (MSU) and in various RAS institutes: the Institute of Oceanology (Moscow), the Institute of Applied Physics (Nizhny Novgorod), the Institute of Computational Mathematics and Mathematical Geophysics of the RAS Siberian Branch (RAS SB) (Novosibirsk), the Institute of Maritime Geology and Geophysics of the RAS Far-East Branch (RAS FEB) (Yuzhno-Sakhalinsk), the Institute of Vulcanology and Seismology of RAS FEB (Petropavlovsk-Kamchatskii).

Many Russian specialists in tsunami waves, including the authors and the editor of this book, have acquired significant teaching experience not only in the universities of Russia (MSU, MSGU, NSU, NNSU, NSTU, SakhsU), but also in Universities of the USA, France, Guadeloupe, Australia, Columbia. Recently, owing to the development of new computer technologies and software, original models have appeared of rare phenomena in the ocean, that were hitherto beyond the reach of scientific analysis. The experience of elaborating original ideas accumulated by Russian scientists in the research of seaquakes, killer waves, temperature anomalies above underwater earthquakes, the formation of cavitation zones, plumes and surges of water require detailed exposition and physical analysis. The experience of collaboration with foreign colleagues, regular participation in international meetings, as well as experience in organizing international conferences in Russia (the Tsunami conferences of 1996, 2000, 2002) have revealed an increased demand in tsunami wave specialists and in systematization of the knowledge accumulated in this field.

At present, no proof is needed of the fact that the influence of tsunami waves on the coasts of continents and islands is of a global nature. This catastrophic phenomenon cares nothing about the borders of states and of the nationalities of individuals, who happen to be in the zone within reach of the catastrophe. In the nearest future the politicians of civilized countries will be compelled to start

resolving the issue of creating a global tsunami warning system, something similar to the World meteorological organization. This task will require scientists from all countries to make enormous efforts for systematization of the knowledge on tsunami waves, for the preparation of national experts, specialists and teachers in the problem of tsunami waves, for developing new methods and means of monitoring, for publishing series of textbooks, scientific and general-education literature.

The authors hope that this book will contribute to the formation of a general collection of knowledge on tsunami waves. The necessity of such a book has ultimately become evident.

Many of our colleagues have taken part in completing the book and preparing it for publication. Section 6.1 was in part prepared by the Director of the SakhUGMS Tsunami Center T. N. Ivek'skaia (Yuzhno-Sakhalinsk), section 6.2 was written by T. K. Pinegina (Petropavlovsk-Kamchatskii), a well-known specialist in palaeotsunami. The illustrations, used in the book and based on computer graphics, were prepared by the leading scientific researcher of the RAS Institute of Oceanology E.V. Sasorova (Moscow). The image of the word "tsunami" in the form of Japanese hieroglyphs was prepared for the book by Dr. H. Matsumoto (Japan, Tokyo). Certain material, put at our disposal by E. A. Kulikov (Moscow), V. K. Gussyakov (Novosibirsk), V.V. Titov (Seattle, USA) and other colleagues of ours has been included in the book. The authors express their sincere gratitude to all of them.

We are grateful to our teachers S. L. Soloviev and L. N. Rykunov for the good school, and we revere their memory. We are grateful to our pupils and colleagues, whose friendly participation and help promoted the appearance of this book. We wish to express particular gratitude to the referee of this issue Prof. E. N. Pelinovsky. The support of the Russian Foundation for Basic Research and of the Russian Academy of Sciences was an enormous stimulus for the preparation and publication of this issue.

B.W. Levin
M.A. Nosov

Contents

1	General Information on Tsunami Waves, Seaquakes, and Other Catastrophic Phenomena in the Ocean	1
1.1	Tsunami: Definition of Concepts	2
1.2	Manifestations of Tsunami Waves on Coasts	5
1.3	Tsunami Magnitude and Intensity	11
1.4	Tsunami Warning Service: Principles and Methods	16
1.5	Tsunami Catalogs and Databases.	20
1.6	Seaquakes: General Ideas	24
1.7	Hydroacoustic Signals in the Case of Underwater Earthquakes	27
	References	30
2	Source of a Tsunami of Seismotectonic Origin	35
2.1	The Main Parameters and Secondary Effects.	36
2.2	Okada Formulae	51
2.3	Rectangular Fault: Relationship Between the Parameters of a Tsunami Source and the Earthquake Moment Magnitude and Depth	55
2.4	Properties of Coseismic Deformations of the Oceanic Bottom According to Data on the Slip Structure at Tsunamigenic Earthquake Sources	67
2.5	Distribution of Tsunami Sources in Space and Time	77
	References	84
3	Hydrodynamic Processes at the Source of a Tsunami of Seismotectonic Origin: Incompressible Ocean	89
3.1	Hydrodynamic Description of Tsunami Waves: The Two Principal Approximations	90
3.1.1	General Formulation of the Hydrodynamic Problem	90
3.1.2	The Long-Wave Theory.	92
3.1.3	The Potential Theory	95

3.2	General Solution of the Problem of Excitation of Gravitational Waves in a Layer of Incompressible Liquid by Deformations of the Basin Bottom	98
3.2.1	Cartesian Coordinates	98
3.2.2	Cylindrical Coordinates	101
3.3	Plane Problems of Tsunami Excitation by Deformations of the Basin Bottom	104
3.3.1	Construction of the General Solution	105
3.3.2	Piston and Membrane Displacements	109
3.3.3	Running and Piston-Like Displacements	119
3.3.4	The Oscillating Bottom	126
3.4	Generation of Tsunami Waves and Peculiarities of the Motion of Ocean Bottom at the Source	132
3.5	Calculation of the Initial Elevation at the Tsunami Source	144
3.6	Residual Hydrodynamic Fields that Accompany the Generation of a Tsunami by an Earthquake	156
3.6.1	Definition of Concepts	156
3.6.2	Basic Mathematical Model for a Homogeneous Ocean	157
3.6.3	The Properties of Residual Fields in the Case of a Homogeneous Ocean of Constant Depth: Analysis of Analytical Solutions	159
3.6.4	Features of Residual Fields Due to the Existence of Stable Stratification	164
3.6.5	Methods for Calculation of Residual Potential Fields for Real Events	171
3.6.6	Estimation of Residual Horizontal Displacements of Water Particles Caused by the Tsunamigenic Earthquake of March 11, 2011	172
	References	175
4	Role of the Compressibility of Water and of Nonlinear Effects in the Formation of Tsunami Waves	181
4.1	Excitation of Tsunami Waves with Regard to the Compressibility of Water	182
4.1.1	Preliminary Estimates	182
4.1.2	Hydrodynamic Formulation of the Problem: Analytic Solutions	186
4.1.3	Piston and Membrane Displacements	193
4.1.4	The Running Displacement	198
4.1.5	Peculiarities of Wave Excitation in a Basin of Variable Depth	202
4.2	Observations of Tsunamigenic Earthquakes Using Ocean Bottom Stations	210
4.2.1	Character of the Water Layer Response to Bottom Oscillations in Dependence of Frequency	211

- 4.2.2 The 2003 Tokachi-Oki Earthquake 216
- 4.2.3 The 2011 Tohoku-Oki Earthquake. 226
- 4.3 Nonlinear Mechanism of Tsunami Generation. 240
 - 4.3.1 Base Mathematical Model 240
 - 4.3.2 Nonlinear Mechanism of Tsunami Generation
by Bottom Oscillations in an Incompressible Ocean. 244
 - 4.3.3 Nonlinear Tsunami Generation Mechanism
with Regard to the Compressibility of Water 252
- References 258
- 5 The Physics of Tsunami Formation by Sources of Nonseismic
Origin. 263**
 - 5.1 Tsunami Generation by Landslides 264
 - 5.2 Tsunami Excitation Related to Volcanic Eruptions 276
 - 5.3 Meteotsunamis 283
 - 5.4 Cosmogenic Tsunamis 294
 - References 305
- 6 Propagation of a Tsunami in the Ocean and Its Interaction
with the Coast. 311**
 - 6.1 Traditional Ideas Concerning the Problem of Tsunami
Propagation 312
 - 6.2 Numerical Models of Tsunami Propagation 329
 - 6.3 Tsunami Run-Up on the Coast 345
 - References 352
- 7 Methods of Tsunami Wave Registration 359**
 - 7.1 Coastal and Deepwater Measurements of Sea Level. 360
 - 7.2 The Investigation of Coasts After Tsunamis:
Tsunami Deposits 366
 - 7.3 Tsunami Detection in the Open Ocean by Satellite
Altimetry 373
 - 7.4 Tsunami Wave Manifestations in the Ionosphere. 381
 - References 384

Chapter 1

General Information on Tsunami Waves, Seaquakes, and Other Catastrophic Phenomena in the Ocean

Abstract Fundamental information on the physics and geography of tsunami waves is presented. Examples are given of known historical events, illustrating the character of tsunami manifestation on coasts. Quantitative characteristics are introduced that describe tsunami strength: magnitude and intensity. Physical principles of the operation of tsunami warning systems are described. Information is provided on tsunami catalogs and electronic databases. The seaquake phenomenon is defined and a synthesized description is given. Information is presented on the main hydroacoustic effects, related to underwater earthquakes: the T-phase, low-frequency elastic oscillations, and cavitation.

Keywords Tsunami · Seaquake · Surface gravitational waves · Long waves · Run-up · Sudden inundation · Impact of waves · Erosion · Damage · Fires · Environment pollution · Epidemics · Human casualties · Local tsunami · Regional tsunami · Teletsunami · Tsunami catalog · Historical tsunami database · Tsunami magnitude · Tsunami intensity · Tsunami warning · Hydroacoustic signals · T-phase · Cavitation

Catastrophic oceanic waves, termed “tsunami” back in the 1960s of the past twentieth century, were considered a mysterious and inexplicable phenomenon of the life of the ocean. The sudden onslaught on the coast by a rabid giant wave would take the lives of tens of thousands people and leave memories engraved for a long time on the minds of those who remained alive. Scientists of many countries have united their efforts to understand the secret of this awe-inspiring phenomenon and to bring nearer a resolution of the problem of tsunami waves. At present, scientists have at their disposal information about 2,528 events in oceans and seas that have given rise to tsunami waves (Global Historical Tsunami Database at NGDC, as of June 2015).

The Pacific is considered the most tsunami-dangerous region, in which 1,589 tsunami source events are known. 470 tsunami source events are known to have taken place in the Mediterranean Sea. There exists information on tsunamis sources in the Atlantic Ocean (181) and in the Caribbean Sea (107), in the Black and Caspian Seas (23). Europe was exposed to the action of the catastrophic tsunami of 1755, during which the city of Lisbon was destroyed. This event was reflected in an old engraving

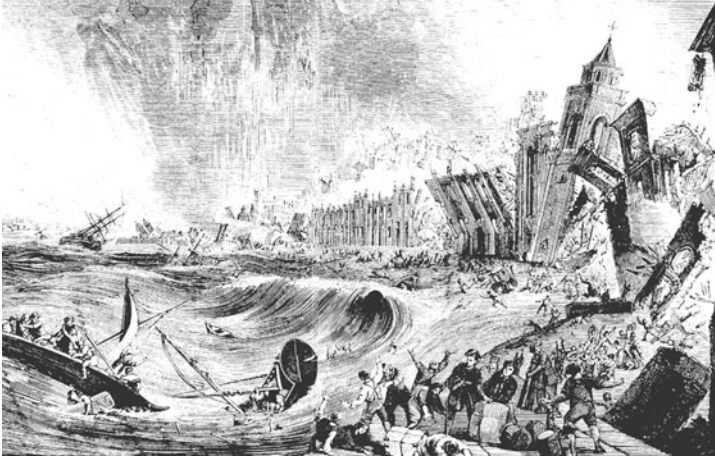


Fig. 1.1 The 1755 Lisbon earthquake and tsunami. Old engraving by unknown author

(Fig. 1.1). At present, researchers are paying particular attention to the Indian Ocean, although in the past, also, its coasts were repeatedly attacked by tsunami waves (152 tsunami source events).

The seaquake phenomenon caused by seismic oscillations of the seafloor is only known to specialists and to experienced seafarers. Even the edition of the Grand Soviet Encyclopedia had no place for this term, although the amount of registered natural events of this type already exceeded 250. Investigation of the entire complex of earthquake-related phenomena in the ocean sheds light on the interaction mechanisms of various media in the communicating and interpenetrative lithosphere–hydrosphere–atmosphere system.

1.1 Tsunami: Definition of Concepts

The word tsunami originates from a combination of two Japanese hieroglyphs (Fig. 1.2), translated together as a “wave in the harbour”. This term has already been conventionally adopted in the scientific literature, although in mass media one may still encounter terms that prevailed some time ago, such as “high-tide wave”, “seismic sea wave”, “seaquake”. Sometimes, the antique European terms “zeebeben” and “maremoto” are used.

Fig. 1.2 Japanese hieroglyphs, pronounced as “tsu-nami” and literally translated as a “wave in the harbour”

津波

Usually, tsunami waves are understood to be surface gravitational waves exhibiting periods within the range $T \sim 10^2\text{--}10^4$ s. Tsunamis pertain to long waves, therefore not only the subsurface layer, but the entire thickness of water becomes involved in the motion. Here, the term “surface” signifies that the presence of a free surface is a necessary condition for these kinds of waves to exist.

Tsunami waves differ from other natural calamities in that they are capable of retaining their destructive force while propagating many thousands of kilometers. Thus, for example, the Hawaiian Islands are repeatedly subjected to the effect of tsunami waves generated by distant sources—earthquakes occurring around the perimeter of the Pacific Ocean inside the so-called Ring of Fire. The catastrophic manifestations of the 1960 Chilean Tsunami on the Pacific ocean coast (at a distance of about 17,000 km!) across from Japan (138 deaths and \$50 million damage—according to data from USGS, Historic Earthquakes) and on the Far East coast of Russia (0 deaths and Soviet Rubles 30 million damage—according to data from Sakhalin Hydrometeorological Service, Russia) are well known to specialists. An impressive example of the long-range destructive action of a tsunami is related to the wave caused by the 1946 Aleutian Islands earthquake. After having covered a distance of about 16,000 km the wave damaged the hut of the British expedition on Winter Island off the west coast of Graham Land (Fuchs 1982; Gusiakov 2014). The Atlantic ocean has its own example of a transoceanic tsunami: the 1755 Lisbon earthquake was accompanied by waves of amplitudes exceeding 3 m on the Caribbean sea islands (the distance from the source was more than 5000 km) (Okal 2011; Zahibo et al. 2011).

The formation of tsunamis is primarily considered to be related to seismic motions of the seafloor, slides, and collapses (underwater, also), underwater volcanic eruptions. Waves exhibiting similar characteristics may be due to sharp changes in the atmospheric pressure (meteotsunami) and due to powerful underwater explosions. Recently, the issue has been actively discussed of tsunami originating as a result of falling meteorites. One must bear in mind the possibility of combinations of various causes. Thus, for example, underwater slides, provoked by earthquakes, may provide an additional contribution to the energy of the tsunami waves, formed by displacements of the seafloor. We stress that the main cause for the destructive tsunami consists in sharp vertical displacements of parts of the seafloor due to strong underwater earthquakes. Considering all the causes together, it may be asserted that any coast of a large water reservoir is potentially dangerous from the point of view of tsunamis.

Modern ideas of the sources of tsunami waves are not unambiguous. Usually, the source of tsunami waves is characterized by its horizontal dimension $L \sim 100$ km, which significantly exceeds the typical depth of the World Ocean, $H \sim 4$ km. A certain quite rapid transient process results in gravitational waves originating at the source with a wavelength $\lambda \sim L$. From the point of view of hydrodynamics these waves are long ($\lambda \gg H$). The propagation velocity of long waves in a reservoir of depth H is determined by the formula $c = \sqrt{gH}$, where g is the free-fall acceleration of gravity. In the case of a depth $H \sim 4$ km the tsunami wave propagates with a velocity of the order of magnitude of 200 m/s, or about 720 km/h, which is comparable to

the velocity of a modern jet aircraft. From the tsunami wavelength and its propagation velocity one can readily estimate the tsunami wave period $T = \lambda/c \approx 500$ s (actually, it varies within the limits of 10^2 – 10^4 s). The tsunami wave amplitude in the open ocean, even in the case of catastrophic events, is usually limited to tens of centimeters and rarely exceeds 1 m. The small amplitude together with the large period renders the tsunami wave in open ocean practically imperceptible for an observer on board a ship. Nevertheless, the displacement amplitude of the water surface at the tsunami source may amount to 10 m and more. But in this case, it is also essentially inferior to the depth of the ocean.

Dependence of the tsunami wave propagation velocity on the depth renders these waves sensitive to the shape of the seafloor. Effects peculiar to tsunamis include the capture of wave energy both by underwater ridges and by the shelf, focusing and defocusing exhibited when waves propagate above underwater elevations and depressions. Irregularities of the seafloor lead to the scattering of tsunami waves.

In fact, the propagation velocity of gravitational waves depends not only on the depth, but also on the wavelength. The formula presented above for the velocity of long waves is the limit case (for $\lambda \gg H$) of the more general expression $c = \sqrt{g \tanh(kH)/k}$, where $k = 2\pi/\lambda$. Wave dispersion results in transformation of the initial perturbation into a wave packet, with the most rapid long waves leading. Note that this effect is manifested in the case of tsunami wave propagation over quite extended routes. Dispersion, resonance properties of the coastal relief, phenomena such as reverberation (i.e., when the wave perturbation reaches a certain coastal site via different routes), the peculiarities of wave formation at the source—all these, as a rule result in a tsunami being manifested not as a solitary wave but as a series of waves with a period amounting to tens of minutes. In this case, the first wave is often not the strongest. The absence of knowledge of precisely this property of tsunami waves often leads to human casualties, which could have been avoided.

The tsunami wave amplitude increasing as it approaches the coast—which to great extent is what determines the danger of these waves, is also related to the relief of the seafloor. A decrease in the water depth leads to a decrease in the wave propagation velocity and, consequently, to compression of the wave packet in space and an increase in its amplitude. In the case of catastrophic tsunamis the run-up height reaches several tens of meters, while the wave is capable of inland (horizontal) inundation of several kilometers from the coastline. A scheme of the tsunami onshore run-up, explaining the main parameters of this process, is shown in Fig. 1.3. Note that the maximal wave height can be achieved at the shoreline, at the inundation boundary, or at any point between them.

The danger carried by tsunami waves is primarily related to the following three factors: the sudden inundation of part of the land, the impact of waves on buildings, and erosion. Strong flows of water, reaching velocities of tens of meters per second, are capable of breaking up houses and of displacing them, washing out substructures of buildings, destroying bridges, and buildings in ports. The flows of water often carry pieces broken off buildings and other structures, trees, small, and large vessels, which leaves people picked up by the fast moving water no chance of survival. The

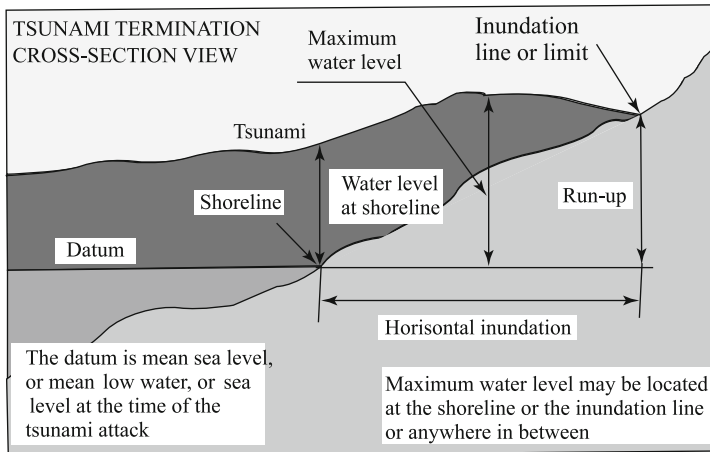


Fig. 1.3 Scheme of tsunami onshore run-up. Adapted from [UNESCO-IOC. Tsunami Glossary (2006)]

damage caused by tsunamis may also be due to fires, pollution of the environment, and epidemics resulting from devastation of the coastal infrastructure.

Depending on the scale of the area in which the destructive force of tsunamis is manifested, one conventionally distinguishes local, regional, and remote (teletsunami) events. The latter are sometimes termed transoceanic tsunamis. Local tsunamis include events, the destructive effect of which is concentrated within distances not exceeding 100 km from the source. If destruction occurs at distances up to 1000 km from the source, then such an event is classified as regional, when above 1000 km it is a teletsunami. Most catastrophic events pertain precisely to local or regional tsunamis. The occurrence of transoceanic tsunamis is much less frequent, but they are, naturally, much more dangerous. After having caused a significant destruction in the immediate vicinity of the source, these waves are capable of traveling many thousands of kilometers from the source and continue carrying with them death and devastation. In the past millennium at least 15 such events took place in the World Ocean (Gusiakov 2014).

1.2 Manifestations of Tsunami Waves on Coasts

There exist numerous descriptions of the effect of tsunamis on a coast, which are due to eyewitnesses or scientists investigating the consequences of these events.

Detailed information about tsunami manifestations can be found in tsunami catalogs (e.g. Soloviev and Go 1974, 1975; Soloviev et al. 1986, 1992, 1997, 2000) and databases Historical Tsunami Database for the World Ocean (HTDB/WLD) and NOAA/WDS Global Historical Tsunami Database at NGDC (GHTD/NGDC).

We present brief descriptions of some of the outstanding events.

The 1868 tsunami near the city of Arica (Chile) was caused by an underwater earthquake of magnitude $M = 8.8$. In the evening, after it became dark, an enormous “wall” of phosphorescent foamy water mixed up with sand arrived from the ocean with a thunderous noise. The height of the waves amounted to 15–18 m. Upon hitting the coast with an enormous force, the wave then carried the large US warship “Watee” from the harbor two miles inland and gently put it down at the rocky foot of the Andes. This event permitted Gabriel Garcia Marquez to depict the fantastic scene of an encounter with a three-mast sailboat among trees in the remote jungles (selva) of South America.

The tsunami reduced the site, where the city of Arica with about 5000 inhabitants had been, to a smooth sandy valley without any signs of buildings. Only individual structures remained here and there on the mountain slopes.

The catastrophic 1908 Messina tsunami, was caused by an earthquake of magnitude 7, the source of which was located under the bottom of the Messina Strait (in between continental Italy and Sicily). The tsunami started nearly immediately after the shaking stopped with a withdrawal of the seawater. Part of the seafloor, adjacent to the coast, happened to be drained, in some places the seafloor opened up for nearly 200 m. Then, all of a sudden, waves started to advance, the first three being the strongest. The tsunami was preceded by a strong noise, similar to the noise of a tempest or of waves hitting rocks with force. The maximum run-up height on the coast of Sicily amounted to 11.7 m, on the Calabrian coast to 10.6 m. Noticeable waves reached the coasts of Libya and Egypt. Of the mareographs that were not damaged, the one closest to the tsunami source was located on the Malta island. It recorded a tsunami of amplitude 0.9 m.

The number of tsunami waves observed varied from place to place from 3 to 9, and the period of the waves from 5 to 15 min. The waves washed out the structures destroyed by the earthquake and destroyed many buildings that had survived. Of the buildings and structures only the foundations, sliced off at land level, remained.

Many vessels, having been damaged, either sank or were stranded inland. The tsunami stirred up seafloor sediments; bubbles of gas came up from the seafloor to the surface of the strait; sea animals and fish, including deep-water inhabitants, unknown to fishermen, were thrown up onto the beach. Sailors on vessels moored several miles from the coast felt a strong seaquake, but could not understand why all the lights had gone out in the towns along the coast.

After the tsunami all of the strait was full of broken and overturned boats, other vessels, floating debris, bodies of human beings and of animals washed off the coasts of Messina and Calabria.

The 1952 tsunami that occurred near the eastern coasts of Kamchatka and off the Island of Paramushir is considered one of the most destructive tsunamis of the twentieth century. We present the description of this event given in the article by Soloviev (1968). On the night between November 4 and 5 the inhabitants of Severo-Kurilsk were woken up by an earthquake: stoves were destroyed, chimneys and household utensils fell down. Forty minutes after the earthquake stopped

a rumble was heard from the ocean, and a water bore moving with a high velocity fell upon the city. In several minutes the water retreated, carrying away what it had destroyed, and the ocean bottom opened up for several hundred meters. In 15–20 min a wall of water 10 m high once again advanced upon the city. It practically washed away everything in its way, at the most leaving only concrete foundations of various structures. Old pillboxes were wrenched out of the ground and thrown around, in the harbor the walls of a bucket were turned upside down, and launches that happened to be there were stranded hundreds of meters inland.

Several minutes later, after this strongest wave, a third relatively weak wave ran up the devastated coast, leaving much debris after it.

The events of 1952 were totally unexpected for most of the population. Thus, for example, some of the vessels moored near the Island of Paramushir transmitted messages that the island was sinking into the ocean waters.

A. E. Abaev, captain of a detachment of hydrographic vessels sent to Severo-Kurilsk immediately after the catastrophe, witnessed the strait between the islands of Shumshu and Paramushir to be completely crammed with floating wreckage of wooden houses, logs, and barrels. The bodies of human beings were seen on the wreckage—it was practically impossible to survive in the ice-cold water.

Another witness of this tsunami, A. Shabanov, who lived in Severo-Kurilsk and at the time was 14-years old, told one of the authors of this book that soon after the earthquake the water receded from the coast and left the ocean bottom open. When Shabanov's mother saw this sudden ebb tide she ran with her two sons toward the hills, which saved their lives. Their family was the only family in which no one was killed. On their way they had difficulty in crossing a deep ditch across which the Japanese in former times had thrown several narrow wooden footbridges. By 1952 most of the footbridges had been used as firewood, since it was not clear to the people arriving from the continent what they were for.

The wave, which in some parts of the coastline reached a height of 10–15 m ($H_{\max} = 18.6\text{ m}$), totally destroyed many buildings and port structures of Severo-Kurilsk (Island of Paramushir) and carried them out to sea, taking the lives of 2336 people. The source of the tsunami wave generated by an underwater earthquake of magnitude $M_w = 9.0$ extended over 800 km and was about 100 km wide.

The fantastic event that gave rise to a tsunami wave of record height took place on July 9 of 1958 in Lituya Bay (Alaska) (Soloviev and Go 1975). The bay exhibits a T-like shape. Its length amounts to 11 km, its width in the main external part—up to 3 km, and its maximum depth is about 200 m. The internal part of the bay is part of the Fairweather canyon. Here the bay resembles a fjord, and its steep walls rise up to heights between 650 and 1800 m. During the earthquake a gigantic slide of snow-and-ice together with local rock of volume about 0.3 km^3 took place. The water ousted by the falling mass splashed out onto the opposite coast and reached a height of 524 meters! The displacement of water was so rapid that all the trees in the flooded wood were wrenched up and the bark and leaves of the trees were rubbed off. Besides this enormous splash, a wave formed that crossed the whole bay right up to the ocean, devastating the bay's shores. Three fishing-launches were caught by the wave in the bay; one of them sank together with two crewmen. The two other

crews were lucky to escape. The fishermen spoke of a wave about 30 m high. Signs of the run-up and of trees broken by the wave remained on the slope for decades after the catastrophe. Note that the expedition led in 1786 by G.-F. La Perouse encountered a similar phenomenon in the French Harbor (presently known as Lituya Bay). An enormous wave carried the two-mast vessel of the expedition through the narrow strait and smashed it against the underwater rocks. Of all the 21 crewmen no one was left alive.

The Chilean tsunami of May 22, 1960 was caused by the strongest earthquake of the twentieth century ($M = 9.4$), the source of which was located in the southern part of central Chile. The maximum elevation of water amounted to 25 m in Chile, 10.5 m on the Hawaiian islands, 9 m in the Oceania, 6.5 m in Japan and the USSR, and 3.5 m in the USA. About 1000 persons lost their lives in Chile, 60 on the Hawaiian islands, 200 in Japan. It took approximately 15 h for the waves to cover 10,000 km and to reach the Hawaiian islands and nearly a day and a night to reach Japan and the far-east coast of the USSR. Naturally, the earthquake was felt neither on the Hawaiian islands, nor in Japan, nor in the USSR, so the wave turned out to be unexpected.

The 1994 tsunami, caused by an earthquake of magnitude $M = 8.3$ near the Island Shikotan, resulted in the destruction of numerous coastal structures. Part of the island subsided by 60 cm, which was recorded by the mareograph in the village of Malokurilsk. In the city of Yuzhno-Kurilsk, located at a distance of 120 km from Shikotan, the tsunami wave tore down a single-storeyed block of flats from its foundation and carried it 300 m inland. The wave's maximum run-up amounted to 10.4 m. It was pure luck that this tsunami resulted in no human casualties.

The 1998 tsunami that occurred in the region of Papua New Guinea gave rise to particular interest among specialists. A relatively small earthquake of magnitude $M_w = 7.1$ resulted in an unexpectedly large wave of height amounting to 15 m. The tsunami attacked the coast with three waves about 18 min after the earthquake. The area influenced was limited to part of the coastline 30 km long, where several fishing villages were destroyed and about 3000 people lost their lives. The formation of such a gigantic wave was mainly due to the colossal underwater slide caused by the earthquake, rather than to the earthquake itself.

The catastrophic tsunami of December 26, 2004 that occurred in the Indian ocean was caused by an exceptionally strong earthquake of magnitude $M_w = 9.1$ (USGS), the epicenter of which was near the northern extremity of Island Sumatra. Comparable magnitudes were exhibited during the past 100 years only by several seismic events (Kamchatka 1952; Aleutian Islands 1957; Chile 1960; Alaska 1964). The manifestation of the tsunami was of a global character. Besides the catastrophic consequences in the vicinity of the source (the coast of Sumatra), where the run-up amounted to 35 m, waves were registered all over the World Ocean. Tsunami waves of significant amplitudes were registered in remote parts both of the Pacific coast (Manzanillo, Mexico—0.5 m, New Zealand—0.5 m, Chile—0.5 m, Severo-Kurilsk, Russia—0.3 m, British Columbia, Canada—0.2 m, San Diego,

California—0.2 m) and of the Atlantic coast (Halifax—0.4 m, Atlantic City—0.2 m, the Bermuda islands—0.1 m, San Juan, Puerto Rico—0.05 m). The worst hit were countries of the basin of the Indian Ocean: Indonesia, Thailand, India, Sri Lanka, Kenya, Somalia, South Africa, the Maldive Islands. The total number of victims exceeded 227,000 people, the damage was enormous and it still has to be estimated. The number of casualties makes this catastrophe the largest of all known catastrophes in the history of tsunamis.

Central Kuril Islands Tsunamis. An extremely strong earthquake of magnitude $M_w = 8.3$ took place on November 15, 2006, in the Central-Kuril segment of the Kuril-Kamchatka seismofocal zone. The epicenter of the earthquake was located in the Pacific Ocean at about 85 km from the northern extremity of Simushur Island. Before this event, the Central-Kuril segment was considered a “seismic gap” zone, an earthquake of such strength was registered here for the first time in the history of seismic observations. Nearly two months later, on January 13, 2007, another earthquake of practically the same strength, $M_w = 8.1$, occurred in the same region. Both seismic events were accompanied by tsunami waves, noted over the entire area of the Pacific Ocean: Shikotan Isl., Malokurilsk—1.55(0.72) m, Kunashir Isl., Yuzhno-Kurilsk—0.55(0.11) m, Alaska, Shemya—0.93(0.69) m, Crescent City, California—1.77(0.51) m, Hawaii, Kahului—1.61(0.24) m, Peru, Callao—0.73(0.3) m, Chile, Talcahuano—0.96(0.23) m (the wave heights indicated in brackets correspond to the event of January 13, 2007). However, owing to the absence of mareographic stations and inhabitants on the Central Kuril Islands, no information about the wave heights in the immediate vicinity of the sources was available. During the period from July 1 to August 14, 2007, two seafaring expeditions were organized with one of their main tasks consisting in the investigation of the coasts of the islands so as to determine the tsunami run-up heights (Levin et al. 2008). The participants of the expedition were the first people to visit the islands after the tsunamis and to estimate the scale of the natural disaster. The time for the expedition depended on the complicated weather conditions in the area. Landing on the coasts of the islands earlier (before April–May) was practically impossible to realize. The highest tsunami run-ups (up to 20 m) were revealed on Matua Island. The tsunami strongly altered the morphology of the coast in the Ainu Bay (South-West of Matua Island) by washing away a section of the sea terrace 20–30 m wide. The maximum run-up height in Dushnaya Bay (North-East part of Simushur Island) amounted to 19 m; here the tsunami left numerous scours. Besides erosion on the coasts investigated, accumulation was also observed everywhere. Tsunami deposits consisted of marine sand, pebbles, boulders, floating debris shifted toward the land. The vegetation on steep slopes was partly destroyed, and the soil washed away. If waves of such strength were to hit a densely populated coast, casualties could certainly not be avoided. The only reason the tsunamis of November 15, 2006 and of January 13, 2007 did not become an awful tragedy was the total absence of population on the Central Kuril Islands. These two events can rightfully be considered the strongest tsunamis that were not accompanied by human casualties.

The 2011 Tohoku-Oki tsunami. On March 11, 2011, at 14.46 (local time—JST) an earthquake occurred in the Pacific Ocean east of the island Honshu, which turned

out to be unprecedented in strength for the region of Japan. This catastrophic event is conventionally called the 2011 Tohoku-Oki earthquake or the Great East Japan earthquake. Data of the U.S. Geological Survey (USGS) show the epicenter of the seismic event (38.322°N, 142.369°E) to have been located 129 Km east of the city of Sendai, the depth of its hypocenter was 32 km, its moment magnitude $M_W = 9.0$.

The Japan Meteorological Agency (JMA) issued a tsunami warning only 3 min after the earthquake onset. The first strong wave reached the nearest coast in about 30 min. The consequences of the tsunami turned out to be terrible. The hazard of the catastrophe was clearly underestimated. At many points of the Honshu island coast closest to the tsunami source the run-up height exceeded 20 m. Currents of sea water ran several kilometers up the land literally obliterating entire settlements from the Earth. The record characteristics of the tsunami run-up onto the shore are kept in the Iwate Prefecture (Tohoku Region): the maximum run-up height was 55.88 m and the maximum inundation distance was 7900 m (according to HTDB/WLD and GHTD/NGDC data). The number of victims amounted to 18,482 persons, the mater-

Table 1.1 Twenty-first-century tsunamis

No	Date	Earthquake magnitude (M_W)	Maximum water height (m)	Number of victims	Location of event
1	23/06/2001	8.4	8.8	26	Peru
2	24/12/2004	9.1	50.9	227899	Indonesia, Sumatra
3	17/07/2006	7.7	20.9	802	Indonesia, South Of Java
4	15/11/2006	8.3	21.9	0	Russia, Central Kuril Islands
5	13/01/2007	8.1			
6	01/04/2007	8.1	12.1	52	Solomon Islands
7	21/04/2007	6.2	7.6	10	Chile
8	15/08/2007	8.0	10.05	3	Peru
9	29/09/2009	8.1	22.35	192	Samoa
10	27/02/2010	8.8	29	156	Chile
11	25/10/2010	7.8	16.9	431	Indonesia, Sumatra
12	11/03/2011	9.0	55.88	18482	Japan
13	28/10/2012	7.7	12.98	1	Canada, British Columbia
14	06/02/2013	7.9	11	10	Solomon Islands
15	01/04/2014	8.2	4.4	0	Chile

ial damage was nearly a quarter of a trillion USA dollars (220085 \$Mill). An important feature of this event consisted in that both the loss of life and the material damage were mainly due to the tsunami waves, and not to the seismic event itself.

The natural catastrophe was accompanied by serious ecological consequences related to the disaster at the nuclear power-station Fukushima-1. The earthquake and tsunami damaged the external electric power system and the reserve diesel generators, which resulted in failure of both the regular and emergency core cooling systems. The subsequent overheating led to a series of explosions and, ultimately, to a release of radioactive material.

Once again the 2011 Tohoku-Oki tsunami revealed that even such a highly technological country, possessing the most rich historical experience of practical investigations of tsunami waves, regrettably happens to be vulnerable to natural calamities.

Table 1.1 presents several examples of twenty-first-century tsunamis (according to GHTD/NGDC data).

1.3 Tsunami Magnitude and Intensity

Estimation of the degree of tsunami danger for one or another coast (long-term tsunami forecast) is primarily based on the statistical analysis of events that occurred in the past. Tsunamis evidently vary in strength within wide limits: from weak waves that can be registered only with the aid of instruments, up to terrible catastrophic events devastating the coast along hundreds of kilometers. How can one estimate the strength of a tsunami? The point is that without the introduction of some quantitative characteristic of this strength it is not only impossible to perform any statistical analysis, but even to speak of estimating the degree of danger. The determination of such a quantitative characteristic is quite a nontrivial problem, the ultimate resolution of which has not yet been achieved. Similar difficulties are encountered by seismologists determining the strength of an earthquake. On the one hand, an earthquake is characterized by objective physical parameters showing the energy emitted by the source, or the released seismic moment. These parameters are measured quantitatively, and the scale of earthquake magnitudes is made to correspond to them. On the other hand, there exists a descriptive scale of earthquake intensities, which is related to the so-called macroseismic data based on the results of in situ studies. Clearly, in practice, it is precisely the intensity scale that is important, but contrary to the magnitude scale it is not rigorous from a physical standpoint.

Going back to tsunamis, we note that this phenomenon is also characterized, on the one hand, by objective and quantitatively measurable parameters (energy, amplitude, period, etc.), and on the other hand by subjective descriptions, reflecting the scale and degree of the destructions caused by the wave or the character of its manifestations on the coast. Like in the case of earthquakes, for estimation of the tsunami danger precisely these subjective descriptions are more important than abstract physical parameters. The inhabitants of coastal regions are not interested in the energy of the approaching wave in joules, they are interested in whether the wave

is dangerous to their lives, what damage may be done, and how it can be avoided. And, until further modeling is realized of the entire process starting from the actual formation of a wave up to its run-up onto the shore, such a situation will remain intact.

The first attempt at classification of tsunamis was made by Sieberg, who introduced a six-point scale of tsunami intensities by analogy with the scale of earthquake intensities (Sieberg 1927). This scale was not related to the measurement of physical parameters (wave heights, run-up lengths, etc.), it was based on the description of effects revealing the degree of destruction. Subsequently, the Sieberg scale was somewhat modified (Ambraseys 1962).

The Sieberg–Ambraseys tsunami intensity scale

1. **Very light.** Waves can only be registered by special tide gauges (mareographs).
2. **Light.** Waves noticed by those living along the shore. On very flat shores waves are generally noticed.
3. **Rather strong.** Waves generally noticed. Flooding of gently sloping coasts. Light sailing vessels carried away on shore. Slight damage to light structures situated near the coasts. In estuaries, reversal of the river flow some distance upstream.
4. **Strong.** Significant flooding of the shore. Buildings, embankments, dikes, and cultivated ground near coast damaged. Small and average vessels carried either inland or out to sea. Coasts littered with debris.
5. **Very strong.** General significant flooding of the shore. Quay-walls and solid structures near the sea damaged. Light structures destroyed. Severe scouring of cultivated land. Littering of the coast with floating items, fish, and sea animals thrown up on the shore. With the exception of big ships all other types of vessels carried inland or out to sea. Bores formed in estuaries of rivers. Harbor works damaged. People drowned. Wave accompanied by strong roar.
6. **Disastrous.** Partial or complete destruction of manmade structures for some distance from the shore. Strong flooding of coasts. Big ships severely damaged. Trees uprooted or broken. Many casualties.

Numerous attempts were made in Japan to introduce a quantitative characteristic of the tsunami strength. Imamura introduced, and Iida further improved, the concept of tsunami magnitude (Imamura 1942, 1949; Iida 1956, 1970). A proposal was made to estimate the magnitude by the formula

$$m = \log_2 H_{\max},$$

where H_{\max} —is the maximum wave height in meters, observed on the shore or measured by a mareograph. In practice, the Imamura–Iida scale is a six-point scale (from -1 up to 4).

In attempts at improving the Imamura–Iida scale S.L. Soloviev introduced the following tsunami intensity:

$$I = \frac{1}{2} + \log_2 H,$$

where H is the average tsunami height in meters on the coast closest to the source. At present such a definition of the tsunami intensity is widespread, and the corresponding scale is conventionally termed the “Soloviev–Imamura tsunami intensity scale.”

Note that the Imamura–Iida definition of magnitude is, generally speaking, unambiguous. It only requires knowledge of the maximum wave amplitude. The Soloviev–Imamura definition of intensity is not mathematically rigorous and, consequently, provides for much “freedom” in calculating the average height of tsunami waves. At any rate, both scales are not very sensitive to small errors in the determination of wave heights, since it is the logarithms of these quantities that count. It is also important to note that in the case of numerous historical events and, more so, of pre-historic events (paleotsunamis) the only available information comprises estimates of wave heights at a single point or at several points along the coast. Thus, both scales are quite convenient and will still be applied in practice for a long time. Anyhow, as a base characteristic to be measured in calculating the magnitude or intensity one may consider the flooded area, instead of the wave height. This characteristic may turn out to be a successful and promising alternative to the wave heights on the coast. A clear advantage of the flooded area consists not only in that it can be conveniently measured by remote means (from satellites, airplanes, etc.), but also in that this characteristic automatically reflects the scale of the catastrophe that took place.

Abe and Hatori proposed to modify the magnitude scale so as to take into account the weakening of waves, as the distance from the source increases (Abe 1979, 1981, 1985, 1989; Hatori 1986),

$$M_t = a \log h + b \log \Delta + D,$$

where h is the maximum wave amplitude on the coast measured from the foot up to the crest in meters, Δ is the distance from the earthquake epicenter to the point of measurement in kilometers, a , b , and D are constants. Such a definition resembles the definition of magnitude in seismology.

An essentially different approach to the definition of tsunami magnitude was put forward in Murty and Loomis (1980). Here, the calculation of magnitude is based on estimation of the tsunami’s potential energy E (in ergs),

$$ML = 2(\log E - 19).$$

The definition of magnitude based on the wave energy is, naturally, the most adequate definition from a physical point of view. However, it is not always possible to calculate the wave energy. At any rate, at the present-day stage calculations can be based on the potential energy of the initial elevation of the water’s surface, considering it to be identical to the residual displacements of the seafloor. These displacements are calculated from the earthquake parameters by the Okada formulas (Okada 1985).

It must be noted that the Imamura–Iida magnitude or the Soloviev–Imamura intensity gives an idea of the wave height on the coast and, consequently, permits to judge the scale of destructions. But although the Murty–Loomis tsunami magnitude ML is

a physically correct quantity, it cannot be unambiguously related to the manifestation of a tsunami on the coast.

Recently, a new detailed 12-point descriptive tsunami intensity scale was proposed in Papadopoulos and Imamura (2001). Its elaboration was based on the more than 100-years-long experience, accumulated by seismologists in drawing up earthquake intensity scales. This scale is not related to any quantitative physical parameters (wave amplitudes, energy and so on), it is organized in accordance with the following three features:

- (a) its influence upon people,
- (b) its impact on natural and artificial objects, including boats of different sizes,
- (c) the damage caused to buildings.

Therefore, a tsunami of large amplitude that hits a weakly inhabited coast may be assigned a low intensity in accordance with the Papadopoulos–Imamura scale. Contrarily, a tsunami of moderate amplitude that hits a densely populated coast may be characterized by quite a high intensity.

It is useful to present the Papadopoulos–Imamura intensity scale here completely. A consistent and systematic description of tsunami manifestations on the coast provides a full picture of the phenomenon.

The Papadopoulos–Imamura tsunami intensity scale

I. Not felt¹

- (a) Not felt even in most favorable circumstances;
- (b) No effect;
- (c) No damage;

II. Scarcely felt

- (a) Felt by some people in light boats. Not observed on the shore;
- (b) No effect;
- (c) No damage;

III. Weak

- (a) Felt by most people in light boats. Observed by some people on the shore;
- (b) No effect;
- (c) No damage;

IV. Largely observed

- (a) Felt by all people in light boats and some on large vessels. Observed by most people on shore;
- (b) Some light boats are slightly carried onto the shore;
- (c) No damage;

¹Registered only by special instruments.

V. Strong

- (a) Felt by all people on large vessels. Observed by all people on shore. Some people are frightened and run-up elevations;
- (b) Many light vessels are carried inland over significant distances, some of them collide with each other or are overturned. The wave leaves layers of sand in places with favorable conditions. Limited flooding of cultivated land along the coast;
- (c) Limited flooding of coastal structures, buildings and territories (gardens, etc.) near residential houses;

VI. Slightly damaging

- (a) Many people are frightened and run-up elevations;
- (b) Most light vessels are carried inland over significant distances, undergo strong collisions with each other, or are overturned;
- (c) Some wooden structures are destroyed and flooded. Most brick buildings have survived;

VII. Damaging

- (a) Most people are frightened and try to run away onto elevations;
- (b) Most light vessels are damaged. Some large vessels undergo significant vibrations. Objects of varying dimensions and stability (strength) are overturned and shifted from their positions. The wave leaves layers of sand and accumulates pebbles. Some floating structures are washed away to sea;
- (c) Many wooden structures are damaged, some are totally wiped away or carried out to sea by the wave. Destructions of first degree and flooding of some brick buildings;

VIII. Heavily damaging

- (a) All people run-up elevations, some are carried out to sea by the wave;
- (b) Most light vessels are damaged, many are carried away by the wave. Some large vessels are carried upshore and undergo collisions with each other. Large objects are washed away. Erosion and littering of the coast. Widespread flooding. Insignificant damage in antitsunami plantations of trees. Many floating structures are carried away by the wave, some are partially damaged;
- (c) Most wooden structures are carried away by the wave or completely wiped off the earth's surface. Destructions of second degree in some brick buildings. Most concrete buildings are not damaged, some have undergone destruction of first degree and flooding;

IX. Destructive

- (a) Many people are carried away by the wave;
- (b) Most light vessels are destroyed and carried away by the wave. Many large vessels are carried inland over large distances, some are destroyed. Broad

erosion and littering of the coast. Local subsidence of the ground. Partial destruction of antitsunami plantations of trees. Most floating structures are carried away, many are partially damaged;

- (c) Destructions of third degree in many brick buildings. Some concrete buildings have undergone destructions of second degree;

X. Very destructive

- (a) General panic. Most people are carried away by the wave;
- (b) Most large vessels are carried inland over large distances, many are destroyed or have undergone collisions with buildings. Small rocks (pebbles, stones) have been carried onshore from the seafloor. Vehicles are overturned and displaced. Petroleum spilt, fires. Widespread subsidence of ground;
- (c) Destructions of fourth degree in many brick houses, some concrete buildings have undergone destructions of third degree. Artificial dams (embankments) destroyed and harbor wavebreakers damaged.

XI. Devastating

- (b) Vital communications destroyed. Widespread fires. Reversed flows of water wash away to sea vehicles and other objects. Large rocks of different kinds are carried onshore from the seafloor;
- (c) Destructions of fifth degree in many brick buildings. Some concrete buildings suffer damage of fourth degree, many of third degree.

XII. Completely devastating

- (c) Practically all brick buildings are wiped out. Most concrete buildings have suffered destructions of degrees not lower than third.

1.4 Tsunami Warning Service: Principles and Methods

The extremely long and sad experience of Japan's population with many thousands of lives lost to tsunamis and earthquakes is expressed in the short inscription on the stone stellae often found near the coastline. The hieroglyphs on the stellae say the following:

Don't forget about earthquakes. If you feel an earthquake, don't forget about tsunamis. If you see a tsunami, run up a high slope.

The following legend is told by the inhabitants of the city of Wakayama, situated not far from Kyoto, the former capital of Japan and a most beautiful city. The mayor of Wakayama once felt an earthquake. He understood he had no time to warn the people on the shore of the tsunami danger, so he ran up the slope to the rice fields where the rice had been harvested, and set the granaries on fire. People, seeing the burning supplies of rice, hurried up to put the fire out and, thus, they happily evaded the lethal strike of the tsunami wave against the coast. The grateful inhabitants of the city erected a monument to the wise ruler.

The first tsunami warning in the far field, based on the interpretation of seismic data, seems to be related to the Kamchatka earthquake of February 3, 1923 (Okal 2011). When Thomas Jaggard, Director of the Hawaiian Volcano Observatory, entered the laboratory in the morning, he found that the seismometer intended for monitoring volcanic tremors had registered a strong and distant earthquake. It was not possible to determine the epicenter position from the data provided by a sole seismometer. But by the difference between the onsets of P and S waves one could estimate the distance from the epicenter. Estimates revealed an earthquake of great strength to have occurred somewhere in the Pacific Ocean basin. Several months earlier (November 11, 1922) the Hawaiian Islands had already been assaulted by tsunami waves with run-up heights of about 2 m, and the source of which was off the Chilean coast. From an analysis of this event, Thomas Jaggard knew the tsunami propagation velocity in the ocean. From the known distance to the epicenter, he calculated the arrival time of the tsunami caused by the Kamchatka earthquake of February 3, 1923, at the Hawaiian Islands and informed the local authorities in Hilo of his forecast. Regretfully, this forecast was simply considered the fantasy of “a gentleman scientist.” In the meantime the tsunami waves reached the Hawaiian Islands and caused damage of 1.5 million dollars as well as the death of a person. 10 years later, during the earthquake of March 2, 1933 (Sanriku), the story repeated itself. This time the local authorities treated the forecast with greater respect and evacuated the population from dangerous areas. The tsunami was destructive, but nobody died.

By the 1960s of the twentieth century many countries of the Pacific region had organized national tsunami warning systems. The tsunami service organizations include a whole network of seismic and hydrometeorological stations, special systems for operative alert transmission, administrative organs for adopting resolutions, and regional organizations for implementing evacuation plans of the population.

In past years the work of a tsunami warning service (TWS) was based on routine and/or urgent dispatches from operators on duty at seismic stations with round-the-clock tsunami services. If a nearby strong earthquake (of magnitude $M_S \geq 7$) is registered, the operator had, within 10 min, to determine the distance to its epicenter, the earthquake’s magnitude, and the approximate region of its location. The operator had then to transmit the signal “TSUNAMI warning” to the administrative organ, to the tsunami headquarters, and to the meteorological station. The oceanologist on duty at the meteorological station applied additional information to decide whether to announce the warning or not. The all-clear signal was announced by the tsunami headquarters upon agreement with specialists.

In modern TWS this technology is automatized. However, the main physical principles of operative tsunami forecasting remain the same. The possibility itself of warning is based on the propagation velocity of seismic waves being many times larger than the velocity of a tsunami wave. A warning is issued if a submarine earthquake is registered of magnitude M_S exceeding a threshold, the value of which varies depending on the region where the earthquake took place.

It must be stressed that estimation of a tsunami intensity based on seismic information is characterized by quite a low precision (see Sect. 2.1). Therefore, a significant number of the tsunami warnings issued happen to be false. A false warning has

at least two negative consequences. First, it results in economic damage (actions undertaken for evacuation, interruption in the operation of enterprises) and, second, it leads to a rise in concerns of the population over the tsunami warning service (TWS) trustworthiness.

An important success achieved in the operative tsunami prognosis consists in the possibility of rapid (real-time) calculation, with a precision and reliability sufficient for practical purposes, of the arrival time of a wave at a given (protected) point of the coast. Such a calculation can be performed applying simple ray theory. To this end it is only necessary to know the location of the tsunami source and the distribution of depths in the basin considered. We recall that the tsunami propagation velocity depends on the ocean depth, $c = \sqrt{gH}$. Data on the bathymetry of the World Ocean are free for a grid with step of 30 arc-seconds, and for many regions even with a significantly improved spatial resolution.

The situation concerning calculation of a tsunami run-up height at a given point of the coast is much worse. The calculation precision and speed required for practical purposes in resolving this problem has not been achieved yet. On the one hand, this is due to the enormous volume of calculations to be performed in estimating the evolution of a wave starting from its rise at the source up to its running up the shore. On the other hand, in the real-time mode it is impossible to calculate what happened at the tsunami source with necessary precision. The time required for the reliable determination of seafloor deformations, due to an earthquake, essentially exceeds the minutes or even hours available for operative forecasting. And in these cases, when underwater landslides participate in the tsunami generation, operative resolution of the problem turns out to be practically impossible.

An original way of resolving this problem was developed and implemented within the Japanese tsunami forecast system (Tatehata 1998; Handbook for Tsunami Forecast 2001). The method is based on tsunami sources exhibiting the property of recurrence. Therefore the problem, requiring long-time calculations, has been resolved beforehand. The results of calculations are presented in a special database. When a real underwater earthquake takes place, then in accordance with its magnitude and epicenter location necessary data are extracted from the database and used for calculating the possible run-up heights applying the interpolation method.

An operative forecast technique making use of preliminary tsunami calculations based on “unit sources” was developed in PMEL/NOAA (e.g. Titov et al. 2003; Gica 2008). At present this technique termed SIFT (Short-term Inundation Forecasting for Tsunamis) is used for guarding the US coast. In the case of a potentially tsunamigenic earthquake a composition approximating the tsunami source is made up of the “unit sources.” From the series of numerical calculations carried out in advance for the chosen “unit sources” a linear combination is formed, which is the tsunami forecast for the given segment of the coast. This technique reminds one of the aforementioned Japanese forecast system, although there also exists an essential difference. A most important progressive feature of the SIFT system consists in its inherent possibility of correcting a forecast, while the tsunami wave is registered first by the nearest to and then the more distant from the source ocean-bottom sealevel stations DART (Deep-ocean Assessment and Reporting of Tsunamis).

Here, it must be noted that the very idea of in-advance registration of tsunami waves far from the coast by bottom pressure sensors was put forward back in the 1960–1970s of the past century by Soloviev (1968), Jaque and Soloviev (1971). But only at the beginning of the twenty-first century did technological developments provide for broad practical implementation of this idea in such systems as DART (Bernard and Meinig 2011), GITEWS (Münch et al. 2011), NEPTUNE (Thomson et al. 2011), EMSO (Favali and Beranzoli 2009), DONET (Kaneda 2010; Matsumoto and Kaneda 2013). It may be said without any doubt whatsoever that the main progress achieved during the past decade in the tsunami warning system is related precisely to development of the networks of ocean-bottom sealevel stations. Indeed, real data on the actual origination of a tsunami and on its parameters permits with quite a high degree of reliability, inaccessible to seismic methods, to estimate the tsunami threat and to make a justified decision concerning the issue or cancellation of a warning.

Ocean-bottom sealevel stations have certainly proven to be the basis of a reliable and convenient method for the registration of tsunami waves in the open ocean. But this is not the only possible method. A tsunami wave can also be measured using satellite altimeters (radioaltimeters). Thus, for example, the catastrophic tsunami that occurred in December 2004, in the Indian Ocean was detected by a radioaltimeter established on the satellite JASON-1 [e.g., Kulikov et al. (2005)]. One more promising method for revealing tsunamis consists in the analysis of ionospheric perturbations generated by displacement of the water surface. Thus, a description of the ionospheric manifestations of the 2011 Tohoku tsunami can be found in Refs. (e.g. Makela et al. 2011; Kunitsyn et al. 2011).

The activities of national Tsunami Warning Systems during the catastrophic tsunami of December 26, 2004 in the Indian ocean clearly revealed the regional approach to creating services, when the “zone of responsibility” is only restricted to the coastal segment under control, to be irrational and insecure. The events in the Indian Ocean have actually made it necessary to alter the attitude toward both the investigation of tsunami waves and the measures taken for reducing the risk of the impact of this catastrophic phenomenon upon coastal communities and objects of the coastal infrastructure. The International Tsunami Information Center (ITIC, NOAA USA) took the initiative of proposing the most rapid creation of a World Tsunami Warning System. Within the framework of this initiative regular international tsunami exercises are being carried out since 2006. Such exercises are extremely important for supporting the high level of readiness of the personnel of tsunami warning services. Catastrophic tsunamis are characterized by a high degree of danger, but they occur rarely. In this connection it is reasonable to perfect the necessary procedures within the framework of specially organized exercises, instead of real events.

1.5 Tsunami Catalogs and Databases

It would be difficult to overestimate the importance of historical data on tsunami manifestations. As a rule, the estimation of tsunami risks, to which one or another coast happens to be exposed, is mainly based on data concerning historical events. In preparing operative tsunami forecasts use is also made of historical data, which permit to establish the threshold earthquake magnitude value that separates tsunamigenic and non-tsunamigenic seismic events in the region of interest. Moreover, historical data are of utmost importance for understanding the physical nature of tsunamis and of related phenomena.

Although mankind has been familiar with the phenomenon of tsunamis as least since antiquity (Marinatos 1939; Ambraseys 1962; Gusiakov 2009), data on historical events for a long time remained scattered among different sources and were never accumulated in a dedicated catalog. The first historical tsunami catalog was, apparently, created by N.H. Heck, who collected and systematized data on tsunami waves found in seismic catalogs (Gusiakov 2009). The first version of the catalog was published in French (Heck 1934). The English-language version, probably inspired by the April 1, 1946 Aleutian tsunami, was published 13 years later as an article in a periodical (Heck 1947). This first catalog contained data on 270 events that occurred in the World Ocean during the period of 479 B.C.–1946 A.D.

At the time, Heck's catalog was the only global tsunami catalog. In spite of it being short and incomplete it remained the only source of information for a long time. Later, numerous catalogs were created in Russia, Japan, the USA, and other countries. At present the list of catalogs numbers over 100 items (http://tsun.sccc.ru/tsulab/tsu_catalogs.htm).

Catalogs are divided into two classes: descriptive and parametric (Gusiakov 2009). Descriptive catalogs (e.g. Heck 1934, 1947; Imamura 1949; Takahasi 1951; Agostinho 1953; Iida 1956; Berninghausen 1962, 1964, 1966, 1968, 1969; deLange and Healy 1986; Zayakin and Luchinina 1987; Murty and Rafiq 1991; Lander et al. 2002) contain original descriptions of tsunami manifestations along coasts (including data on destructions) collected from most diverse sources. Such descriptions can be quite informative, and in a number of cases they even represent a certain substitution for photo/video materials or mareographic data. Descriptive catalogs, however, have an annoying disadvantage: the quantitative information on a phenomenon is spread over the entire text, so it is not easy to identify and submit it to processing. This disadvantage, naturally, does not belittle the role of descriptive catalogs, which always were and still remain a most important source of data on tsunamis and related phenomena.

Catalogs of the second type, parametric catalogs (e.g. Soloviev 1978; Iida 1984; Papadopoulos and Chalkis 1984; Hamzan et al. 2000; Papadopoulos 2001), are usually organized in the form of tables, which include all the main parameters of an event, such as, for example, its date, the coordinates of its earthquake epicenter, its depth, its magnitude, and, also, various quantitative tsunami parameters (measured run-ups, intensities, etc.). The main problem of parametric catalogs consists in

reducing the descriptive information involved to a minimum, which compels the user to rely totally on the interpretation of initial data (including descriptions) provided by the author of the catalog.

Some catalogs are composed of both descriptive and parametric sections. Such catalogs, besides tables including all basic quantitative parameters of a phenomenon, also contain a descriptive historical part (e.g., Soloviev and Go 1974, 1975; Everingham 1977, 1987; Watanabe 1989; Soloviev et al. 1992, 2000; Lander et al. 1993; Lander 1996; Fernandez et al. 2000; Papadopoulos 2000; Lockridge et al. 2002; O’Loughlin and Lander 2003; Fokaefs and Papadopoulos 1986; Papadopoulos et al. 2007; Stephenson et al. 2007).

“Paper” catalogs served as the main sources of information on tsunamis up to the 1970s of the twentieth century. Searching for data, their systematization, and verification were quite laborious. Therefore, with the development of computer technology electronic databases started to be created, which were, doubtless, more convenient for storing and processing large arrays of information.

The first steps toward the creation of a computerized tsunami database were undertaken at the International Tsunami Information Center (ITIC) in Honolulu, Hawaii (USA) in the middle of the 1970s (Pararas-Carayannis 1991; Gusiakov 2009). In the middle of the 1980s at the National Geophysical Data Center (NGDC/NOAA) in Boulder, Colorado (USA) the creation was initiated of a tsunami database, which integrated data from all the available catalogs and studies of tsunamis. For many years the NGDC/NOAA World-Wide Tsunami Database (Lockridge and Dunbar 1995) remained the only digital resource of information on tsunamis. At present the NGDC/NOAA World-Wide Tsunami Database is the most cited source of information on tsunamis.

At the beginning of the 1990s, within the framework of the project GITEC (Genesis and Impact of Tsunamis on the European Coast), initiated by the University of Bologna, Italy (GITEC 1992), the comprehensive historical tsunami database for the Mediterranean and other European surrounding seas was created, which integrated the data from numerous historical catalogs published for this region (Tinti et al. 2001, 2004). This database, termed the European Tsunami Catalog (ETC), underwent further development within the framework of the project TRANSFER (Tsunami Risk AND Strategies For the European Region) (TRANSFER 2005). At present this informational resource is known as the Euro-Mediterranean Tsunami Catalogue (EMTC) (Maramai et al. 2014).

In the middle of the 1990s, at the Novosibirsk Tsunami Laboratory (NTL) of the Institute of Computational Mathematics and Mathematical Geophysics of the Siberian Division of the Russian Academy of Sciences (ICM&MG SD RAS), the Expert Tsunami Database (ETDB) was created (Gusiakov et al. 1997; Gusiakov 2009). The main idea of this project was to integrate, within the framework of a unique system, not only historical data on tsunamis, but also means for analyzing these data as well as means for numerical simulation. Particular attention is paid to developing the geographical mapping subsystem that significantly simplifies data retrieval and visualization. Initially, the region embraced by ETDB was limited to the

Pacific ocean. The development of ETDB resulted in the well-known to specialists informational resource for tsunamis—Historical Tsunami Database for the World Ocean (HTDB/WLD).

Thus, at present, there exist two principal worldwide informational resources that contain information about tsunami waves. The first resource—Historical Tsunami Database for the World Ocean (HTDB/WLD)—contains information about approximately 2400 tsunamis that occurred in the World Ocean since 1628 B.C. The address of the accessible Internet version of the database is http://tsun.sccc.ru/Online_Cat.htm. The second resource—NOAA/WDS Global Historical Tsunami Database at NGDC (GHTD/NGDC)—contains information about 2500 tsunamis that occurred since 2000 B.C. The database GHTD/NGDC can be accessed at the address http://www.ngdc.noaa.gov/hazard/tsu_db.shtml. Both historical tsunami databases are constantly replenished, both owing to newly occurring tsunamis and to events of previous years for which new information is revealed.

Both historical databases contain information about the event date, the suspected tsunami source (in the case of an earthquake: its magnitude, the coordinates of its epicenter, its depth), the tsunami intensity, tsunami magnitude, the wave height, the tsunami cause, damage, validity, number of run-ups (and the very results of measurements), and other parameters. Moreover, various auxiliary information can be found on the bathymetry, seismicity, tectonics, volcanism, on settlements in coastal regions, and also on the network of mareographic observations. The databases provide users with convenient means for data selection (by dates, earthquake magnitudes, the intensity or height of waves, the level of damage, etc.) and visualization of geographic information (the Interactive Map).

On the whole, the contents of the informational resources HTDB/WLD and GHTD/NGDC are quite close to each other. No essential differences exist in time or spatial coverage. However, in the case of many historical events there do exist differences in their types of origin, the number of available run-up observations, resulting fatalities, and their degree of validity (Gusiakov 2009).

As an example of graphic representation of materials from the HTDB/WLD database, Fig. 1.4 shows the distribution of all tsunami sources in the World Ocean, known by 2014. The main tsunamigenic regions are clearly seen in the map. In most cases they are related to known seismically active regions.

An idea about the tsunami recurrence frequency can be obtained from Fig. 1.5, which shows how the number of tsunamis varied (within 10-year periods) between 1800 and 2014. All events are divided into two categories: significant tsunamis of intensity $I \geq 1$ are shown in red (Soloviev–Imamura scale), all known tsunamis are shown in blue. The recurrence rate of significant tsunamis is seen to be conserved at an approximately constant level (about two events per year). Here, the total number of tsunamis tends to increase, which is related to the progress in registering weak waves and to the exchange of information, and also to the development of the coastal zone. Similar comments can be made with respect to Fig. 1.6, in which the tsunami intensity is shown versus time.

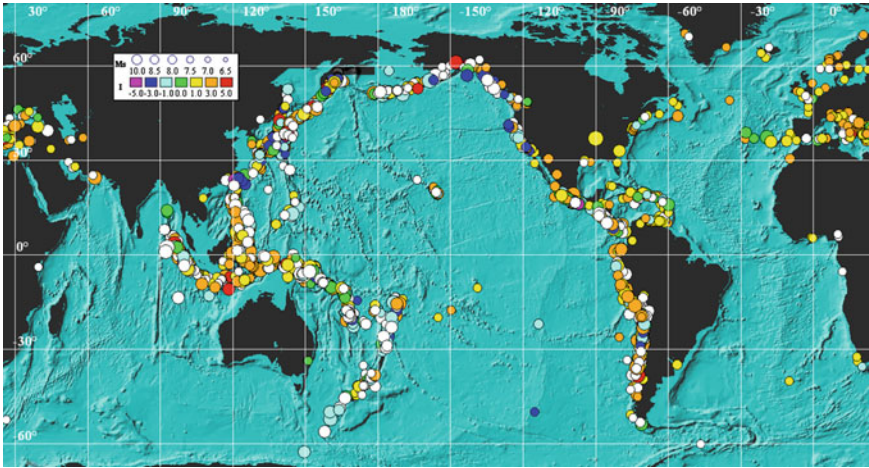


Fig. 1.4 Distribution of tsunami sources in the World Ocean within the period from 2000 B.C. up to 2014. The sizes of the circles correspond to earthquake magnitudes and their colors to the tsunami intensities

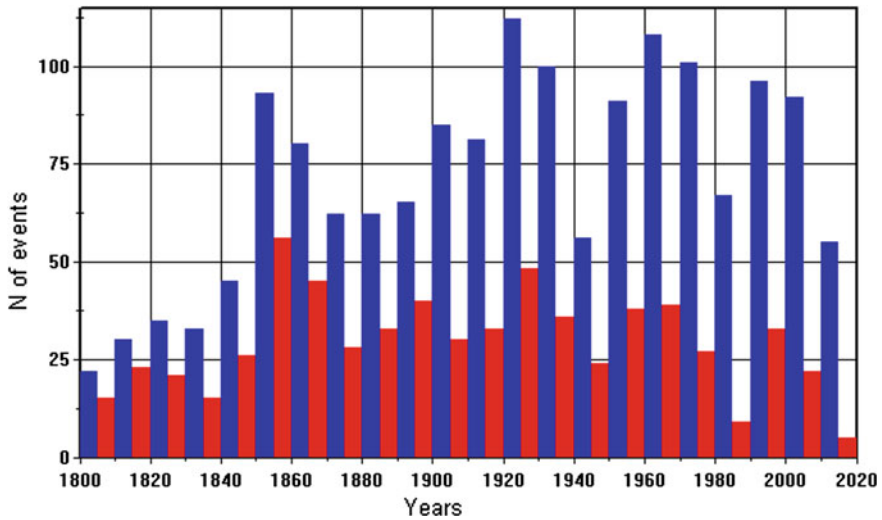


Fig. 1.5 Recurrence of tsunamis (number of events per decade) in the World Ocean between 1800 and 2014. The *blue* color shows all the known tsunamis, the *red* color indicates tsunamis of intensity $I \geq 1$ according to the Soloviev–Imamura scale

It must be underlined here that it would be wrong to draw a conclusion from Figs. 1.5 and 1.6 concerning enhancement of the tsunami recurrence rate in the past centuries. The tsunami recurrence rate can only vary significantly within geological time periods.

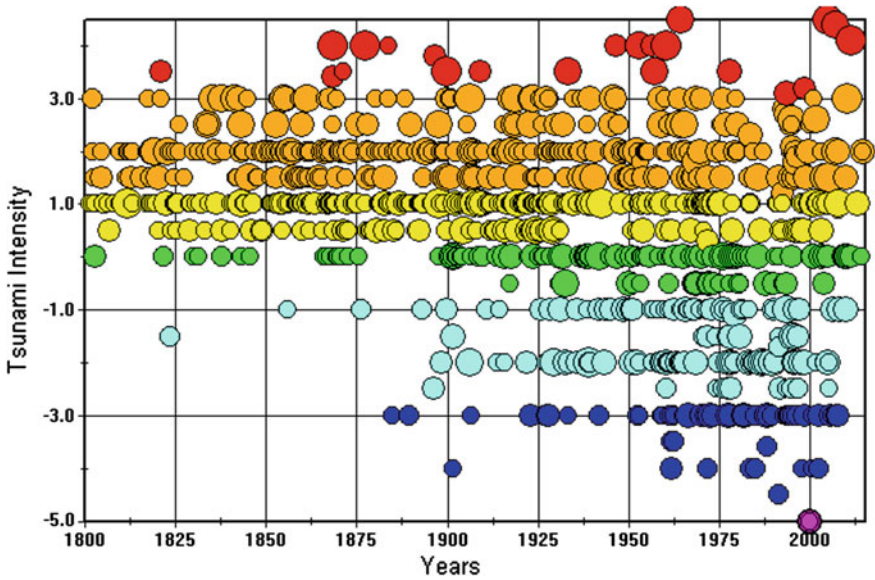


Fig. 1.6 Tsunamis of the World Ocean in the ‘intensity–time’ plane

To conclude this section we point out certain problems peculiar, generally speaking, to any informational tsunami sources. The issue involves the inaccuracy and fragmentarity of data (Gusiakov 2009). In most cases this concerns bygone events, the lack of information which often does not permit to make a reliable conclusion on the nature of the phenomenon described and, even more so, to achieve its quantitative estimation. For example, errors may arise when a totally different natural phenomenon, characterized by similar manifestations (e.g., a storm surge, high tide, river flood, rogue waves), is perceived as a tsunami. Errors may also be due to inaccurate interpretation of available descriptions, when attempts are made to extract from such descriptions quantitative or factual information on an event (e.g., its date and time, location, intensity, type of source). The use of different metric systems and of different calendars also serves as a source of errors in dating or in determining quantitative characteristics of events.

1.6 Seaquakes: General Ideas

Strong ocean bottom earthquakes result in the appearance near the coasts of gigantic devastating tsunami waves, while in the region of the earthquake epicenter unusual hydrodynamic phenomena are observed, which are known to seafarers by the term seaquakes. In certain cases the terms tide race, wave crowd are also used.

The transverse dimension of the perturbed region of the sea surface during a seaquake usually exceeds 10–100 km, while the duration of a strong seaquake may amount to 10 min. During a seaquake sets of very steep standing waves form on the surface of the aquatorium, there arise individual vertical columns of water, solitary water formations arise, and strong acoustic effects are noted. Spray sultans may be observed, as well as cavitational layers of water separating from each other and flying apart. A ship that happens to be in the zone of influence of a seaquake turns out to be surrounded by giant standing waves filling up the entire visible space. Terrible thunderous rumbling and howling are enhanced by sharp blows to the bottom, the most strong shaking of the vessel and the destruction of deck structures that had in the past endured more than a few storms.

From the point of view of the influence upon a human being and the danger for seafaring, a seaquake can compete with tsunamis and killer waves. Seaquakes lead to the destruction of structures on board ships, demoralization of the crew, the rise of critical and emergency situations on vessels, and the mass death of fish and other inhabitants of the ocean.

From general arguments it is clear that a seaquake results from the influence of seismic oscillations of the ocean bottom on the water column, as this process undergoes development in the epicentral zone and terminates when the action of the earthquake finishes. The effects of a seaquake, as a natural phenomenon, and their influence on ship constructions were studied by the renown geophysicists B. Gutenberg and A. Zieberg (Richter 1963). Below, we present the intensity scale for seaquakes developed by A. Zieberg and modified in Levin and Soloviev (1985).

- I A vibration, a light crackling of the deck.
- II A clear crackle, like a light scratching.
- III A strong jolt, as if running aground in shallow water, or on rocky bottom, or onto reef. Loud crack, vibration of objects.
- IV The vessel cracks and is shaken, unstable subjects fall.
- V People cannot stand up, large objects turn over, and fall out of supports, vessel loses speed, constructions creak painfully.
- VI The vessel may be thrown out of the water, masts and deck constructions are broken, emergency situation.

In the opinion of C.F. Richter, one of the founding fathers of seismology, “although the problem of seaquakes contains no unresolvable riddles, to the best of our knowledge, it was neglected for so long, that at present it represents a promising field of studies for new individuals with new ideas.”

Modern catalogs, articles, and scientific publications contain over 250 descriptions of seaquakes in various regions of the World Ocean. Among the recent events one must note the strong damage of eight fishing boats in the region of the South Kuril islands after the Shikotan earthquake of 1994 and the destruction of the huge tanker “Exxon” in the Gulf of Alaska resulting from a seaquake in 1988. Below, follows a scenario of the development of a “generalized” seaquake based on materials of individual descriptions due to witnesses (Levin 1996).

Synthesized description of a seaquake

On a totally breezeless day the smooth mirror-like sea surface became all of a sudden covered with bumps. These aquatic bumps that looked like waves did not move away in any direction, but they did not remain motionless either. They grew rapidly up to a height of about 8m and then shrank down forming deep craters in the place of the recent bumps.

The oscillations were rapid, we were dazzled by these unusual boiling waves filling up all the visible sea space. The aquatic surface seethed and jumped up and down, as if it were in a red-hot kettle with salt brine. The boat was thrown up and down, and it rocked ominously on these jumping waves. They were as steep as the most ferocious storm waves, but no longer than 20m. The keel rocking was so strong that the propeller was several times seen to be completely dry in air, and the wheel of the ship compass fell off its pivot.

All the passengers and crew poured out on deck. The bright sunshine and total calm only enhanced the tension of this terrifying spectacle of a sea gone crazy.

Less than a minute passed but no willpower was left to resist this monstrous galloping, which once in a while weakened, then strengthened again. Hands clinging to the ship's sides felt how unreliable this plaintively creaking vessel was in front of the mysterious and incomprehensible sea catastrophe.

The aquatic bumps started to become smaller, while the frequency of their blinking increased. At the same time from somewhere out of the depth a low thunderous rumble arose that suppressed all willpower and reason. People started thrashing around the ship full of panicky fear. Many passengers, and even sailors, could not bear such torture and, having evidently lost their minds, started to jump overboard. Against the background of these blinking waves there started to appear very high jets of water that collapsing created a strange rustling sound.

All of a sudden the ship was shaken by a most strong blow. Several persons were thrown overboard. The blows to the bottom of the ship came one after another. The ship seemed to batter the rocky seafloor, although the depth of the water exceeded 100m. The impression was that enormous barrels full of water were jumping up and down in the hold and that the sheathing was on the brink of breaking. The shrouds trembled, the handrails of the ladder broke down, the windows of the deck cabin crumbled, the deck superstructures started to move and fall to pieces.

The vessel prepared for its unavoidable death.

Suddenly the din stopped. The sea continued to vibrate, gradually calming down. The vessel that had suffered in 2 minutes more than from the most monstrous storm was rocking quietly on the breezeless sunlit surface of the sea. If the seaquake had continued for half a minute more, then it would have surely led to the appearance of still another "Flying Dutchman", abandoned by its crew, or to the mysterious disappearance in the ocean of one more vessel together with its crew.

Most regions of the World Ocean are known to be characterized by a clearly pronounced stable temperature stratification—the cold lower column several kilometers thick is separated from the atmosphere by a relatively thin (measured by hundreds of meters) warm 'film', comprising a thermocline and a mixed layer. The possibility of cold deep-water masses being transferred up to the surface layer of the ocean

by nonlinear flows in the seaquake zone was first mentioned in Levin et al. (1993) in relation to the identification of a tsunami source from outer space. Later it was pointed out that a seaquake can cause the development of such powerful turbulence as to result in the warm film destruction and in the formation on the surface of the ocean of a cold 'spot' with an area exceeding 1000km^2 ; it was noted that such a 'spot' is capable of exerting significant influence on the structure of the temperature field of near-the-water layer of the atmosphere and to lead to weather anomalies (Levin et al. 1998; Nosov 1998a, b).

1.7 Hydroacoustic Signals in the Case of Underwater Earthquakes

The capability of underwater earthquakes to excite hydroacoustic signals has been known long ago (Ewing et al. 1950; Soloviev et al. 1968; Kadykov 1986). Hydroacoustic waves propagating in the ocean from the epicentral zone of an earthquake are called the T-phase or T-waves. Investigation of this phenomenon traditionally pertains to the scientific activity of seismologists. The term T-phase originated from seismological classification, as this wave is registered as the third phase (*tertia*) after the appearance of phases P (*prima*) and S (*secunda*). A classical definition of the T-phase to be found, for example, in Okal et al. (2003) sounds as follows: "T-phases are seismic waves recorded by seismometers, which have travelled the major part of the source-to-receiver path as acoustic waves channelled in the ocean water column by the SOFAR low velocity waveguide." The SOFAR waveguide that was discovered independently in the 1940s by Maurice Ewing (USA) and Leonid Brekhovskikh (USSR) represents a practically perfect natural waveguide that is conducive to the propagation of hydroacoustic waves over thousands of kilometers from their source. The property of a T-phase to cover large distances from the source provides for the possibility of registering this phenomenon by many, including distant, seismic stations and precisely for this reason the T-phase has been known already for more than half a century.

The conditions for an acoustic signal to propagate along the SOFAR channel are such that the wavelength must not exceed the waveguide thickness. Hence follows the restriction on the T-phase frequency; in most cases the frequency must be superior to 2 Hz.

At the beginning the T-phase phenomenon even gave rise to certain hopes of resolving the problem of operative tsunami forecasting (Ewing et al. 1950). These hopes, however, were not to be fulfilled. The relationship between tsunamis and the T-phase turned out to be no less complex and ambiguous than the relationship of tsunamis and seismic waves. Moreover, a peculiar "anticorrelation" was revealed between tsunamis and the T-phase (Okal et al. 2003). Slow earthquakes, characterized by a lack of high-frequency seismic wave emission and, consequently, a T-phase deficit, were found to be capable of exciting gravitational tsunami waves quite effectively. We recall that slow earthquakes are also conventionally called "tsunami earthquakes."

The spectrum of bottom seismic motions covers quite a broad range from 0.001 up to 100 Hz. Therefore, in the case of underwater earthquakes, besides high-frequency hydroacoustic waves (the T-phase), low-frequency hydroacoustic waves for which the entire water column serves as a waveguide may also originate. Such low-frequency waves were observed relatively not long ago during analysis of the tsunamigenic 2003 Tokachi-Oki earthquake (Nosov et al. 2005; Nosov and Kolesov 2007; Li et al. 2009; Ohmachi and Inoue 2010; Bolshakova et al. 2011). Since the water layer limited from below by the elastic rough bottom and from above by the excited free surface was not a perfect natural waveguide (unlike the SOFAR channel), low-frequency elastic oscillations were not capable of propagating through long distances and they were only observed in the vicinity of the source that generated them. Moreover, owing to the existence of a cutoff frequency elastic oscillations of the water layer produced in the deep-water region could not penetrate shallow water, and, consequently, they could not contribute directly to the tsunami run-up height. But the contribution of hydroacoustic effects to the tsunami wave height on a coast can be indirect—due to nonlinear effects (Novikova and Ostrovsky 1982; Nosov and Kolesov 2005; Nosov et al. 2008). These effects are dealt with in detail in Chap. 4.

Registration of the T-phase is possible not only with the aid of seismographs, but also using hydrophones. The latter method, for instance, is actively used in the American system SOSUS (SOund SURveillance System) (Fox and Hammond 1994), operating from the middle of the 1950s and initially intended for searching for submarines. The system represents a set of hydrophones connected to the coastal services by a cable line. Registration of a T-phase signal by the SOSUS system permits to successfully determine the coordinates of epicenters of underwater earthquakes, which serves as a successful alternative to traditional seismological methods (<http://www.pmel.noaa.gov/vents>). Similar hydroacoustic systems were also created some time ago in the USSR) (From the history 1998).

In Russia, several recent years saw the revival of research aimed at making use of hydroacoustic signals from underwater earthquakes for tsunami warning (Sasorova et al. 2002). If a tsunami is excited by a nearby earthquake, the modern tsunami warning system has very little chance of providing a timely alert signal, as the time provided by Nature for reacting (the time interval between the arrival of the seismic signal and the first tsunami wave) amounts to less than 5 min. At present, the only promising way of withstanding local tsunamis consists in making use in good time of available information on the preparatory stages of a developing underwater earthquake.

Analysis of the records of oceanic hydroacoustic noises, obtained by the Russian multipurpose antenna AGAM within the framework of the international program ATOC (Acoustic Thermometry of the Ocean's Climate) between 1998 and 1999 revealed promising results. The set of hydrophones established on the Pacific shelf of Kamchatka registered hydroacoustic signals of seismic origin in the 3–70 Hz frequency range, which appeared much earlier than the first blow from the earthquake (from hours down to several minutes) (Lappo et al. 2003). The signals were generated by microearthquakes in the preparation area of a strong earthquake and were evidence of the development of the event's critical stage.

It must be noted that signals of a similar type caused by microdestructions of rock (acoustic emission and so on) and propagating in ground and rock dampen very rapidly and are practically imperceptible by land stations already at a distance of several kilometers from the source. The amplitude of an acoustic signal drops exponentially with the distance, and the exponent is proportional to the signal's frequency. The damping factor in water for a signal of frequency 100 HZ amounts to 0.0006 dB/km, in magmatic rock it is approximately 0.01 dB/km, in sedimentary rock and sand of the order of 0.1 and 0.5 dB/km, respectively. A signal of frequency 30 HZ dies out completely in sand at a distance of 2 km from the source, in consolidated sedimentary rock at a distance of 10 km. In water such a signal is reliably registered at distances of up to 1000 km.

Hence follows the important conclusion that hydroacoustic monitoring of the preparation process of an oceanic earthquake may lead to success in resolving the difficult problem of revealing in good time a nearby earthquake at its preparation stage and of issuing a timely and effective warning of the possible rise of a local tsunami.

During strong underwater earthquakes the ocean bottom in the epicentral area is deformed, and the deformation not only has a horizontal component, but a vertical one as well. If the motion is directed vertically upward, then a wave of compression forms in the water and propagates toward the surface; if the motion is downward, then a decompression wave forms. When reflected from a free surface of water, an elastic wave changes its polarity; therefore, independently of the sign of the deformation there may always be realized a wave of decompression which tends to "tear apart" the liquid. The amplitude of pressure variations related to elastic waves can be calculated by the formula

$$p_d = \rho c U,$$

where ρ is the water density, c is the velocity of sound in the water, U is the velocity of motion of the ocean bottom. If the bottom moves with a velocity of 1 m/s, the pressure amplitude will amount to $p_d = 1.5$ MPa.

Besides variations of pressure due to elastic waves, in the water layer there exists a hydrostatic pressure, the increase of which with the depth is approximately linear,

$$p_{st} = p_{atm} + \rho g z.$$

The total pressure $p_d + p_{st}$ at large depths is always positive, but in the layer near the surface (for $U = 1$ m/s down to $z \approx 140$ m) a situation may arise when the dynamic pressure exceeds the hydrostatic pressure in absolute value, hence the total pressure turns out to be negative.

The limit strength of water under tension is known to be about 0.25 MPa. Therefore, in the subsurface layer where the total pressure $p_d + p_{st}$ exceeds in absolute value the limit strength of water, violation of the water continuity is possible and it is called cavitation. The influence of the described mechanism taking place above the epicenter of an underwater earthquake results in the formation of a zone of cavitating (partly foaming) water. This zone has a reflection coefficient (albedo) differing from the reflection coefficient of all the remaining surface of the aquatorium. In this

case the perturbed zone of the water surface can be registered by remote methods (from satellites, airplanes, etc.). Note that cavitation effects in the subsurface layer are observed in the case of underwater explosions.

References

- Abe, K.: Tsunami propagation on a seismological fault model of the 1952 Kamchatka earthquake. *Bull. Nippon Dental Univ.* **8**, 3–11 (1979)
- Abe, K.: Physical size of tsunamigenic earthquakes of the northwestern Pacific. *Phys. Earth Planet. Inter.* **27**, 194–205 (1981)
- Abe, K.: Quantification of major earthquake tsunamis of the Japan Sea. *Phys. Earth Planet. Inter.* **38**, 214–223 (1985)
- Abe, K.: Quantification of tsunamigenic earthquakes by the M_t scale. *Tectonophysics* **166**, 27–34 (1989)
- Agostinho, J.: Notes on some tsunamis of the Azores. *Annales de la Commission Pour l'Etude des Raz de Maree. Internat. Union Geod. Geophys.* **5**, 21–24 (1953)
- Ambraseys, N.N.: Data for investigation of the seismic sea-waves in the eastern Mediterranean. *Bull. Seismol. Soc. Am.* **52**, 895–913 (1962)
- Bernard, E., Meinig, C.: History and future of deep-ocean tsunami measurements. In: *Proceedings of Oceans' 11 MTS/IEEE, Kona, 7 p. IEEE, Piscataway, NJ, No 6106894 (2011), 19–22 September 2011*
- Berninghausen, W.H.: Tsunamis reported from the west coast of South America, 1562–1960. *Bull. Seismol. Soc. Am.* **52**(4), 915–921 (1962)
- Berninghausen, W.H.: Tsunamis and seismic seiches reported from the Eastern Atlantic ocean south of the Bay of Biscay. *Bull. Seismol. Soc. Am.* **54**(1), 439–442 (1964)
- Berninghausen, W.H.: Tsunamis and seismic seiches reported from regions adjacent to the Indian Ocean. *Bull. Seismol. Soc. Am.* **56**(1), 69–74 (1966)
- Berninghausen, W.H.: Tsunamis and seismic seiches reported from the Western North and South Atlantic and the coastal waters of Northwestern Europe. U.S. Naval Oceanographic Office, Washington D.C., Informal Report, vol. 6885, 48 pp. (1968)
- Berninghausen, W.H.: Tsunamis and seiches of Southeast Asia. *Bull. Seismol. Soc. Am.* **59**(1), 289–297 (1969)
- Bolshakova, A., Inoue, S., Kolesov, S., Matsumoto, H., Nosov, M., Ohmachi, T.: Hydroacoustic effects in the 2003 Tokachi-Oki tsunami source. *Russ. J. Earth Sci.* **12**, ES2005 (2011). doi:[10.2205/2011ES000509](https://doi.org/10.2205/2011ES000509)
- de Lange, W.P., Healy, T.R.: New Zealand tsunamis, 1840–198. *N. Z. J. Geol. Geophys.* **29**, 115–134 (1986)
- Everingham, I.B.: Preliminary Catalog of Tsunamis for the New Guinea-Solomon Islands Region, 1768–1972. Report No. 180, Department of Minerals and Energy, Bureau of Mineral Resources: Geology and Geophysics, 85 pp. Canberra, Australia (1977)
- Everingham, I.B.: Tsunamis in Fiji. Ministry of Lands, Energy & Mineral Resources, Mineral Resources Department, Suva, Fiji, Report 62, ISSN 0250-7234; Second Printing, August 1988, 27 pp. (1987)
- Ewing, W.M., Tolstoy, I., Press, F.: Proposed use of the T phase in tsunami warning systems. *Bull. Seismol. Soc. Am.* **40**, 53–58 (1950)
- Favali, P., Beranzoli, L.: EMSO: European multidisciplinary seafloor observatory. *Nucl. Instrum. Methods Phys. Res. Sect. A: Accel. Spectrom. Detect. Assoc. Equip.* **602**(1), 21–27 (2009)
- Fernandez, M.A., Molina, E., Havskov, J., Atakan, K.: Tsunamis and tsunami hazards in Central America. *Nat. Hazards* **22**, 91–116 (2000)

- Fokaefs, A., Papadopoulos, G.A.: Tsunami hazard in the Eastern Mediterranean: strong earthquakes and tsunamis in Cyprus and the Levantine Sea. *Nat. Hazards* **40**, 503–526 (2007)
- Fox, C.G., Hammond, S.R.: The VENTS program T-phase project and NOAA's role in ocean environmental research. *MTS J.* **27**(4), 70–74 (1994)
- From the history of our home hydroacoustics (in Russian). In: Karlik, Ya.S., Krylov, A.N.: (eds.) Collection. TsNII Publishing house, St.Petersburg (1998)
- Fuchs, V.: *Of Ice and Men: The Story of the British Antarctic Survey 1943–1973*. The Bath Press, Avon, Great Britain (1982)
- Gica, E., Spillane, M.C., Titov, V.V., Chamberlin, C.D., Newman, J.C.: Development of the forecast propagation database for NOAA's Short-Term Inundation Forecast for Tsunamis (SIFT), Technical Memorandum OAR PMEL–139, 89 pp. Government Printing Office, Seattle, WA (2008)
- GITEC—Genesis and Impact of Tsunamis on the European Coast, 1992. A Research Proposal Submitted to the Commission of the European Communities, January 1992
- Gusiakov, V.K., Marchuk, A.G., Osipova, A.V.: Expert tsunami database for the Pacific: motivation, design and proof-of-concept demonstration. In: Hebenstreit, G. (ed.) *Perspectives on Tsunami Hazard Reduction: Observations, Theory and Planning*, pp. 21–34. Kluwer Academic Publisher, Dordrecht (1997)
- Gusiakov, V.K.: Tsunami history-recorded. In: Robinson, A., Bernard, E. (eds.) *The Sea, Tsunamis*, vol. 15, pp. 23–53. Harvard University Press, Cambridge (2009)
- Gusiakov, V.K.: Strongest Tsunamis in the World Ocean and the problem of marine coastal security. *Izv. Atmos. Ocean. Phys.* **50**(5), 435–444 (2014)
- Hamzan, L., Puspito, N., Imamura, F.: Tsunami catalog and zones in Indonesia. *J. Nat. Disaster Sci.* **22**(1), 25–43 (2000)
- Handbook for Tsunami Forecast in the Japan Sea. Earthquake and Tsunami Observation Division, Seismological and Volcanological Department, Japan Meteorological Agency, 22 pp. (2001)
- Hatori, T.: Classification of tsunami magnitude scale. *Bull. Earthq. Res. Inst. Univ. Tokyo* **61**, 503–515 (1986) (in Japanese with English abstract)
- Heck, N.H.: List of seismic waves. *Annales de la Commission pour l'Etude des Raz de Maree* **4**, 20–41 (1934)
- Heck, N.H.: List of seismic sea waves. *Bull. Seismol. Soc. Am.* **37**(4), 269–286 (1947)
- Iida, K.: Earthquakes accompanied by tsunamis occurring under the sea off the islands of Japan. *J. Earth Sci. Nagoya Univ.* **4**, 1–43 (1956)
- Iida, K.: Catalog of tsunamis in Japan and its neighboring countries. Special Report, Aichi Institute of Technology, Japan, 52 pp. (1984)
- Iida, K.: The generation of tsunamis and the focal mechanism of earthquakes. In: Adams, W.M. (ed.) *Tsunamis in the Pacific Ocean*, pp. 3–18. East-West Center Press, Honolulu (1970)
- Imamura, A.: History of Japanese tsunamis. *Kayo-No-Kagaku (Oceanography)* **2**, 74–80 (1942). (in Japanese)
- Imamura A.: List of tsunamis in Japan. *J. Seismol. Soc. Jpn.* **2** 23–28 (in Japanese) (1949)
- Jaque, V.M., Soloviev, S.L.: Remote registration of tsunami type weak waves on the shelf of the Kuril Islands. *Dokl. Akad. Nauk USSR* **198**(4), 816–817 (1971). (in Russian)
- Kadykov, I.F.: *The Acoustics of Submarine Earthquakes* (in Russian). Nauka, Moscow (1986)
- Kaneda, Y.: The advanced ocean floor real time monitoring system for mega thrust earthquakes and tsunamis—application of DONET and DONET2 data to seismological research and disaster mitigation. In: *Proceedings of the OCEANS Conference* (2010). doi:[10.1109/OCEANS.2010.5664309](https://doi.org/10.1109/OCEANS.2010.5664309)
- Kulikov, E.A., Medvedev, P.P., Lappo, S.S.: Satellite recording of the Indian Ocean tsunami on 26 December 2004. *Dokl. Earth Sci.* **401**(3), 444–448 (2005)
- Kunitsyn, V.E., Nesterov, I.A., Shalimov, S.L.: Japan megathrust earthquake on 11 March 2011: GPS-TEC evidence for ionospheric disturbances. *JETP Lett.* **94**(8), 616–620 (2011)
- Lander, J.F.: *Tsunamis Affecting Alaska, 1737–1996*. National Geophysical Data Center (NGDC), Boulder, CO, NGDC Key Geophys. Res. Doc. 31, Nat. Geophys. Data Center, NOAA, Boulder, CO, 195 pp. (1996)

- Lander, J.F., Lockridge, P.A., Kozuch, M.J.: Tsunamis Affecting the West Coast of the United States, 1806–1992. National Geophysical Data Center (NGDC), Boulder, CO, NGDC Key to Geophysical Records Doc. vol. 29, 242 pp. (1993)
- Lander, J.F., Whiteside, L.S., Hatori, P.: The tsunamis history of Guam, 1849–1993. *Sci. Tsunami Hazards* **20**(3), 158–174 (2002)
- Lappo, S.S., Levin, B.W., Sasorova, E.V., et al.: Hydroacoustic location of an oceanic earthquake origin area. *Dokl. Earth Sci.* **389**, 2 (2003)
- Levin, B.W.: Tsunamis and seaquakes in the ocean (in Russian). *Priroda* **5**, 48–61 (1996)
- Levin, B., Kaistrenko, V., Kharlamov, A., Chepareva, M., Kryshny, V.: Physical processes in the ocean as indicators for direct tsunami registration from satellite. In: Proceedings of the IUGG/IOC International Tsunami Symposium Wakayama, Japan, pp. 309–319 (1993)
- Levin, B.W., Nosov, M.A., Pavlov, V.P., Rykunov, L.N.: Cooling of the ocean surface as a result of seaquakes. *Dokl. Earth Sci.* **358**(1), 132–135 (1998)
- Levin, B.W., Soloviev, S.L.: Variations of the field of mass velocities in the pleistoseist zone of an underwater earthquake (in Russian). *DAN SSSR* **285**(4), 849–852 (1985)
- Levin, B.W., Kaistrenko, V.M., Rybin, A.V., Nosov, M.A., Pinegina, T.K., Razzhigaeva, N.G., Fitzhugh, B.: Manifestations of the tsunami on November 15, 2006, on the Central Kuril Islands and results of the runup heights modeling. In: *Doklady Earth Sciences*, Vol. 419, No. 1, pp. 335–338. MAIK Nauka/Interperiodica (2008)
- Li, W., Yeh, H., Hirata, K., Baba, T.: Ocean-bottom pressure variations during the 2003 Tokachi-Oki earthquake. In: Lynett, P. (ed.) *Nonlinear Wave Dynamics*, pp. 109–126. World Scientific Publishing Co., Singapore (2009)
- Lockridge, P.A., Whiteside, L.S., Lander, J.F.: Tsunamis and tsunami-like waves of the eastern United States. *Sci. Tsunami Hazards* **20**(3), 120–157 (2002)
- Lockridge, P.A., Dunbar, P.: *World-Wide Tsunamis, 2000 B.C.–1990 World Data Center A for Solid Earth Geophysics*. Boulder, Colorado 31 pp. (1995)
- Makela, J.J., Lognonné, P., Hébert, H., Gehrels, T., Rolland, L., Allgeyer, S., Lamouroux, J.: Imaging and modeling the ionospheric airglow response over Hawaii to the tsunami generated by the Tohoku earthquake of 11 March 2011. *Geophys. Res. Lett.* **38**(24), 1–5 (2011)
- Maramai, A., Brizuela, B., Graziani, L.: The Euro-Mediterranean tsunami catalogue. *Ann. Geophys.* **57**(4), S0435 (2014)
- Marinatos, S.: The volcanic destruction of Minoan Crete. *Antiquity* **13**, 425–439 (1939)
- Matsumoto, H., Kaneda, Y.: Some features of bottom pressure records at the 2011 Tohoku earthquake—Interpretation of the far-field DONET data. In: Proceedings of the 11th SEGJ International Symposium, Yokohama, Japan, p. 493, (2013). doi:[10.1190/segj112013-124](https://doi.org/10.1190/segj112013-124)
- Münch, U., Rudloff, A., Lauterjung, J.: Postface “The GITEWS project—results, summary and outlook”. *Nat. Hazards Earth Syst. Sci.* **11**, 765–769 (2011). doi:[10.5194/nhess-11-765-2011](https://doi.org/10.5194/nhess-11-765-2011)
- Murty, T.S., Loomis, H.G.: A new objective tsunami magnitude scale. *Mar. Geod.* **4**, 267–282 (1980)
- Murty, T.S., Rafiq, M.: Tentative list of tsunamis in the marginal seas of the North Indian Ocean. *Nat. Hazards* **4**(1), 81–83 (1991)
- Nosov, M.A.: Effect of submarine earthquake on a stratified ocean. *Mosc. Univ. Phys. Bull.* **53**(4), 23–27 (1998a)
- Nosov M.A.: Ocean surface temperature anomalies from underwater earthquakes. *Volcanol. Seismol.* **19**(3), 371–375 (1998b)
- Nosov, M. A., Kolesov, S.V. (2005): Nonlinear tsunami generation mechanism in compressible ocean. *Vestnik Moskovskogo Universita. Ser. 3 Fizika Astronomiya* (3) 51–54
- Nosov, M.A., Kolesov, S.V.: Elastic oscillations of water column in the 2003 Tokachi-oki tsunami source: in-situ measurements and 3-D numerical modelling. *Nat. Hazards Earth Syst. Sci.* **7**, 243–249 (2007)
- Nosov, M.A., Kolesov, S.V., Ostroukhova, A.V., Alekseev, A.B., Levin, B.W.: Elastic oscillations of the water layer in a tsunami source. *Dokl. Earth Sci.* **404**(7), 1097–1100 (2005)
- Nosov, M.A., Kolesov, S.V., Denisova, A.V.: Contribution of nonlinearity in tsunami generated by submarine earthquake. *Adv. Geosci.* **14**, 141–146 (2008)

- Novikova, L.E., Ostrovsky, L.A.: On the acoustic mechanism of tsunami wave excitation (in Russian). *Oceanology* **22**(5), 693–697 (1982)
- Ohmachi, T., Inoue, S.: Dynamic tsunami generation process observed in the 2003 Tokachi-oki, Japan, earthquake. *Adv. Geosci. Ocean Sci.* **18**, 159–168 (2010)
- Okal, E.A., Alasset, P.J., Hyvernaud, O., Schindel , F.: The deficient T waves of tsunami earthquakes. *Geophys. J. Int.* **152**(2), 416–432 (2003)
- Okada, Y.: Surface deformation due to shear and tensile faults in a half-space. *Bull. Seismol. Soc. Am.* **75**(4), 1135–1154 (1985)
- Okal, E.A.: Tsunamiogenic earthquakes: past and present milestones. *Pure Appl. Geophys.* **168**(6–7), 969–995 (2011)
- O’Loughlin, K.F., Lander, J.F.: Caribbean Tsunamis. A 500 year history from 1498–1998. *Advances in Natural and Technological Hazards Research*, 263 pp. Kluwer Academic Publishers, Dordrecht (2003)
- Papadopoulos, G.A., Imamura, F.: A proposal for a new tsunami intensity scale. In: *Proceedings ITS*, pp. 569–577 (2001)
- Papadopoulos, G.A. (ed.): *Historical earthquakes and tsunamis in the Corinth Rift, Central Greece*, vol. 12, 129 pp. National Observatory of Athens, Institute of Geodynamics Publisher (2000)
- Papadopoulos, G.A.: Tsunamis in the East Mediterranean: a catalogue for the area of Greece and adjacent seas. In: *Proceedings of the Joint IOC-IUGG International Workshop “Tsunami Risk Assessment Beyond 2000: Theory, Practice and Plans. In memory of Professor S.L. Soloviev. Moscow, Russia, 14 to 16 June 2000”*, Moscow, pp. 34–43 (2001)
- Papadopoulos, G.A., Chalkis, B.J.: Tsunamis observed in Greece and the surrounding area from antiquity up to the present times. *Mar. Geol.* **56**, 309–317 (1984)
- Papadopoulos, G.A., Daskalaki, E., Fokaefs, A., Giraleas, N.: Tsunami hazards in the Eastern Mediterranean: strong earthquakes and tsunamis in the East Hellenic Arc and Trench system. *Nat. Hazards Earth Syst. Sci.* **7**, 57–64 (2007)
- Pararas-Carayannis, G.: *ITIC Progress Report for 1989–1991*, 66 pp. Honolulu, ITIC/NOAA (1991)
- Richter, C.F.: *Elementary Seismology* (in Russian). Foreign literature Publishing House, Moscow (1963)
- Sasorova, E.V., Didenkulov, I.N., Karlik, Y.S., Levin, B.W., et al.: Underwater earthquakes near shorelines: acoustic methods for identifying the preparation process of an earthquake and the prospects of their application for tsunami warning systems (in Russian). In: *Collection of Articles “Local Tsunamis: Warning and Risk Mitigation*, pp. 167–180. Yanus-K, Moscow (2002)
- Sieberg, A.: *Geologische. Physikalische und Angewandte Erdbebenkunde*. Verlag von Gustav Fischer, Jena (1927)
- Soloviev, S.L.: The tsunami problem and its significance for the Kamchatka and the Kuril islands (in Russian). In: *The Tsunami Problem*, pp. 7–50. Nauka, Moscow (1968)
- Soloviev, S.L.: Basic data on tsunamis on the Pacific coast of the USSR. *Izuchenie Tsunami v Otkrytom Okeane*, pp. 61–135. “Nauka” Publishing House, Moscow (1978) (in Russian)
- Soloviev, S.L., Voronin, P.S., Voronina, S.I.: Seismic hydroacoustic data on the T wave (review of the literature) (in Russian). In: *The Tsunami Problem*, pp. 142–173. Nauka, Moscow (1968)
- Soloviev, S.L., Go, C.N.: *Catalogue of Tsunamis on the Western Coast of the Pacific Ocean (173–1968)* (in Russian). Nauka, Moscow (1974)
- Soloviev, S.L., Go, C.N.: *Catalogue of Tsunamis on the Eastern Coast of the Pacific Ocean (1513–1968)* (in Russian). Nauka, Moscow (1975)
- Soloviev, S.L., Go, C.N., Kim, KhS: *Catalogue of tsunamis in the Pacific Ocean, 1969–1982* (in Russian). Izd. MGK, USSR AS, Moscow (1986)
- Soloviev, S.L., Go, Ch.N., Kim, Kh.S., *Catalog of Tsunamis in the Pacific, 1969–1982*. (translated from Russian to English by Amerind Publishing Co., Pvt. Ltd., New Delhi 1988), Academy of Sciences of the USSR, 208 pp. Soviet Geophysical Committee, Moscow (1992)
- Soloviev, S.L., Go, C.N., Kim, Kh.S., et al.: *Tsunamis in the Mediterranean Sea, 2000 B.C.–1991 A.D.* (in Russian), Nauchnyi mir, Moscow (1997)

- Soloviev, S.L., Solovieva, O.N., Go, Ch.N., Kim, Kh.S., Shchetnikov, N.A.: *Tsunamis in the Mediterranean Sea: 2000 B.C.–2000 A.D.* Translation from Russian to English by Gil B. Pontecorvo and Vasiy I. Tropin, 237 pp. Kluwer Academic Publishers, Dordrecht (2000)
- Soloviev, S.L., Go, Ch.N.: *A catalogue of tsunamis on the western shore of the Pacific Ocean*, Moscow, “Nauka” Publishing House, 308 p. English translation: Soloviev S.L., Go Ch.N. (1984). *A catalogue of tsunamis on the western shore of the Pacific ocean*, Translation by Canada Institute for Scientific and Technical Information, National Research Council, Ottawa, Canada KIA OS2 (1974)
- Soloviev, S.L., Go, Ch.N.: *Catalog of Tsunamis on the Eastern Shore of the Pacific Ocean*. Academy of Science of the USSR, Nauka Publishing House, Moscow, Translated from Russian to English by Canadian Institute for Science and Technical Information, No. 5078, National Research Council, Ottawa, Canada, 1984, 293 pp. (1975)
- Stephenson, F., Rabinovich, A.B., Solovieva, O.N., Kulikov, E.A., Yakovenko, O.I.: *Catalogue of tsunamis*, British Columbia, Canada, 1700–2007, 133 pp. Institute of Oceanology RAS, Moscow (2007)
- Takahasi, R.: *An estimate of future tsunami damage along the Pacific coast of Japan*. Bull. Earthq. Res. Inst. Tokyo Univ. **29**(1), 71–95 (1951)
- Tatehata, H.: *The new tsunami warning system of the Japan Meteorological Society*. Sci. Tsunami Hazards **16**(1), 39–49 (1998)
- Tinti, S., Maramai, A., Graziani, L.: *A new version of the European tsunami catalogue: updating and revision*. Nat. Hazards Earth Syst. Sci. **1**, 255–262 (2001)
- Tinti, S., Maramai, A., Graziani, L.: *The new catalogue of the Italian tsunamis*. Nat. Hazards **33**, 439–465 (2004)
- Titov, V.V., González, F.I., Mofjeld, H.O., Newman, J.C.: *Short-term inundation forecasting for tsunamis*. Submarine Landslides and Tsunamis, pp. 277–284. Springer, Netherlands (2003)
- Thomson, R., Fine, I., Rabinovich, A., et al.: *Observation of the 2009 Samoa tsunami by the NEPTUNE-Canada cabled observatory: test data for an operational regional tsunami forecast model*. Geophys. Res. Lett. **38**, L11701 (2011). doi:[10.1029/2011GL04](https://doi.org/10.1029/2011GL04)
- TRANSFER—*Tsunami Risk ANd Strategies For the European Region*, 2005. Research Proposal presented to Sixth Framework Programme Sustainable Development, Global and Ecosystems Priority. 6.3.IV.2.2: *Assessment and Reduction of Tsunami Risk in Europe*, October 2005
- Watanabe, H.: *Comprehensive list of tsunamis to hit the Japanese Islands*, 2nd edn, 206 pp. University Tokyo Press, Japan (1989) (in Japanese)
- Zahibo, N., Pelinovsky, E., Yalciner, A., Zaitsev, A., Talipova, T., Nikolkina, I., Chernov, A., Insel, I., Dilmen, D.I., Ozer, C.: *Trans-Atlantic propagation of 1755 tsunami and its effects on the French West Indies*. Open Oceanogr. J. **5**, 30–41 (2011)
- Zayakin, Yu.A., Luchinina, A.A.: *Catalog of Tsunamis in Kamchatka*, Obninsk, Russia, VNIIGMI-WDC, 51 pp. (1987) (in Russian)

Chapter 2

Source of a Tsunami of Seismotectonic Origin

Abstract Modern ideas are presented concerning the source of an earthquake and the seismotectonic source of a tsunami. The main physical processes taking place at a tsunami source are described. Estimation is performed of the role of secondary effects: of displacements of the bottom, occurring in its own plane, of the Coriolis force, of density stratification of the water. The Okada formulae are presented and the technique is exposed for calculating coseismic ocean bottom deformations caused by an underwater earthquake. The dependence of the properties of coseismic ocean bottom deformation at the tsunami source upon the earthquake magnitude and depth is analyzed applying the Okada formulae in the case of a rectangular fault. Formulae are presented that relate the maximum values of the ocean bottom deformation amplitude, the displaced volume, and the initial elevation energy to the moment magnitude of the earthquake. From the slip distribution, adopted from the SRCMOD database, the vector fields of coseismic ocean bottom deformations were calculated applying the Okada formulae for the sources of 75 underwater earthquakes that occurred during the period between 1923 and 2013. It was shown that horizontal deformation components of an inclined bottom, as a rule, provide an additional and noticeable contribution to the displaced water volume and to the potential energy of the initial elevation (the tsunami energy). The relationships were analyzed between the ocean bottom deformation amplitude, the displaced volume and the tsunami energy, and the moment magnitude of the earthquake; the respective regression dependences were plotted. The part of the earthquake energy transferred to the tsunami waves was shown to increase with its moment magnitude, but even in the case of catastrophic earthquakes it does not exceed 0.1%. From HTDB/WLD and GHTD/NGDC data the peculiarities were investigated of the space–time distribution of tsunamis.

Keywords Tsunami source · Tsunami generation · Bottom earthquake · Moment magnitude · Rectangular fault · Finite fault model · Slip distribution · Coseismic deformation · Initial elevation · Water displacement · Tsunami energy · Tsunami intensity

According to historical data on tsunamis in the World Ocean (HTDB/WLD, GHTD/NGDC) most of the events (more than 70%) are due to strong underwater earthquakes. In this connection, ideas of the seismotectonic origin of tsunamis are on the

whole certainly of supreme importance for the issue of tsunamis. In this chapter we shall mainly deal with problems of solid-state (-earth) physics, in particular, with problems relevant to the physics of earthquake sources. At the same time, in the first section of this chapter certain hydrodynamic estimates will, nevertheless, be presented, that are necessary for a tsunami-oriented analysis of underwater earthquakes.

2.1 The Main Parameters and Secondary Effects

According to modern ideas, an earthquake is the abrupt release of strain accumulated in the Earth's crust, resulting from the relatively slow motion of lithosphere plates (Kanamori and Brodsky 2004). The source of an earthquake can be represented as a displacement that occurs owing to a fault along one or several planes. In the case of large shallow events the rupture speed amounts to 75–95% of the velocity of S-waves. An earthquake is characterized by the seismic moment

$$M_0 = \mu DS[\text{N} \cdot \text{m}], \quad (2.1)$$

where μ is the shear modulus of the medium, D is the displacement amplitude between the opposite edges of the fault, S is the area of the fault surface. The earthquake's moment magnitude is related to the seismic moment by the following relationship:

$$M_w = \frac{\log_{10} M_0}{1.5} - 6.07. \quad (2.2)$$

Some seismic events (for example, Sanriku, 1896, the Aleutian earthquake, 1946) caused tsunamis of intensities higher than could be expected from the available seismic data. Kanamori (1972) termed such earthquakes “tsunami earthquakes” and presumed them to occur, when the process at the earthquake source underwent unusually slow development. This case is characterized by a low emission efficiency of the high-frequency component of seismic waves, which is not so important for the process of tsunami generation.

Figure 2.1 presents the relationships between the tsunami intensity (Soloviev–Imamura scale) and the earthquake magnitudes M_S (a) and M_w (b) for the World Ocean constructed by means of the Historical Tsunami Database for the World Ocean (HTDB/WLD) (see Sect. 1.5). The large spread between the data signifies that the relationship between tsunamis and earthquakes is complex and ambiguous. Comparison of the plots presented in Fig. 2.1 permits to conclude that the tsunami intensity dependence upon the magnitude M_S is characterized by a noticeably larger spread than the dependence on the magnitude M_w . The advantage of a moment magnitude scale is quite evident in the case of strong seismic events, which is apparently due to the known saturation problem peculiar to the scale of magnitudes M_S . However, the data spread remains quite significant, also, when the moment magnitude is

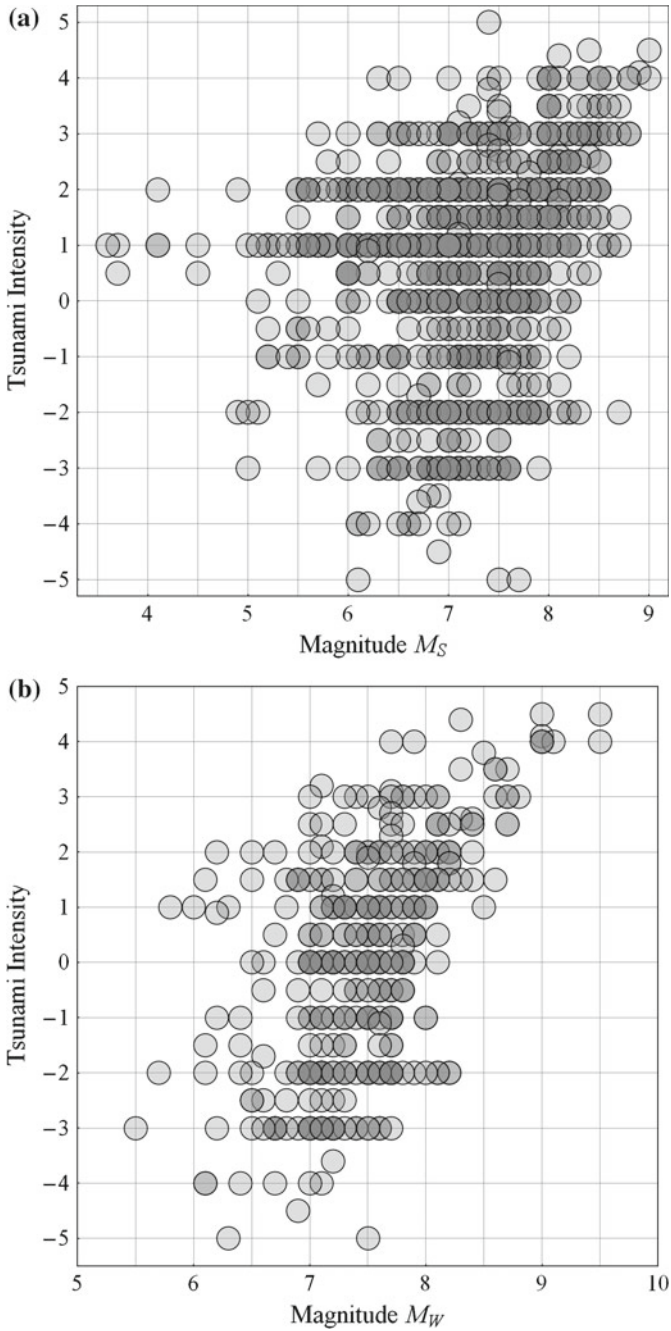


Fig. 2.1 Dependence of the tsunami intensity, according to the Soloviev–Imamura scale, upon the earthquake magnitudes M_S (a) and M_W (b) for the World Ocean

used: if the value of M_w is fixed, the difference in tsunami intensities may differ by several units. For example, if $M_w = 8$, the tsunami intensity varies within 6 units (from -2 up to $+4$). This means that the average heights of tsunami runups may differ by a factor of 64 (2^6)! Hence it becomes evident that a tsunami prognosis based only on seismic data is extremely unreliable. It is also important, here, to note that in the case of strong seismic events the moment magnitude often turns out to be primarily underestimated.

According to Gusiakov (2011) such a significant uncertainty in the tsunami intensity for a fixed earthquake magnitude is due to the following four reasons: (1) the difference in water depths within a source area; (2) the difference in earthquake source mechanisms; (3) the difference in earthquake focus depths; (4) the difference in tectonic settings of the source area (marginal seas, subduction zones, deep-water oceanic plate, etc.).

It is seen that success in the investigation of tsunami generation is related not only to resolution of the hydrodynamic part of the problem, but also to progress in resolving such a difficult problem as description of the earthquake source. It must be noted, that the large spread is also due to the tsunami intensity not being a rigorously defined physical quantity, like, for example, energy. At any rate, a certain positive correlation within the dependences under consideration can be identified: earthquakes of higher magnitudes are generally accompanied by tsunamis of higher intensities. The dependences presented is a good illustration of the magnitude criterion applied in the tsunami warning system. It is seen that the formation of practically all significant tsunamis ($I > 2$) was due to earthquakes of magnitudes $M_w > 7$. Moreover, from Fig. 2.1b one can conclude that earthquakes with magnitudes $M_w \geq 9$ are always accompanied by catastrophic tsunamis of intensities $I \geq 4$.

Figure 2.2 presents distributions of the number of events (tsunamis) over the earthquake source depth and magnitudes M_S (a) and M_w (b). The distributions are based on data from the Historical Tsunami Database for the World Ocean (HTDB/WLD). The HTDB/WLD database contains information on a total of over 2400 tsunamis. The magnitudes M_S and the depths of earthquake sources are known simultaneously for approximately 800 events, while the values of the magnitude M_w and the source depth are known for about 500 events. Most known tsunamis are seen from the figure to originate from strong and shallow earthquakes. The maxima of the distributions lie within the range of magnitudes (M_S or M_w) between 7 and 8 and within the range of source depths from 30 up to 50 km. The rapid decrease in the distributions with the increase of depths and decrease in magnitudes reveals that weak and deep seismic events are rarely accompanied by tsunami waves. The distributions decreasing as the magnitude increases is related to very strong underwater earthquakes occurring extremely rarely, although such seismic events, naturally, always give rise to tsunami waves.

Until the end of the twentieth century, studies of the process of tsunami generation by an earthquake were impeded by the absence of any direct measurements in the source zone. Indeed, all the information on processes proceeding at a tsunami source has been obtained by remote measurements done with mareographs (coastal and deep-water devices), seismographs or hydroacoustic systems. Evidence provided

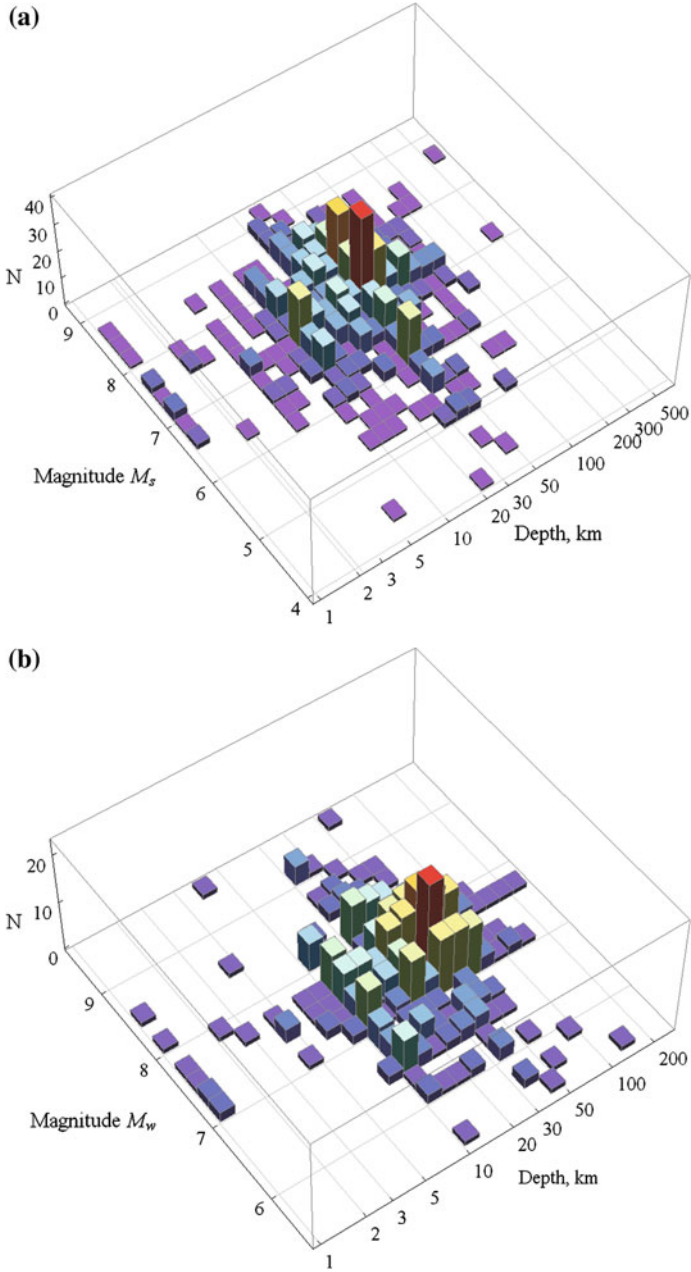


Fig. 2.2 Distributions of the number of events (tsunamis) over the earthquake source depth and magnitudes M_S (a) and M_w (b), based on data from the Historical Tsunami Database for the World Ocean (HTDB/WLD)

by witnesses of underwater earthquakes is quite scarce, and it, naturally, concerns phenomena that took place at the ocean surface. At the beginning of the present century the situation with measurements at a tsunami source changed drastically owing to a sharp rise in the number of deep-water observatories, especially close to Japan. This resulted in the first measurements in history being performed with the aid of sea-bottom stations JAMSTEC (Japan Agency for Marine-Earth Science and Technology) directly at the source of the tsunami Tokachi-Oki of 2003 (Watanabe et al. 2004, Nosov et al. 2005, Mikada et al. 2006). After 7.5 years no less interesting measurements were implemented in 2011 using sea-bottom stations at the source of the catastrophic tsunamigenic earthquake Tokhoku (e.g., Ito et al. 2011).

In simulating a tsunami of seismic origin a convenient method is usually applied that permits not to deal with the description of the generation process in a straightforward manner. The “roundabout maneuver” consists of the following. An earthquake is considered to suddenly cause residual deformations of the ocean bottom (actually the duration of the process at the source may amount to 100 s and more). The residual deformations of the bottom are deduced from the parameters of the earthquake source. Then, the assumption is made that the displacement of the bottom is simultaneously accompanied by formation at the surface of the ocean of a perturbation, the shape of which is fully similar to the residual deformations of the bottom. The perturbation of the water surface (the initial elevation), thus obtained, is then applied as the initial condition in resolving the problem of tsunami propagation.

It is interesting that the possibility to transfer sea-floor perturbations up to the surface is based on the actual structure of the equations for shallow water requiring the sole condition that the sea-floor deformation process be rapid. If, contrariwise, one applies, for instance, potential theory, then, even if the process is instantaneous, the perturbation of the liquid’s surface and the residual deformation will differ from each other.

In general, it is evidently not correct, from a physical point of view, to transfer sea-floor deformations up to the surface. Such an approach turns out to be imperfect, since within its framework at least the following eight factors are neglected: (1) dynamics of the bottom deformation, (2) water compressibility, (3) nonlinear effects, (4) the contribution of horizontal deformations of the sloping (uneven) sea-floor, (5) the smoothing effect of a water layer, (6) stratification, (7) rotation of the Earth, (8) horizontal momentum transfer to the water layer.

The significance of some of the factors mentioned above is quite evident. Thus, for example, in the case of deformation of the seafloor, lasting for a long time, i.e., when a long wave has time to propagate over a noticeable distance, as compared with the horizontal dimension of the source, elevation of the surface will at no particular moment of time coincide with the residual displacements of the seafloor. But this effect could still be taken into account within the framework of the long-wave theory. If, on the other hand, the duration of the deformation is small, then the motion of the water layer must be described within the framework of the theory of a compressible liquid. Here, the theory of long waves turns out to be totally inapplicable. In the case of high-speed displacement of the seafloor an additional contribution to the tsunami wave can also be given by nonlinear effects.

Note the paradoxical effect manifested when tsunami generation is considered as a process proceeding in an incompressible liquid. For definiteness we shall assume an earthquake resulting in area S ($\sqrt{S} \gg H$) of the seafloor being displaced vertically with a constant velocity by a quantity η_0 during a time interval τ . According to the theory of an incompressible liquid, practically all the water layer immediately above the moving part of the seafloor acquires a vertical velocity $\eta_0 \tau^{-1}$, and, consequently, the kinetic energy

$$W_k = \frac{\rho S H \eta_0^2}{2\tau^2}. \quad (2.3)$$

The displacement results in a perturbation forming on the water surface (we shall consider it identical to the deformation of the seafloor), which contains the potential energy

$$W_p = \frac{\rho S g \eta_0^2}{2}. \quad (2.4)$$

The paradox consists in that the kinetic energy involved in the process has a fixed value, but immediately after its completion the kinetic energy disappears without leaving a trace. The paradox is readily resolved, naturally, if the condition $W_p \gg W_k$ is applied. But in reality the kinetic energy may not only be comparable to the potential energy, but even significantly exceed it. Indeed, from formulae (2.3) and (2.4) we have

$$\frac{W_k}{W_p} = \frac{\tau_0^2}{\tau^2},$$

where $\tau_0 = (H/g)^{1/2}$ is the propagation time of a long gravitational wave over a distance equal to the depth of the ocean, ($\tau_0 \approx 20$ s for $H = 4000$ m). In many cases $\tau < \tau_0$, and, consequently, $W_k > W_p$. An accurate resolution of the said paradox is possible within the framework of the theory of compressible liquids.

For an adequate mathematical description of the processes occurring when waves are generated it is necessary to have a clear idea of the characteristic values of the main parameters defining the problem. The range of tsunami wave periods has already been indicated above. The depth of the ocean in area of a tsunami source may vary from several kilometers to zero (when the area of the seafloor deformation extends onto the land). The horizontal size of the tsunami source usually amounts to tens and even hundreds of kilometers. The empirical dependence, that relates the mean radius R_{TS} [km] of the tsunami source and the earthquake magnitude M , is known (Dotsenko and Soloviev 1990a):

$$\lg R_{TS} = (0.50 \pm 0.07) M - (2.1 \pm 0.6). \quad (2.5)$$

Note that real tsunami sources, naturally, do not exhibit a circular, but instead a more complex, as a rule, elongated shape. At any rate, the boundary of a tsunami source is a concept that is essentially conventional. The source of a tsunami of seismic origin can be defined as the area, within which an earthquake has resulted in noticeable residual deformations of the seafloor. From records of waves made by the method of inverse isochrones it is possible to reconstruct the tsunami source region. It is interesting that a source reconstructed in this manner usually exhibits a reasonable correspondence to the area of aftershock manifestations. It must also be stressed that, as a rule, residual deformations are bipolar, i.e., elevation of the seafloor takes place in one part of the source and it is subsided in another part. Figure 2.3, taken from Satake and Imamura (1995), presents the example of the reconstruction of the 1968 Tokachi–Oki tsunami source.

Figure 2.4 shows the areas of the fault surface at the earthquake source (solid line) and of the tsunami source (dotted line) as functions of the earthquake seismic moment (magnitude). The area of the tsunami source was calculated as the area of a circle with a radius determined by formula (2.5). The area of the tsunami source can be seen to be several times larger than the area of the fault at the earthquake source, which is quite reasonable from a physical point of view. It is interesting to note that the said dependencies are practically parallel.

Another essential parameter characterizing tsunami generation by an earthquake is the displacement amplitude ξ_0 [m] of the oceanic surface at the source. This quantity approximately follows the vertical residual deformations of the ocean bottom. The corresponding regression estimate exhibits the following form:

$$\lg \xi_0 = (0.8 \pm 0, 1) M - (5.6 \pm 1.0). \quad (2.6)$$

Formulae (2.5) and (2.6) were derived in Dotsenko and Soloviev (1990a) for magnitudes within the range of $6.7 < M < 8.5$ by analysis of the wave field at the source, reconstructed from measurements at the coast. The estimates for intervals correspond to a 80 % probability. Note that formula (2.6) seems to yield overestimated values of residual displacements in the case of large magnitudes. The catastrophic tsunamigenic earthquake, that occurred on December 26, 2004, and the magnitude of which was $M_w = 9.1$, exhibited maximal vertical displacements of 7.8 m for the uplift area and of 5.9 m for the subsidence area (see Fig. 2.15b). Formula (2.6) yields a value ~ 48 m.

The duration of processes at the tsunami source also represents an important parameter of the problem. Here, one must distinguish among several characteristic quantities. Earlier, we already introduced the timescale $\tau_0 = (H/g)^{1/2}$ peculiar to problems involving surface gravitational waves. Besides, there also exists the propagation time of a long gravitational wave over a distance, equal to the horizontal extension of the source, $T_{TS} = R_{TS}(gH)^{-1/2}$. Note that the order of the tsunami wave period depends precisely on the quantity T_{TS} . In a similar manner one can also introduce the propagation time of a hydroacoustic wave along the source, $T_S = R_{TS}/c$, where c is the speed of sound in water. The maximum period of normal elastic oscillations of a water layer, $T_0 = 4H/c$, is also related to hydroacoustic waves. And,

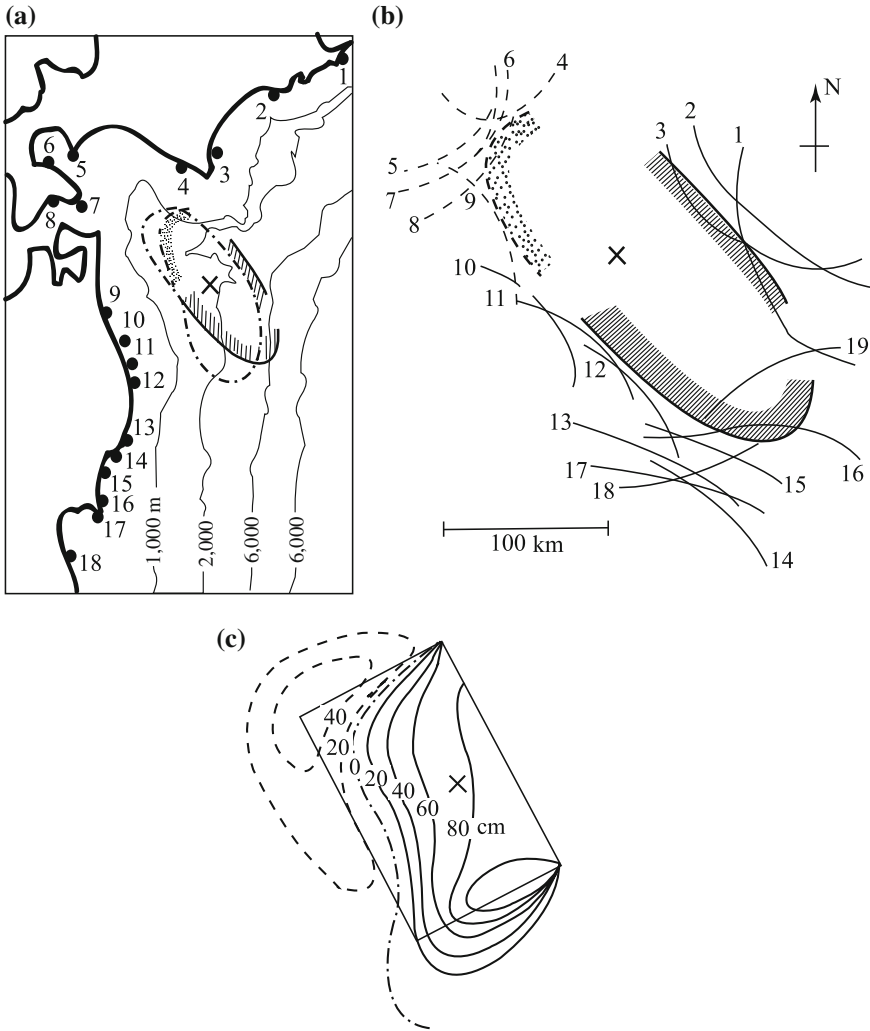


Fig. 2.3 Tsunami source restored applying the method of inverse isochrones (b), and residual deformations of the seafloor (c) for the 1968 Tokachi-Oki earthquake. The figures are the numbers of mareographs, the locations of which are shown in the map (a). The *solid* and *dotted* curves correspond to the positive and negative leading wave, respectively. Adapted from Satake and Imamura (1995)

ultimately, there exists a time, that characterizes the duration of a process occurring at an earthquake source, T_{EQ} . Note that deformation of the seafloor (especially in the case of strong earthquakes) does not proceed simultaneously over the entire area of the tsunami source, but propagates horizontally following the fault that forms at the earthquake source. Therefore, the duration of the seafloor deformation at a

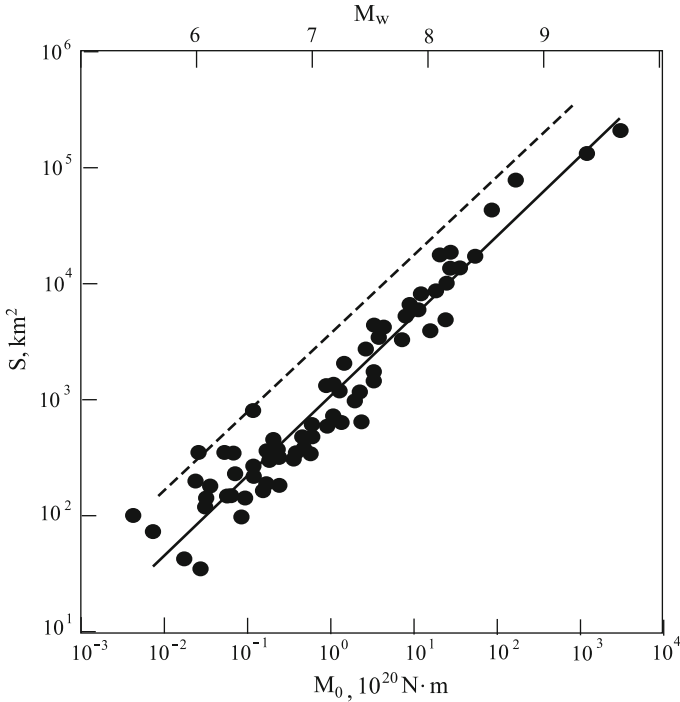


Fig. 2.4 The area of the fault at the source of the earthquake (*solid line*) versus the seismic moment (magnitude). Adapted from Kanamori and Brodsky (2004). The *dotted line* represents an estimation of the area of the tsunami source in accordance with formula (2.3)

certain point may turn out to be significantly shorter than the quantity T_{EQ} . In the Harvard seismic catalogue (<http://www.seismology.harvard.edu/>) a temporal characteristic termed “half duration” is presented, which corresponds to half the duration of the process at an earthquake source. We shall denote this quantity by T_{hd} [s]. Analysis of all the earthquakes of magnitude $M_w > 7$, presented in the Harvard catalogue for the period between January 1976 and March 2005, (370 events) permitted us to obtain the following regression relationship:

$$\lg T_{hd} = (0.42 \pm 0.02) M_w - (1.99 \pm 0.14). \quad (2.7)$$

Such a range of amplitudes was chosen, because significant tsunamis are excited by earthquakes with $M_w > 7$.

Figure 2.5 demonstrates the relation between the above temporal scales and the earthquake magnitude. In constructing the dependences we have applied formulae (2.5) and (2.7) and, besides, for definiteness, we have assumed the ocean depth to vary between 10^2 and 10^4 m.

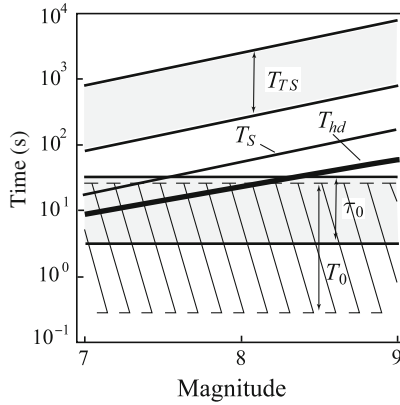


Fig. 2.5 Timescales of a tsunami source as functions of the earthquake magnitude. T_{TS} is the tsunami period, T_{hd} is the duration of the process at the earthquake source (the “half duration”), T_S is the propagation time of the hydroacoustic wave along the tsunami source, T_0 is the maximal period of normal elastic oscillations of the water layer, τ_0 is the timescale for gravitational waves. The ranges correspond to the interval of oceanic depths, 10^2 – 10^4 m

From Fig. 2.5 it can be seen that, as a rule, the duration of processes at the earthquake source, T_{hd} , is significantly inferior to the period of the tsunami wave, T_{TS} , that lies within the range 10^2 – 10^4 s. Therefore, the generation of waves is generally a relatively rapid process. The quantity τ_0 (within the considered range of magnitudes) is always smaller than the period of the tsunami wave, T_{TS} , however, in a number of cases this difference may turn out to be not so significant. In this connection, a tsunami can be considered a long wave, but with certain restrictions: in the case of small-size sources phase dispersion is certain to be manifested. Let us, now, turn to the quantity T_S , which always lies between the quantities T_{TS} and T_{hd} . This reflects the fact that the speed of hydroacoustic waves is always superior to the speed of long waves, but inferior to the speed, with which the fault opens up at the earthquake source. We further turn to elastic oscillations of the water layer. It is readily noted that the quantities T_0 and T_{hd} have very close values, so that effective excitation of elastic oscillations of the water layer is possible at the tsunami source. From the figure it is also seen that the maximal period T_0 of elastic eigen oscillations of the water layer is always smaller than the tsunami period T_{TS} , i.e., elastic oscillations and tsunami waves exist in ranges that do not intersect. This, however, does not mean that elastic oscillations cannot at all contribute to the energy of tsunami waves. Such a contribution can be realized by means of nonlinear effects.

In setting boundary conditions on hard surfaces in hydrodynamic problems one conventionally distinguishes between the normal and tangential components of the flow velocity of the liquid. In the problem of tsunami generation such a hard surface is represented by the ocean bottom, which in the case of an earthquake can undergo motion both in its own plane, and in a perpendicular direction. We will term such displacements tangential and normal. Actually, the surface of the ocean

bottom has a complex structure, therefore the normal is conventionally constructed in a certain plane—the result of averaging either over the entire area of the tsunami source, or over a part of it. We shall consider the differences between this plane and the actual surface of the bottom to be irregularities.

We shall show that, for the excitation of motions in a water layer, normal displacements of the ocean bottom are essentially more effective, than tangential ones. Let each point of the bottom surface at the tsunami source of area S undergo displacement over a distance η_0 during a time τ : once in the tangential direction and then in the normal direction. The normal to the bottom surface is at an angle α to the vertical direction. The slope of the surface of the oceanic bottom rarely exceeds 0.1, therefore the angle α can be considered small.

During tangential shifts the ocean bottom exerts a force on the water layer, equal to $\rho(u^*)^2 S$, where u^* is the friction velocity, ρ is the density of water. The energy transferred to the water layer by the ocean bottom undergoing motion can be estimated as the work performed by this force along the path η_0 :

$$W_t = \rho(u^*)^2 S \eta_0. \quad (2.8)$$

If one passes to the reference frame related to the moving ocean bottom, then one obtains the traditional problem of a logarithmic boundary layer, in which the quantity η_0/τ plays the part of the velocity of the average flow far from the boundary. The friction velocity is known to be essentially smaller than the velocity of the average flow, therefore it is possible to write

$$W_t \ll \rho S \frac{\eta_0^3}{\tau^2}. \quad (2.9)$$

We shall estimate the energy transferred to an incompressible layer of water by a normal displacement as the potential energy of the initial elevation above the water surface. We shall assume the horizontal dimensions of the source to essentially exceed the ocean depth $S^{1/2} \gg H$ and the displacement to be quite rapid, $\tau \ll S^{1/2}(gH)^{-1/2}$. In this case the entire volume of water dislodged by the slip, $\eta_0 S$, will be distributed over an area $S \cos \alpha$ of the ocean surface. Thus, the amplitude of the initial elevation will amount to $\eta_0/\cos \alpha$. Taking into account the smallness of the angle α we obtain the following estimate for the potential energy of the initial elevation:

$$W_n = \rho g S \frac{\eta_0^2}{2}. \quad (2.10)$$

Let us find the ratio between the energies transferred to the water layer by the normal and tangential displacements,

$$\frac{W_n}{W_t} \gg \frac{g\tau^2}{\eta_0}. \quad (2.11)$$

If one assumes $\eta_0 = \xi_0$, $\tau = T_{\text{hd}}$, and applies formulae (2.6) and (2.7), then one can readily show that $g\tau^2/\eta_0 \approx 800 \gg 1$. Hence it follows that tangential motions of the ocean bottom can be neglected in the problem of tsunami generation.

Thus, movements of the seafloor in a direction perpendicular to the sea bottom surface and accompanied by displacements of water happen to be the main effect leading to tsunami generation.

The real ocean is always stratified, and, moreover, owing to rotation of the Earth each moving particle of the water is under the influence of a Coriolis force. Therefore, tsunami generation is, generally speaking, accompanied by the formation of internal waves and vortical motions.

Let us estimate the effect due to rotation of the Earth, when a tsunami is generated by vertical displacements of the ocean bottom. We shall apply the linearized equations of shallow water written with account of the Coriolis force for a horizontally infinite ocean of depth H .

$$\frac{\partial u}{\partial t} = -g \frac{\partial \xi}{\partial x} + f v, \quad (2.12)$$

$$\frac{\partial v}{\partial t} = -g \frac{\partial \xi}{\partial y} - f u, \quad (2.13)$$

$$H \left(\frac{\partial u}{\partial x} + \frac{\partial v}{\partial y} \right) + \frac{\partial \xi}{\partial t} - \frac{\partial \eta}{\partial t} = 0, \quad (2.14)$$

where u, v are the components of the horizontal flow velocity, $f = 2\omega \sin \varphi$ is the Coriolis parameter, η represents small vertical deformations of the ocean bottom (deviations from the initial position), ξ is the displacement of the free surface from the equilibrium position. We differentiate Eq. (2.12) with respect to the coordinate y and Eq. (2.13) with respect to the coordinate x , and, then, we subtract one from the other. With account of the continuity equation (2.14) we ultimately obtain an evolution equation for the vertical curl component of the velocity

$$\frac{\partial}{\partial t} (\text{rot}_z \mathbf{v}) = \frac{f}{H} \left(\frac{\partial \xi}{\partial t} - \frac{\partial \eta}{\partial t} \right). \quad (2.15)$$

We shall assume no motion to exist in the water layer at the time moment $t = 0$ and the surfaces of the water and ocean bottom to be in an unperturbed state ($\mathbf{v} = 0$, $\eta = 0$, $\xi = 0$). We shall further assume deformation of the ocean bottom, arbitrary in space and time, but quite rapid ($\tau \ll R(gH)^{-1/2}$), to take place within a circular area of radius R , which will result in the formation of certain residual displacements. For simplicity we shall consider the residual displacements to differ from zero only inside the circular area of radius R , where they assume the fixed value η_0 . The ocean bottom displacement results in formation of a wave perturbation of the surface, which after a sufficiently long period of time ($T \gg R(gH)^{-1/2}$) will leave the area of the source and the water surface will return to its initial unperturbed state.

The said assumptions make it possible to integrate Eq. (2.15) over time in the time interval from 0 up to T .

$$(\text{rot}_z \mathbf{v})|_{t=T} = -\frac{f}{H} \eta_0. \quad (2.16)$$

Expression (2.16) permits to conclude that influence of the Earth's rotation manifested at the tsunami source area, considering residual displacements of the ocean bottom to form at the site, must result in formation of a certain vortical structure.

Let us estimate the energy of the vortical structure formed by the circular residual deformation. To this end we integrate expression (2.16) over the area of a circle of radius $r \leq R$, the center of which coincides with the center of the source. Applying the known Stokes formula, we pass in the left-hand part of the obtained expression to circulation of the velocity. With account of the radial symmetry of the problem we obtain, for the velocity of vortical motion at a distance r from the center,

$$V(r) = -\frac{f \eta_0}{2H} \begin{cases} r, & r \leq R, \\ R^2/r, & r > R. \end{cases} \quad (2.17)$$

Knowledge of the velocity distribution readily permits to calculate the kinetic energy of the vortex. However, if the kinetic energy is calculated by integration of the quantity $\rho V^2 H \pi r$ over the radius from 0 up to infinity, then the integral diverges. This result, which at first sight seems paradoxical, is explained as follows. The point is that in deriving formula (2.17) we neglected the residual displacement of the free surface, which is actually peculiar to a vortical structure. Resolving the problem (2.12)–(2.14) carefully yields a velocity decrease, that is more rapid than $1/r$, which provides for convergence of the integral (Nosov and Nurislamova 2012; Nosov et al. 2014).

However, application of formula (2.17) makes it possible to calculate the kinetic energy of the central region of the vortical structure easily. To this end it is sufficient to perform integration from 0 up to R . We shall treat the obtained value as the energy of the vortex resulting from bottom deformation in a rotating ocean:

$$W_k = \frac{\pi \rho f^2 \eta_0^2 R^4}{16 H}. \quad (2.18)$$

Let us, now, compare the energy of the vortex with the energy of the tsunami wave, which we estimate as the potential energy of the initial elevation, similar in shape to the residual deformation of the ocean bottom (a circular area of radius R and height η_0),

$$W_p = \frac{\pi \rho g R^2 \eta_0^2}{2}. \quad (2.19)$$

Comparison of formulae (2.18) and (2.19) reveals the ratio of the energy of the vortex, formed at the tsunami source and due to rotation of the Earth, and the energy of the tsunami wave itself to be given by the following expression:

$$\frac{W_k}{W_p} = \frac{f^2 R^2}{8 g H} \sim 10^{-2} - 10^{-4}. \quad (2.20)$$

The part of the energy due to vortical motion is seen to increase quadratically with the horizontal dimension of the source and to decrease as the ocean depth increases. But, in any case, the contribution of this energy does not exceed 1 % of the energy of the tsunami wave. Note that such an estimate is correct for medium or high latitudes; for equatorial regions, where the Coriolis parameter is small, it will be significantly overestimated.

Let us, now, estimate the energy contribution of internal waves that are due to ocean bottom displacements. We shall consider the model of an ocean consisting of two layers: the upper layer of thickness h_1 with a free surface, and the lower layer of thickness h_2 . The density of the upper layer is ρ_1 and of the lower layer ρ_2 ($\rho_2 > \rho_1$). In this case it is convenient to base estimations on the one-dimensional (along the horizontal coordinate) model, constructed within the framework of the linear theory of long waves. We shall consider a segment of the ocean bottom of length L to undergo a vertical displacement η_0 during a time interval $\tau \ll L (g(h_1 + h_2))^{-1/2}$. Such a displacement represents an impulse not only for surface waves, but also for internal waves, since the propagation velocity of the latter is significantly smaller. The displacement results in the formation of initial elevations both on the water surface and on the boundary surface separating the two layers; we shall consider these elevations to be similar in shape to the deformation of the ocean bottom. In principle, it should be possible already at this stage of reasoning to compare the energies of internal, W_{int} , and of surface, W_{sur} , tsunami waves by comparison of the potential energies of the initial elevations. This ratio is evidently given by the formula

$$\frac{W_{int}}{W_{sur}} \approx \frac{\rho_2 - \rho_1}{\rho_2} \sim 10^{-3}. \quad (2.21)$$

But such a value is actually strongly overestimated. The point is that the evolution of initial elevations gives rise to two sets of waves, each of which consists of perturbations on the water surface and on the jump of density. One of the sets of waves propagates rapidly with the velocity of surface waves, the other one is essentially slower and propagates with the velocity of internal waves. As the initial elevation evolves, the water particles on the free water surface in the vicinity of the source are shifted downward. The maximum of this displacement, equal to η_0 , corresponds to the free surface. At the ocean bottom, owing to there being no flow, the displacement equals zero. Assuming the displacement to depend linearly on the vertical coordinate, we obtain the displacement at the level of the density jump, $\Delta\eta = \eta_0 h_2 / (h_1 + h_2)$. The evolution of the elevation on the free surface is seen to result in the initial elevation at the density jump being reduced by the quantity $\Delta\eta$, while its height becomes

equal to $\eta_{int} = \eta_0 h_1 / (h_1 + h_2)$. Naturally, the potential energy, that is proportional to the square height of the initial elevation, also, decreases, here. A more correct estimation yields the following relationship between the energies of the internal and surface tsunami waves:

$$\frac{W_{int}}{W_{sur}} \approx \frac{\rho_2 - \rho_1}{\rho_2} \left(\frac{h_1}{h_1 + h_2} \right)^2 \sim 10^{-5}. \quad (2.22)$$

Estimations reveal that stratification of the ocean and rotation of the Earth cannot significantly influence the process of tsunami generation by an earthquake. But a small part of the earthquake's energy is transferred both to baroclinic motions and to vortical fields.

A complete physical formulation of the problem of tsunami generation by an earthquake should, generally speaking, consider a layer of viscous compressible stratified liquid on an elastic semispace in the gravitational field with account of the Earth's rotation. The above reasoning makes it possible to essentially simplify formulation of the problem. As a first approximation, we shall consider the process of tsunami generation by an earthquake to be a phenomenon occurring in a homogeneous (nonstratified) perfect incompressible liquid in the gravitational field in an inertial (without rotation) reference frame. Deformations of an absolutely rigid ocean bottom of finite duration and small amplitude ($A \ll H$) serve as the source of waves. Owing to tsunami waves being subject to dispersion, it is expedient to resolve the problem within the framework of potential theory.

In conclusion we shall briefly dwell upon one more possible mechanism of tsunami formation in the case of underwater earthquakes. Experience of the investigation of catastrophic and strong seismic events shows that numerous seismic cracks of lengths exceeding tens of kilometers and widths amounting to 5–15 m arise at the epicentral zone. Dilatant changes of the state of rock in the same area develop, enhancement of the specific volume of the medium takes place, as well as revelation of microcracks and growth of its permeability. In the case of underwater earthquakes such processes should clearly take place in the rock of the ocean bottom. Rapid opening of the cracks at the ocean bottom should lead to an impetuous drainage of water.

Evidence provided by witnesses of the 1999 Izmit earthquake revealed that one of the shallow regions of the Sea of Marmara was dried up by the exclusive drainage of water through cracks in the seafloor; large areas of the seafloor were completely uncovered. In scientific literature, such phenomena are conventionally termed the Moses effect, in memory of the biblical Exodus through the Red Sea. Naturally, the dried areas of the seafloor remain for a short time until the water fills up the entire volume formed by the created set of cracks.

The impetuous drainage of water into cracks results in a local lowering of the ocean level. Such an initial perturbation is also capable of generating tsunami waves. The first results of mathematical simulation of the formation mechanism of a tsunami, caused by a fault opening up in the bottom, are presented in Levin and Nosov (2008).

2.2 Okada Formulae

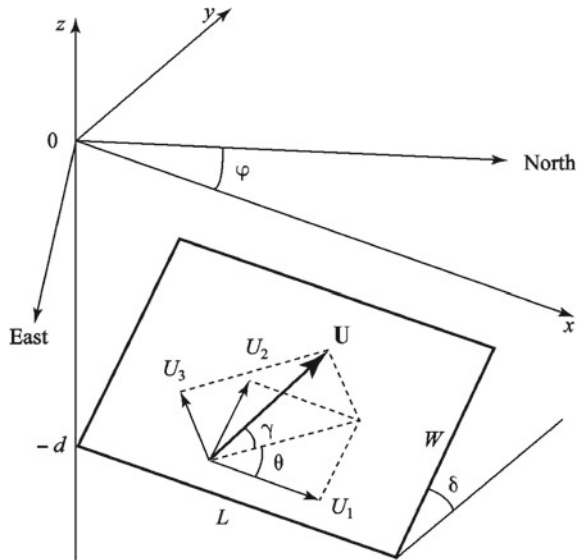
For simulating tsunami waves of seismotectonic origin it is necessary to have realistic data concerning the residual (coseismic or static) deformations of the ocean bottom, resulting from an underwater earthquake. Residual deformations can be calculated on the basis of seismic data, making use of the analytical solution for the stationary problem of elasticity theory. The tensions and displacements caused by sources within the elastic semispace have been studied by many authors (e.g., Chinnery 1961, Maruyama 1964, Press 1965, Savage and Hastie 1966, Gusiakov 1978, Matsu'ura and Tanimoto 1980). In calculations of residual deformations of the ocean bottom at a tsunami source references are usually made to the work of Okada (1985), who brought together, systematized, and checked the calculation formulae carefully. Now these formulae are often termed Okada formulae. It must be stressed that the Okada formulae only permit to calculate static deformations. To reconstruct the dynamics of bottom deformations it is necessary to resolve another, more general, problem.

In this section, formulae are presented for surface displacements due to inclined shear and tensile faults in an isotropic homogeneous elastic half-space. The expressions have been carefully checked to be free from any singularities and misprints.

The Yoshimitsu Okada formulae are quite cumbersome and contain numerous variables. Therefore, in this section, in order to avoid errors, instead of our traditional notation, we shall accurately follow Okada (1985) and apply the original notation adopted therein.

We take the Cartesian reference system as it is shown in Fig. 2.6. The elastic medium occupies the region of $z \leq 0$. The $0x$ axis is taken to be parallel to the strike direction of a finite rectangular fault of length L and width W . Burgers vector

Fig. 2.6 Geometry of the source model (length L , width W , Burgers vector \mathbf{U} , dip angle δ , rake angle θ , angle between Burgers vector \mathbf{U} and the fault plane γ)



$\mathbf{U} = (U_1, U_2, U_3)$ shows the movement of the hanging wall side block relative to the footwall side block. Elementary dislocations U_1 , U_2 , and U_3 are defined so as to correspond to strike-slip, dip-slip, and tensile components of arbitrary dislocations. The tensile component U_3 is normal to the fault plane.

A dislocation is determined by four angles: the strike angle φ (clockwise from North), the dip angle δ , the rake (slip) angle θ , and the angle γ between Burgers vector \mathbf{U} and the fault plane. Elementary dislocations U_1 , U_2 , and U_3 are linked to Burgers vector in the following way: $U_1 = |\mathbf{U}| \cos \gamma \cos \theta$, $U_2 = |\mathbf{U}| \cos \gamma \sin \theta$, $U_3 = |\mathbf{U}| \sin \gamma$.

The final results condensed into compact forms using Chinnery's notation \parallel to represent the substitution

$$f(\xi, \eta) \parallel = f(x, p) - f(x, p - W) - f(x - L, p) + f(x - L, p - W). \quad (2.23)$$

For strike-slip

$$\begin{aligned} u_x &= -\frac{U_1}{2\pi} \left[\frac{\xi q}{R(R + \eta)} + \arctan \left(\frac{\xi \eta}{qR} \right) + I_1 \sin \delta \right] \parallel, \\ u_y &= -\frac{U_1}{2\pi} \left[\frac{\tilde{y}q}{R(R + \eta)} + \frac{q \cos \delta}{R + \eta} + I_2 \sin \delta \right] \parallel, \\ u_z &= -\frac{U_1}{2\pi} \left[\frac{\tilde{d}q}{R(R + \eta)} + \frac{q \sin \delta}{R + \eta} + I_4 \sin \delta \right] \parallel. \end{aligned} \quad (2.24)$$

For dip-slip

$$\begin{aligned} u_x &= -\frac{U_2}{2\pi} \left[\frac{q}{R} - I_3 \sin \delta \cos \delta \right] \parallel, \\ u_y &= -\frac{U_2}{2\pi} \left[\frac{\tilde{y}q}{R(R + \xi)} + \cos \delta \arctan \left(\frac{\xi \eta}{qR} \right) - I_1 \sin \delta \cos \delta \right] \parallel, \\ u_z &= -\frac{U_2}{2\pi} \left[\frac{\tilde{d}q}{R(R + \xi)} + \sin \delta \arctan \left(\frac{\xi \eta}{qR} \right) - I_5 \sin \delta \cos \delta \right] \parallel. \end{aligned} \quad (2.25)$$

For tensile fault

$$\begin{aligned} u_x &= \frac{U_3}{2\pi} \left[\frac{q^2}{R(R + \eta)} - I_3 \sin^2 \delta \right] \parallel, \\ u_y &= \frac{U_3}{2\pi} \left[\frac{-\tilde{d}q}{R(R + \xi)} - \sin \delta \left\{ \frac{\xi q}{R(R + \eta)} - \arctan \left(\frac{\xi \eta}{qR} \right) \right\} - I_1 \sin^2 \delta \right] \parallel, \\ u_z &= \frac{U_3}{2\pi} \left[\frac{\tilde{y}q}{R(R + \xi)} + \cos \delta \left\{ \frac{\xi q}{R(R + \eta)} - \arctan \left(\frac{\xi \eta}{qR} \right) \right\} - I_5 \sin^2 \delta \right] \parallel, \end{aligned} \quad (2.26)$$

where

$$\begin{aligned}
 I_1 &= -\frac{\mu}{\lambda + \mu} \left[\frac{\xi}{(R + \tilde{d}) \cos \delta} \right] - I_5 \tan \delta, \\
 I_2 &= -\frac{\mu}{\lambda + \mu} \ln(R + \eta) - I_3, \\
 I_3 &= \frac{\mu}{\lambda + \mu} \left[\frac{\tilde{y}}{(R + \tilde{d}) \cos \delta} - \ln(R + \eta) \right] + I_4 \tan \delta, \\
 I_4 &= \frac{\mu}{\lambda + \mu} \frac{1}{\cos \delta} \left[\ln(R + \tilde{d}) - \sin \delta \ln(R + \eta) \right], \\
 I_5 &= \frac{\mu}{\lambda + \mu} \frac{2}{\cos \delta} \arctan \left(\frac{\eta(X + q \cos \delta) + X(R + X) \sin \delta}{\xi(R + X) \cos \delta} \right),
 \end{aligned} \tag{2.27}$$

and if $\cos \delta = 0$,

$$\begin{aligned}
 I_1 &= -\frac{\mu}{2(\lambda + \mu)} \frac{\xi q}{(R + \tilde{d})^2}, \\
 I_3 &= \frac{\mu}{2(\lambda + \mu)} \left[\frac{\eta}{R + \tilde{d}} + \frac{\tilde{y} q}{(R + \tilde{d})^2} - \ln(R + \eta) \right], \\
 I_4 &= -\frac{\mu}{\lambda + \mu} \frac{q}{R + \tilde{d}}, \\
 I_5 &= -\frac{\mu}{\lambda + \mu} \frac{\xi \sin \delta}{R + \tilde{d}},
 \end{aligned} \tag{2.28}$$

$$\begin{aligned}
 p &= y \cos \delta + d \sin \delta, \\
 q &= y \sin \delta - d \cos \delta, \\
 \tilde{y} &= \eta \cos \delta + q \sin \delta, \\
 \tilde{d} &= \eta \sin \delta - q \cos \delta, \\
 R^2 &= \xi^2 + \eta^2 + q^2, \\
 X^2 &= \xi^2 + q^2.
 \end{aligned} \tag{2.29}$$

Under special conditions some terms in formulas (2.24)–(2.28) become singular. To avoid all singularities, the following rules should be obeyed:

- i. when $q = 0$, set $\arctan(\xi\eta/qR) = 0$ in Eqs. (2.24)–(2.26);
- ii. when $\xi = 0$, set $I_5 = 0$ in Eq. (2.27);
- iii. when $R + \eta = 0$, set all the terms which contain $R + \eta$ in their denominators to zero in Eqs. (2.24)–(2.28), and replace $\ln(R + \eta)$ by $-\ln(R - \eta)$ in Eqs. (2.27) and (2.28).

To assist the development of a computer program based on expressions (2.23)–(2.29), several numerical results, permitting to check it, are listed in Table 2.1.

Table 2.1 Checklist for numerical calculations

	u_x	u_y	u_z
Case 1: $x = 2; y = 3; d = 4; \delta = 70^\circ; L = 3; W = 2$			
Strike	$-8.689E - 3$	$-4.298E - 3$	$-2.747E - 3$
Dip	$-4.682E - 3$	$-3.527E - 2$	$-3.564E - 2$
Tensile	$-2.660E - 4$	$+1.056E - 2$	$+3.214E - 3$
Case 2: $x = 0; y = 0; d = 4; \delta = 90^\circ; L = 3; W = 2$			
Strike	0	$+5.253E - 3$	0
Dip	0	0	0
Tensile	$+1.223E - 2$	0	$-1.606E - 2$
Case 3: $x = 0; y = 0; d = 4; \delta = -90^\circ; L = 3; W = 2$			
Strike	0	$-1.303E - 3$	0
Dip	0	0	0
Tensile	$+3.507E - 3$	0	$-7.740E - 3$

A medium is assumed to be $\lambda = \mu$ in the all cases, and the results are presented in units of U_i .

When applying Okada formulae in geophysics one should bear in mind that the effect of the Earth's curvature is negligible for shallow events at distances of less than 20° , but that vertical stratification or lateral inhomogeneity can sometimes considerably influence the deformation field. An analysis of the influence exerted on the deformation field by the factors indicated can be found, for example, in Nostro et al. (1999).

The Lamé constants λ and μ enter into expressions (2.27), (2.28) in the form of a combination, which for practical calculations is conveniently expressed via the respective velocities of longitudinal and transverse seismic waves, c_p and c_s ,

$$\kappa \equiv \frac{\mu}{\lambda + \mu} = \frac{c_s^2}{c_p^2 - c_s^2}. \quad (2.30)$$

The following analysis was performed in order to reveal the range of variability of the quantity κ in actual natural conditions. All underwater earthquakes with moment magnitudes $M_w \geq 6$ (about 3600 events during the period of 1976–2012) were selected from the Global CMT Catalog (<http://www.globalcmt.org/>) (Ekström et al. 2012). The quantity κ , we are interested in, was determined for each seismic event from its coordinates and depth in accordance with the global model CRUST2.0 (<http://igppweb.ucsd.edu/~gabi/crust2.html>) (Bassin et al. 2000). It turned out to be that in the case of real underwater earthquakes the quantity κ varies within the range from 0.42 up to 0.52. Variations of the quantity κ within the range indicated weakly affect the result—the residual deformation of the ocean bottom (up to several percent). Therefore, in calculations of residual deformations at tsunami sources the assumption is often made that $\lambda = \mu$, i.e., $\kappa = 0.5$, which, as we see, can be considered quite justified.

2.3 Rectangular Fault: Relationship Between the Parameters of a Tsunami Source and the Earthquake Moment Magnitude and Depth

Many researchers (e.g., Iida 1963, Hatori 1970, Yamashita and Sato 1974, Alekseev and Gusakov 1976, Ward 1980, Kajiura 1981, Dotsenko and Soloviev 1990a, Pelinovsky 1996, Okal 1988, Okal 2003, Bolshakova and Nosov 2011, Poplavskii et al. 2012, Nosov et al. 2014) have been interested in the simple general regularities relating the parameters of a tsunami source and characteristics of the seismic fault area. Usually, in accordance with the approach widely spread in seismology (e.g., Kanamori and Anderson 1975, Kanamori 1977, Sato 1979, Wells and Coppersmith 1994, Okada 1995, Kanamori and Brodsky 2004), attempts were made to relate the parameters of a tsunami source, such as its area (or average radius), the displacement amplitude of the water surface and the initial elevation energy to the earthquake magnitude. In Sect. 2.1, we already presented two such dependences, (2.5) and (2.6), derived from empirical data (Dotsenko and Soloviev 1990b). As another typical example we may note the relation between the tsunami energy (the initial elevation energy) and the magnitude obtained theoretically in Kajiura (1981),

$$\log_{10} E_{TS}[J] = 2.0 M_w - 2.46. \quad (2.31)$$

Making use of the normal mode theory (Okal 2003) analytically obtained an expression relating the tsunami energy within a distant zone to the seismic moment M_0 (dyn \times cm):

$$E_{TS}[\text{ergs}] = 7.4 \times 10^{-17} M_0^{4/3}. \quad (2.32)$$

Passing in formula (2.32) to SI units and expressing the seismic moment via the moment magnitude by means of formula (2.2), formula (2.32) is readily rewritten in terms of the momentary magnitude:

$$\log_{10} E_{TS}[J] = 2.0 M_w - 1.66. \quad (2.33)$$

It is remarkable that in spite of the difference between the approaches applied for obtaining expressions (2.31) and (2.33) they demonstrate an impressive similarity. However, Kajiura's formula (2.31) yields energy values that are underestimated by a factor of approximately 6.3 in comparison to Okal's formula (2.33). What concerns the accuracy of theoretical estimates of the tsunami energy, as noted by Okal himself (2003), there regretfully exist no experimental methods permitting to measure the energy of large transoceanic tsunamis. It may be that the only more or less reliable method for estimating the energy of a tsunami consists in calculating the potential energy of initial elevation.

The interest in general relationships such as (2.5), (2.6), (2.31)–(2.33) is readily explained. They can turn out to be useful not only for operative estimation of an earthquake tsunamigenicity, but also from the point of view of understanding the physical nature of phenomena taking place in the water layer above the underwater earthquake source. On the basis of such relationships, for example, it is possible, from the given earthquake magnitude and depth, to rapidly estimate the maximum possible amplitude of waves at the source, as well as their length, to determine the part of the earthquake energy transferred to the tsunami wave or to some other dynamic process.

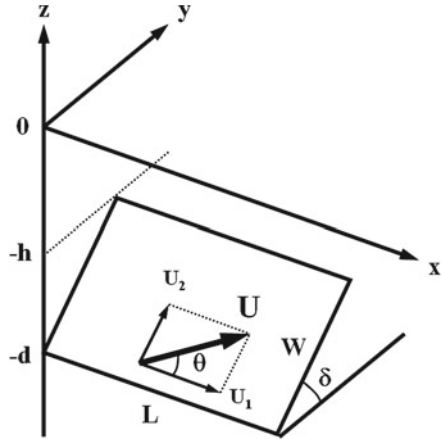
In this section we shall apply the Okada formulae to derive the main regularities relating the parameters of a tsunami source to the respective earthquake magnitude and depth.

In the simplest case the source of a tsunamigenic earthquake can be represented by a rectangular fault with a uniform slip distribution. The Okada formulae presented in the preceding Sect. 2.2 are applicable precisely in the case of such a seismic source. In spite of the Okada formulae being analytical expressions, applying them to reveal general regularities represents a nontrivial problem. The point, here, consists not only in the expressions being cumbersome, but, mainly, in the large number of input parameters. Indeed, the calculation of bottom deformations at the tsunami source with the aid of the Okada formulae requires the following set of input parameters (see Fig. 2.6): the depth d of the fault area, the width W and length L of the fault area, the length of the Burgers vector, $|U|$, the dip angle δ , the angle between the strike direction and the slip direction, θ , the angle between the Burgers vector and the fault plane, γ , and, also, the Lamé coefficients λ and μ , that characterize the elasticity properties of a medium. If calculations are performed for a real event, the above nine parameters must be supplemented with three more quantities: the longitude and latitude of the earthquake epicenter, and, also, the strike angle ϕ . To analyze the general properties of oceanic bottom deformations in a 9-dimensional (11-dimensional) space of input parameters is not only an extremely complicated task, but is also devoid of any practical expediency—it is easier to deal with concrete seismic events, for which all the aforementioned parameters have definite values.

Let us reduce the number of input parameters making use of physically reasonable assumptions and known constraints (Bolshakova and Nosov 2011). We shall, first, assume the Burgers vector to lie in the plane of the fault area: $\mathbf{U} = (U_1, U_2, 0)$ (see Fig. 2.7). Second, we shall consider the Lamé coefficients to be equal to each other, $\lambda = \mu$ (the expediency of this assumption is shown in Sect. 2.2). As additional constraints we shall invoke the definition of the seismic moment (2.1), the relationship between the seismic moment and the moment magnitude (2.2), and, also, the empirical formulae given by Kanamori and Anderson for parameters of the fault area (Kanamori and Anderson 1975):

$$L/W = 2, \quad U/L = 5 \times 10^{-5}. \quad (2.34)$$

Fig. 2.7 Geometry of the source model of an earthquake. L is the length of the fault plane, W is the width of the fault plane, U is the Burgers vector, δ is the dip angle, θ is the rake angle, h is the depth of the upper edge of the fault plane



Formulae (2.1), (2.2) and (2.34) permit to express the dimensions of the fault area and the slip value (the length of the Burgers vector) via the earthquake moment magnitude

$$\log_{10} L[\text{km}] = 0.5 M_w - A_L, \tag{2.35}$$

$$\log_{10} W[\text{km}] = 0.5 M_w - A_W, \tag{2.36}$$

$$\log_{10} U[\text{m}] = 0.5 M_w - A_U. \tag{2.37}$$

The shear modulus entering into formula (2.1) for the seismic moment varies within the range of $3 - 8 \times 10^{10}$ Pa. As a consequence the coefficients involved in formulae (2.35)–(2.37) also undergo insignificant variations: $A_L = 1.92 - 2.07$, $A_W = 2.22 - 2.37$, $A_U = 3.22 - 3.37$. The lower boundaries of the ranges indicated correspond to the minimal value of the shear modulus $\mu = 3 \times 10^{10}$ Pa that is typical for crustal faults. In all further calculations we shall make use of precisely these minimal values ($A_L = 1.92$, $A_W = 2.22$, $A_U = 3.22$)—in this case formulae (2.35)–(2.37) are equivalent to the known expressions presented, for example, in the Handbook for Tsunami Forecast (2001).

Taking into account the adopted assumptions and constraints (2.35)–(2.37), we arrive at a reduced set of input parameters for the Okada formulae, which only includes four quantities: the moment magnitude M_w , the angles Dip (δ), and Rake (θ), as well as the depth d of the earthquake source. In the case of strong shallow earthquakes, which are precisely the most interesting ones as tsunami sources, the source depth and the width W of the fault area are often comparable quantities. If the source depth is set equal to the depth of the lower edge of the fault area and the Dip angle and/or moment magnitude, upon which the width of the fault area depends, are varied, then in a number of cases the fault may emerge at the surface. To prevent the fault from emerging at the surface, it is convenient to consider the source depth

to be equal to the depth of the upper edge of the fault area, $h = d - W \sin \delta$ (see Fig. 2.7). We shall choose precisely this characteristic as a measure of the depth of an earthquake source.

The small number of input parameters permits to apply the Monte Carlo method quite efficiently to reveal general properties of bottom deformations. For example, one of the parameters can be fixed, while variations of the remaining ones are random and statistically uniform within given ranges. Such an analysis was performed by Yoshimitsu Okada in Okada (1995) for a point double-couple source. But these results cannot be applied in analyzing the properties of oceanic bottom deformations in the case of tsunamigenic earthquakes, which, as a rule, are strong and shallow. The source of a tsunamigenic earthquake can evidently not be represented by a point. It is always quite an extended region, the dimensions of which amount to tens and even hundreds of kilometers and in certain cases (for example, Sumatra 2004) exceed a thousand kilometers.

To obtain the relationships between the earthquake parameters and the tsunami characteristics it is additionally necessary to adopt a number of assumptions concerning the mechanism of wave generation. As it was shown in Sect. 2.1, the main effect resulting in the generation of tsunami waves in the case of earthquakes consists in the displacement of water by the residual (coseismic) bottom deformation. Consider a water layer limited by a free surface from above and by the bottom surface of arbitrary form from below. Consider the origin of the reference frame to be situated on the unperturbed water surface. Let the $0z$ axis be directed vertically upward, and the $0x$ and $0y$ axes to the East and North, respectively. Consider the position of the bottom before the earthquake to be determined by the formula

$$z = -H(x, y). \quad (2.38)$$

After the earthquake the bottom occupies a new position:

$$z = -H(x, y) + \eta(x, y), \quad (2.39)$$

where $\eta(x, y)$ is the residual displacement of the bottom surface. To determine the relationship between the vector field of bottom deformations, $\mathbf{D} \equiv (D_x, D_y, D_z)$, and function $\eta(x, y)$ consider a certain point situated on the unperturbed bottom surface, $P_0 = (x_0, y_0, z_0)$. The coordinates of this point satisfy Eq. (2.38). As a result of coseismic deformation after the earthquake the point moves to a new position $P_1 = (x_0 + D_x, y_0 + D_y, z_0 + D_z)$, continuing to remain on the bottom surface. Now, the coordinates of this point satisfy Eq. (2.39) which assumes the following form:

$$z_0 + D_z = -H(x_0 + D_x, y_0 + D_y) + \eta(x_0 + D_x, y_0 + D_y). \quad (2.40)$$

In the practice of numerical tsunami simulation functions, $H(x, y)$ and $\eta(x, y)$, involved in Eq. (2.40), are represented discretely on a certain grid with a spatial increment Δ . This means that the structure of these functions in between the nearest

nodes of the grid remain beyond consideration. It is reasonable to assume that in between nodes functions $H(x, y)$ and $\eta(x, y)$ are sufficiently smooth, for example, linear, otherwise the choice of the grid increment would have to be acknowledged to be erroneous. The grid increment is usually $\Delta \sim 10^3$ m. The coseismic deformation amplitude is significantly inferior to this value: $|\mathbf{D}| \ll \Delta$. Consequently, function $H(x, y)$ in Eq. (2.40) can be expanded into a Taylor series at the point (x_0, y_0) , retaining only linear terms in the expansion. For function $\eta(x, y)$ it is reasonable to adopt an even more simple assumption: $\eta(x_0 + D_x, y_0 + D_y) \approx \eta(x_0, y_0)$. As a result, taking into account Eq. (2.38), we obtain a relationship between the residual displacement of the bottom surface and the vector field of bottom deformations as well as the distribution of depths (Nosov et al. 2014)

$$\eta = \frac{\partial H}{\partial x} D_x + \frac{\partial H}{\partial y} D_y + D_z. \quad (2.41)$$

A similar formula was previously obtained in Tanioka and Satake (1996) on the basis of arguments of a intuitive physical character.

From formula (2.41) it is seen that calculation of the residual displacement of the bottom surface, generally speaking, not only requires information concerning the vector field \mathbf{D} , but also information on the distribution of depths, which is, naturally, individual for each tsunami source. In this connection analysis of the contribution of horizontal components (the first two terms in formula (2.41)) cannot be performed in the general case, i.e., without being related to real tsunami sources. This problem will be dealt with in the next Sect. 2.4. Here, in order to obtain general relationships we shall restrict ourselves to applying the model of an ocean of fixed depth $H = \text{const}$. In this case, only the vertical component of the bottom deformation vector contributes to the generation of tsunami waves: $\eta = D_z$.

Function $\eta(x, y)$, describing displacement of the bottom surface, may exhibit quite a complex structure even in the idealized case of a uniform distribution of the slip along a rectangular fault area (see Fig. 2.8). In the case of real events, with account of bathymetry ($H \neq \text{const}$) and of slip inhomogeneities along the fault surface, the structure of function $\eta(x, y)$, may, evidently, be even more complex.

Which tsunami source parameters, determined by deformation of the bottom, $\eta(x, y)$, should be considered? Generally speaking, quite a significant number of parameters, such as, for example, a set of amplitudes of Fourier harmonics, may be required for a complete description of function $\eta(x, y)$. We must, naturally, not take the path of calculating Fourier harmonics, but will take advantage of a limited number of parameters, each of which has a clear physical meaning and is unambiguously determined by function $\eta(x, y)$. Of all the multitude of such parameters we have found it reasonable to consider the following set of quantities:

1. the double amplitude of vertical bottom deformation:

$$A = \text{Max} [\eta(x, y)] - \text{Min} [\eta(x, y)], \quad (2.42)$$

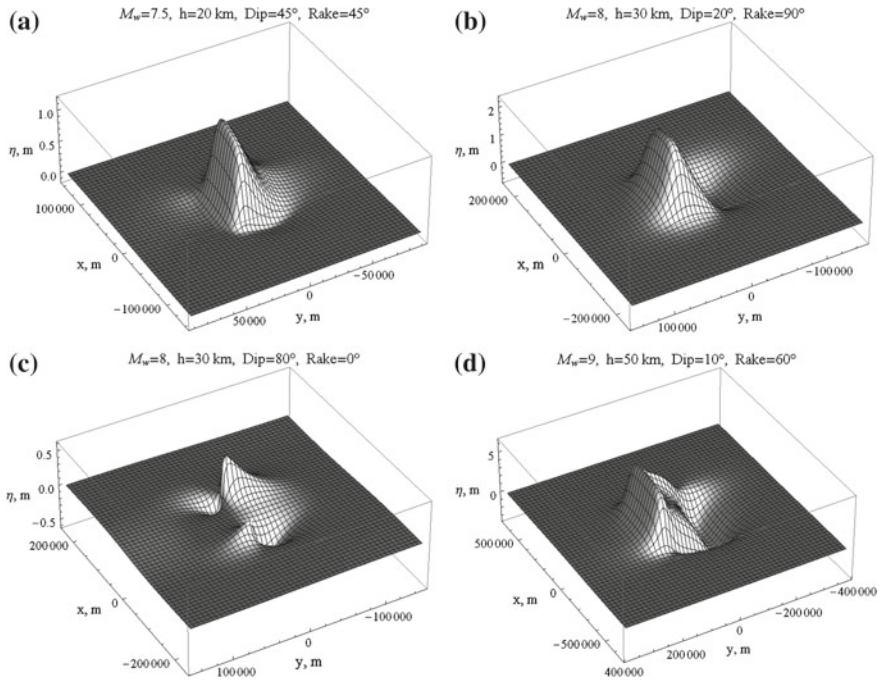


Fig. 2.8 Examples of calculations of the coseismic bottom deformation by the Okada formulae (Okada 1985). The parameters of the rectangular source with uniform distribution of the slip are indicated in figure

2. the absolute value of the displaced water volume:

$$V = \left| \iint \eta(x, y) dx dy \right|, \quad (2.43)$$

3. the potential energy of the initial elevation:

$$E = \frac{\rho g}{2} \iint \eta^2(x, y) dx dy, \quad (2.44)$$

where g is the gravity acceleration, ρ is the density of water (in calculations we assumed $g = 9.8 \text{ m/s}^2$, $\rho = 1000 \text{ kg/m}^3$). In determining energy E we apply the traditional approximation, according to which a bottom deformation immediately gives rise to a perturbation of equivalent shape at the water surface: $\xi = \eta$. The search for extreme values in formula (2.42) and integration in formulae (2.43) and (2.44) was performed over the entire region, where noticeable bottom deformations were observed. In practice this region was defined as follows: $-2L - 2h < x < 3L + 2h$, $-2W - 2h < y < 3W + 2h$. Integration was carried out numerically by the methods of rectangles. The number of rectangular cells in the region amounted to 100×100 .

Let us note a “subtle point” related to calculation of integral (2.43). From the Okada formulae it follows that at large distances from the source the amplitude of the oceanic bottom deformation decreases inversely proportional to the square epicentral distance: $\eta \sim r^{-2}$ (Okada 1995). Consequently, the integral in formula (2.43), if calculated within infinite limits, will diverge. In this connection, the value of the displaced volume, generally speaking, depends on the chosen integration region. However, only significant bottom deformations, occurring in the nearby zone, influence tsunami generation. Calculation of the energy integral (2.44) gives rise to no problems. The drop of the integrand function with distance in formula (2.44) is significantly more rapid ($\eta^2 \sim r^{-4}$), therefore the integral is sure to converge, even in the case of integration within infinite limits.

The amplitude of bottom deformation, A , to a significant extent determines the tsunami runup amplitude—the importance of this characteristic cannot give rise to any doubt. As to the displaced volume V and initial elevation energy E , the significance of these characteristics is confirmed by the fact that in the problem of tsunami propagation in an open ocean both quantities are integrals of motion. Indeed, certain “losses” of displaced volume may occur, but only during the runup process and in the case of sufficiently strong tsunamis, when the waves cover significant distances of land and flood local depressions. Noticeable dissipation of tsunami energy also takes place only in the runup zone (or in shallow water), especially if the propagation of waves is accompanied by their collapse (Li and Raichlen 2002; Bernatskiy and Nosov 2012).

To reveal the dependence of quantities A , V , and E upon the earthquake moment magnitude M_w and depth use was made of the Monte Carlo method. In the first series of calculation variations of the Dip and Rake angles, as well as of the magnitude, were statistically uniform within the following ranges: $0 \leq \delta \leq \pi/2$, $-\pi/2 \leq \theta \leq \pi/2$, $6.5 \leq M_w \leq 9.5$. The depth of the upper edge of the fault area, h , was made to assume fixed values: 0, 10, 30, 100 and 300 km. For each depth value 5000 numerical experiments were performed. The results of calculations, namely the dependencies of quantities A , V and E upon the moment magnitude M_w , are shown in Figs. 2.9, 2.10 and 2.11, respectively.

A common property of the dependences presented consists in that all the parameters investigated tend to exhibit a rapid exponential rise as the earthquake magnitude increases. The dependences are characterized by a significant spread in the data, related to the influence of the orientation of the fault area (the Dip angle) and the slip direction (the Rake angle) on the parameters investigated. The “clouds” of points are characterized by clearly defined upper limits that are determined by the following simple formulae (Bolshakova and Nosov 2011):

$$\log_{10} A_{\max}[m] = 0.5 M_w - 3.22, \quad (2.45)$$

$$\log_{10} V_{\max}[m^3] = 1.5 M_w - 1.8, \quad (2.46)$$

$$\log_{10} E_{\max}[J] = 2.0 M_w - 1.7. \quad (2.47)$$

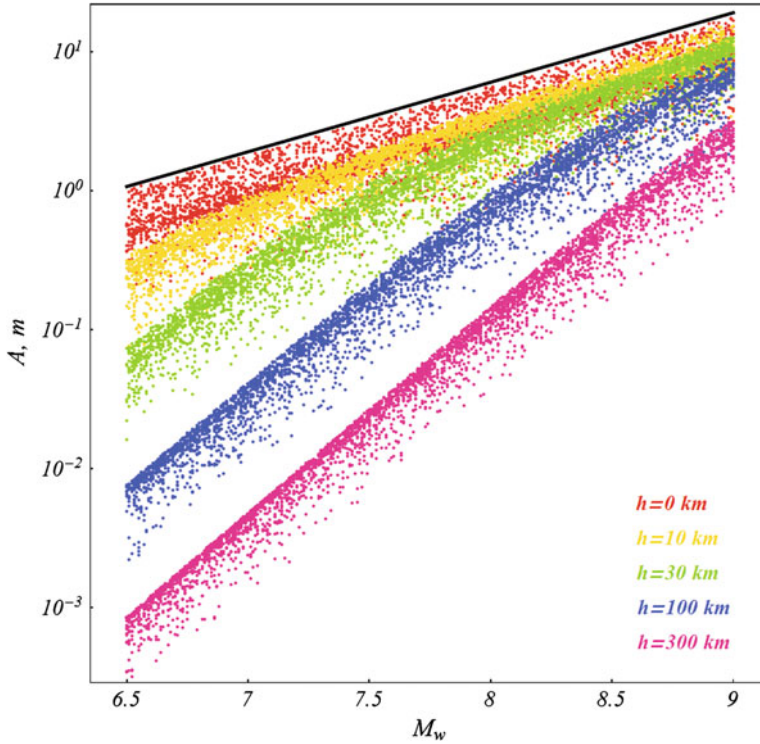


Fig. 2.9 Double amplitude of coseismic bottom deformation at tsunami source versus moment magnitude. The calculation is performed for fixed depth values of the upper edge of the fault area, $h = 0, 10, 30, 100,$ and 300 km. Variations of the Dip and Rake angles and, also, of the magnitude were random and statistically uniform within the ranges: $0 \leq \delta \leq \pi/2$, $-\pi/2 \leq \theta \leq \pi/2$, $6.5 \leq M_w \leq 9.5$. The color of the points varies depending on the depth h in accordance with the legend shown in the figure. The black line, marking the upper edge of the “cloud” of points is constructed in accordance with formula (2.45)

The dependences (2.45)–(2.47) are shown by solid lines in the figures. Note that the slip value serves as an upper limit for the amplitude of bottom deformations: the numerical coefficients in formulae (2.37) and (2.45) coincide.

In the case of amplitude A and energy E the dependence upon the earthquake source depth is quite clear. As the depth increases, both quantities decrease noticeably, and the drop is more rapid at smaller magnitudes.

Unlike the amplitude and energy, the displaced volume does not depend on the depth of the earthquake source. This feature can be explained by the drop in the deformation amplitude in the case of a pointlike source (i.e., for each element of the fault area) being inversely proportional to the square distance $\eta \sim r^{-2}$ Okada (1995). Within the area $dx dy$ the elementary volume $dV = \eta dx dy$ is displaced. If one passes to spherical coordinates with the origin at the chosen pointlike source, then $dx dy \sim r^2 d\varphi d\psi$. The quantity dV is seen to be independent of the distance from

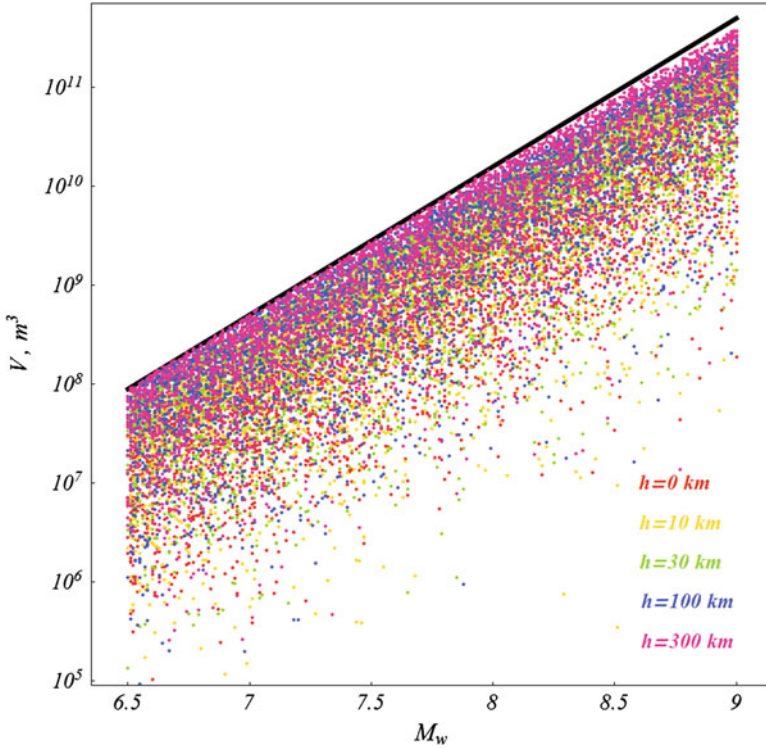


Fig. 2.10 Displaced water volume (its absolute value) at tsunami source versus moment magnitude. The calculation is performed for fixed depth values of the upper edge of the fault area, $h = 0, 10, 30, 100,$ and 300 km. Variations of the Dip and Rake angles and, also, of the magnitude were random and statistically uniform within the ranges: $0 \leq \delta \leq \pi/2, -\pi/2 \leq \theta \leq \pi/2, 6.5 \leq M_w \leq 9.5$. The color of the points varies depending on the depth h in accordance with the legend shown in the figure. The black line, marking the upper edge of the “cloud” of points is constructed in accordance with formula (2.46)

the source, r . Consequently, the whole displaced volume should also be independent of the source depth.

By combining formulae (2.45) and (2.46) it is possible to obtain an estimate for the average radius of the tsunami source, ($R_{ts} \equiv \sqrt{V_{max}/A_{max}}$):

$$\log_{10} R_{ts}[\text{km}] = 0.5 M_w - 2.29. \tag{2.48}$$

The obtained estimate is in good agreement with the empirical formula (2.5).

From formulae (2.45)–(2.48) it follows that in the case of a magnitude $M_w = 7$ the tsunami source parameters have an upper limit defined by the following values: $A_{max} = 1.9$ m, $V_{max} = 5.0 \times 10^8$ m³, $E_{max} = 2.0 \times 10^{12}$ J, $R_{ts} = 16$ km, while, if $M_w = 9$: $A_{max} = 19$ m, $V_{max} = 5.0 \times 10^{11}$ m³, $E_{max} = 2.0 \times 10^{16}$ J, $R_{ts} = 162$ km.

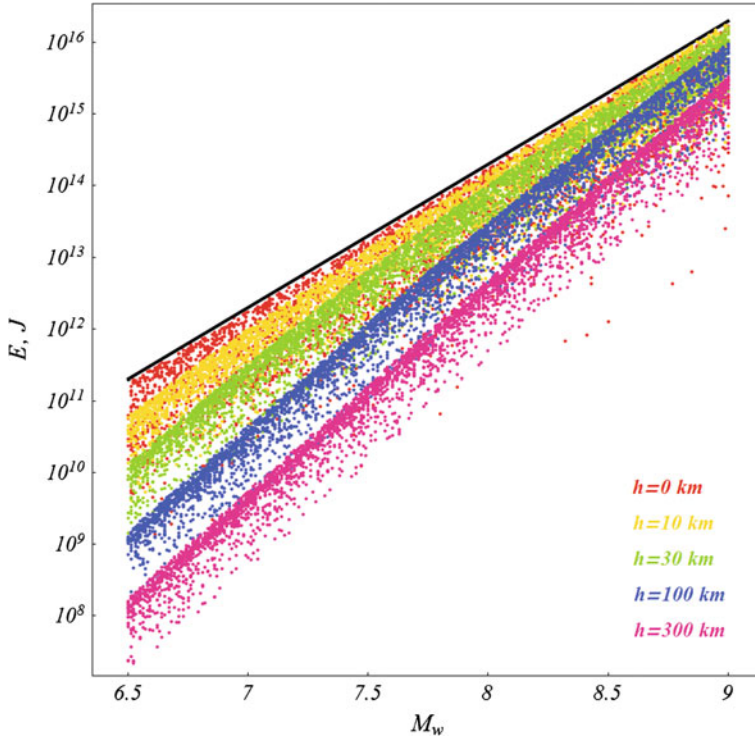


Fig. 2.11 Potential energy of the initial surface elevation at tsunami source versus moment magnitude. The calculation is performed for fixed depth values of the upper edge of the fault area, $h = 0, 10, 30, 100,$ and 300 km. Variations of the Dip and Rake angles and, also, of the magnitude were random and statistically uniform within the ranges: $0 \leq \delta \leq \pi/2$, $-\pi/2 \leq \theta \leq \pi/2$, $6.5 \leq M_w \leq 9.5$. The color of the points varies depending on the depth h in accordance with the legend shown in the figure. The black line, marking the upper edge of the “cloud” of points is constructed in accordance with formula (2.47)

Comparison of the tsunami energy determined by formula (2.47) with the known estimate of an earthquake energy (Kanamori 1977)

$$\log_{10} E_{EQ}[J] = 1.5 M_w + 4.8, \quad (2.49)$$

gives an estimate of the part of an earthquake energy contributing to the formation of tsunami waves,

$$\log_{10} E_{\max}/E_{EQ} = 0.5 M_w - 6.5. \quad (2.50)$$

In accordance with formula (2.50) one can conclude that usually quite a small part of the energy of an earthquake is passed on to tsunami waves: between 0.1 % ($M_w = 7$) and 1 % ($M_w = 9$). Hence follows an important world-outlook conclusion. From the point of view of energy, tsunami waves, that carry an enormous destructive potential, only represent a weak “echo” of a catastrophic earthquake.

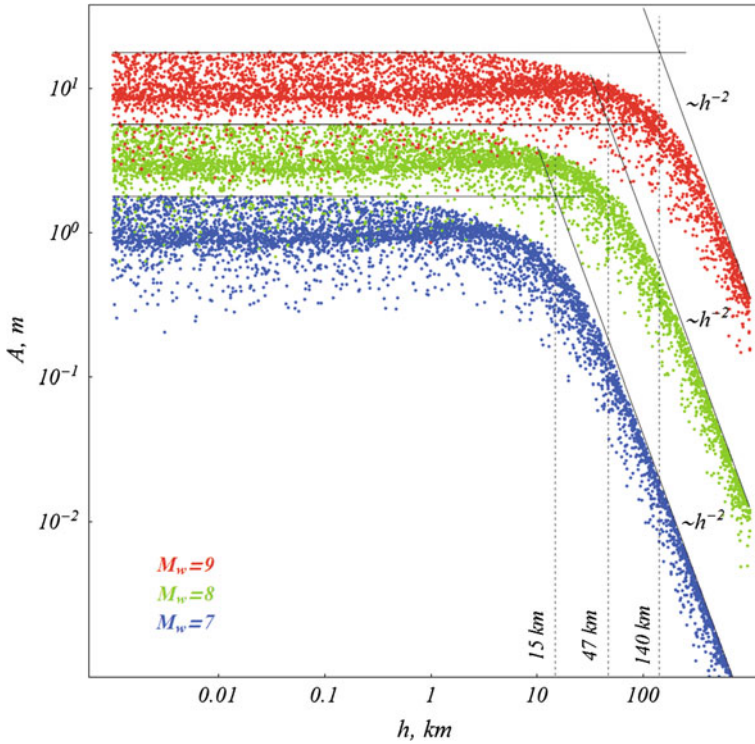


Fig. 2.12 Double amplitude of coseismic bottom deformation at tsunami source versus depth of earthquake. The calculation was performed for fixed values of the moment magnitude $M_w = 7, 8,$ and 9 . Variations of the Dip and Rake angles and, also, of the quantity $\log_{10} h$ were random and statistically uniform within the ranges: $0 \leq \delta \leq \pi/2, -\pi/2 \leq \theta \leq \pi/2, 0 < \log_{10} h[m] < 5.8$. The color of the points varies depending on the magnitude M_w in accordance with the legend shown in the figure

The aim of the second series of Monte Carlo calculations was to reveal the character of the dependence of the amplitude A and energy E on the earthquake depth. Three fixed values were chosen for the magnitude: $M_w = 7, 8, 9$. The angles Dip and Rake, as well as the quantity $\log_{10} h$, underwent variations that were statistically uniform within the following ranges: $0 \leq \delta \leq \pi/2, -\pi/2 \leq \theta \leq \pi/2, 0 < \log_{10} h[m] < 5.8$ ($1 \text{ m} < h < 700 \text{ km}$). For each value of the magnitude 5000 numerical experiments were performed. The results of calculations are shown in Figs. 2.12 and 2.13.

From Figs. 2.12 and 2.13 it is seen that in spite of a significant spread in the data a general tendency can be clearly traced: the amplitude and energy are independent of the earthquake source depth up to certain critical values of the quantity h . In the case of large depths both quantities undergo a decrease that is inversely proportional to the square source depth: $A \sim h^{-2}, E \sim h^{-2}$. The first regularity follows directly from the law, according to which the deformation amplitude decreases with distance: $\eta \sim r^{-2}$ (Okada 1995). To obtain the second regularity it is necessary to take into

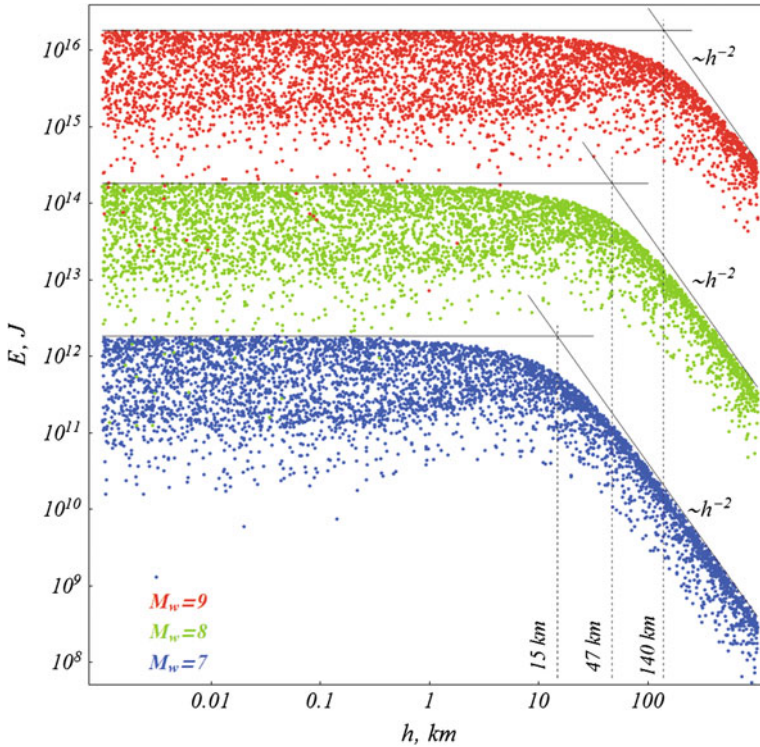


Fig. 2.13 Potential energy of the initial surface elevation at tsunami source versus earthquake depth. The calculation was performed for fixed values of the moment magnitude $M_w = 7, 8$ and 9 . Variations of the Dip and Rake angles and, also, of the quantity $\log_{10} h$ were random and statistically uniform within the ranges: $0 \leq \delta \leq \pi/2$, $-\pi/2 \leq \theta \leq \pi/2$, $0 < \log_{10} h[m] < 5.8$. The color of the points varies depending on the magnitude M_w in accordance with the legend shown in the figure

account that the area encompassing noticeable deformations increases with the source depth: $S \sim h^2$. Therefore, the energy, that is proportional to the product of the square deformation times area, decreases according to the indicated law: $E \sim \eta^2 S \sim h^{-2}$.

From Figs. 2.12 and 2.13 it is possible for each magnitude to determine the critical source depth h_c , beyond which the amplitude and energy start to decrease sharply with the depth. Let us describe the scheme for determining critical values of h_c . At small depths a horizontal straight line is constructed along the upper edge of the “cloud” of points, at large depths a straight line corresponding to the h^{-2} law is constructed. The intersection point of the straight lines determines the sought value of h_c . The critical depth h_c increases with the moment magnitude. It is remarkable that the values of h_c , determined from the dependences for the amplitude and for the energy, are practically equivalent. The critical depths have the following values: $h_c^{M_w 7} \approx 15 \text{ km}$, $h_c^{M_w 8} \approx 47 \text{ km}$, $h_c^{M_w 9} \approx 140 \text{ km}$. The weakening influence of the earthquake source depth starts to manifest itself precisely at these critical values.

To conclude this section we wish to warn against direct application of the theoretical regularities obtained herein in practice, for example, in tsunami warning systems. Real tsunamigenic earthquakes are significantly more complex objects than the model rectangular seismic source dealt with here. The properties of realistic tsunami sources, the coseismic bottom deformations at which are reconstructed with account of the slip structure at the earthquake source, will be analyzed in the following section.

2.4 Properties of Coseismic Deformations of the Oceanic Bottom According to Data on the Slip Structure at Tsunamigenic Earthquake Sources

Publications dedicated to reconstruction of the structure of an earthquake source from the seismic wave field first appeared in the 70s–80s of the twentieth century (Alewine and Jordan 1973, Jovanovich 1975, Pavlov and Gusev 1980, Ward and Barrientos 1986). The significant progress achieved in recent years has provided the possibility of obtaining unique information, namely realistic estimates of slip distributions at earthquake sources (Bassin et al. 2000, Ji et al. 2002, Lay et al. 2011, Shao et al. 2011, Yagi and Fukahata 2011). At present, not only “teleseismic data” are applied in reconstruction of coseismic slip distributions. Here, methods for the inversion of “geodetic data” (e.g., Ozawa et al. 2011, Pollitz et al. 2011), of “strong motion data” (e.g., Kurahashi and Irikura 2011, Suzuki et al. 2011), of “tsunami data” (e.g., Satake 1987, Fujii et al. 2011), and, also, for the “joint inversion of multiple data sets” (e.g., Koketsu et al. 2011, Wei et al. 2012) have proved to be quite opportune.

For reasons of brevity we shall further simply call coseismic slip distributions “slip distributions” or FFM (Finite Fault Model) distributions.

In the case of underwater earthquakes data on slip distributions are particularly valuable: they permit to reconstruct coseismic ocean bottom deformations at the tsunami source, which, in turn, provides the possibility of describing tsunami wave generation. That such a method of reconstructing bottom deformations is adequate is confirmed by the decent agreement between calculated and measured (using the deep-water stations DART, JAMSTEC, and others) waveforms (Laverov et al. 2009, Lay et al. 2011, Nosov et al. 2011). It is precisely for this reason that FFM data are widely used by different scientific groups in simulating concrete tsunamis (e.g., Newman et al. 2011, Poisson et al. 2011, Kim et al. 2013, Nosov et al. 2014).

The slip structure at an earthquake source is represented as follows. The fault surface at the source is approximated by one or several plane rectangular fault segments. Each such segment is characterized by its dimensions as well as position and orientation in space (its geographical coordinates, depth, Dip and Strike angles). The segment is divided into a finite number of subfaults of the same size (usually several hundred rectangular subfaults). Set for each subfault are its coordinates (longitude, latitude), depth and Burgers vector, that characterizes the slip extent and direction (as a rule, the length of the Burgers vector and the Rake angle are given). Further-

more, the activation time of each subfault and its rise time are determined—thus is description performed of the fault rupture dynamics.

As an example, Fig. 2.14a presents the slip distribution (the spatial picture) for the tsunamigenic earthquake that took place on November 15, 2006, on the Central Kuril Islands. The source of the data is the site of the US Geological Survey (Ji 2006). In this particular case, the fault surface is represented by a single segment of dimensions 400 km (along the strike) by 137.5 km. The segment is divided into 220 subfaults (20 km by 12.5 Km each). The maximum slip was 8.9 m.

Figure 2.14b demonstrates the example of a slip distribution, when the fault surface is represented by six fault segments. In this case the data used were obtained in Rhie et al. (2007) the 2004 Sumatra–Andaman earthquake. The total number of subfaults amounted to 201 (66 + 55 + 20 + 20 + 20 + 20). The dimensions of the subfaults were approximately 30 × 30 km (the size of a subfault varied insignificantly from one segment to another). The maximum slip related to the southern fault segment amounted to 35.32 m.

The vector field of coseismic deformation \mathbf{D} can be calculated by the slip distribution, for example, applying the Okada formulae (see Sect. 2.2). The contribution of each subfault to the deformation is calculated independently. The resulting deformation is obtained by summing up the contributions from all the elements (subfaults).

In Fig. 2.15, examples are presented of the calculation of coseismic ocean bottom deformations based on the slip distribution data shown in Fig. 2.14. The black dotted line shows the projection of fault segments onto the surface of the oceanic bottom. The vertical deformation component D_z is shown by isolines (uplifts by red lines, subsidences by blue lines). The green arrows indicate the horizontal deformation component $D_{xy} \equiv (D_x, D_y)$. The maximum uplift and subsidence values, as well as the horizontal deformation amplitude, are indicated in the lower parts of the figures.

Attempts to study the general properties of bottom deformations at tsunami sources, reconstructed from slip distribution data, were first made in Bolshakova and Nosov (2011), Nosov et al. (2014). These works were based on a relatively small set of data presented on the sites of the California Institute of Technology (Caltech), the University of California, Santa Barbara (UCSB), and the US Geological Survey (USGS). Recently, access became open to the database SRCMOD (Finite-Source Rupture Model Database, <http://equake-rc.info/SRCMOD/>), which integrates practically all presently available information on FFM. In this section we shall analyze the general properties of residual bottom deformations at underwater earthquake sources on the basis of a largest possible sample from the database SRCMOD: 200 source models (slip distributions), constructed by different scientific groups for 75 earthquakes during the period between 1923 and 2013 (Bolshakova et al. 2015). In the statistical analysis presented below we shall consider each such source model as an independent realization.

The vector field of oceanic bottom deformations was calculated from slip distributions for each one of the 200 models using the Okada formulae. Then, with the use of formula (2.41) the functions describing displacement of the bottom surface were reconstructed. In calculations, the GEBCO-08 bathymetry with a resolution of 30 ang. sec. was used.

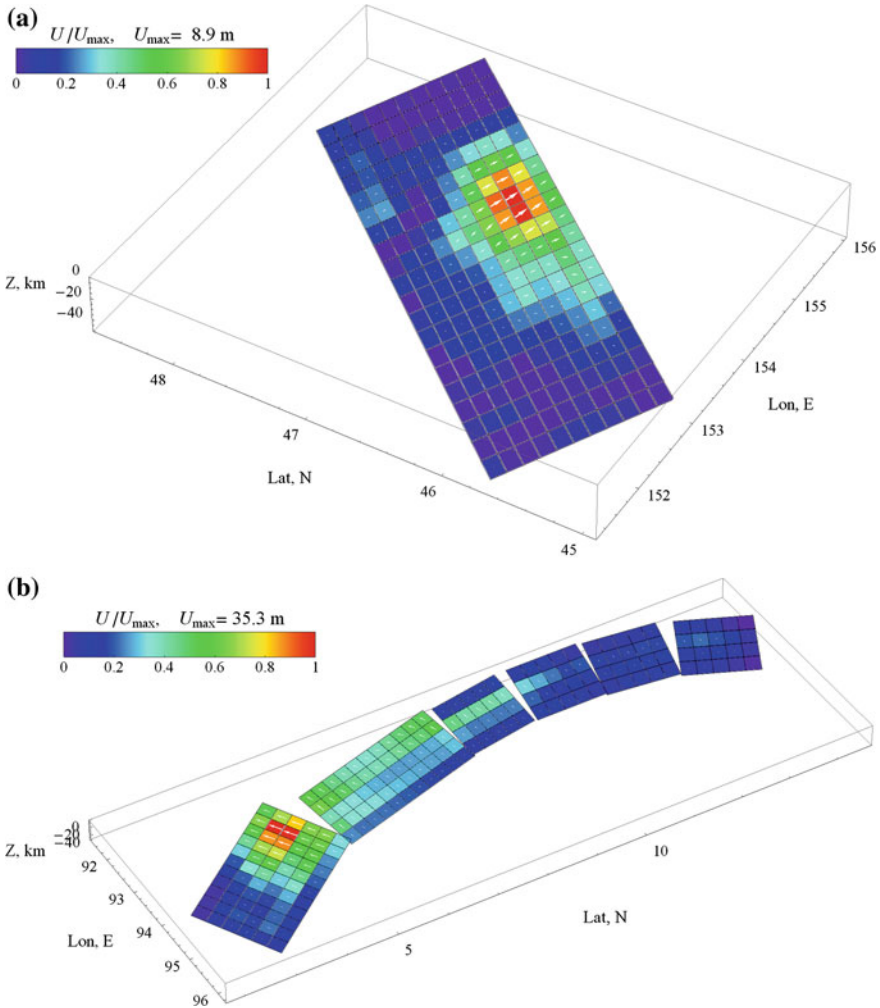


Fig. 2.14 Slip distributions at the 2006 earthquake source on the Central Kuril Islands (a) and at the 2004 Sumatra–Andaman earthquake source (b), based on the data of Ji (2006) and Rhie et al. (2007), respectively. The colors show the amplitudes of dislocations and the white arrows represent the motion of the hanging wall relative to the footwall. The color scale and the maximum slip (dislocation) are presented in the figures

We shall consider the following as the parameters of a tsunami source: the double amplitude of the vertical bottom deformation, A , the displaced water volume V and the initial elevation potential energy E . The quantities indicated are determined by formulae (2.42)–(2.44) in Sect. 2.3. Calculation of the maximum and minimum values, as well as integration in formulae (2.42)–(2.44) was performed over the entire region, where bottom deformations had noticeable values. For coastal sources the land region was not taken into account in calculations. We note that in calculat-

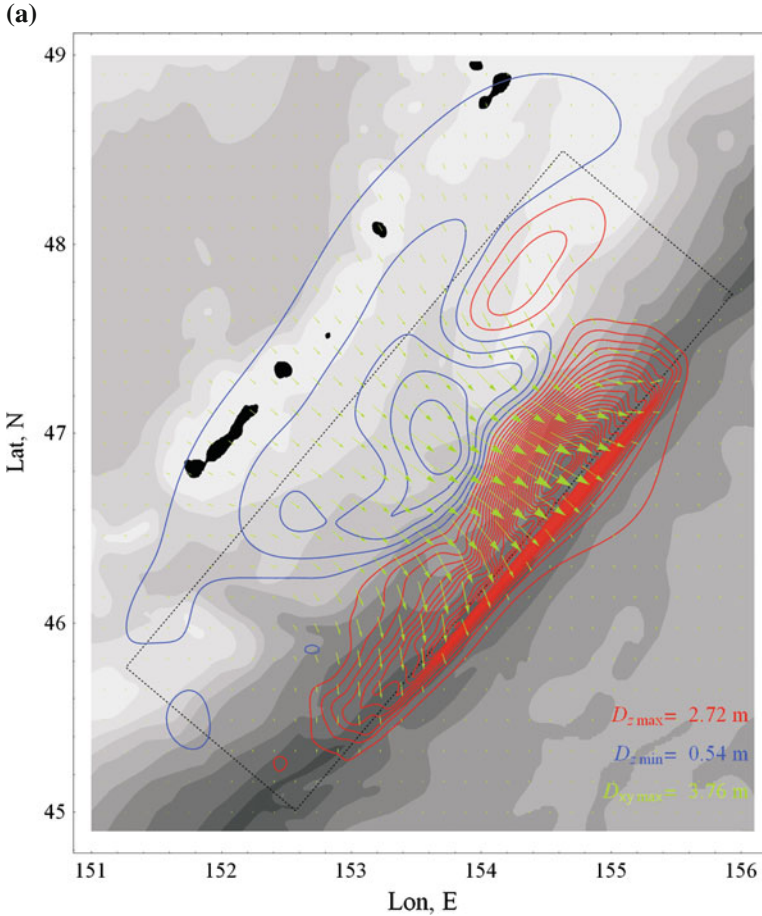


Fig. 2.15 Bottom topography and vector fields of coseismic ocean bottom deformation for the 2006 earthquake on the Central Kuril Islands (a) and the 2004 Sumatra–Andaman earthquake (b). The isobaths are drawn with an interval of 1 km. The vertical bottom deformation is shown by isolines (uplifts in red, subsidences in blue) drawn in steps of 0.1 m (a) and 0.5 m (b). The green arrows stand for the horizontal bottom deformation. The dashed rectangles represent projections of the fault segments onto the surface of the ocean bottom. The maximum uplift and subsidence values, as well as the horizontal deformation amplitudes, are shown in the lower parts of the figures

ing energy we conventionally assume the initial elevation ξ to be equivalent to the coseismic displacement of the bottom surface, η : $\xi = \eta$. Strictly speaking, owing to a “smoothing effect” functions ξ and η may differ from each other (e.g., Kajiura 1963, Nosov and Kolesov 2009, 2011). Neglecting the “smoothing effect” leads to a certain overestimation of the energy. This effect will be dealt with in detail in Sect. 3.5.

(b)

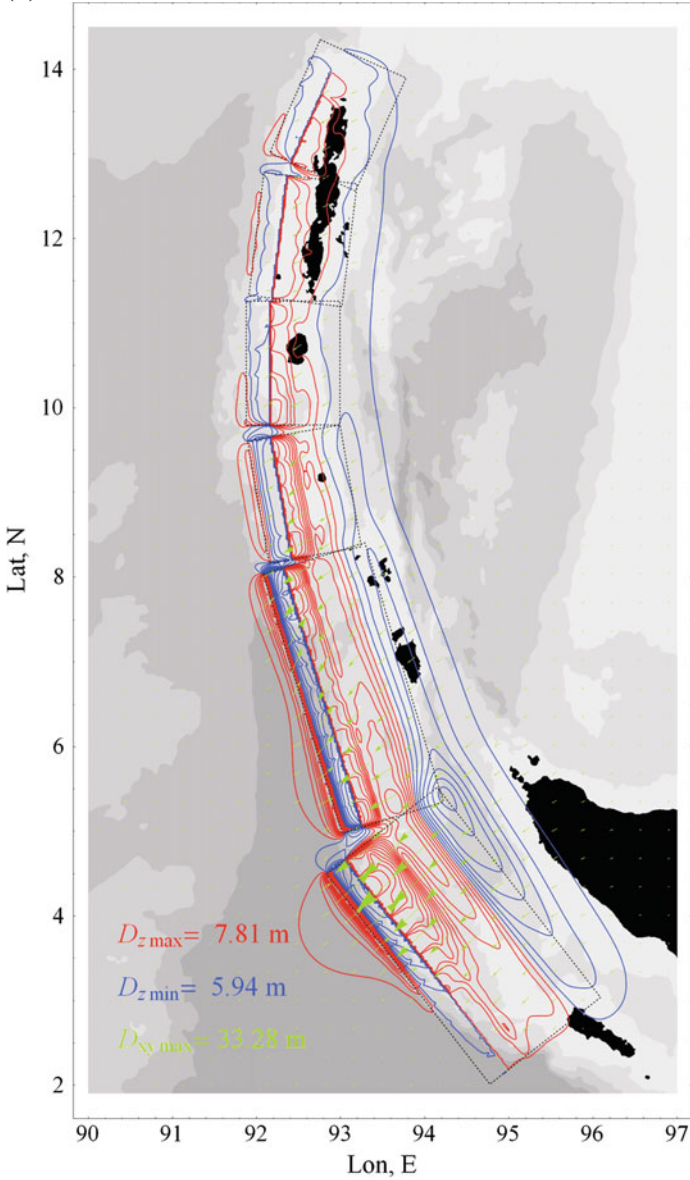


Fig. 2.15 (continued)

Figure 2.16 presents the bottom deformation amplitude versus the moment magnitude of earthquake. The dependence is characterized by quite a significant spread in the data: the correlation coefficient amounts to 0.8. The spread in the data is due to the bottom deformation being sensitive not only to the magnitude, but, also, to the

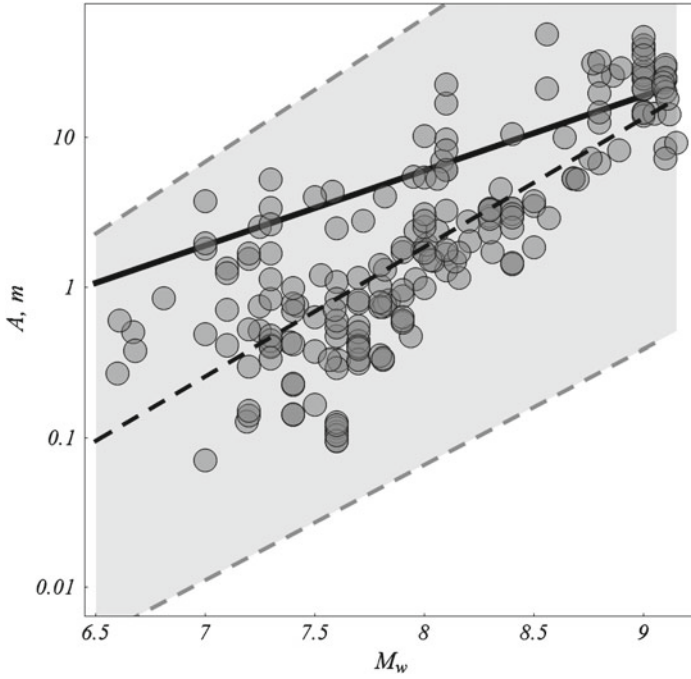


Fig. 2.16 Amplitude of bottom deformation versus earthquake moment magnitude: points—calculation based on data on slip distribution, *dotted line*—regression dependence, *gray band*—95 % confidence interval, *solid line*—theoretical maximum calculated by formula (2.45)

fault area orientation, to the slip direction and distribution, to the earthquake depth. The double amplitude is seen from the figure to vary between several centimeters (7 cm) and several tens of meters (48.5 m) and on the average to rapidly increase exponentially with the magnitude. The regression dependence, constructed by the least-squares method exhibits the following form:

$$\log_{10} A[m] = (0.86 \pm 0.09) M_w - (6.61 \pm 0.73), \quad (2.51)$$

The interval estimates correspond to 95 % probability. The regression dependence (2.51) is shown in Fig. 2.16 by the black dotted line. The gray band within gray dotted lines corresponds to the confidence interval. The solid black line in Fig. 2.16 is the theoretical dependence for the maximum possible deformation amplitude that was obtained in the previous section for the model of a uniform slip along a rectangular fault area (see formula (2.45) from Sect. 2.3). It can be seen that for a significant part of real events, and especially in the case of events with large magnitudes, the bottom deformation amplitude can exceed the theoretically maximum value. This fact is not a paradox. It is due to slip concentration within a narrow region of the fault area.

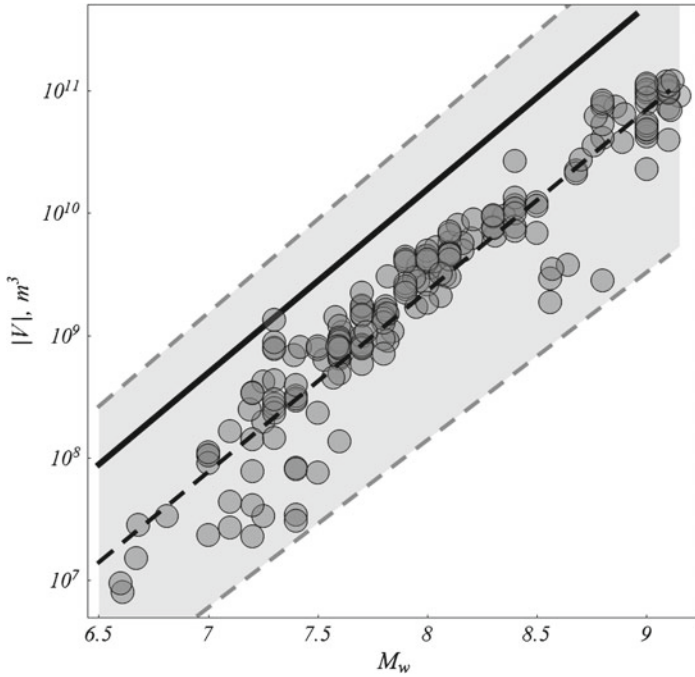


Fig. 2.17 Absolute value of water volume displaced by residual bottom deformation versus earthquake moment magnitude: points—calculation based on data on slip distribution, *dotted line*—regression dependence, *gray band*—95 % confidence interval, *solid line*—theoretical maximum calculated by formula (2.46)

The uniform slip distribution along the whole fault area, the seismic moment (and the moment magnitude) being conserved, would evidently lead to a decrease in the bottom deformation amplitude.

The relationship between the absolute value of the entire displaced volume and the moment magnitude is presented in Fig. 2.17. The displaced volume varies between 0.08 and 121 km³ and on the average exhibits a rapid exponential rise as the moment magnitude increases. As compared to the bottom deformation amplitude the displaced volume is noticeably better correlated with the moment magnitude: the correlation coefficient amounts to 0.95. The respective regression dependence, constructed by the least-squares method, has the following form:

$$\log_{10} V[m^3] = (1.48 \pm 0.09) M_w - (2.45 \pm 0.89), \tag{2.52}$$

The dependence (2.52) is shown in Fig. 2.17 by the black dotted line. The gray band within gray dotted lines corresponds to a 95 % confidence interval.

The solid black line in Fig. 2.17 represents the theoretical dependence for the maximum possible value of the displaced volume, that was obtained within the framework

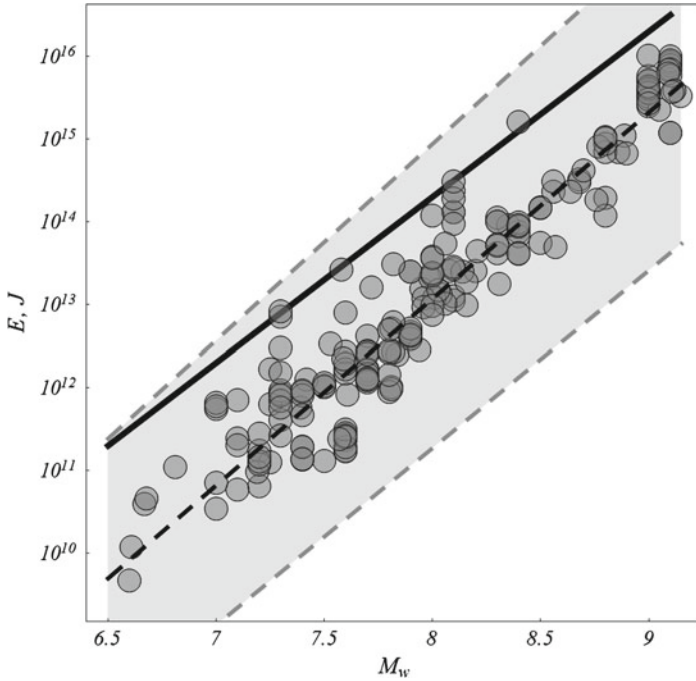


Fig. 2.18 Potential energy of water surface elevation equivalent in shape to residual bottom deformation (the tsunami energy) versus the earthquake moment magnitude: points—calculation based on data on slip distribution, *dotted line*—regression dependence, *gray band*—95% confidence interval, *solid line*—theoretical maximum calculated by formula (2.47)

of the uniform slip distribution model (see formula (2.46) from Sect. 2.3). The displaced volume, calculated for real events, is seen to never exceed the theoretical maximum value, and, on the average, it usually turns out to be several times smaller than this value.

The dependence of the initial elevation potential energy E upon the moment magnitude is presented in Fig. 2.18. In the case of real events the energy estimate varies within the range from 4.62×10^9 up to 1.01×10^{16} J. On the average, the energy increases exponentially with the moment magnitude. The dependence is characterized by quite a high correlation coefficient—0.94. The regression dependence has the following form:

$$\log_{10} E[J] = (2.26 \pm 0.13) M_w - (4.93 \pm 0.92). \quad (2.53)$$

Dependence (2.53) is shown in the figure by the black dotted line. The gray band within dotted lines corresponds to a 95% confidence interval. It is seen that, like in the case of the displaced volume, the potential energy calculated for real sources never exceeds the maximum theoretical value (see formula (2.47) from Sect. 2.3).

Applying the regression dependence for the energy of the initial elevation, (2.53), and the Kanamori formula (2.49) for the energy of an earthquake, we obtain the improved (as compared to formula (2.50) from Sect. 2.3) estimate of the part of the earthquake energy that is transmitted to tsunami waves,

$$\log_{10} E/E_{EQ} = 0.75M_w - 9.73. \quad (2.54)$$

From formula (2.54) it follows that the part of energy transmitted to the tsunami increases with the magnitude from 0.003% (when $M_w = 7$) up to 0.1% (if $M_w = 9$). On the whole, from the analysis of realistic oceanic bottom deformations at a tsunami source it follows that the part of energy transmitted to tsunami waves turns out to be noticeably smaller than what follows from their theoretical estimates (2.50), presented in Sect. 2.3.

To conclude this section we shall deal with revelation of the role of horizontal deformation components of an uneven (inclined) oceanic bottom in the case of tsunami wave generation. We note that analysis of the double amplitude A is of no particular interest in this case. This is so because the quantity A is actually determined by the values of function η at only two points, at which function η assumes its maximum and minimum values. The components of function η , that are due to the horizontal and vertical components of the bottom deformation, are characterized by nearly a total absence of correlation and by significant variability. Contrary to the versatile “point” quantity A , integral characteristics, such as the displaced volume V and the initial elevation energy E , evidently exhibit greater stability, which permits, on their basis, to introduce quantitative characteristics describing the contribution to tsunami waves of horizontal deformation components in the case of an uneven bottom.

The structure of formula (2.41) itself immediately permits to unambiguously determine the contribution of horizontal deformations of an inclined bottom to the total displaced volume:

$$V_{xy} = \iint \left(\frac{\partial H}{\partial x} D_x + \frac{\partial H}{\partial y} D_y \right) dx dy. \quad (2.55)$$

We determine the contribution of horizontal deformations to the initial elevation potential energy as follows:

$$E_{xy} = E - E_z, \quad (2.56)$$

$$E_z = \frac{\rho g}{2} \iint (D_z)^2 dx dy, \quad (2.57)$$

where E is the potential energy calculated with account of all the bottom deformation components by formula (2.44).

Figure 2.19 illustrates the contribution of horizontal deformations of an inclined bottom, V_{xy} , to the total displaced volume V . Both quantities can be either positive or negative. For clarity we present linear equivalents of the volumes retaining their

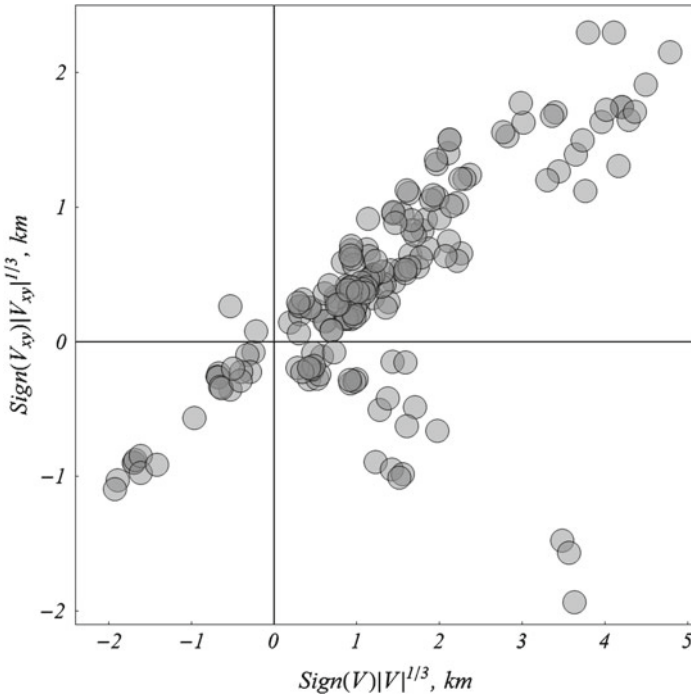


Fig. 2.19 Volume of water displaced by horizontal deformation components of inclined bottom, V_{xy} , versus total displaced volume V . The axes represent linear equivalents of the displaced volumes with their signs retained

signs: $Sign(V) |V|^{1/3}$ and $Sign(V_{xy}) |V_{xy}|^{1/3}$. From the figure it is seen that in most cases (163 out of 200) the signs of quantities V_{xy} and V coincide. This impressive result signifies that, as a rule, horizontal bottom deformations provide an additional contribution to the displaced volume. This result was first obtained in Nosov et al. (2014). In absolute value, the contribution of horizontal bottom deformation components to the displaced volume V_{xy}/V varies between 0.1 and 88%, while its mean value amount to 15%. Hence follows an important, from a practical point of view, conclusion: neglecting the horizontal bottom deformation components in simulating a tsunami in most cases leads to noticeable, while sometimes to significant, underestimation of the wave.

Figure 2.20 presents the part of potential energy of the water surface elevation, that is due to the contribution of horizontal deformation components of an inclined bottom, E_{xy}/E , versus the total potential energy E . The value of E_{xy}/E can be either positive or negative ($-0.08 < E_{xy}/E < 0.41$). In most cases (173 out of 200) the contribution of horizontal deformation is positive. In other words, horizontal components of the bottom deformation, as a rule, give an additional contribution to the tsunami energy. It is remarkable that not only for the displaced volume, but for the tsunami energy, also, this contribution is not negligible.

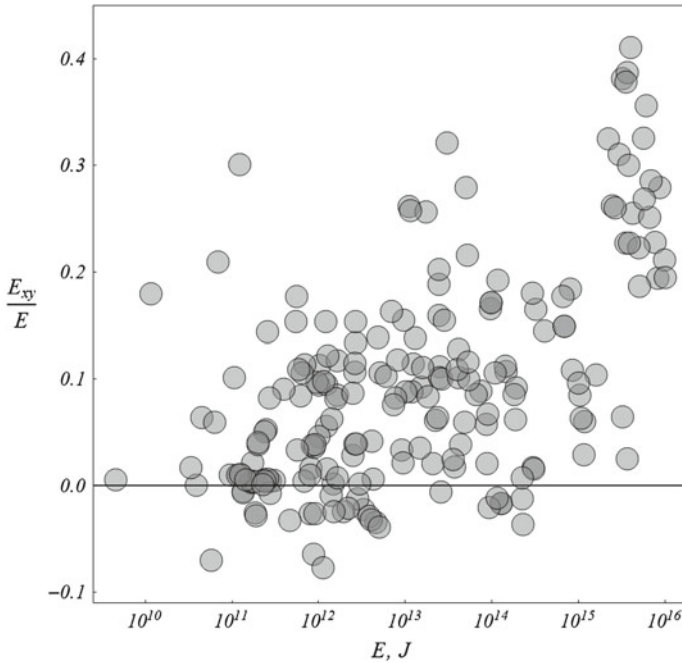


Fig. 2.20 Relative contribution of horizontal bottom deformation components to tsunami energy versus total energy value

The fact that in most cases horizontal deformations of an inclined bottom provide an additional contribution both to the volume of water displaced at the source and to the tsunami energy points to the existence of a certain correlation between the ocean bottom relief and coseismic deformations. To explain the existence of such a correlation it suffices to recall that most tsunamigenic earthquakes are related to subduction zones (e.g., Satake and Tanioka 1999, Gusiakov 2014), which are characterized by certain inherent shapes of the oceanic bottom, such as, for example, deep-water trenches. And, although each seismic event is individual, the occurrence of earthquakes in subduction zones is on the whole consistent with certain “scenarios”, a manifestation of which consists precisely in the observed correlation between vertical and horizontal coseismic shifts of underwater slopes.

2.5 Distribution of Tsunami Sources in Space and Time

The problem of studying the origination periodicity of tsunami sources in space and time continues to be one of the hitherto unresolved fundamental scientific problems, and it is also very important from the point of view of applications (Mogi 1979, Kasahara 1981, Riguzzi et al. 2010, Levin and Sasorova 2012). Sources of tsunami-

genic earthquakes cannot arise at any point whatever of the World Ocean. Thus, for example, practically no tsunami sources have ever existed within regions between latitudes 70 and 90 North as well as between latitudes 40 and 90 South. In other words, from the point of view of the origination of seismotectonic tsunamis high latitudes are sort of forbidden zones. Still another natural event must be noted: at low latitudes, where the occurrence of tsunami sources is quite customary, there also exists a clearly identifiable forbidden zone between latitudes 20 and 30 North. No tsunamis were observed to arise within this band during the past 100 years. Why? Of course, we cannot provide an answer to this question in the present section, and we will only present a number of observed facts, that in the future may facilitate comprehension of the physics of the Earth's seismicity and, in particular, explanation of the existing space–time regularities characteristic of the distribution of tsunami sources.

Analysis of the space–time distributions of tsunamigenic earthquake sources was performed taking advantage of the material provided by two known tsunami databases, NOAA/WDS Global Historical Tsunami Database at NGDC (http://www.ngdc.noaa.gov/hazard/tsu_db.shtml) and Historical Tsunami Database for the World Ocean (<http://tsun.sccc.ru/tsunami-database/index.php>).

The aforementioned databases were used to form an operational catalogue for the period from 1900 up to 2012 containing events involving tsunamigenic earthquakes (EQ) of magnitude $M \geq 7.5$, intensity $I \geq 1.0$, and validity $V = 4$ (i.e., only authentically registered events). After the elimination of duplicates, a cross-check and correction of both databases 99 events were ultimately singled out and identified as tsunamis of tectonic origin.

The statistical peculiarities of tsunamigenic events revealed with account of geographical and magnitude parameters of the distributions permit to answer the following question: what fraction of strong EQ happens to be tsunamigenic EQ when a change occurs in the threshold value of the magnitude.

In Table 2.2 the numbers of events over all the Earth and, separately, the individual hemispheres are presented for the following variations in the magnitude threshold: $M \geq 7.5$; $M \geq 8.0$; $M \geq 8.5$. On the average, tsunamigenic earthquakes are seen to compose 16% (of the entire number of strong EQ, equal to 615), and in the case of events with $M \geq 7.5$ and events with $M \geq 8.0$ the relative amount of events in the Southern hemisphere is greater than in the Northern hemisphere for both bands of magnitudes. This means that the relative number of tsunamigenic earthquakes does not increase with the magnitude.

However, all catastrophic events (with $M \geq 8.5$) are tsunamigenic. The sources of these events are situated in the region of the Pacific Ocean (4 in South America, 3 in the northern part of the subequatorial region, 1 in the Kamchatka region, 1 in Japan). We note that the above features of the distribution of tsunamigenic earthquakes were dealt with in a series of publications (Levin 2006, Levin and Sasorova 2010, Levin and Sasorova 2014).

Table 2.2 Comparison of the number of strong earthquakes (EQ) with the number of tsunamigenic earthquakes (TEQ) of the same magnitude

	The whole Earth	Northern hemisphere	Southern hemisphere
Events with $M \geq 7.5$			
Total number of EQ	615	390	225
Number of TEQ, with $I \geq 1$	99 (16%)	51 (13%)	48 (21%)
Events with $M \geq 8.0$			
Total number of EQ	292	192	100
Number of TEQ, with $I \geq 1$	47 (16%)	28 (15%)	19 (19%)
Events with $M \geq 8.5$			
Total number of EQ	9	5	4
Number of TEQ, with $I \geq 1$	9 (100%)	5 (100%)	4 (100%)

Construction of the spatial distributions of tectonic tsunami sources was based on division of the Earth’s surface into 18 latitudinal bands, the size of each latitudinal band being 10°. Separation was also performed of events that occurred in the Northern and Southern hemispheres of the Earth. In analyzing time distributions the entire interval of observation was divided into 5-year intervals, and the total number of events as well as the total energy released was considered for each 5-year interval.

Since most seismic events occur near the boundaries of lithospheric plates, use was made in the work of the event density and of the energy density (the number of earthquakes and the energy released normalized to the boundary length of the lithospheric plates in each latitudinal band). Such normalization yields the “power” of the given segment of a plate boundary: the mean number of earthquakes or the mean energy value per each 100 kilometers of plate boundary. Utilization of these characteristics, that have a clear physical meaning, permits to compare the seismic activities of latitudinal bands and of different parts of the terrestrial globe (Levin and Sasorova 2012).

Figure 2.21 shows the latitudinal distribution of the number of tsunami sources of tectonic origin. In this distribution one can clearly identify two maxima at latitudes 40°–50°N and 0°–10°S, a local minimum in the region of 20°–30°N and practically zero values at the polar caps and at high latitudes.

Figure 2.21b presents the latitudinal density distribution of the sources of tsunamigenic EQ. The main features of the distribution in Fig. 2.21b are similar to those of the distribution in Fig. 2.21a. However, the maximum in the Northern hemisphere is more sharply outlines, while in the Southern hemisphere the maximum in the region of 0°–10°S disintegrates into two maxima: at 0°–10°S and 30°–40°S. The second maximum is pronounced more weakly.

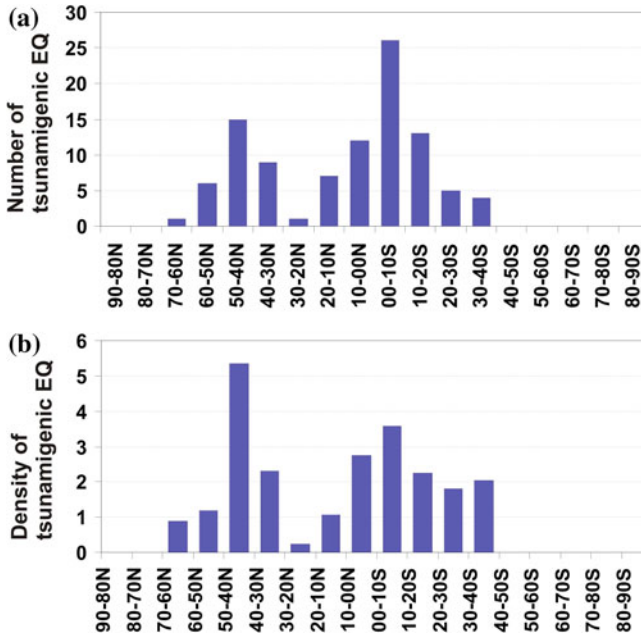


Fig. 2.21 Latitudinal distribution of number of tsunamigenic earthquake sources (a), latitudinal density distribution of tsunamigenic earthquakes (b)

Further, we shall consider latitudinal distributions of the energy released from tsunamigenic EQ (Fig. 2.22a) and of the energy density (Fig. 2.22b). Here, distributions are revealed with three clearly identified local maxima: at 40° – 30° N, 10° – 00° N and 30° – 40° S; in between them there are local minima with practically zero values of energy (and of energy density) at the polar caps and at high latitudes. Of all the energy released from tsunamigenic EQ 22% is released within the 40° – 30° N band of latitudes, 30% within the 10° – 00° N band, and 14% is released at latitudes of 30° – 40° S. All together 66% of the energy is released at latitudes corresponding to local maxima (three latitudinal bands out of 18).

We shall now present the distribution of events over time. Figure 2.23 shows the source density distributions for tsunamigenic earthquakes over 5-year intervals for the entire Earth (a), for the Northern (b) and Southern (c) hemispheres of the Earth. The scale of the vertical axis remains constant for all three fragments. The periodicity in the increase and decrease of the event density in time is clearly seen. Moreover, an asymmetry is apparent in the increase and decrease of tsunami activity in the Northern and Southern hemispheres. Enhancement of tsunamigenic earthquake activity is displayed alternately in the Northern hemisphere and, then, in the Southern hemisphere (and vice versa).

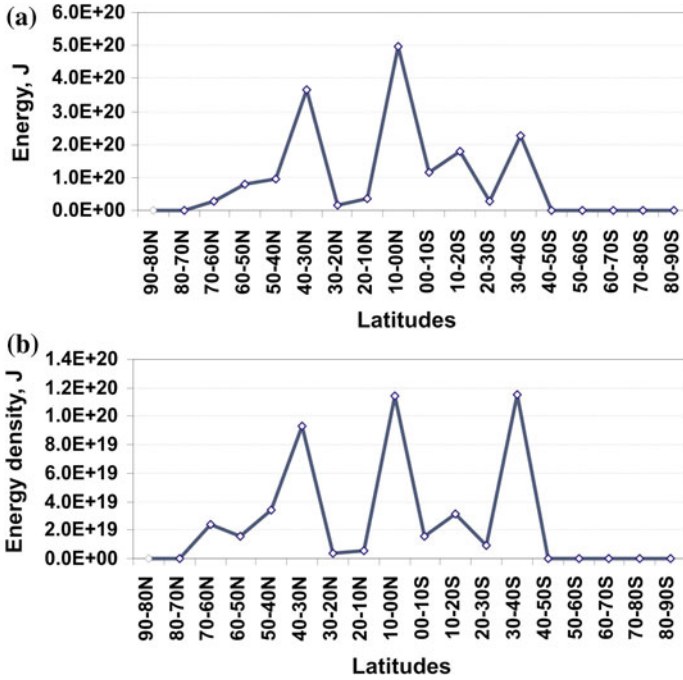


Fig. 2.22 Latitudinal distribution of energy released in tsunamigenic earthquakes (a), latitudinal density distribution of this energy (b)

The most powerful tsunamigenic EQ (from the point of view of the energy release) were observed at the beginning of the twenty-first century. They occurred both in the Northern and Southern hemispheres of the Earth, but within different 5-year intervals. The weakest (in energy) peaks of tsunami activity were at the beginning of the 20 century and at its middle (1950–1965).

Above we dealt separately with latitudinal (spatial) and time distributions of the sources of tectonic tsunamigenic events and with the energy released by these events. However, the most complete picture is provided by two-dimensional (space–time) distributions of events. Such a technique for representing the distributions of seismic activity was first applied in Levin and Sasorova (2010).

The two-dimensional density distribution of tsunamigenic EQ (Fig. 2.24) reveals the existence of regions (polar caps and high latitudes) within which not a single tsunamigenic event occurred during a period more than a hundred years long. The region of high latitudes, where no tsunami sources with $I \geq 1$ were observed, is much more extended in the Southern hemisphere, it starts at 40°S and continues up to the Southern Pole, while in the Northern hemisphere such a region only starts from 70°N. The region with practically zero activity is also found within the latitudinal band of 30°–20°N.

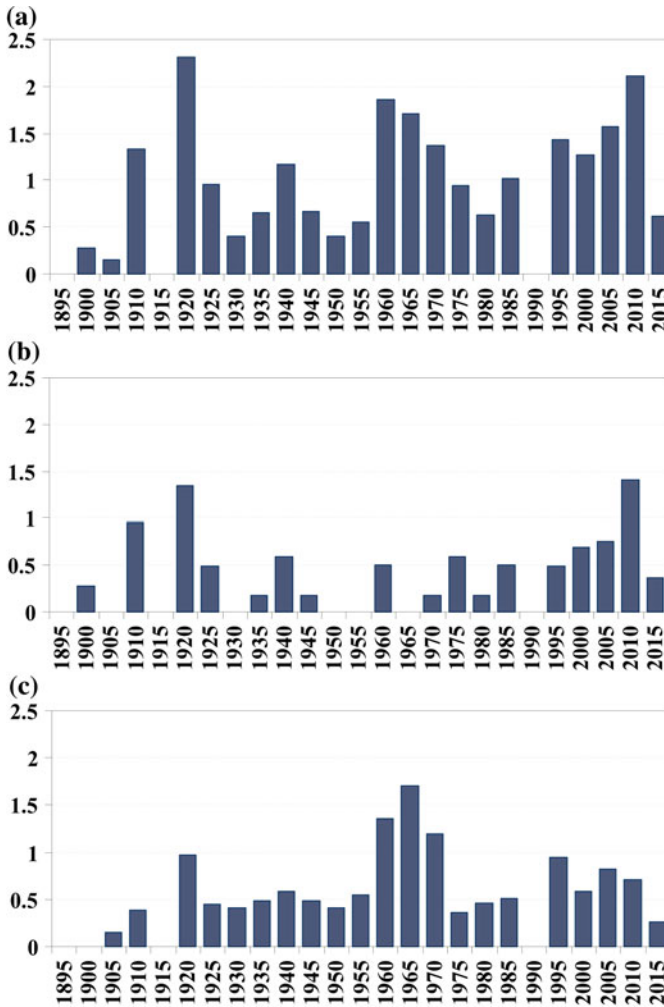


Fig. 2.23 Density distributions of tsunamigenic earthquake sources over 5-year intervals for the entire Earth (a), for the Northern hemisphere (b), for the Southern hemisphere (c)

Periodicity in the origination of tsunamigenic earthquakes is quite pronounced in Fig. 2.24, and this periodicity differs in different latitudinal bands. In the Northern hemisphere powerful peaks of activity were observed, when within a relatively short time interval several significant events took place. Such was the middle of the twentieth century from year 1955 up to 1975, then after a 20-year pause there were events during the period from 1990 up to 2010. Two less powerful clusters were also noted during the period of 1915–1920 and the 1980–1985 time intervals.

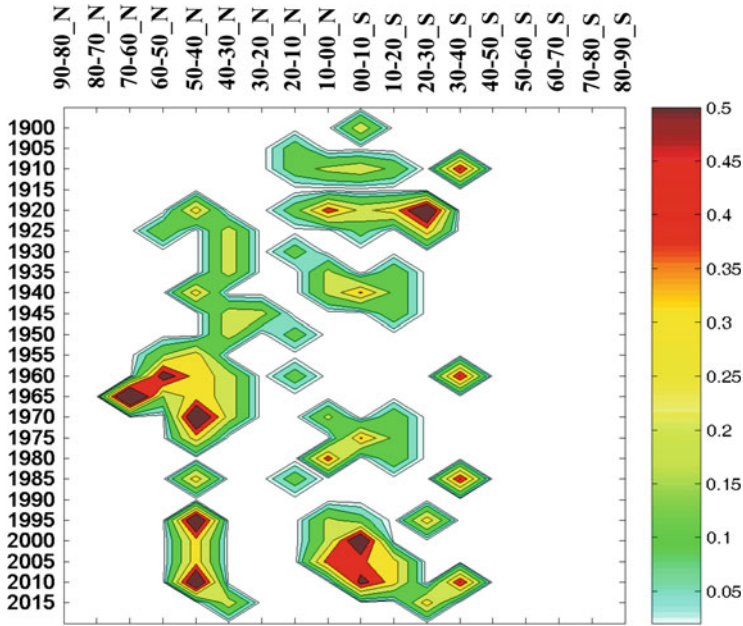


Fig. 2.24 Two-dimensional density distribution of tsunamigenic earthquakes. The *vertical axis* shows time, and the *horizontal axis* shows latitudinal bands. The density of tsunamigenic earthquakes is shown in accordance with the *color scale*

In the subequatorial region peaks of tsunami activity are noted with 25-year intervals (during the first half of the twentieth century), then with 30–40-year intervals (in the middle of the century) and again with an interval of 25 years by the end of the twentieth century. In the Southern hemisphere bursts of tsunami activity, practically identical in power, are noted with a periodicity of 50 years in the first half of the twentieth century, and, then, with a 25-year periodicity between 1960 and present time.

The analysis presented of the distribution of tsunami sources permits to identify the cyclic character of enhancement and attenuation of tsunami activity. Cyclicity is revealed not only in the grouping of events in time, but also in their spatial (latitudinal) grouping. On the one hand, regions are singled out on the surface of the terrestrial globe that exhibit minimal (or zero) tsunami activity—these are regions of high latitudes and Polar Regions. On the other hand, zones are revealed of alternating activity of the process, when adjacent latitudinal zones manifest activity enhancement during different periods of time. High activity in one zone is accompanied by activity attenuation in the adjacent region, and vice versa. Thus, high activity in a certain zone, corresponding to a given time period, is exchanged for a period of relaxation in the neighboring zone.

References

- Alekseev, A.S., Gusakov, V.K.: Numerical modeling of tsunami and seismic surface wave generation by a submarine earthquake. In: Heath, R.A., Creswell, M.M. (eds.) *Proceedings of Tsunami Res. Symposium*, pp. 243–252. Roy. Soc. New Zealand, Wellington (1976)
- Alewine, R.W., Jordan, T.H.: Generalized inversion of earthquake static displacement fields. *Geophys. J. R. Astron. Soc.* **35**, 357–380 (1973)
- Bassin, C., Laske, G., Masters, G.: The current limits of resolution for surface wave tomography in North America. *EOS. Trans. Am. Geophys. Un.* **81**, F897 (2000)
- Bernatskiy, A.V., Nosov, M.A.: The role of bottom friction in models of nonbreaking tsunami wave runup on the shore. *Izv. Atmos. Ocean. Phys.* **48**(4), 427–431 (2012)
- Bolshakova, A.V., Nosov, M.A.: Parameters of tsunami source versus earthquake magnitude. *Pure Appl. Geophys.* **168**, 2023–2031 (2011). doi:[10.1007/s00024-011-0285-3](https://doi.org/10.1007/s00024-011-0285-3)
- Bolshakova, A.V., Nosov, M.A., Kolesov, S.V.: The properties of co-seismic deformations of the ocean bottom as indicated by the slip-distribution data in tsunamigenic earthquake sources. *Mosc. Univ. Phys. Bull.* **70**(1), 62–67 (2015)
- Chinnery, M.A.: The deformation of ground around surface faults. *Bull. Seism. Soc. Am.* **51**, 355–372 (1961)
- Dotsenko, S.F., Soloviev, S.L.: Mathematical modelling of tsunami excitation processes by slides of the ocean bottom. *Tsunami Res. (in Russian)*, 4, 8–20. Moscow (1990a)
- Dotsenko, S.F., Soloviev, S.L.: Comparative analysis of tsunami excitation by “piston” and “membrane” bottom slides. *Tsunami Res. (in Russian)*, 4, 21–27 (1990b)
- Ekström, G., Nettles, M., Dziewonski, A.M.: The global CMT project 2004–2010: centroid-moment tensors for 13,017 earthquakes. *Phys. Earth Planet. Int.* **200–201**, 1–9 (2012). doi:[10.1016/j.pepi.2012.04.002](https://doi.org/10.1016/j.pepi.2012.04.002)
- Fujii, Y., Satake, K., Sakai, S.I., Shinohara, M., Kanazawa, T.: Tsunami source of the 2011 off the Pacific coast of Tohoku earthquake. *Earth Planets Space* **63**(7), 815–820 (2011)
- Gusiakov, V.K.: Residual displacements on the surface of an elastic half-space. In: *Conditionally Well-Posed Problems of Mathematical Physics in the Interpretation of Geophysical Observations (VTs SO RAN, Novosibirsk, 1978)*, pp. 23–51 (in Russian)
- Gusiakov, V.K.: Relationship of tsunami intensity to source earthquake magnitude as retrieved from historical data. *Pure Appl. Geophys.* **168**, 2033–2041 (2011)
- Gusiakov, V.K.: Strongest tsunamis in the World Ocean and the problem of marine coastal security. *Izv. Atmos. Ocean. Phys.* **50**(5), 435–444 (2014)
- Handbook for tsunami forecast in the Japan sea. Earthquake and Tsunami observation division, seismological and volcanological department, Japan meteorological agency, 22 pp. (2001)
- Hatori, T.: Vertical crustal deformation and tsunami energy. *Bull. Earthq. Res. Inst.* **48**, 171–188 (1970)
- Iida, K.: Magnitude, energy and generation mechanism of tsunamis and a catalogue of earthquakes associated with tsunamis In: *Proceedings of Tsunami Meeting Association 10th Pacific Scientific Congress, 1961, I.U.G.G. Monograph vol. 24*, pp. 7–18 (1963)
- Ito, Y., Tsuji, T., Osada, Y., Kido, M., Inazu, D., Hayashi, Y., Tsushima, H., Hino, R., Fujimoto, H.: Frontal wedge deformation near the source region of the 2011 Tohoku-Oki earthquake. *Geophys. Res. Lett.* **38**, L00G05 (2011). doi:[10.1029/2011GL048355](https://doi.org/10.1029/2011GL048355)
- Ji C (UCSB, Kuril 2006). Rupture process of the 15 November 2006 magnitude 8.3—KURIL island earthquake (Revised), http://earthquake.usgs.gov/earthquakes/eqinthenews/2006/usvcam/finite_fault.php
- Ji, C., Wald, D.J., Helmberger, D.V.: Source description of the 1999 Hector Mine, California earthquake; part I: wavelet domain inversion theory and resolution analysis. *Bull. Seism. Soc. Am.* **92**(4), 1192–1207 (2002)
- Jovanovich, D.B.: An inversion method for estimating the source parameters of seismic and aseismic events from static strain data. *Geophys. J. Astron. Soc.* **43**, 347–365 (1975)

- Kajiura, K.: The leading wave of tsunami. *Bull. Earthq. Res. Inst. Tokyo Univ.* **41**(3), 535–571 (1963)
- Kajiura, K.: Tsunami energy in relation to parameters of the earthquake fault model. *Bull. Earthq. Res. Inst.* **56**, 415–440 (1981)
- Kanamori, H.: Mechanism of tsunami earthquakes. *Phys. Earth Planet Int.* **6**, 346–359 (1972)
- Kanamori, H.: The energy release in great earthquakes. *J. Geophys. Res.* **82**, 2981–2987 (1977)
- Kanamori, H., Anderson, D.L.: Theoretical basis of some empirical relations in seismology. *Bull. Seismol. Soc. Am.* **65**, 1073–1095 (1975)
- Kanamori, H., Brodsky, E.E.: The physics of earthquakes. *Rep. Prog. Phys.* **67**, 1429–1496 (2004)
- Kasahara, K.: *Earthquake Mechanics*, p. 284. Cambridge University Press, Cambridge (1981)
- Kim, D.C., Kim, K.O., Pelinovsky, E., Didenkulova, I., Choi, B.H.: Three-dimensional tsunami runup simulation for the port of Koborinai on the Sanriku coast of Japan. *J. Coast. Res.* **65**, 266–271 (2013)
- Koketsu, K., Yokota, Y., Nishimura, N., Yagi, Y., Miyazaki, S., Satake, K., Fujii, Y., Miyake, H., Sakai, S., Yamanaka, Y., Okada, T.: A unified source model for the 2011 Tohoku earthquake. *Earth Planet. Sci. Lett.* **310**, 480–487 (2011)
- Kurahashi, S., Irikura, K.: Source model for generating strong ground motions during the 2011 off the Pacific coast of Tohoku earthquake. *Earth Planets Space* **63**, 571–576 (2011)
- Laverov, N.P., Lobkovsky, L.I., Levin, B.W., Rabinovich, A.B., Kulikov, E.A., Fine, I.V., Thomson, R.E.: The Kuril tsunamis of 15 November 2006, and 13 January 2007: two trans-pacific events. *Dokl. Earth Sci. MAIK Nauka/Interperiodica* **426**(1), 658–664 (2009)
- Lay, T., Yamazaki, Y., Ammon, C.J., Cheung, K.F., Kanamori, H.: The 2011 Mw 9.0 off the Pacific coast of Tohoku earthquake: comparison of deep-water tsunami signals with finite-fault rupture model predictions. *Earth Planets Space* **63**(7), 797–801 (2011)
- Levin, B.W.: On the nature of some periodic changes in the Earth's seismic regime. *Vestn. Dal'nevost. Otd. Ross. Akad. Nauk* **1**, 51–58 (2006)
- Levin, B.W., Nosov, M.A.: On the possibility of tsunami formation as a result of water discharge into seismic bottom fractures. *Izv. Atmos. Ocean. Phys.* **44**(1), 117–120 (2008)
- Levin, B.W., Sasorova, E.V.: General regularities in the distribution of seismic events on the Earth and on the Moon. *Dokl. Earth Sci.* **434**(1), 1249–1252 (2010)
- Levin, B.W., Sasorova, E.V.: Seismicity of the Pacific: Revealing Global Regularities. *Yanus-K, Moscow* (2012) (in Russian)
- Levin, B.W., Sasorova, E.V.: Spatiotemporal distributions of tsunami sources and discovered periodicities. *Izv. Atmos. Ocean. Phys.* **50**(5), 485–497 (2014). doi:[10.1134/S0001433814050065](https://doi.org/10.1134/S0001433814050065)
- Li, Y., Raichlen, F.: Non-breaking and breaking solitary wave run-up. *J. Fluid Mech.* **456**, 295–318 (2002)
- Maruyama, T.: Static elastic dislocations in an infinite and semi-infinite medium. *Bull. Earthq. Res. Inst. Tokyo Univ.* **42**, 289–368 (1964)
- Matsu'ura, M., Tanimoto, T.: Quasi-static deformations due to an inclined, rectangular fault in a viscoelastic half-space. *J. Phys. Earth* **28**(1), 103–118 (1980)
- Mikada, H., Mitsuzawa, K., Matsumoto, H., Watanabe, T., Morita, S., Otsuka, R., Sugioka, H., Baba, T., Araki, E., Suyehiro, K.: New discoveries in dynamics of an M8 earthquake—phenomena and their implications from the 2003 Tokachi-Oki earthquake using a long term monitoring cabled observatory. *Tectonophysics* **426**, 95–105 (2006)
- Mogi, K.: Global variation of seismic activity. *Tectonophysics* **57**, 43–50 (1979)
- Newman, A.V., Hayes, G., Wei, Y., Convers, J.: The 25 October 2010 Mentawai tsunami earthquake, from real-time discriminants, finite-fault rupture, and tsunami excitation. *Geophys. Res. Lett.* **38**(5), L01307 (2011)
- Nosov, M.A., Kolesov, S.V.: Method of specification of the initial conditions for numerical tsunami modeling. *Mosc. Univ. Phys. Bull.* **64**(2), 208–213 (2009)
- Nosov, M.A., Kolesov, S.V.: Optimal initial conditions for simulation of seismotectonic tsunamis. *Pure Appl. Geophys.* **168**(6–7), 1223–1237 (2011)

- Nosov, M.A., Nurislamova, G.N.: The potential and vortex traces of a tsunamigenic earthquake in the ocean. *Mosc. Univ. Phys. Bull.* **67**(5), 457–461 (2012)
- Nosov, M.A., Bolshakova, A.V., Kolesov, S.V.: Displaced water volume, potential energy of initial elevation and tsunami intensity: analysis of recent tsunami events. *Pure Appl. Geophys.* **171**, 3515–3525 (2014)
- Nosov, M.A., Kolesov, S.V., Levin, B.W.: Contribution of horizontal deformation of the seafloor into tsunami generation near the coast of Japan on 11 March 2011. *Dokl. Earth Sci.* **441**(1), 1537–1542 (2011). SP MAIK Nauka/Interperiodica
- Nosov, M.A., Kolesov, S.V., Ostroukhova, A.V., Alekseev, A.B., Levin, B.W.: Elastic oscillations of the water layer in a tsunami source. *Dokl. Earth Sci.* **404**(7), 1097–1100 (2005)
- Nosov, M.A., Nurislamova, G.N., Moshenceva, A.V., Kolesov, S.V.: Residual hydrodynamic fields after tsunami generation by an earthquake. *Izv. Atmos. Ocean. Phys.* **50**(5), 520–531 (2014)
- Nostro, C., Piersanti, A., Antonioli, A., Spada, G.: Spherical versus flat models of coseismic and postseismic deformations. *J. Geophys. Res.* **104**(B6), 13,115–13,134 (1999)
- Okada, Y.: Surface deformation due to shear and tensile faults in a half-space. *Bull. Seism. Soc. Am.* **75**(4), 1135–1154 (1985)
- Okada, Y.: Simulated empirical law of coseismic crustal deformation. *J. Phys. Earth* **43**, 697–713 (1995)
- Okal, E.A.: Seismic parameters controlling far-field tsunami amplitudes: a review. *Nat. Hazards* **1**, 67–96 (1988)
- Okal, E.A.: Normal mode energetics for far-field tsunamis generated by dislocations and landslides. *Pure Appl. Geophys.* **160**, 2189–2221 (2003)
- Ozawa, S., Nishimura, T., Suito, H., Kobayashi, T., Tobita, M., Imakiire, T.: Coseismic and postseismic slip of the 2011 magnitude-9 Tohoku-Oki earthquake. *Nature* **475**(7356), 373–376 (2011)
- Pavlov, V.M., Gusev, A.A.: On possibility of motion restoring in the deep earthquake source according to bulk wave field in Fraunhofer region. *Dokl. Akad. Nauk* **255**, 828–834 (1980)
- Pelinovsky, E.N.: *Hydrodynamics of Tsunami Waves* (in Russian). Institute of Applied Physics, RAS, Nizhniy Novgorod (1996)
- Poisson, B., Oliveros, C., Pedreros, R.: Is there a best source model of the Sumatra 2004 earthquake for simulating the consecutive tsunami? *Geophys. J. Int.* **185**(3), 1365–1378 (2011)
- Pollitz, F.F., Bürgmann, R., Banerjee, P.: Geodetic slip model of the 2011M9.0 Tohoku earthquake. *Geophys. Res. Lett.* **38**, L00G08 (2011)
- Poplavskii, A.A., Zolotukhin, D.E., Khramushin, V.N.: A macroseismic model of a tsunami source and estimation of its efficiency by numerical modeling. *J. Volcanol. Seismol.* **6**(1), 58–64 (2012)
- Press, F.: Displacements, strains and tilts at tele-seismic distances. *J. Geophys. Res.* **70**, 2395–2412 (1965)
- Riguzzi, F., Panza, G., Varga, P., Doglioni, C.: Can Earth's rotation and tidal despinning drive plate tectonics? *Tectonophysics* **484**, 60–73 (2010)
- Rhie, J., Dreger, D., Bürgmann, R., Romanowicz, B.: Slip of the 2004 Sumatra-Andaman earthquake from joint inversion of long-period global seismic waveforms and GPS static offsets. *Bull. Seism. Soc. Am.* **97**(1A), S115–S127 (2007)
- Satake, K.: Inversion of tsunami waveforms for the estimation of a fault heterogeneity: method and numerical experiments. *J. Phys. Earth* **35**(3), 241–254 (1987)
- Satake, K., Imamura, F.: Tsunamis: seismological and disaster prevention studies. *J. Phys. Earth* **43**(3), 259–277 (1995)
- Satake, K., Tanioka, Y.: Sources of tsunami and tsunamigenic earthquakes in subduction zones. *Pure Appl. Geophys.* **154**, 467–483 (1999)
- Sato, R.: Theoretical basis on relationships between focal parameters and earthquake magnitude. *J. Phys. Earth* **27**, 353–372 (1979)
- Savage, J.C., Hastie, L.M.: Surface deformation associated with dip-slip faulting. *J. Geophys. Res.* **71**, 4897–4904 (1966)

- Shao, G., Li, X., Ji, C., Maeda, T.: Focal mechanism and slip history of the 2011 Mw 9.1 off the Pacific coast of Tohoku earthquake, constrained with teleseismic body and surface waves. *Earth Planets Space* **63**(7), 559–564 (2011)
- Suzuki, W., Aoi, S., Sekiguchi, H., Kunugi, T.: Rupture process of the 2011 Tohoku-Oki mega-thrust earthquake (M9.0) inverted from strong-motion data. *Geophys. Res. Lett.* **38**(7) (2011)
- Tanioka, Y., Satake, K.: Fault parameters of the 1896 Sanriku tsunami earthquake estimated from tsunami numerical modeling. *Geophys. Res. Lett.* **23**(13), 1549–1552 (1996)
- Ward, S.N.: Relationships of tsunami generation and an earthquake source. *J. Phys. Earth* **28**, 441–474 (1980)
- Ward, S.N., Barrientos, S.E.: An inversion for slip distribution and fault shape from geodetic observations of the 1983 Borah Peak, Idaho earthquake. *J. Geophys. Res.* **91**, 4909–4919 (1986). doi:[10.1029/JB091iB05p04909](https://doi.org/10.1029/JB091iB05p04909)
- Watanabe, T., Matsumoto, H., Sugioka, H., Mikada, H., Suyehiro, K., Otsuka, R.: Offshore monitoring system records recent earthquake off Japan's northernmost island. *Eos* **85**(2) (2004)
- Wei, S., Graves, R., Helmberger, D., Avouac, J.P., Jiang, J.: Sources of shaking and flooding during the Tohoku-Oki earthquake: a mixture of rupture styles. *Earth Planet Sci. Lett.* **333–334**, 91–100 (2012)
- Wells, D.L., Coppersmith, K.J.: New empirical relationships among magnitude, rupture length, rupture width, rupture area, and surface displacement. *Bull. Seismol. Soc. Am.* **84**(4), 974–1002 (1994)
- Yagi, Y., Fukahata, Y.: Introduction of uncertainty of Green's function into waveform inversion for seismic source processes. *Geophys. J. Int.* **186**(2), 711–720 (2011)
- Yamashita, T., Sato, R.: Generation of tsunami by a fault model. *J. Phys. Earth* **22**, 415–440 (1974)

Chapter 3

Hydrodynamic Processes at the Source of a Tsunami of Seismotectonic Origin: Incompressible Ocean

Abstract The process of tsunami generation by dynamic bottom deformations is treated as a hydrodynamical problem of an incompressible liquid. Two basic approximations are presented, which are used in describing gravitational waves on water—the theory of long waves and the potential theory. Within the framework of linear potential theory of an incompressible liquid in a basin of fixed depth, the general analytical solution is constructed for the two-dimensional (2D) and three-dimensional (3D) problems of tsunami generation by bottom deformations of small amplitudes. The solution of the 3D problem is constructed in both Cartesian and cylindrical coordinates. For a series of model bottom deformation laws (piston, membrane and running displacements, bottom oscillations and alternating-sign displacement) physical regularities are revealed that relate the amplitude, energy, and direction of tsunami wave emission to peculiarities of the bottom deformation at the source. In some cases, the theoretical regularities, obtained within potential theory, are compared with dependences following from the linear theory of long waves and, also, with the results of laboratory experiments. The practical problem of calculating the initial elevation on a water surface at a tsunami source is considered within the framework of the assumption of instantaneity of bottom deformation. Exact analytic solutions of this problem are presented for flat horizontal and inclined bottoms. Within the framework of the linear theory of long waves on account of the Earth's rotation, investigation is performed of horizontal motions of the water layer accompanying tsunami generation by an earthquake in a homogeneous and stratified ocean. The displacement of water by coseismic bottom deformations is shown to serve as the cause of formation not only of tsunami waves, but also of long-lived “traces” of the tsunamigenic earthquake in the ocean—of potential and eddy residual hydrodynamical fields. The field of residual horizontal displacements of water particles is calculated and analyzed for the 2011 Tohoku-Oki earthquake.

Keywords Hydrodynamic description · Gravity waves · Long-wave theory · Potential theory · Fluid velocity potential · Coseismic deformation · Tsunami source · Tsunami generation · Initial elevation · Ocean bottom displacement · Laplace transformation · Fourier transformation · Analytical solution · Phase dispersion · Directional diagrams · Residual hydrodynamic fields · Coriolis force · Geostrophic vortex · Rossby radius of deformation

The model of an incompressible homogeneous liquid is conventionally applied in describing tsunami waves. Remaining within the framework of conventional ideas, we have devoted this chapter to various types of hydrodynamical problems related to the generation of movements in a layer of liquid in the case of dynamic deformations of the basin bottom.

The general formulation of the problem is expounded in Sect. 3.1, and, also, the equations are derived of long-wave theory and of potential wave theory. In the subsequent three sections (3.2–3.4), exact analytic solutions are constructed for a series of linear problems relevant to tsunami generation by an earthquake. A method for calculating the initial elevation at the tsunami source is presented and theoretically substantiated in Sect. 3.5. Peculiarities of horizontal movements of a water layer accompanying tsunami generation are analyzed in Sect. 3.6. In this section the formation is mainly dealt with residual hydrodynamic fields, an effect that is often wrongly disregarded by tsunami researchers. It is shown that in situ revelation and analysis of horizontal movements may turn out to be useful, together with data on the ocean level, for estimating the tsunamigenicity of underwater earthquakes.

The analytic solutions of model problems presented in this chapter can be used not only in analyzing fundamental regularities of tsunami formation by earthquakes, but also for testing numerical models.

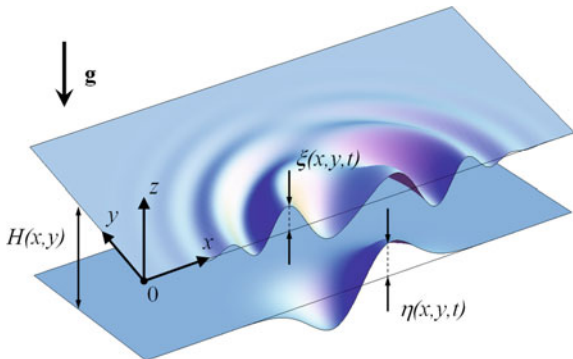
3.1 Hydrodynamic Description of Tsunami Waves: The Two Principal Approximations

In this section we shall expound the general hydrodynamic approach to describing waves excited in a layer of water by dynamic deformations of the ocean bottom. We shall separately present two key approaches applied in describing the dynamics of tsunami waves: *the long-wave theory* and *the potential theory*. Both nonlinear and linear versions of the mentioned theories will be presented.

3.1.1 General Formulation of the Hydrodynamic Problem

We shall consider a layer of ideal (nonviscous) homogeneous incompressible liquid ($\rho = \text{const}$) of variable depth on a rotating Earth. The layer of liquid is limited from above by its free surface and from below by the mobile impermeable bottom. Let the origin of the rectangular reference frame (see Fig. 3.1) be on the unperturbed water surface. We shall direct the Oz -axis vertically upward and the Ox and Oy axes eastward and northward, respectively. The bottom surface will be assumed to be fixed before the moment of time $t = 0$ and its position to be described by the equation $z_b = -H(x, y)$. When $t > 0$ —during the earthquake—the surface of the bottom undergoes motion, and then its position is determined by the equation $z_b = -H(x, y) + \eta(x, y, t)$,

Fig. 3.1 Mathematical formulation of the 3D problem



where $\eta(x, y, t)$ represents dynamic deformation of the bottom. We shall characterize movements of the water layer caused by dynamic deformation of the bottom by the following quantities: displacement of the free surface of water from its equilibrium position, $\xi(x, y, t)$, the scalar pressure field $p(x, y, z, t)$, and the vector flow velocity field $\mathbf{v}(x, y, z, t) \equiv (u, v, w)$, where u , v , and w are velocity components along the $0x$, $0y$, and $0z$ axes, respectively. To describe movements of the water layer we shall take advantage of the Euler equation, written with account of the force of gravity, and of the Coriolis force, and of the continuity equation (e.g., Lamb 1932; Murty 1977; Marchuk et al. 1983; Landau and Lifshits 1987; Pelinovsky 1996)

$$\frac{\partial \mathbf{v}}{\partial t} + (\mathbf{v}, \nabla) \mathbf{v} = -\frac{\nabla p}{\rho} + \mathbf{g} + 2[\mathbf{v} \times \boldsymbol{\omega}], \quad (3.1)$$

$$\operatorname{div} (\mathbf{v}) = 0, \quad (3.2)$$

where \mathbf{g} is the acceleration vector of gravity, $\boldsymbol{\omega}$ is the angular velocity vector of the Earth's rotation.

Equations (3.1) and (3.2) are supplemented with the classical boundary conditions on the free water surface and on the ocean bottom. On the water surface (the “water-atmosphere” partition surface) pressure continuity (a dynamic condition) is assumed,

$$p = p_{atm}(x, y, t) \quad \text{for} \quad z = \xi(x, y, t), \quad (3.3)$$

where $p_{atm}(x, y, t)$ is a function describing the space–time distribution of atmospheric pressure along the free water surface. Besides the dynamic condition, the free surface is also subjected to the kinematic boundary condition

$$\frac{\partial \xi}{\partial t} + u \frac{\partial \xi}{\partial x} + v \frac{\partial \xi}{\partial y} - w = 0, \quad (3.4)$$

the physical meaning of which consists in that particles of the liquid, that belong to the surface, cannot move freely within the liquid layer.

The condition is set that no-normal flow takes place across the ocean bottom: the velocity component normal to the bottom surface must be equal to the motion velocity of the bottom in the same direction (no-normal flow boundary condition):

$$(\mathbf{v}, \mathbf{n}) = (\mathbf{v}_b, \mathbf{n}) \quad \text{for } z = -H(x, y) + \eta(x, y, t), \quad (3.5)$$

where \mathbf{v}_b is the velocity vector of the bottom, \mathbf{n} is the normal to the bottom surface.

In tsunami simulation, which in principle can be performed by straightforward numerical integration of equations (3.1)–(3.5), it is possible to use, as the initial conditions, zero free surface displacement, $\xi_0 = 0$, the zero velocity field $\mathbf{v}_0 = 0$, and the hydrostatic pressure distribution determined from the equation $\nabla p_0 = \rho \mathbf{g}$. The source of waves consists in dynamic deformation of the bottom, $\eta(x, y, t)$, and/or variations in the atmospheric pressure $p_{atm}(x, y, t)$.

Although straightforward numerical simulation based on the equations of hydrodynamics has the doubtless advantage of providing a completeness of description, its application always involves cumbersome calculations. Moreover, it is regrettably impossible to obtain an analytic solution of the set of equations (3.1)–(3.5). Here, it must be pointed out that an analytic solution, even if obtained for a particular case and under certain assumptions, can provide more information on the physical essence of a process than hundreds of numerical experiments. In this connection, it is opportune to analyze tsunami wave dynamics within the framework of different approximations, one of which is the hydrostatics approximation that underlies the long-wave theory.

3.1.2 The Long-Wave Theory

The long-wave theory, sometimes called the shallow-water theory, is based on the assumption that the depth of the ocean is significantly smaller than the wavelength: $H/\lambda \ll 1$. Treating the ocean depth as a vertical space scale, and the tsunami wavelength as the horizontal scale, we obtain from the continuity equation (3.2) written in terms of individual components,

$$\frac{\partial u}{\partial x} + \frac{\partial v}{\partial y} + \frac{\partial w}{\partial z} = 0, \quad (3.6)$$

a simple expression that relates the amplitudes of the vertical (U_z) and horizontal (U_{xy}) velocities,

$$U_z \sim \frac{H}{\lambda} U_{xy}. \quad (3.7)$$

From relationship (3.7) it follows that, if the condition $H/\lambda \ll 1$ is fulfilled, then the horizontal velocities are significantly superior to the vertical ones: $U_{xy} \gg U_z$. A similar conclusion can be made, also, with respect to the dominance of horizontal over vertical accelerations. Consequently, the insignificant vertical accelerations in the vertical component of the Euler equation may be neglected.

We further write out components of the Coriolis force applying the so-called conventional approximation. In accordance with this approximation the vertical component of the Coriolis force is considered negligible as compared to the force of gravity, while in the x -component of the Coriolis force it is the term proportional to the vertical flow velocity that is neglected:

$$2[\mathbf{v} \times \boldsymbol{\omega}] = 2 \begin{pmatrix} v|\omega| \sin \varphi - w|\omega| \cos \varphi \\ -u|\omega| \sin \varphi \\ u|\omega| \cos \varphi \end{pmatrix} \approx \begin{pmatrix} 2v|\omega| \sin \varphi \\ -2u|\omega| \sin \varphi \\ 0 \end{pmatrix} \equiv \begin{pmatrix} fv \\ -fu \\ 0 \end{pmatrix}, \quad (3.8)$$

where $f = 2|\omega| \sin \varphi$ is the Coriolis parameter, φ is the latitude.

Thus, upon discarding the vertical accelerations and the vertical component of the Coriolis force in the Euler equation, we arrive at the equation of hydrostatics,

$$\frac{\partial p}{\partial z} = -\rho g. \quad (3.9)$$

Integrating Eq. (3.9) over the vertical coordinate from a certain point z within the layer of water up to the free surface, we obtain the following for calculating the pressure:

$$p(x, y, z, t) = p_{atm} + \rho g(\xi(x, y, t) - z). \quad (3.10)$$

We shall now turn to the horizontal components of the Euler equation (3.1)

$$\frac{\partial u}{\partial t} + u \frac{\partial u}{\partial x} + v \frac{\partial u}{\partial y} = -\frac{1}{\rho} \frac{\partial p}{\partial x} + fv, \quad (3.11)$$

$$\frac{\partial v}{\partial t} + u \frac{\partial v}{\partial x} + v \frac{\partial v}{\partial y} = -\frac{1}{\rho} \frac{\partial p}{\partial y} - fu. \quad (3.12)$$

Substituting formula (3.10) into Eqs. (3.11) and (3.12), we obtain

$$\frac{\partial u}{\partial t} + u \frac{\partial u}{\partial x} + v \frac{\partial u}{\partial y} = -g \frac{\partial \xi}{\partial x} - \frac{1}{\rho} \frac{\partial p_{atm}}{\partial x} + fv, \quad (3.13)$$

$$\frac{\partial v}{\partial t} + u \frac{\partial v}{\partial x} + v \frac{\partial v}{\partial y} = -g \frac{\partial \xi}{\partial y} - \frac{1}{\rho} \frac{\partial p_{atm}}{\partial y} - fu. \quad (3.14)$$

From Eqs. (3.13) and (3.14) follows a most important feature of long waves: the horizontal velocity components are independent of the vertical coordinate. With

account of this property we integrate the continuity Eq. (3.6) over the vertical coordinate from the bottom, $z = -H + \eta$ up to the surface $z = \xi$. As a result, we obtain

$$\frac{\partial \xi}{\partial t} - \frac{\partial \eta}{\partial t} + \operatorname{div}((H + \xi - \eta)\mathbf{v}) = 0, \quad (3.15)$$

where the operator div operates in the horizontal plane, and the velocity vector has only two components: $\mathbf{v} \equiv (u, v)$.

Equations (3.13)–(3.15) represent a set of equations of the nonlinear long-wave (shallow-water) theory, which is often applied in tsunami wave simulation. The excitation of waves can be described by specifying the function $\eta(x, y, t)$ that describes displacement of the bottom surface. Another version of wave excitation consists in specifying the function $p_{\text{atm}}(x, y, t)$ that describes atmospheric pressure variations. However, Eqs. (3.13)–(3.15) are most often resolved under the assumption that $\eta = 0$, $p_{\text{atm}} = \text{const}$ with initial conditions representing a certain initial elevation of the free surface, $\xi_0(x, y)$, in the case of a zero velocity field $\mathbf{v}_0 = 0$.

If the deformation amplitude of the ocean bottom is small, ($|\eta|/H \ll 1$), then the free surface displacement can also be considered a small quantity: $|\xi|/H \ll 1$. The significance of the nonlinear term is estimated as follows: $|(\mathbf{v}, \nabla) \mathbf{v}| / |\partial \mathbf{v} / \partial t| \sim U_{xy}T/\lambda \sim U_zT/H \sim |\xi|/H \ll 1$. Neglecting small quantities in equations (3.13)–(3.15), we arrive at the linear equations of the long-wave theory,

$$\frac{\partial u}{\partial t} = -g \frac{\partial \xi}{\partial x} - \frac{1}{\rho} \frac{\partial p_{\text{atm}}}{\partial x} + fv, \quad (3.16)$$

$$\frac{\partial v}{\partial t} = -g \frac{\partial \xi}{\partial y} - \frac{1}{\rho} \frac{\partial p_{\text{atm}}}{\partial y} - fu. \quad (3.17)$$

$$\frac{\partial \xi}{\partial t} - \frac{\partial \eta}{\partial t} + \operatorname{div}(H\mathbf{v}) = 0. \quad (3.18)$$

The linear equations (3.16)–(3.18) can be successfully used for describing tsunami dynamics at large depths. These equations can also be applied in the case of shallow water, but only if the wave amplitudes are insignificant.

If the Coriolis force is neglected in the set of equations (3.16)–(3.18), then they can be reduced to a single equation, namely, to an inhomogeneous wave equation. Setting $f = 0$ in equations (3.16) and (3.17) we rewrite them in a vector form,

$$\frac{\partial \mathbf{v}}{\partial t} = -g \nabla \xi - \frac{\nabla p_{\text{atm}}}{\rho}, \quad (3.19)$$

where the operator ∇ operates in the horizontal plane. Owing to the only vortex-generating factor (the Coriolis force) in the case under consideration having been discarded it is possible, without loss of generality, to express the velocity field via the flow velocity potential,

$$\mathbf{v} \equiv (u, v) = \nabla F. \quad (3.20)$$

Substituting representation (3.20) into Eq. (3.19), we obtain

$$\xi = -\frac{1}{g} \frac{\partial F}{\partial t} - \frac{p_{atm}}{\rho g} \quad (3.21)$$

Substitution of expressions (3.20) and (3.21) into Eq. (3.18) gives the sought inhomogeneous wave equation

$$\frac{\partial^2 F}{\partial t^2} - \operatorname{div}(gH\nabla F) = -\frac{1}{\rho} \frac{\partial p_{atm}}{\partial t} - g \frac{\partial \eta}{\partial t}. \quad (3.22)$$

The form of wave equation (3.22) permits to conclude that long waves propagate with a velocity $c = \sqrt{gH}$ —the square of precisely this quantity is found at the proper place in the wave equation. The right-hand part of equation (3.22) describes two sorts of tsunami sources: bottom movements and atmospheric pressure variations. The source of waves is seen to differ from zero only when either bottom displacements take place or changes occur in the atmospheric pressure. The flow velocity field and the free surface displacement are calculated from the known potential making use of formulae (3.20) and (3.21), respectively.

In certain cases it is convenient to take advantage of the wave equation written, instead of the flow velocity potential, in terms of the free surface displacement. The equation in such a form can be obtained as follows. We differentiate equation (3.18) with respect to time, then substitute into it the acceleration $\partial \mathbf{v} / \partial t$, expressed by formula (3.19). As a result of elementary transformations, we obtain the following:

$$\frac{\partial^2 \xi}{\partial t^2} - \operatorname{div}(gH\nabla \xi) = \frac{\partial^2 \eta}{\partial t^2} + \operatorname{div}\left(\frac{H}{\rho} \nabla p_{atm}\right). \quad (3.23)$$

The boundary conditions along the coastline for equations of the linear long-wave theory usually represent the condition of total reflection (no-normal flow): $(\mathbf{v}, \mathbf{n}) = 0$, where \mathbf{n} is the normal to the coastline. In terms of the potential (free surface displacement) this condition has the form $\partial F / \partial \mathbf{n} = 0$ ($\partial \xi / \partial \mathbf{n} = 0$). Initial conditions must be imposed both on the function itself and on its time derivative at $t = 0$: $F = F_0$, $\partial F / \partial t = G_0$ ($\xi = \xi_0$, $\partial \xi / \partial t = q_0$). Actually, these conditions signify setting the initial free surface displacement and the initial flow velocity field.

3.1.3 The Potential Theory

In a number of cases tsunami waves may be insufficiently long to be fully consistent with the requirement that $H/\lambda \ll 1$. Here, assistance will be rendered by the potential theory, which imposes no restrictions on the wavelength. Figuratively speaking, the

potential theory occupies a higher position in the hierarchy of approximations than the long-wave theory. The effect exerted by the Coriolis force cannot be taken into account in potential theory, though.

In accordance with the Helmholtz theorem an arbitrary vector field is expressed via the scalar (F) and vector (\mathbf{G}) potentials: $\mathbf{v} = \nabla F + \nabla \times \mathbf{G}$. The potential theory is based on the assumption that the flow velocity field can be represented by a sole scalar quantity, namely, the flow velocity potential:

$$\mathbf{v} \equiv (u, v, w) = \nabla F. \quad (3.24)$$

Naturally, representation (3.24) not always holds valid, but only under the condition that the flow is vortex-free. In this connection, we shall further make use of equation (3.1) in the following form, without taking into account the vortex-generating factor—the Coriolis force:

$$\frac{\partial \mathbf{v}}{\partial t} + (\mathbf{v}, \nabla) \mathbf{v} = -\frac{\nabla p}{\rho} + \mathbf{g}. \quad (3.25)$$

Substituting representation (3.24) into the continuity equation (3.2), we arrive at the main equation of potential theory—the Laplace equation,

$$\Delta F = 0. \quad (3.26)$$

Let us now formulate boundary conditions for the Laplace equation. The boundary condition on the free surface $z = \xi$ is derived applying the dynamic equation (3.25) from which follows

$$\nabla \left(\frac{\partial F}{\partial t} + \frac{\mathbf{v}^2}{2} + \frac{p}{\rho} + gz \right) = 0. \quad (3.27)$$

The expression under the gradient symbol in formula (3.27) does, evidently, not depend on space coordinates, but it may depend on time,

$$\frac{\partial F}{\partial t} + \frac{\mathbf{v}^2}{2} + \frac{p}{\rho} + gz = f(t), \quad (3.28)$$

where $f(t)$ is an arbitrary function. In equation (3.28), called the unsteady Bernoulli equation, function $f(t)$ can, without loss of generality, be set equal to zero

$$\frac{\partial F}{\partial t} + \frac{\mathbf{v}^2}{2} + \frac{p}{\rho} + gz = 0. \quad (3.29)$$

Indeed, owing to the velocity field being determined by derivatives of the potential with respect to the space coordinates, the quantity F may be supplemented with any function of time, which will have no effect whatsoever on the velocity field.

The boundary condition on the free water surface (for $z = \xi$) with account of the pressure continuity condition (3.3) has the form:

$$\frac{\partial F}{\partial t} + \frac{(\nabla F)^2}{2} + \frac{p_{atm}}{\rho} + g\xi = 0. \quad (3.30)$$

Expression (3.30) must be supplemented with the kinematic condition (3.4), which in terms of the potential is written as follows:

$$\frac{\partial \xi}{\partial t} + \frac{\partial F}{\partial x} \frac{\partial \xi}{\partial x} + \frac{\partial F}{\partial y} \frac{\partial \xi}{\partial y} - \frac{\partial F}{\partial z} = 0. \quad (3.31)$$

We shall also write the no-normal flow boundary condition (3.5), that is in force on an impermeable mobile oceanic bottom, in terms of the potential:

$$\frac{\partial F}{\partial \mathbf{n}} = (\mathbf{v}_b, \mathbf{n}) \quad \text{for } z = -H(x, y) + \eta(x, y, t). \quad (3.32)$$

As to the initial conditions, at $t = 0$ we can set the initial perturbation of the free surface, that is defined by an arbitrary function $\xi_0(x, y)$. Moreover, we can specify a certain velocity potential that naturally satisfies the Laplace equation and the boundary conditions, thus determining the initial velocity field $\mathbf{v}_0(x, y, z)$.

The problem (3.26), (3.30)–(3.32) is essentially simplified if the bottom deformations, as well as the free surface displacements caused by them, and the flow velocities are assumed to be small quantities. In this case, by discarding nonlinear terms in formulae (3.30) and (3.31) we obtain

$$\frac{\partial F}{\partial t} + \frac{p_{atm}}{\rho} + g\xi = 0, \quad (3.33)$$

$$\frac{\partial \xi}{\partial t} - \frac{\partial F}{\partial z} = 0. \quad (3.34)$$

We further assume the atmospheric pressure to be constant along the free surface ($p_{atm} = const$). Then, the potential is opportunely redefined (by subtraction of the quantity $p_{atm}t/\rho$) and expression (3.33) is transformed into

$$\xi = -\frac{1}{g} \frac{\partial F}{\partial t}. \quad (3.35)$$

Substituting formula (3.35) into Eq. (3.34) we obtain a linearized boundary condition on the free surface,

$$\frac{\partial^2 F}{\partial t^2} + g \frac{\partial F}{\partial z} = 0 \quad \text{for } z = 0. \quad (3.36)$$

We note that, owing to the free surface displacement being small, the boundary condition (3.36) may be adopted not for an unknown surface $z = \xi$, but for the fixed surface $z = 0$, that is close to it.

The boundary condition on the bottom (3.32)—also owing to bottom displacements being small—become related to the unperturbed bottom surface,

$$\frac{\partial F}{\partial \mathbf{n}} = (\mathbf{v}_b, \mathbf{n}) \quad \text{for } z = -H(x, y). \quad (3.37)$$

Here, the ocean depth as well as the field of normals to the bottom surface are assumed not to undergo changes during the process of small bottom deformations.

The Laplace equation (3.26) with boundary conditions (3.36) and (3.37), supplemented with the initial conditions described above, represents a Cauchy–Poisson problem formulated within the framework of the linear potential theory of waves. A large part of this chapter is devoted to an analysis of precisely this problem.

3.2 General Solution of the Problem of Excitation of Gravitational Waves in a Layer of Incompressible Liquid by Deformations of the Basin Bottom

3.2.1 Cartesian Coordinates

The goal of this section is the construction of a mathematical model describing the motion of a layer of homogeneous incompressible liquid in the case of deformation of the basin bottom, proceeding in accordance with a certain given space–time law. The liquid is limited from above by its free surface and is in a gravitational field, characterized by the acceleration of gravity, g . We shall only deal with the case of a basin of constant depth H —such an approach will permit to obtain an analytical solution of the problem. We shall consider the amplitude of motions of the basin bottom, η_0 , a small quantity as compared to the depth, $\eta_0 \ll H$. In practice, this condition is actually always satisfied (the average depth of the ocean is $H \sim 4000$ m, while $\eta_0 < \sim 10$ m even in the case of catastrophic earthquakes). The amplitude of gravitational surface waves, A , excited by one or another motion of the basin bottom with the amplitude η_0 , will clearly be of the same order of magnitude: $A \sim \eta_0$. The amplitude of the wave being small in comparison with its length $A \ll \lambda$ makes it possible to apply linear theory. The motion of the liquid will be considered potential.

Consider a layer, infinite in the Oxy plane, of an ideal incompressible homogeneous liquid of constant depth H in the field of gravity. We shall put the origin of the Cartesian reference frame, $Oxyz$, in the unperturbed free surface and direct the Oz -axis vertically upward. The liquid is at rest until the time moment $t = 0$. To find the wave perturbation $\xi(x, y, t)$, formed on the surface of the liquid, and the velocity

field, $\mathbf{v}(x, y, z, t)$, throughout the thickness of the layer in the case of motions of the basin floor, occurring in accordance with the law $\eta(x, y, t)$, we shall resolve the problem with respect to the velocity potential $F(x, y, z, t)$ (see Sect. 3.1.3 or Landau and Lifshits 1987),

$$\frac{\partial^2 F}{\partial x^2} + \frac{\partial^2 F}{\partial y^2} + \frac{\partial^2 F}{\partial z^2} = 0, \quad (3.38)$$

$$g \frac{\partial F}{\partial z} = - \frac{\partial^2 F}{\partial t^2}, \quad z = 0, \quad (3.39)$$

$$\frac{\partial F}{\partial z} = \frac{\partial \eta}{\partial t}, \quad z = -H. \quad (3.40)$$

The physical meaning of the boundary condition (3.39) consists in the pressure on the free surface of the liquid being constant. The boundary condition (3.40) signifies equality of the vertical component of the flow velocity to the velocity of motion of the basin floor. Displacement of the free surface and the flow velocity vector are related to the potential of the flow velocity by the following known formulae:

$$\xi(x, y, t) = - \frac{1}{g} \frac{\partial F}{\partial t} \Big|_{z=0}, \quad (3.41)$$

$$\mathbf{v}(x, y, z, t) \equiv \{u(x, y, z, t), v(x, y, z, t), w(x, y, z, t)\} = \nabla F(x, y, z, t). \quad (3.42)$$

The Laplace equation (3.38) is resolved by the standard method of separation of variables. We shall omit elementary calculations and write out the general solution of the problem in the form of Laplace and Fourier expansions over the time and space coordinates:

$$F(x, y, z, t) = \int_{s-i\infty}^{s+i\infty} dp \int_{-\infty}^{+\infty} dm \int_{-\infty}^{+\infty} dn \exp\{pt - imx - iny\} \\ \times (A(p, m, n) \cosh(kz) + B(p, m, n) \sinh(kz)), \quad (3.43)$$

where $k^2 = m^2 + n^2$.

Substitution of the general solution (3.43) into the boundary condition on the surface, (3.39), yields the relationship between the coefficients,

$$B(p, m, n) = -A(p, m, n) \frac{p^2}{gk}. \quad (3.44)$$

Applying the formulae for the direct and inverse Laplace and Fourier transformations, we obtain the integral representation for the laws, satisfied by motion of the basin floor,

$$\eta(x, y, t) = \frac{1}{8\pi^3 i} \int_{s-i\infty}^{s+i\infty} dp \int_{-\infty}^{+\infty} dm \int_{-\infty}^{+\infty} dn \exp\{pt - imx - iny\} H(p, m, n), \quad (3.45)$$

where

$$H(p, m, n) = \int_0^{\infty} dt \int_{-\infty}^{+\infty} dx \int_{-\infty}^{+\infty} dy \exp\{-pt + imx + iny\} \eta(x, y, t). \quad (3.46)$$

Substituting expression (3.43), written with the aid of formula (3.44), into the boundary condition on the basin floor, (3.40), one can calculate the coefficient $A(p, m, n)$. As a result, one obtains the following expression for the potential of the flow velocity, which corresponds to motions of the basin floor, satisfying the law $\eta(x, y, t)$.

$$F(x, y, z, t) = -\frac{1}{8\pi^3 i} \int_{s-i\infty}^{s+i\infty} dp \int_{-\infty}^{+\infty} dm \int_{-\infty}^{+\infty} dn \times \frac{p \exp\{pt - imx - iny\} \cosh(kz) (gk - p^2 \tanh(kz))}{k \cosh(kH) (gk \tanh(kH) + p^2)} H(p, m, n). \quad (3.47)$$

Applying formulae (3.41) and (3.42), we obtain expressions describing the behavior of the free surface,

$$\xi(x, y, t) = \frac{1}{8\pi^3 i} \int_{s-i\infty}^{s+i\infty} dp \int_{-\infty}^{+\infty} dm \int_{-\infty}^{+\infty} dn \frac{p^2 \exp\{pt - imx - iny\}}{\cosh(kH) (gk \tanh(kH) + p^2)} H(p, m, n), \quad (3.48)$$

horizontal, $u(x, y, z, t)$, $v(x, y, z, t)$, and vertical, $w(x, y, z, t)$, components of the flow velocity,

$$u(x, y, z, t) = \frac{\partial F}{\partial x} = \frac{1}{8\pi^3} \int_{s-i\infty}^{s+i\infty} dp \int_{-\infty}^{+\infty} dm \int_{-\infty}^{+\infty} dn \times \frac{mp \exp\{pt - imx - iny\} \cosh(kz) (gk - p^2 \tanh(kz))}{k \cosh(kH) (gk \tanh(kH) + p^2)} \times H(p, m, n); \quad (3.49)$$

$$\begin{aligned}
v(x, y, z, t) &= \frac{\partial F}{\partial y} = \frac{1}{8\pi^3} \int_{s-i\infty}^{s+i\infty} dp \int_{-\infty}^{+\infty} dm \int_{-\infty}^{+\infty} dn \\
&\times \frac{np \exp\{pt - imx - iny\} \cosh(kz) (gk - p^2 \tanh(kz))}{k \cosh(kH) (gk \tanh(kH) + p^2)} \\
&\times H(p, m, n)
\end{aligned} \tag{3.50}$$

$$\begin{aligned}
w(x, y, z, t) &= \frac{\partial F}{\partial z} = -\frac{1}{8\pi^3 i} \int_{s-i\infty}^{s+i\infty} dp \int_{-\infty}^{+\infty} dm \int_{-\infty}^{+\infty} dn \\
&\times \frac{p \exp\{pt - imx - iny\} \cosh(kz) (gk \tanh(kz) - p^2)}{\cosh(kH) (gk \tanh(kH) + p^2)} H(p, m, n).
\end{aligned} \tag{3.51}$$

In principle, expressions (3.48)–(3.51) provide an exhaustive solution of problem (3.38)–(3.40), but obtaining concrete results requires the calculation of sixfold integrals, which represents quite a realistic, but extremely labor-consuming (from the point of view of the volume of calculations) and irrational task. To be able to perform part of the calculations analytically it is necessary to set the concrete form of function $\eta(x, y, t)$.

3.2.2 Cylindrical Coordinates

In a number of cases, when the model displacement of the basin floor exhibits appropriate symmetry, it may turn out to be convenient to apply a cylindrical reference system, which we shall introduce in a standard manner with respect to the Cartesian system, described in the preceding section. In this case the Laplace equation (3.38) assumes the following form:

$$\frac{1}{r} \frac{\partial}{\partial r} \left(r \frac{\partial F}{\partial r} \right) + \frac{1}{r^2} \frac{\partial^2 F}{\partial \varphi^2} + \frac{\partial^2 F}{\partial z^2} = 0, \tag{3.52}$$

while the boundary conditions (3.39), (3.40) remain intact.

For resolving equation (3.52) we apply the traditional method of variable separation, i.e., we shall assume that

$$F(r, \varphi, z) = R(r) \Phi(\varphi) Z(z). \tag{3.53}$$

Substitution of expression (3.53) into equation (3.52) results in the following set of ordinary differential equations:

$$r^2 \frac{\partial^2 R}{\partial r^2} + r \frac{\partial R}{\partial r} + (r^2 - n^2) R = 0, \quad (3.54)$$

$$\frac{\partial^2 \Phi}{\partial \varphi^2} + n^2 \Phi = 0, \quad (3.55)$$

$$\frac{\partial^2 Z}{\partial z^2} - k^2 Z = 0. \quad (3.56)$$

The Bessel equation (3.54) is written with account of the substitution of variable $r^* = rk$ (the asterisk “*” is dropped). The solutions of equations (3.54)–(3.56) are well known and can be written as follows:

$$\begin{aligned} R(rk) &= C_1 J_n(kr) + C_2 Y_n(kr), \\ \Phi(\varphi) &= C_3 \cos(n\varphi) + C_4 \sin(n\varphi), \\ Z(z) &= C_5 \cosh(kz) + C_6 \sinh(kz), \end{aligned}$$

where J_n and Y_n are Bessel functions of the first and second kinds and of the n th order, C_i are arbitrary constants.

Functions $\Phi(\varphi)$ must satisfy the periodicity condition,

$$\Phi(\varphi) = \Phi(\varphi + 2\pi),$$

from which it follows that parameter n is an integer, $n = 0, \pm 1, \pm 2, \dots$. The condition, that function $R(rk)$ be limited at $r = 0$, requires the coefficient of the Bessel function of the second kind to be equal to zero: $C_2 = 0$.

Thus, it is expedient to seek for the general solution of the problem in the form of a Fourier expansion and of Laplace and Fourier–Bessel transformations (Nikiforov and Uvarov 1984),

$$\begin{aligned} F(r, \varphi, z, t) &= \int_0^\infty dk \int_{s-i\infty}^{s+i\infty} dp \\ &\times \exp\{pt\} J_0(kr) \frac{C_5^0}{2} \left(C_5^0(p, k) \cosh(kz) + C_6^0(p, k) \sinh(kz) \right) \\ &+ \int_0^\infty dk \int_{s-i\infty}^{s+i\infty} dp \exp\{pt\} \sum_{n=1}^\infty J_n(kr) (C_3^n \cos(n\varphi) + C_4^n \sin(n\varphi)) \\ &\times (C_5^n(p, k) \cosh(kz) + C_6^n(p, k) \sinh(kz)). \end{aligned} \quad (3.57)$$

Substitution of equation (3.57) into the boundary condition on the surface, (3.39), yields the relationship between the coefficients,

$$C_6^n(p, k) = -C_5^n(p, k) \frac{p^2}{gk}. \quad (3.58)$$

We shall now write the integral representation for the function describing the space-time law of motion of the basin floor, $\eta(r, \varphi, t) = \eta^r(r) \eta^\varphi(\varphi) \eta^t(t)$

$$\begin{aligned} \eta(r, \varphi, t) = & \int_0^\infty dk \int_{s-i\infty}^{s+i\infty} dp \exp\{pt\} J_0(kr) k \frac{A_0}{2} H^0(p, k) + \int_0^\infty dk \int_{s-i\infty}^{s+i\infty} dp \\ & \times \exp\{pt\} \sum_{n=1}^\infty J_n(kr) k (A_n \cos(n\varphi) + B_n \sin(n\varphi)) H^n(p, k), \quad (3.59) \end{aligned}$$

where

$$\begin{aligned} A_n &= \frac{1}{\pi} \int_{-\pi}^{\pi} \eta^\varphi(\varphi) \cos(n\varphi) d\varphi, \\ B_n &= \frac{1}{\pi} \int_{-\pi}^{\pi} \eta^\varphi(\varphi) \sin(n\varphi) d\varphi, \\ H^n(p, k) &= \frac{1}{2\pi i} \int_0^\infty dt \int_0^\infty dr \eta^r(r) \eta^t(t) \exp\{-pt\} r J_n(kr). \end{aligned}$$

Substitution of formulae (3.57) and (3.59) into the boundary condition on the basin floor, (3.40), reveals that equality of the left-hand and right-hand parts is possible, only when the following three conditions are fulfilled:

$$\begin{aligned} C_3^n &= A^n, \quad C_4^n = B^n, \\ C_5^n(p, k) &= -\frac{pH^n(p, k)}{k \left(\sinh(kH) + \frac{p^2}{gk} \cosh(kH) \right)}. \end{aligned}$$

It is now possible to write out the resultant expression for the potential, which is the solution of equation (3.52) with the boundary conditions (3.39) and (3.40)

$$\begin{aligned}
F(r, \varphi, z, t) = & - \int_0^{\infty} dk \int_{s-i\infty}^{s+i\infty} dp \exp\{pt\} \frac{p \left(\cosh(kz) - \frac{p^2}{gk} \sinh(kz) \right)}{\left(\sinh(kH) + \frac{p^2}{gk} \cosh(kH) \right)} \\
& \times \left(J_0(kr) \frac{A_0}{2} H^0(p, k) + \sum_{n=1}^{\infty} J_n(kr) \left(A_n \cos(n\varphi) \right. \right. \\
& \left. \left. + B_n \sin(n\varphi) \right) H^n(p, k) \right). \tag{3.60}
\end{aligned}$$

Making use of expression (3.60), it is not difficult to obtain formulae for calculation of the displacement of the surface and of the velocity components $v_r = \frac{\partial F}{\partial r}$, $v_\varphi = \frac{1}{r} \frac{\partial F}{\partial \varphi}$, $v_z = \frac{\partial F}{\partial z}$, the explicit expressions for which will not be written out here, because they are too cumbersome.

Below we shall turn to the case, when the source of waves exhibits axial symmetry. The solution of the problem, here, will be of the following form:

$$\begin{aligned}
F(r, z, t) = & - \int_0^{\infty} dk \int_{s-i\infty}^{s+i\infty} dp \exp\{pt\} J_0(kr) \frac{p \left(\cosh(kz) - \frac{p^2}{gk} \sinh(kz) \right)}{\left(\sinh(kH) + \frac{p^2}{gk} \cosh(kH) \right)} X(p, k), \tag{3.61}
\end{aligned}$$

where

$$X(p, k) = \frac{1}{2\pi i} \int_0^{\infty} dt \int_0^{\infty} dr \exp\{-pt\} J_0(kr) r \eta(r, t).$$

3.3 Plane Problems of Tsunami Excitation by Deformations of the Basin Bottom

In this section two-dimensional models (in the vertical plane) are dealt with. Solution of the plane problem permits to demonstrate clearly many important peculiarities of the physical processes taking place during tsunami generation. A significant part of the results, obtained within the framework of the two-dimensional model, remains valid in the three-dimensional case, also. The 2D \Rightarrow 3D transition for problems of the type considered actually permits to investigate only two new points: the direction of wave radiation and changes in their characteristics, as the distance from the source increases.

3.3.1 Construction of the General Solution

We shall consider (Fig. 3.2) a layer of ideal incompressible homogeneous liquid, infinite along the $0x$ -axis, of constant depth H , and in the field of gravity. We shall put the origin of the Cartesian reference system, $0xz$, on the unperturbed free surface, the $0z$ will be directed vertically upward. To find the perturbation of the free surface, $\xi(x, t)$, and the field of flow velocities $\mathbf{v}(x, z, t)$, arising in the layer of liquid, when the basin floor undergoes motion in accordance with the law $\eta(x, t)$, we shall resolve the problem with respect to the potential of the flow velocity, $F(x, z, t)$:

$$\frac{\partial^2 F}{\partial x^2} + \frac{\partial^2 F}{\partial z^2} = 0, \tag{3.62}$$

$$g \frac{\partial F}{\partial z} = - \frac{\partial^2 F}{\partial t^2}, \quad z = 0, \tag{3.63}$$

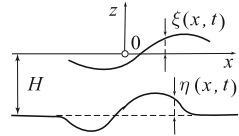
$$\frac{\partial F}{\partial z} = \frac{\partial \eta}{\partial t}, \quad z = -H. \tag{3.64}$$

Without dwelling on the details of resolving the problem (3.62)–(3.64), which were exposed above for the three-dimensional case, we shall present the resultant formulae.

$$F(x, z, t) = -\frac{1}{4\pi^2 i} \int_{s-i\infty}^{s+i\infty} dp \int_{-\infty}^{+\infty} dk \times \frac{p \exp\{pt - ikx\} \cosh(kz) (gk - p^2 \tanh(kz))}{k \cosh(kH) (gk \tanh(kH) + p^2)} H(p, k), \tag{3.65}$$

$$\xi(x, t) = \frac{1}{4\pi^2 i} \int_{s-i\infty}^{s+i\infty} dp \int_{-\infty}^{+\infty} dk \frac{p^2 \exp\{pt - ikx\}}{\cosh(kH) (gk \tanh(kH) + p^2)} H(p, k), \tag{3.66}$$

Fig. 3.2 Mathematical formulation of the 2D problem



$$u(x, z, t) = \frac{\partial F}{\partial x} = \frac{1}{4\pi^2} \int_{s-i\infty}^{s+i\infty} dp \int_{-\infty}^{+\infty} dk \times \frac{p \exp\{pt - ikx\} \cosh(kz) (gk - p^2 \tanh(kz))}{\cosh(kH) (gk \tanh(kH) + p^2)} H(p, k), \quad (3.67)$$

$$w(x, z, t) = \frac{\partial F}{\partial z} = -\frac{1}{4\pi^2 i} \int_{s-i\infty}^{s+i\infty} dp \int_{-\infty}^{+\infty} dk \times \frac{p \exp\{pt - ikx\} \cosh(kz) (gk \tanh(kz) - p^2)}{\cosh(kH) (gk \tanh(kH) + p^2)} H(p, k), \quad (3.68)$$

where

$$H(p, k) = \int_0^{\infty} dt \int_{-\infty}^{+\infty} dx \exp\{-pt + ikx\} \eta(x, t).$$

In the case of arbitrary motion of the basin floor the solution of the problem involves a cumbersome procedure—the calculation of a fourfold integral. Therefore, for physical interpretation of the obtained integral representations it is expedient to select several concrete versions of function $\eta(x, t)$. This will permit to calculate a large part of the integrals analytically.

Consider the following three types of deformation of the basin floor:

1. A linear (in time) displacement

$$\eta_L(x, t) = \eta_0 (\theta(x+a) - \theta(x-a)) \theta(t) t \tau^{-1}, \quad (3.69)$$

2. Running displacement

$$\eta_R(x, t) = \eta_0 (\theta(x) - \theta(x-b)) (1 - \theta(x-vt)), \quad (3.70)$$

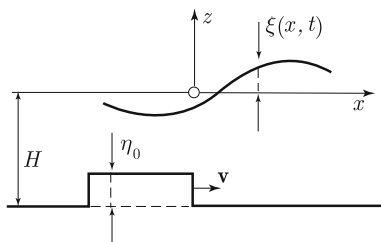
3. Harmonic oscillations of the basin floor

$$\eta_{osc}(x, t) = \eta_0 (\theta(x+a) - \theta(x-a)) \sin(\omega t). \quad (3.71)$$

where η_0 is the amplitude of the basin floor displacement, θ is the Heaviside function, $2a$ and b are the horizontal dimensions of the source. In all cases we consider the rectangular distribution of deformations of the basin floor. The scheme of motions of the basin floor in the case of a running displacement is shown in Fig. 3.3.

For the tsunami problem the linear displacement itself has no physical significance—it is useful only as a mathematical model. But from the function $\eta_L(x, t)$ it is possible to “construct” the two principal model laws of deformation

Fig. 3.3 Model of running displacement of basin floor



of the basin floor at the tsunami source: a motion of the basin floor involving residual displacement,

$$\eta_1(x, t) = \eta_L(x, t) - \eta_L(x, t - \tau) \tag{3.72}$$

and a motion of the basin floor without residual displacement,

$$\eta_2(x, t) = 2\eta_L(x, t) - 4\eta_L(x, t - 0.5\tau) + 2\eta_L(x, t - \tau). \tag{3.73}$$

Complying with the terminology proposed in (Dotsenko and Soloviev 1990a, b), we call the two indicated types of motion “piston” and “membrane” displacements.

The problem considered is linear, therefore, the solutions for the piston and membrane displacements can be expressed through the solution for the linear displacement, making use of the superposition principle:

$$F_1(x, z, t) = F_L(x, z, t) \theta(t) - F_L(x, z, t - \tau) \theta(t - \tau), \tag{3.74}$$

$$F_2(x, z, t) = 2F_L(x, z, t) \theta(t) - 4F_L(x, z, t - 0.5\tau) \theta(t - 0.5\tau) + 2F_L(x, z, t - \tau) \theta(t - \tau), \tag{3.75}$$

where $F_L(x, z, t)$ is the solution of the problem (3.62)–(3.64) in the case of $\eta(x, t) = \eta_L(x, t)$. The perturbation of the free surface and of the velocity component corresponding to the piston or membrane displacements, is obviously, calculated by formulae, similar to (3.74) and (3.75). Only a formal substitution of F_L for ξ_L, u_L or w_L is required.

Calculation of the intermediate integrals, performed applying residue theory, results in the following expressions for the linear displacement:

$$F_L(x, z, t) = -\frac{1}{2\pi\tau} \int_{-\infty}^{+\infty} dk \times \frac{\exp\{-ikx\} \cosh(kz) (1 - (1 + \tanh(kH) \tanh(kz)) \cos(t p_0))}{k \sinh(kH)} X(k). \tag{3.76}$$

$$\xi_L(x, t) = \frac{1}{2\pi\tau} \int_{-\infty}^{+\infty} dk \frac{\exp(-ikx) \sin(tp_0)}{p_0 \cosh(kH)} X(k), \quad (3.77)$$

$$u_L(x, z, t) = \frac{i}{2\pi\tau} \int_{-\infty}^{+\infty} dk \times \frac{\exp\{-ikx\} (\cosh(kz) - [\cosh(kz) + \tanh(kH) \sinh(kz)] \cos(tp_0))}{\sinh(kH)} X(k), \quad (3.78)$$

$$w_L(x, z, t) = -\frac{1}{2\pi\tau} \int_{-\infty}^{+\infty} dk \times \frac{\exp\{-ikx\} (\sinh(kz) - [\sinh(kz) + \tanh(kH) \cosh(kz)] \cos(tp_0))}{\sinh(kH)} X(k), \quad (3.79)$$

where $p_0 = (gk \tanh(kH))^{1/2}$, $X(k) = \eta_0 2 \sin(ka)/k$.

In the case of a running displacement of the basin floor the solution is given by the following formulae:

$$F_R(x, z, t) = -\frac{\eta_0}{4\pi} \int_{-\infty}^{+\infty} dk \frac{\exp\{-ikx\}}{k \cosh(kH)} \times \frac{(gk \cosh(kz) + p_0^2 \sinh(kz))}{p_0} \times \left(\exp\{-ip_0 t\} \frac{\exp\left\{ib\left(k + \frac{p_0}{v}\right)\right\} - 1}{k + \frac{p_0}{v}} - \exp\{ip_0 t\} \frac{\exp\left\{ib\left(k - \frac{p_0}{v}\right)\right\} - 1}{k - \frac{p_0}{v}} \right), \quad (3.80)$$

$$\xi_R(x, t) = \frac{\eta_0}{4\pi i} \int_{-\infty}^{+\infty} dk \frac{\exp\{-ikx\}}{\cosh(kH)} \times \left(\exp\{-ip_0 t\} \frac{\exp\left\{ib\left(k + \frac{p_0}{v}\right)\right\} - 1}{k + \frac{p_0}{v}} + \exp\{ip_0 t\} \frac{\exp\left\{ib\left(k - \frac{p_0}{v}\right)\right\} - 1}{k - \frac{p_0}{v}} \right), \quad (3.81)$$

$$\begin{aligned}
u_R(x, z, t) = & \frac{\eta_0 i}{4\pi} \int_{-\infty}^{+\infty} dk \frac{\exp\{-ikx\}}{\cosh(kH)} \times \frac{(gk \cosh(kz) + p_0^2 \sinh(kz))}{p_0} \\
& \times \left(\exp\{-ip_0 t\} \frac{\exp\left\{ib\left(k + \frac{p_0}{v}\right)\right\} - 1}{k + \frac{p_0}{v}} \right. \\
& \left. - \exp\{ip_0 t\} \frac{\exp\left\{ib\left(k - \frac{p_0}{v}\right)\right\} - 1}{k - \frac{p_0}{v}} \right), \quad (3.82)
\end{aligned}$$

$$\begin{aligned}
w_R(x, z, t) = & -\frac{\eta_0}{4\pi} \int_{-\infty}^{+\infty} dk \frac{\exp\{-ikx\}}{\cosh(kH)} \times \frac{(gk \sinh(kz) + p_0^2 \cosh(kz))}{p_0} \\
& \times \left(\exp\{-ip_0 t\} \frac{\exp\left\{ib\left(k + \frac{p_0}{v}\right)\right\} - 1}{k + \frac{p_0}{v}} \right. \\
& \left. - \exp\{ip_0 t\} \frac{\exp\left\{ib\left(k - \frac{p_0}{v}\right)\right\} - 1}{k - \frac{p_0}{v}} \right). \quad (3.83)
\end{aligned}$$

We stress that expressions (3.80)–(3.83) are valid only, if the condition $t \geq b/v$ is fulfilled. At any rate, this fact gives rise to no essential complications in calculations for time periods inferior to b/v , since, from a physical point of view, the solution of the problem involving a running displacement at $t = t_0 < b/v$ is equivalent to the solution of a similar problem for $b = vt_0$.

3.3.2 Piston and Membrane Displacements

As it was already shown above, tsunami waves are generated by motions of the ocean bottom occurring along the normal to its surface (normal displacements). Motions of the ocean bottom in its own plane (tangential displacements) are not effective, from the standpoint of tsunami generation. The term “vertical displacement” is often encountered in the literature. In the case of small slope angles of the ocean bottom the difference between vertical and normal displacements is, naturally, insignificant.

The goal of this section consists in the revelation of relationships between the main parameters of a tsunami wave and the characteristics of the source generating it—the deformation area of the ocean bottom. The wave parameters of interest to us comprise its amplitude, its length, and the energy of the wave perturbation. The source is characterized by the amplitude and duration of the ocean bottom deformation, as well as its horizontal extension.

The mechanisms of wave generation by ocean bottom displacements, both of impulse and finite duration, have been investigated analytically (Kajiura 1970; Murty 1977; Dotsenko and Soloviev 1990a, b; Dotsenko et al. 1993; Dotsenko and Soloviev 1995), and numerically (Marchuk et al. 1983). There also exists a small number of publications devoted to laboratory simulation of the generation process (Takahasi 1934, 1963; Hammack 1973; Nosov and Shelkovnikov 1997). A review of experimental works can be found in (Levin 1978).

We shall first deal with elementary results that can be obtained within the framework of linear theory of long waves. The one-dimensional wave equation, describing displacements of the free surface, ξ , in the case of deformations η of the ocean bottom, exhibits the following form:

$$\frac{\partial^2 \xi}{\partial t^2} - gH \frac{\partial^2 \xi}{\partial x^2} = \frac{\partial^2 \eta}{\partial t^2}. \quad (3.84)$$

Let deformations of the ocean bottom be given by the formula

$$\eta(x, t) = (\theta(x + a) - \theta(x - a)) \eta(t), \quad (3.85)$$

where $\eta(t)$ represents an arbitrary law of motion of the ocean bottom. Note that the piston and membrane displacements, (3.72) and (3.73), respectively, are special cases of formula (3.85). Deformations of the ocean bottom of the form (3.85) result in the formation of two identical waves, traveling in opposite directions. In the one-dimensional case a long linear wave does not undergo transformation during propagation, so it suffices to know its characteristics at any single point, for instance, close to the right boundary of the generation area ($x = a + \varepsilon$, $\varepsilon > 0$, $\varepsilon \ll a$). The solution of equation (3.84) is readily found analytically. Thus, for example, at $x = a + \varepsilon$ the wave perturbation is described by the following simple formula:

$$\xi(t) = \frac{1}{2}(\eta(t) - \eta(t - 2a(gH)^{-1/2})). \quad (3.86)$$

In Fig. 3.4 examples are presented of the shapes of wave perturbations formed by piston and membrane displacements (solid lines). Calculations are performed in accordance with formula (3.86). A piston-like displacement always forms a sole wave of trapezoidal shape, the polarity of which coincides with the polarity of the seabed displacement. In the case of a membrane-like displacement a bipolar wave arises that comprises a crest and a trough. We shall present the formulae relating the main parameters of waves and the characteristics of a displacement,

- wave amplitude in the case of piston-like displacement

$$A_{\max}^1 = \eta_0 \begin{cases} 1/2, & \tau^* \leq 2, \\ 1/\tau^*, & \tau^* > 2, \end{cases} \quad (3.87)$$

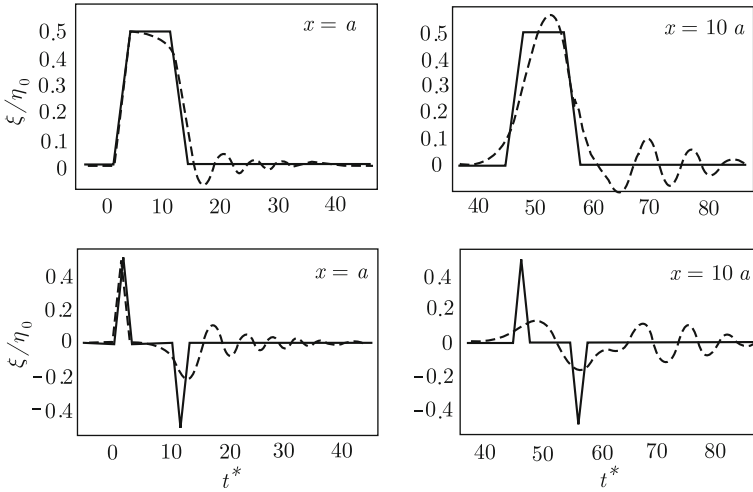


Fig. 3.4 Waves formed by piston (*upper row*) and membrane (*lower row*) displacements of duration $\tau^* = 3$ close to the *right* boundary of the generation area ($x = a$) and at a significant distance from it ($x = 10a$). The horizontal extension of the source $2a = 10$. The *solid line* represents the linear theory of long waves, the *dotted* one the linear potential theory

- crest and trough amplitude in the case of membrane-like displacement

$$A_{\max}^2 = A_{\min}^2 = \eta_0 \begin{cases} 1/2, & \tau^* \leq 4, \\ 2/\tau^*, & \tau^* > 4, \end{cases} \quad (3.88)$$

- wave energy in the case of piston-like displacement

$$W_1 = 2ag\rho\eta_0^2 \begin{cases} \frac{1}{2} - \frac{\tau^*}{12}, & \tau^* \leq 2, \\ \frac{1}{\tau^*} - \frac{2}{3} \left(\frac{1}{\tau^*}\right)^2, & \tau^* > 2, \end{cases} \quad (3.89)$$

- wave energy in the case of membrane-like displacement

$$W_2 = 2ag\rho\eta_0^2 \begin{cases} \frac{\tau^*}{6}, & \tau^* \leq 2, \\ \frac{\tau^*}{6} - \frac{2}{3} \left(\left(\frac{\tau^*}{2}\right)^{1/3} - \left(\frac{\tau^*}{2}\right)^{-2/3} \right)^3, & 2 < \tau^* \leq 4, \\ \left(\frac{4}{\tau^*}\right) \left(1 - \frac{2}{\tau^*}\right), & \tau^* > 4. \end{cases} \quad (3.90)$$

- period of wave perturbation for piston-like and membrane-like displacements

$$T_1 = T_2 = \frac{a(2 + \tau^*)}{(gH)^{1/2}}, \quad (3.91)$$

- wavelength of perturbation for piston-like and membrane-like displacements

$$\lambda_1 = \lambda_2 = a(2 + \tau^*). \quad (3.92)$$

The formulae presented contain the dimensionless displacement duration $\tau^* = \frac{\tau}{a}(gH)^{1/2}$. Below, we shall make use of dimensionless time, determined by a similar formula, $t^* = \frac{t}{a}(gH)^{1/2}$. The energy of the wave (per unit “channel” width) was calculated by the Kajiura formula (Kajiura 1970),

$$W = \rho g (gH)^{1/2} \int_0^T \xi^2 dt, \quad (3.93)$$

where T is the duration of the wave perturbation. From formulae (3.89), (3.90) it is seen that the wave energy is conveniently normalized to the quantity $W_0 = 2a g \rho \eta_0^2$, representing the potential energy of a free surface rectangular elevation of length $2a$ and height η_0 . Precisely, such an elevation should arise on the water surface in the case of an impulse piston-like displacement of the seabed (if the process is described within the framework of the linear theory of long waves).

Owing to the problem considered being linear, the tsunami wave amplitude is proportional to the seabed (ocean bottom) deformation amplitude. In the case of short motions the amplitude is independent of the duration of the displacement or the horizontal size of the source and amounts to half the amplitude of the seabed deformation. When the displacements are longer in time ($\tau^* \gg 1$), the amplitude drops monotonously according to the law $(\tau^*)^{-1}$. The dependencies (3.87) and (3.88) are shown in Figs. 3.5 and 3.6, respectively, by broken lines.

From formulae (3.89) and (3.90) it follows that the energy of a tsunami wave is proportional to the square amplitude of the seabed deformation η_0 and to the horizontal dimension of the source a . The respective dependences are shown in Fig. 3.7 (curve 3). In the case of a piston-like displacement the wave energy decreases monotonously as the duration of the seabed deformation increases. In the case of a membrane-like displacement the corresponding dependence is not monotonous: as the duration of the displacement increases, the energy starts to increase and then drops. The maximum corresponds to $\tau^* = 4$.

As to the wave periods and lengths, these quantities increase monotonously with the displacement duration, in accordance with formulae (3.91) and (3.92). Actually, $\tau^* \ll 1$, therefore both the period and length of a tsunami wave mostly depend on the horizontal dimension of the area of seabed deformation.

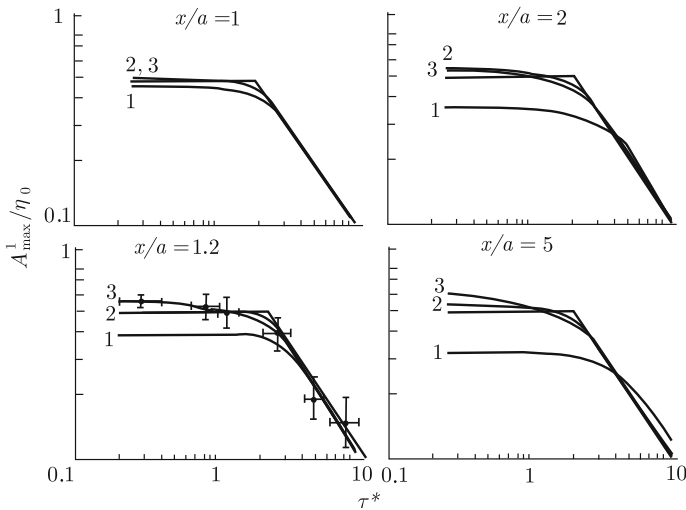


Fig. 3.5 Maximum amplitude of wave, excited by piston-like displacement of seabed, versus displacement duration for various distances from the generation area. Curves 1–3 correspond to values of parameter $a/H = 1, 3, 9$. The broken line represents linear theory of long waves

The results expounded above follow from the linear theory of long waves, which actually describes the process of wave generation and propagation not quite adequately. Figure 3.4 demonstrates waves formed by identical sources, but calculated within the frameworks of two different linear theories: long-wave and potential. In calculations we applied formulae (3.86) and (3.74), (3.75). Note that in the calculations presented in Fig. 3.4, use was made of quite an extended source, the length of which amounted to ten ocean depths.

In the case of a membrane-like displacement the wave shape is essentially different, especially at significant distances from the source. But in the case of a piston-like displacement one can see a noticeable difference in the wave shape and amplitude. In accordance with potential theory, the main perturbation is followed by an oscillating “tail”, due to phase dispersion. A small enhancement of the wave amplitude at large distances from the source (piston-like displacement) is also explained by dispersion. Actually, as the distance from the source increases, the wave amplitude first increases and only subsequently starts to decrease. The physical interpretation of this phenomenon consists in the following: the sharp wave front includes shortwave components traveling slower than the main wave, and, therefore, as the wave propagates, the front “overtakes” it, thus causing enhancement of the amplitude. Variation of the wave amplitude, as it travels away from the source, is shown in Fig. 3.8. Dispersive amplification can be seen to be capable of enhancing the wave amplitude by 25%, but it is not always present and exists only in such cases, when the size of the source is noticeably greater than the basin depth. The effect of dispersive

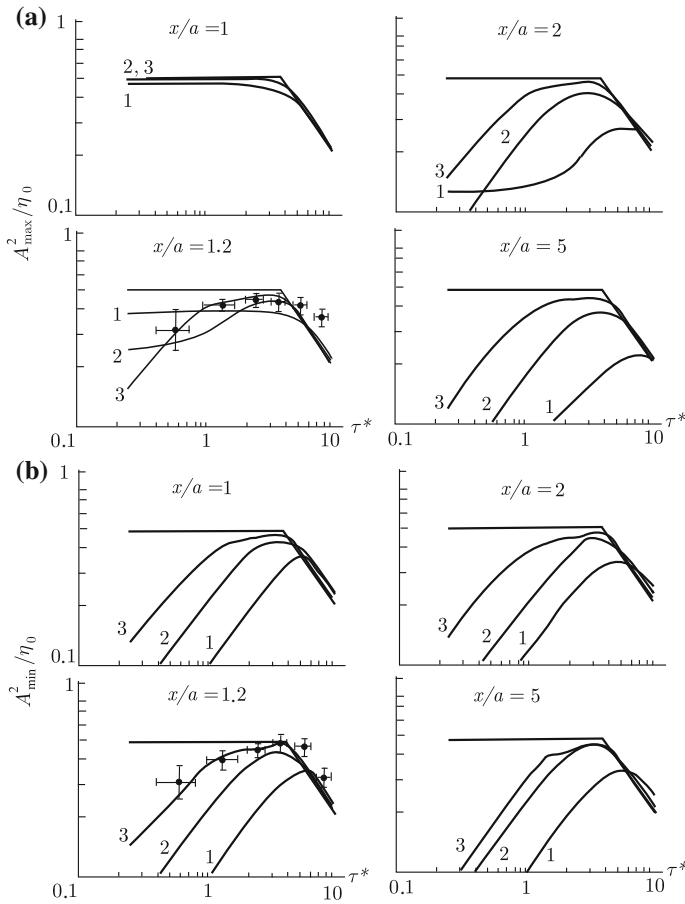


Fig. 3.6 Maximum amplitude of first crest (a) and first trough (b) of wave, excited by membrane-like displacement of seabed, versus displacement duration for various distances from the generation area. Curves 1–3 correspond to values of parameter $a/H = 1, 3, 9$. The broken line represents linear theory of long waves

tsunami amplification was first dealt with in (Mirchina and Pelinovsky 1987) for volcanogenic tsunamis.

Figures 3.5 and 3.6 show the dependences of wave amplitudes upon the displacement duration (curves 1, 2, and 3), calculated within the framework of potential theory. In the case of a piston-like displacement the behavior of these dependencies does not differ very strongly from the broken line, corresponding to the long-wave theory. Significant differences are observed only in the case of small-size sources and at large distances from it. In the case of waves due to a membrane-like displacement, also, no noticeable difference exists at the boundary of the generation area between calculations performed by the long-wave and potential theories. But,

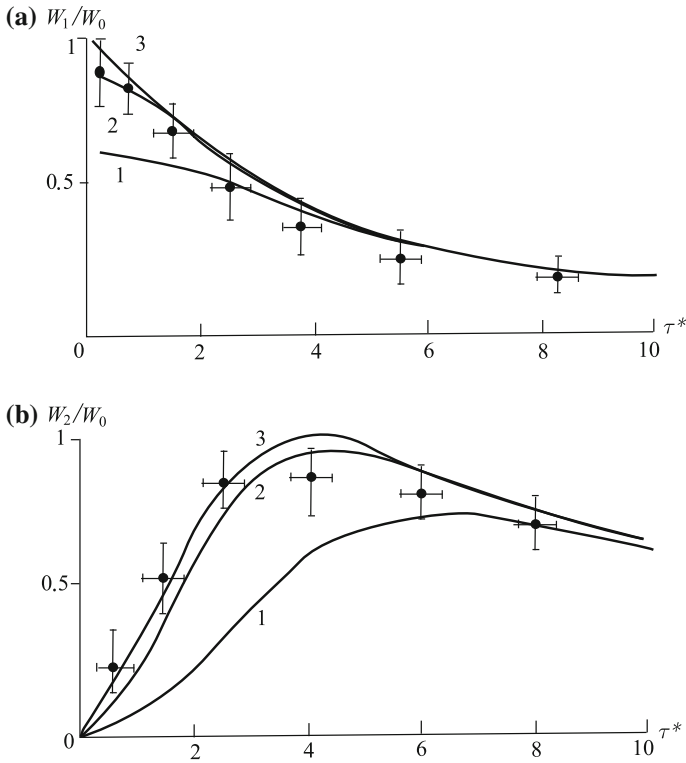
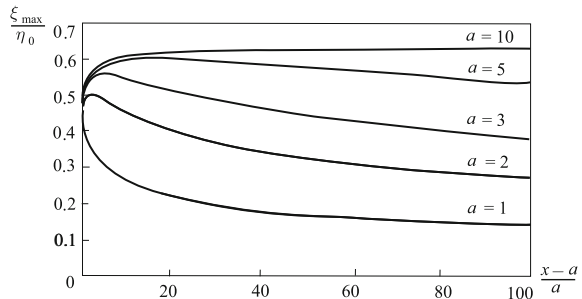


Fig. 3.7 Energy of wave, excited by piston-like (a) and membrane-like (b) displacements of seabed, versus displacement duration. Curves 1, 2 correspond to values of parameter $a/H = 1, 3$. Curve 3 corresponds to linear theory of long waves

Fig. 3.8 Maximum amplitude of wave caused by piston-like displacement, $\tau = 1$, versus distance from the boundary of the source for different source sizes



already at a small distance from the source the dependence of the amplitude essentially changes in character and becomes monotonous. Such a character of the dependence is conserved for any horizontal dimensions of the source. It is important to note that rapid membrane-like displacements do not cause tsunami waves of significant amplitudes.

We shall now turn to the relationship between the wave energy and the source parameters, presented in Fig. 3.7. It can be seen that in the case of a large-size source or of significant displacement durations, the energy values calculated by potential and long-wave theories comply quite well with each other. The most essential difference is again observed in the case of short membrane-like displacements. Taking into account that in the case of real tsunami sources $\tau^* < 1$ clarifies the leading role of seabed motions with residual displacements in the excitation of strong tsunamis. A similar conclusion is made, for example, in Dotsenko and Soloviev (1990a, b) from analysis of a source with axial symmetry.

In conclusion of this section, we shall turn to experimental tests of the theoretical relationships found between wave parameters and source characteristics. We shall briefly describe the layout of laboratory experiments. The setup was an open rectangular wave tank with transparent walls of organic glass of dimensions $0.15 \times 0.15 \times 3.3$ m (Fig. 3.9). As the source of waves, imitating vertical displacements of the basin bottom, use was made of a pneumatic generator representing a rectangular volume with rigid upper and lower sides, and elastic lateral sides. Model displacements of the basin bottom were registered by a sensor, representing a fixed inductance coil and a ferrite core, connected to the moving upper side. Several generators of the same type of dimensions 0.3×0.15 and 0.7×0.15 m were used. The inclined plane at the end of the wave tank served as a wave damper. The depth of the water varied between 0.04 and 0.1 m.

The described system permitted to simulate not only single piston-like and membrane-like displacements, but oscillations of the basin bottom, also. For simulation of a running displacement, use was made of three identical generators, driven sequentially (Fig. 3.10). The registration of waves on the free water surface was performed with the aid of optical sensors—infra-red (IR) wave gauges (Nosov and Shelkovnikov 1991). Unlike traditional contact methods of wave measurements on a water surface, an IR wave gauge introduces no distortion in the surface at the point of measurement, therefore, it can measure waves of small amplitude (0.1 mm and less). Measurement of waves of such small amplitudes is essential in physical simulation of tsunamis in the open ocean. Observation of geometrical similarity (Basov

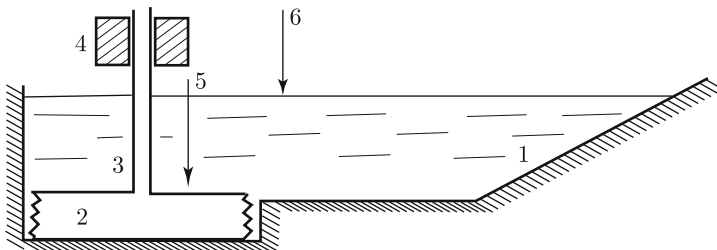


Fig. 3.9 Layout of laboratory setup for simulating tsunami generation by deformations of the basin bottom. 1 Wave damper (slope), 2 pneumatic wave generator, 3 main line of pressure supply, 4 guiding cylinder, 5 sensor of basin bottom motion, 6 IR wave gauge

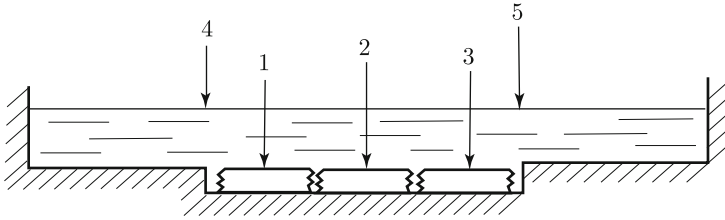


Fig. 3.10 Layout of laboratory setup for simulating tsunami generation by a running displacement. 1, 2, 3 pneumatic wave generators, 4, 5 IR wave gauges

et al. 1984) requires conservation of the relationship between the wave amplitude and the basin depth, $A/H \sim 10^{-3}$, while the depth and wave length are related as $H/\lambda \sim 10^{-2}-10^{-1}$. It is extremely difficult to establish such relationships in laboratory conditions. Owing to application of the IR wave gauge we have succeeded to perform the first investigation in the case of realistic relationships between the basin depth, wave length, and amplitude.

Figure 3.11 presents examples of waves, registered in the experiment (dotted line) and calculated in accordance with linear potential theory (solid line). The theory is seen to describe the wave perturbations quite adequately. Explanation of the small discrepancy between experiment and theory consists in that the actual time dependences of the basin motion differed insignificantly from the theoretical dependences, the first time derivatives of which exhibit discontinuities. The experimental points shown in Figs. 3.5, 3.6 and 3.7 were obtained as a result of analyzing several hundreds of experiments. The experimental data are seen to confirm the main peculiarities of the obtained theoretical dependences.

Once again it must be stressed that not to take into account dispersion in describing the process of tsunami generation may result in significant errors in determining amplitude and energy characteristics of waves, especially in the case of displacements of the basin bottom not accompanied by residual deformations.

For comparison, Fig. 3.12 demonstrates the results of experiments and of theoretical calculations, performed in Hammack (1973). Note that Hammack only investigated waves excited by piston-like displacements. Moreover, he applied a somewhat different, smoother time law of the basin bottom deformation. The main characteristics of the dependences, obtained by Hammack and by us for the piston-like displacement, are identical.

In his experiments Hammack applied the traditional method of wave registration on water, making use of a parallel wire resistance gauge. For this reason he had to excite waves of higher amplitudes. From Fig. 3.12 it is seen that the points, corresponding to positive (empty circles) and negative (full circles) displacements of the basin bottom, are stratified, i.e., lie, respectively, below and above the theoretical dependence obtained within the framework of linear theory. Note that the “stratification” effect of experimental points is observed only in the case of large dimensions of the generation area (for instance, $b/h = 12.20$ or 6.10). This is readily explained

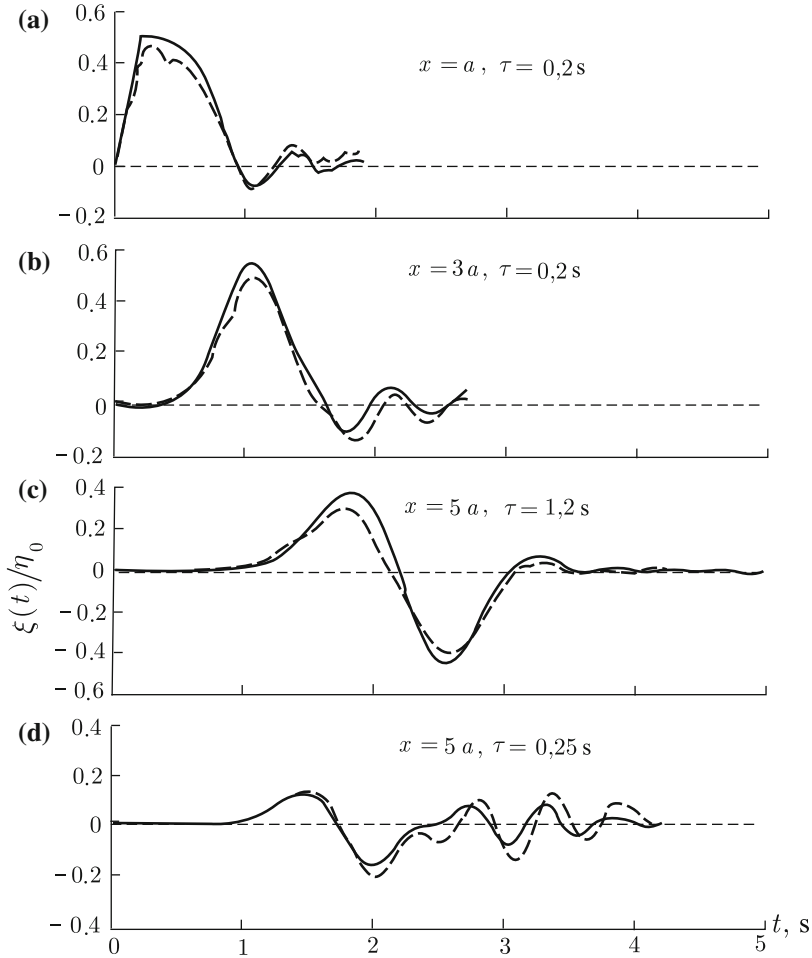


Fig. 3.11 Examples of time evolvents of waves generated by piston-like (a, b) and membrane-like (c, d) displacements of the basin bottom. *Solid line* linear potential theory, *dotted line* experiment; $a = 0.3\text{ m}$, $H = 0.1\text{ m}$

by the large relative dimensions of the generation area (the quantity b/h) being achieved by the choice of a small depth of water in the wave tank, h , owing to which the relative amplitude of the displacement became comparable to the depth. Large relative amplitudes were accompanied by manifestation of nonlinear effects (Kostitsyna et al. 1992). Attention must also be drawn to the fact, that in the case of prolonged displacements the “stratification” effect became noticeably smaller, which was evidently related to the drop in the relative wave amplitude. Figure 3.13 clearly demonstrates the manifestation of nonlinearity in the case of tsunami generation by piston-like displacements of large amplitude.

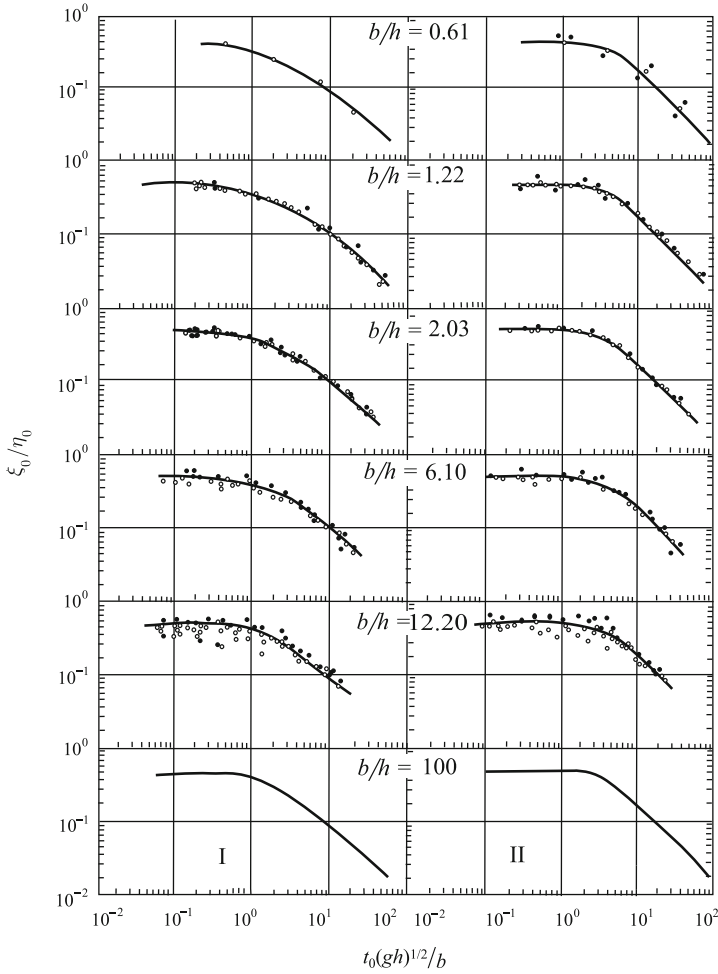


Fig. 3.12 Amplitude ξ_0 of wave, excited by piston-like basin bottom displacement of amplitude η_0 as function of the displacement duration τ . Adapted from Hammack (1973)

3.3.3 Running and Piston-Like Displacements

The idea of the deformation of a basin bottom being a process taking place simultaneously throughout the entire active region is, naturally, far from reality, although it does serve as an illustrative model of tsunami generation. Actually, deformation of a basin bottom is a consequence of the fault at the earthquake source propagating along a certain plane. In the case of strong earthquakes the fault plane may extend over hundreds of kilometers, exhibiting a small angle to the horizontal plane. Therefore, a displacement of the basin bottom, as a rule, has a component that can be

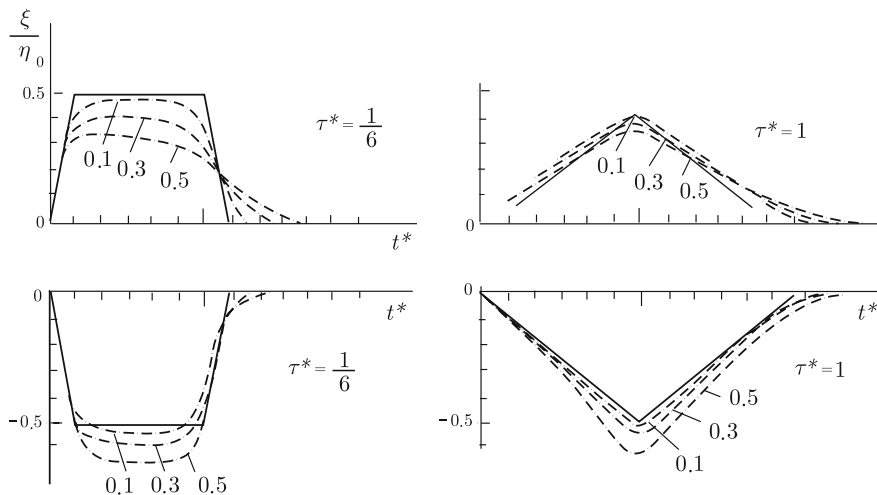


Fig. 3.13 Waves formed by a piston-like displacement of large amplitude. Calculations are performed within the framework of long-wave theory: *solid line* linear theory, *dotted line* nonlinear theory. The *numbers*, indicating the curves show the ratio of the basin bottom deformation amplitude and the basin depth

represented as a perturbation propagating in the horizontal direction. In the literature, such perturbations of the ocean bottom are conventionally termed “running displacements” (Novikova and Ostrovsky 1978; Vasilieva 1981; Marchuk et al. 1983). Let us name several other natural prototypes of the running displacement. This role may be assumed by a nonsimultaneous (sequential) displacement of blocks of the bottom (Lobkovsky and Baranov 1982), a crack propagating over the basin bottom (Bobrovich 1988), surface seismic waves (Belokon’ et al. 1986), the motion of an underwater landslide (Garder et al. 1993; Kulikov et al. 1998; Watts et al. 2001). Similar effects may be observed, also, in the case of wave generation by a moving area of low or elevated pressure (Pelinovsky et al. 2001).

The interest in running displacements arose, because when the propagation velocity of a displacement coincides (even approximately) with the velocity of long waves, $(gH)^{1/2}$, a resonance pumping is realized of energy into the tsunami wave. Like in the preceding section, we shall first turn to the linear theory of long waves. We shall take advantage of the one-dimensional wave equation (3.84), describing perturbation of the surface, $\xi(x, t)$, that arises with deformation of the basin bottom, $\eta(x, t)$. Assume a deformation of the basin bottom, the shape of which is set by a certain function f , to propagate in the positive direction of the $0x$ -axis with a constant velocity v : $\eta(x, t) = f(x - vt)$. Consider the motion to be established, therefore the solution of equation (3.84) will also have the form of a perturbation $\xi(x, t) = A_0 f(x - vt)$ running over the surface, where A_0 is a constant. Substituting the form of the solution, $\xi(x, t)$, and function $\eta(x, t)$ into the wave equation, we find the dependence of

the constant A_0 upon the velocity of long waves and upon the propagation velocity of the perturbation,

$$\xi(x, t) = \frac{v^2}{v^2 - gH} f(x - vt). \quad (3.94)$$

From formula (3.94) it is seen that over a deformation of the basin bottom, traveling horizontally, there always exists a similar in shape perturbation of the water surface. Given the condition $v < (gH)^{1/2}$, the perturbations of the surface and of the basin bottom exhibit different polarities, while when $v > (gH)^{1/2}$, their polarities coincide. The velocities of the perturbation and of long waves being close to each other result in a sharp enhancement of the amplitude of the surface perturbation.

If the problem of an established running displacement is considered within the framework of linear potential theory, then the main conclusion concerning resonance pumping of energy into the wave, when $v \approx (gH)^{1/2}$, does not change. At velocities $v > (gH)^{1/2}$ there will exist over the displacement a perturbation of similar polarity. But for velocities $v < (gH)^{1/2}$, besides the perturbation of opposite polarity located over the displacement, there also exists behind it a periodic in space and stationary in time perturbation with a wavelength determined by the velocity v . Standing waves, similar in nature, form, when underwater obstacles are bypassed by the flow (Sretensky 1977).

Problems of established motion are doubtless expedient for understanding the peculiarities of physical processes taking place during wave generation by running displacements. But in reality a tsunami forms during a certain finite time interval. Therefore, we shall further consider models assuming deformations of the basin bottom to be limited in time.

It must be noted that practically all prototypes of the running displacement (with the exception of underwater landslides) exhibit velocities superior to the velocity of sound in water, therefore, the model of an incompressible liquid, considered here, is often not adequate for describing the process. Nevertheless, the solution of this problem is certainly not without significance, for the following reasons. Earlier, the running displacement as a tsunami generator was studied exclusively within the framework of the theory of long waves (Novikova and Ostrovsky 1978), which occupies a lower position than potential theory in the hierarchy of models. The theory of incompressible liquids is a special case (and limit for $c \rightarrow \infty$) of the more general theory of compressible liquids. Consequently, the solution of the problem for an incompressible liquid will be a convenient bench mark in the construction of a more complex theory, and, moreover, the possibility arises of direct comparison of solutions of one and the same problem, obtained within the frameworks of different theories.

Making use of solutions (3.74) and (3.81), obtained within the framework of linear potential theory, we shall perform comparative analysis of dispersive tsunami waves excited by piston-like and running displacements of the basin bottom and subject to dispersion. We shall also compare such piston-like and running displacements that form identical residual deformations during the same time period, which, evidently, is expressed by the condition $b = v\tau$, where b is the horizontal size of the source, τ

is the duration of the process at the source, v is the propagation velocity of a running displacement. In other words, we are attempting to compare the efficiency of wave excitation, when the area filled exhibits a rectangular shape and is adjacent to the basin bottom, by two methods: from below upward and from left to right. Figure 3.14 presents the profiles of waves calculated at time moment $t = 50(H/g)^{1/2}$ for the value of parameter $b = 10H$, which is characteristic of real tsunami sources. An ordinary piston-like displacement forms identical waves in the positive and negative directions of the Ox -axis, while waves, excited by running displacements of the basin bottom, manifest an explicit asymmetry: a more intense train of waves runs in the direction of propagation of the displacement. The clearest asymmetry is revealed at propagation velocities of displacements, v , close to the velocity of long waves, $(gH)^{1/2}$. In the case of sufficiently large velocities v the profiles of waves, corresponding to piston-like and running displacements, actually become identical.

As a measure of the intensity of wave generation by the two mechanisms investigated, we shall take advantage of energy (per unit “canal” width), calculated by the formula,

$$W = \rho g \int \xi^2 dx. \quad (3.95)$$

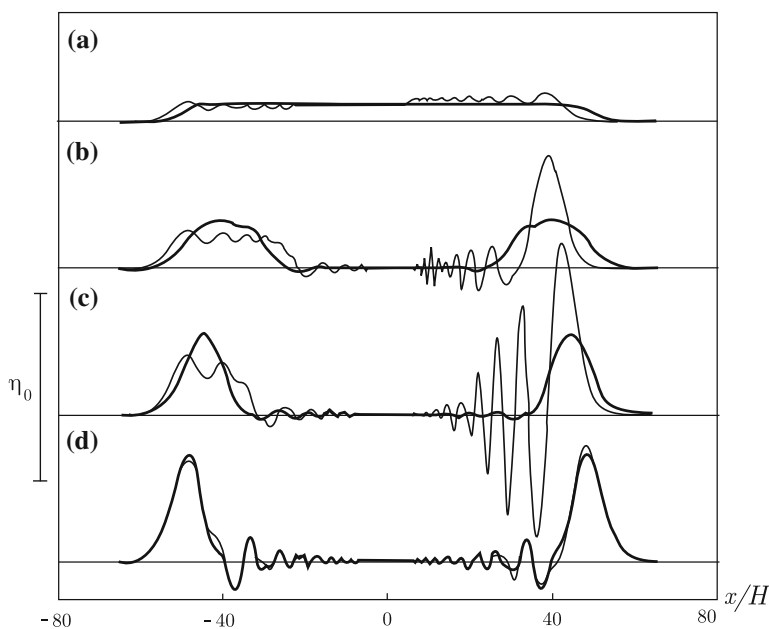
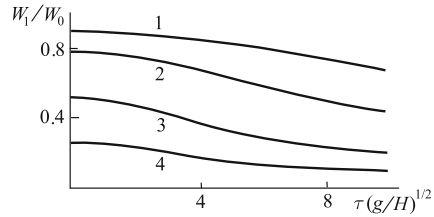


Fig. 3.14 Profiles of waves formed by running (*thin line*) and piston-like (*thick line*) displacements at time moment $t = 50$ for $L = 10$; **a–d** correspond to $v = 0.2, 0.5, 1, \text{ and } 10$; $\tau = 50, 20, 10,$ and 1

Fig. 3.15 Energy of waves excited by piston-like displacement versus displacement duration for various linear dimensions of the active region. Curves 1–4 correspond to $L = 10, 5, 2, 1$



The quantity W equals twice the potential energy of the wave. The calculation of energy was performed for the time moment $t = 50(H/g)^{1/2}$, when energy redistribution between the potential and kinetic energies had been totally completed and the value of W no longer depended on time.

The results of calculations are presented in Fig. 3.15 as dependences of the energy of a wave excited by a piston-like displacement of the basin bottom, W_1 , upon the displacement duration τ . The energy values are normalized to the quantity $W_0 = \rho g b \eta_0^2 / 2$, representing the specific potential energy of a rectangular elevation of height η_0 and length b of the free surface of a liquid. As the duration of a piston-like displacement increases the wave energy undergoes a monotonous decrease. Moreover, the energy depends essentially on the size of the generation area. Curves 1–4 in Fig. 3.15 correspond to values of parameter $b/H = 10, 5, 2, 1$. Note that these results, naturally, do not contradict the data presented in Fig. 3.7.

Figure 3.16 shows the dependence of the energy W_2 of a wave, excited by a running displacement, upon the velocity of the displacement propagation, v . When the parameter $b/H > 2$, the dependence exhibits a maximum, determined by the value of b/H , in the region of $v \sim (gH)^{1/2}$. The figure presents the relationship between the fractions of energy attributed to waves running along (W^+) and against (W^-) the direction of propagation of the running displacement versus the displacement velocity. This dependence also has a maximum in the vicinity of $v \sim 1$. When

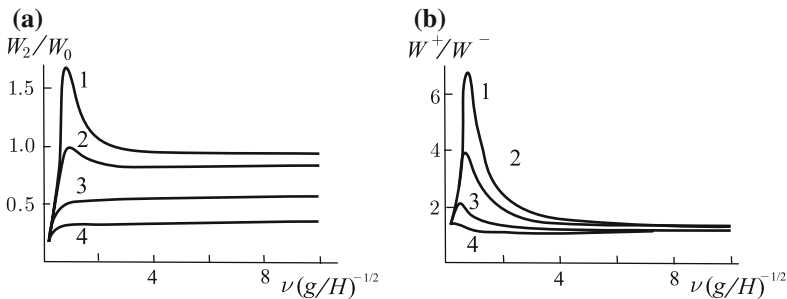
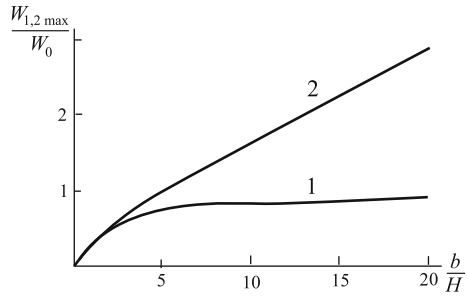


Fig. 3.16 Energy of waves (a), excited by a running displacement versus the propagation velocity of the displacement. b The relationship between the fractions of energy attributed to waves running along (W^+) and against (W^-) the direction of propagation of the running displacement versus the displacement velocity for $L = 10, 5, 2$, and 1 (1–4, respectively)

Fig. 3.17 Dependence of maximum possible energy of waves, excited by piston-like (1) and running (2) displacements, versus the size of the generation area



the parameter b/H decreases, the maximum is shifted noticeably toward smaller velocities. When the propagation velocity of the displacement increases, the curves in Fig. 3.16b asymptotically tend toward unity, independently of the value of b/H , which points to a loss of orientation by the energy emission at large values of v .

Figure 3.17 presents the dependence of the maximum possible energy of waves, excited by piston-like and running displacements of the basin bottom, upon the parameter b/H . In the case of $b/H < 2$ the type of displacement is seen to be irrelevant. When $b/H > 2$, a running displacement turns out to be capable of exciting waves more effectively than a piston-like displacement and while curve 1 tends asymptotically toward an evident long-wave limit equal to unity, the maximum energy of a wave excited by a running displacement actually increases linearly with the parameter b/H . It must be noted that in this case the linear increase of dimensionless energy signifies a quadratic dependence of its dimensional value upon the size of the generation area, b .

Laboratory simulation of a running displacement (Nosov and Shelkovnikov 1995) was performed with the setup depicted in Fig. 3.10. As the wave source, use was made of three identical basin bottom wave generators (of length $l = 0.3$ m) located at the center of the wave tank and driven sequentially. The motion of each of the generators simulated a vertical displacement of the basin bottom, involving residual displacement, and was controlled by its individual sensor. The amplitude of motions of the generators did not exceed 2 mm. The duration of motion of each generator, τ , was chosen so as to have pulsed displacements: $\tau \ll l(gH)^{-1/2}$ (usually, ~ 0.2 s). The depth of the water in experiments amounted to 3, 5, 7, and 10 cm.

Perturbations of the free water surface were registered with the aid of two IR wave gauges, located at the boundaries of the generation area. Records of the generator motions and of signals arriving from the wavegraphs were used in determining the maximum amplitude of the wave perturbations running along and against the direction of propagation of the displacement; the vertical displacement of each of the generators is η_i and the propagation velocity of the displacement, $v = (l/t_{12} + l/t_{23})/2$, where t_{12} and t_{23} are the time intervals between the connections of the first and second and of the second and third generators.

The results of experiments and of calculations, performed in accordance with formula (3.81), are presented in Fig. 3.18 as dependences of the maximum amplitude

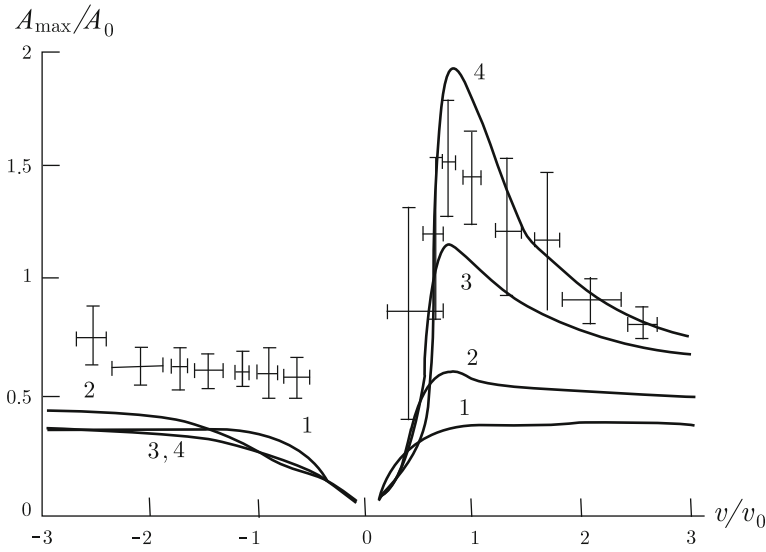


Fig. 3.18 Experimental and calculated dependences of the maximum wave amplitude at the boundary of the generation area at points $x = 0$ ($v/v_0 < 0$) and $x = b$ ($v/v_0 > 0$) versus the propagation velocity of the displacement. Curves 1–4 correspond to values of parameter $b = 1, 2, 5,$ and 10

of the wave perturbation, A_{\max} , upon the propagation velocity of the basin bottom displacement. The dependence is presented in dimensionless coordinates: the wave perturbation amplitude is normalized to the amplitude of the bottom displacement, $A_0 = (\eta_1 + \eta_2 + \eta_3)/3$, averaged for each given experiment, while the velocity v is normalized to the propagation velocity of long waves, $v_0 = (gH)^{1/2}$. The data on the maximum amplitude of the wave, running against the direction of propagation of the displacement, correspond to negative values of the dimensionless velocity. The large spread of experimental data, due to the amplitudes of bottom displacements, η_i , not being strictly equal to each other, did not permit to separate the experimental dependences for different water depths, so the experimental points in Fig. 3.18 reflect the data averaged over all the indicated water depths H .

Motions of the basin bottom in laboratory and theoretical models somewhat differed from each other. Therefore, one cannot expect perfect coincidence of theory and experiment, which is particularly noticeable, when $v/v_0 < 0$. This is also related to the fact that the difference between displacement amplitudes of bottom wave generators could amount to 30%, while the maximum amplitude of the wave, running against the direction of propagation of the displacement, is determined by the amplitude of the largest of η_i . Consequently, in connection with the wave amplitude being normalized to the quantity $A_0 = (\eta_1 + \eta_2 + \eta_3)/3$, the dimensionless amplitude will certainly be overestimated as compared with the case of identical bottom displacement amplitudes.

Theory and experiment show that a running displacement can indeed serve as an effective mechanism for the excitation of tsunami waves. In the case of propagation velocities of bottom displacements close to the velocity of long waves, $(gH)^{1/2}$, sharp enhancement occurs with the amplitude and energy of waves running in the direction of the displacement propagation. It is known that a tsunami amplitude in the open ocean cannot exceed the amplitude of a piston-like displacement of the ocean bottom. Contrariwise, in the case of a running displacement the wave amplitude can significantly exceed the bottom displacement amplitude. In the case of identical residual deformations of the bottom, a running displacement may turn out to be many times more effective than a piston-like displacement. The energy transferred by a running displacement to gravitational waves, when $v = (gH)^{1/2}$, increases in proportion to the square distance covered by the displacement.

3.3.4 The Oscillating Bottom

In the case of established harmonic oscillations of the bottom (3.71) we cannot directly take advantage of the general solution, obtained applying the Laplace transformation (3.65), since the oscillations take place at times $t < 0$. But in the case considered this is not necessary. For established oscillations it is possible to obtain a fully analytical solution, which does not require numerical calculation of integrals (Nosov 1992). Owing to the response of a linear system existing only at the frequency of inducing oscillations, we know the frequency of excited waves. Therefore, the solution of the problem is expediently sought in the following form:

$$F_{osc}(x, z, t) = \exp\{i\omega t\} \int_{-\infty}^{+\infty} dk \exp\{-ikx\} (A(\omega, k) \cosh(kz) + B(\omega, k) \sinh(kz)). \quad (3.96)$$

Taking advantage of the boundary conditions on the surface (3.63) and on the bottom (3.64), we obtain

$$F_{osc}(x, z, t) = \frac{\eta_0 \omega H}{2\pi} \exp\{i\omega t\} \int_{-\infty}^{+\infty} dk \times \frac{(\exp\{-ik(x-a)\} - \exp\{-ik(x+a)\}) (k \cosh(kz) + \omega^2 \sinh(kz))}{k^2 (\omega^2 \cosh(k) - k \sinh(k))}. \quad (3.97)$$

Expression (3.97) contains dimensionless variables under the integral sign that were introduced in accordance with the formulae (the sign “*” has been dropped),

$$\begin{aligned} (x^*, z^*, a^*) &= (x, z, a) H^{-1}; & t^* &= t g^{1/2} H^{-1/2}; \\ \omega^* &= \omega g^{-1/2} H^{1/2}; & k^* &= k H, \end{aligned}$$

but the multiplier before the integral and the velocity potential itself are dimensional quantities.

To calculate the integral (3.97) it suffices to know the value of an integral of the following form:

$$\int_{-\infty}^{+\infty} dk \frac{\exp\{-ik\alpha\} (k \cosh(kz) + \omega^2 \sinh(kz))}{k^2 (\omega^2 \cosh(k) - k \sinh(k))}, \tag{3.98}$$

where the parameter $\alpha = x \pm a$ may assume positive, negative, and zero values.

Let us continue the integrand function in (3.98) analytically from the real axis onto the entire complex plane ($\{\text{Re}(k), \text{Im}(k)\}$). The integrand has two singular points on the real axis, $k = \pm k_0$, and an infinite number of singular points on the imaginary axis, $k = \pm i k_j$. The singular points are poles of the first order, and their positions are determined from the solutions of the two following transcendental equations:

$$\cosh(k) \omega^2 - k \sinh(k) = 0, \tag{3.99}$$

$$\cos(k) \omega^2 + k \sin(k) = 0. \tag{3.100}$$

The integrand function in (3.98) has no other singular points, which is readily demonstrated with the aid of the theorem on counting the number of zeros of an analytical function (Sveshnikov and Tikhonov 1999).

Since the integrand function has poles on the real axis, the integral (3.98) must be understood in the sense of its principal value (p.v.), according to Cauchy. For its calculation the theorem of residues was applied. The ultimate expression, determining the velocity potential of a liquid flow in the case of established oscillations of a part of the bottom, has the following form:

- for $|x| \leq a$

$$\begin{aligned} \frac{F_{osc}(x, z, t)}{H \eta_0 i \omega} &= \exp\{i\omega t\} \left(\frac{1}{\omega^2} + z - 2 \sum_{j=1}^{\infty} Q \exp\{-k_j a\} \cosh(k_j x) \right) \\ &+ P (\exp\{i(\omega t + k_0(x - a))\} + \exp\{i(\omega t - k_0(x + a))\}), \end{aligned} \tag{3.101}$$

- for $x \geq a$

$$\begin{aligned} \frac{F_{osc}(x, z, t)}{H \eta_0 i \omega} &= \exp\{i \omega t\} \left(2 \sum_{j=1}^{\infty} Q \exp\{-k_j x\} \sinh(k_j a) \right) \\ &+ P \left(-\exp\{i(\omega t - k_0(x - a))\} + \exp\{i(\omega t - k_0(x + a))\} \right) \end{aligned} \quad (3.102)$$

- for $x \leq -a$

$$\begin{aligned} \frac{F_{osc}(x, z, t)}{H \eta_0 i \omega} &= \exp\{i \omega t\} \left(2 \sum_{j=1}^{\infty} Q \exp\{k_j x\} \sinh(k_j a) \right) \\ &+ P \left(\exp\{i(\omega t + k_0(x - a))\} - \exp\{i(\omega t + k_0(x + a))\} \right), \end{aligned} \quad (3.103)$$

where

$$\begin{aligned} P &= \frac{k_0 \cosh(k_0 z) + \omega^2 \sinh(k_0 z)}{k_0^2 ((\omega^2 - 1) \sinh(k_0) - k_0 \cosh(k_0))}, \\ Q &= \frac{k_j \cos(k_j z) + \omega^2 \sin(k_j z)}{k_j^2 ((\omega^2 - 1) \sin(k_j) - k_j \cos(k_j))}. \end{aligned}$$

With knowledge of the velocity potential of the flow it is not difficult to obtain expressions for the displacement of a free surface and for the velocity components,

- for $|x| \leq a$

$$\begin{aligned} \xi_{osc}(x, t) &= \eta_0 \exp\{i \omega t\} \left(1 - 2 \omega^2 \sum_{j=1}^{\infty} Q \exp\{-k_j a\} \cosh(k_j x) \right) \\ &+ \eta_0 \omega^2 P \left(\exp\{i(\omega t + k_0(x - a))\} + \exp\{i(\omega t - k_0(x + a))\} \right), \end{aligned} \quad (3.104)$$

- for $x \geq a$

$$\begin{aligned} \xi_{osc}(x, t) &= \eta_0 e^{i \omega t} 2 \omega^2 \sum_{j=1}^{\infty} Q \exp\{-k_j x\} \sinh(k_j a) \\ &+ \eta_0 \omega^2 P \left(-\exp\{i(\omega t - k_0(x - a))\} + \exp\{i(\omega t - k_0(x + a))\} \right), \end{aligned} \quad (3.105)$$

- for $x \leq -a$

$$\begin{aligned} \xi_{osc}(x, t) = & \eta_0 \exp\{i\omega t\} 2\omega^2 \sum_{j=1}^{\infty} Q \exp\{k_j x\} \sinh(k_j a) \\ & + \eta_0 \omega^2 P (\exp\{i(\omega t + k_0(x - a))\} - \exp\{i(\omega t + k_0(x + a))\}). \end{aligned} \quad (3.106)$$

- for $|x| \leq a$

$$u(x, z, t) = \eta_0 i\omega \exp\{i\omega t\} \left(-2 \sum_{j=1}^{\infty} Q k_j \exp\{-k_j a\} \sinh(k_j x) \right), \quad (3.107)$$

$$w(x, z, t) = \eta_0 i\omega \exp\{i\omega t\} \left(1 - 2 \sum_{j=1}^{\infty} \frac{\partial Q}{\partial z} \exp\{-k_j a\} \cosh(k_j x) \right), \quad (3.108)$$

- for $|x| \geq a$

$$u(x, z, t) = \eta_0 i\omega \exp\{i\omega t\} \left(-2 \operatorname{sign}(x) \sum_{j=1}^{\infty} Q k_j \exp\{-k_j |x|\} \sinh(k_j a) \right), \quad (3.109)$$

$$w(x, z, t) = \eta_0 i\omega \exp\{i\omega t\} \left(2 \sum_{j=1}^{\infty} \frac{\partial Q}{\partial z} \exp\{-k_j |x|\} \sinh(k_j a) \right), \quad (3.110)$$

Note that, owing to the discontinuity exhibited by the function, describing the space distribution of oscillations of the basin bottom, expressions (3.107)–(3.110) do not yield adequate values of the flow velocity at the points with coordinates $\{x = \pm a, z = -1\}$. To obtain the exact velocity values in the immediate vicinity of the points indicated it is necessary to take into account quite a large number of terms of the expansion in j .

From the structure of the obtained formulae it is seen that perturbation of a liquid consists of forced oscillations, occurring in the immediate vicinity of the source (and exponentially dying away with the distance from it), and a series of progressive waves starting at points $x = \pm a$.

From the point of view of tsunami generation precisely the amplitude of progressive waves is important. From formulae (3.105) and (3.106) it is seen that this

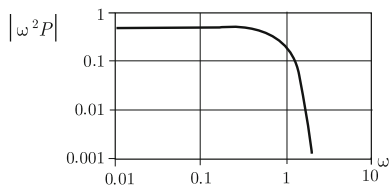


Fig. 3.19 Dependence of the quantity $|\omega^2 P|$, determining the amplitude of a gravitational wave upon the cyclic frequency of oscillations of the basin bottom

amplitude is largely determined by the quantity $|\omega^2 P|$, the dependence of which upon the cyclic frequency is shown in Fig. 3.19. A most important peculiarity of the response of the liquid to oscillations of a part of the ocean bottom consists in the existence of a certain boundary frequency, which, when surpassed, the efficiency of wave emission drops drastically. Thus, at high frequencies all the motion of the liquid is concentrated exclusively in the vicinity of the source and represents forced oscillations.

But the amplitude of emitted waves, A , does not depend only on the frequency of basin bottom oscillations, but on the horizontal extension of the oscillating area of the bottom, also. In accordance with formula (3.105), we can write

$$A(\omega) = \eta_0 \omega^2 \frac{2 \sin(k_0 a) \cosh(k_0)}{k_0 [k_0 + \sinh(k_0) \cosh(k_0)]}, \tag{3.111}$$

where $\omega^2 = k_0 \tanh(k_0)$. The dependence of the absolute value of the amplitude upon the dimensionless oscillation frequency of the ocean bottom $(\nu(H/g)^{1/2})$ is presented in Fig. 3.20. Calculations were performed for three different values of parameter a .

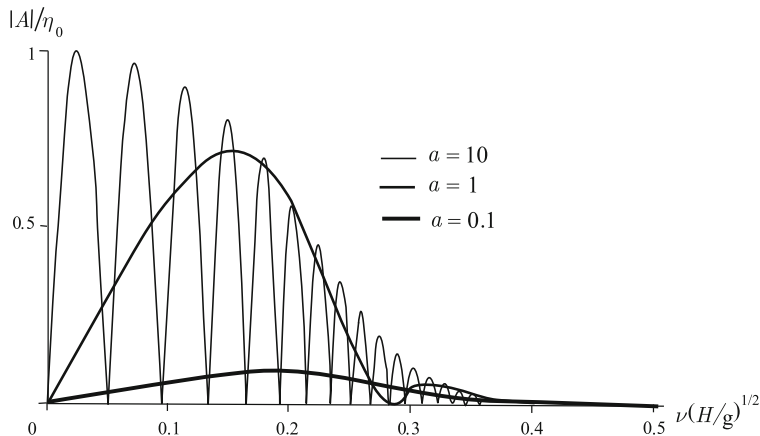


Fig. 3.20 Amplitude of progressive wave excited by oscillating area of ocean bottom versus the frequency of bottom oscillations for different sizes of the source, a

Surface manifestation of the oscillations of a part of the ocean bottom with linear dimensions, smaller than the depth of the layer of liquid, will be relatively weak. The existence of a set of frequencies, at which the amplitude of the emitted wave turns to zero, is related to the interference of waves forming at points $x = \pm a$. The automatic locking of the source is a consequence of the rectangular space distribution of the amplitude of bottom oscillations. Actually, manifestation of the automatic locking effect in nature is extremely improbable.

The dependence (3.111) permits to reveal parameters determining the limits of the tsunami frequency spectrum, ν_{\min} and ν_{\max} . We shall find the limit frequencies from the solution of equation $A(\nu) = \eta_0/10$. From Fig. 3.20 it is not difficult to conclude that $\nu_{\max} \sim 0.3$, while the quantity ν_{\max} does not depend on the size of the generation area, a .

We shall now determine ν_{\min} . At small oscillation frequencies of the ocean bottom (which also corresponds to small values of k_0), expression (3.111) is essentially simplified and assumes the following form: $A(\omega) = \eta_0 a \omega$. Thus, the quantity ν_{\min} can be estimated as $\nu_{\min} \sim (20 \pi a)^{-1}$. Passing to dimensional quantities, we obtain the following formulae for the limits of the tsunami frequency spectrum:

$$\nu_{\max} \sim 0.3 \left(\frac{g}{H} \right)^{1/2}, \quad (3.112)$$

$$\nu_{\min} \sim \frac{(gH)^{1/2}}{20 \pi a}. \quad (3.113)$$

The lower frequency limit is seen to be related both to the ocean depth and to the horizontal dimension of the source, while the upper limit only to the depth. For a depth $H \sim 10^3$ m and size of the source equal to $a \sim 10^4$ m we obtain $\nu_{\max} \sim 10^{-2}$ Hz, $\nu_{\min} \sim 10^{-4}$ Hz. The spectrum of real tsunami waves lies precisely within these limits (Murty 1977; Pelinovsky 1996).

The theoretical dependence (3.111) has been tested experimentally (Nosov and Shelkovnikov 1992). Use was made of the setup shown in Fig. 3.9. The pneumatic generator 30 cm long simulated harmonic oscillations of an area of the ocean bottom. Practically, all the remaining part of the wave tank was occupied by the wave damping system representing a gentle slope covered with a plastic mesh. The wave was registered by the IR wave gauge at a distance of 10 cm from the boundary of the generation area. The results of experiments and of theoretical calculations for three different water depths in the wave tank are presented in Fig. 3.21. The experimental data are seen to comply with the theoretical dependence.

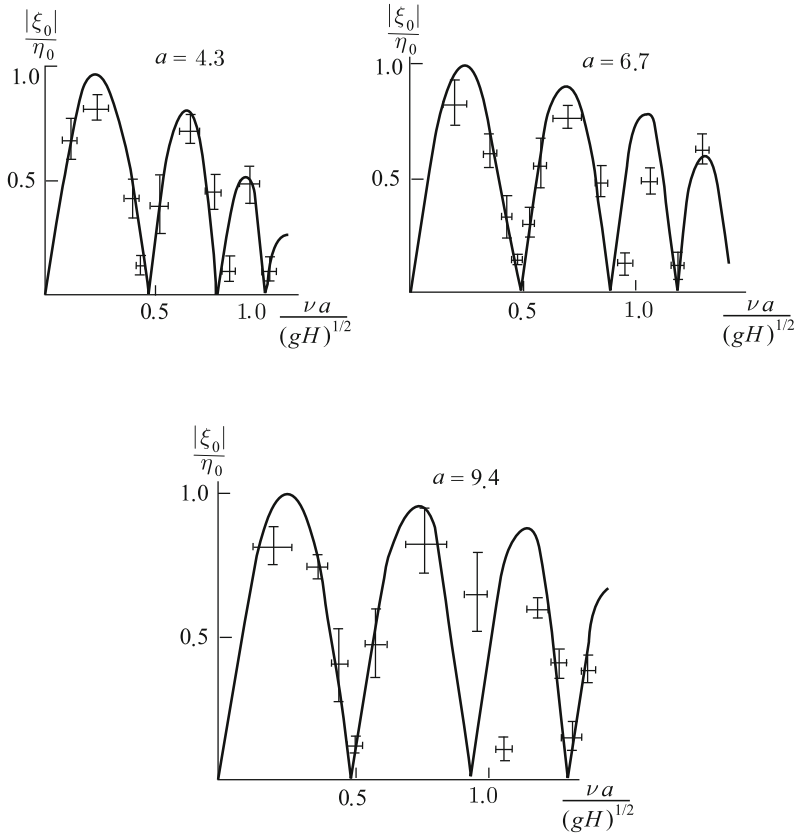


Fig. 3.21 Comparison of experimental and theoretical dependences of amplitudes of excited progressive wave versus frequency of bottom oscillations

3.4 Generation of Tsunami Waves and Peculiarities of the Motion of Ocean Bottom at the Source

In this section we shall deal with the space (3D) problem of tsunami generation by ocean bottom displacements. Transition from plane (2D) models to the more realistic three-dimensional problem makes it possible to investigate the most important issue of the directivity of wave emission and of its relation to parameters of the source. The effect of directed emission of tsunami waves from the source area can be due to various reasons, which are usually considered to comprise the geometrical shape of the deformation area of the ocean bottom, the transfer of horizontal momentum to masses of water, and the waveguide properties of the bottom relief (Voight 1987; Dotsenko and Soloviev 1990a, b). The last reason, generally speaking, is related to the tsunami propagation, and not to wave generation. The directivity of tsunami emission, due to source asymmetry, has been studied theoretically (Kajiura 1963, 1970;

Dotsenko et al. 1993), experimentally (Takahasi 1963), and numerically (Marchuk and Titov 1993).

The strikingly clear directivity of the Chilean tsunami of May 22, 1960, when the amplitude of the wave traveling in a direction, perpendicular to the South American coast, was several times larger than the amplitudes of waves propagating in other directions, initiated the appearance of a series of publications (Voight et al. 1980, 1981, 1982; Lebedev and Sebekin 1982), in which the role was estimated of a horizontal motion of the ocean bottom in forming an directed tsunami wave. In these works, the influence of a horizontal motion on the ocean was simulated by applying an effective mass force in the vicinity of the source, and, then, the properties of waves at a large distance from the generation area were studied. Thus, for example, it was established, that a wave, caused by a vertically directed mass force, exhibits axial symmetry at long distances from the source, in spite of the perturbing force not being axially symmetric, while at the same time the wave front of a tsunami caused by a transfer of horizontal momentum remains anisotropic.

Numerical models of tsunamis, that gained well-known popularity as powerful means for investigations (Chubarov et al. 1992; Kato and Tsuji 1995; Satake 1995; Satake and Imamura 1995; Tanioka and Satake 1996b; Titov et al. 1999; Myers and Baptista 1995; Suleimani et al. 2003; Zaitsev et al. 2005; Kowalik et al. 2005; Titov et al. 2005; Horrillo et al. 2006; Rivera 2006; Gisler 2008), seem to have achieved a certain limit in their perfection, in the sense that for their further successful development it is necessary to introduce a number of essentially novel features, one of which consists in the following: wave excitation must be described realistically, i.e., it must be dealt with as a process extended in time. As a rule, in describing tsunami generation impulse displacements are considered, and, consequently, only geometric characteristics of the source, i.e., the distribution of residual bottom displacements in space, are taken into account. Here, the actual method (the time law followed by motions of the ocean bottom), by which the different residual displacements came about, is totally neglected. At the same time, the duration of processes at the source may amount to 100 seconds, and more (Satake 1995). For example, the process at the source of the Sumatran catastrophic tsunami of 2004 went on for about 1000 s. In such a long period of time, a long wave is capable of covering a distance comparable to the size of a tsunami source, which means that a displacement cannot be assumed to exhibit an impulse character. Moreover, in (Dotsenko 1996; Nosov et al. 1997; Nosov 1998a, b) it was established that the energy, amplitude, and even directivity of tsunami waves are not only related to the geometric characteristics of the source, but to the time law of motion of the ocean bottom, also.

In Sect. 3.2.1 the general solution was obtained, within the framework of potential theory, for the linear response of a layer of incompressible liquid of fixed depth to deformations of the ocean bottom, $\eta(x, y, t)$. We shall consider the following three model laws of ocean bottom deformation:

- piston-like displacement

$$\eta_1(x, y, t) = \eta_S(x, y) (\theta(t)t - \theta(t - \tau)(t - \tau)) \tau^{-1}, \quad (3.114)$$

- membrane-like displacement

$$\eta_2(x, y, t) = \eta_S(x, y) (2\theta(t) t - 4\theta(t - \tau/2) (t - \tau/2) + 2\theta(t - \tau) (t - \tau)) \tau^{-1}, \quad (3.115)$$

- running displacement

$$\eta_3(x, y, t) = \eta_S(x - a, y) (1 - \theta(x - vt)), \quad (3.116)$$

where $\eta_S(x, y) = \eta_0 (\theta(x + a) - \theta(x - a)) (\theta(y + b) - \theta(y - b))$ is the space distribution of ocean bottom deformations, $\theta(z)$ is the Heaviside step function. The active region has the shape of a rectangle of length $2a$ and width $2b$. The piston-like and membrane-like displacements are characterized by amplitude η_0 and duration τ , the running displacement by its amplitude η_0 and propagation velocity \mathbf{v} . In the case of a running displacement the area of bottom deformations is shifted in the positive direction of axis Ox by the quantity \mathbf{a} , so as to have motions of the ocean bottom start at the time moment $t = 0$.

We now introduce dimensionless variables (the sign “*” will be further dropped),

$$\begin{aligned} (m^*, n^*) &= H(m, n); & (x^*, y^*, z^*, a^*, b^*) &= H^{-1}\{x, y, z, a, b\}; \\ \{t^*, \tau^*\} &= \{t, \tau\} g^{1/2} H^{-1/2}; & \{\xi^*, \zeta^*\} &= \eta_0^{-1} \{\xi, \zeta\}. \end{aligned} \quad (3.117)$$

Part of the integrals, present in formula (3.48), can be calculated analytically. Zipping intermediate calculations, we shall write out the formulae describing the perturbation of a free surface in the case of ocean bottom deformations of the form (3.114)–(3.116),

- piston-like displacement

$$\xi_1(x, y, t) = \theta(t) \zeta_1(x, y, t) - \theta(t - \tau) \zeta_1(x, y, t - \tau), \quad (3.118)$$

- membrane-like displacement

$$\begin{aligned} \xi_2(x, y, t) &= 2\theta(t) \zeta_1(x, y, t) \\ &\quad - 4\theta(t - \tau/2) \zeta_1(x, y, t - \tau/2) + 2\theta(t - \tau) \zeta_1(x, y, t - \tau), \end{aligned} \quad (3.119)$$

where

$$\begin{aligned} \zeta_1(x, y, t) &= \frac{4}{\pi^2 \tau} \int_0^\infty \int_0^\infty dm dn \\ &\quad \times \frac{\sin(ma) \sin(nb) \cos(mx) \cos(ny) \sin((k \tanh k)^{1/2} t)}{mn \cosh k (k \tanh k)^{1/2}}, \end{aligned} \quad (3.120)$$

$$k^2 = m^2 + n^2,$$

- running displacement

$$\begin{aligned} \xi_3(x, y, t) = & \frac{\eta_0}{2\pi^2} i \int_0^\infty dn \int_{-\infty}^{+\infty} dm \frac{\exp\{i m x\} \sin(nb) \cos(ny)}{\cosh(k) n} \\ & \times \left(\frac{1 - \exp\left\{-i2a \left(m + \frac{(k \tanh(k))^{1/2}}{v}\right)\right\}}{m + \frac{(k \tanh(k))^{1/2}}{v}} \exp\left\{i(k \tanh(k))^{1/2} t\right\} \right. \\ & \left. + \frac{1 - \exp\left\{-i2a \left(m - \frac{(k \tanh(k))^{1/2}}{v}\right)\right\}}{m - \frac{(k \tanh(k))^{1/2}}{v}} \exp\left\{-i(k \tanh(k))^{1/2} t\right\} \right). \end{aligned} \tag{3.121}$$

Formula (3.121) is valid, when $t \geq 2a/v$ (the reason that such a restriction exists is expounded in Sect. 3.3.1). The integrals in expressions (3.120) and (3.121) were calculated numerically.

Figure 3.22 presents the space structure of waves excited by piston-like and running displacements, which have ultimately resulted in identical residual deformations ($a = 6, b = 2$). The propagation velocity of a running displacement, $v = 2$, and the duration of a piston-like displacement, $\tau = 6$, satisfy the relationship $\tau v = 2a$. Calculations are performed in accordance with formulae (3.118) and (3.121). From the figure it is seen that in the case of a piston-like displacement the waves of maximum amplitude propagate in the negative and positive directions of axis Oy , i.e., in a direction perpendicular to the direction of maximum extension of the source. In the case of a running displacement the source emits waves of maximum amplitude at the Mach angle to the direction of propagation of the displacement, (Ox). Moreover, attention is immediately drawn to the fact that the amplitude of waves caused by a running displacement is significantly superior to the amplitude of waves in the case of a piston-like displacement.

For detailed investigation of the directivity of waves emitted from the source area wave time bases were calculated at points lying on a circle of a certain radius ($r > \max[a, b]$), with its center coinciding with the origin of the chosen reference frame. Examples of such time bases are presented in Fig. 3.23. The azimuthal angle was counted off from the positive direction of axis Ox . From the wave time bases amplitude characteristics were determined, and the energy was estimated by the formula proposed in (Kajiura 1970),

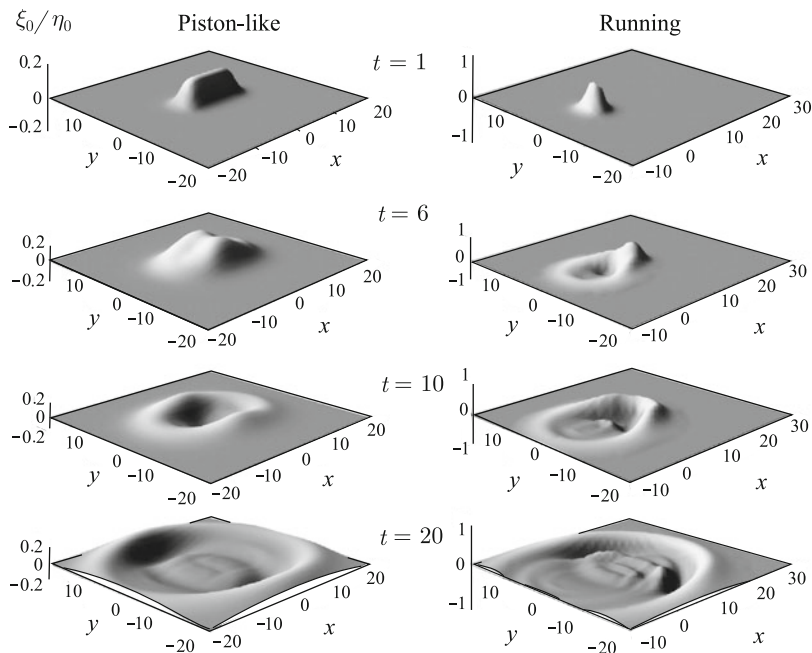


Fig. 3.22 Free surface perturbations caused by piston-like and running displacements of the *bottom* with parameters $a = 6, b = 2, \nu = 2$ ($\tau = 6$). Calculations are performed for the time moments t indicated in the figure

$$W = \rho g (gH)^{1/2} \int_0^T \int_{\gamma} \xi^2(t) dt d\gamma. \tag{3.122}$$

Formula (3.122) yields the energy that passed through the contour γ in time T . In our case, the contour γ was chosen to be the segment of a circle of radius \mathbf{r} , given $\Delta\alpha = 10^\circ$. Energy values were normalized to the quantity $W_0 = 2\rho g a b \eta_0^2$. The quantity W_0 corresponds to the potential energy of the initial free surface elevation, exhibiting the shape of the residual bottom displacement.

Figure 3.24 presents, in the form of directional diagrams, the dependences of the amplitude of the first crest A_1 (a, b), of the “maximum span” $A_{\max} - A_{\min}$ (c, d), and of the wave energy W_α (e, f) upon the azimuthal angle. Calculations are performed for piston-like and running displacements, the durations of which are chosen so as to satisfy the relationship $\tau = 2a\nu^{-1}$. Thus, the process of wave excitation can be investigated by varying the parameter, common to both piston-like and running displacements, namely, the duration of the process in the active area. The dotted line in the figure shows the shape and orientation of the active area. From Fig. 3.24 the orientation is seen to be manifested most weakly for the amplitude of the first crest. The evolution of directional diagrams differs essentially for piston-

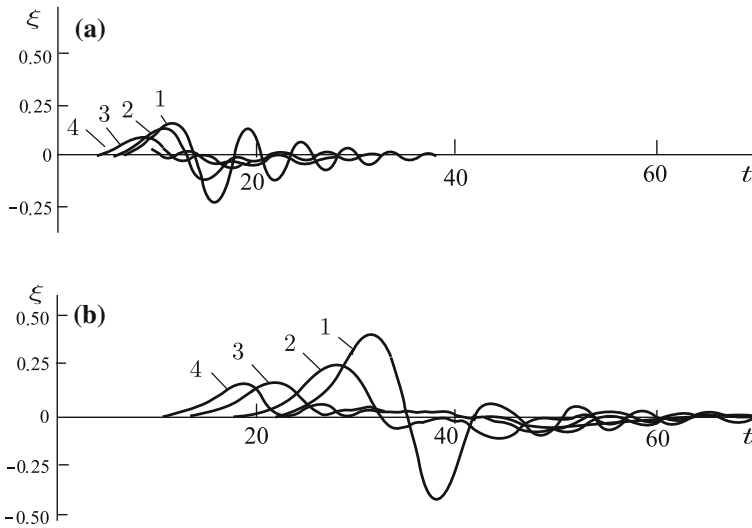


Fig. 3.23 Time base of waves caused by piston-like displacement. Calculations are performed at points lying on a circle of radius $r = 10$ (a) and $r = 30$ (b) with its center at the origin of the reference frame, for azimuthal angles $\alpha = 0, 30, 60, 90^\circ$ (curves 1–4, respectively). The parameters of the *bottom* displacement: $a = 1, b = 5, \tau = 1$ (a) and $a = 3, b = 15, \tau = 1$ (b)

like and running displacements, as the duration of the process at the source varies. When the duration of a piston-like displacement increases, the amplitude and energy of waves monotonously decrease, while their distribution over the azimuthal angle tends to be isotropic. Here, the wave of largest amplitudes and energy are always emitted in a direction, perpendicular to the largest extension of the source. In the case of a running displacement, as the duration of the process at the source increases (the propagation velocity of the displacement decreases), the directional diagrams gradually transform from two-pronged into single-pronged diagrams, and the main part of energy starts to be emitted in the direction of propagation of the displacement. When the duration of the process at the source is small ($\tau = 2$), the directional diagrams for both cases investigated are practically identical. But in the case of large values of τ , the character of motion of the ocean bottom already exerts significant influence on the parameters of the excited wave.

Figure 3.25 presents the dependence of the total wave energy (integrated over all directions) upon the duration of the process at the source. In the case of a piston-like displacement (curve 1) the dependence is monotonous—the energy falls as the duration of the process increases. In the case of a running displacement (curve 2) the dependence reveals a maximum, which corresponds to coincidence of the propagation velocity of the displacement and the velocity of long waves. The running displacement is also seen to be noticeably more effective than the piston-like displacement within a wide range of τ values. When durations of the process at the source are

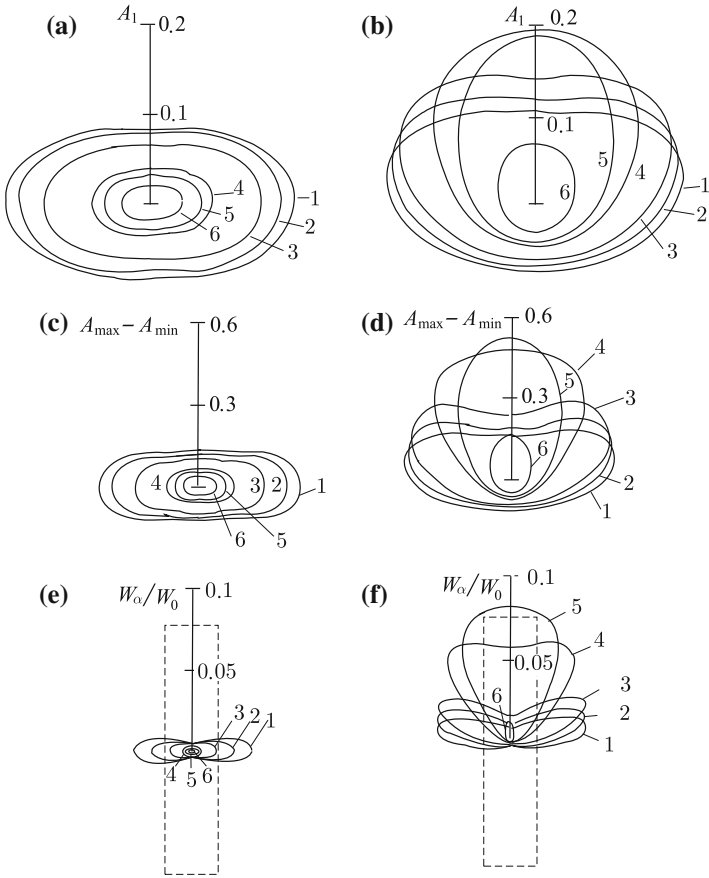
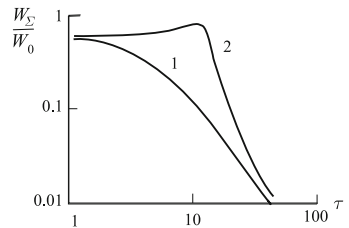


Fig. 3.24 Distribution of amplitude of the first crest (a, b), of the “maximum span” (c, d) and of the energy (e, f) of a wave over the azimuthal angle. Curves 1–6 correspond to piston-like displacements (a, c, e) of durations $t = 2, 3.3(3), 5, 10, 12.5, 20$ and to running displacements (b, d, f) with propagation velocities $v = 5, 3, 2, 1, 0.8, 0.5$. The durations and propagation velocities are chosen so as to have $\tau = 2av^{-1}$. The dotted line shows the shape and orientation of the active area

Fig. 3.25 Total energy of waves generated by piston-like (1) and running (2) displacements versus duration of the process in the active area. In the case of a running displacement $\tau = 2av^{-1}$



small or large the efficiencies of both mechanisms of wave generation are approximately identical.

Figure 3.26 presents energy directional diagrams for waves due to piston-like and membrane-like displacements. The dotted line shows the shape and orientation of the model source. Calculations have been performed for various deformation durations of the bottom. The main part of energy is seen to be emitted in a direction, perpendicular to the direction of maximum extension of the source, independently of the time law satisfied by motion of the bottom. But as the displacement duration increases, the diagram undergoes significant changes, the character of which does depend on the type of time law of motion of the bottom.

We shall now introduce the directional coefficient of emission as the ratio of energy fractions emitted in directions $\alpha = 0^\circ$ and 90° . Figure 3.27 shows the dependence of the directional coefficient upon the displacement duration. For a piston-like displacement the quantity $W^{0^\circ} / W^{90^\circ}$ decreases monotonously as the duration increases. But the corresponding dependence for a membrane-like displacement exhibits a non-monotonous character. It is interesting to note that in the case of a membrane-like displacement the directional coefficient may assume larger values, than for a piston-like displacement. From the figure it can also be concluded that a decrease in the size of a source, if its shape (the ratio a/b) is conserved, results in a weakening of the directionality, especially when its size becomes comparable to the depth.

Why does the duration of the bottom deformation (or type of time law) influence the orientation of wave emission? The point is that an asymmetric source forms waves of differing wavelengths in different directions. In other words, there exists an effec-

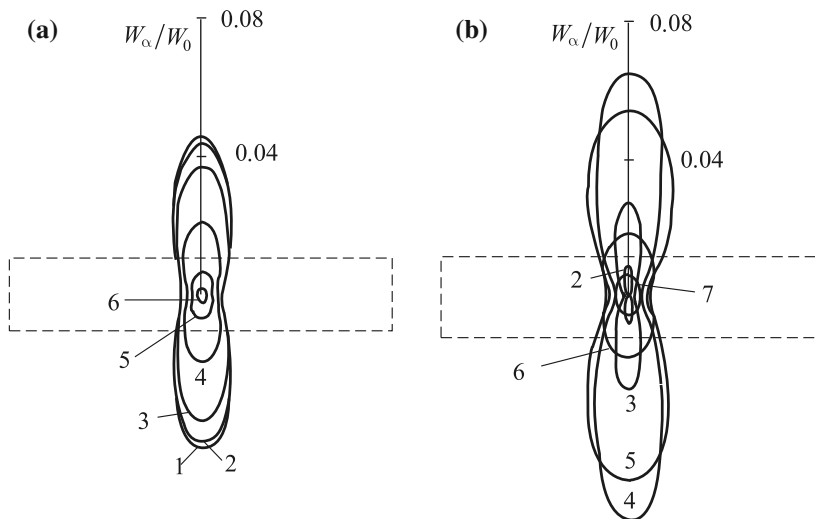
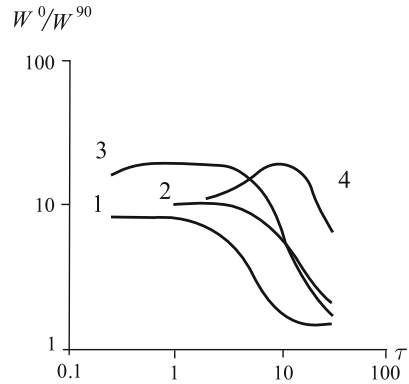


Fig. 3.26 Directional diagrams for emission energy of waves caused by piston-like (a) and membrane-like (b) displacements of ocean bottom. Curves 1–7 correspond to $\tau = 0.5, 1, 2, 4, 8, 16, 32$

Fig. 3.27 Directional coefficient versus duration of bottom displacement. Curves 1, 2 correspond to piston-like displacement, 3, 4 to membrane-like displacement. Curves 1, 3 are obtained for $a = 1, b = 5, r = 10$, curves 2, 4 for $a = 3, b = 15, r = 30$

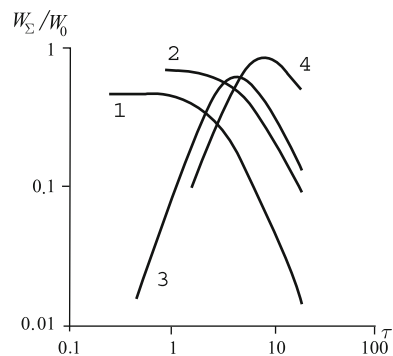


tive horizontal size of a source, depending on the direction. It was shown in Sect. 3.3.2 (Fig. 3.5) that when the displacement duration increases, the wave amplitude falls more rapidly in the case of a source of smaller horizontal extension. Therefore, if the source is elongated, then the degree of emission orientation inevitably decreases, as the displacement duration rises. The behavior of the directional coefficient in the case of a membrane-like displacement is explained in a similar manner.

Figure 3.28 presents the total wave energy (integrated over all directions) versus the duration of the bottom displacement. In the case of a piston-like displacement the energy monotonously decreases as the duration increases, while in the case of the membrane-like displacement there exists a certain “optimal” duration, for which the energy is maximal. For this “optimal” duration the membrane-like displacement turns out to be more effective, than even a piston-like displacement of small duration. Similar dependences were obtained in Refs. (Dotsenko and Soloviev 1990a, b, 1995) within the framework of linear theory of long waves.

Analysis of space distribution of vertical residual displacements shows that at the tsunami source there usually exist two regions: an uplift and a subsidence of the ocean bottom (Van Dorn 1964; Dotsenko et al. 1986; Satake 1995; Kato and

Fig. 3.28 Total energy of waves due to piston-like and membrane-like displacements versus displacement duration. The curves are numbered like in Fig. 3.27



Tsuji 1995). We shall term such a displacement alternating in sign. We shall briefly dwell upon certain peculiarities of the directionality of wave emission, related to such bipolar deformation of the ocean bottom. Consider the displacement alternating in sign to be described by the formula (Nosov et al. 1999),

$$\begin{aligned} \eta_4(x, y, t) = & \left(\eta_1 a_1^{-1} (x + a_1) (\theta(x + a_1) - \theta(x)) \right. \\ & \left. + \eta_2 a_2^{-1} (x - a_2) (\theta(x) - \theta(x - a_2)) \right) \\ & \times \left(\theta(y + b) - \theta(y - b) \right) \left(t \tau^{-1} \theta(t) - (t - \tau) \tau^{-1} \theta(t - \tau) \right). \end{aligned} \quad (3.123)$$

The space distribution of the deformation amplitude of the bottom, determined by formula (3.123), is shown in Fig. 3.29. As to the time law of bottom deformation, we consider a displacement with residual deformation.

The perturbation of a free surface in the case of a displacement alternating in sign is calculated in accordance with the following formula:

$$\xi_4(x, y, t) = \theta(t) \zeta_4(x, y, t) - \theta(t - \tau) \zeta_4(x, y, t - \tau),$$

where

$$\begin{aligned} \zeta_4(x, y, t) = & \frac{2}{\pi^2 \tau} \int_0^\infty \int_0^\infty dm dn \frac{\sin[k \tanh(k)]^{1/2} t}{\cosh(k) (k \tanh(k))^{1/2}} \frac{\cos(ny) \sin(nb)}{n} \\ & \times \left[\cos(mx) \left(\frac{\eta_1}{a_1 m^2} [1 - \cos(ma_1)] - \frac{\eta_2}{a_2 m^2} [1 - \cos(ma_2)] \right) \right. \\ & \left. + \sin(mx) \left(\frac{\eta_1}{a_1 m^2} \sin(ma_1) - \frac{\eta_1}{m} + \frac{\eta_2}{a_2 m^2} \sin(ma_2) - \frac{\eta_2}{m} \right) \right]. \end{aligned} \quad (3.124)$$

Integration over the components m and n of the wave vector in formula (3.124) was performed numerically.

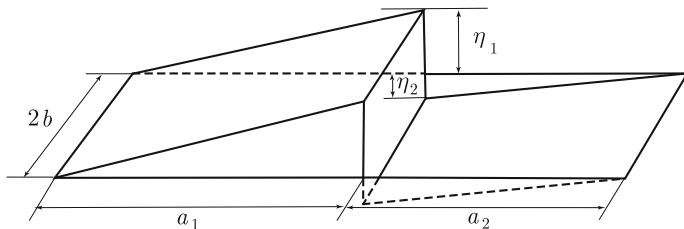


Fig. 3.29 Model of residual deformations of the *bottom* for a displacement alternating in sign

Fig. 3.30 Perturbation of free surface caused by displacement of *bottom* alternating in sign. Calculations are performed for a sequence of time moments (indicated in the figure) for $a_1 = 7$, $a_2 = 3$, $b = 10$, $\tau = 1$

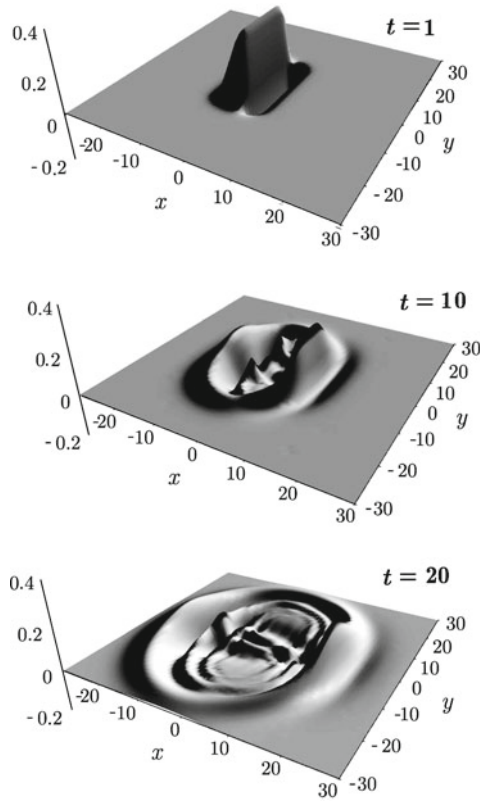


Figure 3.30 shows the example of the space structure of waves, excited by a bottom displacement alternating in sign with parameters $a_1 = 7$, $a_2 = 3$, $b = 10$, $\tau = 1$. The active area (its horizontal projection) exhibits the shape of a rectangle of size 10×20 (along axes Ox and Oy , respectively). The “fault” passes along the axis Oy , the elevation and depression areas of the ocean bottom correspond, respectively, to negative and positive values of the x coordinate. From the figure it is seen that waves of maximum amplitude propagate in a direction, perpendicular to the “fault” direction. Besides the above, attention must be drawn to the following nontrivial peculiarity: the leading wave in the train exhibits negative polarity, not throughout the entire semiplane $x > 0$, but only in a certain sector, the angle of which is noticeably smaller than 180° . Note, that in accordance with the theory of long waves the polarity of the leading tsunami wave is determined by the sign of deformation of the ocean bottom at the nearest point of the source. Potential theory provides a more precise result, demonstrating that the polarity of the leading wave is related to a greater number of parameters.

Figure 3.31 presents wave profiles, calculated for various azimuthal angles α and for two displacement durations $\tau = 1, 10$ (solid and dotted lines, respectively). The waves are characterized by significant dispersion, and their amplitudes

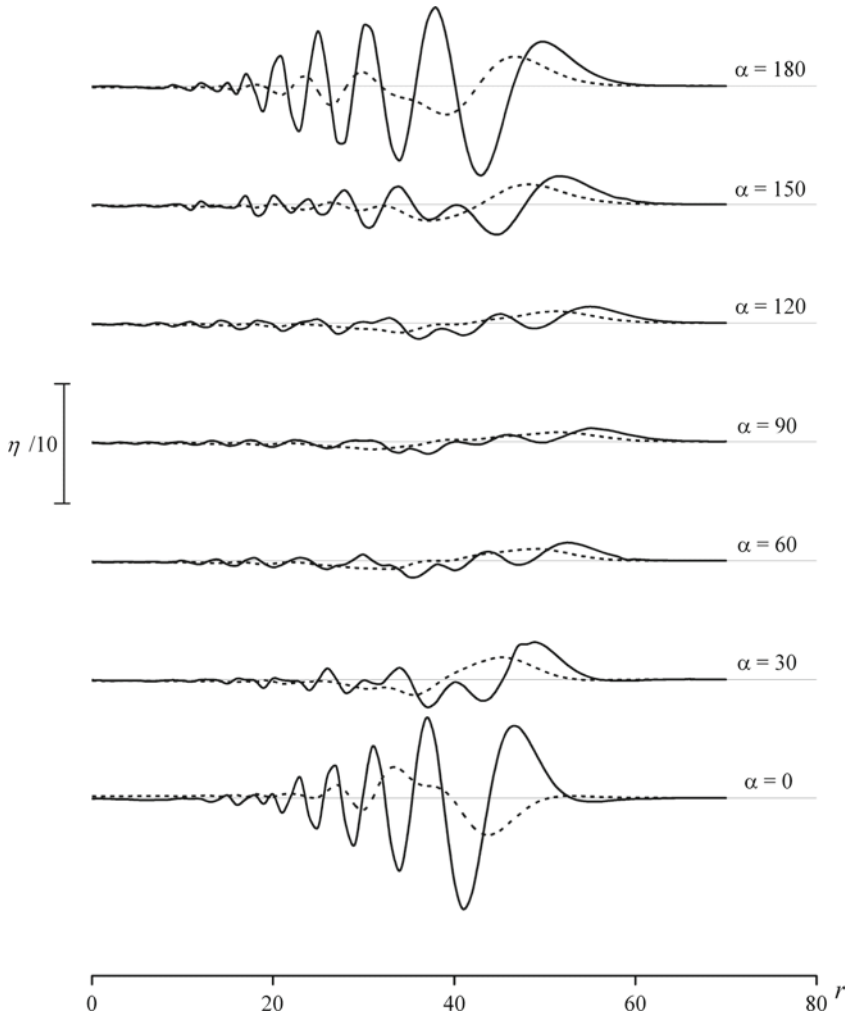


Fig. 3.31 Wave profiles (perturbation of free surface as function of radius r) for various azimuthal angles α at time moment $t = 50$. The parameters of the displacement are $a_1 = 7$, $a_2 = 3$, $b = 10$, $\tau = 1$ (solid line), $\tau = 10$ (dotted line)

depend essentially upon the direction of propagation. The energy directional diagrams are presented in Fig. 3.32. The energy values were normalized to the quantity $W_0 = \rho g b (\eta_1^2 a_1 + \eta_2^2 a_2) / 3$, the physical meaning of which consists in it representing the potential energy of the initial elevation of the water, similar in shape to the residual deformation of the ocean bottom. From Fig. 3.32 it is seen that in the case of symmetry ($a_1 = a_2 = 5$) no wave whatever is emitted in the “fault” direction (90° and 270°). This effect is evident from general arguments: perturbations that happen to be identical in shape, but differ in their signs of bottom deformations, cancel each

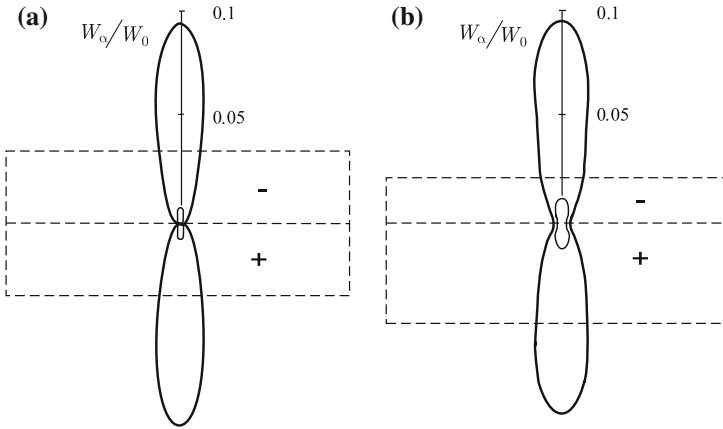


Fig. 3.32 Directional diagrams of energy emission for waves, caused by a *bottom* displacement alternating in sign. The shape and orientation of the source ($a_1 = a_2 = 5$ (a), $a_1 = 7, a_2 = 3$ (b)) are shown by the *dotted line*. Calculations are performed for $b = 10, \tau = 1$ (*thick line*), $\tau = 10$ (*thin line*)

other out along the symmetry axis. Such a symmetry is, naturally, quite improbable in nature. Nevertheless, for the nonsymmetric case ($a_1 = 7, a_2 = 3$), also, the prevalent part of wave energy is emitted perpendicularly to the “fault”, while the energy flux along the “fault” direction is nearly 40 times smaller. An increase of the duration of the bottom deformation reduces the energy of the generated waves and weakens their directionality.

In conclusion it must be stressed that the characteristics of tsunami waves may depend essentially not only on the shape of the source and on the space distribution inside it of residual deformations of the ocean bottom, but also on how these deformations developed in time.

3.5 Calculation of the Initial Elevation at the Tsunami Source

As a rule, numerical models of tsunami waves, applied in practical calculations, are constructed on the basis of the theory of long waves, making use of the equations of hydrodynamics averaged along the vertical coordinate (see Sects. 3.1.2 and 6.2). The process of tsunami formation by an underwater earthquake is considered to be instantaneous. Therefore, the set of equations of the long-wave theory is resolved with initial conditions representing a certain displacement of the free water surface from the equilibrium position (the initial elevation), given a zero flow velocity field. The initial elevation is conventionally set equal to the vertical coseismic (residual) deformation of the oceanic bottom due to the underwater earthquake.

The conventional way of formulating initial conditions is widely applied in the numerical simulation of real events (e.g., Titov et al. 2003; Alasset et al. 2006; Zaytsev 2010; Popinet 2012), since it more or less adequately reconstructs the main mechanism of tsunami generation—the displacement of water by a bottom deformation. At the same time, the conventional approach to formulating initial conditions is far from being perfect owing to the following two reasons (Nosov and Kolesov 2009, 2011). First, at the moment when deformation of the bottom stops, the water surface deviation from the equilibrium position and the vertical residual deformation will not be equal to each other, even in the case of a flat horizontal bottom and an instantaneous deformation—which is a manifestation of the “smoothing effect” of a layer of water. Second, in the case of an inclined bottom horizontal deformation components also lead to a displacement of water and, consequently, contribute to the initial elevation. The significance of the contribution of horizontal components is demonstrated in Sect. 2.4 by numerous examples of real events.

The existence of a “smoothing effect” is explained as follows. From the analytical solution of the problem of tsunami generation in a basin of constant depth by small vertical bottom deformations (3.48) it follows that the spatial spectrum of the water surface displacement is modulated by the rapidly decaying function $1/\cosh(kH)$, where k is the wavenumber. Consequently, movements of the bottom cannot create surface perturbations of a wavelength $\lambda < H$. Therefore, a direct transfer of bottom deformations to the water surface leads to artificial saturation of the tsunami spectrum with shortwave components that are actually nonexistent. For adequate reproduction of these nonexistent shortwave components in numerical models a nonrational reduction of the steps in space and time is required, which leads to an increase of the computation time. Consequently, taking the smoothing effect into account not only permits to avoid errors in calculating the initial elevation, but also helps to enhance the efficiency of numerical models.

The idea of the smoothing influence of a water layer was first put forward by Kajiura even before the era of numerical tsunami simulation (Kajiura 1963). Different versions of initial elevation smoothing were applied in numerical tsunami simulation or were analyzed theoretically by different scientific groups (e.g., Tinti et al. 1999; Tanioka and Seno 2001; Rabinovich et al. 2008; Saito and Furumura 2009; Nosov and Kolesov 2009, 2011; Fine and Kulikov 2011; Nosov and Sementsov 2014). The contribution of horizontal deformations of an inclined bottom to a tsunami wave was also dealt with in a whole number of studies (e.g., Iwasaki 1982; Tanioka and Satake 1996a; Nosov et al. 2011, 2014a; Bolshakova et al. 2015).

Before the end of the twentieth century an earthquake source was in most cases represented simplistically as a rectangular fault area with a uniform slip distribution. Such a simplified representation permitted to obtain an approximate estimate of the bottom deformation at the tsunami source, but no precise calculations were intended. During the past decade a breakthrough took place in the reconstruction of the slip structure at an earthquake source (see Sect. 2.4). Detailed data on the slip structure already permit to hope for accurate calculation of the vector field of the bottom deformation at the tsunami source. In this connection, taking into account the contribution of horizontal deformations and the smoothing effect becomes at present

an urgent necessity. Neglecting these factors will invariably result in errors in the determination of tsunami amplitudes amounting to ten percent and even more.

In this section we shall present a modified method for formulating the initial conditions, which, if the assumption of the bottom deformation being instantaneous is retained, takes into account not only the vertical, but also horizontal deformations of an uneven bottom as well as the “smoothing effect” of a water layer.

We shall consider a uniform incompressible layer of water of variable depth H . Consider the origin of the reference system, $0xyz$, to be situated on the unperturbed free water surface. Let the $0z$ -axis be directed vertically upward, and the $0x$ and $0y$ axes horizontally. Before the earthquake the position of the bottom is determined by the formula $z_b = -H(x, y)$. After the earthquake the bottom is displaced to a new position $z_b = -H(x, y) + \eta(x, y)$, where $\eta(x, y)$ is the residual displacement of the bottom surface ($|\eta| \ll H$). We recall that function η is related to the components of the oceanic bottom deformation vector $D = (D_x, D_y, D_z)$ and to the distribution of depths H by the following formula (see Sect. 2.3):

$$\eta = D_x \frac{\partial H}{\partial x} + D_y \frac{\partial H}{\partial y} + D_z. \quad (3.125)$$

In principle, calculation of the initial elevation can be based on the solution of the three-dimensional problem of gravitational waves in a liquid with account of all three components of the oceanic bottom deformation vector and of the distribution of depths in the vicinity of the source. This problem can be considered within the framework of the linear potential theory formulated as follows (see Sect. 3.1.3):

$$\Delta F = 0, \quad (3.126)$$

$$\frac{\partial^2 F}{\partial t^2} = -g \frac{\partial F}{\partial z}, \quad z = 0, \quad (3.127)$$

$$\frac{\partial F}{\partial \mathbf{n}} = (\mathbf{v}_b, \mathbf{n}) \quad \text{for } z = -H(x, y). \quad (3.128)$$

where F is the flow velocity potential, \mathbf{n} is the normal to the bottom surface, and \mathbf{v}_b is the velocity vector of the bottom. The sought initial elevation is calculated via the potential by the formula,

$$\xi(x, y, \tau) = -\frac{1}{g} \left. \frac{\partial F}{\partial t} \right|_{(x, y, 0, \tau)},$$

where τ is the bottom deformation duration.

In the case, when the deformation can be considered instantaneous, the dynamic problem (3.126)–(3.128) is readily reduced to the more simple static one (Nosov and Kolesov 2009, 2011). Integrating equations (3.126)–(3.128) over time from 0 up to

τ , we obtain the following set of equations:

$$\Delta \Phi = 0, \quad (3.129)$$

$$\Phi = 0, \quad z = 0, \quad (3.130)$$

$$\frac{\partial \Phi}{\partial \mathbf{n}} = (\mathbf{D}, \mathbf{n}), \quad z = -H(x, y), \quad (3.131)$$

$$\Phi \equiv \int_0^\tau F dt,$$

where Φ is the displacement potential. The sought initial elevation is calculated by the displacement potential as follows:

$$\xi_0 = \left. \frac{\partial \Phi}{\partial z} \right|_{z=0}. \quad (3.132)$$

Equation (3.129) and the boundary condition at the bottom, (3.131), are straightforward and evident consequences of equations (3.126) and (3.128). The boundary condition on the surface, (3.130), is derived from formula (3.127), if the process of bottom deformation is assumed to be transient. To obtain formula (3.130) we choose as the spatial and time scales the oceanic depth H and the deformation duration τ , respectively, upon which we pass in expression (3.127) to the dimensionless variables $t^* = t/\tau$ and $z^* = z/H$,

$$\frac{\partial^2 F}{\partial t^{*2}} = -\frac{g \tau^2}{H} \frac{\partial F}{\partial z^*}. \quad (3.133)$$

In the case of an instantaneous deformation, $\tau = 0$, the right-hand part of expression (3.133) turns to zero. Taking into account the zero initial condition $\frac{\partial F}{\partial t} = -g\xi(x, y, 0) = 0$, we integrate formula (3.127) twice over time with the zero right-hand part. As a result, we arrive at the expression $F = C$, where C is the integration constant. In accordance with the definition of the displacement potential it assumes the value $\Phi = C \cdot \tau$ on the surface $z = 0$. The sought initial elevation is determined as the derivative of the potential Φ with respect to the vertical coordinate. Consequently, the displacement potential can be redefined (by subtraction of the constant $C \cdot \tau$), so as to have it assume zero values on the surface: $\Phi = 0$.

Usually, to justify considering the process of tsunami generation by an earthquake to be instantaneous one takes advantage of the condition $\tau \ll R/\sqrt{gH}$, where R is the horizontal dimension of the tsunami source. This condition is always fulfilled quite well. But from formula (3.133) it is seen that the ‘‘instantaneity condition’’ should actually be more rigorous: $\tau \ll \sqrt{H/g}$. And even if, instead of the fault rupture

duration at the earthquake source, the quantity τ is understood to be the significantly shorter rise time, in this case, also, the “instantaneity condition” $\tau \ll \sqrt{H/g}$ will often be violated. In this connection, the solution of the problem (3.129)–(3.131) is to be considered the next approximation which is doubtless more accurate than the traditional transfer of bottom deformations to the water surface, but is nevertheless inferior in precision to the solution of the complete dynamic problem (3.126)–(3.128).

To determine the initial elevation at a real tsunami source the problem (3.129)–(3.131) can be resolved by numerical methods. Numerical calculation is also performed within a limited region of space. Therefore, the formulation is required of boundary conditions for the external boundary of the calculation region, which runs through the ocean. The external boundary must evidently be chosen to be at such a distance from the tsunami source, where displacement of the free surface as well as bottom deformation can be neglected. In this case the Dirichlet boundary condition, that is easily realized, can be established on the external boundary: $\Phi = 0$.

For testing numerical models it may turn out to be expedient to use analytical solutions of problem (3.129)–(3.131) on a flat horizontal bottom and on a flat inclined bottom, to be dealt with below.

For a basin with a flat *horizontal* bottom ($H = \text{const}$) and bottom deformation of a rectangular form of dimensions $2a \times 2b$ and amplitude η_0

$$\eta(x, y) = \eta_0 [\theta(x+a) - \theta(x-a)] [\theta(y+b) - \theta(y-b)], \quad (3.134)$$

where θ is the Heaviside step function, problem (3.129)–(3.131) has the following analytical solution (Nosov and Kolesov 2011):

$$\xi(x, y) = \frac{4\eta_0}{\pi^2} \int_0^{+\infty} dm \int_0^{+\infty} dn \frac{\cos(mx) \cos(ny) \sin(ma) \sin(nb)}{m n \cosh(kH)}, \quad (3.135)$$

$$k^2 = m^2 + n^2,$$

where m and n are components of the vector \mathbf{k} . The integral in formula (3.135) is readily calculated numerically. The integrand function decreases rapidly as the quantities m and n increase, therefore integration can be performed within finite limits.

An example of calculation of the initial elevation by formula (3.135) is presented in Fig. 3.33. It is seen that as compared to the bottom deformation of rectangular form the surface elevation is essentially more smooth. Here, the water volume, displaced by the bottom deformation, is equal to the volume occupied by the initial elevation.

The solution of the equivalent two-dimensional problem in the Oxz plane has the following form (the analog of formula (3.135)):

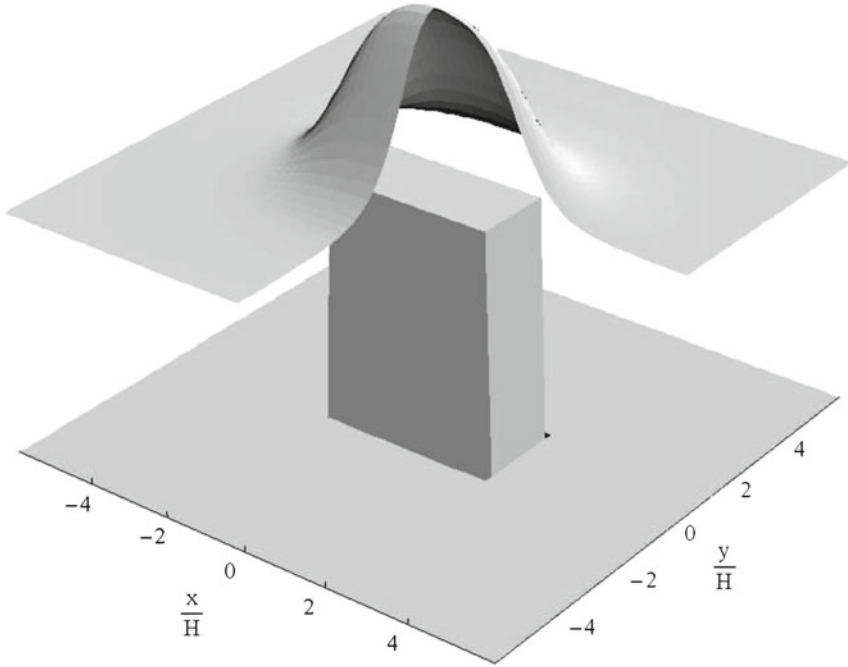


Fig. 3.33 Free surface disturbance caused by residual *bottom* deformation of rectangular shape with parameters $a = 2H$, $b = H$. Calculations are performed using formula (3.135). The surface disturbance and *bottom* deformation are shown on the same scale

$$\xi(x) = \frac{2\eta_0}{\pi} \int_0^{+\infty} dk \frac{\cos(kx) \sin(ka)}{k \operatorname{ch}(kH)}. \tag{3.136}$$

Formula (3.136) describes the free surface displacement caused by a bottom deformation exhibiting a rectangular spatial distribution $\eta(x) = \eta_0 [\theta(x+a) - \theta(x-a)]$ in a basin with a flat horizontal bottom.

For resolving the two-dimensional problem in a basin with a flat *inclined* bottom (see Fig. 3.34) we make use of cylindrical coordinates, in which equations (3.129)–(3.132) assume the form below.

$$r^2 \frac{\partial^2 \Phi}{\partial r^2} + r \frac{\partial \Phi}{\partial r} + \frac{\partial^2 \Phi}{\partial \varphi^2} = 0, \tag{3.137}$$

$$\Phi = 0, \quad \text{for } \varphi = 0, \tag{3.138}$$

$$\frac{1}{r} \frac{\partial \Phi}{\partial \varphi} = (D, n), \quad \text{for } \varphi = -\alpha, \tag{3.139}$$

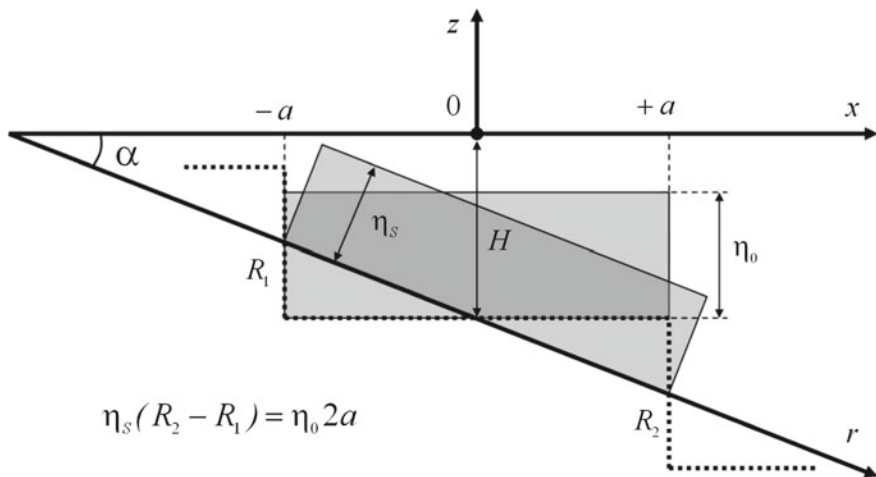


Fig. 3.34 Formulation of 2D problem. Equivalence of sources on inclined and horizontal bottom

$$\xi(r) = \frac{1}{r} \frac{\partial \Phi}{\partial \varphi} \quad \text{for } \varphi = 0, \tag{3.140}$$

where α is the inclination angle of the bottom, $n = (\sin \alpha, \cos \alpha)$ is the normal to the bottom surface.

Like in the case of a horizontal bottom, we take advantage of a rectangular spatial distribution of residual deformations (see Fig. 3.34). The right-hand part of formula (3.139) for such a source has the form,

$$(D, n) = \eta_s [\theta(r - R_1) - \theta(r - R_2)], \tag{3.141}$$

where η_s is the deformation amplitude in a direction perpendicular to its surface, R_1 and R_2 are the respective positions of the left and right boundaries of the source.

Let us introduce a dimensionless space variable $r^* = r/L$, where L is a certain length scale. The structure of equation (3.137) is such that transition to the dimensionless variable does not change the form of the equation,

$$r^{*2} \frac{\partial^2 \Phi}{\partial r^{*2}} + r^* \frac{\partial \Phi}{\partial r^*} + \frac{\partial^2 \Phi}{\partial \varphi^2} = 0.$$

Evidently, the boundary condition on the surface, (3.138), also remains unchanged. As a result of transition to the dimensionless variable only the forms of expressions (3.139), (3.140) change. The right-hand part of the boundary condition on the bottom, describing the source (bottom deformation), now turn out to be multiplied by the quantity L :

$$\frac{1}{r^*} \frac{\partial \Phi}{\partial \varphi} = L \cdot (D, n), \quad \text{for } \varphi = -\alpha.$$

At the same time the displacement sought of the free surface must now be divided by the quantity L :

$$\xi(r) = \frac{1}{L \cdot r^*} \frac{\partial \Phi}{\partial \varphi} \quad \text{for } \varphi = 0.$$

Obviously, these two actions (multiplication and division by L), that mutually compensate each other, may just not be performed at all.

Thus, an interesting feature peculiar to the problem considered consists in the fact that transition to the dimensionless variable r^* does not alter the form of the equations. For reasons of convenience and definiteness we shall further set $L = 1$ m.

We shall further consider equations (3.137)–(3.140), assuming them to be written in dimensionless coordinates (r , R_1 , and R_2 are dimensionless quantities). Here and below we shall drop the symbol “*”.

The analytical solution of problem (3.137)–(3.139) is constructed by the method of separation of variables. The resulting formula, describing the initial elevation generated on the water surface in a basin with a flat inclined bottom in the case of a rectangular bottom deformation (3.141), has the following form (Nosov and Sementsov 2014):

$$\xi(r) = \frac{\eta_S}{\pi r} \int_0^{+\infty} \frac{R_2 \cos q\delta_2 - R_1 \cos q\delta_1 - qR_2 \sin q\delta_2 + qR_1 \sin q\delta_1}{(1 + q^2) \cosh(q\alpha)} dq, \quad (3.142)$$

where $\delta_1 = \ln(r/R_1)$, $\delta_2 = \ln(r/R_2)$. The integral (3.142) can be readily calculated numerically. Owing to the rapid exponential decay of the integrand function numerical integration can be performed up to a finite limit.

Examples of calculation of the shapes of initial elevations generated on a water surface by sources on an inclined bottom (solid lines) and equivalent sources on a horizontal bottom (dotted lines) are presented in Fig. 3.35. The calculation was performed for $t g \alpha = 0.3$ and two depths at the source center: 500 m and 2000 m. The gray rectangles indicate the positions of the sources. The size of the source (half-width $a = 1000$ m) approximately corresponds to the typical grid increment in numerical tsunami simulation (1 ang.min.). As equivalent sources on an inclined or horizontal bottom we intend sources, involving a rectangular space distribution of residual deformation, the depths at the centers of which are identical and the parameters of which are related as follows: $2a = (R_2 - R_1) \cos \alpha$ and $\eta_S = \eta_0 \cos \alpha$. Note that these relationships correspond to the physically reasonable requirement that the displaced volumes be identical.

In all cases, the initial elevations generated by rectangular bottom deformations are seen from Fig. 3.35 to have smooth forms. The greater the depth in the vicinity of the source the smoother becomes the initial elevation. If the calculation is performed with the horizontal bottom model, then the initial elevation is symmetric with respect

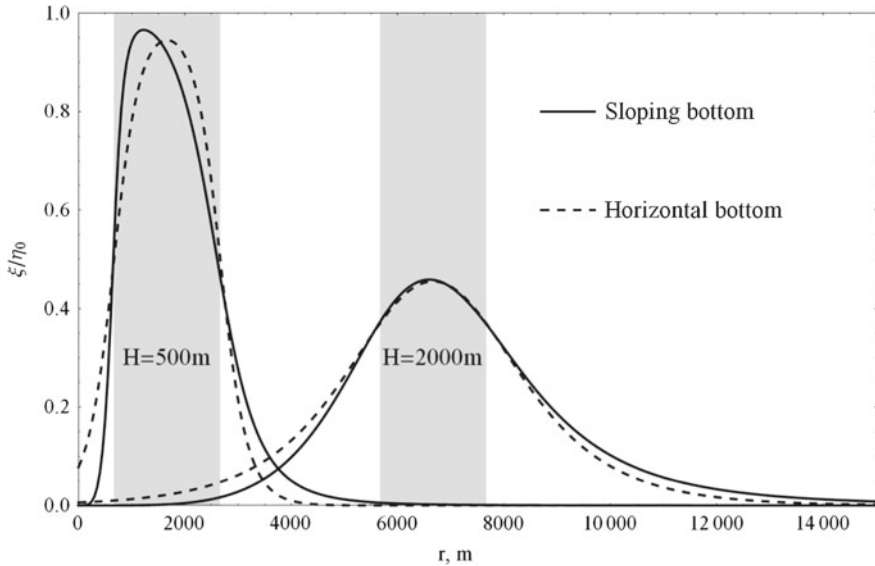


Fig. 3.35 Comparison of initial elevation forms generated on the water surface by source on inclined bottom (solid line) and by equivalent source on horizontal bottom (dotted line). The calculation is performed by formulae (3.136) and (3.142) for $a = 1000$ m, $tg\alpha = 0.3$ in the case of two sources situated at depths $H = 500$ m and $H = 2000$ m. The positions of the sources are shown by gray rectangles

to the source center. In the case of the sloping bottom model the initial elevation is always asymmetric. In the region where the depth is smaller (on the left) the drop in the curve is sharper than in the deepwater region. At small source depths the difference between the inclined and horizontal bottom models is quite noticeable. The difference becomes less significant as the source depth increases.

The maximum difference between the horizontal and inclined bottom models should obviously be observed in the case of significant bottom inclinations. Therefore, the choice of the maximum value of $tg\alpha$ requires justification. In Fig. 3.36 an example is presented of the distribution of bottom inclinations in the region the 2011 Tohoku-Oki tsunami source. The bottom inclination was calculated from the data in the numerical atlas GEBCO (<http://www.gebco.net/>) in steps of 1 ang.min. as the absolute value of the depth gradient ($tg\alpha = |grad H|$). Only those points were processed, the depth at which exceeded 10 m. From Fig. 3.36 the bottom inclinations are seen, as a rule, to be limited by a value of 0.2, and only in extremely rare cases they amount to 0.3.

Thus, the examples of calculations presented in Fig. 3.35 correspond to slopes of maximum inclination. Even in this case the difference between the horizontal and inclined bottom models is seen not to be critical (Nosov and Sementsov 2014). Consequently, calculation of the initial elevation at real tsunami sources must rely on analytical solution of the three-dimensional problem on a flat horizontal bottom. Such

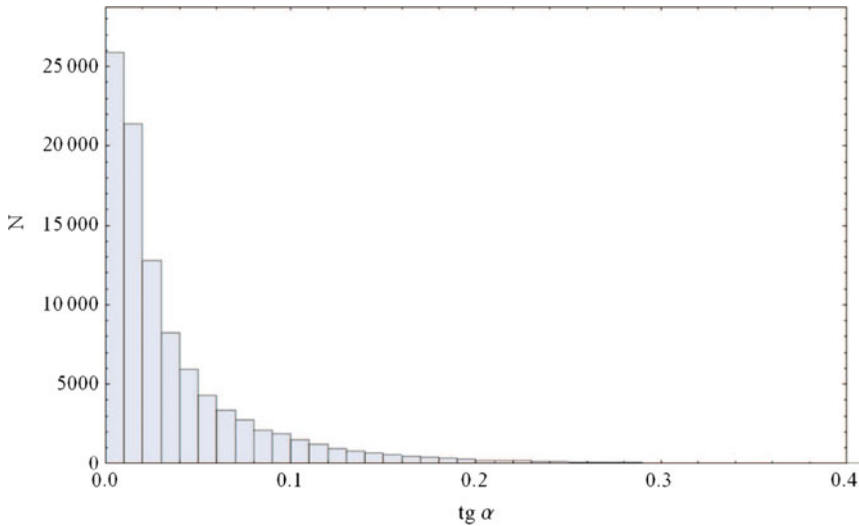


Fig. 3.36 Distribution of ocean *bottom* slopes in the region of the 2011 Tohoku tsunami source. The calculation was performed for the region 140–145 E, 35–42 N on the basis of data from the numerical atlas GEBCO

an approach (analytical–numerical algorithm) was proposed in Refs. (Nosov and Kolesov 2011; Nosov and Sementsov 2014), and it represents a possible alternative to straightforward numerical solution of problem (3.129)–(3.131).

The analytical–numerical algorithm (ANA) is based on the application of formula (3.135) and of the superposition principle. ANA consists in the following: (1) the region of the tsunami source in a basin of variable depth is divided into identical rectangular subregions of fixed dimensions $2a \times 2b$; (2) each subregion is considered an independent elementary source characterized by a certain depth H and a certain bottom surface displacement amplitude η , calculated by formula (3.125); (3) elevation of the free surface, generated by the elementary source at the point with coordinates (x, y) with respect to its center, is calculated numerically by formula (3.135); (4) the final initial elevation is determined as the superposition of the contributions of all the elementary sources.

The perturbation created by an elementary source decays exponentially as the distance from its boundary increases: already at a distance of the order of three depths the perturbation becomes negligibly small. This fact justifies taking into account only the contributions of the elementary sources nearest to the point dealt with, which significantly facilitates the numerical calculation procedure.

Figure 3.37a presents function η that describes coseismic deformation of the oceanic bottom surface at the 2011 Tohoku-Oki tsunami source. The calculation of function η was performed using formula (3.125). The coseismic deformation vector field was calculated from data on the slip distribution obtained by Gavin Hayes (Hayes 2011). Figure 3.37b shows the respective initial elevation of the water surface

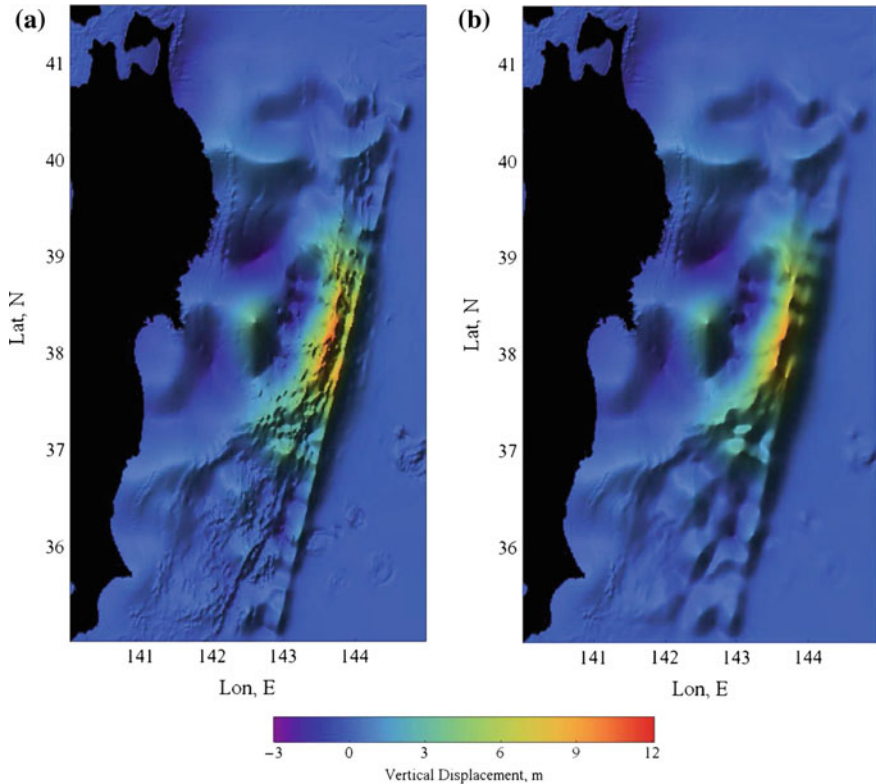


Fig. 3.37 The 2011 Tohoku-Oki tsunami source: coseismic ocean bottom deformation (a) and initial elevation of water surface (b), obtained applying the analytical–numerical algorithm

(function ξ), obtained with the aid of the analytical–numerical algorithm described above. It is seen that far from the coast, where the ocean depths are significant, the structure of the initial elevation is essentially more smooth than the structure of the coseismic bottom deformation. At small depths the difference between functions ξ and η is practically not noticeable. Owing to the size of the 2011 Tohoku-Oki tsunami source being many times larger than the ocean depth the difference between functions ξ and η is not really significant. Actually, this difference represents a “fine structure”, namely, shortwave perturbations that are peculiar to function η , but are absent in function ξ . The negative role of such shortwave perturbations, that, as we recall, are actually nonexistent, were already discussed at the beginning of this section.

Manifestations of the smoothing effect may be more impressive in those cases, when the size of the tsunami source and the ocean depth turn out to be commensurable. A typical example, here, is presented by the tsunamigenic earthquake that took place on the Central Kuril Islands on January 13, 2007. The tsunami source was related to the deepwater Kuril–Kamchatka trench and at the same time had an insignificant

width (Fig. 3.38a). The amplitude of the vertical bottom deformation, calculated from the slip distribution, reconstructed by Ji C. (2007), amounted to the following: uplift—1.8 m, subsidence—7.7 m. The initial elevation calculated applying ANA (Fig. 3.38b) differs quite strongly from the coseismic deformation. The deviation of the water surface at the initial elevation turns out to be nearly two times smaller than the vertical bottom deformation amplitude (uplift—0.9 m, subsidence—4.6 m). Most likely, in this case neglecting the “smoothing effect” leads to overestimation of the tsunami wave amplitude nearly by a factor of two.

In conclusion we note that the initial elevation calculated from the solution of problem (3.129)–(3.131) is, naturally, free from small-scale spatial inhomogeneities, which may be peculiar to coseismic bottom deformation, but anyhow it involves components of wavelength $\lambda \gtrsim H$. Such waves, unlike long waves ($\lambda \gg H$), are subject to phase dispersion, and, consequently, their propagation, especially over transoceanic distances, cannot be described adequately by the theory of long waves.

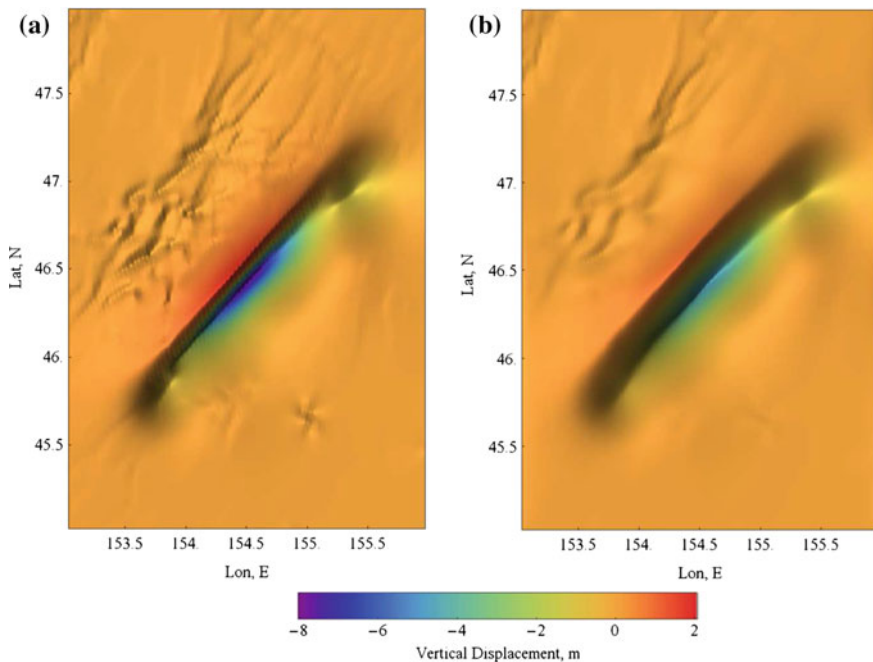


Fig. 3.38 The 2007 Central Kuril Islands tsunami source: coseismic *bottom* deformation (a) and initial elevation of water surface (b), obtained applying the analytical–numerical algorithm

3.6 Residual Hydrodynamic Fields that Accompany the Generation of a Tsunami by an Earthquake

In this section we shall deal with horizontal movements of water layers that accompany the generation of a tsunami by an earthquake in a rotating ocean. The spatial structure of the potential and eddy residual fields will be analyzed within the framework of the linear theory of long waves based on the analytical solution of the model axially symmetrical problem for an ocean of constant depth. Estimates are obtained for the horizontal displacements of particles of water, for the eddy flow velocity and for the geostrophic vortex energy in the case of conditions peculiar to real tsunami sources. Features are examined that are peculiar to residual fields due to stable stratification. Static and dynamic numerical models are described that permit to calculate the potential residual field and its evolution for real events. The field of residual horizontal movements of water particles is calculated and analyzed for the catastrophic earthquake that occurred on March 11, 2011, at the coast of Japan.

3.6.1 Definition of Concepts

The main mechanism underlying the origination of tsunami waves consists in the displacement of water by residual (coseismic) deformations of the oceanic bottom, caused by strong submarine earthquakes. In the case of very strong tsunamigenic earthquakes, such as, for example, the earthquakes that occurred at the coast of Sumatra on December 26, 2004 or Japan on March 11, 2011 the volume occupied by the displaced water may even amount to $\sim 100 \text{ km}^3$ (Grilli et al. 2007; Bolshakova and Nosov 2011; Nosov et al. 2014a; Bolshakova et al. 2015). Gravity leads to the displaced volume being distributed in the ocean over a region adjacent to the source of the tsunami. This process is accompanied by a “residual” displacement of water particles in a horizontal direction from their initial position. At the same time the Coriolis force gives rise to a “residual” geostrophic vortex. Figuratively speaking, a tsunamigenic earthquake leaves two traces in the ocean: a potential trace (of the displacement of water particles) and an eddy one. We shall further call such displacements of water particles and the geostrophic vortex *potential and eddy residual hydrodynamic fields* (Nosov et al. 2014a). We note that these fields are only conventionally residual, since they actually exist against the background of other oceanic currents, and, besides, the eddy field must slowly attenuate owing to the influence of dissipative processes.

The first analytical works devoted to the formation of eddy fields at the sources of tsunamis appeared more than 30 years ago (Dotsenko 1982, 1999; Voit et al. 1986; Bobrovich 1990; Pelinovsky 1996; Ingel 1998; Dotsenko and Shokin 2001). But the potential residual field, which seems more promising from the point of view of its revelation in nature, was, for some strange circumstances, left without any attention up to recent years (Nosov et al. 2011, 2014a; Nosov and Nurislamova 2012, 2013).

At present decisions to announce a tsunami warning are based on a magnitude–geographical criterion (UNESCO/IOC 2009; Poplavskii et al 2009). The strong dependence of the tsunami parameters on the tsunami source mechanism and its depth, on the depth of the ocean and on the tectonic peculiarities of the region render this criterion insufficiently reliable (Gusiakov 2011; Bolshakova and Nosov 2011; Nosov et al. 2014a). In the case of one and the same magnitude the height of the tsunami run-up can vary tens of times. Therefore, in order to improve the prognosis additional information is always made use of: data from deepwater stations or onshore stations at sea level. Expansion of the pool of measured parameters should, doubtless, contribute to enhancement of the tsunami prognosis. Besides variations of the sea level (vertical movements of the water layer) estimation of the tsunami-genicity level of submarine earthquakes can take horizontal movements into account as well and, also, residual hydrodynamic fields. A remarkable property of the residual fields consists in their direct relation to the tsunami generation mechanism: the displacement of water by coseismic deformation of the oceanic bottom.

Owing to the horizontal scale of the phenomenon considered being significantly superior to the vertical one, the velocities of currents forming residual fields are practically independent of the vertical coordinate—the entire water layer is involved in the motion. And, moreover, the horizontal movements significantly exceed the vertical ones in amplitude (e.g., Lighthill 1978). Maybe, precisely these two properties will subsequently permit to effectively reveal residual fields against the background of other oceanic processes. It is important, here, to note that in the case of a stratified ocean residual fields may exhibit an inhomogeneous vertical structure (see Sect. 3.6.4).

At the present stage of development of oceanography residual fields can be registered in situ in several ways. First, to this end one can apply surface or subsurface drifters equipped with a system of satellite positioning or with accelerometers (Okal and Mac Ayeal 2006). We stress the importance of making use of precisely freely floating systems, following the movements of the water layer. Anchored GPS buoys, the use of which in the registration of tsunami (variations of the sea level) (e.g., Nagai 2010; Fujii et al. 2011) started recently, are evidently not suitable for measuring horizontal movements. Second, horizontal movements can be revealed with the aid of acoustic Doppler current profilers (ADCP), placed on the oceanic bottom (Mikada et al. 2006). And, finally, the picture of the residual field can be reconstructed by processing successive satellite high-resolution images (Etaya et al. 2005; Crocker et al. 2007).

3.6.2 Basic Mathematical Model for a Homogeneous Ocean

Consider a layer of incompressible liquid of variable depth H on the rotating Earth. We shall neglect the Earth's sphericity. We choose the origin of the rectangular reference system to be situated on the unperturbed water surface. The Oz -axis will be directed vertically upward, and the Ox and Oy axes will point to the east and north,

respectively. We shall base our mathematical model on equations of the linear theory of long waves that are extensively applied in describing tsunami waves in the open ocean (see Sect. 3.1.2),

$$\frac{\partial \xi}{\partial t} - \frac{\partial \eta}{\partial t} + \frac{\partial (uH)}{\partial x} + \frac{\partial (vH)}{\partial y} = 0, \quad (3.143)$$

$$\frac{\partial u}{\partial t} = -g \frac{\partial \xi}{\partial x} + fv, \quad (3.144)$$

$$\frac{\partial v}{\partial t} = -g \frac{\partial \xi}{\partial y} - fu, \quad (3.145)$$

where ξ is the displacement of the free water surface with respect to its equilibrium position, η is the displacement of the seafloor surface relative to its initial position, u and v are components of the horizontal velocity of the current along the Ox and Oy axes, respectively, g is the acceleration of gravity, f is the Coriolis parameter. We shall assume $f = \text{const}$ (the f-plane approximation) (Gill 1982).

Consider the surface of the bottom to be described at the initial moment of time by the equation $z_b = -H(x, y)$, and let the water layer be in a state of equilibrium $u = v = \xi = 0$. As the result of an earthquake the bottom is shifted to a new position $z_b = -H(x, y) + \eta_\infty(x, y)$, where $\eta_\infty(x, y)$ is the residual bottom deformation of small amplitude ($|\eta_\infty| \ll H$). Note that the smallness of the deformation amplitude means that the change in profile of the bottom can be neglected.

We shall represent the velocity field of the current initiated by deformation of the bottom as the superposition of a potential and an eddy field, (Nosov and Nurislamova 2012, 2013; Nosov et al. 2014b)

$$u = \frac{\partial \varphi}{\partial x} + \frac{\partial \psi}{\partial y}, \quad v = \frac{\partial \varphi}{\partial y} - \frac{\partial \psi}{\partial x}, \quad (3.146)$$

where φ is the velocity potential, ψ is the stream function. Using formulas (3.146) we rewrite the set (3.143)–(3.145) in terms of φ , ψ and ξ ,

$$\frac{\partial \xi}{\partial t} - \frac{\partial \eta}{\partial t} + H \Delta \varphi + \frac{\partial H}{\partial x} \frac{\partial \varphi}{\partial x} + \frac{\partial H}{\partial y} \frac{\partial \varphi}{\partial y} + \frac{\partial H}{\partial x} \frac{\partial \psi}{\partial y} - \frac{\partial H}{\partial y} \frac{\partial \psi}{\partial x} = 0, \quad (3.147)$$

$$\frac{\partial \psi}{\partial t} = f \varphi, \quad (3.148)$$

$$\frac{\partial \varphi}{\partial t} = -g \xi - f \psi. \quad (3.149)$$

Integrating equations (3.147) and (3.148) over time from $t = 0$ to $t = T$ with account of the zero initial conditions ($\xi_0 = 0$, $\eta_0 = 0$), we obtain

$$\xi_T - \eta_T + H\Delta\Phi_T + \frac{\partial H}{\partial x} \frac{\partial \Phi_T}{\partial x} + \frac{\partial H}{\partial y} \frac{\partial \Phi_T}{\partial y} + \int_0^T \left(\frac{\partial H}{\partial x} \frac{\partial \psi}{\partial y} - \frac{\partial H}{\partial y} \frac{\partial \psi}{\partial x} \right) dt = 0, \quad (3.150)$$

$$\psi_T = f \Phi_T, \quad (3.151)$$

where $\Phi_T = \int_0^T \varphi dt$ is the displacement potential, ψ_T is the stream function at $t = T$.

Consider deformation of the bottom to have come to an end by the moment of time $t = T$, and consider the tsunami waves to have left the region examined. From equation (3.150) it is seen that the existence of residual (i.e., stationary) fields is possible under the condition,

$$\frac{\partial H}{\partial x} \frac{\partial \psi}{\partial y} - \frac{\partial H}{\partial y} \frac{\partial \psi}{\partial x} = 0. \quad (3.152)$$

Condition (3.152) signifies that the velocity of the stationary eddy current is directed precisely along isobaths, i.e., the eddy current must be adapted to the bottom relief (Zyryanov 1995; Nosov et al. 2011). Note that in stationary conditions, when potential movements have stopped and eddy movements have steadied, Eq. (3.149) assumes the following form:

$$g \xi_T + f \psi_T = 0. \quad (3.153)$$

From formula (3.153) it is seen that the existence of a residual eddy field requires a nonzero displacement of the free surface.

3.6.3 The Properties of Residual Fields in the Case of a Homogeneous Ocean of Constant Depth: Analysis of Analytical Solutions

When the condition $H = const$ is fulfilled, problem (3.150), (3.151), (3.153) is significantly simplified. The nonstationary term in equation (3.150) automatically turns to zero, which provides for the absolute possibility of the existence of stationary fields.

To identify residual fields we set $T = \infty$ in Eqs. (3.150), (3.151), (3.153). As a result the set of equations assumes the following form:

$$\xi_\infty - \eta_\infty + H\Delta\Phi_\infty = 0, \quad (3.154)$$

$$\psi_\infty = f \Phi_\infty, \quad (3.155)$$

$$g \xi_\infty + f \psi_\infty = 0. \quad (3.156)$$

Excluding functions ψ_∞ and Φ_∞ from Eqs. (3.154)–(3.156) we arrive at the inhomogeneous Helmholtz equation (Nosov and Nurislamova 2012),

$$R_0^2 \Delta \xi_\infty - \xi_\infty = -\eta_\infty, \quad (3.157)$$

where $R_0^2 = gH/f^2$ is a squared barotropic Rossby radius of deformation.

We shall now set the residual deformation in the form of an axially symmetric elevation of the radius R and amplitude $\eta_{0 \max}$

$$\eta_0(r) = \eta_{0 \max} [1 - \theta(r - R)], \quad (3.158)$$

where θ is the Heaviside step function. We shall further pass in Eq. (3.157) to cylindrical coordinates and to the dimensionless variable $r^* = r/R$

$$\frac{\partial^2 \xi_\infty}{\partial r^{*2}} + \frac{1}{r^*} \frac{\partial \xi_\infty}{\partial r^*} - \mu_0^2 \xi_\infty = -\mu_0^2 \eta_\infty, \quad (3.159)$$

where $\mu_0^2 = R^2/R_0^2$ is the only dimensionless parameter of the problem that varies between 0 at the equator up to ~ 1 at high latitudes in the case of an extended source and shelf depths. A typical value of parameter $\mu_0 \sim 0.1$ (for $f \sim 10^{-4} \text{ s}^{-1}$, $R \sim 10^5 \text{ m}$, $H \sim 10^3 \text{ m}$). For presentation of the results we have chosen the range $10^{-3} < \mu_0 < 10^1$, within which the most interesting features of the solution manifest themselves.

The solution of equation (3.159) is expressed via the Infeld and Macdonald functions I_i and K_i , respectively, (Polyanin 2002),

$$\xi_\infty = \eta_{0 \max} \begin{cases} 1 - \mu_0 K_1(\mu_0) I_0(\mu_0 r^*), & 0 \leq r^* < 1, \\ \mu_0 K_0(\mu_0 r^*) I_1(\mu_0), & r^* \geq 1. \end{cases} \quad (3.160)$$

In Fig. 3.39 the form of function ξ_∞ , calculated by formula (3.160) for a typical value of $\mu_0 = 0.1$ is presented. Function ξ_∞ reaches a maximum at the source center and remains practically unchanged right up to its boundary. In typical natural conditions the amplitude of the surface displacement in a geostrophic vortex amounts to $\sim 1\%$ of the bottom deformation amplitude. Outside the source the function ξ_∞ decreases monotonically, and at large radius values it decreases exponentially in accordance with the asymptotic of the Macdonald function: $\xi_\infty \sim \exp(-\mu_0 r^*)/\sqrt{r^*}$.

Knowing function ξ_∞ , we find from Eqs. (3.155) and (3.156) functions Φ_∞ and ψ_∞ , which are used in determining the residual displacements of water particles in

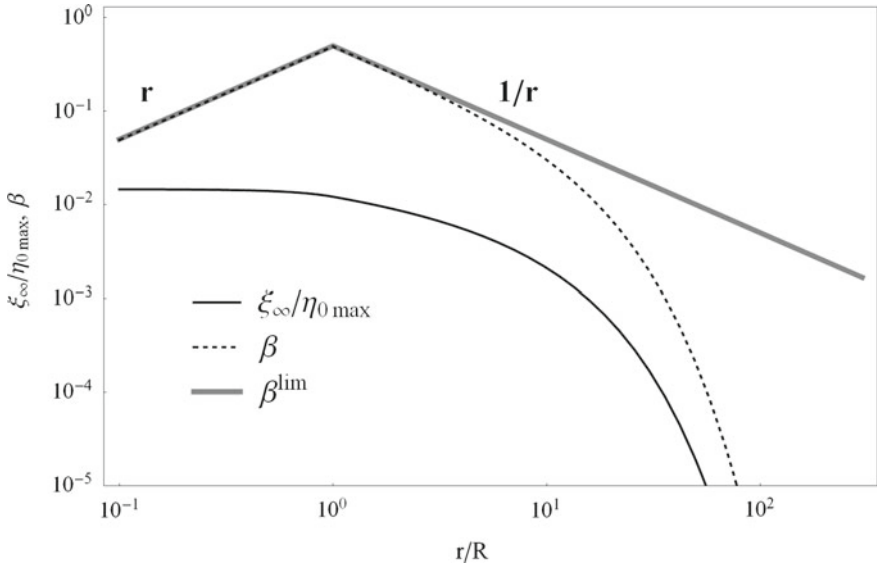


Fig. 3.39 Displacement of free water surface in a residual geostrophic vortex, ξ_∞ ; function β (at $\mu_0 = 0.1$) and its limit value β^{lim} (for $\mu_0 \rightarrow 0$)

the radial direction, D_∞ , and the velocity in the geostrophic vortex, v_∞

$$D_\infty = \frac{\partial \Phi_\infty}{\partial r} = \frac{\eta_{0 \text{ max}} R}{H} \beta, \tag{3.161}$$

$$v_\infty = -\frac{\partial \psi_\infty}{\partial r} = -\frac{\eta_{0 \text{ max}} R f}{H} \beta. \tag{3.162}$$

Function β , that determines the spatial structure of residual fields, is given by the following expression:

$$\beta = \begin{cases} I_1(\mu_0 r^*) K_1(\mu_0), & 0 \leq r^* < 1, \\ I_1(\mu_0) K_1(\mu_0 r^*), & r^* \geq 1. \end{cases} \tag{3.163}$$

The form of function β , calculated for a typical value of $\mu_0 = 0.1$, is presented in Fig. 3.39. Function β is always positive. This means that the uplift of the bottom, ($\eta_{0 \text{ max}} > 0$) is accompanied by a displacement of water particles in the positive direction—from the center of the source. In the northern hemisphere, where the Coriolis parameter $f > 0$, the bottom elevation gives rise to a vortex rotating in the negative direction (anticyclonic). Subsidence of the bottom ($\eta_{0 \text{ max}} < 0$) leads to an opposite result—to displacement of particles toward the center and to a cyclonic vortex.

At any values of parameter μ_0 function β turns to zero at the source center and reaches a maximum at its boundary. Outside the source function β decreases monotonically, and at large values of the radius—like function ξ_∞ —it decreases exponentially: $\beta \sim \exp(-\mu_0 r^*)/\sqrt{r^*}$. Hence follows an interesting conclusion: rotation of the Earth limits the region of manifestation of both the eddy and the potential fields. In other words, contrary to “common sense”, the displaced volume does not spread about the entire basin, but remains inside the region limited by the barotropic Rossby radius of deformation ($R_{0*} \equiv R_0/R = 1/\mu$). Outside this region residual displacements turn out to pertain to zero, which naturally does not revoke seesaw movements of water particles at any distance from the source in the case of propagating gravitational waves.

Tending the Coriolis force toward zero, we find the limit of function β

$$\beta^{\text{lim}}(r^*) \equiv \lim_{\mu_0 \rightarrow 0} \beta(r^*, \mu_0) = 0.5 \begin{cases} r^*, & 0 \leq r^* < 1, \\ 1/r^*, & r^* \geq 1. \end{cases} \quad (3.164)$$

The limit function β^{lim} is shown in Fig. 3.39 by the solid gray line. It is seen that in typical natural conditions ($\mu_0 = 0.1$) rotation of the Earth affects the potential field weakly right up to distances of the order of R_0

$$\beta(r^*, \mu_0) \approx \beta^{\text{lim}}(r^*) a r^* < 1/\mu_0.$$

From the displacement of the free surface and the velocity field we calculate the potential energy $W_p = \pi \rho g \int_0^\infty \xi^2 r dr$ and the kinetic energy $W_k = \pi H \rho \int_0^\infty v^2 r dr$ of the geostrophic vortex (ρ is the water density). Calculating the integrals analytically we obtain

$$W_p/W_0 = 1 - \mu_0^2 I_1^2(\mu_0) K_0^2(\mu_0) - 4I_1(\mu_0) K_1(\mu_0) + \mu_0^2 I_0^2(\mu_0) K_1^2(\mu_0), \quad (3.165)$$

$$W_k/W_0 = \mu_0 [I_1(\mu_0) K_2(\mu_0) - I_0(\mu_0) K_1(\mu_0)], \quad (3.166)$$

where $W_0 = 0.5\pi\rho g R^2 \eta_{0\text{max}}^2$ is the potential energy of the free surface perturbation, equivalent in form to the residual bottom deformation.

Figure 3.40 presents components of the geostrophic vortex energy versus parameter μ_0 . When μ_0 increases, the potential energy increases monotonically, tending to 1. The dependence of the kinetic energy is not monotonic, it exhibits a maximum at $\mu_0 \approx 1.587$. At small μ_0 values the potential energy is essentially smaller than the kinetic energy. At $\mu_0 \approx 0.956$ the two energies become equal. When $\mu_0 > 0.956$, the potential energy exceeds the kinetic energy. The total energy monotonically increases with parameter μ_0 , and tends toward 1. In typical conditions ($\mu_0 \sim 0.1$) $\sim 1\%$ of the initial elevation energy (the tsunami energy) is linked to the geostrophic vortex.

Figure 3.40 also shows the free surface displacement amplitude $\xi_{\infty\text{max}}/\eta_{0\text{max}} \equiv \xi_\infty(r^* = 0)/\eta_{0\text{max}} = 1 - \mu_0 K_1(\mu_0)$, and the quantity $\beta_{\text{max}} \equiv \beta(r^* = 1) =$

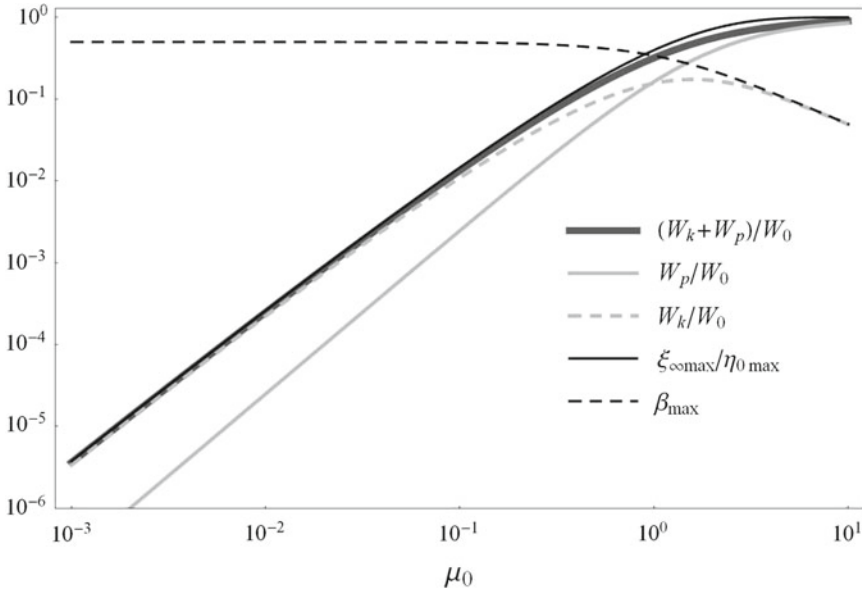


Fig. 3.40 Total ($W_k + W_p$), potential (W_p), and kinetic (W_k) energies of a residual geostrophic vortex; maximum value of free water surface displacement in a geostrophic vortex, $\xi_{\infty \max}$, and value of β_{\max} versus parameter μ_0

$I_1(\mu_0)K_1(\mu_0)$ versus parameter μ_0 . An increase in μ_0 leads to an increase of the free surface displacement $\xi_{\infty \max}/\eta_{0 \max}$, while the value of β_{\max} monotonically decreases. In typical natural conditions ($\mu_0 < 0.1$) one can assume with a good accuracy that $\beta_{\max} \approx 0.5$ and, instead of expressions (3.161)–(3.163), use for estimation of the maximal values of horizontal displacements of water particles approximate formulas: $D_{\infty \max} \approx 0.5\eta_{0 \max}R/H$, $v_{\infty \max} \approx 0.5\eta_{0 \max}Rf/H$. Substituting typical values of tsunami source parameters ($\eta_{0 \max} = 1$ m, $R = 10^5$ m, $H = 10^3$ m, $f = 10^{-4}$ s), into them, we obtain $D_{\infty \max} = 50$ m, $v_{\infty \max} = 0.005$ m/s.

Horizontal displacements of ~ 50 m can be registered in the ocean, for example, using drifters equipped with a Global Positioning System or an accelerometer (Okal and Mac Ayeal 2006). But the velocity at the geostrophic vortex, ~ 0.005 m/s, turns out to be so small, that it will not be so simple to reveal it against the background of other oceanic currents.

A separate comment is due to the situation of $\mu_0 > 1$, hypothetical for the conditions of our planet, when an eddy residual, instead of potential, field is dominant. This situation is interesting in that, when it is realized, the main part of energy transmitted to the water layer by the seismic source is not transferred to gravitational waves (tsunami), but is accumulated in the geostrophic vortex. However, for the realization of such exotic modes it is necessary that the horizontal dimension of the tsunami source, R be noticeably superior to the barotropic Rossby radius of deformation

R_0 , which is practically impossible in the conditions of our planet (typical values: $R \sim 10^5$ m (Pelinovsky 1996; Bolshakova and Nosov 2011), $R_0 \sim 10^6$ m (Gill 1982).

Let us point out the main results of this section. In the case of a homogeneous ocean and on the basis of a fully analytical solution of the model axially symmetric problem it has been established that residual horizontal displacements of water particles in typical natural conditions amount to ~ 50 m, the velocity of the current in the residual geostrophic vortex is ~ 0.005 m/s, the free surface displacement is $\sim 1\%$ of the bottom displacement, the vortex energy is $\sim 1\%$ of the tsunami energy, the dimensions of the vortex are of the order of the barotropic Rossby radius of deformation ($R_0 \sim 10^6$ m). Rotation of the Earth restricts the “spread” region of the displaced water volume over the tsunami source to the limits of the barotropic Rossby radius of deformation.

3.6.4 Features of Residual Fields Due to the Existence of Stable Stratification

In Sects. 3.6.2 and 3.6.3 we assumed the ocean to be homogeneous. A feature of the real ocean is stable stratification. In advance, we note that taking into account stratification not only leads to correction of the estimates obtained above, but also provides for the possible existence of a new sort of residual fields, namely, of stationary perturbations of the stratification structure at the tsunami source (Dotsenko and Shokin 2001; Nosov and Nurislamova 2013; Nosov et al. 2014a). Such perturbations can originate both as a result of the displacement of water by the residual bottom deformation and as a result of the intensification of the vertical exchange above the source of a submarine earthquake (Levin et al 1998; Nosov 1998a, b). In dealing with evolution of the stratification structure one must consider the baroclinic, instead of barotropic, Rossby radius of deformation as a horizontal scale. Contrary to the barotropic radius ($R_0 \sim 10^6$ m), the baroclinic radius ($R_1 \sim 10^4$ m (Gill 1982) is inferior to the dimension of the tsunami source ($R \sim 10^5$ m). Therefore, rotation of the Earth is to be expected to effectively bind perturbations of the stratification structure at the tsunami source and to prevent them from decaying into a series of internal waves, as described, for example, in the classical work (Hammack 1980). However, as it follows from the concluding part of this work, Joseph Hammack, doubtless, understood the importance of the “Coriolis effect” for the evolution of perturbations of the stratification structure.

As the simplest model of a stratified ocean we shall consider a two-layer liquid. Let the upper layer have a thickness H_1 and density ρ , and the lower layer a thickness H_2 and density $\rho + \delta\rho$ ($\delta\rho > 0$). To describe movements of the liquid we shall again apply equations of the linear theory of long waves, written with account of the assumption $\delta\rho/\rho \ll 1$:

$$\frac{\partial u_1}{\partial t} = -g \frac{\partial \xi_1}{\partial x} + f v_1, \quad \frac{\partial v_1}{\partial t} = -g \frac{\partial \xi_1}{\partial y} - f u_1, \quad (3.167)$$

$$\frac{\partial u_2}{\partial t} = -g \left(\frac{\partial \xi_1}{\partial x} + \frac{\delta \rho}{\rho} \frac{\partial \xi_2}{\partial x} \right) + f v_2, \quad \frac{\partial v_2}{\partial t} = -g \left(\frac{\partial \xi_1}{\partial y} + \frac{\delta \rho}{\rho} \frac{\partial \xi_2}{\partial y} \right) - f u_2, \quad (3.168)$$

$$\left(\frac{\partial u_1}{\partial x} + \frac{\partial v_1}{\partial y} \right) H_1 + \frac{\partial \xi_1}{\partial t} - \frac{\partial \xi_2}{\partial t} = 0, \quad \left(\frac{\partial u_2}{\partial x} + \frac{\partial v_2}{\partial y} \right) H_2 + \frac{\partial \xi_2}{\partial t} - \frac{\partial \eta}{\partial t} = 0, \quad (3.169)$$

where u_i and v_i are components of the horizontal current velocity of the i th layer ($i = 1, 2$) along axes Ox and Oy , respectively, ξ_i is the surface displacement of the i th layer from the equilibrium position. All other notations remain intact.

Like in the problem for a homogeneous ocean, we shall assume that before the earthquake the ocean was in a state of rest, $u_i = v_i = \xi_i = 0$, and that all movements in the ocean are initiated by small deformations of the bottom, $\eta_\infty(x, y)$ ($|\eta_\infty| \ll H_i$). The approach to the transformation of equations (3.167)–(3.169) is also similar to the approach adopted in Sects. 3.6.2 and 3.6.3. The velocity field is expressed via the velocity potential and the stream function, and the equations are integrated over time from 0 up to ∞ . As the result of simple transformations we arrive at a set of equations describing residual fields in a two-layer rotating liquid,

$$H_1 \Delta \Phi_{1\infty} = \xi_{2\infty} - \xi_{1\infty}, \quad H_2 \Delta \Phi_{2\infty} = \eta_\infty - \xi_{2\infty}, \quad (3.170)$$

$$\Delta \psi_{i\infty} = f \Delta \Phi_{i\infty}, \quad (3.171)$$

$$g \Delta \xi_{1\infty} + f \Delta \psi_{1\infty} = 0, \quad g \Delta \xi_{1\infty} + g \frac{\delta \rho}{\rho} \Delta \xi_{2\infty} + f \Delta \psi_{2\infty} = 0, \quad (3.172)$$

where $\xi_{i\infty}$ is the residual displacement of the i th surface, $\psi_{i\infty}$ is the stream function that describes the residual eddy field in the i th layer, $\Phi_{i\infty} \equiv \int_0^\infty \varphi_i dt$ is the displacement potential from which the vector is calculated of residual displacement of water particles in the horizontal direction in the i th layer: $\mathbf{D}_{i\infty} = \nabla \Phi_{i\infty}$.

Upon eliminating functions $\psi_{i\infty}$ and $\Phi_{i\infty}$, in Eqs. (3.170)–(3.172), we obtain

$$R_0^2 \Delta \xi_{1\infty} = (1 + \gamma)(\xi_{1\infty} - \xi_{2\infty}), \quad (3.173)$$

$$R_1^2 \Delta \xi_{2\infty} - \xi_{2\infty} = -\frac{1}{1 + \gamma}(\eta_\infty + \gamma \xi_{1\infty}), \quad (3.174)$$

where $R_0 = c_0/f$ and $R_1 = c_1/f$ are the respective barotropic and baroclinic Rossby radii of deformation, $c_0 = \sqrt{g(H_1 + H_2)}$ is the velocity of long gravitational waves in a homogeneous liquid, $c_1 = \sqrt{g \delta \rho H_1 H_2 / \rho (H_1 + H_2)}$ is the velocity of inter-

nal waves in a two-layer liquid (Gill 1982), $\gamma = H_2/H_1$ is the ratio between the thicknesses of the lower and upper layers.

Having determined from the set of equations (3.173) and (3.174) functions $\xi_{1\infty}$ and $\xi_{2\infty}$, it is also possible, using equations (3.171) and (3.172), to calculate all the remaining functions sought,

$$\psi_{1\infty} = -\frac{g}{f}\xi_{1\infty}, \quad \Phi_{1\infty} = -\frac{g}{f^2}\xi_{1\infty}, \quad (3.175)$$

$$\psi_{2\infty} = -\frac{g}{f}\left(\xi_{1\infty} + \frac{\delta\rho}{\rho}\xi_{2\infty}\right), \quad \Phi_{2\infty} = -\frac{g}{f^2}\left(\xi_{1\infty} + \frac{\delta\rho}{\rho}\xi_{2\infty}\right). \quad (3.176)$$

As a model of residual bottom deformation we shall consider axially symmetric elevation described by formula (3.158). But even in the case of cylindrical symmetry it is not possible to construct an analytical solution for the set (3.173)–(3.174). Therefore, we shall further resolve the problem approximately, assuming stratification to weakly affect the free surface displacement in a geostrophic vortex. To confirm the efficiency of such an assumption we approximate the Laplace operator in Eqs. (3.157), (3.173) and (3.174) applying the dimensional analysis ($\Delta \sim R^{-2}$). From the obtained resulting algebraic equations follows the estimate:

$$\frac{\xi_{\infty} - \xi_{1\infty}}{\xi_{\infty}} \sim \frac{R_1^2(R_0^2 + R^2(1 + \gamma))}{(R^2 + R_0^2)(R^2 + R_1^2) + R^2R_1^2\gamma}. \quad (3.177)$$

Substituting into formula (3.177) typical parameter values ($R = 10^5$ m, $R_0 = 10^6$ m, $R_1 = 10^4$ m, $\gamma = 10$), we obtain $(\xi_{\infty} - \xi_{1\infty})/\xi_{\infty} \sim 0.01$. Consequently, the existence of stratification indeed weakly affects free surface displacement in the geostrophic vortex.

Thus, to obtain an approximate solution we shall assume $\xi_{1\infty} = \xi_{\infty}$, where ξ_{∞} is a known function determined by formula (3.160). Equation (3.173) will no longer be necessary to obtain the solution. We write equation (3.174) in cylindrical dimensionless coordinates ($r_* = r/R$)

$$\frac{\partial^2 \xi_{2\infty}}{\partial r_*^2} + \frac{1}{r_*} \frac{\partial \xi_{2\infty}}{\partial r_*} - \mu_1^2 \xi_{2\infty} = -\frac{\mu_1^2}{1 + \gamma} (\eta_{\infty} + \gamma \xi_{1\infty}), \quad (3.178)$$

where $\mu_1 = R/R_1$. Equations (3.178) and (3.159) coincide in form. The solution of equation (3.178) has the following form:

$$\xi_{2\infty} = \frac{\eta_0 \max}{1 + \gamma} (\zeta_1 + \gamma \zeta_2), \quad (3.179)$$

$$\zeta_1 = \begin{cases} 1 - \mu_1 K_1(\mu_1) I_0(\mu_1 r^*), & 0 \leq r^* < 1, \\ \mu_1 K_0(\mu_1 r^*) I_1(\mu_1), & r^* \geq 1, \end{cases}$$

$$\zeta_2 = \begin{cases} 1 + \frac{\mu_0 \mu_1 (-\mu_1 I_0(r^* \mu_0) K_1(\mu_0) + \mu_0 I_0(r^* \mu_1) K_1(\mu_1))}{\mu_1^2 - \mu_0^2}, & 0 \leq r^* < 1, \\ \frac{\mu_0 \mu_1 (\mu_1 I_1(\mu_0) K_0(r^* \mu_0) - \mu_0 I_1(\mu_1) K_0(r^* \mu_1))}{\mu_1^2 - \mu_0^2}, & r^* \geq 1. \end{cases}$$

Upon determining functions $\xi_{i\infty}$, with the use of formulas (3.175), (3.176), we calculate functions $\Phi_{i\infty}$ and $\psi_{i\infty}$, from which we find the residual water particle displacement in the radial direction, $D_{i\infty} = \partial \Phi_i / \partial r$, and the eddy current velocity $v_{i\infty} = -\partial \psi_{i\infty} / \partial r$.

Owing to the adopted simplifying assumption ($\xi_{1\infty} = \xi_\infty$), the sought quantities in the upper layer correspond to the case of a homogeneous ocean, $D_{1\infty} = D_\infty$, $v_{1\infty} = v_\infty$ —they can be calculated from formulas (3.161) and (3.162).

The solution for the lower layer has the form,

$$D_{2\infty} = \frac{\eta_0 \max R}{H_1 + H_2} (\beta + \Delta\beta), \quad (3.180)$$

$$v_{2\infty} = -\frac{\eta_0 \max R f}{H_1 + H_2} (\beta + \Delta\beta), \quad (3.181)$$

$$\Delta\beta = \frac{\delta\rho}{\rho} \frac{(\sigma_1 + \gamma\sigma_2)}{(1 + \gamma)}, \quad (3.182)$$

$$\sigma_1 = \frac{\mu_1^2}{\mu_0^2} \begin{cases} I_1(\mu_1 r^*) K_1(\mu_1), & 0 \leq r^* < 1, \\ I_1(\mu_1) K_1(\mu_1 r^*), & r^* \geq 1. \end{cases}$$

$$\sigma_2 = \frac{\mu_1^2}{\mu_1^2 - \mu_0^2} \begin{cases} I_1(\mu_0 r^*) K_1(\mu_0) - I_1(\mu_1 r^*) K_1(\mu_1), & 0 \leq r^* < 1, \\ I_1(\mu_0) K_1(\mu_0 r^*) - I_1(\mu_1) K_1(\mu_1 r^*), & r^* \geq 1. \end{cases}$$

From formulas (3.180), (3.181) it is seen that the influence of stratification on the residual fields in the lower layer is described by function $\Delta\beta$.

The solution describing residual fields in the two-layer ocean depends on three dimensionless parameters: γ , μ_0 and μ_1 . These parameters are convenient for obtaining an analytical solution, but they are not independent. In particular, the following relation exists: $\mu_1^2 = \mu_0^2 (1 + \gamma)^2 / (\gamma \delta\rho / \rho)$. To present the results it is more convenient to use a set of independent parameters: $\delta\rho / \rho$, γ and μ_0 .

All calculations to be presented in this section will be based on the fixed quantity $\delta\rho / \rho = 0.003$, which is a typical value of the relative density jump for an ocean (Gill 1982). The ratio of layer thicknesses peculiar to a real ocean ($H_1 \sim 10^2$ m, $H_2 \sim 10^3$ m) determines the typical value of parameter $\gamma \sim 10$. However, the value

of γ can vary within a very wide range from $\gamma_{\min} \sim 10^{-3}$ (a thin benthic mixed layer) to $\gamma_{\max} \sim 10^3$ (a thin upper mixed layer). Like in Sect. 3.6.3, we vary parameter μ_0 within the following limits: $10^{-3} < \mu_0 < 10^1$.

Figure 3.41 presents the shape of the free water surface displacement $\xi_{1\infty}$ and the shape of the interface between layers displacement $\xi_{2\infty}$, calculated by formulas (3.160), (3.179) for typical parameters values $\mu_0 = 0.1$ and $\gamma = 10$. First of all, the fact draws attention that the displacement of the interface surface exceeds by an order of magnitude the displacement of a free surface, i.e., the binding effect is observed of a perturbation of the stratification structure that is due to rotation of the Earth.

The displacements of the free surface, $\xi_{1\infty}$, and of the interface between layers, $\xi_{2\infty}$, reach their respective maximum values $\xi_{1\max}$ and $\xi_{2\max}$ at the source center. Using formulas (3.160), (3.179), we calculate the ratio $\xi_{2\max}/\xi_{1\max}$ in dependence of parameters μ_0 and γ . The results of calculations are presented in Fig. 3.42. In all cases the amplitude of the interface between layers displacement, $\xi_{2\max}$, exceeds the free surface displacement amplitude $\xi_{1\max}$, and, in a number of cases, by several orders of magnitude. The ratio $\xi_{2\max}/\xi_{1\max}$ reaches maximum values at small values of the parameters μ_0 and γ . As the parameters μ_0 and γ increase the value of $\xi_{2\max}/\xi_{1\max}$ tends toward 1.

Figure 3.43 presents the shapes of functions β and $\Delta\beta$, which determine the spatial structure of residual fields. The calculation is performed by formulas (3.163), (3.182) for typical parameter values $\mu_0 = 0.1$, $\gamma = 10$. At all values of the argu-

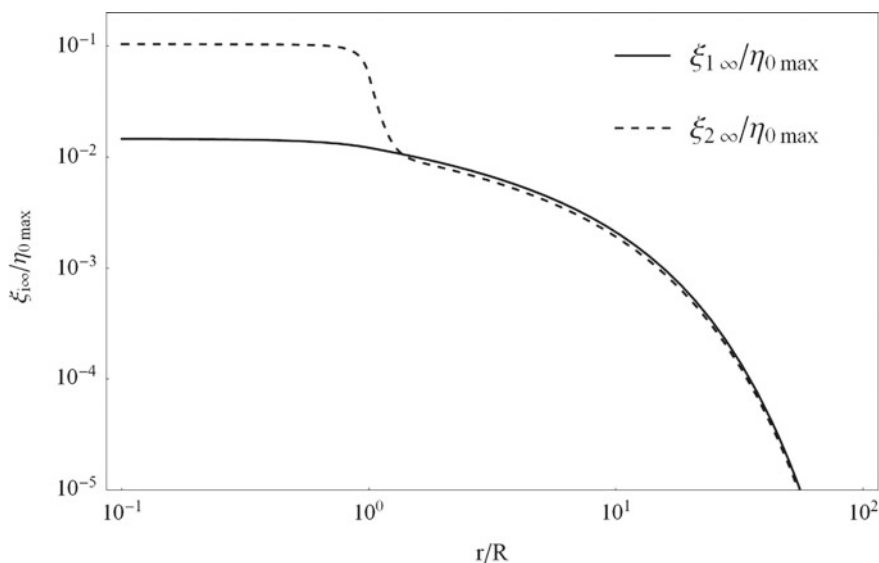


Fig. 3.41 Displacement of free water surface, $\xi_{1\infty}$, and displacement of interface between layers, $\xi_{2\infty}$, in residual geostrophic vortex. The calculation is performed by formulas (3.160) and (3.179) for $\mu_0 = 0.1$, $\gamma = 10$, $\delta\rho/\rho = 0.003$

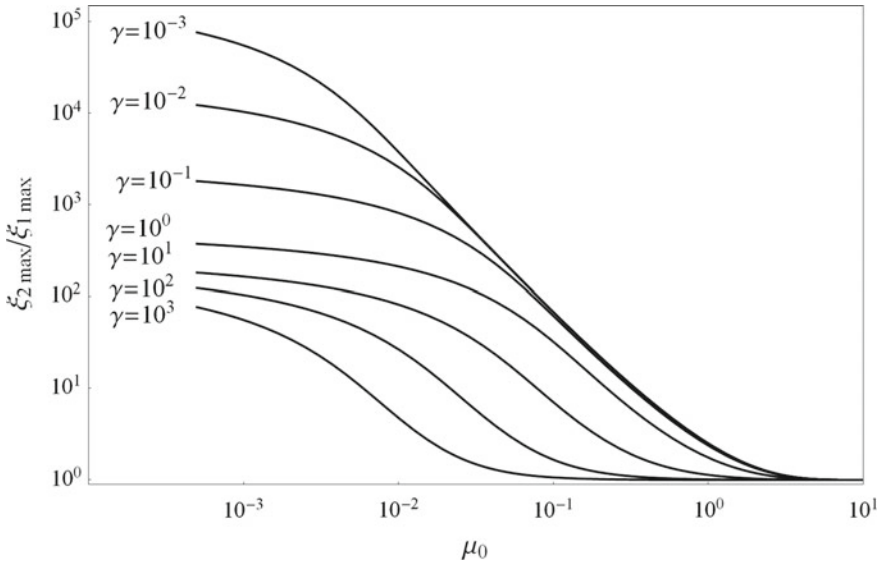


Fig. 3.42 Ratio of residual displacement amplitudes of interface between layers and of free surface, $\xi_{2 \max}$ and $\xi_{1 \max}$, respectively, versus parameter μ_0 . The calculation is performed for $\delta\rho/\rho = 0.003$ for different values of parameter γ (indicated in the figure)

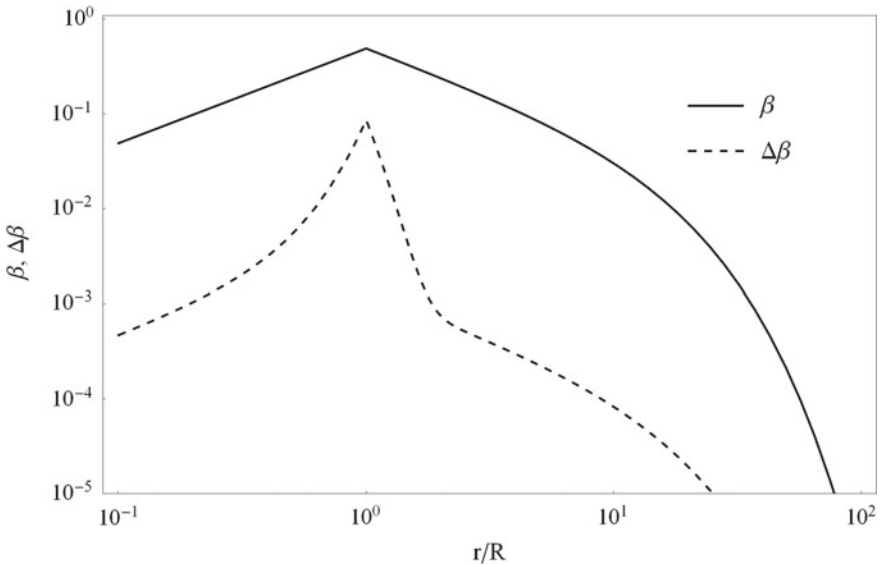


Fig. 3.43 Functions β and $\Delta\beta$, determining the spatial structure of residual fields in a two-layer ocean. The calculation is performed by formulas (3.163) and (3.182) for $\mu_0 = 0.1$, $\gamma = 10$, $\delta\rho/\rho = 0.003$

ment $\beta > 0$ and $\Delta\beta > 0$. This means that the addition $\Delta\beta$, which is due to the influence of stratification, always enhances the residual displacement of water particles and the velocity of the eddy current in the lower layer. We shall calculate the maximal values of these functions, β_{\max} and $\Delta\beta_{\max}$, which are reached at the source boundary ($r^* = 1$). Using formulas (3.163), (3.182) we determine the dependence of ratio $\Delta\beta_{\max}/\beta_{\max}$ on parameters μ_0 and γ . The results of calculations are shown in Fig. 3.44. It can be seen that the role of the correction due to stratification cannot, generally speaking, be characterized as negligible. In typical natural conditions ($\delta\rho/\rho = 0.003$, $\mu_0 = 0.1$) the contribution of the value of $\Delta\beta$ to the amplitude of residual particle displacements and to the velocity of the eddy current, is, of course, not dominant ($\gamma = 100$: $\Delta\beta_{\max}/\beta_{\max} \approx 0.058$; $\gamma = 10$: $\Delta\beta_{\max}/\beta_{\max} \approx 0.176$). However, in the case of a thin lower layer this contribution can become dominant. Thus, for example, for $\mu_0 = 0.1$ and $\gamma = 10^{-3}$ we have: $\Delta\beta_{\max}/\beta_{\max} \approx 18$.

Let us formulate the main results of this section. For a two-layer ocean it is shown, on the basis of the approximate analytical solution of a model axially symmetric problem, that in typical natural conditions a residual displacement forms at the interface between layers with an amplitude noticeably superior to the displacement amplitude of the free surface. Accounting for stratification enhances the residual displacements of water particles and the velocity of the eddy current in the lower layer (by $\sim 10\%$ in typical conditions). If the jump in density is related to large depths, then at the interface between the layers a residual perturbation forms that is comparable in shape and amplitude to the residual ocean bottom deformation. In the case of a thin lower layer even weak stratification is capable of significantly altering the residual fields in the lower layer, enhancing the residual displacements of water particles and the velocity of the eddy current by more than an order of magnitude. In this relation,

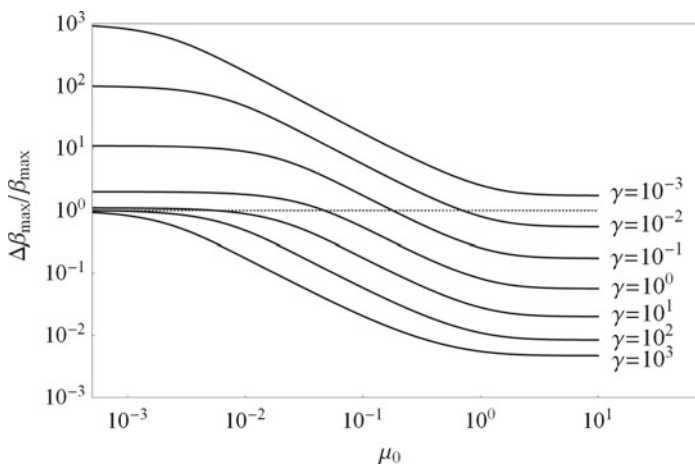


Fig. 3.44 Ratio of maximum values of functions $\Delta\beta$ and β versus parameter μ_0 . The calculation is performed by formulas (3.163) and (3.182) for $\delta\rho/\rho = 0.003$ and different values of parameter γ (indicated in the figure)

estimates of residual fields, obtained using bottom devices for measuring the current velocity, must be interpreted with caution.

3.6.5 Methods for Calculation of Residual Potential Fields for Real Events

To determine residual potential fields with account of real bathymetry and real bottom deformation at the tsunami source we shall take advantage of two numerical models: static and dynamic (Nosov et al. 2014a, b). The static model is intended for calculating the field of residual horizontal displacements of water particles. The dynamic model describes the evolution of these displacements in time. The dynamic model is necessary for understanding in what manner and how fast the field of residual displacements forms. For simplicity, in this section we shall again return to the model of a homogeneous ocean, especially that, as it was shown above, the role of stratification is not dominant in natural conditions.

In the vicinity of the tsunami source—inside the region limited by the barotropic Rossby radius of deformation $R_0 \sim 10^6$ m—rotation of the Earth weakly affects the potential residual field. In this region it is expedient to neglect the Coriolis force in problem (3.143)–(3.145), thus excluding from consideration the eddy component of the velocity field. Expressing the velocity vector of the horizontal current via the velocity potential $\mathbf{v} = \nabla\varphi$, we obtain from the continuity equation (3.143), written in vector form, the following:

$$\frac{\partial \xi}{\partial t} - \frac{\partial \eta}{\partial t} + (\nabla, H\nabla\varphi) = 0. \quad (3.183)$$

Integrating equation (3.183) over time from 0 to ∞ with account of the initial condition $\eta_0 = 0$, we arrive at the following static equation:

$$\xi_\infty - \xi_0 - \eta_\infty + (\nabla, H\nabla\Phi_\infty) = 0. \quad (3.184)$$

Equation (3.184) can be resolved using two types of input data: (1) data on the residual bottom deformation η_∞ (in this case we set $\xi_0 = 0$), (2) data on the initial elevation of the water surface, ξ_0 (in this case we set $\eta_\infty = 0$). Here we shall make use of the data on the initial elevation (Nosov et al. 2014a).

Equation (3.184) was resolved with boundary conditions of the second kind, $\partial\Phi/\partial\mathbf{n} = 0$, where \mathbf{n} is the external normal to the boundary. Physically this condition corresponds to impenetrable boundaries. At the coastline it adequately reflects the physics of the process. But the external boundaries passing through water are, of course, penetrable. In the static problem under consideration it is not possible to realize the condition of “free passage”. To exclude the influence of artificially closed boundaries on the solution we performed a series of preliminary calculations

steadily increasing the calculation region until the results in the region of interest to us stopped changing at the center of the calculation region.

The residual displacement of the water surface, ξ_∞ , was found as the ratio of the displaced water volume and the area of the calculation area. The sought vector of residual horizontal displacement of water particles is calculated via the displacement potential Φ_∞ by the formula $\mathbf{D}_\infty = \nabla \Phi_\infty$.

The dynamic model is based on the wave equation that is obtained by substitution of expression (3.149) into equation (3.183) (at $f = 0$ and $\eta = 0$)

$$\frac{\partial^2 \varphi}{\partial t^2} - g (\nabla, H \nabla \varphi) = 0. \quad (3.185)$$

Equation (3.185) was resolved with initial conditions (at $t = 0$: $\varphi = 0$, $\partial \varphi / \partial t = -g \xi_0$), the physical meaning of which consists in the initial elevation ξ_0 for a zero velocity field being set. At the coastline the condition of impenetrability, $\partial \varphi / \partial \mathbf{n} = 0$, was imposed, and on the boundaries crossing the ocean the condition of free passage for long gravitational waves was adopted.

Owing to the significant size of the calculation region, it was necessary in resolving equations (3.184), (3.185) numerically to take into account the surface curvature of the Earth. Therefore, the differential operator ∇ , entering in the equations was written in a spherical reference system.

Equation (3.184) was resolved numerically by the method of finite elements on a triangular grid with a variable step (Segerlind 1976; Nosov et al. 2014a). Near the coast and in the source region the grid was condensed, and at the periphery of the calculation region the grid step increased. Equation (3.185) was resolved numerically by the explicit method of finite differences on a rectangular grid (Nosov et al. 2014a). The time step was determined from the Courant–Friedrichs–Lewy condition.

3.6.6 Estimation of Residual Horizontal Displacements of Water Particles Caused by the Tsunamigenic Earthquake of March 11, 2011

In this section we shall deal with estimation of the potential residual field initiated by the catastrophic tsunamigenic March 11, 2011 earthquake at the coast of Japan.

The initial elevation of the water surface at the tsunami source was determined by the coseismic bottom deformation and bathymetry with the use of the method expounded in Sect. 3.5. The bathymetry was adopted from the GEBCO numerical atlas (<http://www.gebco.net/>). The coseismic deformation was calculated taking advantage of the Okada formulas (Okada 1985) on the basis of the model distribution of slip presented at the site of the United States Geological Survey (USGS, <http://earthquake.usgs.gov/>). The shape of the initial elevation is shown in Fig. 3.45 by white isolines.

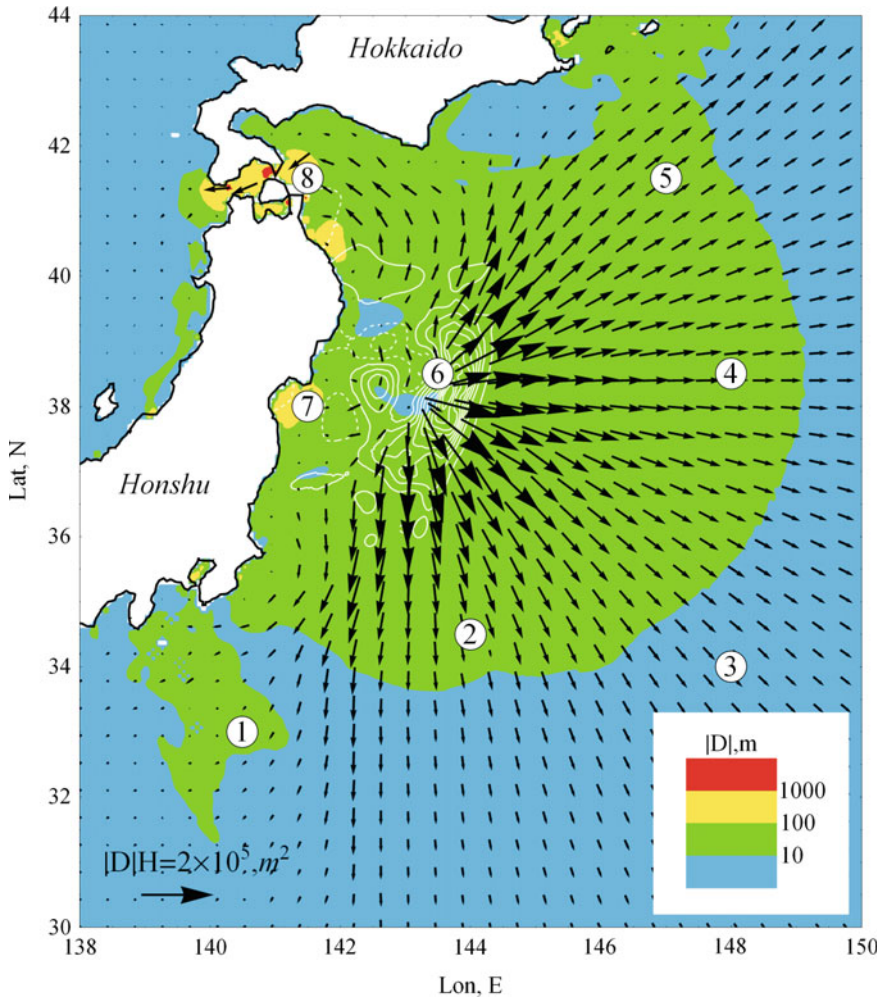


Fig. 3.45 Residual horizontal displacements of water particles (*black arrows*) caused by the tsunamigenic earthquake of March 11, 2011 at the coast of Japan. The length of a vector is proportional to the absolute value of the residual displacement multiplied by the ocean depth. The length scale of the vector is shown in accordance with the color scale depicted in the *lower right* angle of the figure. The initial elevation at the tsunami source is shown by *white* isolines with a step of 1 m (the *solid line* represents an uplift, the *dotted line* represents subsidence). The *white circles* with numbers indicate points at which calculation was performed of the tracks of water particle movements, presented in Fig. 3.46

The results of calculations by the static model are presented in Fig. 3.45. The residual horizontal displacements of water particles are shown by black arrows. The length of an arrow is proportional to the displacement multiplied by the ocean depth ($\mathbf{D}_\infty H$). The distribution of the value of $|\mathbf{D}_\infty|$ is shown in accordance with the color scale placed in the lower right angle of the figure.

The field of residual horizontal displacements depends in a complicated manner on the shape of the initial elevation at the tsunami source, on the bathymetry and on the coastline configuration. Far from the coast the displacement direction of water particles mainly depends on the shape of the initial elevation. The orienting influence of the coast is manifested near islands: vectors tend to be oriented parallel to the coastline. In a region of area of the order of 0.5 million sq. km, which is directly adjacent to the tsunami source and includes a deepwater depression and an abyssal plain, the amplitude of the residual displacement of water particles exceeded 10 m. In shallow-water regions the amplitude of residual displacements exceeded 100 and, in certain individual cases 1000 m.

In Okal and Mac Ayeal (2006) a description is given of the registration of the Indonesian tsunami of December 26, 2004 in a far zone (in the Ross Sea) with the use of an accelerometer placed on an iceberg. The amplitudes measured only amounted to 1.33 m horizontally and to 0.14 m vertically. Clearly, displacements of the order of 10 m can be readily registered by a similar device situated on a drifter.

In Fig. 3.46 characteristic examples are presented of water particle tracks calculated with the use of the dynamic model, and of the vector of residual displacement of water particles calculated by the static model. In an open ocean (points 2, 3, 4) immediately after passage of the leading wave a particle is shifted to a position which corresponds to calculation by the static model. Then, the particle undergoes chaotic motion in the vicinity of this position. It is seen that in these cases the static model

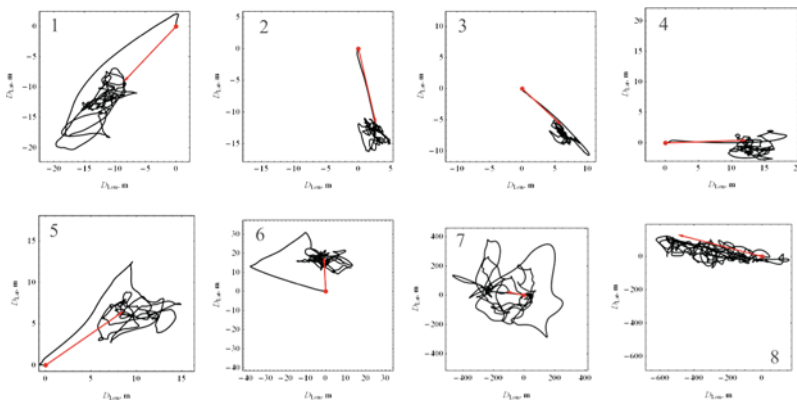


Fig. 3.46 Horizontal movements of water particles caused by the tsunamigenic earthquake of March 11, 2011 at the coast of Japan: tracks calculated by the dynamic model (*curves*) and residual displacement vectors calculated by the static model (*arrows*). Calculations are performed at points, the positions of which are shown in Fig. 3.45

can indeed be used for the rapid estimation of residual displacements. And the data on residual displacements can, in turn, be used for resolving the inverse problem of reconstructing the initial elevation.

At points 1, 5, owing to the vicinity of the coast and the influence of reflected and trapped waves, horizontal motions due to passage of the leading wave do not put particles in a position predicted by the static model. Particles are shifted to this position after a significant time period. At point 6 the horizontal movements of water are of a particular character, which is related to such a point being close to the center of the source. Note that in all three cases the static model quite accurately predicted the residual displacement, but the direction of the initial motion is clearly not consistent with the residual displacement vector.

In shallow-water regions the amplitude of horizontal motions (points 7, 8) significantly increases. But the real residual displacements are apparently achieved only after the decay of waves captured by the shelf. In these cases tracks reveal chaotic wandering of particles with a large amplitude and the static model is only capable of providing an approximate estimate of the amplitude, but not of their direction. The direction of motion is quite versatile and, consequently, not a reliable characteristic.

Let us point out the main results of this section. Numerical calculation shows that the tsunamigenic March 11, 2011 earthquake at the coast of Japan was accompanied by residual horizontal displacements of water particles with an amplitude exceeding 10 m in a region of area ~ 0.5 million sq. km. In shallow water the displacement amplitude could reach 100 and even 1000 m. Analysis of the traces of horizontal movements of water particles performed with the aid of hydrodynamic simulation has permitted to reveal that in open ocean residual displacements form immediately after passage of the leading tsunami wave. Near the coast, although horizontal motions are characterized by a significant amplitude (hundreds of meters), they look complicated and knotty owing to the influence of waves trapped by the shelf.

References

- Alasset, P.J., Hébert, H., Maouche, S., Calbini, V., Meghraoui, M.: The tsunami induced by the 2003 Zemmouri earthquake ($M_w = 6.9$, Algeria): modelling and results. *Geophys. J. Int.* **166**(1), 213–226 (2006)
- Basov, B.I., Kaistrenko, V.M., Levin, B.W., et al.: Some results of physical simulation of tsunami wave excitation and propagation. In: *Tsunami Generation and Wave Runup on Shore*, pp. 68–72. Radiosvyaz, Moscow (in Russian) (1984)
- Belokon', V.I., Goi, A.A., Reznik, B.L., Smal', N.A.: Tsunami excitation by a seismic wave packet subject to dispersion. *Tsunami Res.* (in Russian). Moscow (1), 28–36 (1986)
- Bobrovich, A.V.: Tsunami wave excitation by fissure propagating on the bottom. In: *Theoretical Foundations, Methods and Technical Means of Tsunami Prognosis. Theses of Reports to Symposium* (in Russian), pp. 36–37. Obninsk (1988)
- Bobrovich, A.V.: Generation of waves and vortices in the ocean by underwater earthquakes. *Tsunami Res.* (Mezhvedomstvennyi geofizicheskii komitet AN SSSR, Moscow, 1990), (4), 33–41 (1990) (in Russian)

- Bolshakova, A.V., Nosov, M.A.: Parameters of tsunami source versus earthquake magnitude. *Pure Appl. Geophys.* 2011, **168**, 2023–2031 (2011)
- Bolshakova, A.V., Nosov, M.A., Kolesov, S.V.: The properties of co-seismic deformations of the ocean bottom as indicated by the slip-distribution data in tsunamigenic earthquake sources. *Mosc. Univ. Phys. Bull.* **70**(1), 62–67 (2015)
- Chubarov, L.B., Shokin, Y.I., Simonov, K.V.: Using numerical modelling to evaluate tsunami hazard near the Kuril island. *Nat. Hazard.* (5), 293–318 (1992)
- Crocker, R.I., Matthews, D.K., Emery, W.J., Baldwin, D.: Computing coastal ocean surface currents from infrared and ocean color satellite imagery. *IEEE Trans. Geosci. Remote Sens.* **45**(2), 435–447 (2007)
- Dotsenko, S.F.: Tsunami waves in a continuously stratified ocean. *Tsunami Excit. Propag. Proc.* (IO AN SSSR, Moscow, 1982), 40–52. (1982) (in Russian)
- Dotsenko, S.F.: Effects of earth rotation during tsunami generation by underwater earthquakes. *Izv. Atmos. Ocean. Phys.* **35**(5), 641–647 (1999)
- Dotsenko, S.F., Sergeevsky, B.Yu., Cherkesov, L.V.: Spatial tsunami waves, caused by ocean surface displacements alternating in sign. *Tsunami Res.* (in Russian), Moscow (1), 7–14 (1986)
- Dotsenko, S.F., Sergeevsky, B.Yu.: Dispersion effects during directed tsunami wave generation and propagation. *Tsunami Res.* (in Russian), Moscow (5), 21–32 (1993)
- Dotsenko, S.F., Soloviev, S.L.: Mathematical modelling of tsunami excitation processes by slides of the ocean bottom. *Tsunami Res.* (in Russian), Moscow (4), 8–20 (1990a)
- Dotsenko, S.F., Soloviev, S.L.: Comparative analysis of tsunami excitation by piston and membrane bottom slides. In: *Tsunami Res.* (in Russian), (4), 21–27 (1990b)
- Dotsenko, S.F., Soloviev, S.L.: On the role of residual displacements of the ocean bottom in tsunami generation by submarine earthquakes. *Oceanology* (in Russian) **35**(1), 25–31 (1995)
- Dotsenko, S.F.: The influence of ocean floor residual displacements on the efficiency of directed tsunami generation. *Izv. Atmos. Ocean Phys.* **31**(4), 547–553 (1996)
- Dotsenko, S.F., Shokin, Yu.I.: Generation of vortices in a continuously stratified rotating liquid under displacements of the basin bottom. *Vych. Tekhnol.* (in Russian) (1), 13–22 (2001)
- Etaya, M., Nakano, R., Shimoda, H., Sakata, T.: Detection of ocean wave movements after the northern Sumatra earthquake using SPOT images. *Proc. IGARSS*, 1420–1423 (2005)
- Fine, I.V., Kulikov, E.A.: Computation of ocean surface displacements in the tsunami source, caused by instantaneous vertical bottom motions during an underwater earthquake. *Vych. Tekhnol.* **16**(2), 111–118 (2011) (in Russian)
- Fujii, Y., Satake, K., Sakai, S., Shinohara, M., Kanazawa, T.: Tsunami source of the 2011 off the Pacific coast of Tohoku earthquake. *Earth Planets Space* **63**, 815–820 (2011)
- Ingel', L.Kh.: The vortical trace of an earthquake in the sea. *Dokl. Earth Sci.* **362**(7), 1036–1038 (1998)
- Iwasaki, S.: Experimental study of a tsunami generated by a horizontal motion of a sloping bottom. *Bull. Earthq. Res. Inst. Univ. Tokyo* **57**, 239–262 (1982)
- Garder, O.I., Dolina, I.S., Pelinovsky, E.N., Poplavsky, A.A., Fridman, V.E.: Tsunami wave generation by gravitational lithodynamic processes. *Tsunami Stud.* (5), 50–60 (1993) (in Russian)
- Gill, A.E.: *Atmosphere-Ocean Dynamics*. Academic Press, New York (1982)
- Gisler, G.R.: Tsunami simulations. *Annu. Rev. Fluid Mech.* **40**, 71–90 (2008)
- Grilli, S.T., Ioualalen, M., Asavanant, J., Shi, F., Kirby, J.T., Watts, P.: Source constraints and model simulation of the 26 December 2004, Indian Ocean tsunami. *J. Waterw. Port Coast. Ocean Eng.* **133**(6), 414–428 (2007)
- Gusiakov, V.K.: Relationship of tsunami intensity to source earthquake magnitude as retrieved from historical data. *Pure Appl. Geophys.* 2011, **168**, 2033–2041 (2011)
- Ji., C.: Rupture process of the 13 January 2007 Magnitude 8.1—KURIL Island Earthquake (Revised) (2007). http://earthquake.usgs.gov/earthquakes/eqinthenews/2007/us2007xmae/finite_fault.php
- Hammack, J.L.: A note on tsunamis: their generation and propagation in an ocean of uniform depth. *J. Fluid Mech.* **60**, 769–799 (1973)
- Hammack, J.L.: Baroclinic generation, tsunami. *J. Phys. Oceanogr.* **10**(9), 1455–1467 (1980)

- Hayes, G.: Updated Result of the 11 March 2011 Mw 9.0 Earthquake Offshore Honshu, Japan (2011). http://earthquake.usgs.gov/earthquakes/eqinthenews/2011/usc0001xgp/finite_fault.php
- Horrillo, J., Kowalik, Z., Shighihara, Y.: Wave dispersion study in the Indian Ocean tsunami of 26 December 2004. *Sci. Tsunami Hazards* **25**(1), 42–63 (2006)
- Kajiura, K.: The leading wave of a tsunami. *Bull. Earthq. Res. Inst.* **41**(3), 535–571 (1963)
- Kajiura, K.: Tsunami source, energy and directivity of wave radiation. *Bull. Earthq. Res. Inst.* **48**(5), 835–869 (1970)
- Kato, K., Tsuji, Y.: Tsunami of the Sumba earthquake of 19 August 1977. *J. Nat. Disaster Sci.* **17**(2), 87–100 (1995)
- Kostitsyna, O.V., Nosov, M.A., Shelkovnikov, N.K.: A study of nonlinearity in the process of tsunami generation by sea floor motion. *Mosc. Univ. Phys. Bull.* **47**(4), 83–86 (1992)
- Kowalik, Z., Knight, W., Logan, T., Whitmore, P.: Numerical modelling of the global tsunami: Indonesian tsunami of 26 December 2004. *Sci. Tsunami Hazard* **23**(1), 40–56 (2005)
- Kulikov, E.A., Rabinovich, A.B., Fine, I.V., Bornhold, B.D., Thomson, R.E.: Tsunami generation by slides on the Pacific coast of North America and the role of tides (in Russian). *Oceanology* **38**(3), 361–367 (1998)
- Lamb, H.: *Hydrodynamics*. Cambridge University Press, Cambridge (1932)
- Landau, L.D., Lifshitz, E.M.: *Fluid Mechanics*, 2nd English edn. Pergamon Press, Oxford (1987)
- Lebedev, A.N., Sebekin, B.I.: Directed tsunami wave generation in the coastal zone (in Russian). *Izv. AN SSSR, FAO* **18**(4), 399–417 (1982)
- Levin, B.W.: Review of works on experimental modelling of the tsunami excitation process (in Russian). In: *Methods for Calculating Tsunami Rise and Propagation*, pp. 125–139. Nauka, Moscow (1978)
- Levin, B.V., Nosov, M.A., Pavlov, V.P., Rykunov, L.N.: Cooling of the ocean surface as a result of seaquakes. *Dokl. Earth Sci.* **358**(1), 132–135 (1998)
- Lighthill, J.: *Waves in Fluids*, p. 504. Cambridge University Press, Cambridge (1978)
- Lobkovsky, L.I., Baranov, B.V.: On tsunami excitation in subduction zones of lithospheric plates (in Russian). In: *Processes of Tsunami Excitation and Propagation*, pp. 7–17. Publishing Department, RAS (1982)
- Marchuk, An.G., Chubarov, L.B., Shokin, Yu.I.: *Numerical Simulation of Tsunami Waves* (in Russian). Nauka, Siberian Branch, Novosibirsk (1983)
- Marchuk, An.G., Titov, V.V.: Influence of the source shape on tsunami wave formation (in Russian). *Tsunami Research*, (5), 7–21 (1993)
- Mikada, H., Mitsuzawa, K., Matsumoto, H., Watanabe, T., Morita, S., Otsuka, R., Sugioka, H., Baba, T., Araki, E., Suyehiro, K.: New discoveries in dynamics of an M8 earthquake—phenomena and their implications from the 2003 Tokachi-oki earthquake using a long term monitoring cabled observatory. *Tectonophysics* **426**, 95–105 (2006)
- Mirchina, N.P., Pelinovsky, E.N.: Dispersive amplification of tsunami waves (in Russian). *Oceanology* **27**(1), 35–40 (1987)
- Murty, T.S.: Seismic sea waves—tsunamis. *Bull. Fish. Res. Board Canada Ottawa* **198** (1977)
- Myers, E.P., Baptista, A.M.: Finite element modeling of the 12 July 1993 Hokkaido Nansei-Oki tsunami. *Pure Appl. Geophys.* **144**(3/4), 769–802 (1995)
- Nagai, T.: Introduction of Japanese coastal wave monitoring network. In: *Joint Conference Proceedings, 7th International Conference on Urban Earthquake Engineering (7CUEE) and 5th International Conference on Earthquake Engineering (5ICEE)*, pp. 1649–1653, 3–5 March, Tokyo Institute of Technology, Tokyo, Japan (2010)
- Nikiforov, A.f., Uvarov, V.B.: *Special Functions of Mathematical Physics* (in Russian). Nauka, Moscow (1984)
- Nosov, M.A.: Generation of tsunami by oscillations of a sea floor section. *Mosc. Univ. Phys. Bull.* **47**(1), 110–112 (1992)
- Nosov, M.A., Mironyuk, S.V., Shelkovnikov, N.K.: Directivity of dispersive tsunami radiation and specific features of sea floor motion in the focus area. *Mos. Univ. Phys. Bull. C/c of Vestnik-moskovskii Universitet Fizika I Astronomiia* **52**, 99–102 (1997)

- Nosov, M.A.: On the directivity of dispersive tsunami waves excited by piston-type and traveling-wave sea-floor motion. *Volcanol. Seismol.* **19**, 837–844 (1998a)
- Nosov, M.A. Ocean surface temperature anomalies from underwater earthquakes. *Volcanol. Seismol.* **19**(3), 371–375 (1998b)
- Nosov, M.A.: Tsunami waves of seismic origin: the modern state of knowledge. *Izv. Atmos. Ocean. Phys.* **50**(5), 474–484 (2014)
- Nosov, M.A., Mironyuk, S.V., Shelkovnikov, N.K.: Bottom slides of alternating signs and leading tsunami wave (in Russian). In: Collection “Interaction in the Lithosphere–hydrosphere–atmosphere System”, vol. 2, pp. 193–200. Publishing Department of MSU Physics Faculty, Moscow (1999)
- Nosov, M.A., Kolesov, S.V., Levin, B.W.: Contribution of horizontal deformation of the seafloor into tsunami generation near the coast of Japan on 11 March 2011. *Dokl. Earth Sci.* **441**(1), 1537–1542. SP MAIK Nauka/Interperiodica (2011, November)
- Nosov, M.A., Bolshakova, A.V., Kolesov, S.V.: Displaced water volume, potential energy of initial elevation, and tsunami intensity: analysis of recent tsunami events. *Pure Appl. Geophys.* **171**(12), 3515–3525 (2014a)
- Nosov, M.A., Kolesov, S.V.: Method of specification of the initial conditions for numerical tsunami modeling. *Mosc. Univ. Phys. Bull.* **64**(2), 208–213 (2009)
- Nosov, M.A., Kolesov, S.V.: Optimal initial conditions for simulation of seismotectonic tsunamis. *Pure Appl. Geophys.* **168**(6–7), 1223–1237 (2011)
- Nosov, M.A., Nurislamova, G.N., Moshenceva, A.V., Kolesov, S.V.: Residual hydrodynamic fields after tsunami generation by an earthquake. *Izv. Atmos. Ocean. Phys.* **50**(5), 520–531 (2014b)
- Nosov, M.A., Moshenceva, A.V., Levin, B.W.: Residual hydrodynamic fields near a tsunami source. *Dokl. Earth Sci.* **438**(2), 853–857 (2011)
- Nosov, M.A., Nurislamova, G.N.: The potential and vortex traces of a tsunamigenic earthquake in the ocean. *Mosc. Univ. Phys. Bull.* **67**(5) 457–461 (2012)
- Nosov, M.A., Nurislamova, G.N.: Traces of a tsunamigenic earthquake in a rotating stratified ocean. *Mosc. Univ. Phys. Bull.* **68**(6), 490–496 (2013)
- Nosov, M.A., Sementsov, K.A.: Calculation of the initial elevation at the tsunami source using analytical solutions. *Izv. Atmos. Ocean. Phys.* **50**(5), 539–546 (2014)
- Nosov, M.A., Shelkovnikov, N.K.: Method for measuring submillimeter waves on water surface. *Mosc. Univ. Phys. Bull.* **46**(3), 106–108 (1991)
- Nosov, M.A., Shelkovnikov, N.K.: Generation of surface waves in a fluid layer by periodic motions of the bottom. *Izv. Atmos. Ocean. Phys.* **28**(10–11), 833–834 (1992)
- Nosov, M.A., Shelkovnikov, N.K.: Tsunami generation by traveling sea-floor shoves. *Mosc. Univ. Phys. Bull.* **50**(4), 88–92 (1995)
- Nosov, M.A., Shelkovnikov, N.K.: The excitation of dispersive tsunami waves by piston and membrane floor motions. *Izv. Atmos. Ocean. Phys.* **33**(1), 133–139 (1997)
- Novikova, L.E., Ostrovsky, L.A.: On the excitation of tsunami waves by a running slide of the ocean bottom. In: *Methods for Calculating Tsunami Arisal and Propagation* (in Russian), pp. 88–99. Nauka, Moscow (1978)
- Okada, Y.: Surface deformation due to shear and tensile faults in a half-space. *Bull. Seismol. Soc. Am.* **75**(4), 1135–1154 (1985)
- Okal, E.A., Mac Ayeal, D.R.: Seismic recording on drifting icebergs: catching seismic waves, tsunamis and storms from Sumatra and elsewhere. *Seismol. Res. Letts.* **77**, 659–671 (2006)
- Pelinovsky, E., Talipova, T., Kurkin, A., Kharif, C.: Nonlinear mechanism of tsunami wave generation by atmospheric disturbances. *Nat. Hazards Earth Syst. Sci.* **1**, 243–250 (2001)
- Pelinovsky, E.N.: *Hydrodynamics of Tsunami Waves* (in Russian). Institute of Applied Physics. RAS, Nizhnii Novgorod (1996)
- Polyanin, A.D.: *Handbook of Linear Partial Differential Equations for Engineers and Scientists*. Chapman & Hall/CRC Press, Boca Raton (2002)
- Popinet, S.: Adaptive modelling of long-distance wave propagation and fine-scale flooding during the Tohoku tsunami. *Nat. Hazards Earth Syst. Sci.* **12**, 1213–1227 (2012)

- Poplavskii, A.A., Poplavskaya, L.N., Spirin, A.I., Permikin, Yu, Yu., Nagornyykh, T.V.: Improvements on the magnitude-geographic criterion of tsunami hazard. *J. Volkanol. Seismol.* **3**(1), 59–67 (2009)
- Rabinovich, A.B., Lobkovsky, L.I., Fine, I.V., Thomson, R.E., Ivelskaya, T.N., Kulikov, E.A.: Near-source observations and modeling of the Kuril Islands tsunamis of 15 November 2006 and 13 January 2007. In: *Advances in Geosciences*, vol. 14, pp. 105–116 (2008)
- Rivera, P.C.: Modeling the Asian tsunami evolution and propagation with a new generation mechanism and a non-linear dispersive wave model. *Sci. Tsunami Hazards* **25**(1), 18–33 (2006)
- Segerlind, L.J.: *Applied Finite Element Analysis*. Wiley, New York (1976)
- Saito, T., Furumura, T.: Three-dimensional tsunami generation simulation due to sea-bottom deformation and its interpretation based on the linear theory. *Geophys. J. Int.* **178**(2), 877–888 (2009)
- Satake, K.: Linear and nonlinear computations of the 1992 Nicaragua earthquake tsunami. *PAGEOPH* **144**(3/4), 455–470 (1995)
- Satake, K., Imamura, F.: Tsunamis: seismological and disaster prevention studies. *J. Phys. Earth* **43**(3), 259–277 (1995)
- Sretensky, L.N.: *Theory of Wave Motions of Liquids* (in Russian). Nauka, Moscow (1977)
- Suleimani, E., Hansen, R., Kowalik, Z.: Inundation modeling of the 1964 tsunami in Kodiak Island, Alaska. In: Yalciner, A.C., Pelinovsky, E.N., Okal, E., Synolakis, C.E. (eds.) *Submarine Landslides and Tsunamis*, vol. 21, pp. 191–201. Kluwer Academic Publishers (2003)
- Sveshnikov, A.G., Tikhonov, A.N.: *Theory of Functions of a Complex Variable* (in Russian). Nauka, Fizmatlit, Moscow (1999)
- Takahasi, R.: A model experiment on the mechanism of seismic sea wave generation. Part 1. *Bull. Earthq. Res. Inst.* **12**, 152–178 (1934)
- Takahasi, R.: On some model experiment on tsunami generation. *Int. Union Geodesy Geophys. Monogr.* (24), 235–248 (1963)
- Tanioka, Y., Satake, K.: Tsunami generation by horizontal displacement of ocean bottom. *Geophys. Res. Lett.* **23**(8), 861–864 (1996a)
- Tanioka, Y., Satake, K.: Fault parameters of the 1896 Sanriku tsunami earthquake estimated from tsunami numerical modeling. *Geophys. Res. Lett.* **23**(13), 1549–1552 (1996b)
- Tanioka, Y., Seno, T.: Sediment effect on tsunami generation of the 1896 Sanriku tsunami earthquake. *Geophys. Res. Lett.* **28**(17), 3389–3392 (2001)
- Tinti, S., Bortolucci, E., Armigliato, A.: Numerical simulation of the landslide-induced tsunami of 1988 in Vulcano island, Italy. *Bull. Volcanol.* **61**, 121–137 (1999)
- Titov, V.V., Mofjeld, H.O., Gonzalez, F.I., Newman, J.C.: Offshore forecasting of Alaska-Aleutian subduction zone tsunamis in Hawaii. NOAA Technical Memorandum ERL PMEL-114 (1999)
- Titov, V.V., Gonzalez, F.I., Mofjeld, H.O., Venturato, A.J.: NOAA time seattle tsunami mapping project: procedures, data sources, and products. NOAA Technical Memorandum OAR PMEL-124, 21p (2003)
- Titov, V.V., Gonzalez, F.I., Bernard, E.N., et al.: Real-time tsunami forecasting: challenges and solutions. *Nat. Hazards* **35**(1), 41–58 (2005). (U.S. National Tsunami Hazard Mitigation Program)
- UNESCO/IOC.: *Operational Users Guide for the Pacific Tsunami Warning and Mitigation System (PTWS)*. IOC Technical Series 87, 2nd edn. (2009)
- Van Dorn, W.G.: Source mechanism of the tsunami of March 28, 1964, in Alaska. In: *Proceedings of the 9th Conference on Coastal Engineering*, Lisbon, pp. 166–190 (1964)
- Vasilieva, G.V.: On wave excitation in shallow water. In: *Tsunami Wave Propagation and Runup on Shore*. (in Russian), pp. 67–69. Nauka, Moscow (1981)
- Voight, S.S.: Tsunami waves. *Tsunami Res.* (2), 8–26 (1987). (in Russian)
- Voight, S.S., Lebedev, A.N., Sebekin, B.I.: Certain tsunami wave peculiarities, related to characteristics of the perturbation source. In: *Tsunami Theory and Effective Prognosis* (in Russian), pp. 5–11. Nauka, Moscow (1980)
- Voight, S.S., Lebedev, A.N., Sebekin, B.I.: On the formation of a directed tsunami wave at the perturbation source. *Izv. AN SSSR, FAO* (in Russian) **17**(3), 296–304 (1981)

- Voight, S.S., Lebedev, A.N., Sebekin, B.I.: On the generation of a directed tsunami wave by a horizontal bottom displacement. In: Processes of Tsunami Excitation and Propagation (in Russian), pp.18–23. IO RAN, Moscow (1982)
- Voit, S.S., Lebedev, A.N., Sebekin, B.I.: Earth's rotation effect on energy characteristics of tsunami waves. Tsunami Research (Mezhvedomstvennyi geofizicheskii komitet AN SSSR, Moscow, 1986), (1), 15–20 (1986). (in Russian)
- Watts, P., Grilli, S.T., Imamura, F.: Coupling of tsunami generation and propagation codes. ITS Proc. Session 7(7–13), 811–823 (2001)
- Zaitsev, A.I., Kurkin, A.A., Levin, B.W., et al.: Numerical simulation of catastrophic tsunami propagation in the Indian Ocean (26 December 2004). Dokl. Earth Sci. **402**(4), 614 (2005)
- Zaytsev, A.I., Chernov, A.G., Yalciner, A.C. et al.: MANUAL Tsunami Simulation/Visualization Code NAMI DANCE versions 4.9 (February 2010)
- Zyryanov, V.N.: Topographic Vortices in the Dynamics of Sea Currents. IVP RAN, Moscow (1995) (in Russian)

Chapter 4

Role of the Compressibility of Water and of Nonlinear Effects in the Formation of Tsunami Waves

Abstract The necessity is substantiated for taking into account the compressibility of water in describing behavior of water column in tsunami source. Within the framework of linear potential theory of a compressible liquid in a basin of fixed depth, the general analytical solution is constructed for 2D and quasi-3D (cylindrical symmetry) problems of the generation of acoustic-gravity waves by bottom deformations of small amplitudes. Manifestations of compressibility of the water column in the problem of tsunami generation are studied, making use of the example of model bottom deformation laws (piston, membrane, and running displacements). The main difference between the behavior of a compressible water column as compared to an incompressible model medium is shown to consist in the formation of elastic oscillations exhibiting significant amplitudes and a discrete spectrum. Characteristic features of the dynamics of acoustic-gravity waves in a basin of variable depth are described. Records of ocean bottom pressure gauges and seismometers are used for analyzing manifestations of the 2003 Tokachi-Oki and the 2011 Tohoku-Oki tsunamigenic earthquakes. The mechanism is considered of tsunami formation, related to nonlinear energy transfer from “high-frequency” forced or elastic oscillations of the water column to “low-frequency” gravitational waves.

Keywords Tsunami generation · Water compressibility · Euler’s equations · Acoustic-gravity waves · T-phase · Linear potential theory · Laplace transformation · Fourier transformation · Analytical solution · Ocean bottom displacement · Waveguide · Normal modes · Numerical simulation · The 2003 Tokachi-Oki earthquake · The 2011 Tohoku-Oki earthquake · JAMSTEC · DONET · Nonlinear tsunami source

The issue of accounting for the compressibility of water in the problem of tsunami generation has been raised repeatedly in the literature Sells (1965), Kajiura (1970), Pod’yapolsky (1978), Yanushkauskas (1981), Boorymskaia et al. (1981), Levin (1981), Selezov et al. (1982), Garber (1984), Zhmur (1987), Nosov (1999, 2000), Nosov and Sammer (1998), Panza et al. (2000), Ohmachi et al. (2001), Nosov and Kolesov (2002, 2003, 2007), Nosov et al. (2005, 2007), Gisler (2008), Chierici et al. (2010), Stiassnie (2010), Kadri and Stiassnie (2012), Sammarco et al. (2013), Abdolali et al. (2015). However, in most of the tsunami models the ocean is

considered to be an incompressible medium. Only one of the manifestations of water being compressible in the case of underwater earthquakes, namely the T-phase, has been studied relatively well (e.g., Ewing et al. 1950; Soloviev et al. 1968, 1980; Brekhovskikh 1974; Kadykov 1986; Walker et al. 1992; Kadykov 1999; Lysanov 1997; Okal 2003; Okal et al. 2003). The range of frequencies between 2 and 100 Hz is usual for the T-phase. We note here that in this chapter we will be interested in hydroacoustic phenomena which are related to another frequency range (~ 0.1 Hz) and are localized in the immediate vicinity of the tsunami source.

The necessity of taking into account nonlinear effects during tsunami formation is related to the fact that in the case of seismic motions of the seabed exhibiting small amplitudes, the velocities of these motions may turn out to be quite significant. The nonlinear mechanism of tsunami generation was first considered in Novikova and Ostrovsky (1982). This line of research was further developed in Nosov and Skachko (2001), Nosov and Kolesov (2002, 2005), Nosov et al. (2008).

4.1 Excitation of Tsunami Waves with Regard to the Compressibility of Water

4.1.1 Preliminary Estimates

If the process is treated from a formal physical point of view (e.g., Landau and Lifshits 1987), then a liquid can be considered incompressible only when $\Delta\rho/\rho \ll 1$, where ρ is the density of the liquid. As it is known, the necessary condition for the above to be valid is that the motions of the liquid exhibit small velocities, as compared to the velocity of sound. In the case of stationary motion this condition is sufficient. The problem of tsunami generation is evidently nonstationary so one more additional condition must be fulfilled. In the problem of tsunami generation both conditions are of the following form:

- (1) $v \ll c$;
- (2) $\tau \gg (Hc^{-1}, Lc^{-1})$,

where v is the characteristic mass velocity of motion of water particles or of the ocean bottom, c is the velocity of sound in water, H is the ocean depth, L is the characteristic horizontal size of the source. Note that even in those rare cases, when the authors of one or another investigation substantiate application of the theory of incompressible liquids in the tsunami problem, the second condition is always forgotten. The characteristic values of the indicated parameters are the following: $v \sim 1$ m/s, $c \sim 1500$ m/s, $H \sim 4500$ m, $L \sim 10$ – 100 km, $\tau \sim 1$ – 100 s. The first condition is seen to be well satisfied, while the second can be violated in many cases. In the case of a running displacement (a fault ripped open or a surface seismic wave) the first condition will also be violated.

For problems concerning tsunami propagation in the open ocean and waves running up a coast, the first condition remains the same and is quite fulfilled. The second condition assumes the following form: $T \gg (H c^{-1}, \lambda c^{-1})$, where T is the tsunami period, and λ is the wavelength. With regard to the obvious relationship $T (gH)^{1/2} = \lambda$ and to the fact that the tsunami period is usually tens and even hundreds of minutes long, fulfillment of the second conditions is also doubtless.

It is interesting to compare the energies of acoustic and gravitational waves, excited by one and the same mechanism: by vertical displacement of part of the ocean bottom. We shall consider a column of an ideal homogeneous compressible (or incompressible) liquid with a free upper surface of thickness H located on an absolutely rigid bottom in the field of gravity exhibiting the free-fall acceleration g . At a certain moment of time an area S of the ocean bottom starts to move vertically with a constant velocity v . The motion will take place during a time interval τ , upon which the ocean bottom stops. Such a process results in a residual displacement of the ocean bottom of height $\eta_0 = v \tau$ over an area S . It is known that in an incompressible liquid, when $\tau \ll S^{1/2} (gH)^{-1/2}$, at the time moment $t = \tau$ the shape of the surface perturbation is close to the shape of the residual displacement of the bottom, so the energy transferred to the ocean by the moving bottom can be estimated (from above) as the potential energy of the initial elevation of area S and height $\xi_0 = \eta_0$:

$$E_1 = 0.5 \rho g S \xi_0^2. \quad (4.1)$$

Within the framework of the model of compressible liquids, the energy of acoustic waves (e.g., Landau and Lifshits 1987), excited by the displacement of the ocean bottom, described above, has the following form:

$$E_2 = c \rho S \eta_0^2 \tau^{-1}. \quad (4.2)$$

Note that, when bottom deformations happen to be prolonged, the water layer behaves like an incompressible medium. In such cases estimation by formula (4.2), naturally, has no sense. The critical duration permitting to distinguish between the water layer dynamics of compressible and incompressible character is represented by the quantity $\tau_c = 4H/c$ (justification will be presented in Sect. 4.1.5). This critical duration amounts to $\tau_c = 10$ s for a typical oceanic depth $H = 4500$ m and sonic speed $c = 1500$ m/s.

It is readily verified that within the range of τ values peculiar to real seismic events (1–10 s), the ratio $E_2/E_1 = 2c/(g\tau) \gg 1$. In other words, a significant part of the energy transferred from the moving bottom to the ocean exists in the form of acoustic waves. As time passes, this energy can be transferred to seismic waves or to other forms of motion of the water column. In any case, elastic oscillations represent an energetically significant effect that must be taken into account.

The obtained estimates are expediently compared with natural data. Taking advantage of the empirical relationship (2.53) and of the ratio $E_2/E_1 = 2c/(g\tau)$, it is possible to calculate the energy of a gravitational tsunami wave and the energy of elastic

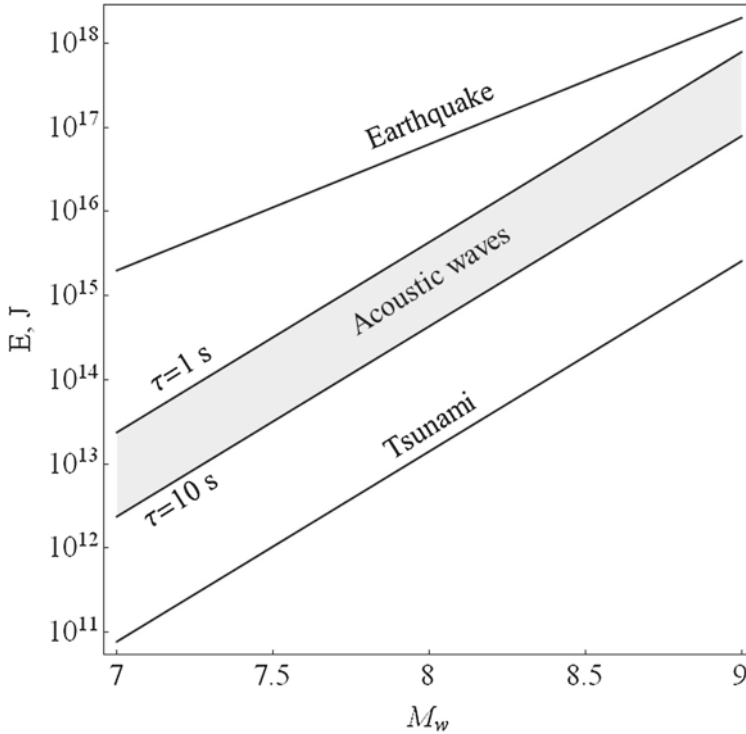


Fig. 4.1 Earthquake energy, energy of gravitational tsunami waves, and energy of acoustic waves in water versus earthquake magnitude

waves in water depending on the earthquake magnitude. We shall compare these quantities with the earthquake energy estimated by the Kanamori formula (1977)

$$\log_{10} E_{EQ}[J] = 1.5 M_w + 4.8. \quad (4.3)$$

Figure 4.1 presents dependences of the earthquake energy, of the energy of the gravitational tsunami wave, and of the energy of acoustic waves upon the earthquake magnitude. In calculating the energy of acoustic waves we assumed the bottom deformation duration to vary between the limits of 1 and 10 s. The dependence of the acoustic wave energy is shown by the gray band, the upper boundary of which corresponds to a duration of $\tau = 1$ s, while the lower one corresponds to $\tau = 10$ s. Formation of the tsunami gravitational wave is seen to consume less than 0.1 % (see Sect. 2.4). But tens and, maybe, even hundreds of times more, up to 10 % of the earthquake energy, may be transformed into the energy of acoustic waves. Thus, submarine earthquakes are capable of exciting powerful acoustic waves and when tsunamis are generated, noticeable manifestations of the compressibility effect of water are to be expected.

Further we shall consider the mathematical model of a compressible water column under the assumption of an absolutely rigid ocean bottom. Such an assumption simplifies the problem noticeably and permits to concentrate on manifestations of the compressibility of the water column. A realistic formulation of the problem should, naturally, take into account the elasticity properties of the ocean bottom. The problem thus formulated was first considered by G.S. Pod'yapolsky (1968a, b, 1978). This topic was further developed in analytical studies Gusyakov (1972, 1974), Alexeev and Gusyakov (1973), Zvolinsky (1986), Zvolinsky et al. (1991, 1994), Sekerzh-Zen'kovich et al. (1999). In recent years publications have appeared, in which attempts are made of numerical simulation of the dynamics of a compressible water column with regard to the elasticity properties of the ocean bottom (Panza et al. 2000; Ohmachi et al. 2001; Balanche et al. 2009; Maeda and Furumura 2013; Maeda et al. 2013). In particular, these properties will be manifested in the time interval, during which elastic oscillations of a water column exist, being limited owing to “leakage” of energy into the ocean bottom.

Consider elastic oscillations to be caused by a horizontally homogeneous vertical deformation of the ocean bottom taking place within quite an extended area. Then the problem becomes one-dimensional along the vertical coordinate. We write the evolution equation for the energy E of elastic waves contained in a water column of thickness H as

$$\frac{dE}{dt} = -\frac{E}{\tau_s}.$$

The energy E obviously decreases exponentially with time. The quantity τ_s , characterizing the damping time, can be deduced from the following arguments. During the propagation of an elastic wave from the ocean bottom to the surface and back ($2H/c$) its energy will be reduced by the quantity D_0E , where $D_0 = 4\rho\rho_bcc_b(\rho c + \rho_b c_b)^{-2}$ is the transition coefficient at the “water–bottom” boundary for a normally incident elastic wave, ρ , ρ_b and c , c_b are the densities of and elastic wave propagation velocities in water and the ocean bottom rock, respectively. In the case of the ocean bottom, longitudinal waves are intended, since in the one-dimensional case considered transverse and surface seismic waves are not excited. The maximum period of elastic oscillations of a water column with a free surface is known to be $T_0 = 4H/c$. Thus, we obtain the following formula for the damping time: $\tau_s = T_0/2D_0$.

We shall consider the density of water and the propagation velocity of sound in water to be $\rho = 1000 \text{ kg/m}^3$ and $c = 1500 \text{ m/s}$, respectively. In the case of rock, making up the ocean bottom, its density and the velocity of longitudinal waves in it vary within the respective limits $1400 < \rho_b < 3500 \text{ kg/m}^3$ and $1700 < c_b < 8000 \text{ m/s}$. Correspondingly, the transition coefficient varies within the limits $0.19 < D_0 < 0.95$. The lower limits of the indicated ranges correspond to friable sedimentary rock. Usually, the ocean bottom has a stratified structure. The effective reflection of elastic waves takes place from the acoustic base—a certain sufficiently dense and high-velocity column. Thus, for example, in the case of $\rho_b = 3000 \text{ kg/m}^3$ and $c_b = 7000 \text{ m/s}$, we obtain $\tau_s \approx 2T_0$. So, it takes two periods for the energy

of elastic oscillations to be reduced by a factor of e , and four periods for the oscillation amplitude.

4.1.2 Hydrodynamic Formulation of the Problem: Analytic Solutions

The general formulation of the problem, considered in this section, remains exactly the same as in Sect. 3.1.1 and is presented in Fig. 3.1. All the notations introduced in Sect. 3.1.1 also remain in force. The main innovation in formulating the problem consists in that we shall now consider the water environment to be a compressible liquid. Moreover, we shall neglect the Coriolis force. Indeed, owing to the longest possible period of hydroacoustic waves, $T_{\max} = 4H/c \sim 10$ s, being certainly many times shorter than the 24h of a solar day, rotation of the Earth is quite unlikely to affect hydroacoustic waves.

To obtain a hydrodynamic description of the movements of a water layer (e.g., Landau and Lifshits 1987) we again take advantage of the Euler equation, in which the density of water is no longer a constant, but depends on pressure,

$$\frac{\partial \mathbf{v}}{\partial t} + (\mathbf{v}, \nabla) \mathbf{v} = -\frac{\nabla p}{\rho} + \mathbf{g}, \quad (4.4)$$

of the continuity equation for a compressible liquid,

$$\frac{\partial \rho}{\partial t} + \operatorname{div}(\rho \mathbf{v}) = 0 \quad (4.5)$$

and of the equation of state for a barotropic liquid,

$$\rho = \rho(p). \quad (4.6)$$

The set of Eqs. (4.4)–(4.6) must be supplemented with boundary conditions. Like in the case of an incompressible liquid, dynamic and kinematic conditions must be set on the free surface of the compressible liquid,

$$p = p_{\text{atm}} \quad \text{for } z = \xi(x, y, t), \quad (4.7)$$

$$\frac{\partial \xi}{\partial t} + u \frac{\partial \xi}{\partial x} + v \frac{\partial \xi}{\partial y} - w = 0 \quad \text{for } z = \xi(x, y, t), \quad (4.8)$$

where p_{atm} is the atmospheric pressure along the free water surface, which we shall consider to be constant. The no-normal flow condition is set on the moving oceanic bottom,

$$(\mathbf{v}, \mathbf{n}) = (\mathbf{v}_b, \mathbf{n}) \quad \text{for } z = -H(x, y) + \eta(x, y, t), \quad (4.9)$$

where \mathbf{v}_b is the velocity vector of the ocean bottom motion, \mathbf{n} is the normal to the ocean bottom surface.

As the initial conditions we shall adopt zero displacement of the free surface, $\xi_0 = 0$ and a zero velocity field, $\mathbf{v}_0 = 0$. Here, the liquid will be in a state of hydrostatic equilibrium, and the initial distributions of pressure $p_0(z)$ and density $\rho_0(z)$ will be related by the equation of hydrostatics,

$$\frac{\nabla p_0}{\rho_0} = \mathbf{g}. \quad (4.10)$$

We shall consider movements of the water layer caused by dynamic deformation of the ocean bottom to be deviations from hydrostatic equilibrium. In this case it is expedient to represent the flow velocity, pressure, and density fields as sums of the respective static ($\mathbf{v}_0 = 0$, $p_0(z)$, $\rho_0(z)$) and dynamic ($\mathbf{v}'(x, y, z, t)$, $p'(x, y, z, t)$, $\rho'(x, y, z, t)$) parts,

$$\mathbf{v} = \mathbf{v}'(x, y, z, t), \quad (4.11)$$

$$p = p_0(z) + p'(x, y, z, t), \quad (4.12)$$

$$\rho = \rho_0(z) + \rho'(x, y, z, t). \quad (4.13)$$

Substitution of representations (4.11)–(4.13) into Eqs. (4.4) and (4.5) gives

$$\frac{\partial \mathbf{v}'}{\partial t} + (\mathbf{v}', \nabla) \mathbf{v}' = -\frac{\nabla p'}{\rho_0 + \rho'} + \frac{\rho' \mathbf{g}}{\rho_0 + \rho'}, \quad (4.14)$$

$$\frac{\partial \rho'}{\partial t} + \text{div}(\rho_0 \mathbf{v}' + \rho' \mathbf{v}') = 0. \quad (4.15)$$

We stress that Eqs. (4.14) and (4.15) are obtained by identical transformations without application of any simplifying assumptions. Therefore, they are just as difficult to resolve as the initial equations. But, if the assumption is made that deviations from hydrostatic equilibrium are due to acoustic and gravitational waves of small amplitudes, then Eqs. (4.14) and (4.15) can be linearized. Neglecting the small quantities \mathbf{v}' , p' , and ρ' , we obtain a set of linear equations describing waves of small amplitude in a compressible liquid,

$$\frac{\partial \mathbf{v}'}{\partial t} = -\frac{\nabla p'}{\rho_0} + \frac{\rho' \mathbf{g}}{\rho_0}, \quad (4.16)$$

$$\frac{\partial \rho'}{\partial t} + \rho_0 \text{div}(\mathbf{v}') = 0. \quad (4.17)$$

Small variations of density ρ' and pressure p' are related to each other by the following formula deriving from the equation of state (4.6):

$$\rho' = p'/c^2, \quad (4.18)$$

where $c = \sqrt{(\partial p / \partial \rho)_s} \approx 1500$ m/s is the velocity of sound in water (the derivative is calculated for constant entropy, since the process of compression and decompression in an acoustic wave is assumed to be adiabatic). Besides the equations, boundary conditions (4.7)–(4.9) must, naturally, also, undergo linearization. The respective procedure is described in Sect. 3.1.3 (see Eqs. (3.36) and (3.37)).

The last term in the right-hand part of Eq. (4.16) describes the force of buoyancy. The significance of the force of buoyancy can be estimated by calculating the ratio of the absolute values of the second and first terms in the right-hand part of Eq. (4.16). With regard to formula (4.18) we obtain the following estimate:

$$\frac{|\rho' \mathbf{g}|}{|\nabla p'|} \sim \frac{g\lambda}{c^2}, \quad (4.19)$$

where λ is the acoustic wavelength. From the obtained expression it follows that the force of buoyancy can exert significant influence on acoustic waves when the wavelength is comparable to the quantity $c^2/g \approx 230$ km. The upper limit of the acoustic wavelength is always noticeably smaller, being determined by the ocean depth, $\lambda_{\max} \leq 4H$. For this reason, it has sense to neglect the force of buoyancy in Eq. (4.16). As a result we arrive at the equation

$$\frac{\partial \mathbf{v}'}{\partial t} = -\frac{\nabla p'}{\rho_0}. \quad (4.20)$$

The set of Eqs. (4.17) and (4.20) represents a classical set of equations of linear hydroacoustics (e.g., Landau and Lifshits 1987; Tolstoy and Clay 1987; Brekhovskikh and Lysanov 2003). This set can be reduced to a single equation, namely, to a homogeneous wave equation. Here, we introduce the flow velocity potential F ,

$$\mathbf{v}' = \nabla F. \quad (4.21)$$

Substitution of representation (4.21) into Eq. (4.20) gives a formula that relates dynamic pressure and the potential,

$$p' = -\rho_0 \frac{\partial F}{\partial t}. \quad (4.22)$$

Expressing variations of the density ρ' in Eq. (4.17) via variations of pressure p' by formula (4.18) we obtain

$$\frac{1}{c^2} \frac{\partial p'}{\partial t} + \rho_0 \operatorname{div}(\mathbf{v}') = 0. \quad (4.23)$$

Substitution of pressure p' and velocity \mathbf{v}' , expressed by formulae (4.22) and (4.21), into expression (4.23) gives the sought wave equation,

$$\frac{\partial^2 F}{\partial t^2} - c^2 \Delta F = 0. \quad (4.24)$$

We supplement wave equation (4.24) with linearized boundary conditions on the free surface and on the oceanic bottom. We write the conditions in terms of the flow velocity potential (see Sect. 3.1.3),

$$\frac{\partial^2 F}{\partial t^2} + g \frac{\partial F}{\partial z} = 0 \quad \text{for } z = 0, \quad (4.25)$$

$$\frac{\partial F}{\partial \mathbf{n}} = (\mathbf{v}_b, \mathbf{n}) \quad \text{for } z = -H(x, y). \quad (4.26)$$

The flow velocity can be calculated from the known potential F making use of formula (4.21), while the dynamic pressure field can be calculated applying formula (4.22). Displacement of the free surface is determined by the following formula (see Sect. 3.1.3):

$$\xi = -\frac{1}{g} \left. \frac{\partial F}{\partial t} \right|_{z=0}. \quad (4.27)$$

As initial conditions for problem (4.24)–(4.26) at $t = 0$ we set the potential equal to zero, $F = 0$, as well as the derivative of the potential with respect to time, $\partial F / \partial t = 0$. Physically, the first condition signifies a zero initial flow velocity field $\mathbf{v}'_0 = 0$, while the second points to zero deviation of the pressure distribution from hydrostatic equilibrium, $p'_0 = 0$.

The wave equation (4.24) with boundary conditions (4.25) and (4.26), supplemented with the initial conditions described above, represents the Cauchy–Poisson problem formulated within the framework of linear potential theory. The solution of this problem describes acoustic and gravitational waves, excited in a water layer by small-amplitude dynamic deformations of the ocean bottom. Note that the problem for an incompressible liquid, (3.26), (3.36), and (3.37), is a limit case of the problem for a compressible liquid, (4.24)–(4.26), when $c \rightarrow \infty$.

The problem (4.24)–(4.26) can be resolved analytically for an ocean of constant depth $H = \text{const}$. In this case the boundary condition on the ocean bottom, (4.26), transforms into the following simple form:

$$\frac{\partial F}{\partial z} = \frac{\partial \eta}{\partial t} \quad \text{for } z = -H, \quad (4.28)$$

where η is the bottom surface deviation from its initial position.

In subsequent sections analytic solutions will be obtained and analyzed for problems of the generation of wave motions in a compressible water layer of fixed depth in the case of dynamic ocean bottom deformations of small amplitude $|\eta| \ll H$. We shall restrict ourselves to resolving the two following two-dimensional problems: the plane problem (in a Cartesian reference frame) and the quasi-three-dimensional problem (exhibiting cylindrical symmetry).

Cartesian Coordinates

In a Cartesian reference frame, the solution of the problem (4.24), (4.25), (4.28) is sought via the respective Laplace and Fourier transformations relative to the time and space coordinates in the following form:

$$F(x, z, t) = \int_{s-i\infty}^{s+i\infty} dp \int_{-\infty}^{+\infty} dk \Phi(z, p, k) \exp\{pt - ikx\}. \quad (4.29)$$

Substituting formula (4.29) into expression (4.24), we obtain an equation for determining function $\Phi(z, p, k)$,

$$\Phi_{zz} - \alpha^2 \Phi = 0, \quad (4.30)$$

where $\alpha^2 = k^2 + p^2 c^{-2}$.

The solution of Eq. (4.30) is well known and can be written in the form,

$$\Phi(z, p, k) = A \cosh(\alpha z) + B \sinh(\alpha z),$$

where A and B are arbitrary numerical coefficients.

Applying the boundary condition for a free surface, (4.25), we find the relationship between the coefficients,

$$B = -A p^2 (g\alpha)^{-1}.$$

With the aid of the boundary condition for the basin bottom, (4.28), we determine the coefficient A :

$$A = -\frac{p \Psi(p, k)}{\alpha \sinh(\alpha H) + p^2 g^{-1} \cosh(\alpha H)},$$

where function $\Psi(p, k)$ represents the Laplace and Fourier transforms of the space-time law of motion of the bottom $\eta(x, t)$,

$$\Psi(p, k) = \frac{1}{4\pi^2 i} \int_0^{\infty} dt \int_{-\infty}^{+\infty} dx \eta(x, t) \exp(-pt + ikx). \quad (4.31)$$

Thus, we have function $\Phi(z, p, k)$ in the following form:

$$\Phi(z, p, k) = \frac{p\Psi(p, k)}{\alpha \sinh(\alpha H) + p^2 g^{-1} \cosh(\alpha H)} \left(p^2 (g\alpha)^{-1} \sinh(\alpha z) - \cosh(\alpha z) \right). \tag{4.32}$$

Substitution of expression (4.32) into formula (4.29) yields the final expression for calculation of the potential corresponding to an arbitrary space–time law determining the displacement of the bottom, $\eta(x, t)$. In investigating analytical models, it is of interest to consider the behavior of the free surface of the liquid (as the most illustrative characteristic), the displacement of which relative to its unperturbed level is expressed via the potential in accordance with formula (4.27). As a result we obtain the following expression:

$$\xi(x, t) = g^{-1} \int_{s-i\infty}^{s+i\infty} dp \int_{-\infty}^{\infty} dk \frac{p^2 \Psi(p, k)}{\alpha \sinh(\alpha H) + p^2 g^{-1} \cosh(\alpha H)} \exp\{pt - ikx\}. \tag{4.33}$$

In choosing the concrete function for describing the space–time law determining the motion of the bottom, part of the integrals in expression (4.33) can be calculated analytically.

Cylindrical Coordinates

The cylindrical reference frame will be introduced in a standard manner with respect to the Cartesian reference frame, described in Sect. 3.1.1. The origin of the cylindrical reference frame will be located on the free unperturbed surface, axis Oz will be directed vertically upward. As a source of elastic gravitational waves we shall consider axially symmetric movements of the bottom proceeding in accordance with the law $\eta(r, t)$. The wave equation in the cylindrical reference system exhibits the following form:

$$r^{-1} (r F_r)_r + F_{zz} = c^{-2} F_{tt}. \tag{4.34}$$

The boundary conditions on the surface, (4.25), and on the bottom, (4.28), retain their form in the cylindrical reference frame.

The solution of the problem (4.34), (4.25), and (4.28) is sought applying the separation of variables in the form of the inverse Laplace transformation,

$$F(r, z, t) = \int_{s-i\infty}^{s+i\infty} dp R(r, p) Z(z, p) \exp\{pt\}. \tag{4.35}$$

Substituting formula (4.35) into (4.34), we obtain equations for determining functions $R(r, p)$ and $Z(z, p)$,

$$r^{-1} (r R_r)_r + k^2 R = 0 \tag{4.36}$$

$$Z_{zz} - \alpha^2 Z = 0, \tag{4.37}$$

where $\alpha^2 = k^2 + p^2 c^{-2}$. The solutions of Eqs. (4.36) and (4.37) are well known (Nikiforov and Uvarov 1984). Making use of this result, one can represent the general solution of Eq. (4.34) as follows:

$$F(r, z, t) = \int_0^\infty dk \int_{s-i\infty}^{s+i\infty} dp \exp\{pt\} J_0(kr) (A(p, k) \cosh(\alpha z) + B(p, k) \sinh(\alpha z)), \tag{4.38}$$

where J_0 is the zeroth-order Bessel function of the first kind.

With the aid of the boundary condition on the free surface, (4.25), we find the relationship between the coefficients A and B ,

$$B(p, k) = -A(p, k) p^2 (g \alpha)^{-1}.$$

The boundary condition on the bottom, (4.28), permits to determine the coefficient $A(p, k)$,

$$A(p, k) = -\frac{p k \Psi(p, k)}{\alpha (\sinh(\alpha H) + p^2 g^{-1} \alpha^{-1} \cosh(\alpha H))}, \tag{4.39}$$

where function $\Psi(p, k)$ represents the Laplace and Fourier–Bessel transforms of the space–time law of movements of the bottom, $\eta(x, t)$,

$$\Psi(p, k) = \frac{1}{2\pi i} \int_0^\infty dr \int_0^\infty dt \eta(r, t) r J_0(kr) \exp\{-pt\}. \tag{4.40}$$

We shall further consider the behavior of a free surface, the displacement of which from its unperturbed level is expressed through the potential as follows:

$$\xi(r, t) = -g^{-1} F_t(r, 0, t). \tag{4.41}$$

With use of formula (4.38) expression (4.41) acquires the following form:

$$\xi(r, t) = -g^{-1} \int_0^\infty dk \int_{s-i\infty}^{s+i\infty} dp p \exp\{pt\} J_0(kr) A(p, k). \tag{4.42}$$

4.1.3 Piston and Membrane Displacements

We shall start exposition of the peculiarities of tsunami formation in a compressible ocean by considering the axially symmetric problem (Nosov 2000). As sources of acoustic-gravity waves we choose two model displacements of the bottom: the piston and membrane displacements,

$$\eta_1(r, t) = \eta_0(1 - \theta(r - R)) \left(\frac{\theta(t) t - \theta(t - \tau)(t - \tau)}{\tau} \right), \quad (4.43)$$

$$\eta_2(r, t) = \eta_0(1 - \theta(r - R)) \times \left(\frac{2\theta(t) t - 4\theta(t - 0,5\tau)(t - 0,5\tau) + 2\theta(t - \tau)(t - \tau)}{\tau} \right), \quad (4.44)$$

where θ is the Heaviside step function. The displacement amplitude η_0 is the same throughout the entire active zone, exhibiting a circular shape of radius R , and is zero outside this region. The duration of the displacement is τ .

We introduce the dimensionless variables (the asterisk "*" will be dropped),

$$\begin{aligned} k^* &= kH; & p^* &= pHc^{-1}; & \alpha^* &= \alpha H; \\ R^* &= RH^{-1}; & r^* &= rH^{-1}; & z^* &= zH^{-1}; \\ t^* &= tH^{-1}; & \tau^* &= \tau cH^{-1}; & c^* &= c(gH)^{-1/2}. \end{aligned} \quad (4.45)$$

Making use of the general solution (4.42), we obtain expressions, describing motion of the free surface of a compressible liquid in the case of piston-like (ξ_1) and membrane-like (ξ_2) displacements of the bottom,

$$\xi_1(r, t) = \theta(t) \zeta(r, t) - \theta(t - \tau) \zeta(r, t - \tau), \quad (4.46)$$

$$\begin{aligned} \xi_2(r, t) &= 2\theta(t) \zeta(r, t) - 4\theta(t - 0,5\tau) \zeta(r, t - 0,5\tau) \\ &\quad + 2\theta(t - \tau) \zeta(r, t - \tau), \end{aligned} \quad (4.47)$$

where

$$\zeta(r, t) = \frac{\eta_0 c^2 R}{2\pi i \tau} \int_0^\infty dk \int_{s-i\infty}^{s+i\infty} dp \frac{\exp\{pt\} J_0(rk) J_1(Rk)}{\alpha \sinh(\alpha) + p^2 c^2 \cosh(\alpha)}. \quad (4.48)$$

As a function of the complex parameter p the integrand in (4.48) has two or an infinite number (depending on the sign of α^2) of poles located on the axis $\text{Im}(p) = 0$. An incompressible liquid ($c = \infty$) represents a special case of the problem dealt with. The solution for an incompressible liquid can be obtained by a formal substitution of $\alpha \rightarrow k$ in formula (4.48). The integrand, here, will have only two first-order poles

$p_0^{1,2} = \pm i c^{-1} (k \tanh(k))^{1/2}$, which permits to perform integration over the parameter p analytically. In the case of an incompressible liquid, this results in the function $\zeta(r, t)$, entering into formulae (4.46) and (4.47), assuming the following form:

$$\zeta(r, t) = \frac{\eta_0 c R}{\tau} \int_0^\infty dk \frac{J_0(rk) J_1(Rk) \sin(tc^{-1} (k \tanh(k))^{1/2})}{\cosh(k) [k \tanh(k)]^{1/2}}. \quad (4.49)$$

The integrals in formulae (4.48) and (4.49) were calculated numerically for $c = 8$ and $R = 1, 5$, and 10 .

Figure 4.2 presents the example of time evolvents, showing the displacement of a free surface at two fixed points (at the center of the active zone and outside it) for compressible and incompressible liquids. The insets show the behavior of the free surface of an incompressible liquid at long times. The theory of a compressible liquid is seen to provide a more reliable description of the movement of the surface from the point of view of moment of time the perturbation arrives at the given point. Before the long gravitational wave arrives at point $r = 20$, acoustic precursors of noticeable amplitude are observed. The main difference in behavior between compressible and incompressible liquids consists in the existence of “fast” oscillations of the surface with a prevalent period, equal to $4H/c$. Oscillations take place against the background of the development of a slower gravitational wave. The origin of surface oscillations is due to the excitation of standing acoustic waves in the natural quarter-wave resonator of a “column of compressible liquid with a free surface on the rigid bottom”. The resonator exhibits a set of frequencies, $f_n = 0.25 c (1 + 2n) H^{-1}$, where $n = 0, 1, 2, 3, \dots$. Precisely, the lowest mode corresponds to the period observed.

It is quite probable that such a resonator plays an important part in the formation of seaquakes (see Sect. 1.6). In the case of depths of several kilometers, usual for oceans, the eigenfrequencies of the resonator lie precisely within the range of frequencies of seismic processes. Therefore, extremely effective transmission of energy is possible from an oscillating ocean bottom to the thick volume of water.

Figure 4.3 presents the dependences of the maximum free surface displacement amplitudes for compressible and incompressible liquids versus the durations of bottom displacements. Calculations were performed for three different sizes of the source ($R = 1, 5$, and 10). The maximum amplitudes were determined from the time evolvents in accordance with the following formulae:

- for model of compressible liquid:

$$A = \eta_0^{-1} \left(\max(\xi_{\text{comp}}(t) - \xi_{\text{incomp}}(t)) - \min(\xi_{\text{comp}}(t) - \xi_{\text{incomp}}(t)) \right);$$

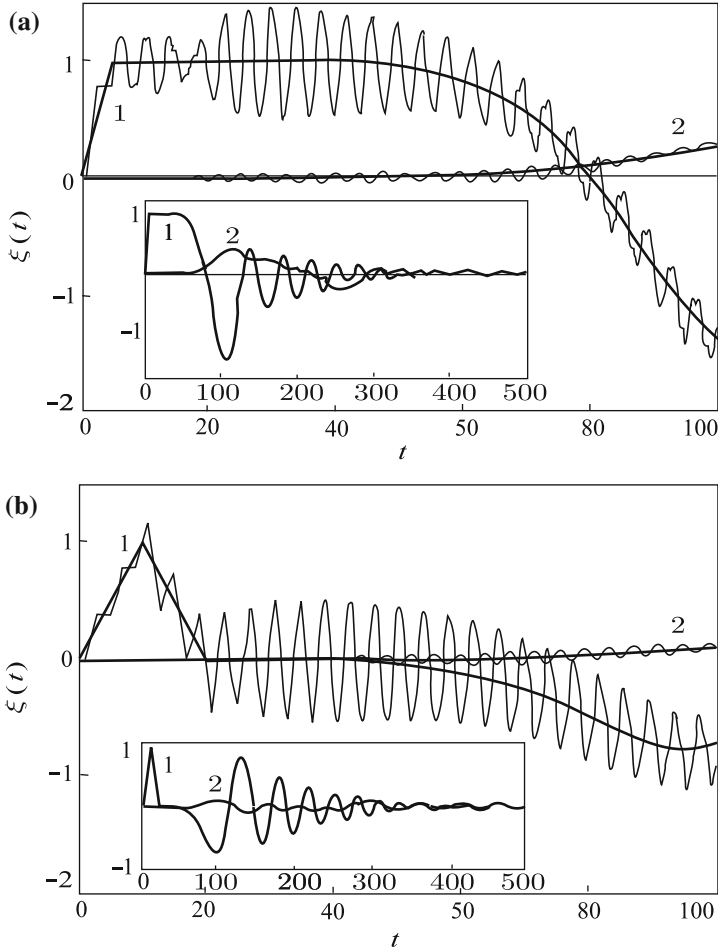


Fig. 4.2 Examples of time evolutions of free surface perturbations of compressible (*thin line*) and incompressible (*thick line*) liquids, caused by displacements of the bottom of duration $\tau = 5$ with a residual deformation (a) and of duration $\tau = 20$ without any residual displacement (b). Curves 1, 2 correspond to $r = 0, 20$, respectively. Calculation were performed for $R = 10$

- for model of incompressible liquid:

$$A = \eta_0^{-1} \left(\max(\xi_{\text{incomp}}(t)) - \min(\xi_{\text{incomp}}(t)) \right).$$

In the case of incompressible liquids the dependences of amplitudes and energies of gravitational waves upon the durations of bottom displacements have been repeatedly investigated theoretically and experimentally by different authors (Hammack 1973; Dotsenko 1995, 1996; Nosov and Shelkovnikov 1997). The

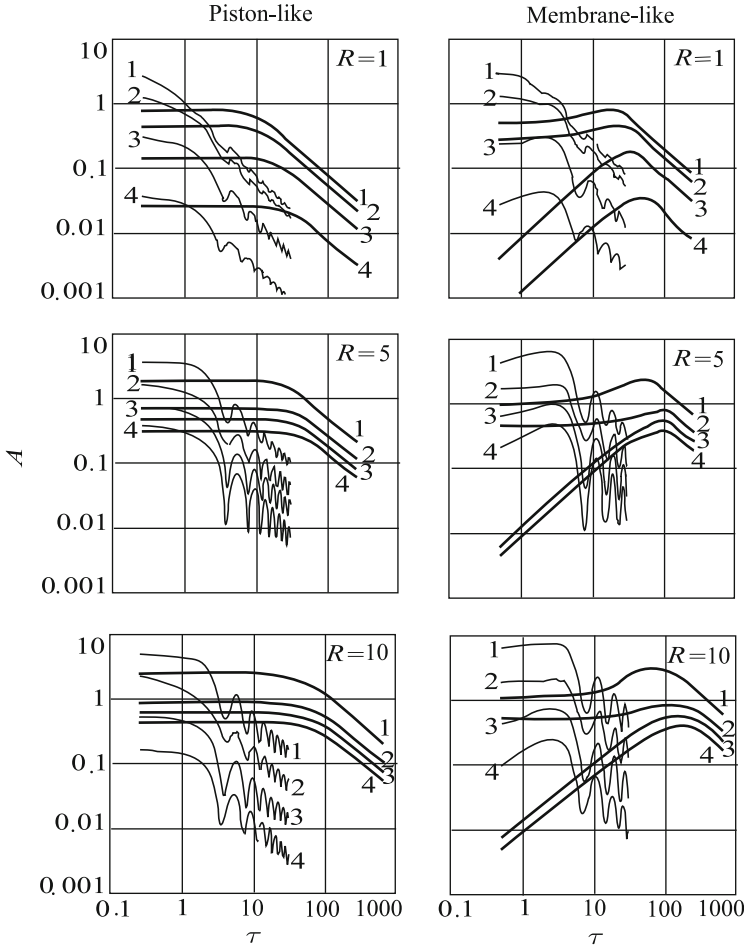


Fig. 4.3 Dependences of maximum amplitude of “fast” surface oscillations (*thin line*) and of maximum amplitude of gravitational waves (*thick line*) upon the durations of bottom displacements with residual deformations (piston-like displacement) and without displacement (membrane-like displacement). Curves 1–4 correspond to distances $r = 0, 10, 20,$ and 40 from the center of the source. Calculations were performed for $R = 1, 5,$ and 10

character of the curves presented in Fig. 4.3 for the case of incompressible liquids is in good agreement with the results of indicated publications and Sects. 3.3 and 3.4.

In the case of an *incompressible* liquid the characteristic features of the amplitude dependence on the displacement duration are the following. When a displacement of the ocean bottom is accompanied by a residual displacement, the dependence is characterized by the presence of a plateau at small values of the parameter τ and by a monotonous drop at large τ values. When no residual displacement accompanies the displacement, the dependence considered has a local maximum that shifts

to the right as the source radius increases. Short displacements of the ocean bottom without residual displacement result in the formation of very weak surface perturbations outside the source.

Enhancement of the size of the active zone leads to an increase in both the amplitude of “fast” surface oscillations and the amplitude of gravitational waves. It must be noted that an increase of the size of the active zone causes a noticeable change in the amplitude only for values of the parameter $R < 5$, after which the dependence reaches saturation.

The specific nonmonotonous character of the curves, related to the model of compressible liquids, is due to the aforementioned resonance properties. As the displacement duration increases, the amplitude of “fast” oscillations tends to decrease. It is interesting to note that in the case of large values of parameter τ all the dependences (both for compressible and incompressible liquids) behave like τ^{-1} . Given other conditions being equal, the amplitude of “fast” surface oscillations above the source may be several times larger than the amplitude of surface displacements of an incompressible liquid.

The duration of real ocean bottom displacements lies within the range 0.4–40 (1–100 s). On the basis of data presented in Fig. 4.3 it is possible to conclude that the maximum amplitude of gravitational waves proper in the case of bottom displacements, involving residual deformation, is weakly sensitive to variations of the parameter τ . In the case of displacements of the ocean bottom without residual deformation the amplitudes of gravitational waves, going beyond the limits of the source, undergo quite significant changes within the range we are interested in. For any type of displacement the amplitude of “fast” surface oscillations depends strongly on the displacement duration.

Figure 4.4 presents the dependences of amplitudes of gravitational waves and of “fast” surface oscillations upon the distance from the source center r . The data correspond to the duration of the ocean bottom displacement, $\tau = 1$, which does not violate the general nature of the conclusions, since the form obtained for the solution of (4.46) and (4.47) reveals that the parameter τ does not affect the decrease of amplitude with distance. In all cases, the amplitude varies weakly immediately above the source zone. Outside the source zone the amplitude of gravitational waves decreases approximately like $r^{-1/2}$ (corresponding to the known asymptotic estimates, see Pelinovsky 1996), while the amplitude of oscillations drops like r^{-2} . Here, displacements of the ocean bottom with and without residual deformation lead practically to the same oscillation amplitude, while the amplitudes of gravitational waves differ noticeably. Figure 4.4 permits to conclude that “fast” surface oscillations are considered local effects, the appearance of which should be noticeable either immediately at the tsunami source, or at relatively small distances, not exceeding several sizes of the source.

The general picture of tsunami excitation in a compressible ocean can be represented as follows. When a vertical displacement of the ocean bottom occurs, the water column is shifted correspondingly, and under the force of gravity it gradually starts to spread out, at the same time undergoing elastic oscillations. Therefore, the tsunami source not only serves as a source of gravitational tsunami waves, but also of

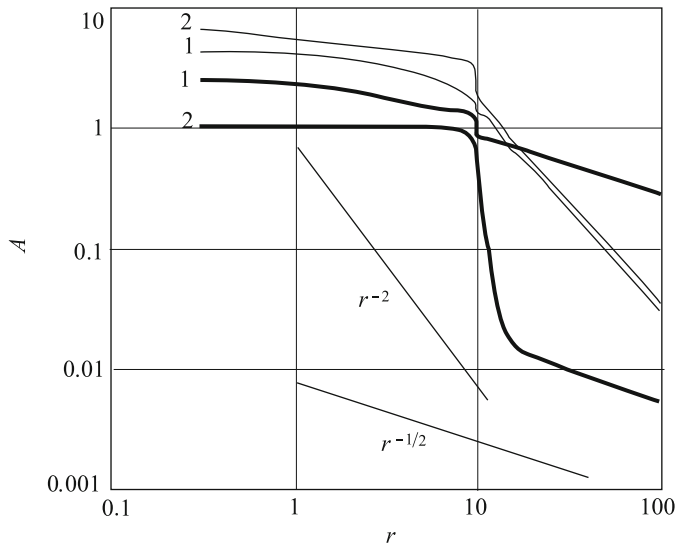


Fig. 4.4 Dependences of maximum amplitude of “fast” surface oscillations (*thin line*) and of maximum amplitude of gravitational waves (*thick line*) upon the distance from the source center. Curves 1, 2 correspond, respectively, to displacements of the bottom with residual deformation (piston-like displacement) and without residual deformation (membrane-like displacement). Calculations are performed for $\tau = 1$, $R = 10$

low-frequency acoustic waves, the emission of which is possible at the characteristic frequencies $f_n = 0.25 c (1 + 2n) H^{-1}$. Waves of low energy-carrying modes exhibit lengths that significantly exceed the width of the underwater acoustic channel and that, consequently, cannot be captured by it. In this case the entire thickness of the ocean must serve as the waveguide, while the elastic waves considered will effectively be scattered on irregularities of the ocean bottom and of the water surface and be absorbed by the elastic ocean bottom. Most likely, it is precisely for this reason that at large distances from the source only relatively weak components of the signal are observed at frequencies $f > 2$ Hz, and precisely they are termed the T-phase.

4.1.4 The Running Displacement

In dealing with the running displacement problem in Sect. 3.3.3 we noted that movements of the ocean bottom of such types are characterized by high propagation velocities, at which the theory of incompressible liquids cannot be applied. The velocity, with which the fault ruptures at the earthquake source, the crack propagating along the bottom, surface seismic waves—all these phenomena are characterized by velocities exceeding the speed of sound in water. And it is only in the case of underwater slumps (landslides) that the velocity of a running displacement is

significantly inferior to the speed of sound in water. Therefore, the aim of this section is the construction of a mathematical model for the excitation of waves by a running displacement of the ocean bottom in a compressible liquid.

Consider a plane problem, the general formulation of which corresponds to (4.24), (4.25), and (4.28). We shall choose the model law of motion of the ocean bottom in the case of a running displacement to be of the form (Fig. 3.3)

$$\eta(x, t) = \eta_0(\theta(x) - \theta(x - a))(1 - \theta(x - vt)), \tag{4.50}$$

where $\theta(z)$ is the Heaviside step function. The residual deformation of the ocean bottom, η_0 , is the same over the entire active zone of length a and equals zero outside this zone. The horizontal propagation velocity of the displacement is v . A similar problem has been resolved in Sect. 3.3.1 for the case of an incompressible liquid.

We shall apply the general solution of the problem (4.33) and pass to dimensionless variables in accordance with formulae (4.45), which in the case of a running displacement must be complemented with the expression $v^* = v(gH)^{-1/2}$ (we drop the asterisk “*”). As a result we arrive at the following expression describing the surface perturbation of a compressible liquid caused by a running displacement of the ocean bottom (Nosov and Sammer 1998),

$$\xi(x, t) = \frac{\eta_0 c^2}{4\pi^2 i} \int_{-\infty}^{+\infty} dk \int_{s-i\infty}^{s+i\infty} dp \frac{p(\exp\{a\gamma\} - 1) \exp\{pt - ikx\}}{\gamma \cosh(\alpha) (\alpha \tanh(\alpha) + p^2 c^2)}, \tag{4.51}$$

where $\gamma = (ik - pcv^{-1})$, $\alpha^2 = k^2 + p^2$.

As a function of the complex parameter p the integrand expression has two or an infinite number (depending on the sign of α^2) of poles located on the axis $\text{Im}(p) = 0$. Since the positions of the poles are determined from the solution of a transcendental equation, and, besides, they depend on the parameter k , over which external integration is performed, further analysis of expression (4.51) was carried out numerically. Formula (3.81), obtained in Sect. 3.3.1, is the analog of expression (4.51) for the case of incompressible liquids.

The following parameter values were chosen for calculations: $c = 8$, $a = 10$, which at ocean depths of 4000 m approximately correspond to the velocity of sound in water, 1500 m/s, and to a horizontal size of the source equal to 40 km. The propagation velocity of the displacement, v , was varied within limits from 0.125 up to 32 (from 23 up to 6000 m/s).

Figure 4.5 presents displacement profiles of the surface of a liquid, $\xi(x)$, for the time moment $t = 10$, calculated within the framework of models for compressible and incompressible liquids for three displacement propagation velocities, $v = 4, 8, 16$. In all cases, an account of the compressibility led to a significantly more subtly structured perturbation of the surface, differing from zero only at those points, at which the elastic wave, formed by the running displacement, had time to arrive. As it is seen from the figure, when $v = 4$, the differences between free

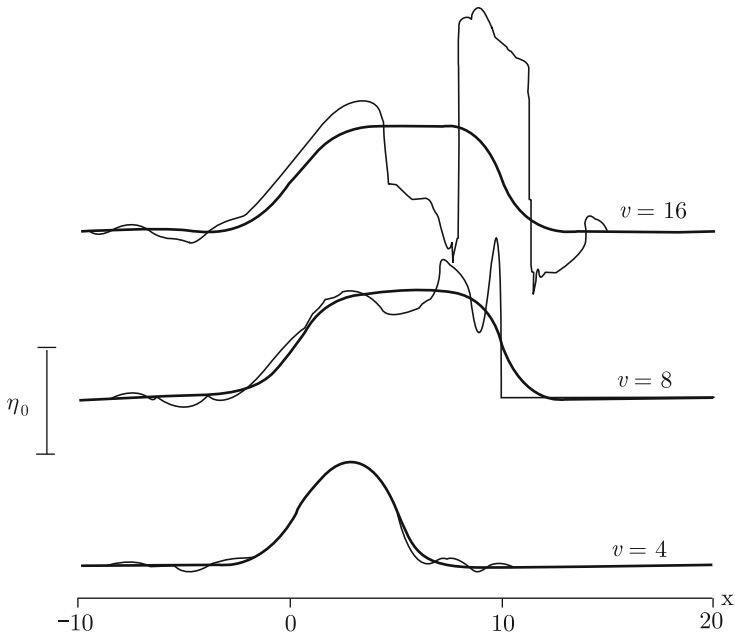


Fig. 4.5 Profiles of surface displacement of a liquid at moment of time $t = 10$ for different propagation velocities of the running displacement, v . The *thick* and *thin* lines correspond to incompressible and compressible liquids, respectively

surface perturbations for compressible and incompressible liquids is not so large, but in the case of high velocities the difference becomes quite significant. When $v \geq c$, the profile is characterized by the presence of steep fronts and of an original periodic structure, that is a consequence of multiple reflections from the surface and from the ocean bottom of the front of the elastic wave, formed by the front edge of the running displacement. From mathematical physics it is known that when an elastic wave is reflected from a free surface, it changes polarity. Thus, for this reason positive and negative fronts alternate.

The results of calculations of time evolvents $\xi(t)$ for the center of the active zone ($x = 5$) are presented in Fig. 4.6. The main feature, distinguishing the behavior of a compressible liquid, consists in the rise in the source area of surface oscillations with a prevalent period equal to four. Oscillations take place against the background of a developing slower gravitational wave. The rise of surface oscillations is due to the excitation of standing acoustic waves in the natural resonator of a “column of compressible liquid with a free surface on the rigid bottom”. Similar oscillations arise in the case of piston-like and membrane-like displacements of the ocean bottom (Fig. 4.2).

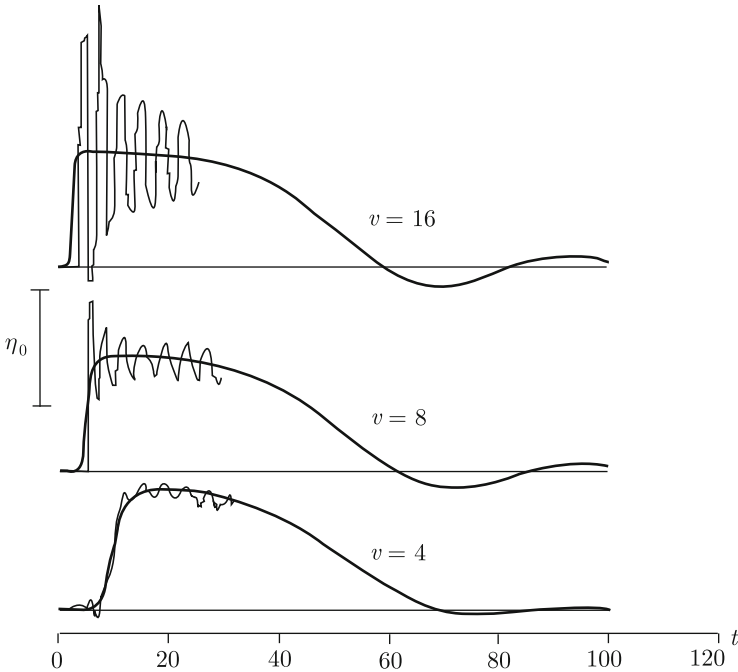
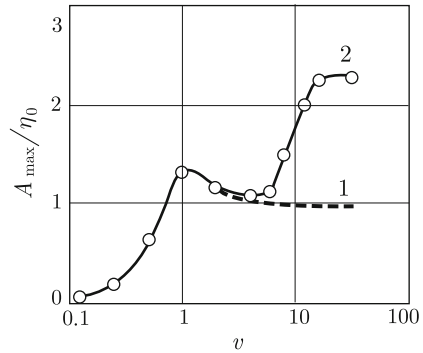


Fig. 4.6 Time evolvents of surface displacements of liquids at the center of the active zone for different displacement propagation velocities v . The *thick* and *thin lines* correspond to incompressible and compressible liquids, respectively

Within the framework of the model applied, the damping of oscillations is due to the outflow of elastic wave energy from the generation area. The oscillation damping process proceeds, in this case, faster than in the case of vertical displacements of the ocean bottom, which is related to the existence of a large number of elastic wave rays deviated from the vertical direction. In real natural conditions the damping will proceed even more rapidly owing to losses occurring, when the elastic waves are reflected and scattered from the boundaries “water–bottom” and “water–atmosphere”.

In Fig. 4.7, the dependence of the maximum amplitude of surface displacement at the center of the active zone ($x = 5$) is presented in a semilogarithmic scale as a function of the velocity v . From the figure it is seen that for propagation velocities of the displacement inferior to $v = 4$ ($v = c/2 \sim 750$ m/s) practically no difference exists between the models for compressible and incompressible liquids. Both theories reveal the presence of a local maximum at $v = 1$, corresponding to resonance excitation of gravitational waves. At high velocities the model for incompressible liquids more than twice underestimates the free surface displacement.

Fig. 4.7 Maximum amplitudes of surface displacements for incompressible (1) and compressible (2) liquids at the center of the active zone versus the propagation velocity of the bottom displacement, v



4.1.5 Peculiarities of Wave Excitation in a Basin of Variable Depth

Analytical resolution of the problem of movements of a compressible liquid in a basin with an irregular bottom encounters significant complications, while in the general case it is not even possible. Therefore, in studying peculiarities of the excitation of elastic gravitational waves in a basin of *variable depth* it is expedient to apply numerical simulation (Nosov and Kolesov 2003, 2007). It must be noted that numerical methods have also to be applied in dealing with analytical solutions (for calculating integrals). Given all the obvious advantages of analytical solutions, direct numerical simulation often turns out to be much more efficient.

We shall consider the plane problem (4.24)–(4.26).

Numerical resolution implies using a region of finite dimensions for calculations. Thus, besides the boundary conditions on the bottom and on the surface, conditions must be formulated for the left and right boundaries of the calculation region. As such conditions for free second-order transition (of elastic waves) were chosen (Marchuk et al. 1983):

$$c \frac{\partial^2 F}{\partial x \partial t} - \frac{\partial^2 F}{\partial t^2} + \frac{c^2}{2} \frac{\partial^2 F}{\partial z^2} = 0, \quad x = x_{\min}, x_{\max}. \tag{4.52}$$

Equation (4.24) and the boundary conditions (4.25), (4.26) and (4.52) were reduced to a dimensionless form in accordance with formulae, $(x^*, z^*) = (x, z)H_{\max}^{-1}$, $t^* = tH_{\max}^{-1}c$, where H_{\max} is the maximum depth of the basin.

The distribution of depths chosen for calculations imitated transition from the shelf zone through the continental slope toward the abyssal plain (Fig. 4.8a). The parameter $L = 80$ km was not varied. The depths H_1 and H_2 varied between 0.5 and 8.5 km. The maximum steepness of the slope amounted to 0.1. The tsunami source was located on the slope and represented a displacement involving residual deformation. The form of the space–time law of motion of the bottom deformation, $\eta(x, t) = X(x)T(t)$, is shown in Fig. 4.8b. Movement of the bottom occurred in a direction normal to the surface of the bottom. The displacement duration varied between 1 and 100 s.

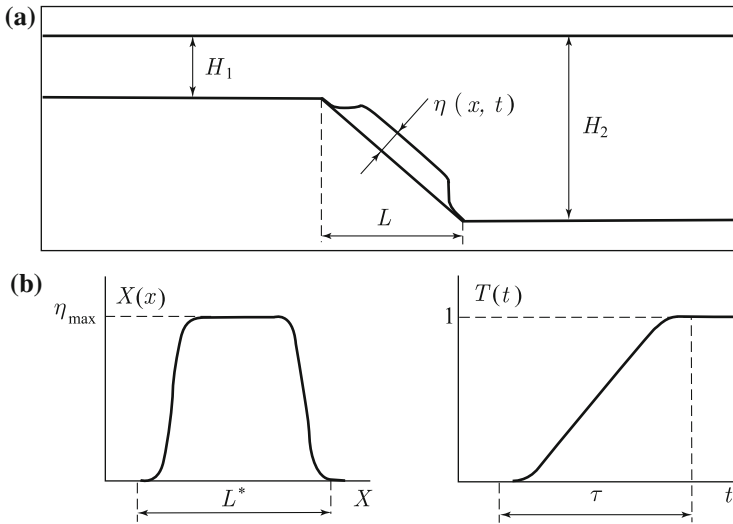


Fig. 4.8 Shape of calculation region (a). Space–time law of motion of bottom (b)

Resolution of the problem (4.24)–(4.26) and (4.52) was performed by the explicit finite difference method on a rectangular mesh with fixed (but not identical) horizontal and vertical steps. As the stability condition we adopted the Courant criterion $\Delta t < \min(\Delta x, \Delta z)/c$, where Δt is the time step, Δx and Δz are the space steps.

Figures 4.9 and 4.10 show the calculated free surface disturbance at time moment $t = 1000$ s for different depth values H_1 and H_2 . The displacement duration was 10 s. Figure 4.9 corresponds to a fixed depth of the shallow-water area, $H_1 = 0.5$ km; here, the depth H_2 is varied. Figure 4.10 demonstrates the results of calculations for the case of a fixed average depth of the calculation region: the slope “rotates” about its central point $x = 0, z = -4.5$ km. Practically, the wave perturbation of the surface in all the cases consists of a slow gravitational component and of a fast acoustic component.

In the case of a horizontal ocean bottom ($H_1 = H_2 = 4.5$ km) elastic oscillations of the water column above the source area continue to be present for a long time. This is due to the wave vectors retaining directions close to vertical, and the energy of elastic oscillations slowly leaves the source area. The appearance of even a very insignificant slope of the bottom (1:160 for $H_1 = 4.25$ km, $H_2 = 4.75$ km) alters the picture drastically. In the deep part of the basin an acoustic precursor is observed of significant amplitude, the amplitude of elastic surface oscillations in the shallow region remains practically intact. Oscillations immediately above the source are already close to conclusion by the time moment $t = 1000$ s. Further enhancement of the slope’s steepness, first, leads to a decrease in the amplitude of the acoustic precursor in the shallow-water part of the basin, and, subsequently, to its total disappearance. Hence follows the important conclusion, that it is impossible to register an acoustic precursor in shallow water, for example, by variations of the sea level.

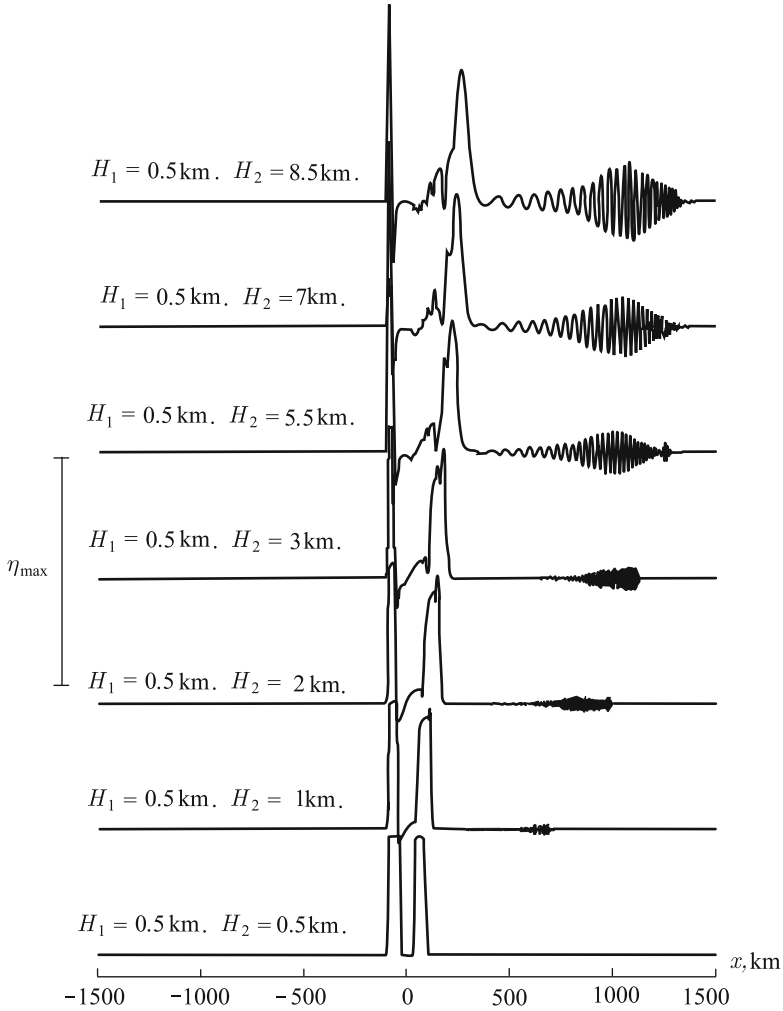


Fig. 4.9 Perturbation of free surface at time moment $t = 1000$ s

The absence is also to be noted of any manifestation of the compressibility effect on the surface in the case of insignificant depths $H_1 = H_2 = 0.5$ km (Fig.4.9). Enhancement of the slope's steepness is accompanied by an increase in the propagation velocity of the acoustic precursor toward the deepwater area. Here, the region of maximum amplitudes is intended, the front of acoustic perturbation, naturally, travels with the velocity of a sonic wave.

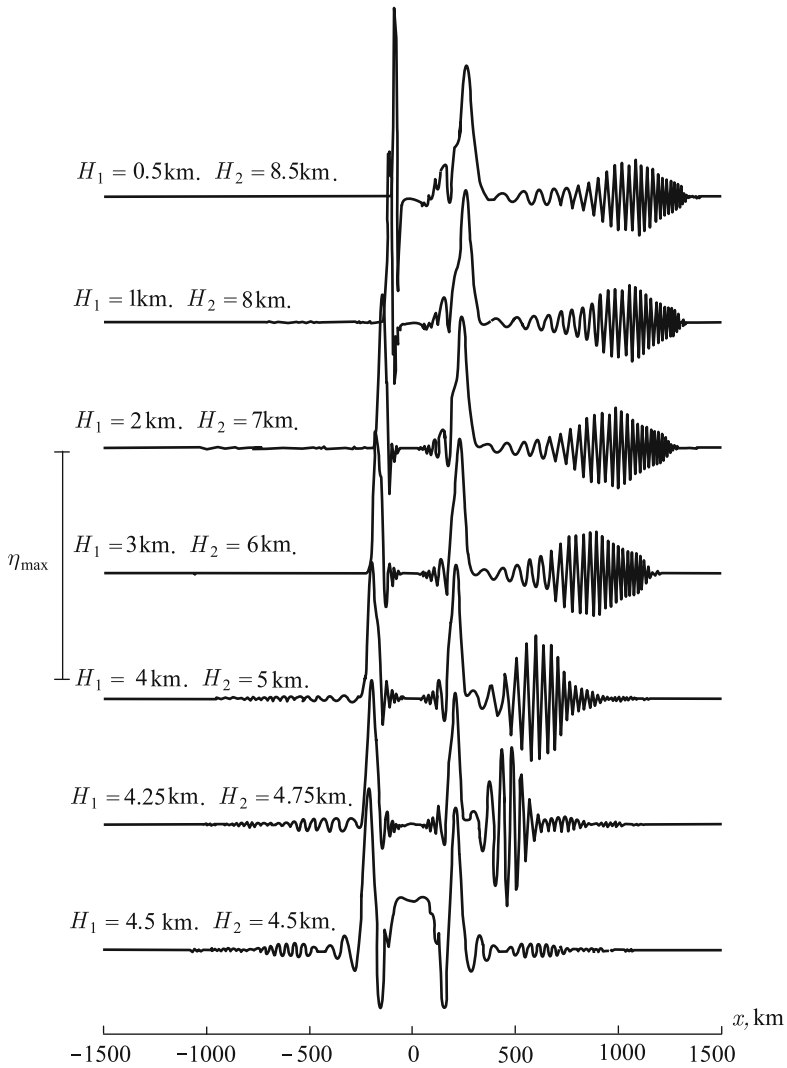


Fig. 4.10 Perturbation of free surface at time moment $t = 1000 \text{ s}$

In the deepwater region, the wavelength of the acoustic precursor and its amplitude may reach values comparable to the length and amplitude of a tsunami gravitational wave. The wavelength of the acoustic precursor in the deepwater area grows starting from the front toward the “tail”. This effect is a direct consequence of the geometrical dispersion (or waveguide dispersion). Indeed, a column of compressible liquid, limited by a free surface and by an absolutely rigid bottom, represents a waveguide.

It is known (Tolstoy and Clay 1987) that the group velocity for each mode n in such a waveguide is determined by the formula,

$$C_{gr} = \frac{c}{\sqrt{1 + (k_z^n/k_x)^2}},$$

where k_x is the horizontal wavenumber, $k_z^n = \pi(1 + 2n)/2H$ is the vertical wavenumber for the n th mode ($n = 0, 1, 2, \dots$). It is seen from the formula that the group velocity rises, as the horizontal wavenumber increases, i.e., as the wavelength decreases.

As compared to the case of elastic surface perturbation, the amplitude characteristics of gravitational waves are not so sensitive to variations in the ocean bottom profile. Nevertheless, the wave of higher amplitude can be seen to propagate into the shallow-water area. Anyhow, the wave entering the deepwater area exhibits greater energy.

The dynamic pressure happens to be the most illustrative characteristic for describing the wave field throughout the thickness of a water column. In natural conditions precisely, the dynamic pressure can be measured in a most simple manner (with the aid of hydrophones). Figure 4.11 presents an example of characteristic dependences of the dynamic pressure versus time, calculated for six fixed points, the location of which is shown in the inset. From the figure it is seen that the amplitude of dynamic pressure related to elastic waves (the short-period component) increases as it approaches the ocean bottom. The contribution given by the gravitational surface wave (long-period component at points 1–3) is noticeable only in the shallow-water region against the background of quite weak elastic oscillations. In the deepwater area the amplitude of dynamic pressure reaches a significantly higher value, and the main contribution to the perturbation is precisely due to the acoustic, but not gravitational, component.

We shall further analyze the peculiarities of the space distribution of the dynamic pressure amplitude for various shapes of the relief of the ocean bottom and conditions for wave generation. We define the amplitude dynamic pressure in accordance with formula,

$$p_{\max}(x, z) = \max_{0 < t < \Theta} [p(t, x, z)],$$

where Θ is the moment of time, when the acoustic and gravitational waves have already had time to leave the point considered.

The influence the ocean bottom slope in the source area has on the space distribution of the dynamic pressure amplitude is illustrated by Fig. 4.12. From the figure it is seen that the amplitude of dynamic pressure reaches its maximum values near the ocean bottom, while the presurface region is characterized by minimum values of the dynamic pressure. This property is a direct consequence of the boundary condition at the free water surface. When the bottom is flat, the region of maximum pressures is localized immediately above the source, and the amplitude of the signal

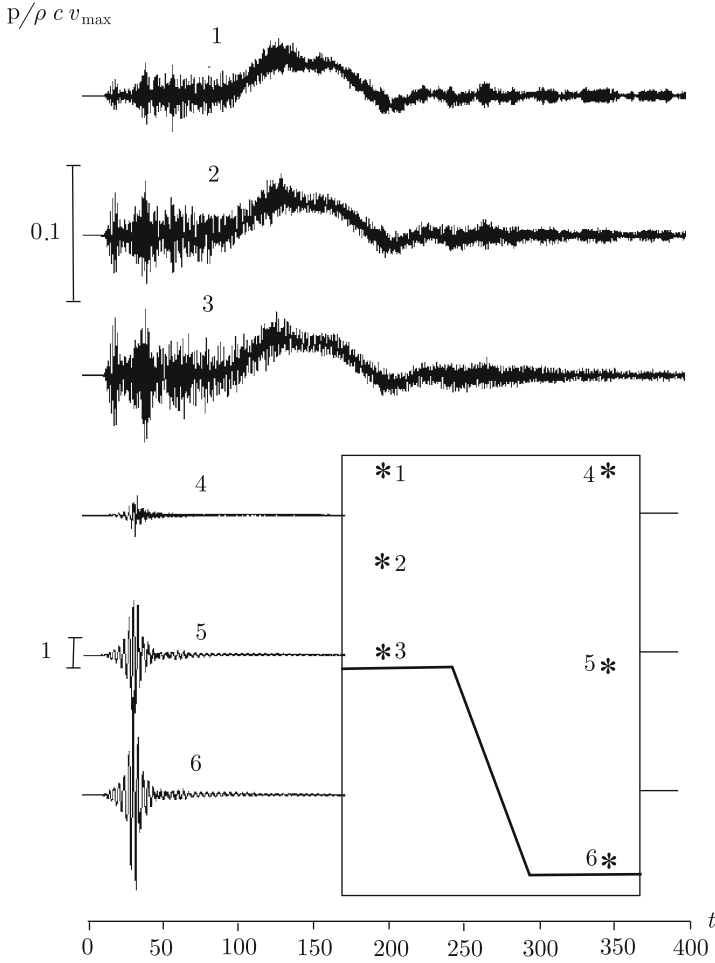


Fig. 4.11 Dynamic pressure, calculated as function of time at fixed points. The pressure is normalized to the quantity $\rho c v_{\max}$, where v_{\max} is the maximum velocity of movement of the ocean bottom. The scale units for realizing 1–3 and 4–6 are different (indicated in the figure for curves 2 and 5, respectively)

reaches noticeable values near the ocean bottom ($p_{\max} \sim 0.5\rho c v_{\max}$) at significant distances from the source, ~ 200 km, also. In Fig. 4.12 the amplitude of the dynamic pressure is normalized to the quantity $\rho c v_{\max}$, where v_{\max} is the maximum velocity of motion of the ocean bottom. The appearance of even a very insignificant slope angle in the vicinity of the source leads to a shift of the region of maximum pressures toward large depths. In this case the amplitude of the signal in the shallow-water region is noticeably reduced. Further enhancement of the ocean bottom slope angle results in the maximum pressure values being achieved already outside the source area (in

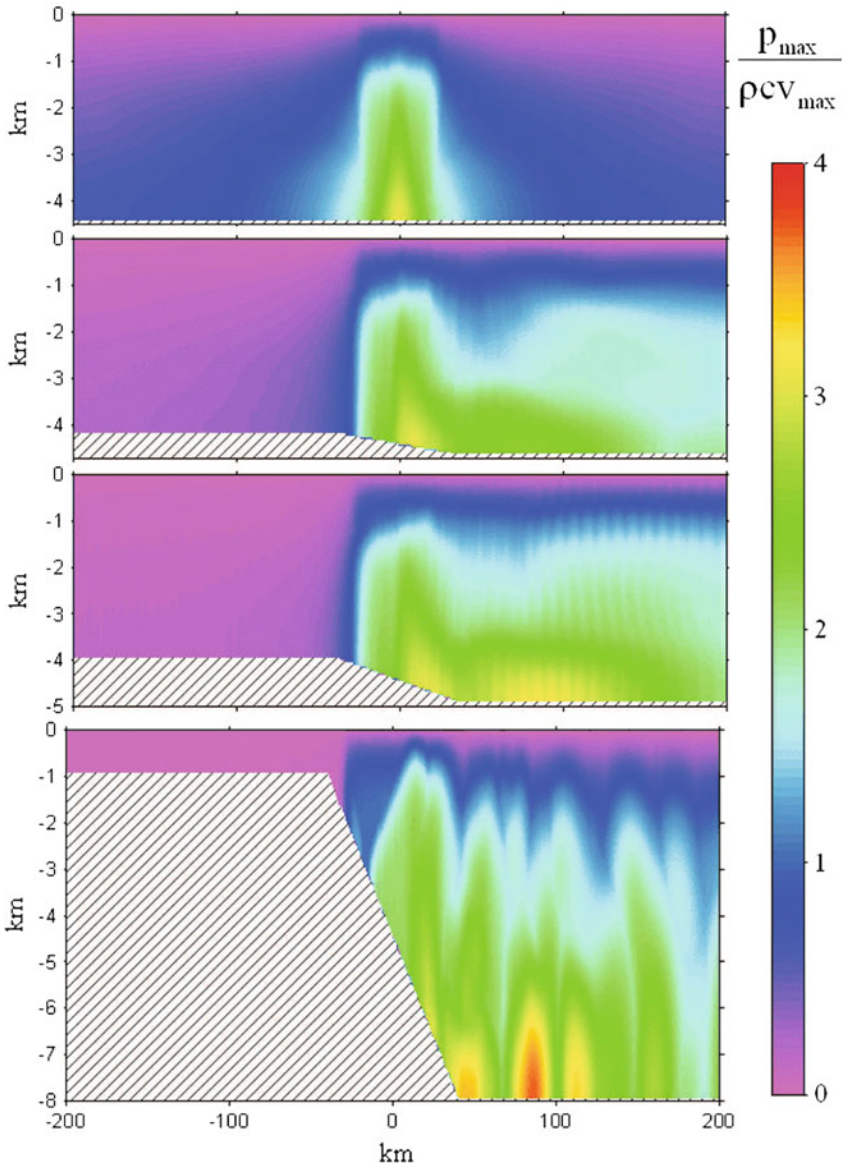


Fig. 4.12 Space distribution of maximum dynamic pressure. The calculation is performed at $\tau = 10$ s for various profiles of the ocean bottom

the deepwater region), while propagation of the acoustic signal into the shallow-water region is strongly suppressed. Thus, for example, if $H_1 = 1$ km and $H_2 = 8$ km in the shallow-water region, then the dynamic pressure remains at a level $\sim 0.02\rho cv_{\max}$, and the main contribution to this quantity is not due to the acoustic, but to the surface gravitational wave. At the same time, in the deepwater area the pressure amounts to $3\rho cv_{\max}$ and more.

In the case of short-duration displacements the region of maximum dynamic pressure may be observed not only near the ocean bottom, but also inside the thick water column, which is due to the excitation of higher modes of elastic oscillations. In the case of long-duration displacements the dynamic pressure becomes homogeneous in the vertical direction, because effects of water compressibility lose their first-priority significance, and the pressure related to gravitational waves starts to prevail.

In the case of a basin of variable depth, for instance, when the source of waves is located on the sloping ocean bottom, a most important result consists in the shallow-water region turning out to be practically closed to the penetration of elastic waves. The acoustic signal in the shallow-water region being suppressed depends on *two reasons*, the *first* of which is trivial: the underwater slope is so oriented that the source emits elastic waves into the deepwater region. But this reason is not the sole and even less the principal one. The *second* reason is related to the waveguide properties of a column of compressible liquid, limited by a free surface and by an absolutely rigid bottom. It is known (Brekhovskikh and Goncharov 1982) or (Tolstoy and Clay 1987), that the dispersion relation for normal modes in such a waveguide has the form,

$$k_x = \sqrt{\omega^2/c^2 - (k_z^n)^2}, \quad (4.53)$$

where k_x is the horizontal wavenumber, $k_z^n = \pi(1+2n)/2H$ is the vertical wavenumber for the n th mode ($n = 0, 1, 2, \dots$), ω is the cyclic frequency ($\omega = 2\pi/T$). It is seen that for fixed frequency (or period T) and depth H the horizontal wave number will be real only for a finite number of modes. These modes will be propagating modes. For modes of higher numbers k_x becomes a purely imaginary quantity, consequently, the perturbation in the wave decreases exponentially in the x direction. The situation is possible, when in the deepwater part of the basin there exist several (or one) propagating modes of period T , while in the shallow-water part no mode exists for such a period. Assuming in expression (4.53) $n = 0$, one can readily find the critical period for the given depth H ,

$$T_c = \frac{4H}{c}. \quad (4.54)$$

The frequency corresponding to the critical period is called the cutoff frequency. Modes of periods superior to T_c do not propagate in the considered waveguide. Formula (4.54) also permits to calculate the critical depth H_c for a given period of elastic waves, T . An elastic wave will not penetrate the region, where the depth is smaller than the critical depth, $H < H_c = cT/4$. A displacement of the ocean bottom

with residual deformation of duration τ forms elastic waves of period $T \sim \tau$, which are capable of penetrating down to depths $H_c \sim c\tau/4$. The examples of calculations presented in Figs. 4.9, 4.10, and 4.12 correspond to $\tau = 10$ s, i.e., the critical depth amounts to $H_c = 3,75$ km. From the figures it is seen that manifestations of compressibility of the water column correspond to those cases, when the depths exceed the critical value H_c .

Note one more interesting effect, related to the shape of the ocean bottom relief. We intend the possibility for the lowest mode of elastic oscillations to be captured by regions of local depressions of the ocean bottom (deepwater trenches or hollows). Indeed, if the lowest mode originates in the region of a local maximum depth, H_{\max} , then it exhibits the period $T_{\max} = 4H_{\max}/c$. This mode cannot leave the region, where it originated, since to do so it would have to propagate up the slope.

In conclusion of this section, we note that in tsunami catalogs (Soloviev et al. 1997; Soloviev and Go 1974, 1975) cases are repeatedly mentioned, when tsunami waves throw out onto the coast deepwater fish (unknown species, "sea monsters"). Moreover, cases have been described, when deepwater fish risen up to the surface before an earthquake. We shall present two quotations from the catalog of tsunamis in the Mediterranean sea.

1783, February, 5, 12 h \pm 30 min. Calabrian Arc. 38°25'N, 15°50'E.

Catastrophic Calabrian earthquake, which initiated a long period of seismic activity in the southwest of Italy that continued for several years.

Unusual events at sea are described, which can be considered short-time precursors of the earthquake. At the beginning of February close to Messina and at other sites deepwater fish Chichirella started appearing in large numbers, although it usually does not leave the seabed and digs into the seabed silt.

1887, February (March), 23, 6 h 20 min. Ligurian sea, Italy, France. 43°42'N, 08°03'E.

Strong earthquake occupied an area of 570 thousand sq. km. Deepwater fish or fish rarely seen in winter were found thrown out onto the beaches of Nizza, San-Remo, Savona.

Such a behavior of the marine inhabitants is readily explained by the distribution of the dynamic pressure amplitude. In attempts at avoiding the influence of uncomfortable changes in pressure, caused by the underwater earthquake, the fish goes to those regions, where the variations in pressure are minimal, i.e., to shallow-water regions or to the surface.

4.2 Observations of Tsunamigenic Earthquakes Using Ocean Bottom Stations

In this section an analysis of in situ data will be presented, for the interpretation of which it is important to take into account the compressibility of water. We shall deal with variations of the bottom pressure and of the accelerations of bottom oscillations

registered by the submarine observatories JAMSTEC during the tsunamigenic 2003 Tokachi-Oki and 2011 Tohoku-Oki earthquakes. In the first case the registrators were established directly at the tsunami source, while in the second at a significant distance (800 km) from the source. In the first subsection the basic theoretical concepts necessary for interpretation of the signals observed are expounded.

4.2.1 Character of the Water Layer Response to Bottom Oscillations in Dependence of Frequency

The spectrum of seismic bottom movements embraces quite a broad frequency range (usually $\sim 10^{-3}$ – 10^2 Hz). The lower boundary of this range is determined by the time required for the rupture at the earthquake source to be ripped open, while the upper boundary depends on the propagation conditions of seismic waves: high-frequency waves die out more rapidly with distance.

How does a water layer react to bottom oscillations occurring with a certain frequency f ? The answer to this, at first glance, absolutely theoretical question is extremely important for adequate interpretation of the signals registered by pressure gauges and seismometers established on the ocean's bottom. Such systems have recently become widespread in the practice of studying and predicting tsunami waves and submarine earthquakes. Evidently, when the frequency varies within a range of several orders of magnitude and the onset of different physical factors takes place, the character of the reaction of a water layer may undergo essential changes. To reveal the character of the linear response of a water layer to bottom oscillations, we shall rely on results of the theoretical analysis expounded in Sects. 3.2.1, 3.3.4 and 4.1.5.

From the analytical solution of the problem of gravitational wave generation in a layer of incompressible liquid by small dynamic bottom deformations, (3.48) it follows that the spatial spectrum of these waves is always modulated by the rapidly decaying function

$$\chi(k) = \frac{1}{\cosh(kH)}. \quad (4.55)$$

The result of such modulation is an exponentially rapid decrease in the amplitude of waves, excited by bottom movements, as the wavenumber k increases (or the wavelength $\lambda = 2\pi/k$ decreases). Thus, the wavelengths of gravitational waves excited in a water layer by bottom movements or by other bottom processes turn out to have a lower limit $\lambda_{\min} \sim H$.

Note that function χ is responsible not only for the suppression of short gravitational waves, excited by movements of the bottom. In the theory of potential gravitational waves of small amplitude (e.g., Lacombe 1965) the relationship is known between displacement of the free surface in a monochromatic wave, ξ , and the

variations in pressure p , created by this wave at the bottom of the basin. This relationship is realized by means of function χ :

$$\frac{p}{\rho g \xi} = \chi. \tag{4.56}$$

Taking into account the character of the behavior of function χ , it is possible to draw the conclusion from formula (4.56) that only long waves ($kH \ll 1$) manifest themselves in variations of the bottom pressure. At the same time, shortwaves ($kH \gg 1$) give rise to no oscillations of the bottom pressure.

In linear gravitational waves the wavenumber k is uniquely related to the cyclic frequency ω ($\omega = 2\pi f$) by the dispersion relation: $\omega^2 = gk \tanh(kH)$. Taking advantage of the dispersion relation one can represent function $\chi(k)$ in the form of a frequency dependence $\chi(f)$. In Fig. 4.13 the quantity χ is presented as a function of the dimensionless frequency $f\sqrt{H/g}$. From the figure it is seen that at low frequencies the quantity χ is close to 1. As the frequency increases, the quantity χ undergoes a sharp decrease.

Since the quantity χ determines the amplitude of gravitational waves caused by bottom movements, an analysis of the dependence depicted in Fig. 4.13 permits to draw the following conclusions. Gravitational waves can be caused by bottom oscillations only of sufficiently low frequencies: $f < f_g$, where $f_g = \alpha\sqrt{g/H}$ is the critical frequency, at frequencies above which the wave amplitude becomes negligible, α is a numerical coefficient. For unambiguous determination of the coefficient α it is necessary to set the amplitude attenuation level of surface waves compared with the

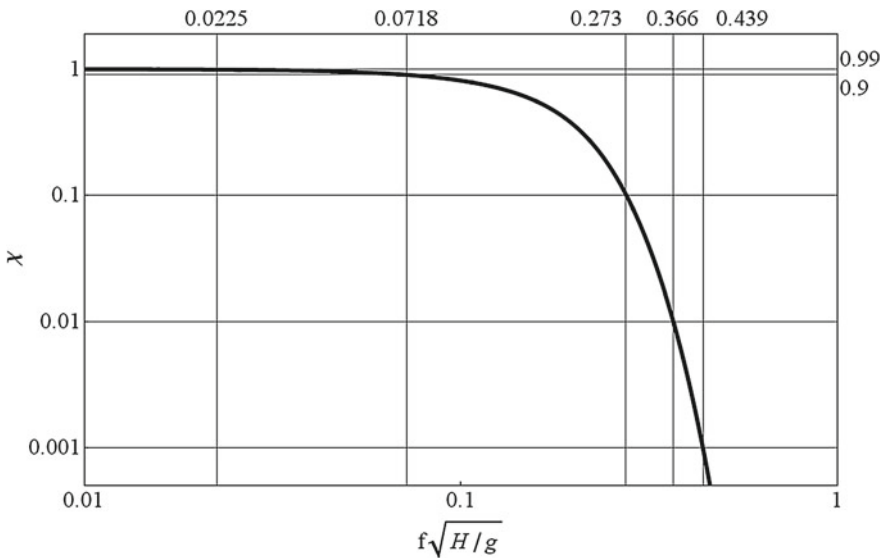


Fig. 4.13 Quantity χ determining the amplitude of gravitational waves excited by bottom oscillations of frequency f in a water layer of depth H versus frequency

amplitude of ocean bottom oscillations (see Fig. 4.13). Thus, for example, a hundredfold attenuation of the wave compared to the amplitude of bottom oscillations corresponds to the value of coefficient $\alpha_{100} \approx 0.366$. For comparison we present values of the coefficient corresponding to a tenfold and thousandfold attenuation: $\alpha_{10} \approx 0.273$, $\alpha_{1000} \approx 0.439$. Owing to function χ dropping quite sharply, coefficients corresponding to different attenuation levels do not differ strongly from each other. For definiteness we shall further use the value of coefficient α_{100} .

Within the “gravity-wave” frequency range of $f < f_g$ it is expedient to single out a subrange of long (low-frequency) waves $f < f_{lw} < f_g$. The long-wave approximation implies fulfillment of the law of hydrostatics, in this case $\chi = 1$. To determine the critical frequency $f_{lw} = \alpha\sqrt{g/H}$, restricting the long-wave range, one must establish the deviation level of function χ from its hydrostatic limit $\chi = 1$. In the case of a deviation of 1% ($\chi = 0.99$) the coefficient $\alpha_{0.99} \approx 0.0225$, while if the deviation is 10% ($\chi = 0.9$) $\alpha_{0.9} \approx 0.0718$. We shall further apply the value $\alpha_{0.99}$.

The above reasoning permits to introduce two critical frequencies for gravitational waves:

$$f_g \approx 0.366\sqrt{g/H}, \quad (4.57)$$

$$f_{lw} \approx 0.0225\sqrt{g/H}. \quad (4.58)$$

Both critical frequencies only depend on the ocean depth and on the gravity acceleration.

The dependences (4.57) and (4.58) are presented in Fig. 4.14. In the “depth-frequency” plane these two curves identify regions, in which the excitation is possible of gravitational waves ($f < f_g$), or of long gravitational waves ($f < f_{lw}$). The region in between the curves ($f_{lw} < f < f_g$) corresponds to relatively short (dispersing) gravitational waves. Here, it is appropriate to note that tsunami waves caused by perturbations at the ocean bottom (seismic movements of the bottom, submarine landslides etc.) by the very nature of their origination are not obliged to be long waves, their spectrum may also involve shortwave dispersing components.

As it was already noted in Sect. 4.1.5, a layer of compressible liquid that is limited from below by an absolutely rigid bottom and from above by a free surface, represents a waveguide, characterized by a cutoff frequency,

$$f_{ac} = c/4H, \quad (4.59)$$

where c is the velocity of sound in water. Hydroacoustic waves are capable of propagating along such a waveguide only if their frequency exceeds the cutoff frequency: $f > f_{ac}$. Thus, the cutoff frequency, determined by formula (4.59), represents a critical frequency that imposes a lower limit on the frequency range for the existence of hydroacoustic waves. Dependence (4.59) is shown in Fig. 4.14 together with dependences (4.57) and (4.58) that are responsible for the critical frequencies of gravitational waves.

From Fig. 4.14 it is seen that the curves corresponding to critical frequencies f_g and f_{ac} never intersect in the conditions of our planet (the inequality $f_g < f_{ac}$ always

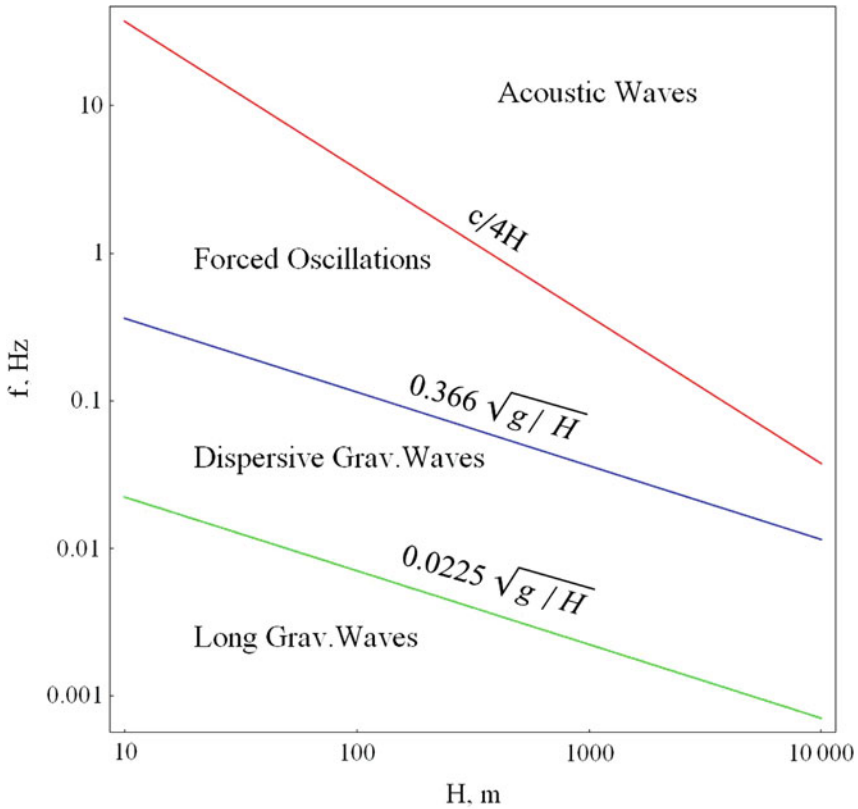


Fig. 4.14 Critical frequencies for gravitational and acoustic waves in a water layer versus depth H . Frequency ranges corresponding to the character of the linear response of a water layer to ocean bottom oscillations of frequency f : “long gravitational waves”, “dispersive gravitational waves”, “forced oscillations”, and “acoustic waves”

holds valid). Consequently, gravitational and hydroacoustic waves excited by seismic movements of the bottom are always related to different (not intersecting) frequency ranges. The intermediate frequency range $f_g < f < f_{ac}$ corresponds to the mode of forced oscillations. If the frequency of bottom oscillations is within the range of “forced oscillations”, then neither gravitational nor hydroacoustic waves arise, and the water layer will follow movements of the bottom like a single whole. In the mode of forced oscillations, when the ocean bottom is flat and horizontal, variations of the bottom pressure p are related to the vertical component of acceleration a of bottom movements, in accordance with Newton’s second law,

$$p_{fo} = \rho H a, \tag{4.60}$$

where ρ is the density of water.

In the frequency range $f_g < f < f_{ac}$ forced oscillations exist in a “pure form”, outside this range they also exist, but in superposition with acoustic or gravitational waves.

The fact that for the “forced oscillations” range there exists an exact formula (4.60), by which it is possible to calculate the dynamic pressure at the bottom is, in a certain sense, unique. The point is that no simple exact formulae exist for the ranges of gravitational and acoustic waves. However, in these cases pressure variations can be estimated applying approximate relationships. For the range of long gravitational waves bottom pressure oscillations are exclusively due to changes in the water layer thickness during the passage of gravitational waves. The amplitude of these waves is approximately equal to the amplitude of bottom oscillations, η . Thus, the following formula may be considered for estimation of the dynamic pressure at the ocean bottom:

$$p_{lw} \sim \rho g \eta. \quad (4.61)$$

Note that the contribution of forced oscillations to pressure variations can be neglected in the frequency range $f < f_{lw}$,

$$\frac{p_{lw}}{p_{fo}} \sim \frac{g}{H\omega^2} > 50.$$

As the frequency of bottom oscillations increases and approaches the value of f_g , forced oscillations start to be dominant in the formation of pressure variations. Manifestations of gravitational waves, contrariwise, become weaker, owing to the “double effect of function χ ”, which consists in that, first, bottom oscillations of frequency $f \sim f_g$ are not capable of effectively exciting gravitational waves, and, second, the waves generated are manifested at the ocean bottom with attenuation.

We shall base estimation of dynamic pressure in the range of “acoustic waves” on the exact formula $p = \rho cu$, well known in acoustics and according to which pressure is calculated in the vicinity of a solid surface, moving with a velocity u along the direction of its normal vector (e.g., Landau and Lifshits 1987). The presence of a free water surface reflecting acoustic waves restricts the possibility of applying this formula as an exact expression for calculating the pressure. But the same expression can quite be used for approximate estimation of bottom pressure variations within the range of acoustic waves,

$$p_{ac} \sim \rho cu, \quad (4.62)$$

where u is the vertical component of the bottom movement velocity.

Thus, in the ranges of “gravitational waves”, “forced oscillations”, and “acoustic waves” the pressure variations are, respectively, proportional to the following parameters of bottom oscillations: the linear amplitude, acceleration, and velocity. Taking into account that the velocity and acceleration are related in a known way to the amplitude η and cyclic frequency ω ($u \sim \eta\omega$, $a \sim \eta\omega^2$), one can expect pressure variations in the range of forced oscillations to increase in proportion to the square frequency

$p_{fo} \sim \omega^2$, and within the range of acoustic waves in proportion to the frequency itself, $p_{ac} \sim \omega$.

In conclusion of this section we shall touch upon an estimate confirming, at least in part, the existence of internal consistency of the reasoning presented above. From general physical arguments, one should expect no drastic changes to occur in the amplitude of the bottom dynamic pressure, if transition takes place from the range of “forced oscillations” to the range of “acoustic waves” owing to gradual changes of frequency in the vicinity of f_{ac} . It is not difficult to verify that the estimates of quantities p_{fo} and p_{ac} , obtained by formulae (4.60) and (4.62), for the critical frequency f_{ac} are, indeed, quite consistent with each other,

$$\frac{p_{fo}}{p_{ac}} \sim \frac{H\omega}{c} = \frac{\pi}{2} \sim 1.$$

4.2.2 The 2003 Tokachi-Oki Earthquake

Till recently all the information on tsunami sources were obtained exclusively by remote measurements using mareographs (coastal or deepwater), hydroacoustic systems, or seismographs. The absence of direct measurements at the tsunami sources in part explains why processes at the epicentral zones of underwater earthquakes have been studied relatively weakly.

The possibility of investigating the formation of a tsunami at its source, in principle, arose at the end of the twentieth century, when a system of bottom stations involving, in particular, pressure gauges and seismometers was established at the Pacific ocean bottom near the Japanese islands. Bottom stations are connected to coastal registration points by cable lines, which makes it possible to transfer data operatively with quite a high sampling frequency.

The aforementioned stations were established by four different organizations: Japan Meteorological Agency (JMA), Japan Agency for Marine-Earth Science and Technology (JAMSTEC), Earthquake Research Institute (ERI), the University of Tokyo and National Research Institute for Earth Science and Disaster Prevention (NIED) (Joseph 2011; Rabinovich 2014). It so happened that the first, in the history of science, registration of a tsunami generation process with the aid of bottom sensors situated precisely at its source, was accomplished by JAMSTEC Watanabe et al. (2004). The analysis and interpretation of these unique data are dealt with in quite a large number of publications (e.g., Nosov et al. 2005, 2007; Mikada et al. 2006; Nosov and Kolesov 2007; Li et al. 2009; Ohmachi and Inoue 2010; Bolshakova et al. 2011; Matsumoto 2011).

The 2003 Tokachi-Oki earthquake was the first strong seismic event, the epicenter of which was located in the immediate vicinity of the JAMSTEC sensors (see Fig. 4.15). According to USGS Significant Earthquake Archive, this event took place on September 25 at 19:50:06 UTC; the coordinates of its epicenter were 41.775 N, 143.904 E; its hypocenter depth was 27 km, its magnitude was 8.3 M_w . The

earthquake gave rise to a tsunami wave, the height of which amounted to 4 m along the southeast coast of Hokkaido island (Tanioka et al. 2004).

In this section, data are analyzed on bottom oscillations and variations of the bottom pressure registered by JAMSTEC sensors at the source of the 2003 Tokachi-Oki tsunami. We consider the water column at the source to behave as a compressible medium—this is essential here. A theoretical analysis of the role, played by water compressibility in the tsunami problem, carried out in Sect. 4.1.1, permits to assert that elasticity effects turn out to be essential only at the stage of tsunami generation by an earthquake, while wave propagation or the runup of a wave onto the coast can be described as the motion of an incompressible liquid. Simple estimation reveals that the energy of elastic oscillations of a water column in the tsunami source area may exceed the energy of the gravitational tsunami wave by more than an order of magnitude.

If the case of a horizontal absolutely rigid ocean bottom is considered, then the main difference in the behavior of a compressible ocean as compared to an incompressible model medium consists in the formation of elastic oscillations of the water column, which are characterized by a discrete set of normal frequencies

$$f_n = \frac{c(1 + 2n)}{4H}, \quad (4.63)$$

where c is the velocity of sound in water, H is the ocean depth, and $n = 0, 1, 2, \dots$

For typical conditions of a tsunami source the minimal normal frequency $f_0 \equiv f_{ac} = c/4H \sim 0.1$ Hz is excited most effectively.

Real tsunami sources are, naturally, located not on a horizontal ocean bottom, but in a region of complex bathymetry. But the slope of the oceanic bottom usually does not exceed the value of 0.1. Therefore, the surface of the bottom can arbitrarily be represented as a set of quasihorizontal segments, each of which is characterized by its own depth and set of normal frequencies, corresponding to this depth. Thus, at a certain fixed point of the source there, first, takes place formation of elastic oscillations with normal frequencies determined by the ocean depth at this point. Then, the spectrum of elastic oscillations can be enriched by high frequencies at the cost of waves arriving from neighboring shallow-water regions. In Sect. 4.1.5 it was shown that owing to the existence of a cutoff frequency low-frequency oscillations formed in adjacent deepwater regions do not propagate up the slope.

Note two features peculiar to compressibility effects that explain why they have been studied weakly. First, elastic low-frequency oscillations of a water column can be revealed only at sufficiently large depths (in the open ocean), which hinders their direct registration. Second, the compressibility effects were not quite within the line of research of tsunamis, since, owing to the significant difference in frequency ranges, elastic oscillations were not considered capable of giving any contribution to a tsunami wave. Probably, such an assertion is erroneous, and the contribution of elastic oscillations to a tsunami wave can be provided for by nonlinear mechanisms (Sect. 4.3).

Till recently the existence of elastic low-frequency oscillations of the water column at a tsunami source had not been confirmed by measurements in natural waters, and, therefore, the effect remained only theoretically predicted. To avoid confusion, the difference must be stressed between such a well-known phenomenon as the T-phase and the effects dealt with here. Not only the T-phase is related to a range of higher frequencies ($f > 2$ Hz), but it is also registered at significant distances from the source (e.g., Okal et al. 2003).

Figure 4.15 shows the region, where the 2003 Tokachi-Oki earthquake occurred. The epicenter of the seismic event is indicated by the asterisk. The vertical coseismic deformation component, which permits to draw conclusions on the location and size of the tsunami source, is shown in the figure by isolines (red lines indicate uplifts, blue lines indicate subsidences, the isoline pitch is 0.1 m). The coseismic deformation is calculated using the Okada formulae (see Sect. 2.2) by the slip distribution model developed in Koketsu et al. (2004) on the basis of joint inversion of strong motion and geodetic data. The triangles indicate the positions of four JAMSTEC bottom

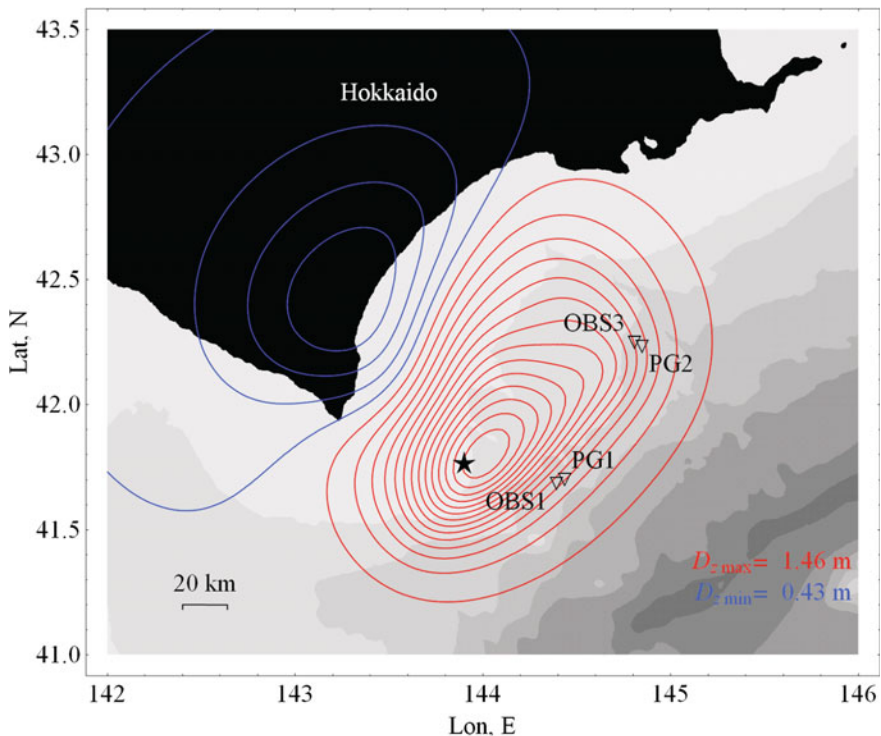


Fig. 4.15 Relative position of epicenter of the 2003 Tokachi-Oki earthquake (*asterisk*) and ocean bottom JAMSTEC stations (*triangles*). The coseismic vertical deformation of the ocean bottom is shown by isolines drawn with a pitch of 0.1 m (uplifts are shown by *red lines*, subsidences are shown by *blue lines*). The maximum uplift and subsidence values are indicated in the *lower right angle*. Isobaths are drawn with a 1 km pitch

stations that registered the tsunami formation process immediately at its source: two pressure gauges, PG1, PG2 and two ocean bottom seismometers, OBS1, OBS3. The registrators are situated in pairs: “OBS1–PG1” and “OBS3–PG2”. The distance between pairs amounts to about 70 km. The seismometers and pressure gauges in each of the pairs are separated by quite significant distances: 4 km (OBS1–PG1) and 3.6 km (OBS3–PG2). According to data presented on the official JAMSTEC site, the ocean depths at the points where the sensors are placed are the following: $H_{PG1} = 2218$ m, $H_{PG2} = 2210$ m, $H_{OBS1} = 2329$ m, $H_{OBS3} = 2124$ m. The data sampling frequency for seismometers is 100 Hz, while for pressure gauges it is 10 Hz.

Signals registered by the seismometers and pressure gauges during the 2003 Tokachi-Oki earthquake are presented in Figs. 4.16 and 4.17, respectively. The vertical acceleration component (accelerogram) of the bottom movement and variations of bottom pressure are shown together with spectrograms constructed with the aid of the Morlet wavelet transformation. On the spectrograms, the positions are indicated of critical frequencies f_g and f_{ac} that restrict the regions of existence of gravitational and hydroacoustic waves (see Sect. 4.2.1).

From the accelerograms presented in Fig. 4.16 one can conclude that the most intensive bottom oscillations lasted about 2 min, and at this phase the acceleration exceeded 1 m/s^2 (the double amplitude amounted to 2.23 m/s^2 according to OBS1 data and to 2.20 m/s^2 according to OBS3 data). During the first few minutes the signal was quite wideband and then frequencies that approximately corresponded to the critical frequency of hydroacoustic waves, f_{ac} , started to dominate. In the region of high frequencies weak splashes were observed that were probably caused by weak aftershocks.

Figure 4.17 presents variations of the bottom pressure during the 15 min time interval after the beginning of the earthquake. Like in the case of acceleration of the bottom motion, the spectral composition of pressure variations is characterized by a wideband beginning and further gradual transition to the singled out frequency, close to f_{ac} . During the first two minutes the dynamic pressure attains an amplitude of 200 kPa and more (the double amplitude amounted to 490 and 518 kPa according to the respective PG1 and PG2 data).

In Fig. 4.18, the variations of bottom pressure are presented for a long time period (2.5 h) that involved both the main seismic event of $M_w 8.3$ and a strong aftershock of $M_w 7.3$ that took place at 21 h 08 min 19.5 s (CMT Catalog). It is remarkable that the “sounding” of the tsunami source at the chosen frequency lasted quite a long time—more than an hour. After the aftershock the evolution picture of the spectral composition is repeated: in several minutes after the shock the signal is localized within a narrow frequency range near the value of f_{ac} .

The prolonged “sounding” of the tsunami source at a fixed frequency, that is observed both in records of pressure variations and in accelerograms, permits to make the conclusion that we are dealing with manifestations of the response of a certain high-Q oscillatory system to the earthquake. The results of a theoretical analysis presented in Sects. 4.1.3–4.1.5 indicate that such a system could be represented by a layer of compressible water restricted from above by a free surface and from below by an absolutely rigid bottom. Indeed, in this case the system will respond at the lowest

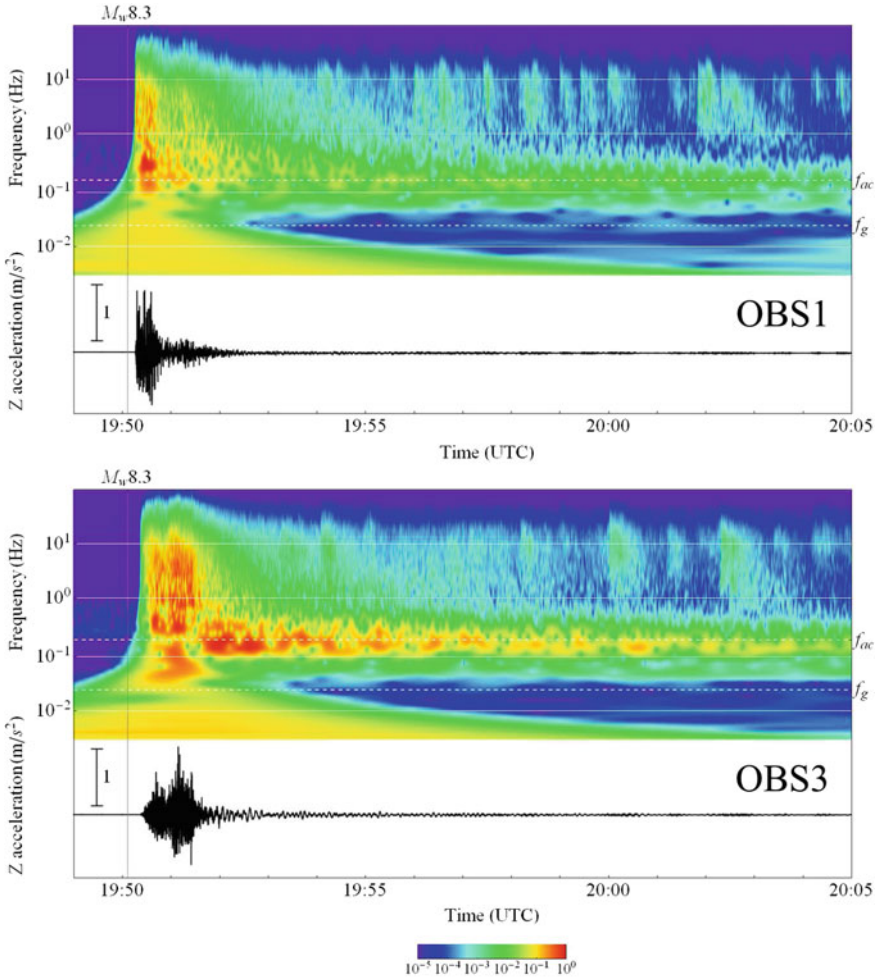


Fig. 4.16 Signals registered during the 2003 Tokachi-Oki earthquake by seismometers OBS1 and OBS3 (the vertical component of acceleration). Spectrograms of signals constructed using the Morlet wavelet transformation. On the spectrograms the position is indicated of critical frequencies f_g and f_{ac} (white dotted lines) that restrict the regions of existence of gravitational and hydroacoustic waves. The beginning of an earthquake of $M_w 8.3$ is indicated by the vertical line

possible normal frequency f_{ac} . However, from the spectrograms shown in Figs. 4.16, 4.17, and 4.18 frequencies somewhat lower than the theoretical value f_{ac} are seen to correspond to the observed oscillations. This fact is explained as follows. The model of a compressible water layer lying on an absolutely rigid horizontal bottom is not quite accurate. Actually, the ocean bottom exhibits elasticity properties, stratified structure, and is certainly not strictly horizontal. Moreover, the acoustic stiffness (product of the density of the medium and the velocity of longitudinal waves) of

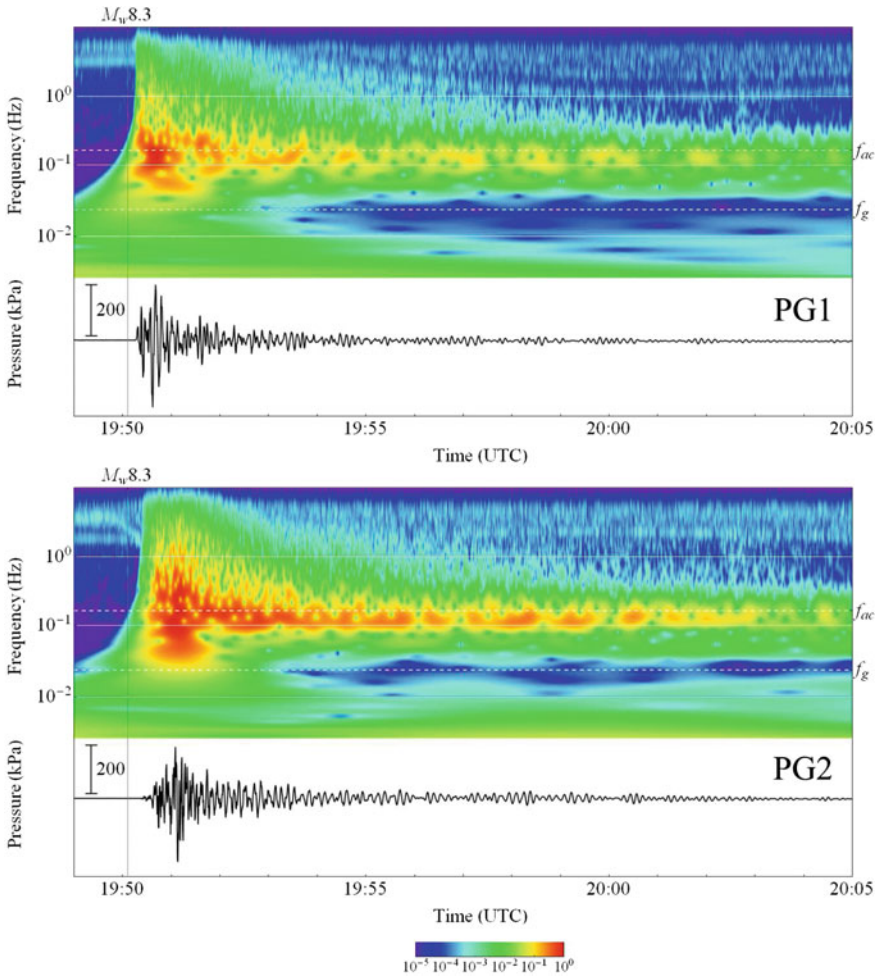


Fig. 4.17 Signals registered during the 2003 Tokachi-Oki earthquake by bottom pressure gauges PG1 and PG2. Spectrograms of signals constructed using the Morlet wavelet transformation. On the spectrograms the position is indicated of critical frequencies f_g and f_{ac} (white dotted lines) that restrict the regions of existence of gravitational and hydroacoustic waves. The beginning of an earthquake of M_w 8.3 is indicated by the vertical line

the upper sedimentary layers does not differ significantly from the corresponding characteristic of sea water. In this connection, an earthquake does not simply excite elastic oscillations of a water layer, but coupled elastic oscillations of the water layer and the upper sedimentary layers.

How significantly do the normal frequencies of such coupled oscillations differ from the normal frequencies of a water layer lying on an absolutely rigid bottom? To answer this question we shall consider the following model. Let a compressible layer

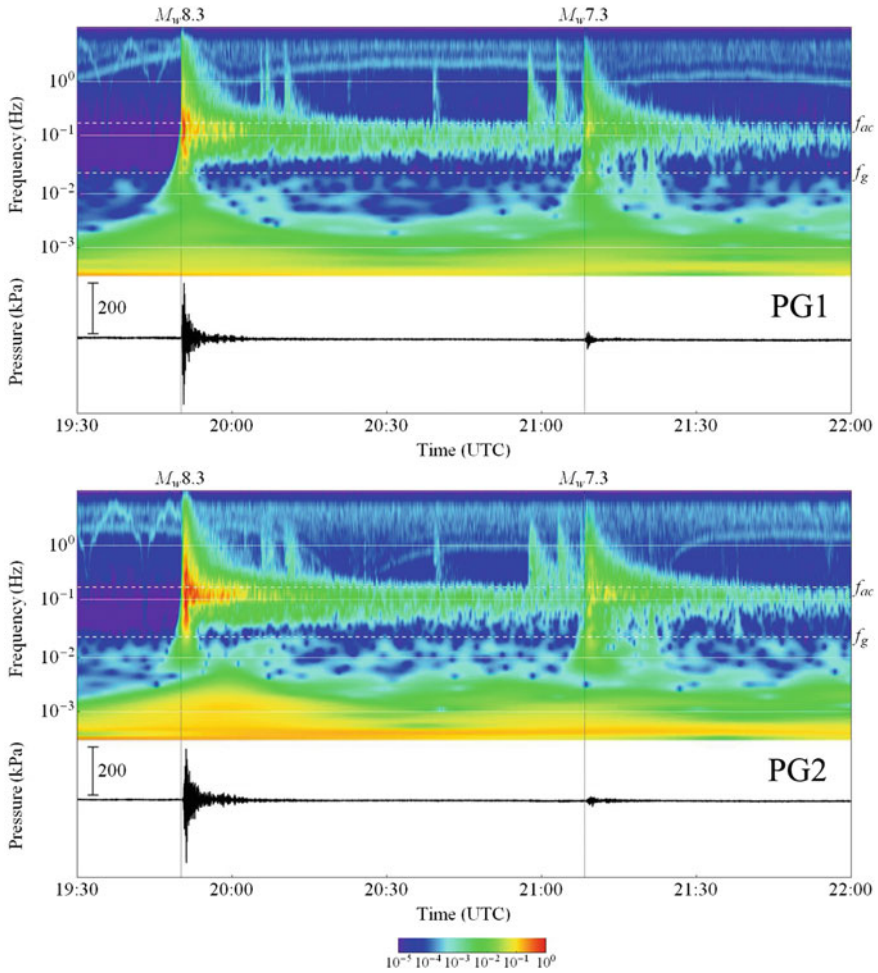


Fig. 4.18 Signals registered during the 2003 Tokachi-Oki earthquake by bottom pressure gauges PG1 and PG2. Recording lasted 2.5 h. *Vertical lines* indicates the beginning moments of the main earthquake of M_w 8.3 and of the aftershock of M_w 7.3. Other notations are similar to the notation in Fig. 4.17

of water of thickness H be restricted from above by a free surface and from below by an elastic sedimentary layer. Let the sedimentary layer have a thickness H_s and let it lie on an absolutely rigid acoustic fundament. Such a system is characterized by a set of normal frequencies f_s , determined by the solution of the following transcendental equation (Nosov et al. 2005, 2007; Bolshakova et al. 2011):

$$\tan\left(\frac{2\pi f_s H}{c}\right) \tan\left(\frac{2\pi f_s H_s}{c_s}\right) = \frac{\rho_s c_s}{\rho c}, \tag{4.64}$$

where c_s is the velocity of elastic longitudinal waves in the sediment, and ρ_s is the density of the sediment.

Let us estimate the minimum normal frequency with and without account of the sedimentary layer for conditions peculiar, for example, to the PG1 station. We shall characterize the water layer by the following parameter values: $\rho = 1030 \text{ kg/m}^3$, $c = 1500 \text{ m/s}$, and $H_{PG1} = 2218 \text{ m}$. In accordance with the Global Crustal Model at 1×1 Degrees (CRUST 1.0, <http://igppweb.ucsd.edu/~gabi/crust1.html>), the sedimentary layer is characterized at the location of the PG1 station by the following set of parameters: $c_s = 1740 \text{ m/s}$, $\rho_s = 1820 \text{ kg/m}^3$, $500 < H_s < 2000 \text{ m}$. Without taking into account the sedimentary layer the minimum normal frequency assumes the value $f_{ac} = 0.169 \text{ Hz}$. If the sedimentary layer is taken into account, the minimum normal frequency turns out to be noticeably smaller, $0.116 \text{ Hz} < f_s < 0.154 \text{ Hz}$ (the lower limit corresponds to a sedimentary layer of maximum thickness). The obtained theoretical estimate for the value f_s is in good agreement with the observed quantity—the frequency at which “sounding” of the tsunami source takes place during an hour and more after the earthquake.

We note one more curious detail that is well seen on the spectrograms presented in Fig. 4.18. Before the beginning of the earthquake the range of frequencies $f > f_g$ contains no noise of natural origin. This is due to natural noise, that is, first of all, due to gravitational surface waves, being capable of manifesting itself in variations of the bottom pressure only at sufficiently low frequencies $f < f_g$ (see formula (4.57) of Sect. 4.2.1). Thus, observational data confirm adequacy of the determined critical frequency, f_g . To avoid misunderstanding we note that the weak signals observed in the range $f > 0.1 \text{ Hz}$, including regular “structures” on the spectrograms, are probably manifestations of instrumental noise.

In Sect. 4.2.1 it was noted that within the “forced oscillations” frequency range the pressure variation and the acceleration of bottom movements must be related by the linear dependence (4.60) that follows from Newton’s second law. In Bolshakova et al. (2011) the indicated relationship was indeed observed for the first time for signals registered by pairs of sensors “OBS1-PG1” and “OBS3-PG2” during the 2003 Tokachi-Oki earthquake. Here, we shall not deal with the analysis of these data, since, owing to the significant distance between the seismometers and the pressure gauges, the correspondence between pressure variations and acceleration was not perfect. A mutual analysis of pressure and acceleration is to be presented in Sect. 4.2.3 using the example of records obtained during the 2011 Tohoku-Oki earthquake by stations of the DONET system, in which seismometers and pressure gauges are located in the immediate vicinity of each other.

In Fig. 4.19, the variations of near-bottom pressure are presented in a magnified scale, permitting to see the formation of residual displacements of the ocean bottom, caused by the earthquake. To discard the high-frequency components ($> 0.02 \text{ Hz}$) initially they were subjected to numerical filtration. The result of filtration is shown in the figures by dotted lines. The smooth decrease of pressure down to the starting point of the earthquake is related to tidal variations of the ocean level. The behavior of the dotted curve clearly shows that the earthquake resulted in the average pressure at sensor PG1 decreasing by $\Delta p_{PG1} \approx 4 \text{ kP}$, and at sensor PG2 by

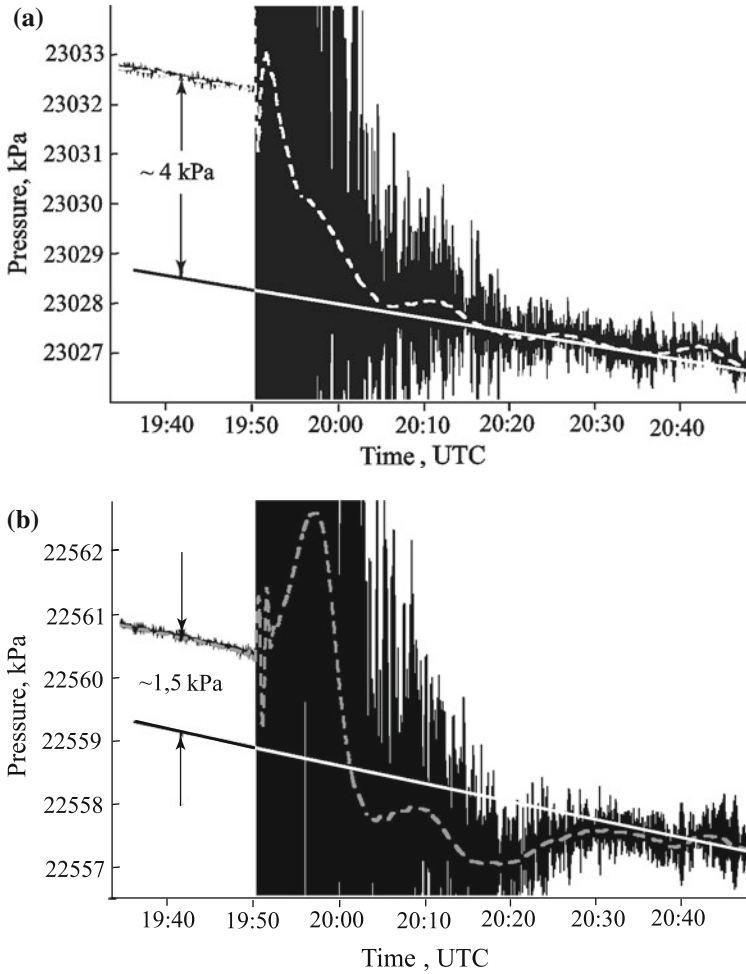


Fig. 4.19 Signals registered during the 2003 Tokachi-Oki earthquake by bottom pressure gauges PG1 (a) and PG2 (b) in magnified scale. The *arrow* indicates variation of the hydrostatic pressure caused by elevation of the ocean bottom. The *dotted line* represents the result of low-pass ($f < 0.02$ Hz) filtration of the initial signal

the quantity $\Delta p_{PG2} \approx 1.5$ kPa, which corresponds to a reduction of the water level (elevation of the bottom) by $\Delta H_{PG1} \approx 0.4$ m and $\Delta H_{PG2} \approx 0.15$ m, respectively, ($\Delta H = \Delta p / \rho g$). Note that residual deformations of the ocean bottom were first revealed from the data considered by the authors of Watanabe et al. (2004).

According to the Harvard CMT Catalog, the half duration of the process at the 2003 Tokachi-Oki earthquake source amounted to $\tau_E = 33.5$ s. But from Fig. 4.19 it is seen that the pressure decreases during an essentially longer period of time (~ 900 s). Evidently, the sensor registers not only the deformation process of the ocean bottom,

but also the tsunami wave formation, which is observed as a relaxation of the water column “elevated” by the displacement.

Section 4.1.2 contains a description of the procedure for linearization of equations describing the dynamics of a compressible water layer. Now, possessing the results of measurements at the tsunami source we can estimate the actual significance of nonlinear effects and quite justify the application of linear equations. To this end we shall need peak values of the mass velocity of water motion and density, as well as the mean values of water density and of sound velocity in water ($\rho_0 = 1030\text{ kg/m}^3$, $c = 1500\text{ m/s}$).

We shall first dwell upon estimation of the double amplitude of water density variations that can be performed with the aid of formula (4.18) by the measured peak value of the double amplitude of bottom pressure variations: $p' \approx 500\text{ kPa}$. Using this quantity we obtain the sought estimate: $\rho' = p'/c^2 \approx 0.2\text{ kg/m}^3$. The density variations are seen to be quite insignificant as compared with the mean value, $\rho' \ll \rho_0$. Consequently, the value ρ' in Eqs. (4.14) and (4.15) can indeed be reasonably neglected.

We shall associate the mass velocity of water particles with the vertical velocity of the ocean bottom motion during an earthquake. The bottom motion velocity can be estimated by the data provided by seismometers OBS1 and OBS3 by integration of the accelerograms over time. Velocities thus reconstructed are presented in Fig. 4.20. From the figures it is seen that accurate reconstruction of the velocities by accelerations, measured in the nearby zone, is, generally speaking, problematic. The point is that in the case of strong bottom motions the spatial orientation of

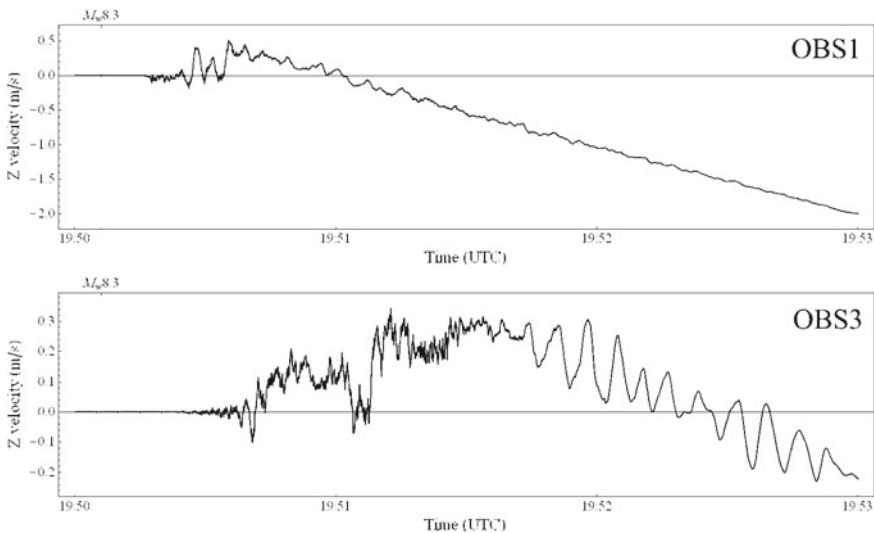


Fig. 4.20 The velocity of bottom motion during the 2003 Tokachi-Oki earthquake reconstructed by integration of accelerograms over time. The onset of the earthquake of $M_w 8.3$ is indicated by a vertical line

accelerometers can change (even if insignificantly), which often results in a statistical error in the determination of acceleration. The existence of statistical errors in the value of acceleration leads to errors increasing with time in the determination of velocity. Such a linear trend is quite noticeable in Fig. 4.20. In spite of the presence of an error (the linear trend) it is not difficult to determine that the double amplitude of vertical velocity of the bottom motion approximately amounted to 0.3–0.5 m/s.

The obtained velocity estimate can be confirmed independently on the basis of data on the measured double amplitude of bottom pressure variations $p' \approx 500$ kPa. Assuming pressure variations to be mainly due to hydroacoustic waves in accordance with formula (4.62) of Sect. 4.2.1 we obtain an estimate for the double amplitude of the bottom motion velocity: $u \sim p' / \rho_0 c \approx 0.32$ m/s (Nosov et al. 2005, 2007).

To make it possible to neglect the nonlinear term $(\mathbf{v}', \nabla)\mathbf{v}'$ in Eq. (4.14) it is necessary to require fulfillment of the following condition:

$$\frac{|(\mathbf{v}', \nabla)\mathbf{v}'|}{\left|\frac{\partial \mathbf{v}'}{\partial t}\right|} \sim \frac{UT}{\lambda} = \frac{u}{c} \ll 1,$$

where λ is the acoustic wavelength, T is the period of the acoustic wave. The estimate obtained above for the mass velocity of a liquid is significantly inferior to the velocity of sound in water, hence at the 2003 Tokachi-Oki tsunami source it is possible, at least in the first approximation, to neglect nonlinear effects.

4.2.3 The 2011 Tohoku-Oki Earthquake

At the beginning of the twenty-first century, bottom pressure gauges started being used extensively for tsunami wave measurements in the open ocean. The most well-known system in this field is the system involving stations DART (Deep-ocean Assessment and Reporting of Tsunamis) (Bernard and Meinig 2011). Records obtained using DART stations or other similar systems always contain a high-frequency noise-like signal observed before the tsunami onset and generated by seismic waves (e.g., Filloux 1983; Heidarzadeh and Satake 2013). Adequate interpretation of this signal is usually rendered complicated both by the large data sampling interval (15 s in the case of DART) and by the absence of data on seismic bottom displacements at the point where the pressure gauge is established.

Detailed analysis of signals preceding a tsunami onset became possible owing to the unique technical potential of the system DONET (Dense Oceanfloor Network System for Earthquakes and Tsunamis), established in 2006–2011 by the Japan Agency for Marine-Earth Science and Technology—JAMSTEC (Kaneda 2010).

The system DONET involves 20 bottom stations connected by cable lines to the coastal center of data processing (within the framework of the project, 29 more bottom stations are to be established in 2013–2015). Each station is equipped with a Pressure Gauge (PG) and an Ocean Bottom Seismometer (OBS—accelerometer

and velocimeter), located practically at the same point—at a distance less than 10 m from each other. The stations are established at depths between 1.9 and 4.4 km, the distance between them varies from 15 to 20 km. The sampling frequency of data amounts to 10 Hz in the case of pressure variations and to 200 Hz for seismograms.

By the time the catastrophic 2011 Tohoku-Oki earthquake occurred close to the coast of Japan on March 11, 2011, 10 DONET stations were functioning—all of them successfully recorded both the seismic event itself and the subsequent tsunami waves that followed it (Matsumoto and Kaneda 2013; Nosov et al. 2015). According to data of the United States Geological Survey (USGS) the Tohoku earthquake occurred at 05:46:24 (UTC), its epicenter (38.297°N , 142.372°E) was located 129 km east of the city of Sendai, the depth of its hypocenter was 30 km, its moment magnitude $M_w = 9.0$. The strong aftershock ($M_w = 7.9$, epicenter: 36.281°N , 141.111°E , depth: 42 km) that occurred at 06:15:40 was also registered by all 10 DONET stations. The relative positions of the epicenters of both seismic events and of the DONET stations are shown in Fig. 4.21. The isolines in the figure image the vertical coseismic bottom deformation (the tsunami source) calculated from the slip structure (Finite Fault Model, USGS) (Nosov et al. 2013).

Since all 10 DONET stations are located quite close to each other, the signals registered by them on the whole differ insignificantly. To present the data we chose two stations, the most shallow-water one, B08 (1924 m), and the most deepwater one, C09 (3511 m). The amplitude of seismic waves from the 2011 Tohoku-Oki earthquake was so significant, that the velocimeters, regretfully, turned out to be saturated. Therefore, we shall further only analyze seismograms obtained with the aid of accelerometers.

In Fig. 4.22 presented are the original seismograms (vertical acceleration component, sampling frequency 200 Hz, and duration 15 min). The signals are presented together with spectrograms normalized to the maximum value (the Morlet wavelet transformation). The positions of the critical frequencies f_g and f_{ac} , limiting the manifestation regions of gravitational and hydroacoustic waves (see Sect. 4.2.1), are indicated in the spectrograms. From the figure it is seen that after the earthquake the onset of high-frequency body waves takes place first, then comes the low-frequency dispersive Rayleigh waves. The peak values of the acceleration double amplitude measured by stations B08 and C09 amounted to 0.0496 and 0.0285 m/s^2 , respectively. Note that these values are nearly two orders of magnitude inferior to the acceleration amplitudes measured immediately at the source of the 2003 Tokachi-Oki tsunami (see Sect. 4.2.2).

The DONET stations were situated at a significant distance from the epicenter (~ 800 km). Therefore, the high-frequency components of the seismic signal (> 10 Hz), that had time to decay while propagating, are actually not manifested in the records. Consequently, the sampling frequency of the initial signal can be down-sampled to 10 Hz without loss of information—precisely such a sampling frequency is peculiar to records of pressure variations.

The results of downsampling are shown in Fig. 4.23. The length of records was 1 h—within this time interval manifestations occur of both the main seismic event of $M_w 9.0$ and of the first strong aftershock of $M_w 7.9$. After its onset the seismic signal

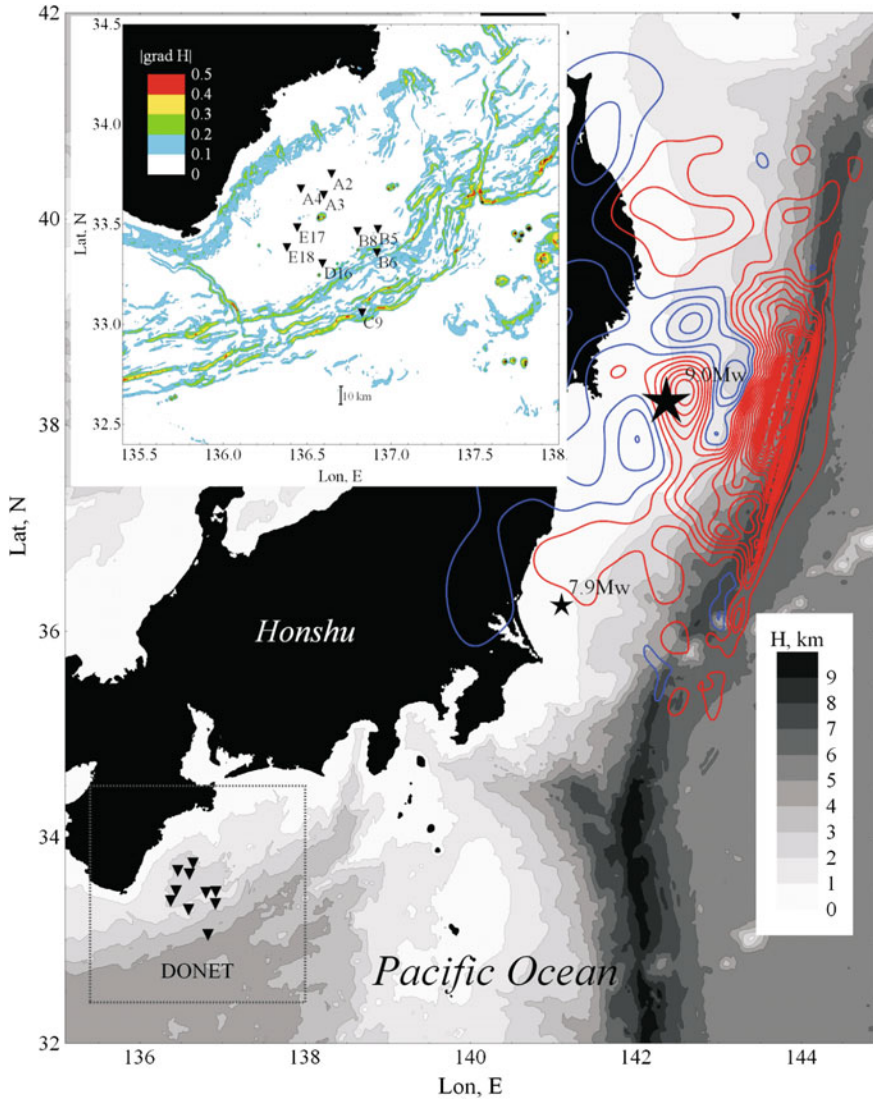


Fig. 4.21 Relative positions of DONET stations (*triangles*) and epicenters of the 2011 Tohoku-Oki earthquake and of the first strong aftershock (*asterisks*). Isolines show coseismic bottom deformation (*red lines* indicate uplift, *blue lines* indicate subsidence, the interval is 0.5 m). Isobaths are drawn with an interval of 1 km, the color scale is shown in the *lower right angle*. The *inset* in the *upper left angle* shows details of the region close to DONET stations. The absolute value of the depth gradient in the inset is depicted in accordance with the color scale (*upper left angle of inset*). The scale of lengths (10 km) is shown at the center of the lower part of the *inset*

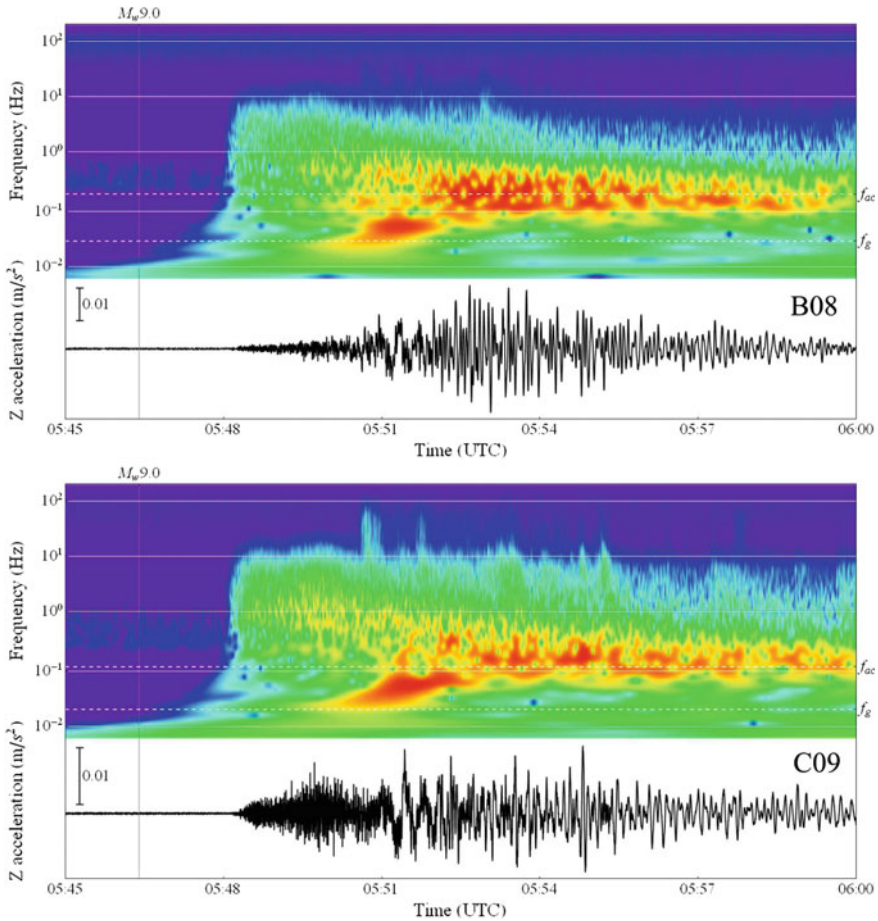


Fig. 4.22 Vertical accelerations, registered by accelerometers of DONET stations B08 and C09 during the 2011 Tohoku-Oki earthquake, and spectrograms of signals. The sampling frequency of data is 200 Hz, recording lasted 15 min. The time moment corresponding to the onset of the main seismic event of $M_w 9.0$ is indicated. *White dotted lines* in spectrograms show positions of critical frequencies for hydroacoustic (f_{ac}) and gravitational (f_g) waves

is quite broadband for the first few minutes. Then, the signal subsequently tends to become localized within a narrow frequency range in the vicinity of the critical frequency f_{ac} (a similar phenomenon was described in Sect. 4.2.2). From our point of view the observed narrowband and long-lived signal is a manifestation of coupled elastic oscillations of the water and the underlying sedimentary layers.

Figure 4.24 shows the signal registered by pressure gauges. The time interval of recording was chosen to be the same as for Fig. 4.23. Manifestations of high-frequency body and of low-frequency dispersive surface waves (Rayleigh waves)

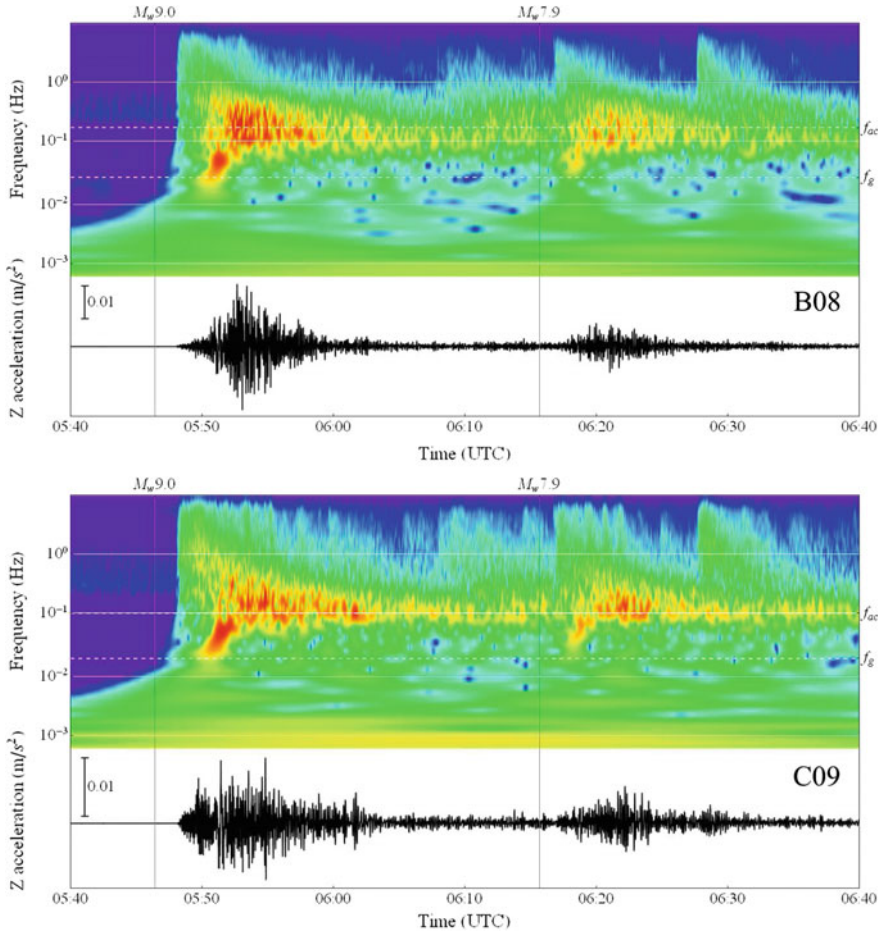


Fig. 4.23 Vertical accelerations obtained by downsampling (200 Hz \rightarrow 10 Hz) of signals, registered by accelerometers of DONET stations B08 and C09 during the 2011 Tohoku-Oki earthquake, and spectrograms of 10 Hz signals. Recording lasted 1 h. Time moments corresponding to the main seismic event of $M_w 9.0$ and the first strong aftershock of $M_w 7.9$ are indicated. *White dotted lines* in spectrograms indicate positions of critical frequencies for hydroacoustic (f_{ac}) and gravitational (f_g) waves

are clearly seen in the spectrograms. The double amplitude of pressure variations due to seismic waves amounts to 62.8 kPa (B08) and 68.6 kPa (C09).

By comparison of the spectrograms presented in Figs. 4.23 and 4.24 it is readily seen that within the range of forced oscillations $f_g < f < f_{ac}$ a complete identity (down to small details) is observed between the acceleration and the pressure spectrograms. Thus, the linear relationship is manifested between pressure variations and bottom acceleration (see Sect. 4.2.1),

$$p_{fo} = \rho H a, \quad (4.65)$$

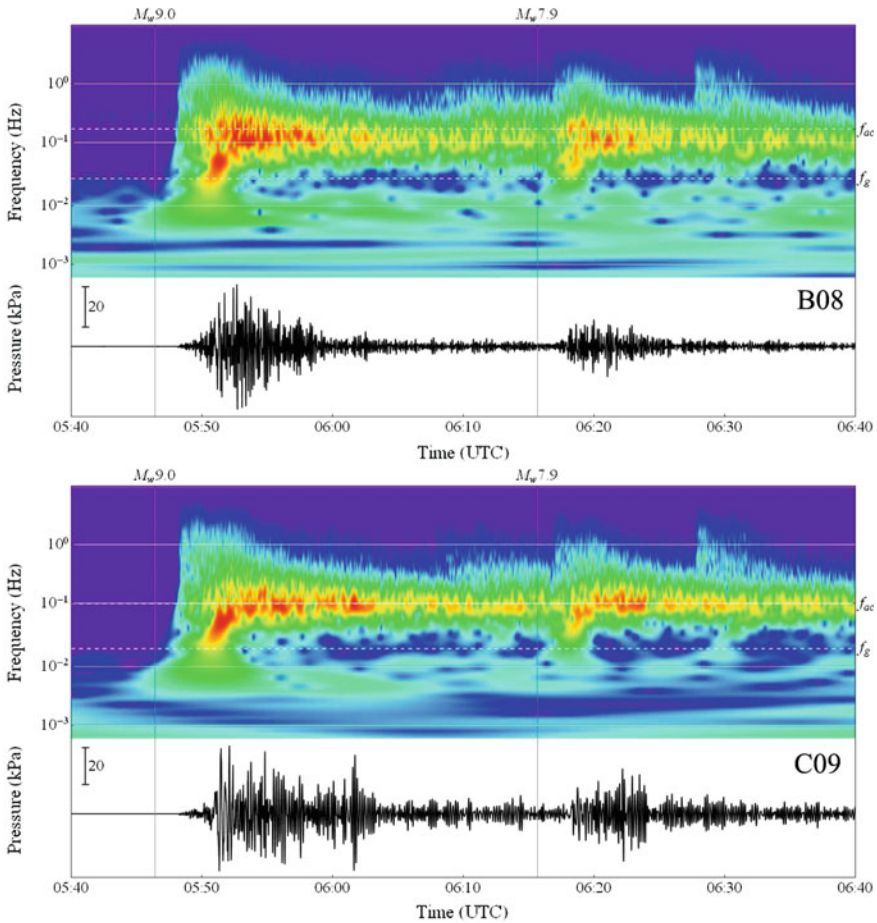


Fig. 4.24 Variations of ocean bottom pressure, registered by DONET stations B08 and C09 during the 2011 Tohoku-Oki earthquake, and spectrograms of signals. The data sampling frequency is 10 Hz, recording lasted 1 h. Time moments corresponding to the main seismic event of $M_w 9.0$ and the first strong aftershock of $M_w 7.9$ are indicated. *White dotted lines* in spectrograms indicate positions of critical frequencies for hydroacoustic (f_{ac}) and gravitational (f_g) waves

which should exist within the range of forced oscillations. We shall trace this correspondence quantitatively by comparison of the power spectra of signals registered by pressure gauges and acceleration sensors.

In order to depict the power spectra of pressure variations and of acceleration on one and the same plot, we shall represent the signal registered by the accelerometer in units of pressure in accordance with formula (4.65). In calculating spectra we made use of fragments of records 15 min long that corresponded to the main seismic event of $M_w 9.0$ (05:46-06:01 UTC) and to the aftershock of $M_w 7.9$ (06:15-06:30 UTC). The smoothed spectral estimates are presented in Fig. 4.25. The red curves show the

power spectra of acceleration, the blue curves show the power spectra of pressure variations.

From Fig. 4.25 it is seen that the red and blue curves indeed exhibit close behaviors within the “forced oscillations” range ($f_g < f < f_{ac}$). Outside this frequency range the curves diverge. The coincidence according to the B08 station is more exact than according to the C09 station. Most likely, this is due to the station C09 being near underwater slopes, where the horizontal component of acceleration must be taken into account to achieve better coincidence. It is remarkable that the degree of

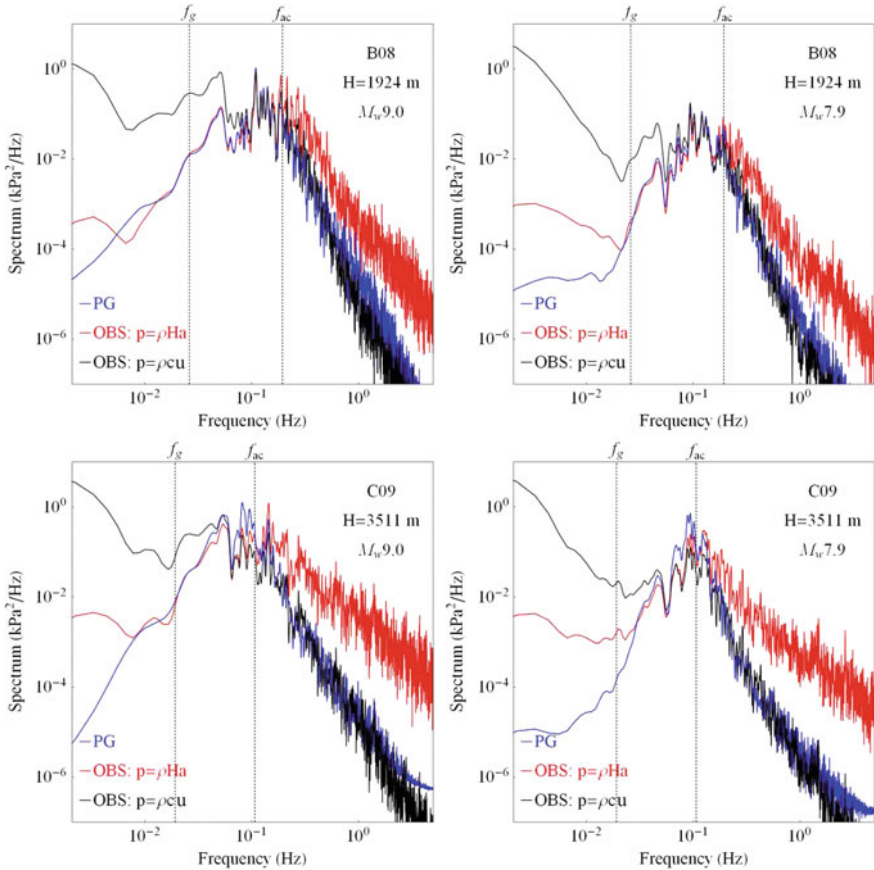


Fig. 4.25 Power spectra of signals registered by pressure gauges (blue curve) and accelerometers (red and black curves) of DONET stations B08 and C09 after the main seismic event of $M_w 9.0$ (05:46-06:01 UTC) and after the first strong aftershock of $M_w 7.9$ (06:15-06:30 UTC). Red curves correspond to vertical acceleration spectrum presented in units of pressure by formula $p = \rho Ha$. Black curves represent power spectra of vertical velocity shown in pressure units. The velocity spectrum is calculated from the acceleration spectrum in accordance with formula $Sp = \rho^2 c^2 S_a / \omega^2$. Vertical dotted lines show positions of critical frequencies for hydroacoustic (f_{ac}) and gravitational (f_g) waves

coincidence between the curves does not depend on which seismic event the observed signals correspond to—the main earthquake of $M_w 9.0$ or the aftershock of $M_w 7.9$.

In Sect. 4.2.1 we noted that within the frequency range of “acoustic waves” ($f > f_{ac}$) pressure variations at the ocean bottom, p_{ac} , should be related to the vertical component of the bottom displacement velocity, u , by the following formula:

$$p_{ac} \sim \rho c u. \quad (4.66)$$

Regretfully, we had no possibility of taking advantage of records provided by velocimeters (owing to saturation) for verifying regularity (4.66). But, owing to the known relationship between velocity and acceleration, $u \sim a/\omega$, where ω is the cyclic frequency, the velocity power spectrum S_u can be readily reconstructed from the acceleration power spectrum S_a : $S_u \sim S_a/\omega^2$. Thus, the spectra of pressure variations and of acceleration within the frequency range $f > f_{ac}$ are to be expected to be related as follows:

$$S_p \sim \rho^2 c^2 S_a / \omega^2. \quad (4.67)$$

Spectra calculated from accelerograms in accordance with formula (4.67) are presented in Fig. 4.25 by black curves. It is clearly seen that the black and blue curves indeed exhibit a common tendency within the range of $f > f_{ac}$. Naturally, no exact correspondence between the curves is intended in this case, since the initial formula (4.66) is itself approximate. At high frequencies (and in the case of very small amplitudes of the signal) a certain systematic difference is observed in the behavior of the black and blue curves, which is probably related to a manifestation of instrumental noises by the pressure gauges.

We shall now proceed to analyze gravitational waves. In Fig. 4.26 pressure variations are presented for a long period (3 h) permitting to observe manifestations of not only seismic waves, but of tsunami waves, also. In this figure the onset is clearly noticeable of the leading tsunami wave, that reached the region, where the DONET stations were established, in more than an hour after the main seismic event. Owing to the significant epicentral distance, the seismic waves and the tsunami waves are separated in time, and for this reason both phases are clearly observed. The amplitude of pressure variations due to tsunami waves (~ 4 kPa) is more than an order of magnitude inferior to the amplitude of seismic wave manifestations.

From the spectrograms presented in Fig. 4.26 it is possible to conclude that before the onset of seismic waves the pressure gauges only register a weak low-frequency noise in the range of $f < f_g$. It can be asserted with certainty that the gauges register nothing but manifestations of background surface gravitational waves. Gravitational waves of higher frequencies, $f > f_g$, are not manifested in bottom pressure variations, owing to reasons indicated in Sect. 4.2.1. It is not difficult to notice that the frequency starting from which the pressure gauge no longer “feels” surface gravitational waves has a lower value in the case of the station C09. This is totally consistent with theoretical views: the critical frequency depends on depth, $f_g \approx 0.366\sqrt{g/H}$, and the station C09 is situated at a large depth.

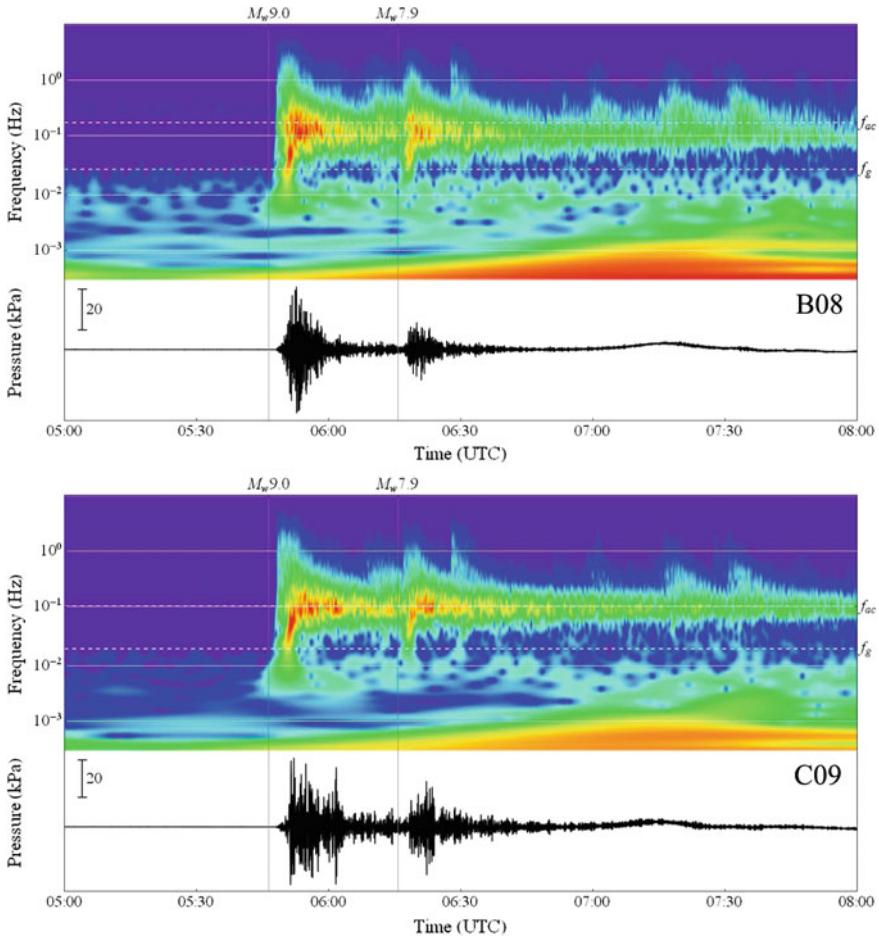


Fig. 4.26 Bottom pressure variations, registered by DONET stations B08 and C09 during the 2011 Tohoku-Oki earthquake and tsunami, and spectrograms of signals. The data sampling frequency is 10 Hz, recording lasted 3 h. Time moments corresponding to the main seismic event of $M_w 9.0$ and the first strong aftershock of $M_w 7.9$ are indicated. *White dotted lines* in spectrograms indicate positions of critical frequencies for hydroacoustic (f_{ac}) and gravitational (f_g) waves

The spectrograms presented in Figs. 4.22 and 4.23 permit to make the conclusion that surface seismic waves from the 2011 Tohoku-Oki earthquakes are manifested in the low-frequency range of $f < f_g$, within which the generation is possible of gravitational waves. From the spectrograms of pressure variations (Figs. 4.24 and 4.26) it is seen that after the onset of Rayleigh waves (both from the main event and from the aftershock) weak pressure variations arise of frequencies ~ 0.01 Hz that last more than an hour and then merge with the manifestations of tsunami waves. These oscillations clearly stand out as an independent “branch” in the pressure

spectrograms, for which there exists no analog in the acceleration spectrograms (Fig. 4.23). The observed low-frequency oscillations represent a manifestation of free surface gravitational waves, generated in the ocean by the propagation of surface seismic waves along the ocean bottom (Nosov et al. 2015). Such gravitational waves leave the leading tsunami wave behind by more than an hour, i.e., they can be arbitrarily termed “tsunami precursors”. It is important, however, to understand that the observed “precursors” actually have no direct relationship to the subsequent tsunami waves, therefore, it is unlikely possible for them to be used in resolving forecasting problems.

Figure 4.27 presents the result of band-pass filtration of signals registered by the pressure gauges of stations B08 and C09. Those signal components are singled out that correspond to the frequency ranges “acoustic waves” ($f > f_{ac}$), “forced oscillations” ($f_g < f < f_{ac}$), and “gravitational waves” ($f < f_g$). For comparison original (not subjected to filtration) signals are also presented. From Fig. 4.27 the conclusion can be made that the maximum amplitudes of bottom pressure variations are due to the high-frequency components of the signal (the ranges of “acoustic waves” and of “forced oscillations”). The signal in the range of “gravitational waves” is an order of magnitude weaker (in Fig. 4.27 this signal is presented upon tenfold amplification). It is remarkable that the signal amplitudes within the ranges of “acoustic waves” and of “forced oscillations” are approximately equal to each other. However, at large depths (C09) the signal in the range of “acoustic waves” is characterized by a somewhat larger amplitude. From the low-frequency component ($f < f_g$, without the tidal component) of pressure variations, registered by stations B08 and C09, it is seen that after the passage of Rayleigh waves oscillations are observed with a period $T \approx 150$ s and of amplitude $p_0 \sim 100$ Pa, which is a manifestation of weak gravitational surface waves or of “tsunami precursors”. Waves of the indicated period can be considered long waves with an accuracy sufficient for estimates. Therefore, for transition from the amplitude of pressure variations to the amplitude of oscillations of the ocean surface, ξ_0 , we shall apply the simple formula $\xi_0 = p_0/\rho g$, where ρ is the density of water, ($\rho = 1030$ kg/m³). Estimation of the wave amplitude yields the value $\xi_0 \sim 0.01$ m. From our point of view formation of the observed gravitational waves occurs in regions, where the ocean depth undergoes sharp changes. The inset of Fig. 4.21 shows the absolute value of the depth gradient. Numerous large-scale underwater slopes are seen in the vicinity of the DONET stations.

Let us discuss possible mechanisms for generation of the observed gravitational waves. Since we only interpret the low-frequency component of registered signals, $f < f_g < f_{ac}$, it is expedient to treat the ocean as an incompressible medium. The most simple model, within the framework of which the generation of a tsunami by bottom displacements is described adequately, is the linear theory of long waves. Equations of this theory reduce to an inhomogeneous wave equation with respect to the displacement ξ of a free surface (see Sect. 3.1.2),

$$\frac{\partial^2 \xi}{\partial t^2} - g \nabla (H \nabla \xi) = \frac{\partial^2 \eta}{\partial t^2}, \quad (4.68)$$

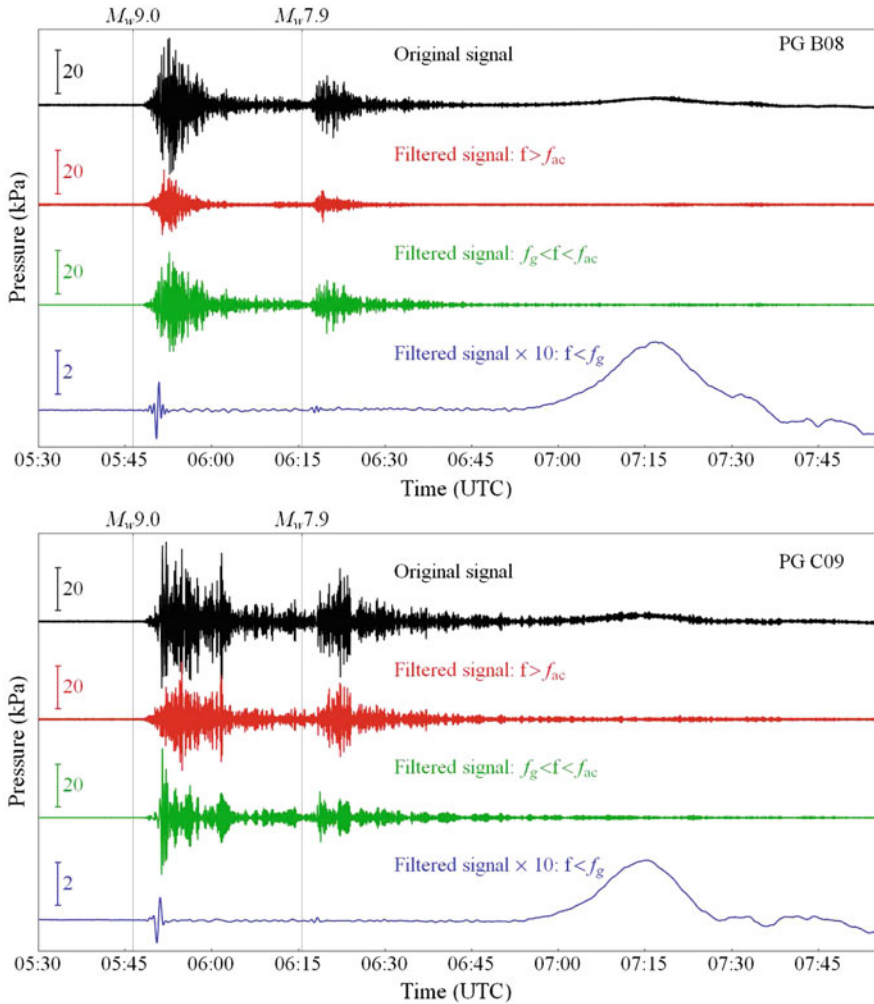


Fig. 4.27 Original signals (*black curves*), registered by pressure gauges of DONET stations B08 and C09 during the 2011 Tohoku-Oki earthquake and tsunami. Band-pass filtered signals (*colored curves*). Frequency ranges are indicated near the *curves* in the figure. The signal from the “gravitational waves” range is shown upon tenfold amplification. Time moments corresponding to the main seismic event of $M_w 9.0$ and the first strong aftershock of $M_w 7.9$ are indicated

where η is the deviation of the bottom surface from its initial position (the source function). Consider the $0z$ -axis to be directed vertically upward, and the $0x$ and $0y$ axes toward the east and north, respectively. Then, the source function η , present in Eq. (4.68), can be expressed via components of the bottom deformation vector $\mathbf{D} \equiv (D_x, D_y, D_z)$ and the distribution of depths by the following formula (see Sect. 2.3):

$$\eta = \frac{\partial H}{\partial x} D_x + \frac{\partial H}{\partial y} D_y + D_z. \quad (4.69)$$

In the low-frequency range of $f < f_g$ the vector field \mathbf{D} represents a superposition of Rayleigh and Love waves, and, consequently, it exhibits the character of a running perturbation. The form of formula (4.69) points to the possibility of dealing separately with the contributions of vertical and horizontal components of bottom movements. Vertical displacements correspond exclusively to Rayleigh waves, while horizontal displacements correspond to both Love and Rayleigh waves.

We shall first estimate the contribution of vertical bottom movements ($\eta = D_z$). By the difference in onset times of low-frequency components of the seismic signal (vertical acceleration) at the DONET stations we determined the propagation velocity of a Rayleigh wave, which amounted to $U \approx 3700$ m/s. By the velocity and the maximum frequency we estimated the minimum Rayleigh wavelength: $\lambda = U/f_g \approx 150$ km. From Fig. 4.21 (the inset) the Rayleigh wavelength is seen to be essentially superior to the typical horizontal extension of steep areas of underwater slopes ($L < 10$ km $\ll \lambda$). In such a situation an underwater slope can be treated like a steplike change in depth.

Consider a flat wave perturbation running with a velocity U along the infinite surface of an even horizontal bottom, and the shape of which is described by the function $\eta(x, y, t) = f(x - UT)$. In this case a forced running perturbation is known to arise (see Sect. 3.3.3) within the water layer involving a free surface displacement $\xi(x, y, t) = Af(x - UT)$, where $A = U^2/(U^2 - gH)$. In such a system no gravitational waves are excited. For free waves to be excited there must be bottom irregularities.

Consider a plane seismic wave traversing a region, in which the ocean depth undergoes a steplike change from H_1 to H_2 . The change in depth will cause a restructurization of the forced perturbation in the water layer, which is certain to be accompanied by the generation of free gravitational waves. The amplitude of these waves can be estimated by equating the free surface displacements and the fluxes of liquid at the point of steplike change in depth,

$$\xi_1 = \frac{g(H_2 - H_1)U^2\eta_0}{(\sqrt{gH_1} + \sqrt{gH_2})(gH_1 - U^2)(\sqrt{gH_2} + U)} \quad (\text{in the region of depth } H_1), \quad (4.70)$$

$$\xi_2 = \frac{g(H_1 - H_2)U^2\eta_0}{(\sqrt{gH_1} + \sqrt{gH_2})(\sqrt{gH_1} - U)(gH_2 - U^2)} \quad (\text{in the region of depth } H_2), \quad (4.71)$$

where η_0 is the running perturbation amplitude. Integrating the accelerogram (the vertical component) twice we obtain an estimate for the amplitude of vertical displacements in the Rayleigh wave, $\eta_0 \sim 0.1$ m. From formulae (4.70) and (4.71) it follows that the amplitude of the arising waves does not exceed several percent of the value η_0 . Thus, for example, in the case of $H_1 = 3000$ m and $H_2 = 2000$ m at the jump in depth there will arise waves of amplitude ~ 0.001 m, which is essentially less than the observed value. Thus, the mechanism related solely to vertical bottom displacements in the Rayleigh wave cannot fully explain the observed amplitudes of gravitational waves.

The contribution of horizontal bottom oscillations to the source function ($\eta = \partial H/\partial x D_x + \partial H/\partial y D_y$) is particular in that its manifestations are only present in narrow ($L \ll \lambda$) areas on large-scale underwater slopes. In this case the source function no longer exhibits the character of a running perturbation, it rather resembles individual oscillating areas of the bottom. The amplitude of waves due to such sources is easy to estimate. It will be of the order of the amplitude of horizontal bottom displacements multiplied by the depth gradient. The amplitude of horizontal bottom movements estimated by the twice integrated horizontal acceleration components was ~ 0.1 m, a typical value of the depth gradient is 0.1. As a result we obtain an estimate for the wave amplitude equal to 0.01 m, that is in good agreement with the observed value.

In conclusion of this section we shall discuss possibilities for operative forecasting of tsunami waves, that have newly opened up owing to the appearance of a dense network of deepwater stations, such as, for example, DONET (Nosov and Grigorieva 2015). The main idea of the forecast method, which dates from the 1960–1970s (Soloviev 1968; Jaque and Soloviev 1971), consists in that tsunami calculations are only based on real data on the sea level obtained from stations located at distances providing the necessary lead time. The data on the sea level are assimilated by a hydrodynamic numerical model, with the aid of which, in the real time mode and on a regular basis, oscillations are calculated of the sea level at the coast. An important condition for such a scheme to be effective consists in the presence of a sufficiently dense network of instruments for measuring the sea level. In principle, there may be exceptions from this rule, but in such cases forecasting will involve resolution of difficult inverse problems (e.g., Tsushima et al. 2009, 2011).

For an absolute and accurate reconstruction of the wave field from measurements made at a set of points the distance between stations must not exceed half the minimum wavelength. The minimum wavelength is calculated from the maximum frequency and the velocity of long waves. As the maximum frequency it is expedient to choose the frequency $f_{lw} = 0.0718\sqrt{g/H}$ that separates the ranges of long and dispersive waves (see Sect. 4.2.1; the numerical coefficient in the formula corresponds to a 10% level of signal attenuation). Thus, we obtain the condition for the distance between stations,

$$d < \sim \frac{\lambda_{\min}}{2} = \frac{\sqrt{gH}}{2f_{lw}} \approx 7H. \quad (4.72)$$

Most of the DONET stations are established at depths of about 2 km. Thus, in accordance with formula (4.72) the distance between stations necessary for reconstructing the tsunami wave field must not exceed 14 km. The actual distance between the DONET stations is quite consistent with this condition. The signal registered by a bottom pressure gauge represents a superposition of manifestations of seismic, hydroacoustic, and gravitational waves, as well as the hydrostatic pressure. Oscillations of the sea level corresponding precisely to long gravitational waves must be introduced into the long-wave prognostic model. Consequently, the initial signal must be subjected to filtration and recalculation to oscillations of the sea level. The maximum frequency of long waves, f_{lw} , is to be chosen as the filter cutoff frequency. Estimation of the maximum frequency (for $H = 2000$ m, $g = 9.8$ m/s²) yields the value $f_{lw} \approx 0.005$ Hz.

The high-frequency ($f > 0.005$ Hz) components of signals registered by pressure gauges of the DONET system were discarded applying the Morlet wavelet transformation. Sea level variations reconstructed from data provided by the DONET stations are shown in Fig. 4.28. The filtered signal is seen to contain only tsunami waves and tides. Manifestations of seismic waves are not observed, although their amplitude in the initial records exceeded the tsunami signal by more than an order of magnitude.

It is remarkable that in the method of tsunami precalculation based on the assimilation of data by a dense network of stations it is not necessary to discard the tidal component of the signal. Contrariwise, reconstruction of a tsunami together with the tide is extremely important from a practical point of view, since the arrival of a tsunami wave during the phase of high tide may have more severe consequences. Details of the tsunami precalculation method based on DONET data are expounded in Nosov and Grigorieva (2015).

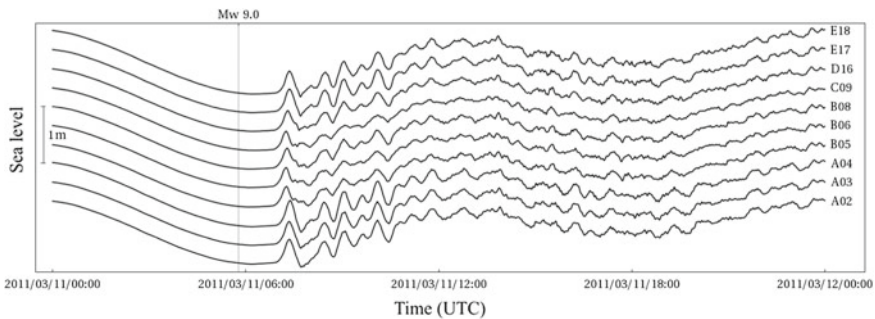


Fig. 4.28 Variations of sea level reconstructed from pressure measurements by DONET bottom stations during the period from 00:00 to 24:00 UTC on March 11, 2011. The vertical line indicates the moment of the 2011 Tohoku-Oki earthquake onset (M_w 9.0)

4.3 Nonlinear Mechanism of Tsunami Generation

This section deals with the formation mechanism of tsunami waves due to the nonlinear transfer of energy from “high-frequency” induced or elastic oscillations of the water column to “low-frequency” surface gravitational waves. Seismic movements of the ocean bottom are considered as the source of “fast” oscillations of the water column. The “traditional” tsunami generation mechanism, related to residual displacements substituting the water, naturally, remains in force, and in most cases precisely it plays the leading part. The nonlinear mechanism provides additional contributions to the tsunami amplitude and energy. It is not excluded that in individual cases nonlinear effects can also provide a determinative contribution to a tsunami wave.

At a first glance formulation of the problem, assuming the presence of periodic oscillations, may seem restricted. Actually, such a restriction is important only under the condition that the water column responds to movements of the ocean bottom like an incompressible liquid. In this case one must indeed consider *periodic* oscillations of a part of the bottom, which lead to corresponding induced oscillations of the incompressible water column. But, if the water column reacts to seismic movements of the ocean bottom like a compressible liquid, the necessity of periodic movements of the bottom vanishes, since any vertical displacements will be accompanied by elastic oscillations of the water column at normal frequencies.

In substantiating the application of linear theory in the tsunami generation problem one usually quotes the condition that the amplitude of the ocean bottom deformation be small as compared to the depth of the basin, $\eta \ll H$. Indeed, this condition is quite fulfilled in reality. But even when the amplitude of the ocean bottom displacement is small, the velocity of its movement may turn out to be sufficiently high for the manifestation of nonlinear effects.

Before our studies were published (Nosov and Skachko 2001; Nosov and Kolesov 2002, 2005; Nosov et al. 2008) there existed only a single work (Novikova and Ostrovsky 1982), in which the possibility was investigated of tsunami formation resulting from a nonlinear effect—the “detection” of acoustic oscillations of the water column.

4.3.1 Base Mathematical Model

Before proceeding with the construction of a model describing nonlinear effects, it is useful to present a description of the character of the linear response of a compressible water column to movements of the ocean bottom without residual displacement. The character of the response varies depending on the position of the spectrum of ocean bottom movements with respect to the two characteristic frequencies f_g and f_{ac} (see Sect. 4.2.1). Further, without losing generality, we shall not speak of a spectrum, but of a certain frequency of bottom oscillations, f . Thus, if the frequency of

bottom oscillations, $f < f_g$, then the linear response of the water column represents a superposition of forced oscillations (in the source area) and of gravitational waves, emitted toward the distant zone. If the frequency lies within the range $f_g < f < f_{ac}$, then no gravitational waves arise, and movements of the water column exist only in the immediate vicinity of the source in the form of forced oscillations. As the frequency increases up to values $f > f_{ac}$, a qualitative change occurs in the dynamics of the linear response—the water column starts to behave like a compressible medium.

The three frequency ranges identified above are shown in the “ocean depth–frequency of bottom oscillations” plane in Fig. 4.14. It is interesting to note that the dependences intersect at the hypothetical ocean depth of $H \approx 107$ km, consequently, in the conditions of the planet Earth the three indicated ranges exist at any point of the world oceans. Nonlinear effects are manifested only in the case of sufficiently high velocities of bottom movements, which can be characteristic of the frequency ranges “Forced Oscillations” and “Acoustic Waves”. Clearly, the low-frequency range “Gravitational Waves” is of no special interest.

The mathematical model of tsunami generation due to nonlinear effects will be constructed on the basis of Euler’s equations, assuming the liquid to be compressible,

$$\frac{\partial \mathbf{v}}{\partial t} + (\mathbf{v}, \nabla) \mathbf{v} = -\frac{\nabla p}{\rho} + \mathbf{g}, \quad (4.73)$$

$$\frac{\partial \rho}{\partial t} + \text{div}(\rho \mathbf{v}) = 0. \quad (4.74)$$

In the case of an incompressible liquid the density ρ will be assumed constant, while for the compressible liquid we shall consider the variations in pressure to be proportional to the variations in density, $p' = c^2 \rho'$.

Applying a device used, for instance, in turbulence theory or nonlinear acoustics, we represent movement of the liquid as the sum of a slow (average) movement and of a fast (oscillatory) movement,

$$\mathbf{v} = \langle \mathbf{v} \rangle + \mathbf{v}', \quad p = \langle p \rangle + p', \quad \rho = \langle \rho \rangle + \rho'. \quad (4.75)$$

Substituting formulae (4.75) into Eqs.(4.73) and (4.74) and averaging over the period of “fast” oscillations, we obtain a set of equations for describing the average movement of the liquid,

$$\frac{\partial \langle \mathbf{v} \rangle}{\partial t} + (\langle \mathbf{v} \rangle, \nabla) \langle \mathbf{v} \rangle = -\frac{\nabla \langle p \rangle}{\langle \rho \rangle} + \mathbf{g} - \langle (\mathbf{v}', \nabla) \mathbf{v}' \rangle + \frac{\langle \rho' \nabla p' \rangle}{\langle \rho \rangle^2}, \quad (4.76)$$

$$\frac{\partial \langle \rho \rangle}{\partial t} + \text{div}(\langle \rho \rangle \langle \mathbf{v} \rangle) = -\text{div} \langle \rho' \mathbf{v}' \rangle. \quad (4.77)$$

In performing the averaging we applied rules, similar to the Reynolds rules, applied in turbulence theory.

In the case of an incompressible liquid (range ‘Forced Oscillations’) the mean is calculated from the period of the ocean bottom oscillations, and the average motion can, obviously, be described as the flow of an incompressible liquid. If the liquid is compressible (range ‘Acoustic Waves’), then as the period for averaging one should take the quantity $4H_{\max}/c$, where H_{\max} is the maximum depth of the basin. It is known that acoustic modes with periods superior to $4H_{\max}/c$ do not exist, consequently, in this case, also, the mean movement can be described as the flow of an incompressible liquid. Taking into account that $\langle \rho \rangle = \text{const}$ and neglecting the term quadratic in the average velocity, $(\langle \mathbf{v} \rangle, \nabla) \langle \mathbf{v} \rangle$, one arrives at the following system:

$$\frac{\partial \langle \mathbf{v} \rangle}{\partial t} = -\frac{\nabla \langle p \rangle}{\langle \rho \rangle} + \mathbf{g} - \langle (\mathbf{v}', \nabla) \mathbf{v}' \rangle + \frac{\langle \rho' \nabla p' \rangle}{\langle \rho \rangle^2}, \quad (4.78)$$

$$\text{div} \langle \mathbf{v} \rangle = -\frac{1}{\langle \rho \rangle} \text{div} \langle \rho' \mathbf{v}' \rangle. \quad (4.79)$$

The expressions obtained differ from the usual linearized Euler equations for an incompressible liquid by the presence of the following new terms:

$$\Phi = -\langle (\mathbf{v}', \nabla) \mathbf{v}' \rangle + \frac{\langle \rho' \nabla p' \rangle}{\langle \rho \rangle^2} \equiv -\langle (\mathbf{v}' \nabla) \mathbf{v}' \rangle + \frac{\langle \nabla p'^2 \rangle}{2c^2 \langle \rho \rangle^2}, \quad (4.80)$$

$$s = -\frac{1}{\langle \rho \rangle} \text{div} \langle \rho' \mathbf{v}' \rangle \equiv -\frac{1}{c^2 \langle \rho \rangle} \text{div} \langle p' \mathbf{v}' \rangle, \quad (4.81)$$

which can be interpreted as a force field Φ and a distributed source of mass, s . The origin of the new terms is due to the nonlinearity of the initial equations. The combined action of the force field and of the distributed source of mass under certain conditions is capable of causing long gravitational waves. We shall speak of this action as of a “nonlinear tsunami source”.

For calculating the waves caused by the action of the force field and of the distributed source of mass, we shall apply the linear theory of long waves. The expedience of choosing this theory is, first of all, explained by the fact that we are interested in large-scale motions correlated in space (i.e., long waves), and, moreover, this way seems the most simple one.

We shall further restrict ourselves to dealing with the plane problem. We write Eqs. (4.78) and (4.79) for the separate components:

$$\frac{\partial u}{\partial t} = -\frac{1}{\rho} \frac{\partial p}{\partial x} + \Phi_x, \quad (4.82)$$

$$\frac{\partial w}{\partial t} = -\frac{1}{\rho} \frac{\partial p}{\partial z} + \Phi_z - g, \quad (4.83)$$

$$\frac{\partial u}{\partial x} + \frac{\partial w}{\partial z} = s. \quad (4.84)$$

Neglecting vertical acceleration $\partial w/\partial t$, we integrate Eq.(4.83) over the vertical coordinate within limits from z to ξ . The result for the pressure is the following:

$$p(z) = p_{\text{atm}} + \rho g \xi - \rho g z - \rho \int_z^\xi \Phi_z dz^*, \quad (4.85)$$

where ξ is the displacement of the free surface, z is the running vertical coordinate, varying within the limits $-H \leq z \leq \xi$. Substituting expression (4.85) into Eq. (4.82), we find,

$$\frac{\partial u}{\partial t} = -g \frac{\partial \xi}{\partial x} + \int_z^\xi \frac{\partial \Phi_z}{\partial x} dz^* + \Phi_x. \quad (4.86)$$

Integration of formula (4.86) over dz within limits from $-H$ to ξ yields the following equation:

$$H \frac{\partial U}{\partial t} = -gH \frac{\partial \xi}{\partial x} + \int_{-H}^\xi dz \int_z^\xi \frac{\partial \Phi_z}{\partial x} dz^* + \int_{-H}^\xi \Phi_x dz, \quad (4.87)$$

where U is the horizontal velocity value averaged along the vertical direction. We further integrate the continuity equation (4.84) over dz within the same limits,

$$H \frac{\partial U}{\partial x} + \frac{\partial \xi}{\partial t} = \int_{-H}^\xi s dz. \quad (4.88)$$

In obtaining expression (4.88) account was taken of the no-flow condition on the ocean bottom, $w(x, -H, t) = 0$ (the ocean bottom is considered motionless for the mean movement), while the vertical velocity at the surface is expressed as the partial time derivative of the displacement ξ .

Further, calculating the partial derivatives with respect to x and t of Eqs. (4.87) and (4.88), respectively, and excluding the mixed derivative $\partial^2 U/\partial x \partial t$ we arrive at the nonuniform wave equation,

$$\frac{\partial^2 \xi}{\partial x^2} - \frac{1}{gH} \frac{\partial^2 \xi}{\partial t^2} = \frac{1}{gH} Q(x, t). \quad (4.89)$$

Considering the free surface to deviate insignificantly from its equilibrium position ($\xi \ll H$), it is correct to perform integration over the vertical coordinate in the right-hand part of Eq. (4.89) not up to $z = \xi$, but to $z = 0$. Thus, to calculate a long wave

caused by the combined action of a force field and distributed sources of mass it is necessary to calculate the following function:

$$Q(x, t) = \int_{-H}^0 dz \left(\frac{\partial \Phi_x}{\partial x} + \int_z^0 \frac{\partial^2 \Phi_z}{\partial x^2} dz^* - \frac{\partial s}{\partial t} \right). \tag{4.90}$$

For a constant depth of the basin the solution of Eq.(4.89) is given by the well-known integral formula (Tikhonov and Samarsky 1999). In the general case, when the depth is a function of the horizontal coordinate, the equation is readily resolved numerically by the finite difference method.

4.3.2 Nonlinear Mechanism of Tsunami Generation by Bottom Oscillations in an Incompressible Ocean

Suppose that in the process of an underwater earthquake a section of the ocean bottom oscillates with a frequency corresponding to range “Forced Oscillations”. In this case the ocean behaves like an incompressible liquid, undergoing forced oscillations following movements of the bottom. From formulae (4.80) and (4.81) the nonlinear tsunami source is seen to be manifested only as a force field,

$$\Phi_{incompr} = -\langle (\mathbf{v}', \nabla) \mathbf{v}' \rangle. \tag{4.91}$$

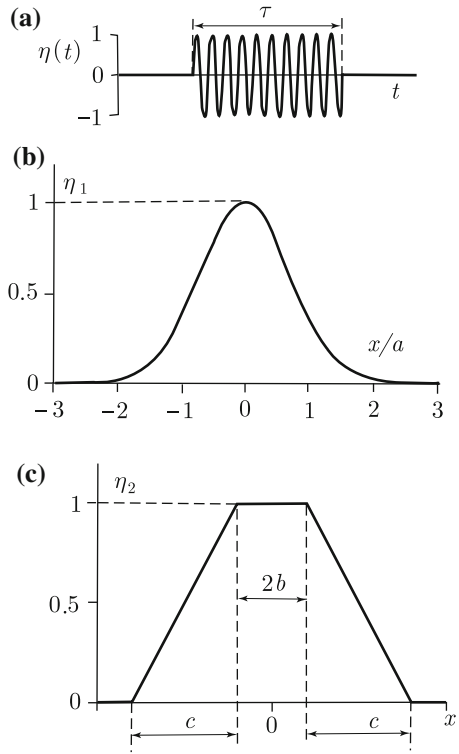
In this case the linear mechanism is not capable of leading to the formation of gravitational waves, but they may arise as a result of the action of the force field.

Calculation of the quantity $\Phi_{incompr}$ requires knowledge of the velocity field in the induced oscillations of the water column. The velocity field can be calculated from the solution of the problem within the framework of linear potential theory, (3.67) and (3.68). Let the law of motion of the ocean bottom, $\eta(x, t)$, have the form

$$\begin{aligned} \eta(x, t) &= \eta_i(x) (\theta(t) - \theta(t - \tau)) \sin(\omega t), \quad i = 1, 2, \\ \eta_1(x) &= \eta_0 \exp\{-x^2 a^{-2}\}, \\ \eta_2(x) &= \begin{cases} \eta_0, & |x| \leq b, \\ \eta_0 [c^{-1}(b - |x|) + 1], & b < |x| \leq b + c, \\ 0, & |x| > b + c, \end{cases} \end{aligned} \tag{4.92}$$

where η_0 and ω are the amplitude and cyclic frequency, respectively, of ocean bottom oscillations, a, b, c are parameters characterizing the horizontal extension and shape of the space distribution of the amplitudes of bottom oscillations, θ is the Heaviside function. The model law of motion of the ocean bottom is shown in Fig.4.29. We shall consider ocean bottom oscillations to always terminate at the same phase, as

Fig. 4.29 Model law of motion of the ocean bottom: time part (a), space distribution of $\eta(x)$ (b) and (c)



when they started, otherwise the residual displacements of the ocean bottom will certainly excite a gravitational wave via the ordinary piston mechanism.

Dropping intermediate calculations, we present formulae for components of the flow velocity and displacement of the free surface in the case of ocean bottom oscillations described by expression (4.92) (for $\tau = \infty$),

$$\begin{aligned}
 u(x, z, t) = & \frac{\eta_0 \omega}{\pi} \int_0^\infty dk \frac{\sin(kx) \cosh(kz) X_i(k)}{\cosh(k)(p_0^2 - \omega^2)} \\
 & \times \left(\cos(\omega t) \left(k + \omega^2 \tanh(kz) \right) - \cos(p_0 t) \left(k + p_0^2 \tanh(kz) \right) \right) \quad (4.93)
 \end{aligned}$$

$$\begin{aligned}
 w(x, z, t) = & -\frac{\eta_0 \omega}{\pi} \int_0^\infty dk \frac{\cos(kx) \cosh(kz) X_i(k)}{\cosh(k)(p_0^2 - \omega^2)} \\
 & \times \left(\cos(\omega t) \left(k \tanh(kz) + \omega^2 \right) - \cos(p_0 t) \left(k \tanh(kz) + p_0^2 \right) \right), \quad (4.94)
 \end{aligned}$$

$$\xi(x, t) = \frac{\eta_0}{\pi} \int_0^\infty dk \frac{\omega \cos(kx)(\omega \sin(\omega t) - p_0 \sin(p_0 t))X_i(k)}{\cosh(k)(\omega^2 - p_0^2)}, \tag{4.95}$$

where

$$p_0^2 = k \tanh(k), \quad X_i(k) = \int_{-\infty}^{+\infty} dx \exp\{ikx\}\eta_i(x).$$

Expressions (4.93)–(4.95) contain under the integral sign dimensionless variables (the asterisk “*” is omitted),

$$\begin{aligned} k^* &= Hk, & t^* &= t \left(\frac{g}{H}\right)^{1/2}, \\ \omega^* &= \omega \left(\frac{H}{g}\right)^{1/2}, & (x^*, z^*, a^*, b^*, c^*) &= \frac{1}{H} (x, z, a, b, c), \end{aligned} \tag{4.96}$$

but the coefficients in front of the integrals are dimensional.

Numerical calculation of the flow velocity components has shown, that in the frequency range considered, immediately after oscillations of the ocean bottom are “switched on”, each point of the liquid starts performing harmonic oscillations with an amplitude depending only on its coordinates,

$$u'(x, z, t) = u'(x, z) \cos(\omega t), \quad w'(x, z, t) = w'(x, z) \cos(\omega t). \tag{4.97}$$

Substituting formulae (4.97) into expression (4.91) and subsequently averaging over the period of oscillations, we obtain formulae for calculating the horizontal and vertical components of the force field, Φ_x and Φ_z , respectively,

$$\Phi_x(x, z) = -\frac{1}{2} \left(u'(x, z) \frac{\partial u'(x, z)}{\partial x} + w'(x, z) \frac{\partial u'(x, z)}{\partial z} \right), \tag{4.98}$$

$$\Phi_z(x, z) = -\frac{1}{2} \left(u'(x, z) \frac{\partial w'(x, z)}{\partial x} + w'(x, z) \frac{\partial w'(x, z)}{\partial z} \right). \tag{4.99}$$

Functions $u'(x, z)$ and $w'(x, z)$ can be calculated from formulae (4.93) and (4.94) at $t = 0$,

$$u'(x, z) = -\frac{\eta_0 \omega}{\pi} \int_0^\infty dk \frac{\sin(kx) \sinh(kz) X_i(k)}{\cosh(k)}, \tag{4.100}$$

$$w'(x, z) = \frac{\eta_0 \omega}{\pi} \int_0^\infty dk \frac{\cos(kx) \cosh(kz) X_i(k)}{\cosh(k)}. \tag{4.101}$$

As a result we arrive at the following expressions for the components of the force field:

$$\begin{aligned} \Phi_x(x, z) = & -\frac{(\eta_0\omega)^2}{4\pi^2H} \int_0^\infty dk_1 \int_0^\infty dk_2 \frac{X_i(k_1)X_i(k_2)k_2}{\cosh(k_1)\cosh(k_2)} \\ & \times (\sin((k_1 - k_2)x) \cosh((k_1 + k_2)z) \\ & - \sin((k_1 + k_2)x) \cosh((k_1 - k_2)z)), \end{aligned} \tag{4.102}$$

$$\begin{aligned} \Phi_z(x, z) = & -\frac{(\eta_0\omega)^2}{4\pi^2H} \int_0^\infty dk_1 \int_0^\infty dk_2 \frac{X_i(k_1)X_i(k_2)k_2}{\cosh(k_1)\cosh(k_2)} \\ & \times (\cos((k_1 - k_2)x) \sinh((k_1 + k_2)z) - \cos((k_1 + k_2)x) \sinh((k_1 - k_2)z)). \end{aligned} \tag{4.103}$$

Figure 4.30 presents a typical form of the force field in the case of the space distribution of the oscillation amplitude calculated for different sizes of the source, a . It is seen, that, as parameter a increases, the vertical component of the force, Φ_z , decreases, while the dependence of the horizontal component Φ_x upon the vertical coordinate z becomes weaker and weaker.

For estimation of the relative contributions of the horizontal and vertical components of the force field to the amplitude of the long gravitational wave we take advantage of formula (4.90) for function $Q(x, t)$, entering into the right-hand part of the wave equation (4.89). With regard to the set of dimensionless variables (4.96), adopted above, we have,

$$Q(x, t) = \int_{-1}^0 dz \left(\frac{\partial \Phi_x}{\partial x} + \int_z^0 \frac{\partial^2 \Phi_z}{\partial x^2} dz^* \right). \tag{4.104}$$

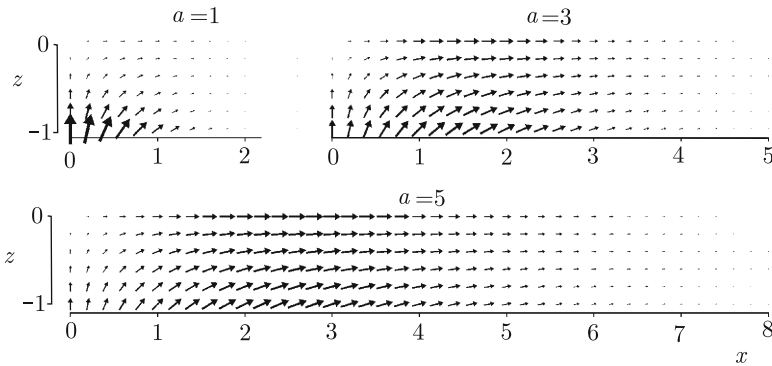


Fig. 4.30 Typical form of force field. The calculation is performed for the space distribution of the ocean bottom oscillation amplitude η_1 for $a = 1, 3,$ and 5 . The direction and length of the arrow corresponds to the vector $a \Phi_{incompr}$

Substituting formulae (4.102) and (4.103) into (4.104) and performing the required differentiation and integration, we obtain

$$Q(x, t) = "X" + "Z", \tag{4.105}$$

where

$$\begin{aligned} "X" = & \frac{(\eta_0 \omega)^2}{4\pi^2 H} \int_0^\infty dk_1 \int_0^\infty dk_2 \frac{X_i(k_1)X_i(k_2)k_2}{\cosh(k_1) \cosh(k_2)} \\ & \times \left(\frac{(k_1 + k_2)}{(k_1 - k_2)} \cos((k_1 + k_2)x) \sinh((k_1 - k_2)) \right. \\ & \left. - \frac{(k_1 - k_2)}{(k_1 + k_2)} \cos((k_1 - k_2)x) \sinh((k_1 + k_2)) \right), \tag{4.106} \end{aligned}$$

$$\begin{aligned} "Z" = & \frac{(\eta_0 \omega)^2}{4\pi^2 H} \int_0^\infty dk_1 \int_0^\infty dk_2 \frac{X_i(k_1)X_i(k_2)k_2}{\cosh(k_1) \cosh(k_2)} \\ & \times \left(\frac{(k_1 - k_2)^2}{(k_1 + k_2)^2} \cos((k_1 - k_2)x) ((k_1 + k_2) - \sinh(k_1 + k_2)) \right. \\ & \left. - \frac{(k_1 + k_2)^2}{(k_1 - k_2)^2} \cos((k_1 + k_2)x) \{(k_1 - k_2) - \sinh(k_1 - k_2)\} \right). \tag{4.107} \end{aligned}$$

The quantity $X(x)$ determines the contribution of the horizontal component of the force field to the formation of long gravitational (tsunami) waves, and the quantity $Z(x)$ determines the contribution of the vertical component.

Figure 4.31 presents functions $Q(x)$, $X(x)$, and $Z(x)$, which were calculated in accordance with formulae (4.105)–(4.107) for the space distribution of the ocean bottom oscillation amplitude $\eta_1(x)$. From the figure it is seen that the terms $X(x)$ and $Z(x)$, as a rule, exhibit differing signs. This means the structure of the force field is such that the contribution of the horizontal force component to the gravitational wave formation is always partly compensated by the vertical component. In the case of a source of small size ($a \sim H$) this effect is capable of significantly reducing the wave amplitude. However, in the case of a large horizontal extension of the source ($a \gg H$) the action of the horizontal component turns out to prevail ($|X| \gg |Z|$). The dimensions of real tsunami sources are always significantly greater than the ocean depth, therefore, the contribution of the vertical component of the force field can be neglected.

Neglecting the contribution of the vertical component of the force field, $Z(x)$, we write Eq. (4.89) in a dimensionless form (in accordance with formulae (4.96)):

$$\frac{\partial^2 \xi}{\partial x^2} - \frac{\partial^2 \xi}{\partial t^2} = \frac{H}{g} \frac{\partial \bar{\Phi}_x}{\partial x}, \tag{4.108}$$

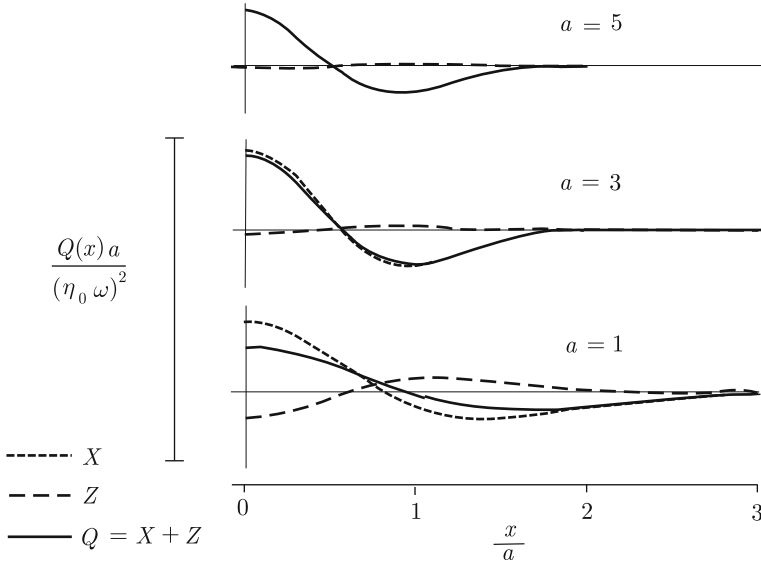


Fig. 4.31 Characteristic form of function $Q(x)$ and of its components $X(x)$ and $Z(x)$. The calculation is performed for the space distribution of the ocean bottom oscillation amplitude η_1 for $a = 1, 3$ and 5

where $\bar{\Phi}_x = \int_{-1}^0 \Phi_x dz$ is the horizontal component of the force field, averaged along the vertical direction, ξ is the displacement of the free surface of the liquid from its equilibrium position, corresponding to the mean movement. We recall that there are, also, present above the oscillating ocean bottom fast oscillations of the surface, which are related to induced oscillations.

The solution of Eq. (4.108) is well known (Tikhonov and Samarsky 1999),

$$\xi(x, t) = \frac{H}{2g} \int_0^t d\hat{t} \int_{x-(t-\hat{t})}^{x+(t-\hat{t})} \frac{\partial \bar{\Phi}_x}{\partial \hat{x}} d\hat{x}. \tag{4.109}$$

Oscillations of the ocean bottom (4.92) take place during a finite period of time τ and exhibit fixed amplitude and frequency. Therefore, we can write

$$\bar{\Phi}_x(x, t) = \bar{\Phi}_x(x) (\theta(t) - \theta(t - \tau)). \tag{4.110}$$

Substituting expression (4.110) into formula (4.109) and performing integration over the space variable, we obtain

$$\xi(x, t) = -\frac{H}{2g} \int_0^t (\theta(\hat{t}) - \theta(\hat{t} - \tau)) (\bar{\Phi}_x(x + (t - \hat{t})) - \bar{\Phi}_x(x - (t - \hat{t}))) d\hat{t}. \tag{4.111}$$

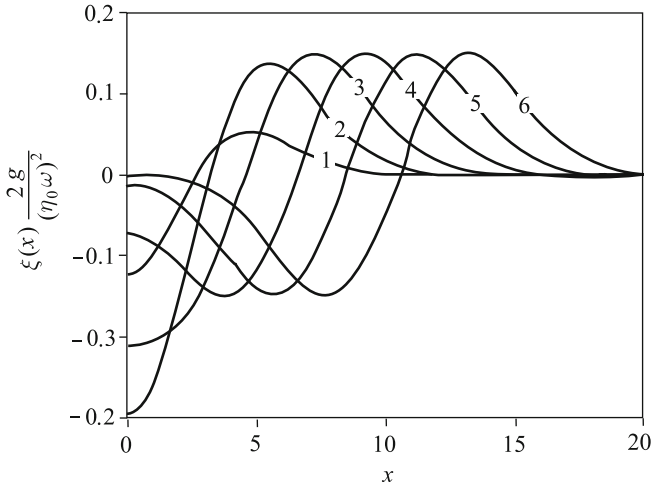
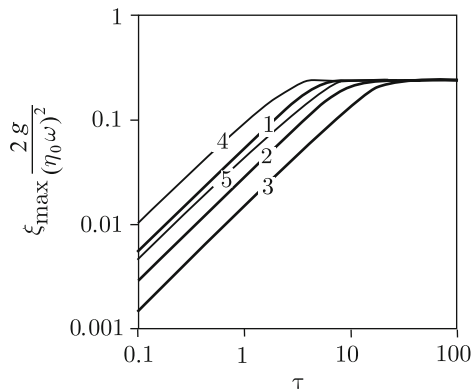


Fig. 4.32 Profile of wave formed by the nonlinear mechanism in an incompressible ocean. The calculation is performed for consecutive moments of time $t = 2, 4, 6, 8, 10, 12$ (curves 1–6) for the case of η_1 and $a = 5, \tau = 3$

The process of tsunami formation by the nonlinear mechanism is shown in Fig. 4.32. Shifts of the surface of the liquid, ξ , were calculated by formula (4.111) as functions of the horizontal coordinate x for consecutive moments of time. A completely formed wave is sure to consist of a hump and depression, which have a zero total volume. The perturbation always starts with a positive phase. The wave length approximately corresponds to the size of the source.

Figure 4.33 presents the wave amplitude ξ_{\max} (the height of the hump) as a function of the duration of ocean bottom oscillations for different shapes of the space distribution of the oscillation amplitude. The quantity ξ_{\max} increases monotonously with the duration of oscillations, but this increase is not without limit: the

Fig. 4.33 Amplitude of long wave versus the duration of the source action. Curves 1–3 are calculated for the space distribution of η_1 for $a = 5, 10, \text{ and } 20$, curves 4 and 5 for η_2 and $b = 2, c = 3$ (4) and $b = 1, c = 9$ (5)



amplitude cannot exceed a certain value, which is practically independent of the shape of the space distribution of $\eta_i(x)$. The horizontal extension of the oscillating area of the ocean bottom noticeably affects the value of τ , at which the maximum amplitude is achieved: when the extension in space of the source is greater, the formation of a wave of maximum amplitude will require prolonged action of the source.

The nonlinear effect considered can be briefly presented as follows. When oscillations of the basin bottom occur, the liquid is “pushed out” of the region of most intense movements (the source), which is precisely what causes the formation of a gravitational wave. The amplitude of such a wave does not depend on the space law, governing variations in the amplitude of the ocean bottom oscillations (providing the law is sufficiently smooth), but depends on the velocity amplitude of oscillations, $\eta_0\omega$, their duration τ and the horizontal size of the oscillating area.

The data presented in Fig. 4.33 permit to estimate the amplitude of a tsunami wave caused by the nonlinear mechanism considered. Thus, for example, when the ocean depth is 1 km, oscillations of an area of the ocean bottom of the characteristic size of 20 km (the space distribution of η_1 , $a = 10$), amplitude of oscillatory velocity of 10 m/s, lasting for 60 s, gives rise to a wave of amplitude 0.8 m.

For illustrative estimation of the contribution of the nonlinear effect to the tsunami amplitude, Fig. 4.34 presents the dependence of the gravitational wave amplitude upon the frequency of ocean bottom oscillations. The wave amplitude is normalized to the amplitude of bottom oscillations. Calculation of the dependence is performed for the case of $\eta_1(x)$ for $a = 10$ km and $H = 1$ km. The oscillations of the ocean bottom,

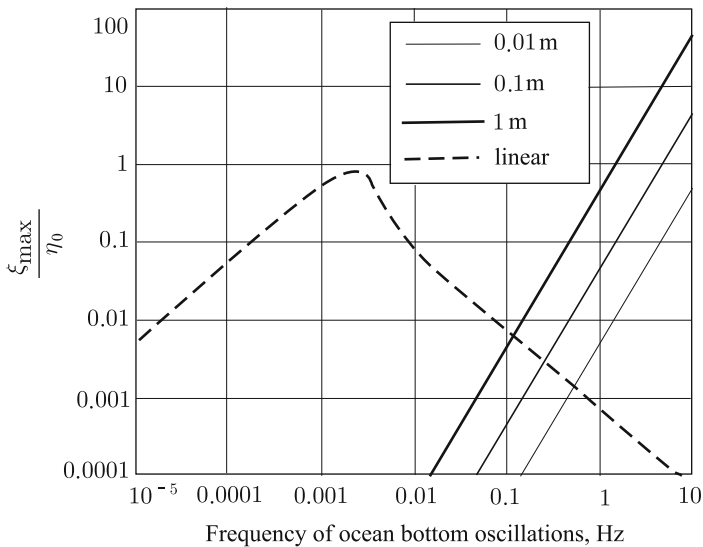


Fig. 4.34 Amplitude of gravitational waves, excited by oscillations of ocean bottom, versus oscillation frequency: linear and nonlinear responses. Calculations are performed for exponential distribution of amplitude of bottom oscillations for $a = 10$ km and ocean depth of 1 km

having started at a certain moment of time, are assumed to continue sufficiently long for the amplitude of the wave, formed by the nonlinear mechanism, to reach the maximum value. The linear response (dotted line) is calculated using formula (4.95). Owing to the auxiliary problem being linear, this dependence is the same for any amplitude of bottom oscillations. The contribution of the nonlinear effect is proportional to the square velocity of bottom oscillations, therefore, it depends on both the amplitude and the frequency of oscillations. Within the range 0.1–1 Hz this contribution is already capable of competing with the linear response and even of exceeding it.

4.3.3 Nonlinear Tsunami Generation Mechanism with Regard to the Compressibility of Water

This section deals with the tsunami generation mechanism related to the nonlinear transfer of energy from “high-frequency” elastic oscillations of the water column to “low-frequency” surface gravitational waves. Elastic oscillations are the reaction of the water column to movements of the bottom of seismic origin. In this case movements of the ocean bottom may not be periodic, it is only important for their frequency spectrum to correspond to frequency range “Acoustic Waves” ($f > c/4H$). Our aim is to find the relationship between characteristics of the “low-frequency” gravitational wave and the parameters determining the ocean bottom displacement, and, also, a comparative analysis of the efficiencies of the piston and nonlinear mechanisms in tsunami generation.

In the case of a compressible liquid, a nonlinear tsunami source is manifested as the action of a force field Φ and of a distributed source of mass, s . For calculation of these quantities knowledge is required of the fields of velocity \mathbf{v}' and of dynamic pressure p' , which we shall find by resolving the plane problem of the linear response of an ideal compressible liquid to small deformations of the ocean bottom, (4.24)–(4.26).

The problem was resolved numerically by the explicit finite difference method, using dimensionless variables ($x^* = x/H$, $t^* = tc/H$). The velocity of ocean bottom deformation was given by the following model laws:

$$U_{pist}(x, t) = v_{\max} \eta \left(\frac{x}{L} \right) \eta \left(\frac{t}{\tau} \right) \quad (\text{piston-like displacement}),$$

$$U_{osc}(x, t) = v_{\max} \eta \left(\frac{x}{L} \right) \sin \left(\frac{2\pi Nt}{\tau} \right) (\theta(t) - \theta(t - \tau))$$

(oscillations of ocean bottom),

where $\eta(\alpha) = 0,5 (\tanh(20(\alpha - 0,15)) - \tanh(20(\alpha - 0,85)))$, v_{\max} is the maximum deformation velocity value, $\theta(t)$ is the Heaviside function, L is the horizontal extension of the deformation area, τ is the duration of the deformation process, N is

the number of oscillation periods (an integer number). The form of function $\eta(\alpha)$ is shown in Fig. 4.35. The piston-like displacement resulted in residual deformations of the ocean bottom, oscillations of the ocean bottom finished without residual deformations.

Numerical calculations and theoretical estimates (Nosov and Kolesov 2002, 2005) reveal the contribution of the force field to tsunami formation to be essentially greater than the contribution of distributed sources of mass. The characteristic form of the field Φ , calculated at consecutive moments of time, is presented in Fig. 4.36. The model parameters chosen for calculations are typical for a real tsunami source.

Fig. 4.35 Form of function determining the space-time law of ocean bottom deformation

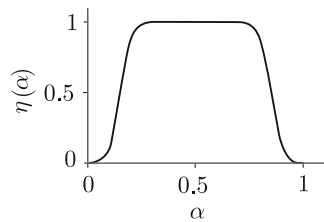
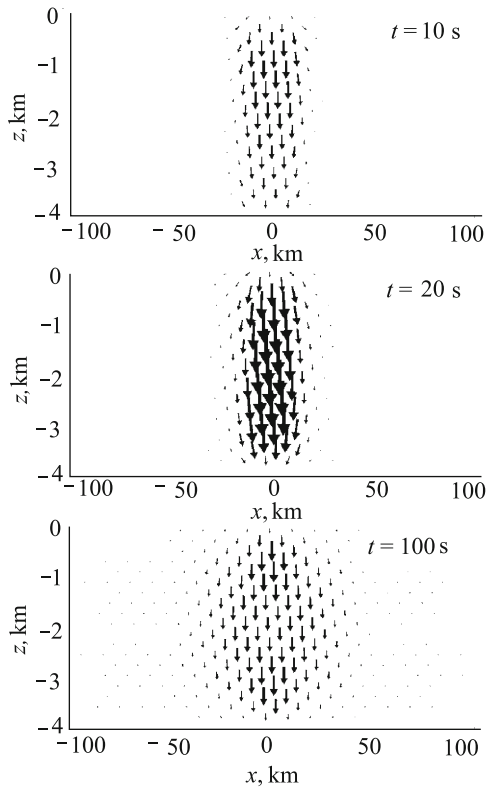


Fig. 4.36 Force field Φ at consecutive moments of time. Calculation for ocean bottom displacement with residual deformation, $\tau = 8$ s, $L = 40$ km, $H = 4$ km



At most of the points the field is directed nearly vertically downward, which leads to the water being pushed out of the area of intense elastic oscillations. Thus, the leading wave, in this case also, is positive. The quantity $|\Phi|$ develops in time as follows. Being equal to zero at the initial moment of time, it reaches its maximum during the first tens of seconds, then, as the elastic waves leave the source area, it tends monotonously toward zero.

For the calculation of gravitational waves, due to the nonlinear mechanism, we applied Eq. (4.89) written in dimensionless variables ($x^* = x/H$, $t^{**} = t\sqrt{g/H}$, $\xi^* = \xi g/v_{\max}^2$)

$$\frac{\partial^2 \xi^*}{\partial x^{*2}} - \frac{\partial^2 \xi^*}{\partial t^{**2}} = Q^*(x^*, t^{**}). \quad (4.112)$$

Equation (4.112) was approximated by the explicit finite difference scheme. At the boundaries of the calculation region the condition of free passage was realized,

$$\frac{\partial \xi^*}{\partial t^{**}} = \mp \frac{\partial \xi^*}{\partial x^*}. \quad (4.113)$$

Since the fields Φ and s , determining the function Q^* , are a result of averaging over the time interval $\Delta t^* = 4$, the output of the model (4.24)–(4.26) was the discrete set: $Q^*(x^*, n\Delta t^*)$, where $n = 1, 2, 3 \dots$. In passing to resolve the problem (4.112) and (4.113) the step in space Δx^* remained the same, while the time steps Δt^* and Δt^{**} were made to comply with each other as follows: within the time interval t^{**} from 0 to $4\sqrt{gH}/c$ function $Q^*(x^*, 4)$ was in force, within the time interval from $4\sqrt{gH}/c$ to $8\sqrt{gH}/c$ it was $Q^*(x^*, 8)$ and so on.

The main part of numerical experiments was carried out for values of the dimensionless parameters, corresponding to $H = 4$ km, $L = 20, 40$ and 80 km, $0.26 < \tau < 26$ s. The vertical step amounted to $\Delta z = 20$ m. The horizontal step was chosen to be such that 100 nodes could occupy the length L of the source ($\Delta x = 200, 400$ and 800 m). The time step was determined by the Courant condition $\Delta t < \Delta z/c$. In calculations the step $\Delta t = 0.009$ s was applied.

Figure 4.37 presents the typical time behavior of function $Q^*(x^*)$, reflecting the action of a “nonlinear tsunami source”. The highest absolute values of $Q^*(x^*)$ are not achieved immediately, but only after the passage of a certain time ($t^* = 8$ in the example considered), upon which the intensity of the “nonlinear source” decreases monotonously, which is explained by elastic waves leaving the region where deformation of the ocean bottom occurred. It is important to note that the time the nonlinear source is in action noticeably exceeds the duration of the ocean bottom displacement.

Figure 4.38 presents typical profiles of surface waves, formed by a “nonlinear source”. The action of this source leads to water being “pushed out” of the source area, therefore, the waves always originate with a positive phase and finish with a negative phase.

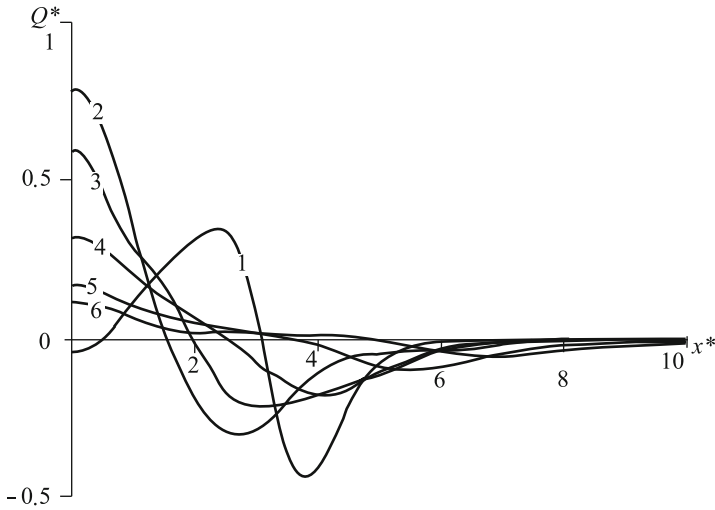


Fig. 4.37 Characteristic form of function $Q^*(x^*, t^*)$. Curves 1–6 correspond to $t^* = 4, 8, 12, 16, 20, 24$. The source parameters: $\tau = 8$ s, $L = 40$ km, $H = 4$ km

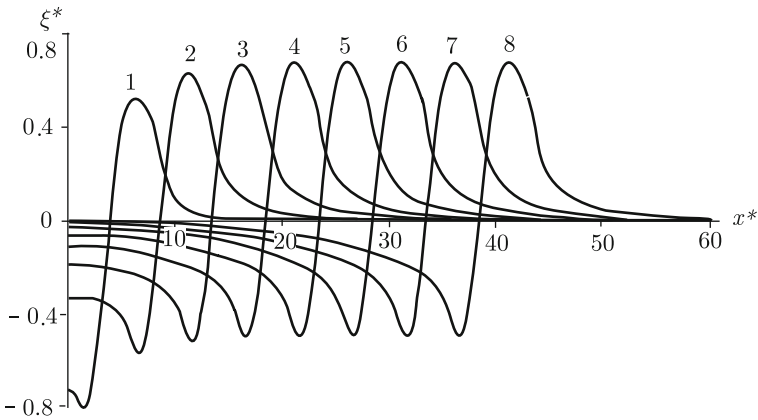


Fig. 4.38 Profiles of gravitational waves formed by a “nonlinear source”. Curves 1–8 are calculated for consecutive moments of time separated by intervals of 100 s. The source parameters: $\tau = 8$ s, $L = 40$ km, $H = 4$ km

From the profiles of the formed waves calculation was performed of the amplitude

$$A_N = \frac{v_{\max}^2}{g} \left(\text{Max}_{x^*}(\xi^*) - \text{Min}_{x^*}(\xi^*) \right) \equiv \frac{v_{\max}^2}{g} A^*(\tau^*, L^*), \tag{4.114}$$

and of the energy

$$W_N = \rho H g^{-1} v_{\max}^4 \int_{-\infty}^{\infty} \xi^2 dx^* \equiv \rho H g^{-1} v_{\max}^4 W^*(\tau^*, L^*). \quad (4.115)$$

The result of calculations carried out for various durations of piston-like displacements, τ^* , and source sizes L^* ($\tau^* = \tau c/H$, $L^{**} = L/H$), were dimensionless functions of the dimensionless arguments $A^*(\tau^*, L^*)$ and $W^*(\tau^*, L^*)$.

Nonlinear effects can, obviously, provide a noticeable contribution to a tsunami wave only in the case of sufficiently high velocities of the ocean bottom deformation, which is equivalent to displacements of small durations. Therefore, in calculations we only dealt with the range of $\tau < 8H/c$. From the point of view of traditional ideas, such displacements can be considered instantaneous ($\tau = 8H/c \ll L/\sqrt{gH}$); in the case of an instantaneous displacement, on the water surface an initial elevation is formed that repeats the shape of residual deformations of the ocean bottom. Precisely the evolution of this elevation generates tsunami waves in their classical sense. We shall term such a tsunami generation mechanism linear. The tsunami amplitude formed by the linear mechanism can be estimated as the amplitude of residual deformations of the ocean bottom,

$$A_L \approx \eta_0 = v_{\max} \tau C_1, \quad C_1 = \int_0^1 \eta(\alpha) d\alpha \approx 0.7, \quad (4.116)$$

and the energy as the potential energy of the initial elevation

$$W_L \approx \frac{\rho g}{2} \int_{-\infty}^{+\infty} \xi^2(x, \tau) dx = \rho g v_{\max}^2 \tau^2 L \frac{C_1^2 C_2}{2}, \quad (4.117)$$

$$C_2 = \int_0^1 \eta^2(\alpha) d\alpha \approx 0.65.$$

Applying formulae (4.116) and (4.117), we obtain relationships permitting to calculate the relative contributions of the nonlinear and the linear mechanisms to the amplitude and energy of tsunami waves:

$$\frac{A_N}{A_L} = \left(\frac{\eta_0 c^2}{gH^2} \right) \frac{A^*(\tau^*, L^*)}{C_1^2 \tau^{*2}}, \quad (4.118)$$

$$\frac{W_N}{W_L} = \left(\frac{\eta_0 c^2}{gH^2} \right)^2 \frac{2W^*(\tau^*, L^*)}{C_1^4 C_2 \tau^{*4} L^*}, \quad (4.119)$$

Fig. 4.39 Ratio between amplitudes of tsunami waves formed by the nonlinear (A_N) and the linear (A_L) mechanisms versus the displacement duration. Curves 1–3 are drawn for $L/H = 20, 10$ and 5

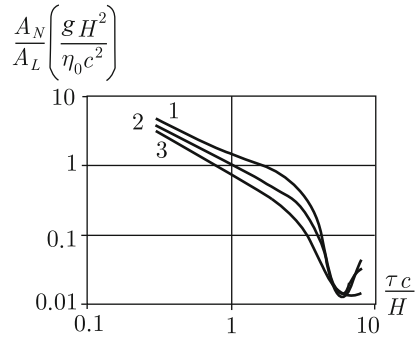
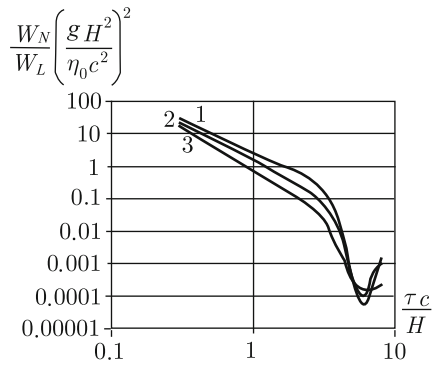


Fig. 4.40 Ratio between energies of tsunami waves formed by the nonlinear (A_N) and the linear (A_L) mechanisms versus the displacement duration. Curves 1–3 are drawn for $L/H = 20, 10$ and 5



where η_0 is the amplitude of the vertical ocean bottom deformation. From formulae (4.118) and (3.2.47) the quantities A_N/A_L and W_N/W_L are seen to be determined to a large extent by the dimensionless combination $\eta_0 c^2 g^{-1} H^{-2}$.

Figures 4.39 and 4.40 present the dependences of quantities A_N/A_L and W_N/W_L upon the piston-like displacement duration. The calculation is performed for three different relationships between the source size and the ocean depth. The curves for three different relationships between the source size and the ocean depth. The curves being nonmonotonous for $\tau^* > 1$ is due to the modal structure of elastic oscillations of the water column (the minimum normal frequency corresponds to $\tau^* = 4$). When $\tau^* < 1$, the dependences investigated behave approximately like the power functions τ^{*-1} and τ^{*-2} . An increase in the horizontal size of the source leads to an insignificant enhancement of the role of the nonlinear mechanism.

Taking advantage of the data presented in Figs. 4.39 and 4.40 one can readily perform the following estimations. For an ocean depth of 1.5 km, displacement duration and amplitude of 1 s and 1 m, respectively, the contribution of the nonlinear mechanism to the tsunami amplitude will be at a level of 10%, and to its energy of 1%. The contribution of the nonlinear mechanism may increase as the amplitude of the ocean bottom displacement increases or the displacement duration decreases, but, most likely, the linear mechanism will continue to prevail in the case of a piston-like displacement.

The nonlinear mechanism may provide for an essential contribution to the amplitude of a tsunami wave in the case of ocean bottom oscillations at one of the normal frequencies, $f_k = c(1 + 2k)/4H$, $k = 0, 1, 2, \dots$ (resonance pumping of energy). According to linear theory, ocean bottom oscillations without residual displacements at frequencies $f > f_g$ do not produce gravitational waves (see Sect. 4.2.1). In conditions of the planet Earth $f_k > f_g$, consequently, in the case of ocean bottom oscillations with frequencies f_k only the nonlinear mechanism can give rise to tsunamis.

Calculations, carried out for $U(x, t) = U_{osc}(x, t)$, have revealed the following. If an area of the ocean bottom of dimension $L = 40$ km at a depth of $H = 4$ km undergoes $N = 10$ oscillations of frequency $f_0 = c/4H \approx 0.094$ Hz and amplitude 0.3 m, then the nonlinear mechanism produces a tsunami of amplitude ~ 0.5 m. In similar conditions, but at a higher frequency $f_3 = 7c/4H \approx 0.65$ Hz, the tsunami amplitude will already amount to ~ 1.2 m. If the frequency of ocean bottom oscillations differs noticeably from the normal frequency, then the efficiency of the nonlinear mechanism decreases significantly. Thus, for example, if $f = 0.55$ Hz ($f_2 < f < f_3$), the tsunami amplitude will only be of the order of 6 cm.

In conclusion we note that the frequencies of seismic oscillations of the ocean bottom lie within the range of several first normal frequencies of the water column, f_k , which creates favorable conditions for realization of the nonlinear mechanism of tsunami generation.

References

- Abdolali, A., Kirby, J.T., Bellotti, G.: Depth-integrated equation for hydro-acoustic waves with bottom damping. *J. Fluid Mech.* **766**, R1 (2015)
- Alexeev, A.S., Gusakov, V.K.: Numerical simulation of the process of tsunami wave and seismo-acoustic wave excitation during earthquakes in the ocean. In: Works of IV All-Union Symposium on Wave Diffraction and Propagation (in Russian), vol. 2, pp. 194–197 (1973)
- Balanche, A., Guennou, C., Goslin, J., Mazoyer, C.: Generation of hydroacoustic signals by oceanic subseafloor earthquakes: a mechanical model. *Geophys. J. Int.* **177**, 476–480 (2009)
- Bernard, E., Meinig, C.: History and future of deep-ocean tsunami measurements. In: Proceedings of Oceans'11 MTS/IEEE, Kona, No. 6106894, 7 pp. IEEE, Piscataway, 19–22 September 2011
- Bolshakova, A., Inoue, S., Kolesov, S., Matsumoto, H., Nosov, M., Ohmachi, T.: Hydroacoustic effects in the 2003 Tokachi-Oki tsunami source. *Russ. J. Earth Sci.* **12**, ES2005 (2011). doi:[10.2205/2011ES000509](https://doi.org/10.2205/2011ES000509)
- Brekhovskikh, L.M. (ed.): *Acoustics of the Ocean* (in Russian). Nauka, Moscow (1974)
- Brekhovskikh, L.M., Goncharov, V.V.: *Introduction to the Mechanics of Continuous Media (as applied to wave theory)* (in Russian). Nauka, Moscow (1982)
- Brekhovskikh, L.M., Lysanov, I.P.: *Fundamentals of Ocean Acoustics*. Springer Science & Business Media, New York (2003)
- Boorymskaia, R.N., Levin, B.W., Soloviev, S.L.: Kinematical criterion for a submarine earthquake to be tsunamigenic (in Russian). *DAN SSSR* **261**(6), 1325–1329 (1981)
- Chierici, F., Pignagnoli, L., Embriaco, D.: Modeling of the hydroacoustic signal and tsunami wave generated by seafloor motion including a porous seabed. *J. Geophys. Res.: Oceans* **115**(C3), 1978–2012 (2010)
- Dotenko, S.F.: Influence of residual displacements of ocean bottom on the efficiency of directed tsunami wave generation. *Izv. AN SSSR, FAO* (in Russian), **31**(4), 570–576 (1995)

- Dotsenko, S.F.: Excitation of tsunami waves during oscillations of a section of the bottom. *Izv. AN SSSR, FAO (in Russian)*, **32**(2), 264–270 (1996)
- Ewing, W.M., Tolstoy, I., Press, F.: Proposed use of the T phase in tsunami warning systems. *Bull. Seismol. Soc. Am.* **40**, 53–58 (1950)
- Filloux, J.H.: Pressure fluctuations on the open-ocean floor off the Gulf of California: tides, earthquakes, tsunamis. *J. Phys. Oceanogr.* **13**(5), 783–796 (1983)
- Garber, M.R.: Improved model for long-period wave excitation in ocean and atmosphere by underwater earthquakes (in Russian). *DVNII Transactions*, No. 103, pp. 14–18. *Gidrometeoizdat, Leningrad* (1984)
- Gisler, G.R.: Tsunami simulations. *Annu. Rev. Fluid Mech.* **40**, 71–90 (2008)
- Gusakov, V.K.: Excitation of tsunami waves and of oceanic Rayleigh waves during a submarine earthquake. In: *Mathematical Problems of Geophysics (in Russian)*. Public Department of Computation Center, SB RAS USSR, Novosibirsk, No. 3, pp. 250–272 (1972)
- Gusakov, V.K.: On the relationship between a tsunami wave and the source parameters of the underwater earthquake. In: *Mathematical Problems of Geophysics (in Russian)*, No. 5, part I, pp. 118–140. Public Department of Computation Center, SB RAS USSR, Novosibirsk (1974)
- Hammack, J.L.: A note on tsunamis: their generation and propagation in an ocean of uniform depth. *J. Fluid Mech.* **60**(04), 769–799 (1973)
- Heidarzadeh, M., Satake, K.: Waveform and spectral analyses of the 2011 Japan tsunami records on tide gauge and DART stations across the Pacific Ocean. *Pure Appl. Geophys.* **170**(6–8), 1275–1293 (2013)
- Jaque, V.M., Soloviev, S.L.: Remote registration of tsunami type weak waves on the shelf of the Kuril Islands. *Dokl. Akad. Nauk USSR* **198**(4), 816–817 (1971) (in Russian)
- Joseph, A.: *Tsunamis: Detection, Monitoring, and Early-Warning Technologies*. Academic Press, Burlington (2011)
- Kadri, U., Stiassnie, M.: Acoustic gravity waves interacting with the shelf break. *J. Geophys. Res.: Oceans* **117**(C3), 1978–2012 (2012)
- Kadykov, I.F.: *The Acoustics of Submarine Earthquakes (in Russian)*. Nauka, Moscow (1986)
- Kadykov, I.F.: *Submarine Low-Frequency Acoustic Noise of the Ocean (in Russian)*. Editorial URSS, Moscow (1999)
- Kajiura, K.: Tsunami source, energy and directivity of wave radiation. *Bull. Earthq. Res. Inst. Tokyo Univ.* **48**(5), 835–869 (1970)
- Kanamori, H.: The energy release in great earthquakes. *J. Geophys. Res.* **82**(20), 2981–2987 (1977)
- Kaneda, Y.: The advanced ocean floor real time monitoring system for mega thrust earthquakes and tsunamis-application of DONET and DONET2 data to seismological research and disaster mitigation. In: *OCEANS*, pp. 1–6. IEEE, September 2010
- Koketsu, K., Hikima, K., Miyazaki, S., Ide, S.: Joint inversion of strong motion and geodetic data for the source process of the 2003 Tokachi-Oki, Hokkaido, earthquake. *Earth Planets Space* **56**(3), 329–334 (2004)
- Lacombe, H.: *Cours d’océanographie physique: Théories de la circulation générale*. Houles et vagues. Gauthier-Villars, Paris (1965)
- Landau, L.D., Lifshitz, E.M.: *Fluid Mechanics*, 2nd edn. Pergamon Press, London (1987)
- Levin, B.W.: On the source and hydromechanics of an underwater earthquake (in Russian). In: *Tsunami Wave Propagation and Runup on Shore*, pp. 5–10. Nauka, Moscow (1981)
- Li, W., Yeh, H., Hirata, K., Baba, T.: Ocean-bottom pressure variations during the 2003 Tokachi-Oki Earthquake. In: Lynett, P. (ed.) *Nonlinear Wave Dynamics*, pp. 109–126. World Scientific Publishing Co., Singapore (2009)
- Lysanov, Y.P.: Trapping of hydroacoustic waves generated by deep ocean earthquakes in an underwater sound channel. *Acoust. Phys.* **43**, 79–83 (1997)
- Maeda, T., Furumura, T.: FDM simulation of seismic waves, ocean acoustic waves, and tsunamis based on tsunami-coupled equations of motion. *Pure Appl. Geophys.* **170**(1–2), 109–127 (2013)
- Maeda, T., Furumura, T., Noguchi, S., Takemura, S., Sakai, S.I., Shinohara, M., Lee, S.J.: Seismic- and tsunami-wave propagation of the 2011 Off the Pacific Coast of Tohoku Earthquake as inferred

- from the tsunami-coupled finite-difference simulation. *Bull. Seismol. Soc. Am.* **103**(2B), 1456–1472 (2013)
- Marchuk, An.G., Chubarov, L.B., Shokin, Yu.I.: *Numerical Simulation of Tsunami Waves* (in Russian). Nauka, Novosibirsk (1983)
- Matsumoto, H.: *Advances for Tsunami Measurement Technologies and its Applications*. INTECH Open Access Publisher (2011)
- Matsumoto, H., Kaneda, Y.: Some features of bottom pressure records at the 2011 Tohoku earthquake—Interpretation of the far-field DONET data. In: *Proceedings of the 11th SEGJ International Symposium, Yokohama, Japan, vol. 2013*, pp. 493–496 (2013). doi:[10.1190/segj112013-124](https://doi.org/10.1190/segj112013-124)
- Mikada, H., Mitsuzawa, K., Matsumoto, H., Watanabe, T., Morita, S., Otsuka, R., Sugioka, H., Baba, T., Araki, E., Suyehiro, K.: New discoveries in dynamics of an M8 earthquake—phenomena and their implications from the 2003 Tokachi-Oki earthquake using a long term monitoring cabled observatory. *Tectonophysics* **426**, 95–105 (2006)
- Nikiforov, A.F., Uvarov, V.B.: *Special Functions of Mathematical Physics* (in Russian). Nauka, Moscow (1984)
- Nosov, M.A.: A model for tsunami generation by bottom movements incorporating water compressibility. *Volcanol. Seismol.* **20**, 731–741 (1999)
- Nosov, M.A.: On the tsunami generation in the compressible ocean by vertical bottom displacements. *Izv. Atmos. Ocean. Phys.* **36**(5), 718–726 (2000)
- Nosov, M.A., Grigorieva, S.S.: Tsunami forecasting based on deepwater-station data. *Mosc. Univ. Phys. Bull.* **70**(4), 326–332 (2015)
- Nosov, M.A., Kolesov, S.V.: Non-linear mechanism of tsunami generation in a compressible ocean. In: *Proceedings of the International Workshop Local Tsunami Warning and Mitigation, Moscow*, pp. 107–114 (2002)
- Nosov, M.A., Kolesov, S.V.: Tsunami generation in compressible ocean of variable depth. In: Yalciner, A.C., Pelinovsky, E., et al. (eds.) *Submarine Landslides and Tsunamis*, pp. 129–137. Kluwer, Boston (2003)
- Nosov, M.A., Kolesov, S.V.: Nonlinear tsunami generation mechanism in compressible ocean (in Russian). *Mosc. Univ. Phys. Bull.* no. 4 (2005)
- Nosov, M.A., Kolesov, S.V.: Elastic oscillations of water column in the 2003 Tokachi-Oki tsunami source: in-situ measurements and 3-D numerical modelling. *Nat. Hazards Earth Syst. Sci.* **7**, 243–249 (2007)
- Nosov, M.A., Sammer, K.: Tsunami excitation by a moving bottom displacement in compressible water. *Mosc. Univ. Phys. Bull.* **53**(6), 67–70 (1998)
- Nosov, M.A., Shelkovnikov, N.K.: The excitation of dispersive tsunami waves by piston and membrane floor motions. *Izv. Atmos. Ocean. Phys.* **33**(1), 133–139 (1997)
- Nosov, M.A., Skachko, S.N.: Nonlinear tsunami generation mechanism. *Nat. Hazards Earth Syst. Sci.* **1**, 251–253 (2001)
- Nosov, M.A., Kolesov, S.V., Ostroukhova, A.V., Alekseev, A.B., Levin, B.W.: Elastic oscillations of the water layer in a tsunami source. *Dokl. Earth Sci.* **404**(7), 1097–1100 (2005)
- Nosov, M.A., Kolesov, S.V., Denisova, A.V., Alekseev, A.B., Levin, B.W.: On the near-bottom pressure variations in the region of the 2003 Tokachi-Oki tsunami source. *Oceanology* **47**(1), 26–32 (2007)
- Nosov, M.A., Kolesov, S.V., Denisova, A.V.: Contribution of nonlinearity in tsunami generated by submarine earthquake. *Adv. Geosci.* **14**, 141–146 (2008)
- Nosov, M.A., Moshenceva, A.V., Kolesov, S.V.: Horizontal motions of water in the vicinity of a tsunami source. *Pure Appl. Geophys.* **170**(9–10), 1647–1660 (2013)
- Nosov, M.A., Sementsov, K.A., Kolesov, S.V., Matsumoto, H., Levin, B.W.: Recording of gravity waves formed in the ocean by surface seismic waves during the earthquake of March 11, 2011, off the coast of Japan. In: *Doklady Earth Sciences*, vol. 461, no. 2, pp. 408–413. Pleiades Publishing April 2015

- Novikova, L.E., Ostrovsky, L.A.: On the acoustic mechanism of tsunami wave excitation (in Russian). *Oceanology* **22**(5), 693–697 (1982)
- Ohmachi, T., Inoue, S.: Dynamic tsunami generation process observed in the 2003 Tokachi-Oki, Japan, earthquake. *Adv. Geosci.* **18**, 159–168 (2010)
- Ohmachi, T., Tsukiyama, H., Matsumoto, H.: Simulation of tsunami induced by dynamic displacement of seabed due to seismic faulting. *Bull. Seismol. Soc. Am.* **91**(6), 1898–1909 (2001)
- Okal, E.A.: T Waves from the 1998 Papua New Guinea earthquake and its aftershocks: timing the tsunamigenic slump. *Pure Appl. Geophys.* **160**, 1843–1863 (2003)
- Okal, E.A., Alasset, P.J., Hyvernaud, O., Schindele, F.: The deficient T waves of tsunami earthquakes. *Geophys. J. Int.* **152**, 416–432 (2003)
- Panza, F.G., Romanelli, F., Yanovskaya, T.B.: Synthetic tsunami mareograms for realistic oceanic models. *Geophys. J. Int.* **141**, 498–508 (2000)
- Pelinovsky, E.N.: *Hydrodynamics of Tsunami Waves* (in Russian). Institute of Applied Physics, RAS, Nizhniy Novgorod (1996)
- Pod'yapolsky, G.S.: Excitation of a long gravitational wave in the ocean by a seismic source inside the crust (in Russian). *Izv. RAS Earth Phys.* no. 1 (1968a)
- Pod'yapolsky, G.S.: On the relationship between a tsunami wave and the underground source, that generated it (in Russian). In: *The Tsunami Problem*. Nauka, Moscow (1968b)
- Pod'yapolsky, G.S.: Tsunami excitation by an earthquake. In: *Methods for Calculating Tsunami Rise and Propagation* (in Russian), pp. 30–87. Nauka, Moscow (1978)
- Rabinovich, A.B.: Tsunami observations in the open ocean. *Izv. Atmos. Ocean. Phys.* **50**(5), 445–458 (2014)
- Sammarco, P., Cecioni, C., Bellotti, G., Abdolali, A.: Depth-integrated equation for large-scale modelling of low-frequency hydroacoustic waves. *J. Fluid Mech.* **722**, R6 (2013)
- Sekerzh-Zen'kovich, S.Ya., Zakharov, D.D., Timokhina, A.O., Shingareva, I.K.: Tsunami wave excitation in an inhomogeneous ocean by seismic-type sources inside the Earth's crust (in Russian). In: *Collection Interaction in the Lithosphere–Hydrosphere–Atmosphere System*, vol. 2. pp. 233–240. Publishing Department of MSU Physics. Faculty, Moscow (1999)
- Selezov, I.T., Tkachenko, V.A., Yakovlev, V.V.: On the influence of water compressibility on tsunami wave generation (in Russian). In: *Processes of Tsunami Excitation and Propagation*, pp. 36–40. Publishing house of USSR AS, Moscow (1982)
- Sells, C.C.H.: The effect of a sudden change of shape of the bottom of a slightly compressed ocean. *Philos. Trans. R. Soc. Lond. (A)* no. 1092, 495–528 (1965)
- Soloviev, S.L.: The tsunami problem and its significance for Kamchatka and the Kuril islands (in Russian). In: *The Tsunami Problem*, pp. 7–50. Nauka, Moscow (1968)
- Soloviev, S.L., Go, C.N.: *Catalogue of Tsunamis on the Western Coast of the Pacific Ocean (173–1968)* (in Russian). Nauka, Moscow (1974)
- Soloviev, S.L., Go, C.N.: *Catalogue of Tsunamis on the Eastern Coast of the Pacific Ocean (1513–1968)* (in Russian). Nauka, Moscow (1975)
- Soloviev, S.L., Voronin, P.S., Voronina, S.I.: Seismic hydroacoustic data on the T wave (review of the literature) (in Russian). In: *The Tsunami Problem*, pp. 142–173. Nauka, Moscow (1968)
- Soloviev, S.L., Belavin, Yu.S., Kadykov, I.F., Ton Il', U.: Registration of T phases in earthquake signals in the north-western part of the Pacific Ocean (in Russian). *Volcanol. Seismol.* no.1, 60–69 (1980)
- Soloviev, S.L., Go, C.N., Kim, Kh.S., et al.: *Tsunamis in the Mediterranean Sea, 2000 B.C.—1991 A.D.* (in Russian). Nauchnyi mir, Moscow (1997)
- Stiassnie, M.: Tsunamis and acoustic-gravity waves from underwater earthquakes. *J. Eng. Math.* **67**(1–2), 23–32 (2010)
- Tanioka, Y., Nishimura, Y., Hirakawa, K., Imamura, F., Abe, I., Abe, Y., Masaka, S.: Tsunami run-up heights of the 2003 Tokachi-Oki earthquake. *Earth Planets Space* **56**(3), 359–365 (2004)
- Tikhonov, A.N., Samarsky, A.A.: *Equations of Mathematical Physics* (in Russian). Publishing house of Moscow University, Moscow (1999)

- Tolstoy, I., Clay, C.S.: *Ocean Acoustics—Theory and Experiment in Underwater Sound*, 2nd edn. American Institute of Physics, New York (1987)
- Tsushima, H., Hino, R., Fujimoto, H., et al.: Near-field tsunami forecasting from cabled ocean bottom pressure data. *J. Geophys. Res.* **114**, B06309 (2009)
- Tsushima, H., Hirata, K., Hayashi, Y., et al.: Near-field tsunami forecasting using offshore tsunami data from the 2011 off the Pacific coast of Tohoku Earthquake. *Earth Planets Space* **63**, 821 (2011)
- Walker, D.A., McCreery, C.S., Hiyoshi, Y.: T-phase spectra, seismic moment and tsunamigenesis. *Bull. Seismol. Soc. Am.* **82**, 1275–1305 (1992)
- Watanabe, O., Matsumoto, H., Sugioka, H., Mikada, H., Suyehiro, K., Otsuka, R.: Offshore monitoring system records recent earthquake off Japan's northernmost island. *Eos Trans. AGU* **85**(2), 14–14 (2004)
- Yanushkauskas, A.I.: Cauchy-Poisson theory for a compressible liquid (in Russian). In: *Tsunami Wave Propagation and Runup on Shore*, pp. 41–55. Nauka, Moscow (1981)
- Zhmur, V.V.: Surface phenomena above the sources of strong underwater earthquakes. *Tsunami studies* (in Russian), no. 2, pp. 62–71 (1987)
- Zvolinsky, N.V.: On the seismic mechanism of tsunami wave generation. *Izv. AN SSSR, Ser. Earth Phys.* (in Russian), no. 3, 3–15 (1986)
- Zvolinsky, N.V., Nikitin, I.S., Sekerzh-Zen'kovich, S.Ya.: Generation of tsunami and Rayleigh waves by a harmonic expansion center. *Izv. AN SSSR, Ser. Earth Phys.* (in Russian), no. 2, 34–44 (1991)
- Zvolinsky, N.V., Karpov, I.I., Nikitin, I.S., Sekerzh-Zen'kovich, S.Ya.: Generation of tsunami and Rayleigh waves by a harmonic two-dimensional rotation center. *Izv. AN SSSR, Ser. Earth Phys.* (in Russian), no. 9, 29–33 (1994)

Chapter 5

The Physics of Tsunami Formation by Sources of Nonseismic Origin

Abstract The physics is described of tsunami formation by sources of nonseismic origin: landslides, volcanic eruptions, meteorological causes, and cosmic bodies falling into the ocean. Short descriptions are given of certain remarkable historical events (with the exception of cosmogenic tsunamis). Approaches to the mathematical description of tsunami generation by these sources are expounded. Basic regularities, relating parameters of a source and of the tsunami wave generated by it are presented.

Keywords Tsunami generation · Gravitational surface wave · Earthquake · Landslide · Slump · Mud flow · River tsunami · Erosion · Sedimentary layer · Viscous fluid · Froude number · Volcano · Volcanic eruption · Caldera collapse · Explosive eruption · Underwater volcano · Pyroclastic flow · Equivalent source · Stationary-phase method · Meteotsunami · Anemobaric waves · Resonance · Proudman resonance · Internal waves · Storm surges · Tension of friction · Atmospheric pressure · Long-wave theory · Meteorite · Cosmogenic tsunami · Asteroid · Kinetic energy · Parametrization · Numerical simulation · Dispersion

Tsunami generation is mainly caused by sharp vertical displacements of separate areas of the ocean bottom, taking place during strong underwater earthquakes. Details of this process are described in Chaps. 2–4. But seismotectonic movements are not the only possible mechanisms of tsunami formation. A significant number of events are caused by landslides (slumps), processes related to volcanic eruptions, and meteorological causes (see Table 5.1). In accordance with the NOAA/WDS Global Historical Tsunami Database at NGDC, 73 % of events were due to earthquakes, 3.4 % to landslides, 4.7 % to volcanic eruptions, and 3.6 % to meteorological causes. The sources of the remaining 10 % of events are still unknown. In some cases, tsunamis were due to combinations of earthquake and landslide (3.6 %), volcanic eruption and earthquake (0.5 %), and volcanic eruption and landslide (0.4 %).

Recently, tsunami generation by meteorites falling into the ocean has been the issue of active discussions. Such events are extremely rare. Such an event may even never have occurred during the whole history of our civilization. But, bearing in mind the scale of such a catastrophe, the authors considered it necessary to present certain results of studies of this tsunami generation mechanism.

Table 5.1 Distribution of the number of events over the cause of tsunami, based on data from NOAA/WDS global historical tsunami database at NGDC, as of June 2015

Cause of tsunami	Number of events
Unknown	258
Earthquake	1838
Questionable earthquake	13
Earthquake and landslide	90
Volcano and earthquake	13
Volcano, earthquake, and landslide	1
Volcano	120
Volcano and landslide	9
Landslide	86
Meteorological	92
Explosion	1
Astronomical tide	2

5.1 Tsunami Generation by Landslides

After tsunamis of seismotectonic origin, most often encountered are so-called *landslide tsunamis* (“Landslide” + “Earthquake and Landslide” + “Volcano, Earthquake, and Landslide” + “Volcano and Landslide” – 7.4%). This term stands for gravitational surface waves caused by underwater landslides and mud flows, fragments of steep coasts, rock and icebergs, and, sometimes, even buildings in harbors, collapsing into the water. At present, in the World Ocean over 186 tsunamis are known to have been caused or contributed by the mechanisms indicated. As a rule, landslide tsunamis are considered local events (Okal and Synolakis 2004; Harbitz et al. 2006). But studies, performed in recent years, reveal that landslides can give essential additional contributions to tsunamis generated by strong earthquakes (Gusiakov 2001; Fryer et al. 2004; Suleimani et al. 2011; Tappin et al. 2014).

As compared to the horizontal dimensions of seismic sources (10^4 – 10^5 m), coastal and underwater landslides usually exhibit smaller scales (10^2 – 10^3 m). The largest known in geological history Storegga landslide took place in the late quaternary period in the region of the steep continental slope off the coast of Norway (Jansen et al. 1987; Harbitz 1992). Its horizontal extension is estimated to have amounted to tens of kilometers.

In spite of their local character, the destructive force of landslide tsunamis is no less than that of waves of seismotectonic origin. Such tsunamis are particularly dangerous in narrow straits, fjords, and closed gulfs and bays (Murty 1977; Jiang and LeBlond 1992). Among the best-known events one must mention the catastrophic tsunamis in Lituya Bay (Lituya Bay, South-East Alaska, 1958) and in Vaiont Valley (Vaiont Valley, Northern Italy, 1963). The tsunami in Lituya Bay was caused by the fall of rock matter at the bay apex into the water, which led to the formation

of a huge wave, the runup height of which amounted to 524 m (Miller 1960; Murty 1977; Lander 1996). The catastrophe in Vaiont Valley resulted in the destruction of an entire city, and about 2000 people died (Wiegel et al. 1970; Murty 1977).

Landslide tsunamis are characterized by a high repetition rate at certain parts of the coast. For example, in situ studies at Lituya Bay, carried out after the catastrophic event of 1958, revealed that gigantic waves, caused by landslides, had also occurred there previously—in 1853–1854 (120 m), in 1874 (24 m), in 1899 (60 m), and in 1936 (150 m) (Miller 1960). Even the Laperouse expedition suffered from a tsunami in this bay—a two-mast schooner of the squadron with a crew of 21 men was shattered by an “unusual wave” against the cliffs of the island in 1787.

It is interesting that landslide tsunamis can occur not only in oceans and seas, but also in large rivers. The description of one such event, that took place in river Volga in 1597, is presented in Didenkulova et al. (2007). We have succeeded in finding reference to another river tsunami, which took place in river Irtysh in 1885. Here, we quote the book of travel notes by K.M. Stanyukovich, the well-known Russian writer on the Sea, “To far lands” (Collection of works in 10 volumes, Vol. 1—Moscow: Pravda, 1977):

...The right sandy bank of the Irtysh, being constantly washed out, once in while caves in, and, then, as the Siberians say, the “landslides”, that fall from the height into the water with a crash and noise, happen to cause accidents and misfortunes. Such a misfortune occurred just three weeks before we passed there. About two hundred versts¹ from the estuary of Irtysh we saw a schooner lying helplessly on its side in the sands. It had been passing one verst from the right bank, precisely when the bank caved in. Such a mass of earth falling together with century-old trees caused the water to shrink back from the bank, thus giving rise to agitation so strong that it capsized the flat-bottomed schooner, which most likely had no appropriate ballast, and threw it toward the left bank. The barge, towed by the schooner, withstood the wave and remained unharmed. Of the crew and passengers of the schooner several peoples died in the river, several were crippled. A day after the catastrophe, cries for help were heard on the “Reytern”, that was passing by. The steamboat stopped and took the people, asking help, on board ...

Studies of landslide tsunamis have a long history; however, until recently publications, devoted to investigation of this phenomenon, were quite rare. One of the first attempts at detailed investigation of tsunami waves, caused by underwater landslides, was made by N.L. Leonidova (1972). This investigation was based on earlier works of B. Gutenberg (1939) and R. Mitchell (1954); however, precisely this work laid the foundation for modern ideas concerning the problem of landslide tsunamis. One must also mention the experimental study, well known to specialists, carried out by R. Wigel (1955), which was devoted to investigating wave generation in a channel, when hard bodies of different shapes were made to slide along the channel bottom.

The recent enhancement of interest in studies of landslide tsunamis was initiated by the catastrophic events in Papua New Guinea and Indonesia. The wave, which demolished the coast of Papua New Guinea on July 17, 1998, was 15 m high. It was due to a relatively moderate earthquake of $M_w = 7.1$, accompanied by a local

¹1 verst = 1.067 km.

underwater landslide (Tappin 1998; Heinrich et al. 2000; Imamura et al. 2001). The earthquake, which took place on December 12, 1992 with magnitude $M_w = 7.7$ on island Flores (Indonesia), also gave rise to an underwater landslide and subsequent tsunamis of heights up to 26 m.

The landslide process is usually the result of a prolonged accumulation of sedimentary material during tens and hundreds of years. With time the sedimentary masses on slopes lose stability. Numerous factors can provoke a landslide (Ren et al. 1996; Kulikov et al. 1998):

- sudden surge of river silt during a freshet;
- erosion of sedimentary layer on a steep underwater slope;
- coastal construction projects;
- prolonged rain, resulting in saturation of coastal land; and
- uncovering of coast during pronounced low tide.

Recently, the role of gas hydrates in provoking underwater landslides is also discussed (Parlaktuna 2003). Earthquakes, naturally, serve as most important causes of landslides and collapses. Volcanic eruptions, also, happen not to play the last part in initiating landslide processes and collapses.

Sedimentary masses, deposited on underwater slopes during many decades, accumulate huge potential energy. As they lose stability, they are capable of moving over the ocean bottom with high velocities, transferring part of the accumulated potential energy to tsunami waves. Precipitations, annually accumulated in some canyons, amount to 10^6 – 10^9 m³, while the bottom slopes often exceed 0.1. Precipitations on slopes of the ocean bottom often exhibit thixotropic properties, i.e., they are capable of becoming fluid in the case of sharp enhancement of the threshold pressure due to blows, shaking, and vibrations. The unstable friable sedimentary material, possessing a high content of subcolloidal fractions, may, when losing stability, form dense suspension (muddy, turbidite) flows. Moving down a bottom slope with a velocity exceeding 10 m/s, such a flow leads to waves of the tsunami type being generated at the water surface, and it also severs underwater cables. The strong earthquake that destroyed the city of Messina on December 28, 1908 gave rise to a landslide or muddy flow, which severed seven underwater cables connecting continental Italy and Sicily.

It must be noted that well-known large underwater canyons were located inside the source areas of some strong tsunamis: the Lisbon canyon (tsunami of 1755), the Messina canyon (tsunamis of 1783 and 1908), the Kamchatka canyon (tsunamis of 1791, 1923, 1937), and others. N.L. Leonidova was, evidently, the first to note that most aftershocks of strong tsunamigenic earthquakes, even when approximately equal in force to the main shock, do not cause noticeable tsunami waves. Thus, the well-known Kanto earthquake, which destroyed Tokyo in 1923, gave rise in the Sagami bay to a tsunami wave 12 m high, while its aftershock, which originated in about the same place and with practically the same energy, was accompanied by waves less than 0.3 m high. Measurements showed that the volume of the landslide, provoked by the first earthquake, amounted to about 7×10^{10} m³, the average width

of the flow was 2 km, its length 350 km, its power (thickness) 100 m, and the flow velocity in the canyon was estimated to be 25 m/s. The potential energy of the landslide, which covered a path from a depth of 1500 m (the average position of the landslide body at the beginning of its movement) down to 7000 m (the bottom of the deepwater depression) can be estimated to have been 10^{18} J. The energy of the tsunami waves generated was of the order of 10^{16} J.

Note that after the earthquake on December 26, 2004 ($M_w = 9.1$), which gave rise to a catastrophic tsunami with runups as high as 50.9 m (HTDB/WLD), another strong earthquake took place in March 2005, ($M_w = 8.7$) approximately in the same region, but caused quite a weak tsunami with heights up to 2.35 m.

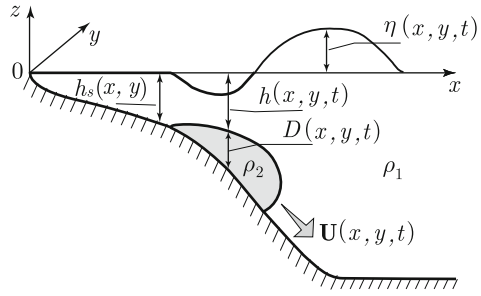
Much of the information on ground or underwater landslides, avalanches, cliff collapses indicate that the models, in which the movement of a landslide is considered just forward displacement of a solid body, not subject to deformation, are too simplistic and do not describe the character of these processes adequately. The idea of a landslide representing a flow of a heavy viscous fluid is much closer to the true nature of landslide dynamics. In the region of river estuaries, the sedimentary silt masses usually consist of diluted fractions, which after the breakdown of an unstable sedimentary mass form a dense dirt (mud) flow, behaving like a viscous fluid.

In problems concerning landslide tsunami generation, the notion of a landslide in the form of a flow of a heavy viscous fluid has started to be applied only quite recently. Such an approach was first proposed in Jiang and LeBlond (1992, 1994). Numerical methods, based on this approach, were successfully applied in analyzing landslide tsunamis in Nizza of 1979 (Assier-Rzadkiewicz et al. 2000), in Skagway Harbour of 1994 (Fine et al. 1998; Rabinovich et al. 1999), and in Papua New Guinea of 1998 (Heinrich et al. 2000; Titov and Gonzalez 2001; Imamura et al. 2001). In these studies, it was shown that the notion of a landslide in the form of a flow of a heavy viscous fluid provides reasonable agreement with data of in situ observations.

The version of the model described here is based on Jiang and LeBlond (1994) and Fine et al. (1998). We shall consider the horizontal scales of surface waves to significantly exceed the basin depth, and the thickness of the landslide to be much smaller than its width and length. In this case, it is possible to apply the long-wave (hydrostatic) approximation both in the case of water and in the case of the fluid forming the landslide. The Coriolis force is usually neglected in such problems.

The scheme of the model is presented in Fig. 5.1. The origin of the Cartesian reference system $Oxyz$ is placed on the unperturbed free surface, and the Oz axis is directed vertically upward. The upper layer of water has a density ρ_1 , a free surface displacement $\eta(x, y, t)$, \mathbf{u} is the horizontal velocity vector with components x and y ; t is time. The lower layer (the landslide body) has a density characteristic of sedimentary deposits, ρ_2 , ν is the kinematical viscosity, and \mathbf{U} is the horizontal velocity vector of the fluid in the lower layer with components U and V . The slope of the ocean bottom and the slope of the landslide surface are considered small, so that the fluid can be considered to undergo purely horizontal movement. The landslide body is limited by the bottom surface $z = -h(x, y, t)$, while its upper surface is given by its thickness $D(x, y, t) = h_s(x, y) - h(x, y, t)$.

Fig. 5.1 Geometry of the model: reference system and notation. The shaded part shows the body of a viscous landslide. Adapted from Rabinovich et al. (2003)



The main assumptions concerning landslide properties, substantiated in Jiang and LeBlond (1992, 1994), are adopted in the form:

1. A landslide consists of an incompressible viscous fluid, and the sea water is considered an incompressible liquid of zero viscosity.
2. The difference between the density of the landslide and the density of water must be large, $(\rho_2 - \rho_1) \geq 0.2 \text{ g/cm}^3$.
3. The flow of a viscous fluid is laminary and quasistationary. For describing the movement of a viscous fluid over an underwater slope, it is, generally speaking, necessary to consider two modes—inertial and viscous (quasistationary) (Simpson 1987). After the landslide body has suddenly become free (from its initial state), the flow of the fluid forming the landslide undergoes transition from the inertial-mode state to the viscous-mode state, when the vertical profile of the flow has already been established. In the given model, we assume the transition time to be negligible, and the flow to be constantly in the quasistationary mode, adapting relatively slowly, in the process of movement, to the shape of the bottom relief.
4. In this model, we neglect mixing effects on the landslide–water boundary. This means that no exchange of mass takes place between the flow of sedimentary material and the water.

Owing to the no-slip boundary condition, the tangential velocity component at the ocean bottom must turn to zero. At the upper boundary of the landslide, absence is assumed of tangential tensions, i.e., the normal component of the velocity gradient turns to zero. Under such conditions, the horizontal velocity of the stationary flow of a fluid exhibits a parabolic vertical profile,

$$\mathbf{U}(x, y, z, t) = \mathbf{U}_m(x, y, t)(2\xi - \xi^2), \tag{5.1}$$

where $\xi = (z + h_s)/D$ is the dimensionless vertical coordinate.

The continuity and momentum balance equations for a viscous flow in a landslide, obtained from the equations of hydrodynamics by integration along the vertical coordinate with account of formula (5.1), have the following form:

$$\frac{\partial D}{\partial t} + \frac{2}{3}(\nabla \cdot D\mathbf{U}) = 0; \quad (5.2)$$

$$\frac{2}{3} \frac{\partial \mathbf{U}}{\partial t} - \frac{2}{15} \frac{\mathbf{U}}{D} \frac{\partial D}{\partial t} + \frac{8}{15} (\mathbf{U} \cdot \nabla) \mathbf{U} = -\frac{g}{\rho_2} ((\rho_2 - \rho_1) \nabla(D - h_s) + \rho_1 \nabla \eta) - \frac{2\nu \mathbf{U}}{D^2}. \quad (5.3)$$

Here, the condition must be fulfilled that the landslide flow across the boundary of the coastal line G always be zero, and that during its movement the landslide does not cross the external (free) boundary Γ .

The upper layer of the fluid (water) is described by nonlinear equations of motion in the approximation of shallow water:

$$\frac{\partial(h + \eta)}{\partial t} + [\nabla \cdot (h + \eta)\mathbf{u}] = 0; \quad (5.4)$$

$$\frac{\partial \mathbf{u}}{\partial t} + (\mathbf{u} \cdot \nabla) \mathbf{u} = -g \nabla \eta. \quad (5.5)$$

Actually, the generation of surface waves by a moving landslide body is only due to the continuity Equation (5.4). The waves further propagate under the condition that boundary conditions and the nonlinear Equation (5.5) be satisfied.

On the open external boundary of the region, Γ , the one-dimensional emission condition for outgoing waves is applied: $u_n = \eta(g/h)^{1/2}$, where u_n is the velocity component, normal to the boundary Γ . Along the coastal line, fulfillment is assumed of the noflow condition through a vertical wall: $u_n = 0$ on G .

As the initial conditions of the problem, the landslide and the water layer are assumed to be at rest at time moment $t = 0$, i.e., all the velocities and the displacement of the free water surface are equal to zero.

The set of Eqs. (5.2)–(5.5) can be resolved by the explicit finite-difference method. Usually, the staggered leap-frog scheme in space and time is used (Imamura and Gica 1996) in calculations.

We shall make use of a hypothetical event in the Malaspina strait (British Columbia, Canada) (Rabinovich et al. 2003) as an example in considering the peculiarities of landslide tsunami formation. Numerical simulation of this tsunami is performed applying the mathematical model, described above. Studies of hypothetical tsunamis are important for estimation of the risk of tsunami hazard. For the demonstration of research methods of this kind, we shall first give a detailed description of the primary geophysical (geomorphological) information and, then, present the results of simulation.

The Malaspina strait (Fig. 5.2), located between the continental coast of British Columbia and Texada island, was about 50 km long and 5 km wide. Its depth along the axis of the strait varies between 300 and 375 m. In the central part of the strait, there is a thick (~ 100 m) sedimentary layer, mainly consisting of silt carried out from the estuary of Fraser River.

In 1946, an earthquake in the central part of Vancouver island, British Columbia, gave rise to a series of landslides and slumps in the coastal area of Malaspina strait.

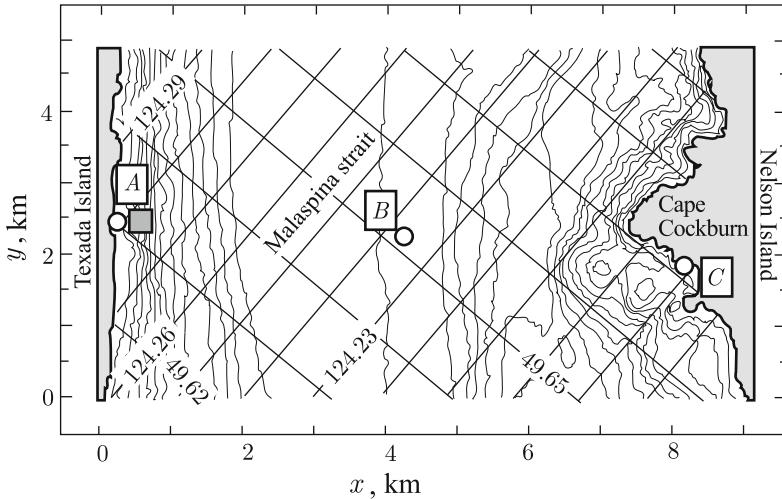


Fig. 5.2 Malaspina strait: map of calculation region. Adapted from Rabinovich et al. (2003)

In the northern part of the strait, banks were observed to crumble and cave in, and underwater cable lines were damaged.

Geophysical studies, performed by the Geological Survey of Canada, revealed the existence of two separate deposition zones of bottom sediments, located between isobaths 30 and 120 m. Identification of these areas was carried out with the aid of echo sounding gear for lateral observation and equipment for seismic profiling of high resolution. Special underwater video shooting, performed in 1996, revealed that lower down the slope there are a number of blocks of well-consolidated sediments several meters thick, which obviously resulted from their breaking away from the main mass and falling down the slope under the force of gravity. The main block of sediments has corresponding areas with a very steep edges left after partial collapse of the sedimentary mass. The lower boundary of this sedimentary layer exhibits a very steep inclination everywhere—practically like a precipice.

The northern zone of the sedimentary cover is up to 38 m thick, and the inclination of the inner boundary toward the sea is, on the average, 7.5° . The layer above it is inclined at approximately 16° relative to the boundary of the base layer and extends about 400 m along the slope, exhibiting a thickness of about 300 m.

The hypothetical scenario of tsunami generation assumes that the earthquake causes all the mass of sediments, accumulated in the northern zone of the sedimentary cover, to break-off from and to slide down the steep slope of the basalt boundary of the bottom. Owing to a lack of geotechnical data on the properties of sediments, simulation of the movement of the landslide is based on a broad set of parameters of the material. The possibility of the southern and northern sedimentary layers collapsing at the same time is not considered. Such a joint scenario would, naturally, lead to the generation of waves of higher amplitudes.

Calculations were performed on a mesh with 365×197 nodes and steps $\Delta x = \Delta y = 25$ m. In the initial state, the landslide body was considered to have a rectangular shape with a parabolic profile over the thickness in both directions. Calculations were performed for the following landslide parameters:

Volume:	1,250,000 M m ³ ;
Width:	200 m;
Average width	30 m;
Coordinates of center:	49°37.94'N, 124°16.80'W;
Average depth:	80 m;
Density (ρ_2):	2.0 g · cm ⁻³ ;
Kinematic viscosity (ν):	0.01 m ² · s ⁻¹ .

Figure 5.3 shows fragments of numerical calculations of the movements of the landslide and of tsunami waves in the strait. Unlike a solid-state body, retaining its size and shape, the viscous landslide moves along the slope, spreading out and assuming the form of a sickle. Displacement of the landslide takes place mostly along the normal to the west bank. Movement of the landslide gives rise to radially diverging surface waves. The leading wave (positive) moves toward the continent, while the negative wave (depression) moves in the opposite direction toward Texada island. The leading wave crosses the Malaspina strait and reaches Cape Cockburn on Nelson island in approximately 132 s after the slide starts moving. As a result, reflected waves form, and the general picture of wave field in the Malaspina strait becomes complex, reminding standing oscillations. The waves leaving through the open boundaries of the strait leads to rapid dampening of the amplitudes of level oscillations.

Figure 5.4 presents examples of calculations of level variations at points A, B, and C, the locations of which are indicated in Fig. 5.2. The maximum wave amplitude is observed at site A, the closest to the landslide zone, and the minimum amplitude turns out to be in the middle of the strait (point B). The tsunami starts with negative phase at point A and positive phase at points B and C.

The amplitude distributions of a tsunami wave at its crest and its depression along the west and east coasts of the strait are shown in Fig. 5.5. According to these calculations, the maximum level reduction (down to -5 m) is observed in the immediate vicinity of the source. Toward the North and South, the wave height rapidly dies out. The maximum at the wave crest on the west boundary is smaller than in the depression, and amounts to $+2.7$ m. At the opposite west coast, these maxima are significantly smaller (by approximately ± 1 m).

Numerical calculations were performed for a wide range of density values of the landslide material ($1.6 \leq \rho_2 \leq 2.2$ g/cm³), its viscosity coefficient ($10^{-3} \leq \nu \leq 1$ m²/s), and the initial positions of the landslide on the slope. It turned out that the results of calculations are least sensitive to variations in the landslide viscosity. An increase of the viscosity from 0.001 up to 0.1 m² · s⁻¹ leads to a change in the wave amplitudes by merely 1%. Their sensitivity to changes in the density of the material turned out to be much higher. Enhancement of the density ρ_2 from 1.6 up to 2.0 g/cm³ leads to an increase of the tsunami amplitude by 20%. The most important characteristic of a landslide, affecting the formation of tsunami waves, turned out

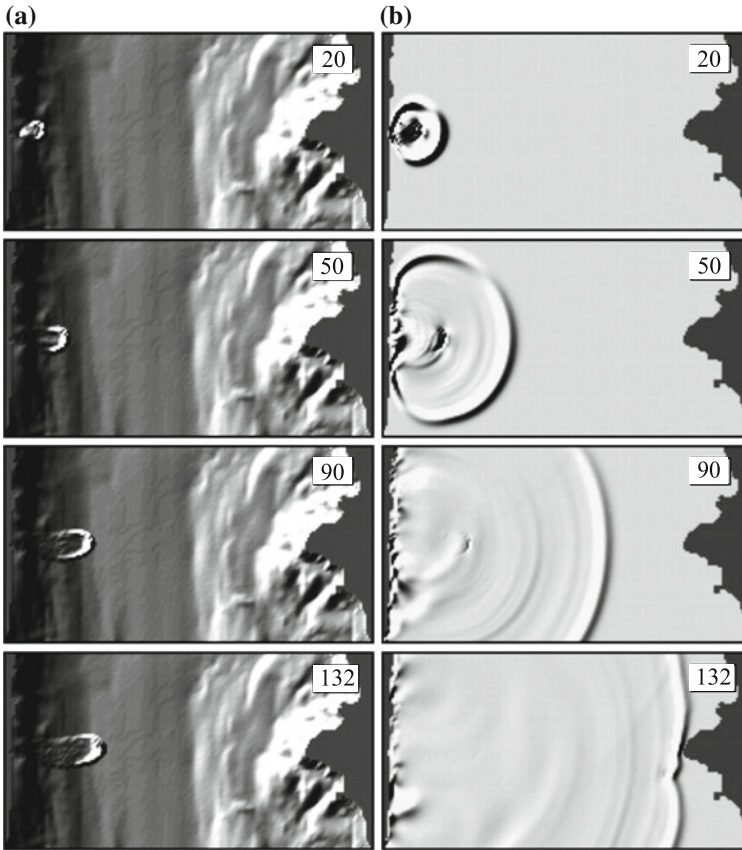


Fig. 5.3 Results of numerical simulation of the movement of a landslide on the *bottom* of Malaspina strait **(a)** and of the resultant surface waves **(b)** for times 20, 50, 90, and 132 s after the landslide collapses. Adapted from Rabinovich et al. (2003)

to be its initial position on the slope. For example, displacement of the center of a landslide by 100 m closer to the coast (the depth over the landslide amounts to about 30 m, here) results in the amplitudes of the tsunami waves increasing by 85%. Displacement of the landslide center toward the sea (a change of depth from 80 down to 118 m) reduces wave heights by 70%. Additional test calculations have shown that the amplitudes of surface waves generated are approximately proportional to the volume of the landslide. Summing up these results, one can conclude that the energy of a landslide tsunami depends, first of all, on the potential energy of the landslide (its

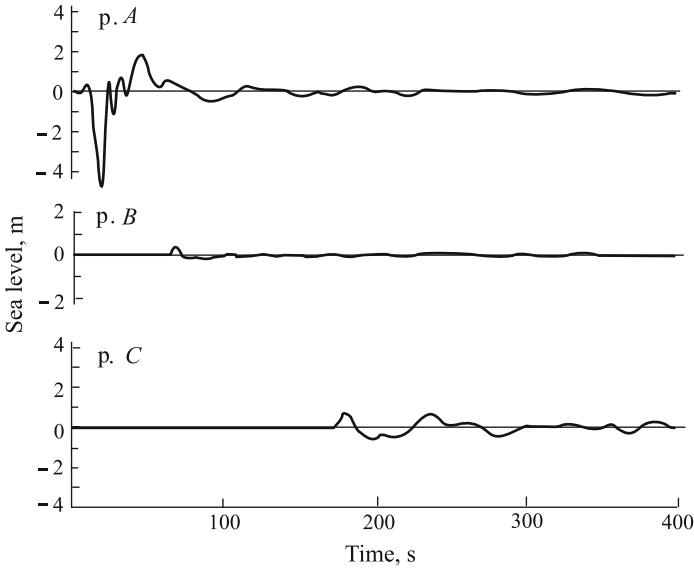


Fig. 5.4 Results of calculations of level oscillations at points A, B, and C, the locations of which are indicated in Fig. 5.2. Adapted from Rabinovich et al. (2003)

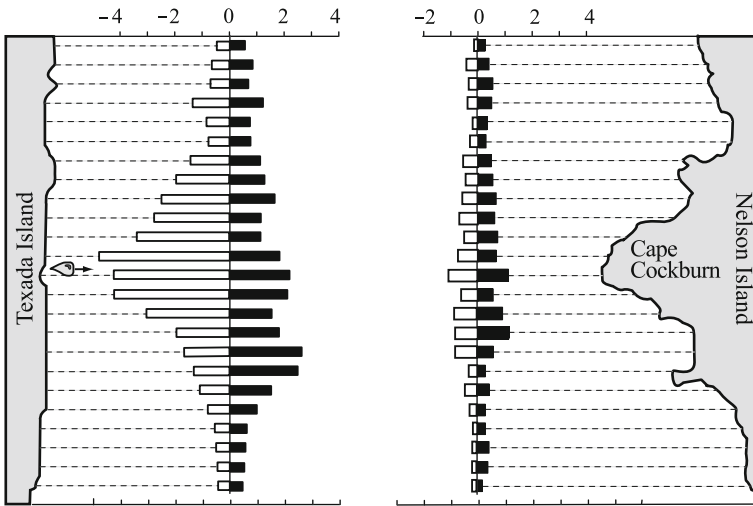


Fig. 5.5 Maximum level deviations at the crest and in the depression of a tsunami wave, calculated for the west and east coasts of Malaspina strait. Adapted from Rabinovich et al. (2003)

density, location on the slope, volume). The viscosity of the landslide body causes no noticeable dissipation of the landslide energy, which leaves a certain freedom in the choice of viscosity coefficient.

The character of interaction between a landslide body and surface waves depends on the relationship between the motion velocities of the landslide and of the surface waves (see Sect. 3.3.3). Actually, the process of wave generation by a landslide is similar to the formation of waves accompanying a ship, when it moves. The effect of resonance excitation of the accompanying wave is well known in the case, when a vessel moves toward shallow water with a velocity $c = \sqrt{gh}$, where h is the depth of the liquid. In this case, the wave resistance increases sharply, and the wave amplitude starts to grow. In this manner, also, a landslide moving on the sea bottom gives rise to perturbations of the water surface, which remind the wave accompanying a ship. Here, a measure of “closeness” to resonance conditions can be the Froude number $Fr = U/c$, where U is the velocity of the landslide, and $c = \sqrt{gh(x, y)}$ is the velocity of gravitational waves on the variable relief of the bottom. The value $Fr = 1$ corresponds to a resonance. For a landslide, representing a solid-state body, not subject to deformation, the notion of “velocity of motion” is unambiguous. But in the case of the flow of a viscous fluid, the particles of which move with differing velocities, it is not simple to introduce the concept of “landslide velocity.” Owing to the no-slip boundary condition, the velocity in the lower part of the landslide is much smaller than at its surface. Moreover, while the landslide body moves, it “spreads”, essentially changing its form. We shall estimate the velocity of a landslide, U_f , as the velocity, with which its *front* moves (the corresponding Froude number $Fr = U_f/c$).

The maximum velocity $U_{f \max}$, obtained in numerical calculations of a landslide in the Malaspina strait, amounted to 19.5 m/s at a distance of about 1 km from the coast of Texada island. The plot in Fig. 5.6a shows the variations in velocity for a gravitational wave, $c = \sqrt{gh(x)}$, and for the motion of a viscous slide front along the horizontal coordinate (across the strait). Figure 5.6b shows the dependence of the corresponding Froude number. The maximum value of the Froude number $Fr_{\max} = 0.46$ is achieved at a distance of 0.85 km from the coast.

For comparison, calculations were performed for the movement of a landslide in the form of a solid body sliding down the slope under the influence of the forces of gravity and of friction (between the landslide and the bottom). The friction coefficient k was set within the range from 0 to 0.2. The results of calculations are presented in Fig. 5.6.

The motion dynamics of a solid body on an inclined plane under the influence of the force of gravity with account of friction is such that there exists a “critical” inclination of the bottom, ψ , at which the down-pulling force is balanced by the force of friction, and the landslide moves without acceleration, $k = \tan \psi$. It can be considered that the “break-off” and subsequent sliding down of the landslide body takes place precisely, when the “holding” forces (of friction) weaken (for instance, owing to erosion at the edge of the sedimentary layer) so much as to allow the down-pulling force to start to exceed the force of friction. The characteristic slope of the bottom near Texada island is $\psi \approx 6^\circ$, which corresponds to $k = 0.1$. For this value, the maximum velocity of the solid landslide amounts to the value $U_{\max}^k = 33.1$ m/s at a distance $x = 1.86$ km from the coast, and here the Froude number $Fr_{\max} = 0.61$ turns out to reach its maximum at a distance $x = 0.95$ km, i.e.,

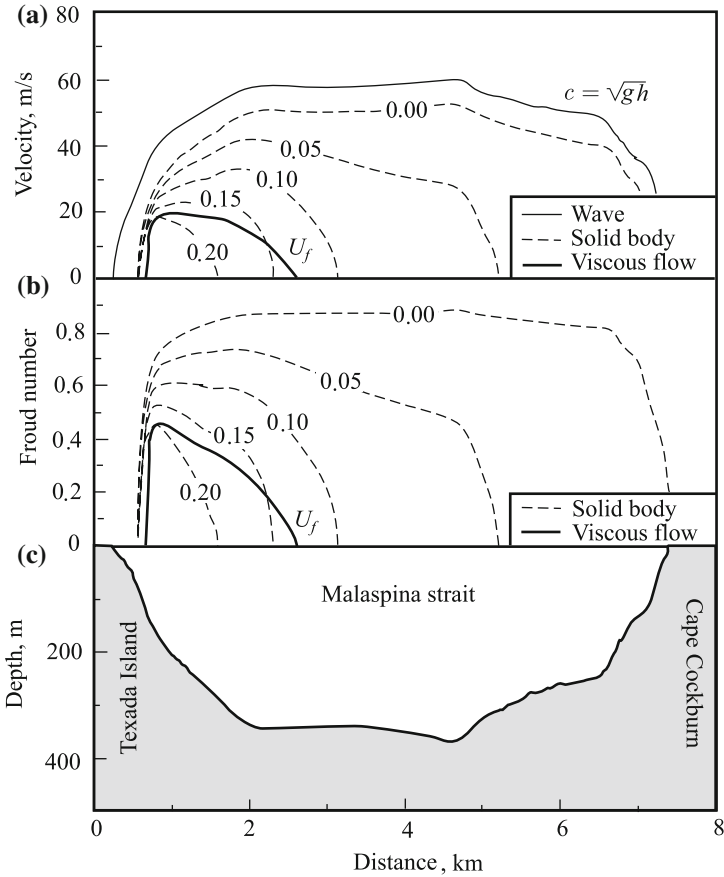


Fig. 5.6 Velocities of long gravitational waves, of a solid slide, and of the front of a viscous slide in the Malaspina strait. Velocities of the solid slide are calculated for various friction coefficients (from 0 to 0.2) (a). Froude numbers, corresponding to these velocities (b). Depth profile in the strait (c). Adapted from Rabinovich et al. (2003)

much closer to the coast. From the figure, it is seen that the Froude number rapidly reaches its maximum along the initial length of sliding down and gradually decreases as the landslide reaches the gently sloping bottom. Ultimately, the landslide stops, when its potential energy has already been spent on friction and wave generation. The “path length” of a solid landslide depends directly on the friction coefficient; thus, for $k = 0.05, 0.10, 0.15,$ and 0.20 , the “path length” amounts, respectively, to $x_s = 5.19, 3.13, 2.29,$ and 1.58 km.

When $k < 0.15$, the velocity of motion and the Froude number for a solid landslide exceed the velocity of motion of the front of a viscous flow everywhere. Here, the “path length” of the viscous landslide amounts to 1.6 km.

We draw attention to the velocity of motion of underwater landslides being, as a rule, smaller than the velocity of long gravitational waves (i.e., $Fr < 1$). This fact follows from elementary physical arguments. If the motion of a landslide is considered without account of the wave resistance and of friction ($k = 0$), then its velocity is determined by the formula

$$U = \sqrt{2g \frac{\rho_2 - \rho_1}{\rho_2} \Delta h}, \quad (5.6)$$

where Δh is the change in vertical position of the center of mass of the landslide. Suppose that, going down the slope, the landslide reaches a certain depth h . Clearly, for an underwater landslide, the inequality $\Delta h < h$ is always satisfied. Comparing the velocity of the landslide, determined by formula (5.6), and the velocity of long waves, \sqrt{gh} , it is not difficult to arrive at the conclusion that equality of these two quantities is possible, only if $\rho_2 > 2.0 \text{ g/cm}^3$, i.e., for well-consolidated sediments and rock. If the force of friction is taken into account, the required density of the landslide body will be even greater. Thus, a “resonance” ($Fr = 1$) is possible only for landslides, consisting of very dense materials, or when the landslide enters the water with a certain initial velocity. In the latter case, one can speak of both subaerial (partially submerged) landslides and of landslides sliding into water from a “dry” coastal slope.

5.2 Tsunami Excitation Related to Volcanic Eruptions

Explosions of volcanic islands (collapses of calderas), explosive (explosion-like) eruptions of underwater volcanoes, pyroclastic flows landing in water are all phenomena capable of giving rise to waves, which in their destructive strength are in no way inferior to tsunamis of seismotectonic origin. At present, 143 tsunamis of volcanic origin (“Volcano” + “Volcano and Earthquake” + “Volcano, Earthquake, and Landslide” + “Volcano and Landslide”—see Table 5.1) are known in the World Ocean.

One of the most striking historical examples of volcanogenic tsunamis is represented by the waves caused by the activity of the Krakatau volcano in August of 1883 (Self and Rampino 1981; Nomanbhoy and Satake 1995; Choi et al. 2003; Paris et al. 2014). On August 26, at 17:00, local time, a series of loud explosions took place, and the volcano ejected an ash cloud to a height of up to 25 km. A small tsunami of 1–2 m high was formed. In the morning of August 27, three colossal explosions took place. The first explosion (at 5:28) destroyed mountain Perboewatan on Krakatau island, which was 130 m high. The caldera produced was immediately filled up with sea water, leading to the generation of a small tsunami. At 6:36, mountain Danan, which was 500 m high, exploded and collapsed, which gave rise to a tsunami wave up to 10 m high. The main (third) explosion took place at 9:58. It literally blew apart what remained of Krakatau island (Rakata island). The volcano threw out

9–10 km³ of tephra (solid material) and 18–21 km³ of pyroclastic deposits, which were distributed over an area of about 300 km² with an average thickness of 40 m. Ash covered a territory of approximately 2.8×10^6 km². In the place of the island, there emerged a caldera 6 km in diameter and 270 m deep. The third explosion came with the most strongest noise ever heard by mankind. Air blasts circumvented the globe seven times. The energy released during the main eruption of the Krakatau volcano amounted to 8.4×10^{17} J. The waves that resulted from the third most strong explosion were 42 m high, and they arrived 5 km inland. The average height of waves on the coast of the Sunda straits (separating islands Java and Sumatra) was about 15 m. At least 36 thousand people were died. About 300 villages were destroyed. The tsunami caused by explosion of the Krakatau volcano was noticed everywhere. Waves were recorded by many mareographs not only in the Indian Ocean, but also in the Pacific and Atlantic, as well. Far from the coasts of Indonesia, wave amplitudes were relatively small.

On the basis of the diameter and depth of the caldera formed as a result of the explosion of the Krakatau volcano, it is not difficult to estimate the volume of the initial perturbation—the “local depression” of the ocean level. It amounts to ~ 7 km³. It is interesting to note that this volume approximately corresponds to the volume of water ousted by ocean bottom deformations in the case of strong earthquakes (100×100 km² \times 1 m = 10 km³). The potential energy corresponding to the initial perturbation, which can be estimated by formula (2.4), amounts to $\sim 6 \times 10^{15}$ J, which is of the order of 1 % of the eruption energy.

Another frequently discussed event took place in the Bronze Age (around 35 centuries ago) in the Aegean sea (Antonopoulos 1992; Dominey-Howes 2004). There exists a hypothesis that explosion of the volcanic Thera island (the Santorini volcano) and the resulting tsunami caused the death of mythical Atlantis, while the explosive eruption itself contributed to destruction of the Cretan-Mycenaean culture. At any rate, geological traces of this tsunami have been found along the coastlines of Greece and Turkey (Minoura et al. 2003).

Of about one thousand volcanoes, known to be active on Earth, some hundreds are underwater volcanoes. Numerous works are devoted to the study of tsunami generation, related to volcanic eruptions (Basov et al. 1981; Egorov 1990; Pelinovsky 1996; Waythomas and Neal 1998; Belousov et al. 2000; Tinti et al. 2003; Ward and Day 2001, 2003; Kurkin and Pelinovsky 2004; Egorov 2007; Mader and Gittings 2006). The main physical mechanisms of volcanogenic tsunami generation comprise the following:

- (1) the discharge into water of a large volume of matter (from slow lava flows to explosive eruptions);
- (2) the collapse of a caldera (explosion of a volcanic island);
- (3) pyroclastic flows, landslides, etc.; and
- (4) volcanic earthquakes.

In the case of underwater volcanoes, the first two mechanisms are prevalent. The third (landslide) mechanism may be more peculiar to volcanoes on coasts, although

the possibility cannot be excluded of underwater landslides and mudslides initiated by an underwater eruption.

In certain cases, volcanic eruptions can provoke enormous collapses. Thus, for example, in Ward and Day (2001) the possibility is indicated for part of the La Palma island (Canary islands) to collapse during the next eruption of the volcano, located there. Geological estimates reveal that the volume of such a collapse may amount to 500 km^3 . A tsunami wave caused by such a colossal collapse would be capable of crossing the Atlantic Ocean and reaching the coasts of America with a height exceeding 10 m.

In the present section, we shall only deal with those original mechanisms of tsunami formation, which are peculiar precisely to volcanic eruptions. Thus, here we shall not consider wave generation by volcanic earthquakes, as well as by volcanogenic landslides.

We shall first dwell upon certain peculiarities of tsunami formation in the case of a caldera collapsing and being subsequently filled up with water. If one speaks of an underwater volcano, then the description of the waves generated fully reduces to the problem of tsunami generation by deformation of the ocean bottom, which has been investigated in detail in Chaps. 3 and 4. Truly, in the case of a collapsing caldera, the amplitude of the “bottom deformation”, $\eta_0 \sim 10^2\text{--}10^3 \text{ m}$, and the horizontal dimension of the deformation area, $D \sim 10^3\text{--}10^4 \text{ m}$, may turn out to be comparable to the ocean depth. Note that underwater volcanoes may be located both at small (shelf) and at large (abyssal) depths. If the explosion of a volcanic island takes place, then the water filling up the caldera, like the waters surrounding the island, are evidently characterized by shelf depths ($\sim 10^2 \text{ m}$).

A suddenly generated caldera (in total absence of obstacles to water entering it) will be filled with water in a time $T \sim D/\sqrt{gH}$, where D is the diameter of the caldera and H is its characteristic depth. Taking advantage of the aforementioned ranges of these parameters, we obtain that the quantity T varies within the limits of 30–300 s. In the case of the most probable development of events, when obstacles to the arrival of water do exist, the time the caldera will take to fill up may increase significantly.

Thus, the caldera collapsing results in a source of waves (a flow of mass) with a characteristic action time of $10^2\text{--}10^3 \text{ s}$. The volume of water, taking part in the process, can be estimated as $V \sim \pi D^2 H/4 \sim 0.3\text{--}30 \text{ km}^3$. The obtained characteristics of the source are quite in agreement with the values for a seismotectonic tsunami source. Caldera collapses are capable of generating powerful long-period tsunami waves. Simulation of tsunami wave propagation, due to activity of the Krakatau volcano in 1883, performed within the framework of long-wave theory (Choi et al. 2003), demonstrated good agreement between the model and observed arrival times of waves at various points of the World Ocean distant from the source. This result testifies that the wave front indeed propagated with a velocity close to the velocity of long waves, \sqrt{gH} , i.e., the waves were sufficiently long. Note that, in the case of abyssal depths, strongly dispersive waves are formed in the area of the caldera collapse, which rapidly die out with the distance from the source.

Further, we shall deal with the most “original” of the tsunami generation mechanisms peculiar to volcanoes. What is meant is the release of a large volume of matter

in the case of an underwater eruption. First, consider the case of a slow outflow of matter. An adequate model for describing the tsunami generation process will consist of a set of hydrodynamic equations with a source of mass (volume). Assume eruption of the underwater volcano to proceed slowly: a volume V_0 is released in time τ from the crater. On the basis of general physical arguments, it is not difficult to estimate the amplitude and energy of surface gravitational waves, caused by such an underwater “eruption”. Consider the ocean depth H to be fixed, the area S of the crater to be small, and the condition $\sqrt{S} \ll H$ to be satisfied. Of course, the model of an ocean of constant depth is limited (the crater of the volcano is usually situated on top of a cone), but for presenting general physical regularities of the process such a simplified model is quite applicable.

The volume thrown out will oust an identical volume of water. This volume will spread over the area of a circle of radius, equal to the distance, which a long wave has time to cover during the eruption time $r = \tau\sqrt{gH}$. As a result, we have the amplitude of the initial water elevation

$$\xi_0 = \frac{V_0}{\pi \tau^2 gH}. \tag{5.7}$$

The potential energy of such an initial elevation is calculated by formula (2.4)

$$W_p = \frac{\rho V_0^2}{2\pi \tau^2 H}. \tag{5.8}$$

From formulae (5.7) and (5.8), the amplitude and especially the energy are seen to increase with the rate V_0/τ , at which volcanogenic material is released from the crater. An increase of the ocean depth reduces the efficiency of tsunami excitation.

For more accurate description of the waves, caused by a flow of material from a hole of radius R in the ocean bottom, it is possible to apply the general solution of the problem, (3.52), (3.39), and (3.40), obtained in Sect. 3.2.2 within the framework of linear potential wave theory. Formulation of the axially symmetric problem is schematically presented in Fig. 5.7. In the case dealt with, the boundary condition on the bottom, (3.40), assumes the following form:

$$\frac{\partial F}{\partial z} = w(r, t) = w_0(1 - \theta(r - R))(\theta(t) - \theta(t - \tau)), \quad z = -H, \tag{5.9}$$

where $w_0 = V_0/(\tau\pi R^2)$ is the outflow velocity of material from the crater. Displacement of the free surface, caused by the flow, released from the ocean bottom, is determined by formula

$$\begin{aligned} \xi(r, t) &= \theta(t) \zeta(r, t) - \theta(t - \tau) \zeta(r, t - \tau), \\ \zeta(r, t) &= \frac{V_0}{\pi R \tau} \int_0^\infty dk \frac{J_0(rk) J_1(Rk) \sin\left(t(gk \tanh(kH))^{1/2}\right)}{\cosh(kH) (gk \tanh(kH))^{1/2}}. \end{aligned} \tag{5.10}$$

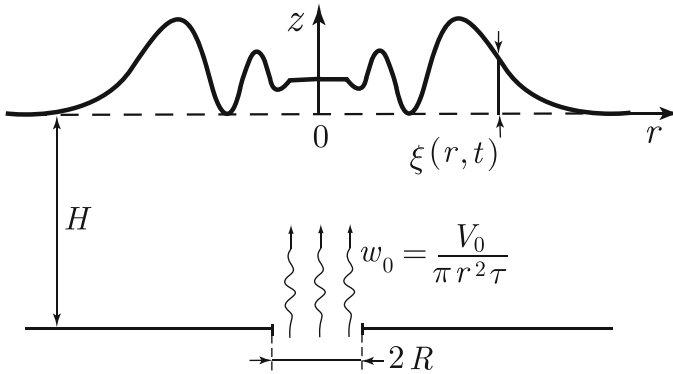


Fig. 5.7 Mathematical formulation of the problem of tsunami generation by an underwater eruption

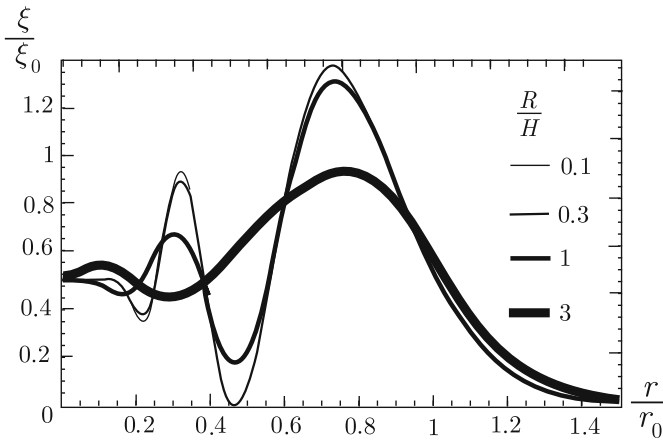


Fig. 5.8 Perturbation of free surface caused by underwater eruption. The calculation is performed at the time moment, when the eruption finishes, $t = 10\sqrt{H/g}$, for various ratios of the crater radius and the ocean depth, R/H (indicated in the figure). The x-axis is normalized to the quantity $r_0 = \tau\sqrt{gH}$, and the y-axis to $\xi_0 = V_0/(\pi\tau^2gH)$

The form of the free surface displacement at the moment, when the eruption finishes ($t = \tau$), calculated by formula (5.10) for $\tau = 10\sqrt{H/g}$ and various radii of the crater, $R/H = 0.1, 0.3, 1,$ and 3 , is shown in Fig. 5.8. The curves are presented in dimensionless coordinates. The x-axis is normalized to the distance covered by a long wave during eruption time $\tau\sqrt{gH}$, and the y-axis is normalized to the free surface perturbation, determined by estimation formula (5.7). From the figure, it is seen that the form and amplitude of the free surface perturbation depend little on the radius of the crater, when $R/H < 1$. Moreover, the quantity ξ_0 , determined by formula (5.7), is indeed seen to represent a good estimate for the surface displacement amplitude.

Note that the application of the theory of incompressible liquids imposes natural limits on the outflow velocity of material from the crater, $w_0 < c$, where c is the velocity of sound in water, and on the relationship between the eruption duration and the ocean depth, $\tau > 4H/c$.

For estimates, we take advantage of the modest, as compared to the 1883 event (Krakatau), eruption of an underwater volcano, located at a depth $H = 1000$ m. Let the release of material amount be $V_0 = 1 \text{ km}^3$, and the eruption duration $\tau = 100$ s. For the indicated duration of the process, the perturbation (elevation) radius of the water surface amounts to $r \approx 10$ km. Its height, calculated in accordance with formula (5.7), amounts to the significant value $\xi_0 \approx 3$ m. And the potential energy, calculated by (5.8), is $W_p = 1.7 \times 10^{13}$ J. A tsunami, generated by such an initial elevation, will evidently represent a serious threat.

In the model, described above, we assumed the eruption to be a slow process. This provided grounds for applying linear theory and considering water to be incompressible. But the eruption of an underwater volcano may exhibit an explosive character. In such a case, the products of eruption form a gaseous bubble in the water, which contains high-temperature gases and water vapor at high pressures. The expansion and floating-up of the bubble lead to the formation of a cupola or plume—an elevation on the water surface. An analog of this process is the formation of a plume in the case of an underwater explosion. It must be stressed that the formation of a gaseous bubble at large depths is not always possible, owing to the colossal hydrostatical pressure.

In this case, description of the wave generation process is a difficult task. But one can select an equivalent source and use it as the initial perturbation in calculating tsunami waves. Reasonable agreement with reality (explosions in water for energies within the range of 2×10^6 – 3×10^{10} J) is achieved for the following form of the initial displacement of the water surface (Kurkin and Pelinovsky 2004):

$$\xi_0(r) = H_S \left(2 \left(\frac{r}{R_s} \right)^2 - 1 \right) (1 - \theta(r - R_s)), \tag{5.11}$$

where R_s is the source radius and H_S is the amplitude of the water level displacement at the source. Both parameters, characterizing the source, can be estimated via the equivalent energy of the explosion (or volcanic eruption) (Le Mehaute and Wang 1996).

In the case of an ocean of constant depth H , evolution of the initial free surface perturbation, exhibiting radial symmetry, is described by the following expression (see general theory in Sect. 3.2.2):

$$\xi(r, t) = \int_0^\infty k dk A(k) J_0(kr) \cos(\omega(k)t), \tag{5.12}$$

$$A(k) = \int_0^\infty r dr \xi_0(r) J_0(kr), \tag{5.13}$$

where $\xi_0(r)$ is a function describing the form of the initial perturbation and J_n is the Bessel function of the first kind of n th order. The relationship between the cyclic frequency and the wave number is determined by the known dispersion relation for gravitational waves on water, $\omega^2 = gk \tanh(kH)$. For an initial elevation, exhibiting the form, determined by formula (5.11), we have

$$A(k) = -\frac{H_S R_S J_3(kR)}{k}. \tag{5.14}$$

For large times, we represent the integral in expression (5.12) with the aid of the stationary-phase method,

$$\xi(r, t) \cong \sqrt{\frac{2\pi}{t |S''(k_0)|}} k_0 A(k_0) J_0(k_0 r) \cos\left(\omega(k_0)t - \frac{\pi}{4}\right), \tag{5.15}$$

where k_0 is the extremum of function $S(k) = \sqrt{gk \tanh(kH)} - kx/t$, which exists under the condition $x < t\sqrt{gH}$.

As an example, Fig. 5.9 shows the profiles of waves generated as a result of evolution of the initial perturbation (5.11). The calculation is performed by formula (5.15) for the moment of time $t = 100\sqrt{H/g}$ for two different radii of the initial perturbation. The waves are seen to be strongly dispersive; therefore, the propagation velocity of the wave packet depends strongly on the radius of the initial perturbation. The existence of such a dependence leads to an interesting effect (dispersion amplification), which was first noted in Mirchina and Pelinovsky (1987). Consider two or more successively amplified eruptions taking place. The radius R_S of the perturbation created on the water surface increases with the strength (energy) of the eruption. In accordance with the growth of the radius, the propagation velocity of the wave packet also increases. Consequently, during the process of wave propagation, the superposition is possible of wave packets from different eruptions, which may lead to

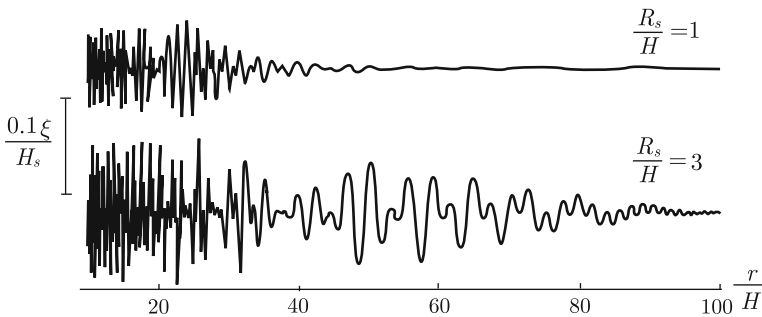


Fig. 5.9 Profile of waves excited by underwater eruption. The calculation is performed for $t = 100\sqrt{H/g}$ for two different ratios of the initial perturbation radius and the ocean depth, R_S/H (the values are indicated in the figure)

significant amplification of the tsunami amplitude. We recall that in August 1883, three eruptions occurred of the Krakatau volcano, each of which was stronger than the preceding one.

5.3 Meteotsunamis

Long waves, similar in characteristics to tsunami waves of seismotectonic origin, can form as a result of the influence of various atmospheric processes upon the water layer. These waves are conventionally termed anemobaric waves or meteotsunamis. The term “meteotsunami” was apparently coined in Nomitsu (1935).

The main causes for meteotsunamis to arise are moving inhomogeneities of the atmospheric pressure or the tension of wind friction (e.g., Monserrat and Rabinovich 2006). We at once note that, unlike other tsunami generation mechanisms, in this case an important role is played by resonance effects, revealed, when the propagation velocity of atmospheric perturbations and their period turn out to be close to the velocity of long waves and to the period of eigen oscillations of the aquatorium, respectively.

Like tsunamis of seismotectonic origin, meteotsunamis represent quite a rare phenomenon. Similar to tsunamis not being excited by each individual earthquake, not every cyclone, atmospheric front, train of internal gravitational waves or other atmospheric perturbation leads to the formation of meteotsunamis. A great number of examples are known, when quite strong atmospheric perturbations were not accompanied by any generation of long waves. Nevertheless, in the World Ocean, 92 events (3.6%) have been registered, which are classified as tsunamis of meteorological origin (see Table 5.1).

The extent, to which the parameters of tsunamis due to meteorological and seismotectonic causes are identical, is such that in a number of cases it is difficult to determine the actual cause of wave generation. Thus, for example, the group of long waves about 60 cm high with a period of 24–60 min, registered at the coast of South Africa on May 11, 1981, was initially identified as a seismotectonic tsunami and described in the September issue of “Tsunami Newsletter”. Later, these waves were classified as a meteotsunami caused by a deep cyclone and atmospheric waves related to it.

From general arguments, it is clear that an intensification of atmospheric processes, for example, in the case of tropical cyclones should lead to perturbations of the water layer and to the generation of long waves. The passage of cyclones is nearly always accompanied by significant oscillations of the atmospheric pressure, enhancement of the wind, and development of storm agitation. Extreme values of pressure and wind velocity in tropical cyclones reach 870 hPa (cyclone “TIP”, October 1979) and 82 m/s (cyclone “LINDA”, September 1997), respectively. Part of the energy of such intense atmospheric processes, doubtless, must be transformed into the energy of long waves. But an analysis of synchronous measurements of ocean level oscillations and of atmospheric pressure fluctuations reveal that the direct relationship

between these processes, with the exception of individual cases, is not essential (Munk 1962; Kovalev et al. 1991; Rabinovich and Monserrat 1996).

At the same time, there exist numerous examples of the observation of long waves, the formation of which is unambiguously related to atmospheric processes. Thus, for example, in Bondarenko and Bychkov (1983) a description is given of the generation of long waves with a period of about 23 min, caused by internal gravitational waves with the same period, that propagated over the Caspian Sea in the region of Svinoi island. Several cases are known of catastrophic waves arising on the Great lakes (Donn and Ewing 1956). On May 5, 1952, June 26, and July 6, 1954 sharp jumps in the atmospheric pressure, which propagated with velocities of 20–40 m/s, led to the formation of strong long waves, which caused significant destruction on the coast and even the death of people.

The anomalous character of seiche oscillations in Nagasaki Bay (Kyusiu island) is renown (Rabinovich 1993). Oscillations of amplitudes ~ 0.5 m and periods of about 30 min in this bay represent quite a typical phenomenon. It is known by the local term “abiki”. In a number of cases, abiki waves are capable of achieving significant amplitudes. Thus, for example, on March 31, 1979, the maximum height of waves that caused significant damage and the death of 3 persons amounted to 4.78 m. In Hibiya and Kajiura (1982), this event was shown to be caused by the passage of a jump of atmospheric pressure from 2 to 6 hPa over the western part of the East-Chinese Sea. The propagation velocity of the pressure jump was about 30 m/s.

Characteristic depths of the sea in between the region, where the perturbation originates, and Kyusiu island lie between 50 and 150 m. The propagation velocities of long waves, corresponding to them, vary within the limits 22–28 m/s, which is close to the propagation velocity of the atmospheric perturbation. The period of the waves, which arrived in Nagasaki Bay, also turned out to be close to the period of eigen oscillations. As a result of the double resonance, the height of waves increased by more than a factor of 100. Thus, a jump in pressure of only several hPa caused the formation of abiki waves in Nagasaki Bay several meters high.

Another well-known example consists in seiche oscillations with periods from several minutes up to several tens of minutes, which are observed regularly in summertime off the south-east coast of Spain in the region of the Balearic islands. From this point of view, the Ciutadella Bay, located in the north-west part of Menorca island, is the most renown. The bay is of the order of 1 km long, about 90 m wide with a practically flat bottom at a depth of 5 m. In certain cases, seiches with typical periods of about 10 min reach heights of 4 m, here, leading to serious damage to ships and coastal structures. This calamity has received the local name “rissaga” (Monserrat et al. 1991). An analysis of synchronous measurements of the atmospheric pressure and of long waves, performed in Rabinovich and Monserrat (1996), has permitted to reveal a series of cases, when strong level oscillations were caused by perturbations of the atmospheric pressure. One of such events is the formation of seiche oscillations in Ciutadella Bay with a amplitude of 0.87 m. Formation of the waves resulted from the passage of a train of intense internal gravitational waves in the atmosphere with an amplitude of about 200 Pa and propagation velocity of about 30 m/s. The period of atmospheric waves was of the order of 1 h, while their length over 100 km, which

essentially exceeds the period of proper oscillations of the bay and its dimensions. These differences exclude a possible resonance response of the bay. Most likely, the formation of the long waves was a result of resonance effects in open sea, after which they approached the coast and caused strong oscillations in the bay. A fact, favoring this assumption, consists in that the velocity of the long waves on the external shelf with depths ~ 100 m was in good accordance with the propagation velocity of atmospheric perturbations.

The meteotsunami phenomenon has much in common with the so-called storm surges. In the monograph of Murty (1984), storm surges are defined as sea-level oscillations in the coastal zone or within internal basins with periods from several minutes up to several days, and caused by atmospheric influence. Note that this definition excludes wind waves and choppy sea, since they are characterized by periods smaller than a minute. Actually, the terms meteotsunami and storm surge denote phenomena of the same scope, which are caused by the same reason—by influence of the atmosphere. The only formal difference between a storm surge and a meteotsunami consists in the difference between their maximum periods. The maximum period for a tsunami does not exceed several hours, while storm surges may last several days.

Strong storm surges of heights up to 5 m are observed off the coast of China in the northern part of the Yellow Sea. This phenomenon results in colossal calamities for the Republic of Bangladesh—only during recent decades, it has brought about the death of several hundreds of people. Storm surges are also known in Europe. The catastrophic storm surge, which occurred in the North Sea in the period between January 31 and February 2, 1953, destroyed protective coastal structures, flooded an area of 25,000 km², and killed 2000 people in Great Britain and Holland (Gill 1982). The famous inundations of St. Petersburg are nothing, but storm surges. Besides St. Petersburg, strong storm surges in Russia also take place off the coasts of the Asov and Okhotsk seas, and the Sea of Japan.

The physical mechanism of meteotsunami formation can be related to the influence upon the water surface of atmospheric pressure and tangential tensions, created by the wind. In principle, there exists, also, the possibility of nonlinear energy transfer from the relatively short wind (storm) waves to the long-wave components, but we shall not deal with this mechanism, here.

From the point of view of mathematical description, the influence of the atmosphere upon a water layer is taken into account by the boundary condition on the free water surface. Instead of the traditional for tsunami problems condition of constant pressure on the free water surface, we shall now assume this quantity to be variable in space and time, $p_{\text{atm}} = p(x, y, t)$. Besides the pressure, acting upon the water surface along the normal direction, there also exists a tangential tension of friction, caused by the wind. The tangential tension per unit surface area, \mathbf{T}_S , is related to the speed of the wind, \mathbf{U} , by the following approximate relationship:

$$\mathbf{T}_S = C \rho_{\text{atm}} \mathbf{U} |\mathbf{U}|,$$

where ρ_{atm} is the density of air and C is a dimensionless empirical coefficient, the value of which usually lies within limits from 0.0012 up to 0.003 (Lichtman 1970).

A similar formula relates the velocity of the water flow near the bottom, \mathbf{v} , and the tension of friction, acting on the water column from the bottom,

$$\mathbf{T}_B = -C_B \rho \mathbf{v} |\mathbf{v}|,$$

where ρ is the density of water and C_B is a dimensionless empirical coefficient, the value of which is usually set equal to 0.0025 (Murty 1984). We recall that in the case of tsunami generation by bottom landslides tangential tensions on the bottom are not taken into account (owing to the short duration of a landslide). But in the case considered the action of tangential tension of the wind may turn out to be prolonged (up to several days) and to transfer significant momentum to the water column.

The presence of tangential tensions on the free water surface and on the bottom is accompanied by the formation of a pronounced vertical flow structure, which in real natural conditions is usually turbulent. Owing to the turbulence, the solution of the problem should, evidently, not be based on the Navier–Stokes equations, but on Reynolds equations. The existence of a vertical flow structure complicates transition from the general nonlinear equations of hydrodynamics to the long-wave equations. But, if the nonlinear term $(\mathbf{v}, \nabla) \mathbf{v}$ is neglected, then the Reynolds equations can be integrated over the vertical coordinate from the bottom, $z = -H$, up to the free water surface, $z = \xi$. As a result, a set of equations will be obtained, which will contain flow velocities averaged over the depth, while the term, describing the vertical turbulent momentum transfer, will be expressed as the difference between tensions on the bottom and on the free surface,

$$\int_{-H}^{\xi} \frac{\partial}{\partial z} \left(K_z \frac{\partial \mathbf{v}}{\partial z} \right) dz = \frac{1}{\rho} (T_S - T_B).$$

Without going into the details of obtaining the equations, expounded, for example in the monograph of Murty (1984), we present a version of the set of equations, applied in practice for calculating meteotsunami generation and propagation (Vilibic et al. 2004):

$$\begin{aligned} \frac{\partial u}{\partial t} + u \frac{\partial u}{\partial x} + v \frac{\partial u}{\partial y} - fv &= -g \frac{\partial \xi}{\partial x} - \frac{1}{\rho} \frac{\partial p_{\text{atm}}}{\partial x} + \frac{(T_S - T_B)_x}{\rho (H + \xi)} + K_L \left(\frac{\partial^2 u}{\partial x^2} + \frac{\partial^2 u}{\partial y^2} \right), \\ \frac{\partial v}{\partial t} + u \frac{\partial v}{\partial x} + v \frac{\partial v}{\partial y} + fu &= -g \frac{\partial \xi}{\partial y} - \frac{1}{\rho} \frac{\partial p_{\text{atm}}}{\partial y} + \frac{(T_S - T_B)_y}{\rho (H + \xi)} + K_L \left(\frac{\partial^2 v}{\partial x^2} + \frac{\partial^2 v}{\partial y^2} \right), \\ \frac{\partial \xi}{\partial t} + \frac{\partial}{\partial x} ((H + \xi) u) + \frac{\partial}{\partial y} ((H + \xi) v) &= 0, \end{aligned}$$

where u and v are velocity components averaged over the depth, ξ is the free surface displacement from equilibrium position, $f = 2\omega \sin \varphi$ is the Coriolis parameter, and K_L is the constant horizontal turbulence viscosity coefficient. In principle, the quantity K_L may be variable, and then it should be present under the derivative sign. In Vilibic et al. (2004), the assumption was made that $K_L = 15 \text{ m}^2/\text{s}$.

Now consider the main physical regularities of the meteotsunami generation process, taking advantage of the example of waves, caused by moving perturbations of atmospheric pressure. For clarity, the problem will be considered within the framework of the simple one-dimensional model. Let $|\xi|$ be the absolute value of the free surface displacement from equilibrium, and consider the ocean depth $H = \text{const}$ and the horizontal scale of atmospheric perturbation a to be related as follows: $|\xi| \ll H \ll a$. With account of such assumptions, the meteotsunami formation process can be described by linear equations of long-wave theory:

$$\frac{\partial u}{\partial t} + g \frac{\partial \xi}{\partial x} = -\frac{1}{\rho} \frac{\partial p_{\text{atm}}}{\partial x}, \quad (5.16)$$

$$\frac{\partial \xi}{\partial t} + H \frac{\partial u}{\partial x} = 0. \quad (5.17)$$

If the atmospheric pressure is constant in time, but depends on the space coordinate ($\partial/\partial t = 0$), then from Eq. (5.16) immediately follows the so-called “inverse barometer law”

$$\xi(x) = -\frac{p_{\text{atm}}(x)}{\rho g}. \quad (5.18)$$

In accordance with this law, the local enhancement of atmospheric pressure “presses down” the free sea surface, forcing the water to occupy those regions, where the atmospheric pressure is lower. And, contrariwise, in the region of local reduction of pressure, for example, in cyclones, an enhancement of the water level should be observed. Extreme variations of atmospheric pressure are observed in tropical cyclones. The pressure at the center of such a gigantic whirlwind can drop by a value of $\sim 100 \text{ hPa}$, which amounts to about 10 % of normal atmospheric pressure. A local elevation of the level by $\sim 1 \text{ m}$ corresponds to such a depression. But in the case of most tropical cyclones and of other atmospheric processes, the amplitude of pressure perturbations and, consequently, the amplitude of the free water surface deviation will be by 1–3 orders of magnitude smaller. Variations of atmospheric pressure with amplitudes exceeding 10 % can, most likely, arise only in the case of powerful explosions of natural (volcanoes, meteorites) or of artificial origin. In such cases, the pressure perturbation will, naturally, not be motionless, but will propagate in the atmosphere, most probably, like a shock wave.

We, now, introduce the dimensionless variables (the asterisk * will be further omitted)

$$\begin{aligned}
 x^* &= \frac{x}{H}, & t^* &= t\sqrt{\frac{g}{H}}, & V^* &= \frac{V}{\sqrt{gH}}, \\
 p_{\text{atm}}^* &= \frac{p_{\text{atm}}}{\rho gH}, & \xi^* &= \frac{\xi}{H}.
 \end{aligned}
 \tag{5.19}$$

Note that the square dimensionless velocity is the well-known Froude number $\text{Fr} = V^2/gH$. With account of transformations (5.19), the set of Eqs. (5.16) and (5.17) is easily reduced to the nonlinear wave equation

$$\frac{\partial^2 \xi}{\partial t^2} - \frac{\partial^2 \xi}{\partial x^2} = \frac{\partial^2 p_{\text{atm}}}{\partial x^2}.
 \tag{5.20}$$

If motion exists only at times $t > 0$, then for zero initial conditions the solution of Eq. (5.20) is determined by the formula (Tikhonov and Samarsky 1999)

$$\xi(x, t) = \frac{1}{2} \int_0^t dT \int_{x-(t-T)}^{x+(t-T)} dX \frac{\partial^2 p_{\text{atm}}}{\partial X^2}.
 \tag{5.21}$$

Let the propagating perturbation of atmospheric pressure be described by the formula

$$p_{\text{atm}}(x, t) = p(x - Vt)\theta(t),
 \tag{5.22}$$

where p is an arbitrary function determining the space distribution of the pressure, θ is the steplike Heaviside function, and V is the propagation velocity of the perturbation. The dynamics of the atmospheric process, described by formula (5.22), is such that at time moment $t = 0$ the atmospheric pressure perturbation is “switched on” and starts movement unlimited in time with constant velocity V in the positive direction of axis $0x$. In the case considered, the integrals in expression (5.21) are calculated analytically, and the solution of the problem is given by the formula

$$\xi(x, t) = \frac{p(x - Vt)}{V^2 - 1} - \frac{p(x - t)}{2(V - 1)} + \frac{p(x + t)}{2(V + 1)}.
 \tag{5.23}$$

From formula (5.23), it follows that the wave perturbation on the water surface has three components. One of them propagates with the velocity V , following the area of altered pressure. The other two components correspond to free waves traveling along axis $0x$ in the positive and negative directions, respectively, with the velocity of long waves. The amplitude of waves on the water surface depends strongly on the propagation velocity of the atmospheric perturbation. Here, the amplitude of waves traveling in the the same direction as the atmospheric perturbation may undergo a sharp increase, when $V \approx 1$. When the equality $V = 1$ is satisfied exactly, the growth of amplitude is without limit, within the model considered. This effect is known as the ‘Proudman resonance’. The amplitude of waves traveling in the

negative direction of axis $0x$ exhibits no such peculiarities. Always remaining a relatively small quantity, it monotonously decreases as the velocity V increases.

It is possible to determine the behavior of a wave perturbation on a water surface in resonance conditions by calculating the limit of expression (5.23), when $V \rightarrow 1$. The resonance effects involve the first two terms of expression (5.23). In the case of resonance, each of these terms tends toward infinity, but their sum has a finite limit. We shall, now, expand function $p(x - Vt)$ in a Taylor series at point $z_0 = x - t$ with an accuracy up to the linear term,

$$p(z_0) \approx p(z_0) + p'(z_0)(z - z_0).$$

Upon performing elementary transformations, we obtain an expression, describing the free surface displacement in the case of resonance,

$$\xi_{\text{res}}(x, t) = \lim_{V \rightarrow 1} \left(\xi(x, t) \right) = -\frac{p'(x-t)t}{2} - \frac{p(x-t)}{4} + \frac{p(x+t)}{4}. \quad (5.24)$$

From formula (5.24), it follows that, when resonance conditions are fulfilled, the wave perturbation comprises three components. The first component represents a wave of amplitude, increasing linearly with time, and the growth rate of the amplitude is proportional to the derivative of the distribution of pressure in space. The other two components describe waves of insignificant and fixed amplitudes.

For definiteness, we shall further consider the distribution of pressure in space in formula (5.22) to have a Gaussian form:

$$p(z) = p_0 \exp \left\{ -\frac{z^2}{a^2} \right\}, \quad (5.25)$$

where p_0 is the pressure amplitude. Figure 5.10 presents the example of the movement of an atmospheric perturbation (in the region of a local enhancement of pressure) and of the evolution of waves, generated by this perturbation. The calculation is performed in accordance with formula (5.23) for three different velocities of the perturbation. From the figure, it is seen that below the critical velocity ($V = 0.75$), immediately under the atmospheric perturbation, a similar in shape, but opposite in sign, perturbation forms of the water surface—an induced wave. Moreover, there arise two free waves, traveling in opposite directions, and the one propagating in the same direction as the atmospheric perturbation has a larger amplitude, while its polarity is opposite to the polarity of the induced wave. When $V \ll 1$, the amplitude and polarity of the induced wave are in accordance with the values determined by the inverse barometer law. Practically, all atmospheric processes in open ocean serve as natural prototypes for slowly propagating atmospheric perturbations. Thus, for instance, the propagation velocity of a tropical cyclone usually amounts to $V \sim 5\text{--}10\text{ m/s}$, which is significantly inferior to the propagation velocity of long waves at large depths $\sqrt{gH} \sim 200\text{ m/s}$ (for $H = 4000\text{ m}$).

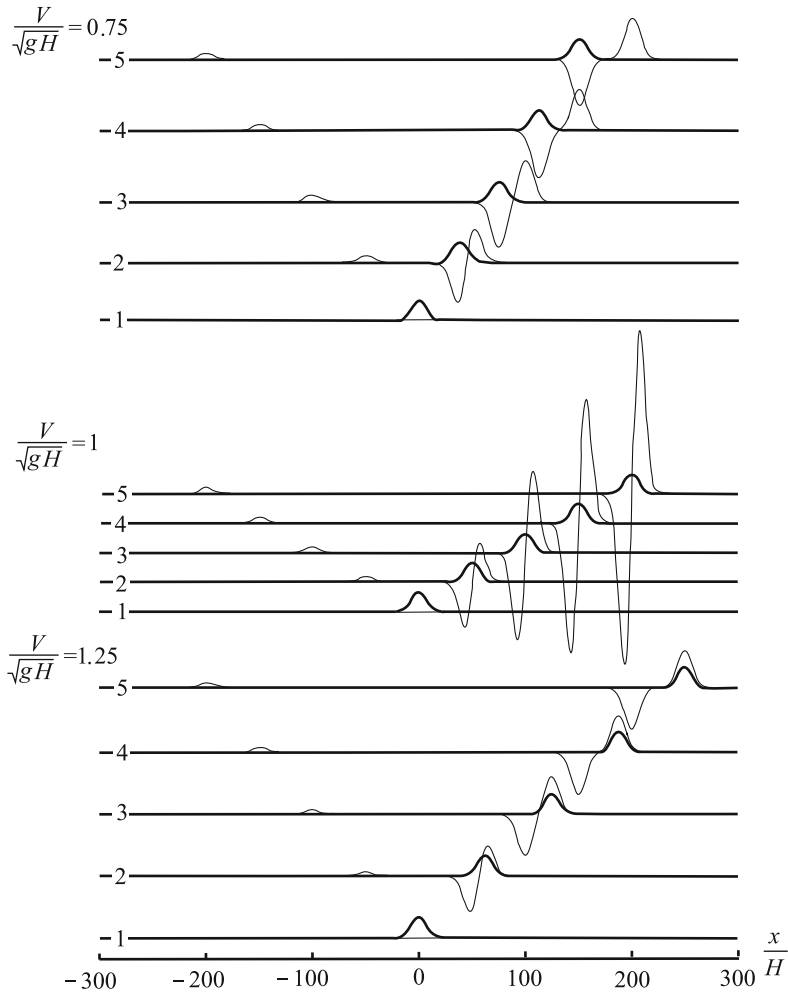
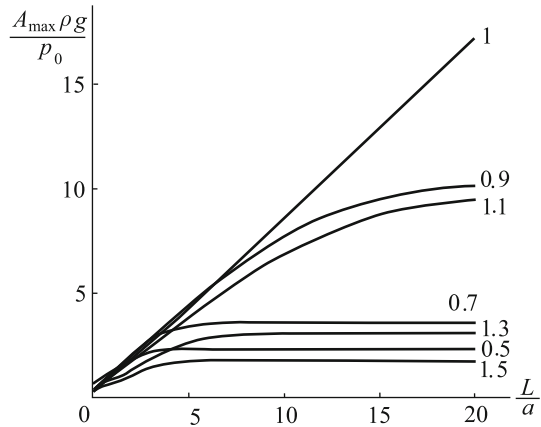


Fig. 5.10 Profiles on free water surface of waves (*thin line*), formed by perturbation of atmospheric pressure (*thick line*), traveling with a velocity V . The calculation is performed at $a = 10$ for fixed time moments $t\sqrt{gH} = 0, 50, 100, 150, 200$ (*curves 1–5*)

In the case of resonance ($V = 1$), only two waves are observed on the water surface. The induced wave follows the atmospheric perturbation, linearly increasing its amplitude with time. The second wave is free. It travels in the opposite direction, and its amplitude is small. We underline that within the framework of the model problem considered, the amplitude of the induced wave grows without limit. Fulfillment of the resonance conditions is possible, for example, in shallow water ($H \sim 10\text{--}100\text{ m}$), where the velocity of long waves ($\sqrt{gH} \sim 10\text{--}30\text{ m/s}$) may turn out to be close to the typical propagation velocity of atmospheric perturbations.

Fig. 5.11 Amplitude (range) of waves on water surface versus distance $L = Vt$, covered by perturbation of atmospheric pressure of amplitude p_0 and with horizontal dimension a . The calculation is performed for different propagation velocities of the atmospheric perturbation. The numbers indicate values of dimensionless velocity V/\sqrt{gH} for respective curves



If the velocity V exceeds the critical velocity (in Fig. 5.10, the case of $V = 1.25$ is presented), then the induced wave turns out to be similar in shape and sign to the perturbation of atmospheric pressure. The polarity of the free wave, traveling in the same direction as the atmospheric perturbation, differs in polarity from the induced wave. The free wave, traveling in the opposite direction, here, like in all other cases, repeats the polarity of the atmospheric perturbation. From formula (5.23), it is seen that at high velocities V the amplitude of the free surface response tends asymptotically toward zero. Note that the similar dependence (3.94) for waves generated by a running landslide of the ocean bottom exhibits a somewhat different character: at high velocities V , the surface displacement tends toward a constant, instead of zero. In reality, the pressure perturbations, corresponding to the velocity range $V \gg 1$, may be related, for example, to acoustic waves in the atmosphere or to the propagation of atmospheric internal waves above shallow-water areas.

Figure 5.11 illustrates the character of variation of the double amplitude of waves on the water surface versus the distance covered by the atmospheric perturbation, $L = Vt$. The double amplitude is calculated by the formula

$$A_{\max}(x) = \max_t \left(\xi(x, t) \right) - \min_t \left(\xi(x, t) \right). \tag{5.26}$$

From the figure, it is seen that for a noticeable increase in the amplitude, it is necessary that the resonance condition be fulfilled along a path the length of which holds several horizontal extensions of the atmospheric perturbation. If the velocity $V \neq 1$, then the growth of the amplitude is limited. At any rate, at the initial stage of wave formation, when $V \approx 1$, the growth rate of the amplitude does not differ strongly from the resonance case. Therefore, if the velocity of the atmospheric perturbation, V , varies within limits $\pm 10\%$ of the resonance velocity, then a tenfold increase is possible of the wave perturbation amplitude as compared with the value determined by the inverse barometer law.

One of the most important properties of meteotsunamis is the proportionality of the wave amplification coefficient to the ratio of the length of the “resonance” area of water and the horizontal size of the atmospheric perturbation. Taking advantage of this property, it is possible to determine in advance the sections of the coast, potentially endangered by meteotsunamis. To this end, it is necessary to analyze the littoral bathymetry and to reveal extended shelf zones, within which the resonance conditions can be fulfilled. For this work, it is, naturally, necessary to know the characteristic propagation velocities of atmospheric perturbations.

Since typical propagation velocities of atmospheric perturbations amount are from units to tens of meters per second, fulfillment of the Proudman resonance conditions is most probable in shallow-water areas of the ocean. But, when meteotsunamis of significant amplitude are excited within shallow-water areas, linear theory is no longer applicable. Therefore, it is expedient to consider the problem of wave generation by atmospheric perturbations within the framework of nonlinear theory of long waves. We shall now assume that the displacement amplitude of the free water surface may be comparable to the basin depth, i.e., the main parameters of the problem are related as follows: $|\xi| \sim H \ll a$. We shall write the equations of nonlinear theory of long waves in dimensionless variables, bearing in mind the formulae (5.19),

$$\frac{\partial u}{\partial t} + u \frac{\partial u}{\partial x} + g \frac{\partial \xi}{\partial x} = - \frac{\partial p_{\text{atm}}}{\partial x}, \quad (5.27)$$

$$\frac{\partial \xi}{\partial t} + \frac{\partial}{\partial x} ((1 + \xi) u) = 0. \quad (5.28)$$

It is not possible to resolve the complete nonlinear problem (5.27) and (5.28) analytically. But, when movement of the atmospheric perturbation is not limited in time ($-\infty < t < +\infty$), it is possible to obtain an analytical relationship between the free surface displacement in the induced wave and the perturbation of atmospheric pressure.

Like in the linear problem, we shall consider a perturbation of the atmospheric pressure (deviation from a certain standard value), which propagates with a constant velocity V in the positive direction of axis Ox ,

$$p_{\text{atm}}(x, t) = p(x - Vt). \quad (5.29)$$

We shall assume the response of the water column to represent an induced wave, traveling with the velocity V in the same direction,

$$u(x, t) = u(x - Vt), \quad (5.30)$$

$$\xi(x, t) = \xi(x - Vt). \quad (5.31)$$

Successive differentiation with respect to time and integration over space of functions with arguments of the form $(x - Vt)$ is similar to multiplication by the quantity $-V$,

$$\int \frac{\partial}{\partial t} f(x - Vt) dx = -Vf(x - Vt).$$

Making use of this fact, we pass from differential equations (5.27) and (5.28) to the algebraic relations (Pelinovsky et al. 2001)

$$-Vu + \frac{u^2}{2} + \xi = -p_{\text{atm}}, \quad (5.32)$$

$$-V\xi + (1 + \xi)u = 0. \quad (5.33)$$

Generally speaking, expressions (5.32) and (5.33) are correct with an accuracy up to certain integration constants. We have chosen the values of these constants so as to have zero flow velocities and zero free surface displacements $u = 0$, $\xi = 0$, respectively, to correspond to zero perturbation of the atmospheric pressure.

Excluding the quantity u from the set of Eqs. (5.32) and (5.33), we obtain the relationship between the moving perturbation of atmospheric pressure and the free water surface response, corresponding to it,

$$p_{\text{atm}} = V^2 \left(\frac{\xi}{1 + \xi} - \frac{\xi^2}{2(1 + \xi)^2} \right) - \xi. \quad (5.34)$$

When $\xi \ll 1$, the problem considered reduces to the linear problem. In this case, formula (5.34) can be written in the form

$$\xi = \frac{p_{\text{atm}}}{V^2 - 1}, \quad (5.35)$$

which fully corresponds to the first term in the analytical solution of the linear problem (5.23).

The free surface displacement ξ can also be expressed explicitly in the nonlinear case via the perturbation of pressure p_{atm} . Equation (5.34) has three solutions, and some of them have no physical sense in the case of certain values of quantities p_{atm} and V . Moreover, the form of the solutions is determined by quite cumbersome formulae. In this connection, it is much more simple to select a certain free surface displacement and, by applying the unambiguous functional relationship (5.34), to determine the pressure perturbation, which could have caused this displacement.

For definiteness, we shall assume the free surface displacement to be determined by the function

$$\xi(x, t) = A_{\text{max}} \exp \left\{ -\frac{(x - Vt)^2}{a^2} \right\}.$$

The perturbation of pressure, corresponding to it, which can be calculated by formula (5.34) in the vicinity of the resonance or for large values of the quantity A_{max} , generally speaking has a form essentially differing from a Gaussian. Therefore, it has sense to introduce a certain quantity p_{max} , characterizing the intensity of

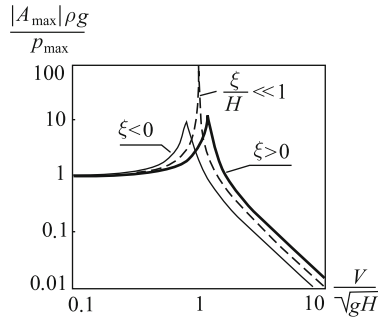


Fig. 5.12 Ratio of free surface displacement amplitude A_{\max} and amplitude of atmospheric pressure perturbation, p_{\max} , versus propagation velocity of atmospheric perturbation. The calculation is performed for positive ($A_{\max}/H = 0.25$), negative ($A_{\max}/H = -0.25$), and infinitesimal (dotted line) displacements of the free surface

pressure variations. Let p_{\max} denote the amplitude of pressure variations, understood in the sense of formula (5.26). The ratio of quantities A_{\max} and p_{\max} (in dimensionless form $A_{\max} \rho g / p_{\max}$) represents the “amplification coefficient” of the wave amplitude.

In Fig. 5.12, the quantity $A_{\max} \rho g / p_{\max}$ is plotted against the propagation velocity V of the atmospheric perturbation. The dotted line in the figure shows the dependence, corresponding to linear theory and calculated with the use of formula (5.35). The amplification coefficient is seen to depend, in accordance with nonlinear theory, not only on the velocity V , but also on the sign of the wave, produced, also. For positive waves, the Proudman resonance point turns out to be shifted to the right as compared with the linear case, while in the case of negative perturbations to the left. Moreover, the growth of the wave amplitude for any fixed values of velocity V turns out to be limited. This fact is a most important manifestation of nonlinearity in the problem dealt with. Let us briefly dwell upon its physical interpretation. Consider the resonance condition $V^2/gH = 1$ to be fulfilled, starting from a certain moment of time. Then, at the initial stage, in accordance with linear theory, an increase in the amplitude of the free surface perturbation will take place. But, as soon as the quantity ξ reaches sufficiently high values, the actual basin depth, present in the resonance condition, will change from H to $H \pm \xi$. As a result, the resonance condition will be violated, and growth of the amplitude will stop. Further enhancement of the amplitude is possible in certain cases, when the resonance conditions are continuously corrected by variation of the velocity V or by realization of a certain particular profile of depths along the route.

5.4 Cosmogenic Tsunamis

Recently, particular interest has been shown in the possibility of catastrophic tsunami waves arising due to bodies falling into the ocean from outer space (Toon et al. 1997;

Ward and Asphaug 2000; Kharif and Pelinovsky 2005; Gusiakov 2007; Bryant et al. 2007; Gisler et al. 2011; Kozelkov et al. 2015).

Such waves are conventionally termed cosmogenic tsunamis in modern scientific literature. Geological structures, reminiscent in shape of craters and found on all continents, have been understood to be traces of collisions of meteor bodies with the Earth only during the past 30–40 years. Such structures called astroblems—star scars, contain rock that was produced under huge pressures (up to a million atmospheric pressures) and exhibit signs of shock-wave transformations of the mineral components and are often related to diamond deposits. According to Expert Database on Earth Impact Structures (<http://tsun.sccc.ru/nh/impact.php>), at present, on Earth, more than one thousand such objects have been found (e.g., Arizona crater, USA, 1.2 km; (Popigai astroblem, East Siberia, Russia, 100 km). The World Ocean occupies approximately 2/3 of the surface of our planet; therefore, a great part of meteorites falls precisely into the ocean, the bottom of which guards the traces of many such collisions, that in the past caused catastrophes of a planetary scale (Kharif and Pelinovsky 2005).

Since in this section we are entering into a field far from oceanology, we shall define some concepts. *Meteorites* are the remains of *meteor bodies*, which survived transition through the atmosphere and that have fallen to the Earth's surface from outer space. According to their composition, meteorites are divided into three main classes: stony (93.3 %), stony-iron (1.3 %), and iron (5.4 %). the atmosphere, air resistance causes the body to heat up strongly and to shine brightly (the *bolide* phenomenon). According to modern ideas, meteorites are fragments of parent bodies—asteroids. *Asteroids* are considered small planets of diameters approximately between 1 and 1000 km.

The task of describing cosmogenic tsunamis can be divided into three stages. First, it is necessary to determine the characteristics (dimensions, density, and velocity) of meteorites, which can fall into the ocean, and to estimate the probability of such an event. Second, the essentially nonlinear process of interaction of a meteorite with the water column must be described, and the relationship between parameters of the initial perturbation of the water column and characteristics of the celestial body must be revealed. At the third stage, an analysis must be performed of the peculiarities of cosmogenic tsunami propagation in open ocean and of waves running up shores. All three stages are connected with numerous uncertainties, which arise primarily because no cosmogenic tsunami has been recorded yet.

Estimates made by specialists reveal that several thousand large objects (asteroids and comets) of diameters over 1 km have a potential possibility of colliding with our planet (Solem 1999). A cosmic body of size superior to 2 km colliding with the Earth will result in a global catastrophe (Paine 1999). Luckily, the probability of such a collision is extremely small, and in all written history of the existence of mankind no such catastrophe occurred. Objects of relatively small dimensions regularly bombard the Earth, but most of them are destroyed and already burn up in the upper layers of the atmosphere. The critical for a stony meteor body size, with which it is capable of reaching the Earth's surface, amounts to about 100 m in

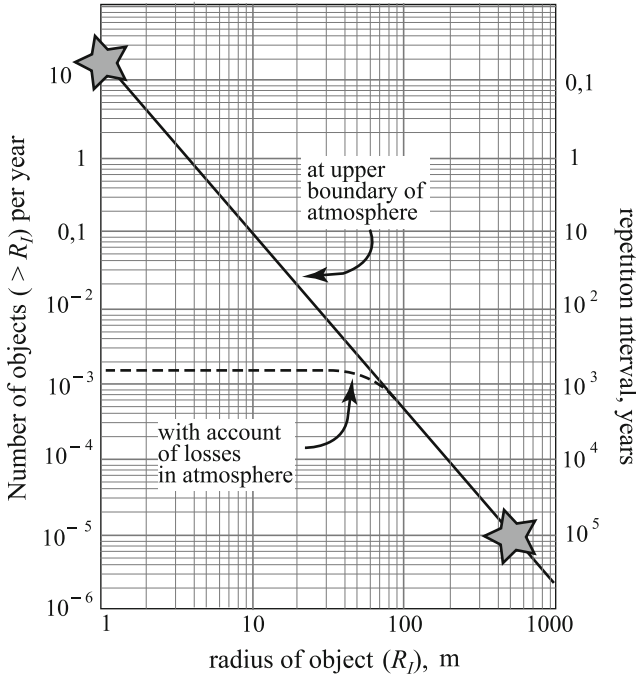


Fig. 5.13 Number of asteroids colliding with the Earth per year versus their radius. *Dotted line* a number of objects reaching the Earth’s surface (with account of losses in the atmosphere). *Stars* show the results of Nemtchinov et al. (1997) and Shoemaker et al. (1990). Adapted from Ward and Asphaug (2000)

diameter. In the case of iron objects, this critical size is significantly smaller (~ 1 m), but they are encountered very rarely, so they will not be dealt with.

From Fig. 5.13, one can judge the collision probability of a celestial body with the Earth depending on the radius of the object. This dependence has been obtained in Ward and Asphaug (2000). Actually, it represents a straight line (in logarithmic scale), which passes through the two points indicated in the figure by stars. The first point is based on existing material—observations from geostationary satellites of meteor bodies with dimensions ~ 1 m exploding in the atmosphere. These data permit to assert that on the average about 25 events of this kind take place in a year (Nemtchinov et al. 1997). The second point is based on estimations of the collision frequency of the Earth with large objects (~ 1 km), made in Shoemaker et al. (1990) and Toon et al. (1994). Large objects collide with our planet approximately once every 100,000 years. The authors of Ward and Asphaug (2000) point out that

the dependence presented in Fig. 5.13 is not quite accurate, but that it is the best estimate of all, which could be made for objects with radiuses of 1–1000 m, using presently available information. The actual collision frequency of the Earth with celestial bodies within the range of dimensions indicated may differ by a factor of 3 as compared to the dependence proposed.

The dotted line in Fig. 5.13 shows the number of objects, which are not destroyed in the atmosphere and are capable of reaching the Earth's surface. From the point of view of tsunami generation, we will be interested precisely in these objects, since they are capable of effectively influencing the water column. Of course, large meteor bodies, exploding in the atmosphere at small heights (such as the Tungus meteorite, 1908) over the surface of the ocean, are probably also capable of causing gravitational waves, but, most likely, their energy will be insufficient for exciting dangerous tsunami waves.

The typical density of stony asteroids amounts to about 3000 kg/m^3 , and their velocity to 20 km/s. Assuming the object to have a spherical shape, it is easy to estimate its kinetic energy. Thus, for example, a meteor body of diameter 100 m will have a kinetic energy $\approx 3 \times 10^{17} \text{ J}$. This value corresponds to the energy of a very strong seismotectonic tsunami (see Fig. 2.18). Now, if the diameter of the object amounts to 1 km, then its energy will be colossal, $\approx 3 \times 10^{20} \text{ J}$. This value is already many times greater than the energy of the source of the strongest earthquake of the 20th century, which occurred in Chile in 1960. It is not difficult to estimate that such an energy is sufficient to evaporate 10^{11} m^3 of water (the heat required to evaporate water is $2.3 \times 10^6 \text{ J/kg}$). It is interesting to note that precisely such a volume of water is ousted by ocean bottom deformations in the case of very strong earthquakes (source area of $1000 \times 100 \text{ km}$, average vertical deformation of bottom of 1 m). At any rate, a relatively small part of the energy is, most likely, spent on the evaporation of water.

Following Ward and Asphaug (2002), we shall assume a meteorite falling into the ocean to create, at the initial stage, a radially symmetric cavity, described by the following function:

$$\xi_0(r) = D_C \left(\frac{r^2}{R_C^2} - 1 \right) \left(1 - \theta(r - R_D) \right), \quad (5.36)$$

where D_C is the depth of the cavity, R_C and R_D are its internal and external radiuses, respectively, and θ is the Heaviside step function. The case, when $R_D = R_C$, corresponds to water being released into the atmosphere (or to its evaporation). The initial perturbation, here, represents a depression (Fig. 5.14a). When $R_D = R_C\sqrt{2}$, the water ejected from the cavity forms an external circular structure (a splash or circular swell), the volume of which is exactly equal to the volume of the water, ejected from the cavity (Fig. 5.14b).

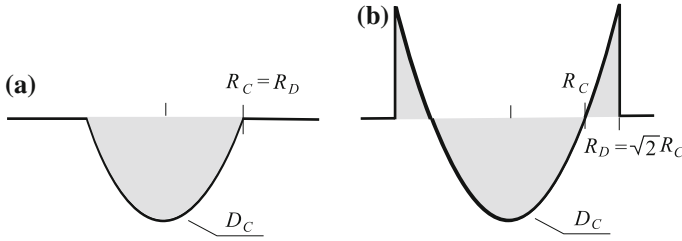


Fig. 5.14 Model shape of perturbation (cavity), resulting from a meteorite falling into the ocean. D_C depth of cavity, R_C and R_D internal and external radiuses of cavity. Adapted from Ward and Asphaug (2000)

From the shape of the cavity, it is possible to estimate the tsunami energy as the potential energy of the initial elevation,

$$E_T = \frac{\pi \rho_w g}{2} (D_C R_D)^2 \left(1 - \frac{R_D^2}{R_C^2} + \frac{R_D^4}{3R_C^4} \right), \quad (5.37)$$

where ρ_w is the density of water, g is the acceleration of gravity. When $R_D = R_C \sqrt{2}$, the general formula (5.37) assumes the more simple form

$$E_T = \frac{\pi \rho_w g}{3} (D_C R_C)^2. \quad (5.38)$$

Only a fraction ε of the meteorite's kinetic energy E_I is transformed into the tsunami energy, so we can write

$$E_T = \varepsilon E_I = \varepsilon \frac{\rho_I (4\pi/3) R_I^3 V_I^2}{2}, \quad (5.39)$$

where ρ_I , R_I , and V_I are the meteorite density, radius, and velocity, respectively. The part of the meteorite energy transferred to the tsunami is not, generally speaking, a constant, but depends on the properties of the water column and of the falling body.

Comparison of expressions (5.38) and (5.39) permits to express the depth of the cavity as follows:

$$D_C = \left(\frac{2\varepsilon \rho_I R_I^3 V_I^2}{\rho_w g R_C^2} \right)^{1/2}. \quad (5.40)$$

We further assume the relationship between the depth of the cavity and its radius to be of the form

$$D_C = q R_C^\alpha, \quad (5.41)$$

where q and α are coefficients related to the properties of the meteorite and of the water column. Substitution of relation (5.41) into formula (5.40) permits to express the radius of the cavity as follows:

$$R_C = R_I \left(2\varepsilon \frac{V_I^2}{gR_I} \right)^\delta \left(\frac{\rho_I}{\rho_w} \right)^{1/3} \left(\left(\frac{\rho_w}{\rho_I} \right)^{1/3-\delta} \left(\frac{1}{q R_I^{\alpha-1}} \right)^{2\delta} \right), \quad (5.42)$$

where $\delta = 1/(2\alpha + 2)$. The form of formula (5.42) corresponds to the known relation for the radius (diameter) of a crater Schmidt and Holsapple (1982)

$$R_C^{SH} = R_I \left(\frac{1}{3.22} \frac{V_I^2}{gR_I} \right)^\beta \left(\frac{\rho_I}{\rho_T} \right)^{1/3} \left(\frac{C_T}{1.24} \right), \quad (5.43)$$

where β and C_T are parameters depending on the properties of the target (water, in this case). For water, their values are $\beta \approx 0.22$ (i.e., $\alpha = 1/(2\beta) - 1 \approx 1.27$), $C_T \approx 1.88$. By comparison of formulae (5.42) and (5.43), one can note that about 16% of the kinetic energy of the falling body is transformed into tsunami energy ($\varepsilon = 1/(2 \cdot 3.22) \approx 0.16$). Of course, this is an approximate estimate, and it is correct only if the quantity ε is actually not subject to strong variations.

The quantity q present in formula (5.41) varies weakly with the size of the falling celestial body, R_I , and of the density ratio ρ_I/ρ_w . By comparison of formulae (5.42) and (5.43), it is not difficult to obtain the following approximate dependence:

$$q \approx 0.39 \left(\frac{\rho_w}{\rho_I} \right)^{0.26} \frac{1}{R_I^{0.27}}. \quad (5.44)$$

In the case, when the density of the celestial body is three times that of the density of water, ($\rho_I/\rho_w = 3$), the value of q varies between 0.1 ($R_I = 50$ m) and 0.054 ($R_I = 500$ m).

To simplify the calculations, it is possible, instead of the cumbersome expressions (5.41) and (5.43) to use approximate formulae, which are valid for $V_I = 20$ km/s and $\rho_I/\rho_w = 3$ (Ward and Asphaug 2002),

$$R_C \approx 98 \cdot R_I^{3/4}, \quad (5.45)$$

$$D_C \approx 0.64 \cdot R_C. \quad (5.46)$$

In Fig. 5.15, the dependences (5.41) and (5.43) are shown by solid lines, the approximate relationships (5.45), and (5.46) by dotted lines. The cavity diameter is usually 2.5–3 times greater than its depth. Thus, for example, a cosmic body of radius 200 m falling into the ocean creates a cavity of diameter about 10 km and depth of the order of 3.5 km. Note that in the case of celestial bodies of radius $R_I > 300$ m the calculated cavity depth D_C will, as a rule, exceed the ocean depth H . In this case, a crater will

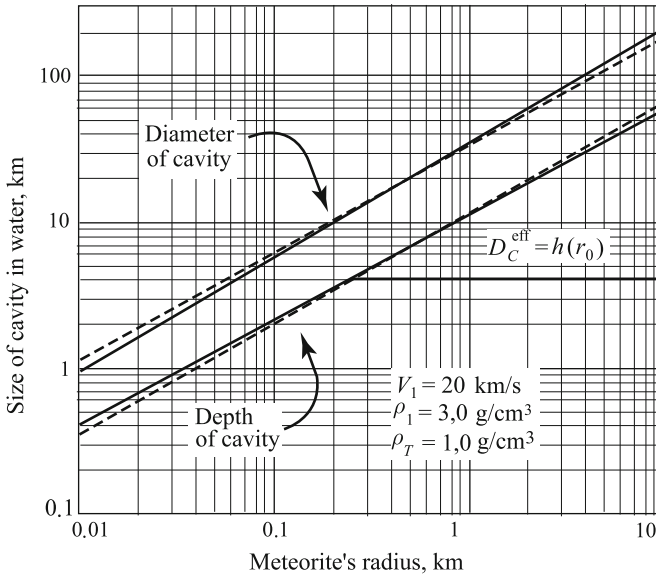


Fig. 5.15 Size of cavity (depth and diameter), produced in water by a falling meteorite, versus the meteorite's radius. Adapted from Ward and Asphaug (2002)

not only form in the water, but in the ocean bottom, also. To avoid overcomplicating the problem, we shall further assume an effective cavity depth D_C^{eff} , equal to the ocean depth, to be applicable, when $D_C > H$. The cavity radius is calculated as previously, in this case.

Figure 5.16 presents a comparison of cavity shapes calculated using the proposed parametrization (5.41) and (5.43) and obtained by detailed numerical simulation of the process, performed in Crawford and Mader (1998). The complex nonlinear model and the parameterizations proposed are seen to be in quite reasonable agreement. Noticeable divergence is only observed in the external circular structure, but for performing tsunami calculations at a level of estimations, it is not too important. Owing to dispersion and dissipation, the shortwave components making up the external circular structure will not play any noticeable role at large distances from the source.

At the next stage, we must describe the evolution of waves from the initial perturbation (5.36), generated by the celestial body. We assume that at the moment, when the cavity and circular swell behind it have formed, the velocity of motion of water particles can be neglected. To describe the waves, we take advantage of linear potential theory. In this problem, it is essential to take into account phase dispersion, so application of the long-wave approximation is not permitted. Note that owing to the large wave amplitudes (comparable to the depth), the application of linear theory is also not quite correct. But for approximate estimation of the properties of a cosmogenic tsunami, such an approach is quite justified.

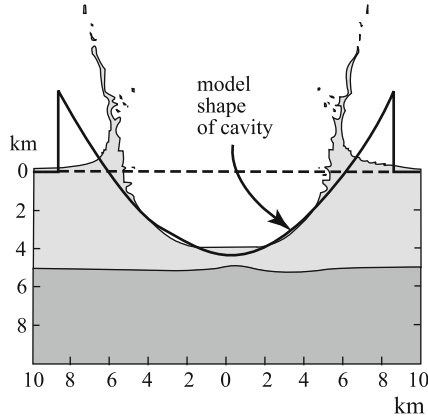


Fig. 5.16 Shape of cavity formed in water by a falling meteorite: comparison of results of numerical simulation (Crawford and Mader 1998) and of idealized model (formula (5.36) with account of relations (5.41) and (5.43)). Calculations are performed for a time moment of 25 s, an asteroid diameter of 500 m, a fall velocity of 20 km/s, a density of 3.32 g/cm³, ocean depth of 5 km. Adapted from Ward and Asphaug (2000)

In the case of an ocean of constant depth, evolution of the initial free surface perturbation, exhibiting radial symmetry, is described by the following expression (see general theory in Sect. 3.2.2):

$$\xi(r, t) = \int_0^\infty k dk A(k) J_0(kr) \cos(\omega(k) t), \tag{5.47}$$

$$A(k) = \int_0^\infty r dr \xi_0(r) J_0(kr), \tag{5.48}$$

where $\xi_0(r)$ is the function describing the form of the initial perturbation and J_0 is the Bessel function of the first kind of zeroth order. The relation between the cyclic frequency and the wave number is determined by the known dispersion relation for gravitational waves on water, $\omega^2 = gk \tanh(kH)$. For an initial perturbation, determined by formula (5.36), the Fourier-Bessel transformation (5.48) yields the following form for the dependence of the amplitude of space harmonics upon the wave number:

$$A(k) = D_C \frac{R_D \left((R_D^2 - R_C^2) k J_1(k R_D) - 2 R_D J_2(k R_D) \right)}{R_C^2 k^2}. \tag{5.49}$$

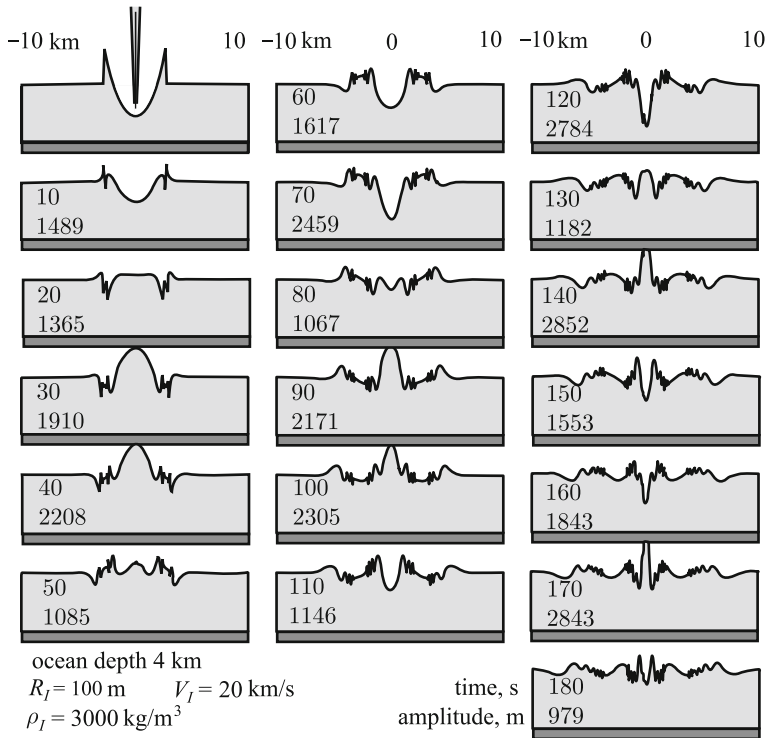


Fig. 5.17 Dynamics of wave perturbation in the vicinity of the incidence point of a meteorite during the first 3 min. Adapted from Ward and Asphaug (2000)

Figure 5.17 presents the example of a calculation of waves caused by the fall into an ocean 4 km deep of a celestial body of radius 100 m and density 3000 kg/m^3 , moving with a velocity of 20 km/s. It is seen that during the first minutes after the fall the waves in the immediate vicinity of the incidence point may reach colossal heights of the order of 1 km and more. Figure 5.18 presents in dimensionless coordinates the wave number dependences of phase and group velocities of surface gravitational waves on water. The same plot shows the amplitude distribution of space harmonics over the wave numbers, calculated in accordance with the form of the initial perturbation (5.36) for an internal cavity radius equal to the ocean depth. The amplitude distribution is determined by function $|k A(k)|$, where $A(k)$ is given by formula (5.49). The position of the space spectrum on the wave number axis is related in an evident manner to the cavity radius. Therefore, on the basis of calculations for $R_C = H$, from which the maximum turns out to be located at the value $kH \approx 2.97$, it is possible to write the formula determining the position of the maximum as function of the cavity radius, $k_{\text{max}} \approx 2.97/R_C$. Recalculation for the wave lengths reveals

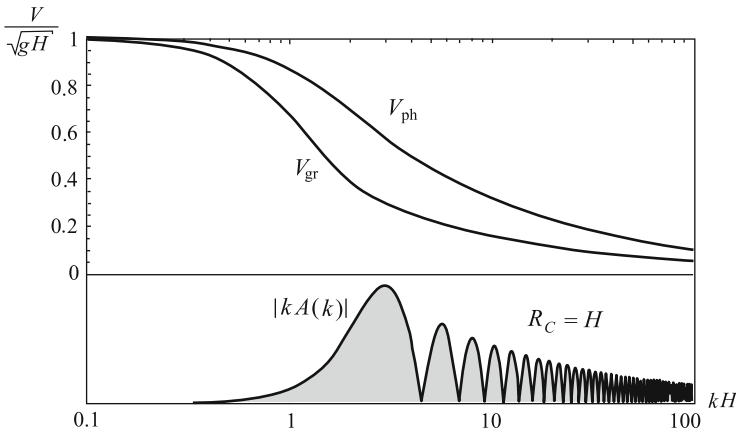


Fig. 5.18 Phase and group velocities of gravitational waves on water versus the wave number, space spectrum (absolute value of function $kA(k)$)

this to correspond to $\lambda_{\max} \approx 2.12R_C$, which somewhat exceeds the cavity diameter. Taking advantage of the dispersion relation, it is not difficult to determine the period corresponding to the maximum of the spectrum, $T_{\max} = 2\pi/\sqrt{gk_{\max} \tanh(k_{\max}H)}$. For typical values of $R_C = H = 5\text{ km}$, the period amounts to $T_{\max} \approx 83\text{ s}$. We recall that the range of tsunami wave periods is $10^2\text{--}10^4\text{ s}$. The orders of magnitude of wave periods caused by falling meteorites can be seen to correspond to the most short-period region of the tsunami spectrum. This fact is essentially reflected in the character of cosmogenic tsunami propagation. Unlike waves of seismotectonic origin, cosmogenic tsunamis have no fronts propagating with the velocity of long waves, \sqrt{gH} . From Fig. 5.18, their spectrum is seen just not to contain components of the necessary wavelength ($kH < 0.1$). As to the components carrying energy, they will propagate significantly slower (about two times slower in the case of $R_C = H$) than usual seismotectonic tsunamis.

Straightforward calculation of waves for long times, the results of which are shown in Fig. 5.19 confirm the arguments, presented above. At the point, corresponding to the position of the front of a long wave, no visible signal is present. The wave packet, in which the long-wave components lead at long times, propagates with a velocity more than 2 times inferior to the velocity of long waves. Here, the amplitude of waves rapidly decreases with time and distance from the area of origin. Thus, while at the third minute after the impact of the celestial body, the amplitude amounts to over 2000m, in 27 min it no longer exceeds 70m. And then, waves of noticeable amplitude only have time to cover 100km. Note that in 27 min long waves cover distances of over 300km.

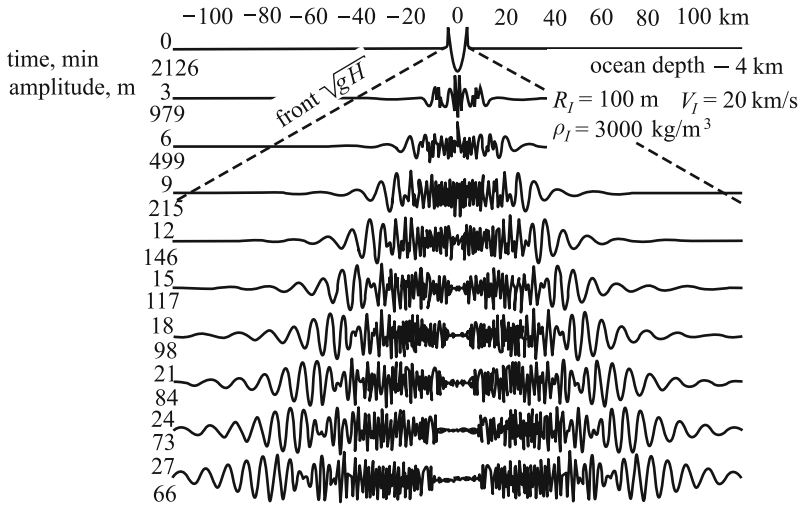


Fig. 5.19 Dynamics of wave perturbation at long times. Adapted from Ward and Asphaug (2000)

Analysis of numerous calculations have permitted the authors of Ward and Asphaug (2000) to propose a formula describing the damping of cosmogenic tsunamis with distance in an ocean of constant depth. These calculations show that variation in the wave amplitude is only related to geometrical factors and phase dispersion. Dissipative factors and the Earth’s sphericity are not taken into account. Moreover, the assumption is made that, independently of the characteristics of the celestial body falling into the ocean, the initial wave amplitude cannot exceed the ocean depth.

$$\xi_{\max}(r) = \min(D_C, H) \left(\frac{1}{1 + r/R_C} \right)^\gamma, \tag{5.50}$$

where $\gamma = 1/2 + 0.575 \exp \{-0.035R_C/H\}$. The dependence (5.50) is shown in Fig. 5.20. It is calculated for various sizes of falling celestial bodies and ocean depths. The data, shown in the figure, permit to estimate the degree of danger (the height of waves) represented by tsunamis of cosmogenic origin at different distances from the point of impact. When one approaches the coast, the wave amplitude (like in all tsunami cases) will increase by several times, owing to a decrease in depth.

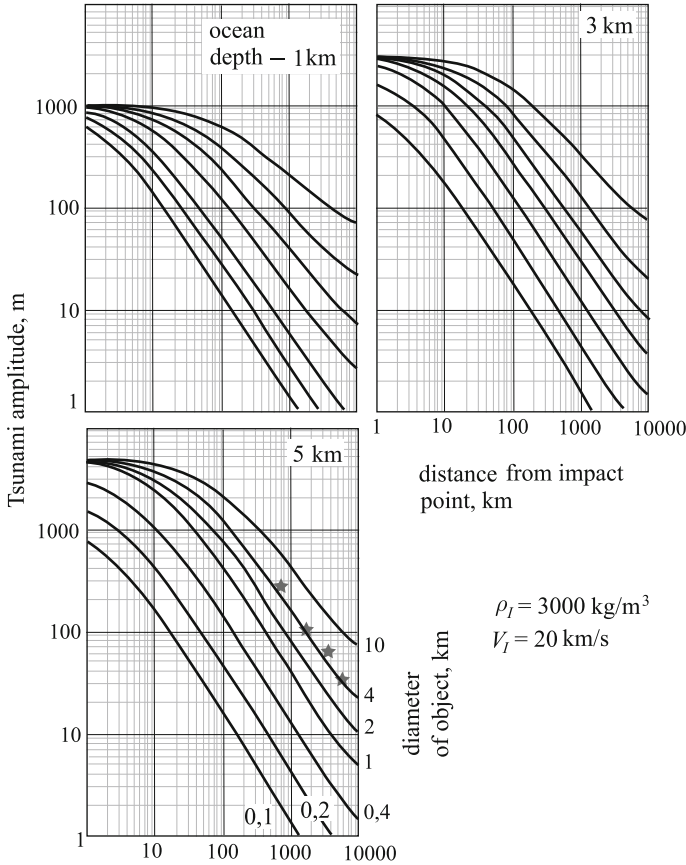


Fig. 5.20 Decrease of cosmogenic tsunami amplitude with distance from impact point of object. Calculations are performed for various sizes of object and ocean depths. Adapted from Ward and Asphaug (2002)

In conclusion, we once again draw attention to the probability of a large meteorite, capable of causing significant tsunami waves, falling on Earth being extremely small. But, if such an event actually does take place, then among other catastrophic consequences tsunami waves will certainly not play the last part.

References

Antonopoulos, J.: The great Minoan eruption of Thera volcano and the ensuing tsunami in the Greek Archipelago. *Nat. Hazards* **5**(2), 153–168 (1992)
 Assier-Rzadkiewicz, S., Heinrich, P., Sabatier, P.C., Savoye, B., Bourillet, J.F.: Numerical modeling of landslide-generated tsunami: the 1979 nice event. *Pure Appl. Geophys.* **157**, 1707–1727 (2000)

- Basov, B.I., Dorfman, A.A., Levin, B.W., Kharlamov, A.A.: On perturbations of the ocean surface, excited by the eruption of an underwater volcano. *Vulcanologia i Seismologia* (in Russian). No. 1, pp. 93–98 (1981)
- Belousov, A., Voight, B., Belousova, M., Muravyev, Y.: Tsunamis generated by subaquatic volcanic explosions: unique data from 1996 Eruption in Karymskoye Lake, Kamchatka, Russia. *Pure Appl. Geophys.* **157**, 1135–1143 (2000)
- Bondarenko, A.L., Bychkov, V.S.: Marine baric waves. *Meteorologia i gidrologia* (in Russian). No. 6, pp. 86–91 (1983)
- Bryant, E.A., Walsh, G., Abbott, D.: Cosmogenic mega-tsunamis in the Australia region: are they supported by Aboriginal and Maori legends? *Faculty of Science-Papers*, 42 (2007)
- Choi, B.H., Pelinovsky, E., Kim, K.O., Lee, J.S.: Simulation of the trans-oceanic tsunami propagation due to the 1883 Krakatau volcanic eruption. *Nat. Hazards Earth Syst. Sci.* **3**, 321–332 (2003)
- Crawford, D.A., Mader, C.: Modeling asteroid impact and tsunami. *Sci. Tsunami Hazards* **16**, 21–30 (1998)
- Didenkulova, I.I., Kurkin, A.A., Pelinovsky, E.N.: Run-up of solitary waves on slopes with different profiles. *Izv. RAN, Atmos. Ocean. Phys.* **43**(3), 384–390 (2007)
- Dominey-Howes, D.: A re-analysis of the Late Bronze age eruption and tsunamis of Santorini, Greece, and the implications for the volcano–tsunami hazard. *J. Volcanol. Geotherm. Res.* **130**(1), 107–132 (2004)
- Donn, W.L., Ewing, M.: Stokes edge waves in Lake Michigan. *Science* **124**, 1238–1242 (1956)
- Egorov, Yu.A.: Hydrodynamic model of tsunami wave generation by eruption of submarine volcano. *Natural catastrophes and disasters in the far-east region. Publishing House of the Far-east Branch of the USSR Academy of Sciences* (in Russian), Vladivostok, vol. 1, pp. 82–93 (1990)
- Egorov, Y.: Tsunami wave generation by the eruption of underwater volcano. *Nat. Hazards Earth Syst. Sci.* **7**, 65–69 (2007)
- Fine, I.V., Rabinovich, A.B., Kulikov, E.A., Thomson, R.E., Bornhold, B.D.: Numerical modeling of landslide-generated tsunamis with application to the Skagway Harbor tsunami of 3 November, 1994. In: *Proceedings of International Conference on Tsunamis, Paris, 26–28 May*, pp. 211–223 (1998)
- Fryer, G.J., Watts, P., Pratson, L.F.: Source of the great tsunami of 1 April 1946: a landslide in the upper Aleutian forearc. *Mar. Geol.* **203**(3), 201–218 (2004)
- Gill A.E.: *Atmosphere and ocean dynamics*. Academic Press, New York (1982)
- Gisler, G., Weaver, R., Gittings, M.: Calculations of asteroid impacts into deep and shallow water. *Pure Appl. Geophys.* **168**(6–7), 1187–1198 (2011)
- Gusiakov, V.K.: “Red”, “green” and “blue” pacific tsunamigenic earthquakes and their relation with conditions of oceanic sedimentation. In: Hebenstreit, G. (ed.) *Tsunamis at the End of a Critical Decade*, pp. 17–32. Kluwer Academic Publishers, Dordrecht (2001)
- Gusiakov, V.K.: Tsunami as a destructive aftermath of oceanic impacts. *Comet/Asteroid Impacts and Human Society*, pp. 247–263. Springer, Berlin (2007)
- Gutenberg, B.: Tsunamis and earthquakes. *Bull. Seismol. Soc. Am.* **29**, 517–526 (1939)
- Harbitz, C.B.: Model simulations of tsunamis generated by the Storegga slides. *Mar. Geol.* **105**, 1–21 (1992)
- Heinrich, P., Piatensi, A., Okal, E., Hébert, H.: Near-field modeling of the 17 July 1998 tsunami in Papua New Guinea. *Geophys. Res. Lett.* **27**, 3037–3040 (2000)
- Hibiya, T., Kajiura, K.: Origin of Abiki phenomena (a kind of seiches) in Nagasaki Bay. *J. Oceanogr. Soc. Jpn.* **38**(3), 172–182 (1982)
- Harbitz, C.B., Lovholt, F., Pedersen, G., Masson, D.G.: Mechanisms of tsunami generation by submarine landslides: a short review. *Nor. Geologisk Tidsskr.* **86**(3), 255 (2006)
- Jansen, E., Befring, S., Bugge, T., et al.: Large submarine slides on the Norwegian continental margin: sediments, transport, and timing. *Mar. Geol.* **78**, 77–107 (1987)
- Jiang, L., LeBlond, P.H.: The coupling of a submarine slide and the surface waves which it generates. *J. Geophys. Res.* **97**(C8), 12731–12744 (1992)

- Jiang, L., LeBlond, P.H.: Three-dimensional modeling of tsunami generation due to a submarine mudslide. *J. Phys. Oceanogr.* **24**(3), 559–572 (1994)
- Imamura, F., Gica, E.C.: Numerical model for tsunami generation due to subaqueous landslide along a coast. *Sci. Tsunami Hazards* **14**(1), 13–28 (1996)
- Imamura, F., Hashi, K., Imteaz Md, M.A.: Modelling for tsunamis generated by landsliding and debris flow. In: Hebenstreit, G.T. (ed.) *Tsunami Research at the End of Critical Decade*, pp. 209–228. Kluwer Academic Publishers, Dordrecht (2001)
- Kharif, Ch., Pelinovsky, E.: Asteroid impact tsunamis. *Comptes Rendus Physique* **6**, 361–366 (2005)
- Kozelkov, A.S., Kurkin, A.A., Pelinovskii, E.N., Kurulin, V.V.: Modeling the cosmogenic tsunami within the framework of the Navier-Stokes equations with sources of different types. *Fluid Dyn.* **50**(2), 306–313 (2015)
- Kovalev, P.D., Rabinovich, A.B., Shevchenko, G.V.: Investigation of long waves in the tsunami frequency band on the southwestern shelf of Kamchatka. *Nat. Hazards* **4**, 141–159 (1991)
- Kulikov, E.A., Rabinovich, A.B., Fine, I.V., Bornhold, B.D., Thomson, R.E.: Tsunami generation by slides on the Pacific coast of North America and the role of tides (in Russian). *Oceanology* **38**(3), 361–367 (1998)
- Kurkin, A.A., Pelinovsky, E.N.: Killer waves: facts, theory and simulation (in Russian). N. Novgorod: Publishing house of Nizhegorod. state Technical University (2004)
- Lander, J.F.: *Tsunamis Affecting Alaska, 1737–1996*. US Department of Community, Boulder (1996)
- Le Mehaute, B., Wang, S.: *Water Waves Generated by Underwater Explosion*. World Science, Singapore (1996)
- Leonidova, N.L.: On the possibility of exciting tsunami waves by muddy flows (in Russian). Works of SakhKNII of Far-East Scientific Center of USSR Academy of Sciences. *Tsunami waves*. No. 29, pp. 262–270. Yuzhno-Sakhalinsk (1972)
- Lichtman, D.L.: *Physics of the atmospheric boundary layer* (in Russian). Hydrometizdat, Leningrad (1970)
- Mader, C.L., Gittings, M.L.: Numerical model for the Krakatoa hydrovolcanic explosion and tsunami. *Sci. Tsunami Hazards* **24**(3), 174–182 (2006)
- Miller, D.J.: The Alaska earthquake on 10 July 1958: giant wave in Lituya Bay. *Bull. Seismol. Soc. Am.* **50**(2), 253–266 (1960)
- Minoura, K., Imamura, F., Kurun, U., et al.: Tsunami hazard associated with explosion-collapse processes of a dome complex on Minoan Thera. *Submarine Landslides and Tsunamis*, pp. 229–236. Kluwer Academic Publishers, Dordrecht (2003)
- Mirchina, N.P., Pelinovsky, E.N.: Dispersive amplification of tsunami waves (in Russian). *Oceanology* **27**(1), 35–40 (1987)
- Mitchel, R.: Submarine landslips of the coasts of Puerto-Rico and Barbados, West-Indies. *Nature* **173**(4394), 119–121 (1954)
- Monserrat, S., Ibbetson, A., Thorpe, A.J.: Atmospheric gravity waves and the “Rissaga” phenomenon. *Q. J. R. Meteorol. Soc.* **117**, 553–570 (1991)
- Monserrat, S., Rabinovich, A.B.: Meteotsunamis: atmospherically induced destructive ocean waves in the tsunami frequency band. *Nat. Hazards Earth Syst. Sci.* **6**(6), 1035–1051 (2006)
- Munk, W.H.: *Long ocean waves. The Sea. Ideas and Observations on Progress in the Study of the Sea*, pp. 647–663. Wiley, New York (1962)
- Murty, T.S.: Seismic sea waves—tsunamis. *Bull. Fish. Res. Board Can. Ott.* **198**, 337 (1977)
- Murty, T.S.: *Storm surges. Meteorological ocean tides*. Department of Fisheries and Oceans, Bulletin 212, Ottawa (1984)
- Nomanbhoy, N., Satake, K.: Generation mechanism of tsunamis from the 1883 Krakatau eruption. *Geophys. Res. Lett.* **22**(4), 509–512 (1995)
- Nemtchinov, I.V., Svetsov, V.V., Kosarev, I.B., et al.: Assessment of kinetic energy of meteoroids detected by satellite-based light sensors. *Icarus* **130**, 259–274 (1997)
- Nomitsu, T.: A theory of tsunamis and seiches produced by wind and barometric gradient. *Met. Coll. Sci. Imp. Univ. Kyoto A* **18**(4), 201–214 (1935)

- Okal, E.A., Synolakis, C.E.: Source discriminants for near-field tsunamis. *Geophys. J. Int.* **158**(3), 899–912 (2004)
- Paine, M.P.: Asteroid impacts: the extra hazard due to tsunamis. *Sci. Tsunami Hazards* **17**(3), 155–166 (1999)
- Paris, R., Switzer, A.D., Belousova, M., Belousov, A., Ontowirjo, B., Whelley, P.L., Ulvrova, M.: Volcanic tsunami: a review of source mechanisms, past events and hazards in Southeast Asia (Indonesia, Philippines, Papua New Guinea). *Nat. Hazards* **70**(1), 447–470 (2014)
- Parlaktuna, H.: Natural gas hydrates as a cause of underwater landslides: a review. *Submarine Landslides and Tsunamis*, pp. 163–169. Kluwer, Dordrecht (2003)
- Pelinovsky, E.N.: Hydrodynamics of tsunami waves (in Russian). Institute of Applied Physics, RAS, Nizhnii Novgorod (1996)
- Pelinovsky, E., Talipova, T., Kurkin, A., Kharif, C.: Nonlinear mechanism of tsunami wave generation by atmospheric disturbances. *Nat. Hazards Earth Syst. Sci.* **1**, 243–250 (2001)
- Rabinovich, A.B.: Long gravitational waves in the ocean: capture, resonance, irradiation (in Russian). *Hydrometeoizdat*, St. Petersburg (1993)
- Rabinovich, A.B., Monserrat, S.: Meteorological tsunamis near the Balearic and Kuril Islands: descriptive and statistical analysis. *Nat. Hazards* **13**, 55–90 (1996)
- Rabinovich, A.B., Thomson, R.E., Kulikov, E.A., et al.: The landslide-generated tsunami of 3 November 1994 in Skagway Harbor, Alaska: a case study. *Geophys. Res. Lett.* **26**(19), 3009–3012 (1999)
- Rabinovich, A.B., Thomson, R.E., Bornhold, B.D., et al.: Numerical modelling of tsunamis generated by hypothetical landslides in the Strait of Georgia, British Columbia. *Pure Appl. Geophys.* **160**(7), 1273–1313 (2003)
- Ren, P., Bornhold, B.D., Prior, D.B.: Seafloor morphology and sedimentary processes, Knight Inlet, British Columbia. *Sediment. Geol.* **103**, 201–228 (1996)
- Self, S., Rampino, M.R.: The 1883 eruption of Krakatau. *Nature* **294**, 699–704 (1981)
- Schmidt, R.M., Holsapple, K.A.: Estimates of crater size for large-body impacts: gravitational scaling results. *GSA Special Paper*, vol. 190, pp. 93–101. GSA, Boulder (1982)
- Shoemaker, E.M., Wolfe, R.F., Shoemaker, C.S.: Asteroid and comet flux in the neighborhood of earth. In: Sharpton, V.L., Ward, P.D. (eds.) *Global Catastrophes in Earth History*. *GSA Special Paper*, vol. 247, pp. 155–170. GSA, Boulder (1990)
- Simpson, J.E.: *Gravity Currents: In the Environment and Laboratory*. Halsted Press, England (1987)
- Solem, J.C.: Comet and asteroid hazards: threat and mitigation. *Sci. Tsunami Hazards* **17**(3), 141–153 (1999)
- Suleimani, E., Nicolisky, D.J., Haeussler, P.J., Hansen, R.: Combined effects of tectonic and landslide-generated tsunami runup at Seward, Alaska during the M w 9.2 1964 earthquake. *Pure Appl. Geophys.* **168**(6–7), 1053–1074 (2011)
- Tappin, D. et al.: Sediment slump likely caused 1998 Papua New Guinea Tsunami. *EOS*, vol. 80, pp. 329, 334, 340 (1998)
- Tappin, D.R., Grilli, S.T., Harris, J.C., Geller, R.J., Masterlark, T., Kirby, J.T., Mai, P.M.: Did a submarine landslide contribute to the 2011 Tohoku tsunami? *Mar. Geol.* **357**, 344–361 (2014)
- Tikhonov, A.N., Samarsky, A.A.: *Equations of mathematical physics* (in Russian). Publishing house of Moscow University (1999)
- Tinti, S., Pagnoni, G., Piatanesi, A.: Simulation of tsunamis induced by volcanic activity in the Gulf of Naples (Italy). *Nat. Hazards Earth Syst. Sci.* **3**, 311–320 (2003)
- Titov, V.V., Gonzalez, F.I.: Numerical study of the source of the 17 July 1998 PNG tsunami. In: Hebenstreit, G.T. (ed.) *Tsunami Research at the End of a Critical Decade*, pp. 197–207. Kluwer, Dordrecht (2001)
- Toon, O.B., Zahnle, K., Turco, R.P., Covey, C.: Environmental perturbations caused by asteroid impacts. In: Gehrels, T. (ed.) *Hazards due to Comets and Asteroids*, pp. 791–826. University of Arizona Press, Tucson (1994)
- Toon, O.B., Zahnle, K., Morrison, D., Turco, R.P., Covey, C.: Environmental perturbations caused by the impacts of asteroids and comets. *Rev. Geophys.* **35**(1), 41–78 (1997)

- Vilibic, I., Domijan, N., Orlic, M., Leder, N., Pasaric, M.: Resonant coupling of a traveling air pressure disturbance with the east Adriatic coastal waters. *J. Geophys. Res.* **109**, C10001 (2004). doi:[10.1029/2004JC002279](https://doi.org/10.1029/2004JC002279)
- Ward, S.N., Asphaug, E.: Asteroid impact tsunami: a probabilistic hazard assessment. *Icarus* **145**, 64–78 (2000)
- Ward, S.N., Asphaug, E.: Impact tsunami—Eltanin. *Deep-Sea Res. Part II* **49**, 1073–1079 (2002)
- Ward, S.N., Day, S.: Cumbre Vieja volcano—potential collapse and tsunami at La Palma, Canary Islands. *Geophys. Res. Lett.* **28**, 397–400 (2001)
- Ward, S.N., Day, S.: Ritter island volcano—lateral collapse and the tsunami of 1888. *Geophys. J. Int.* **154**, 891–902 (2003)
- Waythomas, C.F., Neal, C.A.: Tsunami generation by pyroclastic flow during the 3500-year B.P. caldera-forming eruption of Aniakchak Volcano, Alaska. *Bull. Volcanol.* **60**, 110–124 (1998)
- Wiegel, R.L.: Laboratory studies of gravity waves generated by the movement of a submerged body. *Trans. Am. Geophys. Union* **36**(5), 759–774 (1955)
- Wiegel, R.L., Noda, E.K., Kuba, E.M., et al.: Water waves generated by landslides in reservoirs. *J. Waterw. Harb. Coast. Eng. ASCE* **96**, 307–333 (1970)

Chapter 6

Propagation of a Tsunami in the Ocean and Its Interaction with the Coast

Abstract Traditional ideas of tsunami propagation in the open ocean are dealt with. The significance is estimated of manifestations of phase and amplitude dispersions. Classical problems are considered, concerning variation of the amplitude of a long wave in a basin with gently varying depth (the Green's law) and the reflection of a wave from a step and from a rectangular obstacle. Formulae of the ray method are presented in Cartesian and spherical coordinate systems. Phenomena of long-wave refraction and capture by underwater ridges and the shelf are described. Estimation is performed of linear (viscous) and nonlinear (turbulent) dissipation of the energy of long waves. The effect of a wave amplitude being reduced by scattering on bottom irregularities is considered. Approaches to the numerical simulation of tsunami wave propagation are described. Conventionally applied equations of nonlinear long-wave theory, taking into account the Coriolis force and bottom friction, are presented both in Cartesian and spherical coordinate systems. The technique for formulating initial and boundary conditions in the tsunami propagation problem is described. Brief information is given on certain tsunami models (codes), that are actively applied, at present. Features of transoceanic wave propagation are considered, taking advantage of the December 26, 2004 tsunami as an example. The main results, due to investigation of the issues of a tsunami run-up on the shore, are presented.

Keywords Tsunami propagation · Tsunami run-up · Phase dispersion · Amplitude dispersion · Long-wave theory · Green's law · Refraction · Reflection · Scattering · Trapped waves · Wave attenuation · Numerical tsunami models · Nonlinear long-wave theory · Bottom friction · Coriolis force · Manning coefficient · Cartesian coordinates · Spherical coordinates · Initial elevation · Boundary conditions · Bathymetry · Topography · Waveguide · Breaking waves · Run-up height · Laboratory experiments

The following three stages are traditionally distinguished in the life of a tsunami: generation of the wave, its propagation in open ocean, and its interaction with the coast (run-up). The most simple task is to describe tsunami propagation in the open ocean. In this case, the wave's amplitude $A \sim 10^{-1} - 10^0$ m is significantly smaller than the ocean depth $H \sim 10^3$ m, while the depth, in turn, is much smaller than the wavelength $\lambda = T(gH)^{1/2} \sim 10^4 - 10^6$ m. These two facts permit to apply with success

the simplest linear theory of long waves. At any rate, the manifestations of amplitude and phase dispersion will be insignificant. To describe the run-up of waves is already a more complicated problem pertaining to the class of nonlinear problems in a region with moving boundaries. Indeed, as one approaches the coast, the ocean depth decreases, while the tsunami amplitude increases, so the nonlinearity parameter A/H is no longer a small quantity. Moreover, currents associated with the wave become turbulent, the influence of friction on the seafloor increases, processes resulting in suspension of bottom sediments are activated. A problem of no less complexity is presented by the fact that as the wave propagates over the land, the boundaries of the region, in which the hydrodynamic problem is resolved, alter quite essentially. First of all, this naturally concerns the advancement of the shoreline, but the “water–air” and the “water–bottom” (owing to erosion) boundaries also move. In this chapter, the main physical regularities, determining tsunami propagation in the open ocean and the run-up of waves on a shore, will be dealt with. Significant attention will be devoted to mathematical models, applied in numerical tsunami simulation.

6.1 Traditional Ideas Concerning the Problem of Tsunami Propagation

Right up till the last quarter of the twentieth century all measurements of tsunami waves were performed exclusively by coastal stations. Only during the past decades has the development of engineering reached a level that provides for the possibility of reliable tsunami registration in the open ocean and even at the very source during generation. Measurements of wave parameters, done with the aid of pressure sensors at the ocean bottom (Jacques and Soloviev 1971; Gonzalez et al. 1987; Kulikov and Gonzalez 1995; Milburn et al. 1996; Rabinovich and Eblé 2015), GPS buoys (Kato et al. 2011) and satellite radioaltimeters (Okal et al. 1999; Kulikov et al. 2005) permit to claim with certainty that the amplitude of a tsunami in open ocean, as a rule, lies between several centimeters and several tens of centimeters. In the most strong cases the amplitude of the free water surface displacement in the vicinity of the source may, apparently, reach several meters.

In any case, at great distances from the coast the tsunami amplitude A turns out to be essentially smaller than the ocean depth H . The value of H , in turn, is essentially inferior to the wavelength λ . These two facts permit, in a first approximation, to consider tsunami as long (not subject to dispersion) linear waves, the velocity of which is determined by the simple formula $c = \sqrt{gH}$, where g is the acceleration of gravity. The period of tsunami waves, T , lies within the range 10^2 – 10^4 s. With account of the relationship $\lambda = T\sqrt{gH}$ it is possible to rewrite the condition $\lambda \gg H$ as $T\sqrt{g/H} \gg 1$. It is easy to verify that for the range of periods indicated this condition is always quite satisfied at small (shelf) depths. But for short-period tsunamis, propagating in the open ocean, fulfillment of this condition is not so evident.

The linear theory of long waves, representing the most simple version of a theory of gravitational surface waves on water, serves as quite an applicable approximation for describing the process of tsunami propagation in the open ocean along short routes. But, when waves cover long distances, dispersion and nonlinear effects, that exhibit the property of accumulating, are capable of essentially altering not only the amplitude, but the very structure of the wave perturbation also.

Manifestations of phase dispersion are well observed in measurements of tsunami waves in the open ocean by bottom pressure sensors. In Fig. 6.1 the example is presented of a record of ocean-level variations occurring during the passage of a weak tsunami, caused by an underwater earthquake in Alaska Bay on March 6, 1988 (Milburn et al. 1996). The distance between the earthquake epicenter and the registration point was 978 km. The upper part of the figure shows the original record, in which tidal oscillations of the level prevail. The lower part of the figure presents the filtered signal, from which the tidal component has been removed. From the record two groups of waves are well distinguished. The first group, taking effect practically immediately after the earthquake, represents the response of the pressure sensor to the surface seismic wave. The second group of waves, delayed by over an hour, represents oscillations of the ocean level due to passage of the tsunami. From the tsunami record it is well seen, that at the beginning there are long-period components of the signal, and only subsequently there appear short-period oscillations. This fact is established well by spectral-time analysis, the results of which are shown in Fig. 6.2. The spectral composition of the signal not only changes with time, but the behavior of these changes satisfy the dispersion law for gravitational waves on water (Kulikov and Gonzalez 1995). The dispersion law is shown in the figure by the solid line, calculated by formula $t(\omega) = L/C_{gr}(\omega)$, where L is the distance from the sensor

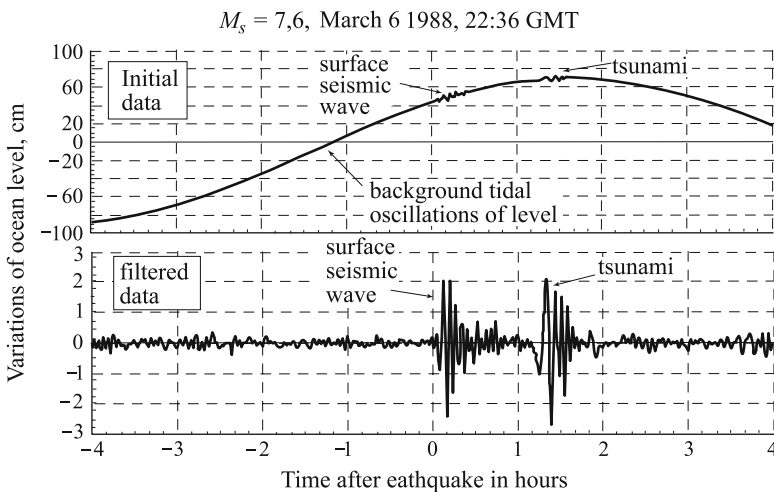


Fig. 6.1 Example of tsunami registration in open ocean by bottom pressure sensor (Adapted from Milburn et al. 1996)

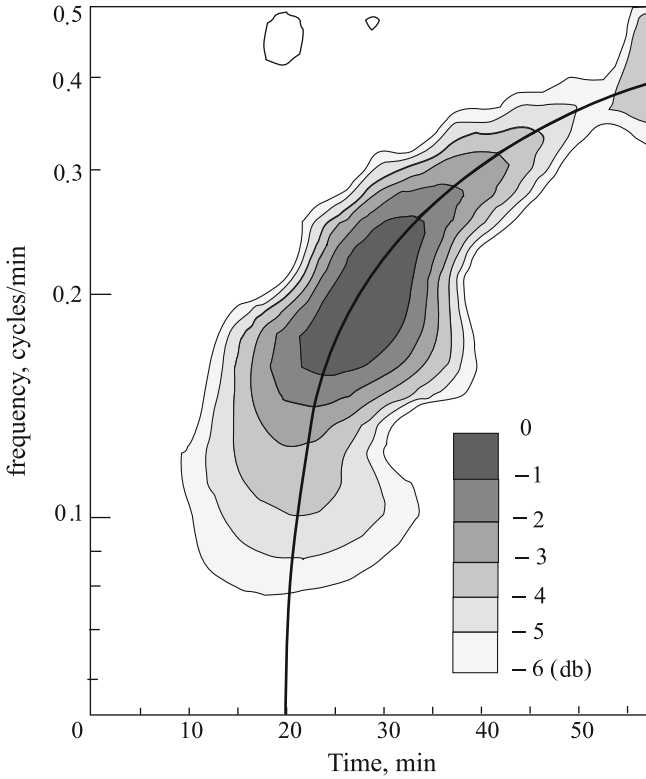


Fig. 6.2 Spectral-time diagram for amplitude of ocean-level oscillations during passage of tsunami of March 6, 1988, tsunami (the record is shown in Fig. 6.1). The *isolines* are drawn in steps of 1 dB. The *solid line* shows theoretical calculation of time spectral components take effect, performed in accordance with the dispersion law for gravitational waves (Adapted from Kulikov and Gonzalez 1995)

to the earthquake epicenter, $C_{gr}(\omega)$ is the group velocity, which is a function of the cyclic frequency ω .

We shall take advantage of the dispersion relation for gravitational surface waves in a liquid, $\omega^2 = gk \tanh(kH)$, where $k = 2\pi/\lambda$ is the wave number according to which the group velocity is determined by the formula

$$C_{gr} = \frac{\partial \omega}{\partial k} = \frac{g \left(\frac{kH}{\cosh^2(kH)} + \tanh(kH) \right)}{2\sqrt{gk \tanh(kH)}}.$$

We recall that in wave physics, besides the group velocity, due to which energy is transported, one also deals with the phase velocity, i.e., the velocity with which the

phase of a wave propagates. The phase velocity of gravitational waves on water is determined by the following expression:

$$C_{ph} = \frac{\omega}{k} = \frac{\sqrt{gk \operatorname{th}(kH)}}{k}.$$

A feature peculiar to gravitational waves is so-called normal dispersion, in the case of which the phase velocity exceeds the group velocity. Moreover, here, both the group and phase velocities are always inferior to the velocity of long waves: $C_{gr} < C_{ph} < \sqrt{gH}$. When the wavelength increases, the group and phase velocities tend asymptotically to a common limit, namely, to the velocity of long waves: $\lim_{kH \rightarrow \infty} C_{gr} = \lim_{kH \rightarrow \infty} C_{ph} = \sqrt{gH}$.

We shall now estimate the distance, at which manifestations of dispersion effects should turn out to be quite significant. The distance of dispersive destruction of a wave, L_{cd} , can be determined as the product of the velocity of long waves by the time, required for a wave packet to lag behind the front at a distance equal to the wavelength (Kulikov et al. 1996),

$$L_{cd} = \frac{\lambda \sqrt{gH}}{\sqrt{gH} - C_{gr}}. \quad (6.1)$$

The following approximate relation follows from formula (6.1), when $\lambda \gg H$:

$$L_{cd} \approx \frac{\lambda^3}{2\pi^2 H^2}. \quad (6.2)$$

For estimates it is often convenient to use the period of a wave, T , instead of its wavelength. The phase velocity of weakly dispersive waves is quite close to the velocity of long waves, so the approximate formula $\lambda \approx T\sqrt{gH}$ holds valid, and taking it into account we obtain from (6.2) the following relationship:

$$L_{cd} \approx \frac{T^3 g^{3/2}}{2\pi^2 H^{1/2}}.$$

This approximate formula can be successfully applied in estimating the dispersive destruction for any values of tsunami periods and ocean depths taken from real natural value ranges. Noticeable deviations from the exact formula (6.1) arise only in the case of small periods and large depths. Thus, for example, in the case of $H = 5$ km and $T = 100$ s the approximate formula only underestimates the value of L_{cd} by 10%.

The dependence (6.1) is presented in Fig. 6.3. The periods of tsunami waves, that vary within limits of 10^2 – 10^4 s, are plotted along the x-axis. Calculations are performed for different depths of the water column (numbers near the curves). The dotted line in the figure shows the length of the Earth's equator, indicating a measure of the limit distance which can be covered by a tsunami wave. For typical depths of the open ocean the whole range of tsunami wave periods can be divided into

two intervals. “Short-period” waves ($T < 10^3$ s), for which the manifestation of dispersion may turn out to be significant, correspond to the first interval. In the second interval ($T > 10^3$ s), along routes not longer than the Earth’s equator, no significant manifestation of dispersion will be observed. In those cases, when the wave periods exceed 100s only slightly, the manifestation of dispersion will already be noticeable at relatively short distances of the order of 100–1000 km.

It must be noted, here, that a recent analysis of the transoceanic propagation of tsunami waves caused by the 2011 Tohoku-Oki and the 2010 Chilean earthquakes revealed an insignificant (below 2%) deviation from the “classical” dispersion law (Watada et al. 2014). The deviation from the “classical” law $\omega^2 = gk \tanh(kH)$, that was obtained assuming a homogeneous incompressible layer of water on an absolutely rigid ocean bottom, is explained by manifestations of the effects of sea-water compressibility, gravitational potential variation, and solid Earth elasticity. It is remarkable that “classical” normal dispersion turned out to be peculiar to tsunami waves with short periods ($T < 10^3$ s), while long-period ($T > 10^3$ s) waves are characterized by anomalous dispersion, in the case of which the phase velocity of waves decreases as the period increases.

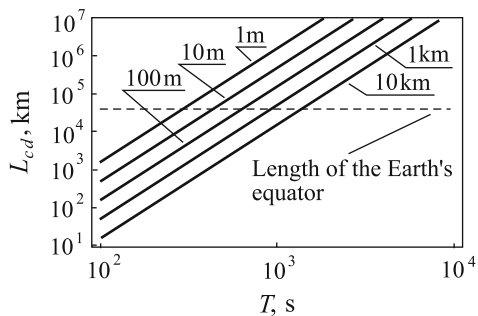
Similar estimation can be performed in the case of transformation of a wave packet due to amplitude dispersion, arising as a consequence of nonlinearity. Consider a wave with a crest of height A . The propagation velocity of the crest will differ from the velocity of linear long waves, its value can be estimated as $\sqrt{g(H + A)}$. By analogy with the distance of dispersive destruction, we introduce the distance of “nonlinear destruction” of a wave,

$$L_{cn} = \frac{\lambda \sqrt{gH}}{\sqrt{g(H + A)} - \sqrt{gH}}. \tag{6.3}$$

If $A/H \ll 1$, then the following approximate relation will be valid:

$$L_{cn} \approx \frac{2H\lambda}{A}. \tag{6.4}$$

Fig. 6.3 Distance of dispersive destruction of a tsunami wave as function of period T and ocean depth (numbers at curves). The dotted line shows a distance equal to the Earth’s equator, as a measure of a limit distance, that can be covered by a tsunami wave



From formula (6.4) it is seen that, even when the tsunami wave height in open ocean is quite significant, $A = 1$ m, in the case of a typical depth $H = 4$ km and wavelength $\lambda = 100$ km, the value of L_{cn} will amount to about 400,000 km, which exceeds the length of the Earth's equator by an order of magnitude. Therefore, nonlinear effects, in the case of tsunami propagation in the open ocean, can indeed be neglected.

The ratio of the quantities L_{cd} and L_{cn} , determined in accordance with the approximate formulae (6.2) and (6.4), gives the Ursell parameter $L_{cd}/L_{cn} \sim A\lambda^2/H^3 = Ur$ (Pelinovsky 1996), known in the theory of nonlinear dispersion waves on water. In open ocean, as a rule, $Ur \ll 1$, which means that phase dispersion prevails over nonlinear effects. Near the coast (in shallow water), if microtsunamis are not considered, the parameter $Ur \gg 1$, i.e., nonlinear effects become predominant. Estimation of the distances of dispersive and nonlinear destruction, yielding formulae similar to (6.2) and (6.4), can be found in the book Pelinovsky (1982).

From the above analysis it follows that in simulating tsunamis, even along extended routes, the application of linear theory is quite justified. Moreover, long-wave theory is also quite appropriate for long-period waves. In this connection, it will be expedient to dwell upon certain partial results, following from the linear theory of long waves.

Tsunami waves are capable of covering enormous transoceanic distances. In this connection, the basic regularities exhibited by wave amplitude variations far from the source are of interest. Consider the ideal case of a limitless ocean with a flat horizontal bottom. We shall consider the water to be an ideal (nonviscous) liquid. In the approximation indicated a decrease in the wave amplitude may be due to two factors: geometrical divergence and phase dispersion.

In those cases, when phase dispersion can be neglected (long waves), a decrease in the wave amplitude A will only be due to geometric divergence. Indeed, the total wave energy is proportional to the square amplitude multiplied by the length of the wave front. As a wave propagates away from its source the length of its wave front increases in proportion to the distance from the source r . From the energy conservation law follows the formula $A^2 r = const$, precisely which determines the sought regularity in the amplitude variation of long waves with distance: $A \sim 1/\sqrt{r}$. Note that, when long waves propagate within a channel, no geometric divergence exists, so, consequently, the wave amplitude remains intact.

Dispersive "smearing" of a wave packet in space serves as an additional factor that reduces the amplitude of waves propagating away from the source. Therefore, the amplitude of dispersing waves should evidently decrease more rapidly than the amplitude of long waves. The analytical solutions of the plane (channel) and space problems of tsunami generation by bottom deformations, obtained in Chap. 3 in an integral form, can be represented at large distances from the source by analytical formulas using the stationary phase method. From these formulas it follows that the amplitude of dispersing waves propagating within a channel falls in accordance with the law $A \sim 1/\sqrt{r}$, while in the case of propagation in space (on the plane) in accordance with the law $A \sim 1/r$.

Since the distance from the source and the wave propagation time are related by $r = t\sqrt{gH}$ (this formula is approximate in the case of dispersing waves), the regularities in the wave variation can be represented in the form of time dependencies. Thus, for example, in the spatial problem the amplitude of dispersing waves decreases with time as $A \sim 1/t$.

The ocean depth is the only variable quantity entering into the formula for the velocity of long waves, $c = \sqrt{gH}$. Therefore, many effects of tsunami propagation and run-up are related to the relief of the ocean bottom.

Consider the one-dimensional problem of the propagation of a long wave in a basin, the depth of which varies along the horizontal coordinate. We consider depth variations to be sufficiently smooth, so the reflection of waves from inclined sections of the bottom can be neglected. For definiteness, we shall consider a sine wave of length λ . Within the linear model, the kinetic and potential energies of the wave are equal to each other, therefore, the total energy attributed to a single space period (and to unit front length) can be calculated as twice the potential energy,

$$W = \rho g \int_0^\lambda \xi^2 dx, \quad (6.5)$$

where ξ is the free water surface displacement from the equilibrium position, ρ is the density of water.

Since in a linear system the perturbation frequency remains unchanged, while the wavelength may change during propagation, it is worthwhile to perform in formula (6.5) integration over time, instead of space,

$$W = \rho g \sqrt{gH} \int_0^T \xi^2 dt = \text{const} \cdot \xi_0^2 \sqrt{H}. \quad (6.6)$$

From energy conservation (we neglect dissipation here) it follows that the quantity $\xi_0^2 \sqrt{H}$ must be conserved along the route of the wave propagation. In other words, if the ocean depth decreases, as the wave propagates, then the wave amplitude will increase by the law $\xi_0 \sim H^{-1/4}$. The relationship obtained is termed as the Green's law or the "one-quarter" rule. This law, for instance, explains why the tsunami amplitude increases as it approaches the coast. Owing to a decrease in depth and, consequently, in propagation velocity, the wave packet shrinks in space, but boosts its amplitude.

Another "classical" effect of the interaction of long waves with the relief consists in their transformation in the region of abrupt changes in the ocean depth. In those cases, when the ocean depth changes over distances much shorter than the wavelength, the distribution of depths is expediently represented in the form of a step (Fig. 6.4a). Such a situation is dealt with in many sectors of classical wave theory (optics, acoustics), and it is known as wave refraction and reflection at the boundary of

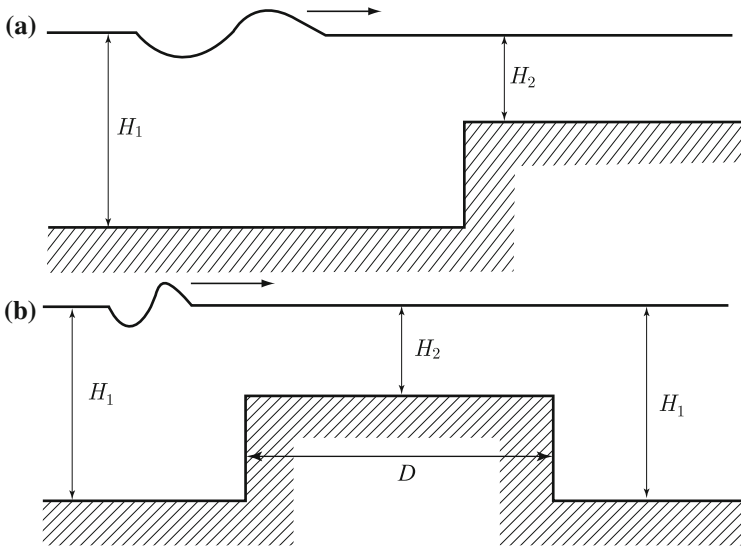


Fig. 6.4 Ocean bottom geometry in problem of long wave transformation on irregularities of the bottom relief: step (a), rectangular obstacle (b)

two media. We shall only consider normal incidence of waves (the one-dimensional problem). We shall determine the amplitude coefficients for reflection, R , and transmission, T . To this end, following the classical book Lamb (1932), we take advantage of the continuity conditions for the free surface displacement, ξ , and the water release (Hu) at the depth jump point. The resulting reflection and transmission coefficients R and T , respectively, are

$$R = \frac{\sqrt{H_1/H_2} - 1}{\sqrt{H_1/H_2} + 1}, \tag{6.7}$$

$$T = \frac{2\sqrt{H_1/H_2}}{\sqrt{H_1/H_2} + 1}. \tag{6.8}$$

The dependences (6.7) and (6.8), calculated within a wide range of depth ratios H_1/H_2 , are shown in Fig. 6.5. If $H_1 > H_2$, then the waves, that are transmitted through and reflected from, respectively, a step, will have the same polarity as the incident wave, and the amplitude of the transmitted wave will increase. In the case of transformation on a step the wave amplitude cannot be more than twice the initial value. When $H_1 < H_2$, the reflected wave changes polarity, and the amplitude of the wave, reaching deepwater, is reduced.

Now, consider the “classical” problem, akin to the previous one, of transformation of a long wave above a rectangular obstacle (Fig. 6.4b), of length D and height $|H_2 - H_1|$. The role of the obstacle can be assumed both by a local elevation of the bottom and by a depression. We note, right away, that this problem cannot be

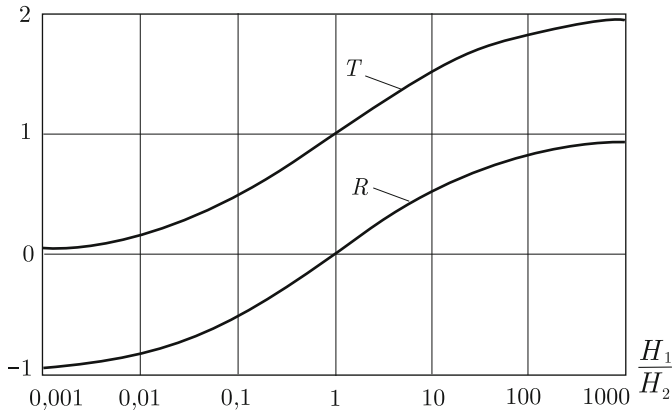


Fig. 6.5 Amplitude coefficients for transmission, T , and reflection, R , versus the depth ratio in the case of wave transformation on a step

reduced to two consecutive independent acts of wave transformation on the front and back edges of the obstacle, i.e., on two steps. Anyhow, in the case of a solitary wave, with a length much shorter than the length of the obstacle, such an approach is quite adequate (Nakoulima et al. 2005).

In the general case, a correct description of wave transformation above a rectangular obstacle requires the examination of a constrained system comprising five waves. Consider a sine wave incident upon the obstacle and traveling in the positive direction of axis $0x$. Then, in the regions $x < 0$ (before the obstacle) and $0 < x < D$ (above the obstacle) there exist two wave perturbations, propagating in both the positive and negative directions, while in the region $x > D$ there is only one perturbation, running in the positive direction. From the continuity condition for the free surface displacement ξ and the water release (Hu) at points $x = 0, D$ the following expression is obtained for the amplitude transmission coefficient (Mofjeld et al. 2000):

$$T = \frac{T_{\min}}{\sqrt{T_{\min}^2 \cos^2 \beta + \sin^2 \beta}}, \tag{6.9}$$

where $T_{\min} = \frac{2\sqrt{H_1/H_2}}{1 + H_1/H_2}$, $\beta = k_2 D$ is the phase difference between the boundaries of the obstacle, k_2 is the wave number over the obstacle. In the case of transformation of a long wave on a step the transmission and reflection coefficients were only determined by the depth ratio and did not depend on any parameters of the wave. In the case of wave transformation above the rectangular obstacle the transmission coefficient turns out to depend on the wave frequency. The phase difference β is related to the wave number and, consequently, to the wave frequency, $\beta = \omega D/\sqrt{gH_2}$.

The dependence (6.9) is presented in Fig. 6.6. Its important peculiarity consists of the existence of a minimum transmission coefficient T_{\min} , the value of which is

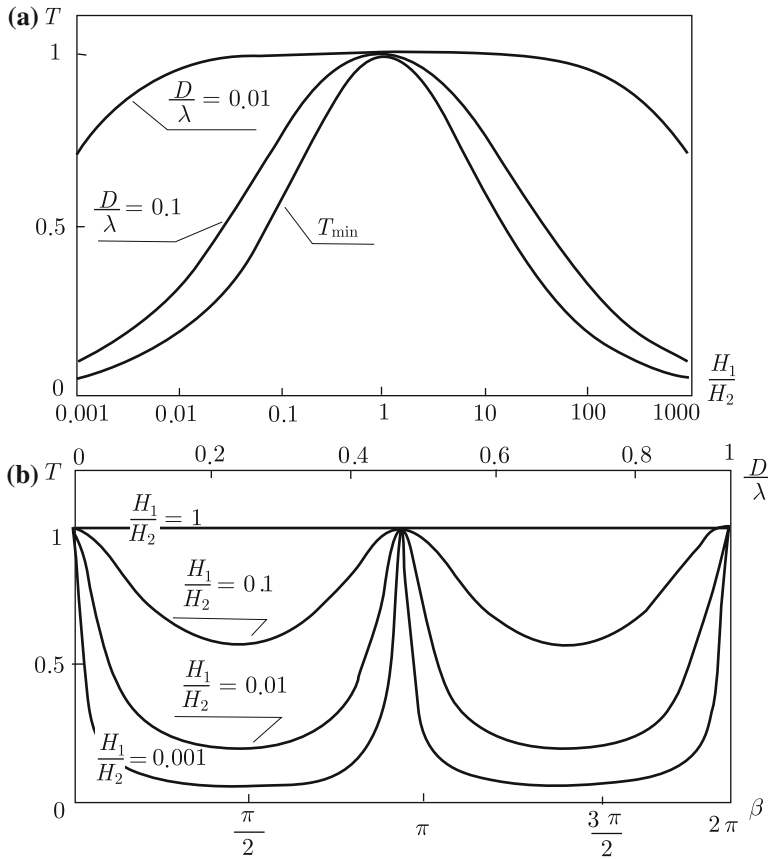


Fig. 6.6 Amplitude transmission coefficient for a long wave on a rectangular obstacle versus the depth ratio (a) and versus the phase difference between the edges of the obstacle (b)

only determined by the depth ratio H_1/H_2 , but does not depend on the width of the obstacle or the wavelength. The transmission coefficient is quite weakly related to the quantity H_1/H_2 . The less the width of the obstacle, i.e., the smaller the ratio D/λ , the weaker this relationship happens to be.

If the width of the obstacle is small as compared to the tsunami wavelength ($D/\lambda < 0.2$), then an increase in the dimensions (width and height) of the obstacle unambiguously results in a decrease of the transmission coefficient. As soon as the width of the obstacle is commensurable with the wavelength, interference effects start to become apparent. When the phase difference β (Fig. 6.6b) changes, the values of coefficient T change periodically from T_{\min} up to 1. These changes are explained as follows. The interference between the waves, reflected from the front and rear boundaries of the obstacle, leads to mutual canceling of the waves and, consequently, to amplification of the transmitted wave intensity. We recall that this effect

is widely applied for producing antireflection optics. As to applications to the tsunami problem, we are, first of all, interested in wave transformation on obstacles of small sizes, $D \ll \lambda$. The point is that the transformation of waves by large-scale bottom irregularities, $D \gtrsim \lambda$, is automatically taken into account in numerical simulations. Therefore, it is practically important to estimate the contribution of small-scale (several kilometers and less) or so-called sub-net inhomogeneities, the size of which turns out to be smaller than the distance between the nodes of the mesh. We shall return to this estimate at the end of the section.

Small-scale inhomogeneities of the open ocean bottom exhibit heights significantly smaller than the thickness of the water column. Therefore, it is reasonable to introduce the relative height of an obstacle,

$$\alpha \equiv \frac{H_1 - H_2}{H_1},$$

that is a small quantity. When $\alpha \ll 1$ and $\beta \ll 1$, from formula (6.9) we obtain the simple approximate relation

$$T \approx 1 - \frac{(\alpha\beta)^2}{8}. \quad (6.10)$$

The expression obtained permits to assert, that in the case of transformation of a wave passing above an obstacle, the decrease in amplitude is proportional to the square area of the obstacle.

We have hitherto considered influence of the bottom relief on tsunami waves within the framework of one-dimensional problems. Actually, tsunami propagation takes place in two-dimensional space: on a plane or on the surface of a sphere. Certain two-dimensional peculiarities of the bottom relief, such as underwater oceanic mountain ridges, the shelf, are capable, for example, of effectively capturing waves, thus creating priority directions for tsunami propagation and providing for prolonged “sounding” of tsunamis at a coast. Phenomena of such kind are readily tracked making use of ray theory, which is also called an approximation of geometrical optics. Ray theory provides an effective instrument for operative calculation of tsunami arrival times. Its application permits to determine the contours of a tsunami source from data of the network of mareograph stations. Ray theory is extremely illustrative and permits to judge about the directions of tsunami energy propagation. Computational methods have been developed for calculating wave amplitudes on the basis of equations written “along the ray” (Pelinovsky 1996).

The velocity of a wave c being a function of two coordinates, x and y , the ray equations for nondispersive waves are written as follows (Lighthill 1978):

$$\frac{dX}{dt} = c \frac{k_x}{\sqrt{k_x^2 + k_y^2}}, \quad (6.11)$$

$$\frac{dY}{dt} = c \frac{k_y}{\sqrt{k_x^2 + k_y^2}}, \tag{6.12}$$

$$\frac{dk_x}{dt} = -\frac{\partial c}{\partial x} \sqrt{k_x^2 + k_y^2}, \tag{6.13}$$

$$\frac{dk_y}{dt} = -\frac{\partial c}{\partial y} \sqrt{k_x^2 + k_y^2}, \tag{6.14}$$

where X, Y are the coordinates of ray points, k_x and k_y are components of the wave vector, t represents time. The ray equations written in this form, permit not only to easily calculate the course of the wave ray, but also the evolution of the wave front. For computing the ray evolution the set of Eqs. (6.11)–(6.14) must be supplemented by initial conditions consisting of determination of the initial coordinates and direction. It is not difficult to note that in the case of a fixed basin depth ($c = \text{const}$) the rays will be straight lines.

Figure 6.7 presents two examples of the computation of ray behavior, performed with the aid of formulae (6.11)–(6.14). The model bottom relief in the first case (Fig. 6.7a) imitates a mountain ridge in the middle of the ocean. Part of the rays emitted by a pointlike source turn out to be captured, these rays further propagate along the underwater eminence. Not all rays happen to be captured, but only those the direction of which does not differ strongly from the axis of the ridge, namely, in this case is the condition of total internal reflection realized.

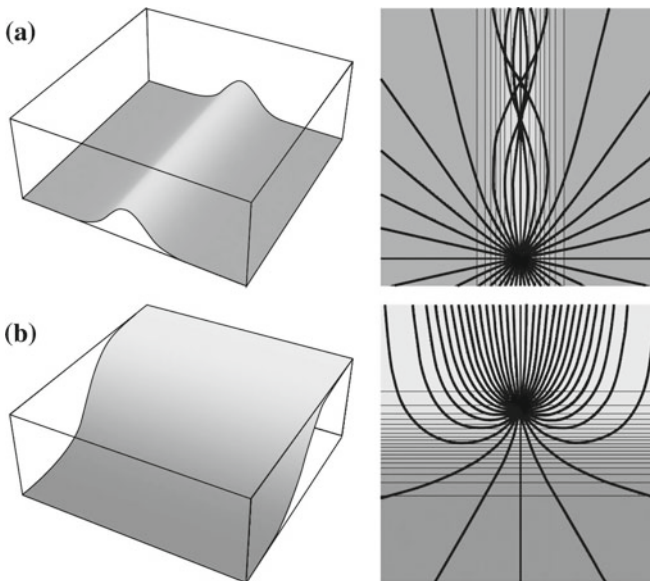


Fig. 6.7 Examples of influence of bottom relief on the course of wave rays emitted by a pointlike source: capture of rays by an underwater ridge (a); refraction and capture of waves in the shelf zone (b)

Figure 6.7b shows the course of rays from a pointlike source, situated on the “shelf”. It is well seen that part of the rays, curved at the beginning toward large depths, turn back to shallow water. Thus, refraction results in a significant part of the wave energy turning out to be captured by the shelf and to propagate along the coast. In Fig. 6.7b, one also observes a classical refraction effect: as the rays arrive in shallow water, they are turned around in the direction normal to the coastline.

A striking example of the role of waves, captured by the shelf is related to the tsunami, that took place in Indonesia on December 12, 1992. This event is known as the tsunami of Flores island. At a distance of 5 km north of the Flores island coast there is a small island (the Babi island) of approximately circular shape and diameter about 2.5 km. The tsunami source was north of Babi island, however, the maximum run-up (7.1 m) was observed on the southern coast of the island. This effect is explained by the fact that the tsunami wave, having approached the island from the north, happened to be captured by the shelf, then turned round the island on both sides and provided maximum run-up on the coast of the back side of the island relative to the tsunami source. This effect has been studied with the use of laboratory simulation (e.g., Yeh et al. (1994); Briggs et al. (1995)) and numerical simulation (e.g., Liu et al. (1995); Choi et al. (2007)).

In the analysis of real events, the use of equations (6.11)–(6.14) is limited to small-scale areas of water. Beam computation for transoceanic routes requires taking into account the Earth’s sphericity. Calculation of the path of a ray on a spherical surface is performed applying the following set of equations (Satake 1988):

$$\frac{d\theta}{dt} = \frac{\cos \zeta}{nR}, \quad (6.15)$$

$$\frac{d\varphi}{dt} = \frac{\sin \zeta}{nR \sin \theta}, \quad (6.16)$$

$$\frac{d\zeta}{dt} = -\frac{\sin \zeta}{n^2 R} \frac{\partial n}{\partial \theta} + \frac{\cos \zeta}{n^2 R \sin \theta} \frac{\partial n}{\partial \varphi} - \frac{\sin \zeta \cot \theta}{nR}, \quad (6.17)$$

where θ is the colatitude (supplement up to the latitude), φ is the ray longitude, t is time, the quantity $n = (gH)^{-1/2}$ is the inverse velocity of long waves, R is the Earth’s radius, ζ determines the ray direction counted anticlockwise from the direction toward the South. For computation of the evolution of wave rays knowledge is required of the distribution of ocean depths over latitude and longitude. At present, information on the global topography and bathymetry with a space resolution of 30 arcsecond (GEBCO) is available on the site of the British Oceanographic Data Centre (<http://www.ngdc.noaa.gov/mgg/gebco/>). An example of the application of equations (6.15)–(6.17) can be found, for example, in Choi et al. (2003).

Any wave motion in a nonideal (viscous) liquid is subject to dissipation. Tsunami waves also lose part of their energy as they travel, owing to its irreversible transformation into heat. We shall estimate the influence of dissipative factors on tsunami propagation.

The damping of long gravitational waves in a viscous liquid is known to be due to energy dissipation within a thin bottom layer. The wave amplitude, here, decreases exponentially with time,

$$A \sim \exp\{-\gamma t\}.$$

The following formula has been obtained in the book Landau and Lifshitz (1987) for the time decrement of amplitude damping for a wave propagating in a basin of constant depth H :

$$\gamma = \left(\frac{\nu\omega}{8H^2} \right)^{1/2},$$

where ν is the molecular kinematic viscosity of the liquid, ω is the cyclic frequency of the wave. If a long wave propagates only in the direction of axis Ox , then its amplitude will also decrease exponentially with the distance,

$$A \sim \exp\left\{-\frac{x}{L_1}\right\},$$

where

$$L_1 = \frac{\sqrt{gH}}{\gamma} = \left(\frac{8gH^3}{\nu\omega} \right)^{1/2}. \quad (6.18)$$

The physical meaning of quantity L_1 is the distance, over which the amplitude of a long wave in a viscous liquid becomes e times smaller. We shall call this quantity the viscous (linear) dissipation length.

Note that formula (6.18) is correct for any constant viscosity coefficient, which, generally speaking, can be both molecular and turbulent. One must, however, bear in mind, that in the bottom boundary layer the turbulent viscosity, as a rule, depends strongly on the vertical component, i.e., is not a constant value. Therefore, it would not be quite correct to substitute into formula (6.18) any values of the turbulent viscosity coefficient. On the other hand, in a real ocean exchange of momentum does not proceed via molecular mechanisms, but by turbulence. Indeed, in spite of the relatively low flow velocity, characteristic of tsunami waves in open ocean, $u \approx A\sqrt{g/H} \sim 10^{-2}$ m/s, the Reynolds numbers turn out to be sufficiently large for the development of turbulence.

Determination of the quantity L_1 from formula (6.18) actually gives an idea of the minimum possible level of tsunami wave energy losses. Actually, owing to turbulence these losses may turn out to be more significant. We shall estimate the damping of tsunami waves on the basis of the known parameterization of frictional tension exerted by the ocean bottom on the water flowing along it with a velocity \mathbf{v} ,

$$\mathbf{T}_B = -C_B \rho \nu |\mathbf{v}|, \quad (6.19)$$

where ρ is the density of water, C_B is a dimensionless empirical coefficient, the value of which is usually set to 0.0025 (Murty 1984). The minus sign in formula (6.19)

indicates that the water flow is hindered by a force directed against the flow velocity vector. The absolute value of the force of friction is proportional to the square flow velocity, therefore, the problem of wave damping under the action of bottom friction is certainly not linear, and, consequently, one can expect the damping not to be exponential in character.

For definiteness, we shall consider the one-dimensional problem of a sine wave propagating in the positive direction of axis $0x$ in a basin of fixed depth H ,

$$u(x, t) = u_0 \sin(x - \sqrt{gH}t).$$

Assume the action of the friction force to be insignificant, so that the amplitude and shape of a wave covering a distance comparable with the wavelength λ undergo no significant changes. We shall estimate the wave energy per period in space (and per unit length of front), as twice the kinetic energy,

$$E = \rho H \int_0^\lambda u^2 dx = \frac{\rho H \lambda u_0^2}{2}. \quad (6.20)$$

Strictly speaking, such an estimate is only valid for linear waves, but, as we have already noted, we consider the nonlinearity to be weak.

The losses of wave energy per unit time in the region from 0 up to λ , that are due to the action of bottom friction, are determined by the following formula (the point above the variable signifies differentiation with respect to time):

$$\dot{E} = \int_0^\lambda (T_B, u) dx = -C_B \rho \int_0^\lambda |u|^3 dx = -\frac{4C_B \rho \lambda u_0^3}{3\pi}. \quad (6.21)$$

Now, pass in formulae (6.20) and (6.21) to specific energy per unit mass of liquid

$$b \equiv \frac{E}{\rho H \lambda} = \frac{u_0^2}{2}, \quad (6.22)$$

$$\dot{b} \equiv \frac{\dot{E}}{\rho H \lambda} = -\frac{4C_B u_0^3}{3\pi H}. \quad (6.23)$$

Excluding the quantity u_0 in expression (6.23), with the aid of the constraint (6.22) one obtains the ordinary differential equation

$$\dot{b} = -\frac{8\sqrt{2} C_B b^{3/2}}{3\pi H}. \quad (6.24)$$

We recall, that we are tracing the energy of a sole space period of the wave. The ordinary differential equation (6.24) describes the variation of this quantity in time.

The solution of Eq. (6.24), written with respect to the wave velocity amplitude u_0 , has the following form:

$$u_0(t) = \frac{u_0(0)}{1 + \frac{4C_B u_0(0)}{3\pi H} t}, \quad (6.25)$$

where $u_0(0)$ is the velocity amplitude at time moment $t = 0$. Taking advantage of the relationship between the free surface displacement and the flow velocity $u \approx \xi \sqrt{g/H}$ and taking into account, that $x = t\sqrt{gH}$, we obtain an expression describing variation of the wave amplitude along the horizontal coordinate,

$$\xi_0(x) = \frac{\xi_0(0)}{1 + x/L_2}, \quad (6.26)$$

where $L_2 = \frac{3\pi H^2}{4C_B \xi_0(0)}$ is the distance, along which the wave amplitude becomes two times smaller.¹ We shall call this quantity the nonlinear dissipation length.

We shall point out a number of special features, distinguishing viscous (linear) and nonlinear damping of long waves from each other. First, the actual character of damping is different: in the first case it is exponential, while in the second it is hyperbolic. Second, the characteristic distance, along which noticeable wave damping occurs (L_1 and L_2), is related to different parameters of the problem. The quantity L_1 depends on the wave frequency and on the basin depth, while the quantity L_2 depends on the wave amplitude and depth. In both cases the distance L_i increases with the depth H , but in the case of nonlinear damping this dependence is stronger.

Figure 6.8 presents the dependences of dissipation lengths L_1 and L_2 upon the ocean depth. Calculations are performed for characteristic ranges of tsunami wave frequencies (10^{-4} – 10^{-2} Hz) and amplitudes (0, 1–10 m) for the coefficient $C_B = 0.0025$, viscosity $\nu = 10^{-6}$ m²/s. From the figure it is seen that for conditions of the open ocean, $H > 10^3$ m, viscous and nonlinear friction cannot influence tsunami wave propagation in any noticeable way. For dissipative effects to be manifested in a noticeable manner the wave must cover a distance exceeding the length of the Earth's equator, which is not possible in practice. From a purely theoretical point of view it is interesting that at large depths the quantities L_1 and L_2 become closer. Anyhow, this fact rather reflects the correct choice of coefficient C_B . The point is that viscous dissipation is not taken into account in tsunami models, applied in practice. At the same time nonlinear dissipation is present in model equations. As it is seen, it provides approximately the same (albeit tiny) contribution to wave damping, which could have been provided by viscous dissipation.

Essential manifestations of dissipation are only possible at small depths $H < 10$ m. Here, the role of viscous linear wave dissipation turns out to be insignificant. Most likely, in shallow water the dissipation lengths will be related as $L_1/L_2 > 10$. There-

¹With a precision up to a numerical coefficient, this quantity is in accordance with the result obtained in the book Pelinovsky (1996).

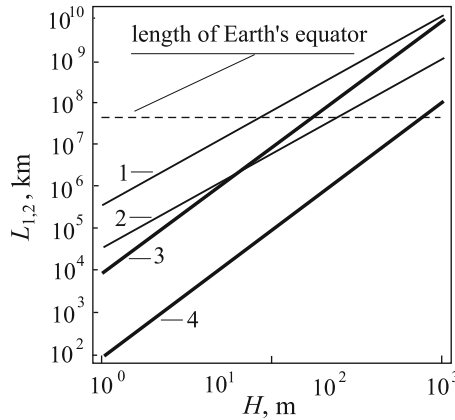


Fig. 6.8 Tsunami wave dissipation length versus ocean depth. Curves 1, 2—viscous (linear) dissipation, 3, 4—nonlinear dissipation. The calculation is performed for $C_B = 0.0025$, $\nu = 10^{-6} \text{ m}^2/\text{s}$. Curve 1— 10^{-4} Hz , 2— 10^{-2} Hz , 3— 0.1 m , 4— 10 m . For comparison, the dotted line shows a distance equal to the length of the Earth’s equator

fore, only taking into account nonlinear dissipation, like it is presently done in practical models, can be considered justified. The role of classical linear dissipation can indeed be neglected. We stress that one can speak of a noticeable influence of dissipation on a tsunami wave only in the case of very small depths. If we were to consider, for example, typical shelf depths $H \sim 100 \text{ m}$, then the dissipation length would, most likely, exceed 1000 km .

The wave amplitude decreasing as it propagates can be related not only to dissipation, but also to waves being scattered on small-scale irregularities of the ocean bottom. For estimating the significance of the scattering effect, we shall make use of the aforementioned results, concerning the transformation of long waves above a rectangular obstacle. Consider a “comb” on the ocean bottom, consisting of rectangular obstacles with a repetition period in space of $2D$. Then, along a route of length x , the number of obstacles encountered by a wave will be $N = x/2D$. Each time interaction with an obstacle takes place, a decrease in the wave amplitude will occur determined by the transmission coefficient T . The law by which the wave amplitude A decreases with distance is written as

$$A(x) = A_0 T^N. \tag{6.27}$$

Formula (6.27) is expediently represented in a more customary exponential form,

$$A(x) = A_0 \exp \left\{ -\frac{x}{L_3} \right\},$$

where $L_3 = -2D/\ln T$ is the characteristic distance, along which the wave amplitude is reduced by e times, owing to scattering on irregularities of the ocean bottom.

In the case of small relative heights of the roughnesses α and a small phase difference β we obtain the simple formula

$$L_3 = \frac{16D}{(\alpha\beta)^2}.$$

Expressing parameter β through the wavelength and the obstacle width, we ultimately obtain

$$L_3 = \frac{4}{\pi^2} \frac{\lambda^2}{\alpha^2 D}. \quad (6.28)$$

Applying expression (6.28), we shall perform a simple estimation showing the negligible role of wave scattering by small-scale irregularities of the ocean bottom. Let the tsunami wavelength be 100km and the ocean depth 4km. Then, if the obstacle has a width $D = 1$ km and is 100m high, then the quantity L_3 will amount to 6.5×10^9 m, which is equivalent to over 160 lengths of the Earth's equator.

6.2 Numerical Models of Tsunami Propagation

The headlong development of computational technologies, taking place in recent decades, has opened up new possibilities for numerical studies of problems of the mechanics of continuous media (MCM). The necessary computational facilities are now available to a wide range of researchers.

Description of tsunami evolution from the moment of generation to arrival of the wave on the shore represents one of the tasks of MCM. The application of analytical models for describing real tsunamis is limited, even if only for the complex topography of the ocean bottom. The only obvious alternative consists of numerical modeling. The efficiency of such means for studying tsunamis has long been unanimously acknowledged by the scientific community. Hopes of resolving the problem of tsunami prediction are also to a great extent related to the development of numerical models.

The "age" of numerical simulation of real tsunamis started at the end of the 1960s of the twentieth century. The first works in this direction were performed by Japanese researchers Aida (1969, 1974), Abe (1978, 1979). One of the first numerical models developed in Russia was described in Gusakov and Chubarov (1982, 1987), Chubarov et al. (1984).

At present there exist numerous software means developed for hydrodynamic simulation of tsunamis. Without claiming to present a full list, we can indicate the most well-known models: TUNAMI (Imamura et al. 2006), MOST (Titov et al. 2003), COMCOT (Liu et al. 1998), NAMI DANCE (Zaytsev et al. 2010), MGC (Shokin et al. 2008), TsunAWI (Harig et al. 2008), NEOWAVE (Yamazaki et al. 2009), GeoClaw (LeVeque et al. 2011), ALASKA (Nicolosky et al. 2011), BOSZ (Roeber and Cheung 2012).

Certain tsunami models do not have special names, but are actively applied by scientific groups—their descriptions can be found in Fine et al. (2005), Fujii and Satake (2007), Kowalik et al. (2007), Nicolsky et al. (2011), Nosov et al. (2013).

The development of all aforementioned models was based on the theory of long waves, within the framework of which the initial 3D hydrodynamic problem reduces to the 2D problem by the integration of equations along the vertical coordinate. In spite of 3D numerical tsunami models undergoing active development and being introduced into practice (Ohmachi et al. 2001; Nosov and Kolesov 2007; Choi et al. 2007, 2008; Maeda and Furumura 2013; Bolshakova et al. 2011; Ma et al. 2012), vertically integrated (2D) models will doubtless continue to be in demand for the following two reasons. First, such models quite adequately reflect the physical essence of the phenomena examined. Second, 2D simulation requires a relatively small computational capability.

In the Cartesian reference system with $0x$ and $0y$ axes directed eastward and northward, respectively, the equations of nonlinear theory of long waves, with account of the bottom friction and the Coriolis force, has the following form:

$$\frac{\partial U}{\partial t} + U \frac{\partial U}{\partial x} + V \frac{\partial U}{\partial y} = -g \frac{\partial \xi}{\partial x} - \frac{C_B U \sqrt{U^2 + V^2}}{D} + fV, \quad (6.29)$$

$$\frac{\partial V}{\partial t} + U \frac{\partial V}{\partial x} + V \frac{\partial V}{\partial y} = -g \frac{\partial \xi}{\partial y} - \frac{C_B V \sqrt{U^2 + V^2}}{D} - fU, \quad (6.30)$$

$$\frac{\partial \xi}{\partial t} + \frac{\partial}{\partial x}(DU) + \frac{\partial}{\partial y}(DV) = 0, \quad (6.31)$$

where U , V are the flow velocity components, along the axes $0x$ and $0y$, respectively, ξ is the free surface displacement from the equilibrium position, $D(x, y, t) = H(x, y) + \xi(x, y, t)$ is the thickness of the water column, g is the acceleration of gravity, $f = 2\omega \sin \varphi$ is the Coriolis parameter, ω is the angular velocity of the Earth's rotation, φ is the latitude, C_B is a dimensionless empirical coefficient, which is usually set to 0.0025. There also exist more precise models, which take into account the dependence of quantity C_B on the thickness of the water column. Thus, for example, the following dependence is applied in Titov et al. (2003):

$$C_B = \frac{gn^2}{D^{1/3}}, \quad (6.32)$$

where n is the Manning coefficient, the value of which depends on the roughness of the bottom surface. A typical value of the Manning coefficient for a coast free from dense vegetation, amounts to $n = 0.025 \text{ s/m}^{1/3}$.

Note that formula (6.32) yields the value $C_B = 0.0025$ for a water column of $D \approx 15 \text{ m}$. The dependence of $C_B(D)$ is weak ($C_B(1 \text{ m}) \approx 0.006$, $C_B(100 \text{ m}) \approx 0.0013$), therefore, the results of calculations of wave dynamics carried out assuming the coefficient C_B to be constant and with account of the dependence (6.32), should

not differ strongly from one another. We recall that the bottom friction does practically not influence tsunami propagation at large depths.

In certain models another form is used for writing the nonlinear equations of the theory of long waves (“in total fluxes”),

$$\frac{\partial M}{\partial t} + \frac{\partial}{\partial x} \left(\frac{M^2}{D} \right) + \frac{\partial}{\partial y} \left(\frac{MN}{D} \right) = -gD \frac{\partial \xi}{\partial x} - \frac{C_B M \sqrt{M^2 + N^2}}{D^2} + fN, \quad (6.33)$$

$$\frac{\partial N}{\partial t} + \frac{\partial}{\partial x} \left(\frac{MN}{D} \right) + \frac{\partial}{\partial y} \left(\frac{N^2}{D} \right) = -gD \frac{\partial \xi}{\partial y} - \frac{C_B N \sqrt{M^2 + N^2}}{D^2} - fM, \quad (6.34)$$

$$\frac{\partial \xi}{\partial t} + \frac{\partial M}{\partial x} + \frac{\partial N}{\partial y} = 0, \quad (6.35)$$

where $M = UD$, $N = VD$ are components of the water release along the $0x$ and $0y$ axes, respectively. Transition from system (6.29)–(6.31) to system (6.33)–(6.35) is performed as follows. Equation (6.29) is multiplied by the quantity D , while Eq. (6.31), in which the partial derivative $\partial \xi / \partial t$ is replaced by the equivalent quantity $\partial D / \partial t$, is multiplied by the velocity component U . Upon adding up the obtained expressions and performing elementary transformations, we obtain Eq. (6.33). Equation (6.34) is derived in a similar manner. Transition from formula (6.31) to (6.35) is trivial and requires no comments.

Note that system (6.29)–(6.31) is not a rigorous consequence of the equations of hydrodynamics. First of all, this is due to the expression for the force of bottom friction having been obtained from an empirical dependence. Moreover, the stopping of the flow is due to tangential tension, acting only on the lower boundary. This circumstance hinders the rigorous derivation of nonlinear equations for long waves. However, linear equations (without advective terms) can be obtained in a rigorous manner by integration of the linearized Reynolds equations along the vertical coordinate from the bottom up to the free water surface.

In calculating tsunami propagation along extended routes account must be taken of the curvature of the Earth’s surface. The form of the surface of our planet can be considered spherical with a precision sufficient for our problem, therefore, it is expedient to write the equations of the theory of long waves in spherical coordinates,

$$\begin{aligned} \frac{\partial U}{\partial t} + \frac{1}{R \cos \varphi} \left(U \frac{\partial U}{\partial \psi} + V \cos \varphi \frac{\partial U}{\partial \varphi} \right) - \frac{UV \tan \varphi}{R} \\ = -\frac{g}{R \cos \varphi} \frac{\partial \xi}{\partial \psi} - \frac{C_B U \sqrt{U^2 + V^2}}{D} + fV, \end{aligned} \quad (6.36)$$

$$\begin{aligned} \frac{\partial V}{\partial t} + \frac{1}{R \cos \varphi} \left(U \frac{\partial V}{\partial \psi} + V \cos \varphi \frac{\partial V}{\partial \varphi} \right) + \frac{U^2 \tan \varphi}{R} \\ = -\frac{g}{R} \frac{\partial \xi}{\partial \varphi} - \frac{C_B V \sqrt{U^2 + V^2}}{D} - fU, \end{aligned} \quad (6.37)$$

$$\frac{\partial \xi}{\partial t} + \frac{1}{R \cos \varphi} \left(\frac{\partial(U D)}{\partial \psi} + \frac{\partial(V D \cos \varphi)}{\partial \varphi} \right) = 0, \quad (6.38)$$

where ψ is the longitude, φ is the latitude, U and V are the flow velocity components, along the parallel (West–East) and along the meridian (North–South), respectively, $R \approx 6371$ km is the mean radius of the Earth.

The serious disadvantages of 2D models, based on the theory of long waves, must be considered to include the neglect of phase dispersion, manifestations of which, as it was already noted in Sect. 6.1, are, generally speaking, peculiar to tsunami waves. Thus, for example, in the case of a typical oceanic depth of 5 km the distance of dispersive destruction due to a wave with a period of 500 s (see formula (6.1)) will amount to about 2800 km, which is significantly inferior to the length of transoceanic tsunami propagation routes. Attempts are known at the simulation of real dispersion in long-wave models on the basis of a numerical effect, namely, numerical dispersion (see, for example, the MOST (Burwell et al. 2007) packet). But such an approach can hardly be acknowledged to be universal and quite correct.

All the advantages connected to 2D simulation can be retained and at the same time weak phase dispersion can be taken into account correctly within the framework of the Boussinesq approximation. Precisely, this approximation serves as a basis for such tsunami models as FUNWAVE-TVD (Shi et al. 2012), COULWAVE (Lynett et al. 2003), GloBouss (Løvholm et al. 2010).

The set of equations of long-wave theory, written in a Cartesian or spherical reference system, is usually resolved with initial conditions (initial elevation), representing a free surface displacement, equivalent to vertical residual deformations of the ocean bottom, resulting from an earthquake. The initial field of flow velocities is assumed to be zero. The method for calculating the initial elevation is discussed in detail in Sect. 3.5.

As a rule, the boundary conditions used for simulating tsunami propagation within the theory of long waves pertain to one of the following three types (Marchuk et al. 1983):

- (1) interaction with the coast,
- (2) free transmission,
- (3) perturbation, arriving from external area.

In the most simple case, the interaction of waves with the coast is described as total reflection from the coast. To this end one considers that on a certain fixed isobath (usually, 10–20 m) the flow velocity component normal to the coastline (or the chosen isobath) turns to zero,

$$V_{\mathbf{n}} = 0.$$

A direct consequence of this condition is the equality to zero of the component normal to the shoreline (or the chosen isobath) of the derivative of the free surface displacement,

$$\frac{\partial \xi}{\partial \mathbf{n}} = 0.$$

The choice of isobathic line H_0 , the condition of total reflection on which is imposed is not, generally speaking, arbitrary. The quantity H_0 is related to the spatial increment, Δ , and, also, to the minimal wave period T_{\min} , that are reproduced by the numerical model. The point is that, when a tsunami approaches shallow water, its wavelength is significantly reduced—sometimes by dozens of times. When the wavelength becomes comparable to the spatial increment, the numerical model no longer describes the tsunami dynamics adequately. The waves evidently exhibit the shortest lengths precisely at those points, where the oceanic depth is the smallest, i.e., on the isobathic line H_0 : $\lambda_{\min} = T_{\min}\sqrt{gH_0}$. In accordance with the Nyquist–Shannon–Kotelnikov theorem, the wavelength should accommodate at least two spatial increment: $\lambda_{\min} \geq 2\Delta$. From this condition follows a restriction on the value of H_0

$$H_0 > \frac{4\Delta^2}{T_{\min}^2 g}. \quad (6.39)$$

Substituting into formula (6.39) the value, often applied in practice, of the spatial increment corresponding to 1 angular minute (at the equator $\Delta \approx 1855$ m), we obtain for the minimal tsunami wave period $T_{\min} = 100$ s the following: $H_0 > 140$ m. Note that this value significantly exceeds the values usually chosen in establishing the reflection condition. Such large H_0 values move the isobathic line too far away from the true coastal line, which may turn out to be inadmissible even in the case of global calculations. The problem is resolved by rendering the spatial increment smaller in the coastal region. From formula (6.39) it follows that the choice of isobath $H_0 = 10$ m in the case of $T_{\min} = 100$ s requires the spatial increment to be set to $\Delta < 500$ m.

The condition of total reflection is usually applied in those cases, when the main goal is to investigate wave propagation in the open ocean. In analyzing tsunami dynamics in the shelf zone a more detailed description is necessary in the interaction of waves with the coast. Here, it has sense to consider partial reflection of waves and to make use of the formula proposed by A.V. Nekrasov (1973),

$$V_n = \frac{1-r}{1+r} \frac{\xi\sqrt{gH}}{H+\xi},$$

where the parameter r , characterizing the degree of reflection, varies within limits from 0 up to 1.

The limited nature and complexity must be noted of practical implementation of the partial reflection conditions. In principle, these conditions could be applied for taking into account the energy losses arising, for example, when waves collapse. In this case the energy losses always turn out to be concentrated within quite a narrow coastal strip, while their absolute value may reach tens of percent (Li and Raichlen 2002). But preliminary estimation of the dependence of parameter r upon time and coordinates represents quite a nontrivial task. If the run-up of waves occurs without them collapsing, then the application of partial reflection conditions no longer has any sense owing to the following two reasons (Bernatskiy and Nosov 2012). First, the tsunami wave energy losses related to bottom friction cannot be treated as an

effect concentrated near the coastal line. Second, in most cases these energy losses are so insignificant (<1 %) that it is quite expedient to neglect them.

A more complex version of the description of tsunami interaction with the coast implies numerical simulation of waves running up the coast. We shall dwell upon methods for resolving this problem in Sect. 6.3.

In those cases, when detailed simulation of the tsunami dynamics within a restricted region is required, the necessity often arises to make use of boundaries that freely transmit incident waves. In other words, the amplitude of a wave, reflected from such a boundary, should be reduced to the minimum. The physical principle for realization of such a “nonreflecting” boundary condition is quite simple. At each moment of time a boundary point is assigned that value, which should be brought to it by the wave incident upon the boundary. However, technical realization of the condition of free transmission turns out to be elementary only in the one-dimensional case. If one considers wave propagation along the $0x$ axis, then the condition of free transmission will be of the form

$$\frac{\partial u}{\partial t} = \pm c \frac{\partial u}{\partial x}, \quad (6.40)$$

where $c = \sqrt{gH}$ is the velocity of long waves. The quantity u in formula (6.40) is understood to be any of the sought functions (the free surface displacement or the flow velocity component).

A condition of the same form as (6.40) is also applicable in resolving two-dimensional problems, but it will no longer provide for ideal free transmission through the boundary $x = \text{const}$ of waves, travelling at a certain angle to the $0x$ axis. Regretfully, no success has been achieved in totally avoiding the reflected wave, when resolving the problem on a plane. It is possible to reduce the amplitude of waves, reflected by the boundary, by enhancing the order of the boundary condition approximation (Marchuk et al. 1983; Ilgamov and Gilmanov 2003),

$$\begin{aligned} c \frac{\partial^2 u}{\partial x \partial t} &= \frac{\partial^2 u}{\partial t^2} - \frac{c^2}{2} \frac{\partial^2 u}{\partial y^2}, \\ c \frac{\partial^2 u}{\partial t^2} - \frac{c^3}{4} \frac{\partial^3 u}{\partial y^2 \partial x} &= \frac{\partial^3 u}{\partial t^3} - \frac{3c^2}{4} \frac{\partial^2 u}{\partial y^2 \partial t}. \end{aligned}$$

In the case of a wave impinging at an incidence angle of 45° the 1-st order condition (6.40) yields an amplitude reflection coefficient $R \approx -0.17$, while at the same time the 2-nd order condition gives $R \approx 0.03$ (Ilgamov and Gilmanov 2003). The 2-nd order condition is seen to provide quite a good precision. Note that one must be careful in imposing boundary conditions of a high order. Unlike the classical boundary conditions, introduced by Dirichlet, Neumann or Robin, a boundary condition of higher order may lead to problems, for which no uniqueness theorem has been proven.

There also exists another approach to realizing nonreflecting boundaries. It consists in the introduction of an absorbing layer in the vicinity of the boundary (Israeli and Orzag 1981; Kosloff and Kosloff 1986).

Let us indicate one more original approach to implementing the nonreflection boundary condition (Ilgamov and Gilmanov 2003). For definiteness we shall assume a plane wave to be incident at a certain angle upon the boundary $x = 0$, reflection from which is to be excluded. The approach consists in superposing two solutions of one and the same problem upon each other, given that at the boundary $x = 0$ they, first, satisfy the Dirichlet condition $\xi = 0$ and, then, the Neumann condition $\partial\xi/\partial x = 0$. The Dirichlet condition is known to provide for an amplitude reflection coefficient $R = -1$, while the Neumann condition gives $R = 1$. Superposition of these two solutions excludes waves reflected by the boundary $x = 0$.

The third type of boundary conditions (perturbation, arriving from external area) is the most simple to realize. If a certain perturbation approaches the boundary from outside of the calculation region, then at all points of the boundary one must set the velocity components and the surface displacement to correspond to this perturbation. Depending on the concrete problem these quantities can either be determined from the solution of another numerical problem or be given by certain functions.

The key information, upon the reliability of which the precision of numerical tsunami calculations depends, comprises data on the ocean bottom bathymetry and on the topography of the coastal area. At present, free access is provided to a 1-minute global database for the Earth's relief (ETOPO1, <http://www.ngdc.noaa.gov/>) and a 30 arcsecond digital atlas (GEBCO, British Oceanographic Data Centre, <http://www.ngdc.noaa.gov/mgg/gebco/>). For some regions data are available with a significantly improved space resolution, for example, like in the NGDC Tsunami Inundation Gridding Project (<http://www.ngdc.noaa.gov/mgg/inundation/tsunami/>). In run-up simulation it may turn out to be useful to take advantage of 3 arcsecond data, obtained by the Shuttle Radar Topography Mission (SRTM). SRTM successfully collected data over 80% of the Earth's land surface, for all the area between 60°N and 56°S latitude. The data are available at the site <http://seamless.usgs.gov/>.

The most widespread approach to the numerical solution of equations describing tsunami dynamics is based on the finite-difference method, which uses structured (regular) grids. In those cases, when a detailed description of the wave dynamics within a region defined beforehand is required, the method of nested grids is applied. Here, inside the computation region one singles out a sole or several (usually rectangular) subregions of the 1-st level, inside which the spatial increment is rendered small. In a 1-st level region it is possible to single out subregions of the 2-nd level, within which the spatial increment is further reduced, and so on. At the boundary between the subregions of levels n and $n + 1$ the solutions are dynamically made to match. Implementation of the method of nested grids is quite simple, so it is widespread (e.g., TUNAMI, MOST, NAMI DANCE, MGC, FUNWAVE-TVD).

Besides the finite-difference method, use is also made in tsunami simulation of the method of finite elements applying unstructured grids (variable step) (Harig et al. 2008; Piatanesi et al. 1999; Walters 2006; Zhang and Baptista 2008; Androsov et al. 2011). Implementation of the method of finite elements is more difficult than of

the finite-difference method. But it does have an important advantage: unstructured grids are readily adapted to the complex form of a computation region and they admit condensation of the grid when enhanced spatial resolution is required.

In recent years, works have appeared, in which dynamically adaptive grids are used in tsunami simulation (LeVeque et al. 2011; Popinet 2012). The main idea of this approach consists in partitioning the grid into smaller cells inside those zones of the computation region and at that time, where and when the solution exhibits a small-scale structure. If the problem is nonlinear and the structure of the solution is unpredictable, then application of dynamically adaptive grids is doubtless one of the most optimal approaches. But the dynamics of tsunami waves in open ocean is linear and all the spatial peculiarities of the wave field are unambiguously related to the distribution of depths. Therefore, the use of dynamically adaptive grids for the description of tsunamis in the open ocean is not most optimal. It is expedient to apply this “fine tool,” for instance, in the shallow-water zone and for describing the run-up, i.e., precisely in those cases, when the manifestations of nonlinearity are certain to be significant. In open ocean, when the grid can be readily adapted to the depth distribution, dynamical adaptation evidently only leads to additional consumption of computational resources.

For numerical description of the dynamics of linear long waves, the velocity of which is determined by the expression \sqrt{gH} , while their period is conserved during propagation, it has sense to vary the spatial increment depending on the depth as follows:

$$\Delta(H) = \Delta_{\max} \sqrt{H/H_{\max}}, \quad (6.41)$$

where Δ_{\max} is the maximum spatial increment, established in the vicinity of the point of maximum depth H_{\max} . The law (6.41) provides for conservation of the number of grid nodes per wavelength. Consequently, the possibility is excluded for the length of a wave in the shallow-water region to drop down to the “dangerous” limit of $\lambda = 2\Delta$. Moreover, application of grids of variable step will permit significant reduction of the computational work content required by the problem.

The law (6.41) can, naturally, not be applied straightforwardly in constructing a plane rectangular computational grid. In this case, only multiple division of the spatial increment is possible. Thus, for example, in the case of depths within the range $H_{\max}/4 < H \leq H_{\max}$ a 1-st level grid is constructed with a spatial increment $\Delta_1 = \Delta_{\max}$; for depths within a range of $H_{\max}/16 < H \leq H_{\max}/4$ a 2-nd level grid is constructed with a spatial increment $\Delta_2 = \Delta_{\max}/2$, and so on. An example of such a grid is shown in Fig. 6.9a. A more or less smooth decrease in the grid step can be achieved, in accordance with law (6.41), if triangular partitioning is applied (see Fig. 6.9b).

Let us estimate the work content required for numerical solution of the problem concerning the propagation of long waves, when grids with constant and variable (in accordance with formula (6.41)) spatial increments are used. By the work content we intend the number of grid nodes multiplied by the necessary number of time steps, $N = N_x N_y N_t$. For our estimation we shall assume the computation region to have a characteristic horizontal extension L . Computation of the tsunami

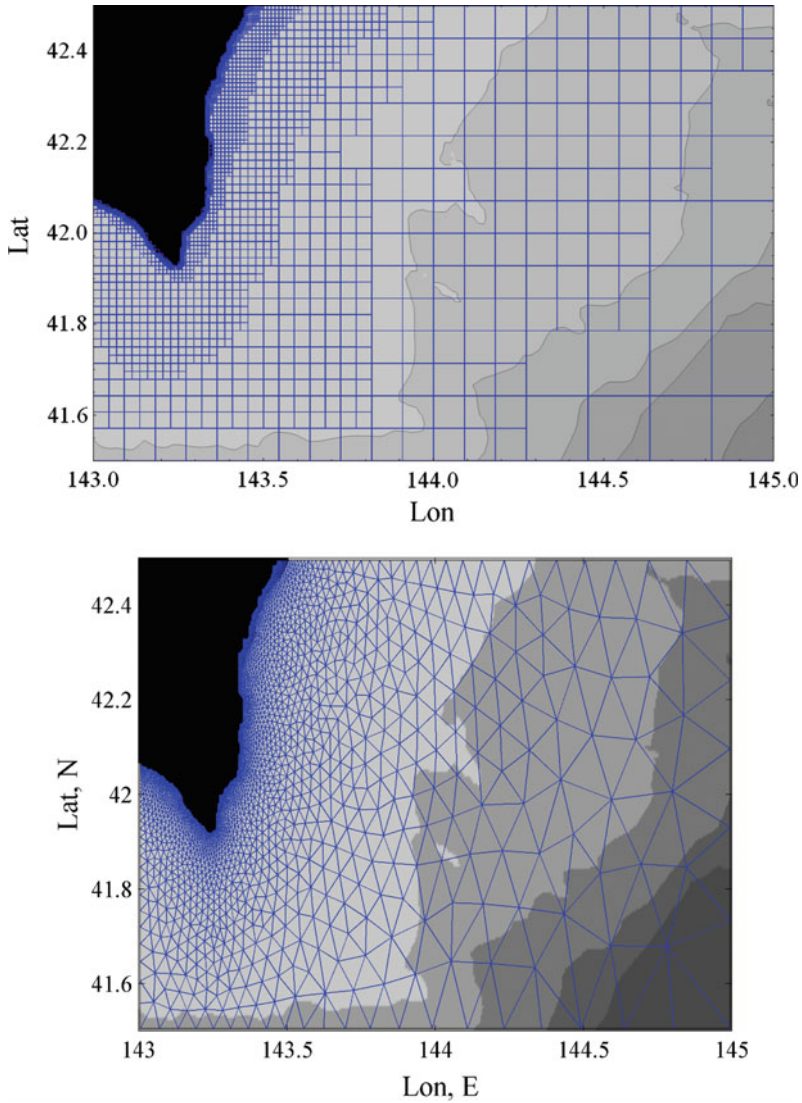


Fig. 6.9 Examples of unstructured grids adapted to the ocean depth

propagation must, evidently, be carried out at least until the time, required for the wave to cover a distance equal to the dimension of the computation region, passes: $T \sim L/\sqrt{gH_{\max}}$.

The amount of nodes in a grid of constant step Δ is determined by the simple formula $N_{xy} \equiv N_x N_y \sim (L/\Delta)^2$. The time step is determined by the Courant–Friedrichs–Lewy Condition: $\Delta t < \Delta/\sqrt{gH_{\max}}$. The number of steps in time is

estimated as $N_t \sim T/\Delta t = L/\Delta$. Thus, when a grid of constant step is used, the computational work content increases vary rapidly—in proportion to the cubic ratio of the size of the computation region and the spatial increment:

$$N \sim \left(\frac{L}{\Delta}\right)^3.$$

Let us further estimate the computational work content of the problem, when a grid of variable step, determined by formula (6.41), is used. We right away note that the advantage of unstructured grids is not only due to significant reduction of the amount of nodes, while the necessary spatial resolution in the shallow-water region is conserved, but, also, to the possibility of setting a large time step and at the same time maintaining stability of the numerical scheme.

To calculate the number of nodes of a unstructured grid we divide the computation region into subregions, the oceanic depth in which varies within the ranges $H_{\max}/4^n < H \leq H_{\max}/4^{n-1}$, where $n = 1, 2, 3 \dots$. The spatial increment in a subregion of level n is determined by the formula $\Delta_n = \Delta_{\max}/2^{n-1}$. The total number of grid nodes is estimated as follows:

$$N_{xy}^U = \sum_n \frac{S_n}{\Delta_n^2} \sim \frac{L^2}{\Delta_{\max}^2} \sum_n \frac{S_n}{S} 4^{n-1}, \quad (6.42)$$

where S_n is the area occupied by a subregion of level n , $S = \sum_n S_n$ is the area of all the region.

The time step is determined by the Courant–Friedrichs–Lewy criterion $\Delta t^U < \Delta(H)/\sqrt{gH}$, from which, with account of relation (6.41), we obtain $\Delta t^U < \Delta_{\max}/\sqrt{gH_{\max}}$. We can now estimate the number of necessary steps in time:

$$N_t^U \sim T/\Delta t^U \sim L/\Delta_{\max}. \quad (6.43)$$

As a result, we have an estimate of the computational work content required for solution of the problem using an unstructured grid,

$$N^U \sim N_{xy}^U N_t^U \sim \frac{L^3}{\Delta_{\max}^3} \sum_n \frac{S_n}{S} 4^{n-1}.$$

The advantage of applying an unstructured grid is determined by the ratio of the work contents N and N^U

$$N/N^U \sim \frac{1}{\sum_n \frac{S_n}{S} 4^{n-1}} \left(\frac{\Delta_{\max}}{\Delta}\right)^3. \quad (6.44)$$

An accurate calculation of the sum present in formula (6.44) requires setting the concrete bathymetry. As an example, consider the region near to the island Hokkaido,

shown in Fig. 6.9a. We shall only single out 6 subregions. In this case the spatial increment varies between Δ_{\max} for large depths and $\Delta_{\max}/32$ in the coastal region. Applying the bathymetry GEBCO08 (30 angular seconds) we obtain the following value for the sum present in formula (6.44):

$$\sum_n \frac{S_n}{S} 4^{n-1} \approx 14.3.$$

When a structured grid is used, in order to achieve a spatial resolution equivalent to the resolution, obtained with an unstructured grid, it is necessary to set the step in space to $\Delta = \Delta_{\max}/32$ over the entire region. As a result, for the example of a computation region, dealt with, we obtain $N/N^U \approx 2300$. Hence follows an important conclusion: application of an unstructured grid permits to reduce the computational work content of the problem by thousands of times, at the same time maintaining the required spatial resolution in the shallow-water region.

The decrease in wavelength upon arrival in a shallow-water region is not the only factor to give rise to short-wave perturbations and to require condensation of the computational grid. If the ocean depth variation is described by a discrete function, situations may occur when a significant change of depth occupies a single grid step in space. In such a case we arrive at an analogy to the classical interaction problem of a long wave propagating within a channel involving a jump in depth. At the jump point of the depth the continuity conditions are fulfilled for the displacement of the free surface $\xi_1 = \xi_2$ (pressure) and for the flow of liquid, $u_1 H_1 = u_2 H_2$ (indices “1” and “2” are related to the regions separated by the depth jump). Consequently, at this point a discontinuity forms in the flow velocity as well as a discontinuity in the spatial derivative of the surface displacement,

$$u_2 - u_1 = u_1 \frac{H_1 - H_2}{H_2}, \quad (6.45)$$

$$\frac{\partial \xi_2}{\partial x} - \frac{\partial \xi_1}{\partial x} = \frac{\partial \xi_1}{\partial x} \frac{H_1 - H_2}{H_2}. \quad (6.46)$$

Naturally, the representation of functions in a discrete form in resolving problems by the finite-difference method implies their saltatory variation. But the validity of the method will clearly be violated if such saltatory variations alter the values of the functions strongly. The computation grid must obviously be partitioned so the calculated functions do not undergo significant changes along distances of the order of the spatial increment. Mathematically, this condition can be written as follows:

$$\left| \frac{u_2 - u_1}{u_1} \right| \ll 1,$$

$$\left| \frac{\frac{\partial \xi_2}{\partial x} - \frac{\partial \xi_1}{\partial x}}{\frac{\partial \xi_1}{\partial x}} \right| \ll 1.$$

With account of formulae (6.45) and (6.46) we obtain a sole condition:

$$\left| \frac{H_1 - H_2}{H_2} \right| \ll 1,$$

which can be rewritten as follows:

$$\frac{|H_1 - H_2|}{H_2} \approx \frac{|gradH| \Delta}{H} \ll 1. \tag{6.47}$$

From formula (6.47) follows the condition to be imposed on the length of the spatial increment, which can be readily applied in practice:

$$\Delta \ll \frac{H}{|gradH|}. \tag{6.48}$$

Figure 6.10 presents the distribution of the quantity $H / |gradH|$, calculated for the region near the island Hokkaido, shown in Fig. 6.9. A typical range of the quantity investigated is $10^3 - 10^6$ m, and in most of the cases it exceeds 10^4 m. Consequently, in

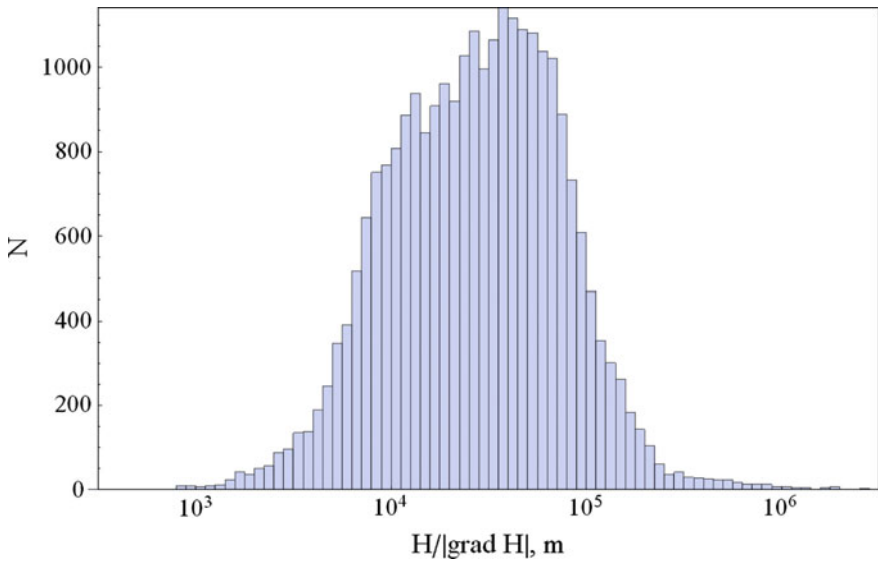


Fig. 6.10 Distribution of quantity $H / |gradH|$ for the region shown in Fig. 6.9. In calculations use was made of the bathymetry GEBCO08 with a resolution of 30 angular seconds

accordance with criterion (6.48), the spatial increment can be set at a level $\Delta \sim 10^3$ m. However, in certain cases the quantity $H/|\text{grad}H|$ may reach $\sim 10^3$ m, which makes it necessary to reduce the spatial increment down to a value $\Delta \sim 100$ m.

In constructing an unstructured grid the spatial increment must, naturally, be chosen to be equal to the smallest of the values specified by formulae (6.41) and (6.48).

We shall further touch upon certain results of numerical simulation of the Indonesian catastrophic tsunami that took place on December 26, 2004. The example of this tsunami will be used in describing characteristic features of tsunami wave propagation for demonstrating the possibilities of modern numerical models. We shall mainly adhere to the results obtained in Titov et al. (2005).

The tsunami of December 26, 2004, happened to be the first global event, for which there were high-quality measurements of the sea level supplemented with data from satellite altimeters. The first instrumental measurement of this tsunami appeared 3 hours after the earthquake—the wave was registered by a station on the Coconut islands (Fig. 6.11) at about 1700 km from the epicenter. According to these data, the first wave was only 30 cm high. The first wave was followed by prolonged level oscillations with a maximum amplitude not exceeding 53 cm. At the same time, at a number of coastal sites of India and Sri Lanka, located at approximately the same distance, waves ten times higher, than on the Coconut islands, were registered. Such a large difference in amplitude, confirmed by the results of numerical simulation, demonstrates a pronounced directivity of the wave energy emission. The data from other mareographs in the Indian Ocean showed wave amplitudes between 0.5 and 3 m, and no noticeable damping was observed as the distance from the source increased.

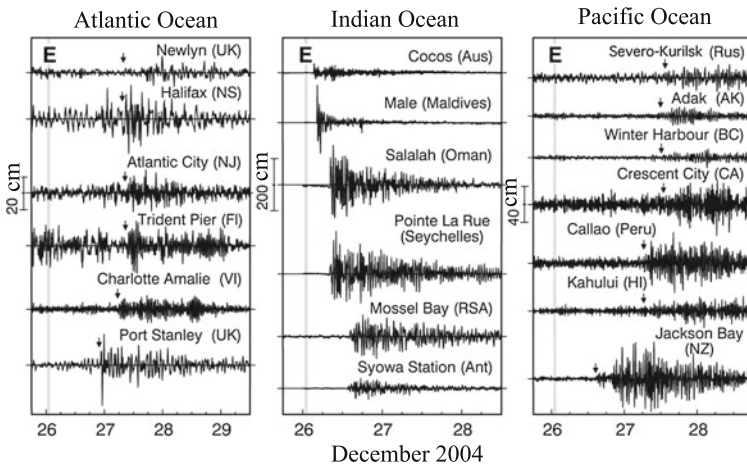


Fig. 6.11 Time series of tsunami wave heights (cm) as recorded at selected tide-gauge stations in the three major ocean basins. *Arrows* indicate first arrival of the tsunami (Reprinted from Titov et al. 2005 by permission of the publisher)

Note that the wave heights measured by mareographs are not always in good accordance with the tsunami run-up heights on the coast. Several records, obtained from regions with significant run-ups, registered wave heights 2–5 times smaller, than actually observed values. Thus, for example, the mareograph at Phuket showed 1.5 m, while the actual run-up height was from 3 to 6 m. This divergence strongly complicates determination of the true tsunami height on the coast. Moreover, many mareographs in the Indian Ocean were destroyed (Thailand) or happened to be strongly damaged (Colombo, Sri Lanka). Therefore, the true maximum wave heights may have remained unknown.

Data on tsunamis in the remote zone revealed that, unlike manifestations near the source, the maximum wave amplitude was not associated with the leading wave. In the North Atlantic and at the North of the Pacific Ocean maximum wave heights were observed with delays from several hours up to several days after the onset of the tsunami front (Fig. 6.11). It is interesting to note, that at Callao (Peru), situated 19,000 km from the source, the waves were higher, than on the Coconut islands, lying significantly closer (1700 km). Moreover, the tsunami amplitude at Halifax (Nova Scotia, Canada) was also greater, while in this case the waves had to cross not only the Indian but also the Atlantic Ocean (longitudinally) and in doing so to cover over 24,000 km.

Model studies of tsunami propagation in the open ocean permit to obtain a picture of energy propagation, which cannot be reconstructed having only the data of coastal measurements at one's disposal. Since the tsunami dynamics in the open ocean is linear, the height of a wave is proportional to the square root of its energy. Thus, the space distribution of calculated maximum wave heights, presented in Fig. 6.12 provides a clear picture of tsunami energy propagation. Numerous versions of calculations, performed for different values of bottom deformations, sizes and orientations of the source, have revealed that all these parameters insignificantly influence wave propagation in the remote zone. We right away note, that in the close zone the shape and orientation of the source happen to be decisive parameters.

A very important fact, testifying in favor of the numerical model being adequate, is the good agreement between wave amplitudes, resulting from calculations, and those registered by coastal stations. Thus, for example, the anomalously high values of amplitudes in the remote zone reflect precisely the main directions of wave energy propagation. The coastal stations in Halifax (Canada), Manzanillo (Mexico), Callao (Peru), Arice (Chile) recorded wave heights exceeding 50 cm. Being at a significant distance from the source (over 20,000 km), each of the sites indicated is to be found in an area, related to the end of one of the "wave rays".

Numerical calculations, corroborated by in-situ data, confirm the assumptions that two main factors influence tsunami propagation: the source configuration (geometry), and the waveguide properties of mid-oceanic ridges. We recall that the continental shelf can also serve as a waveguide. In many cases waves, captured by the shelf, are the cause of prolonged oscillations of the water level at the coast.

In the nearby zone, the orientation of energy emission was related to the large extension of the tsunami source. The long and narrow region (stretched out in the meridional direction), in which deformations of the ocean bottom, caused by

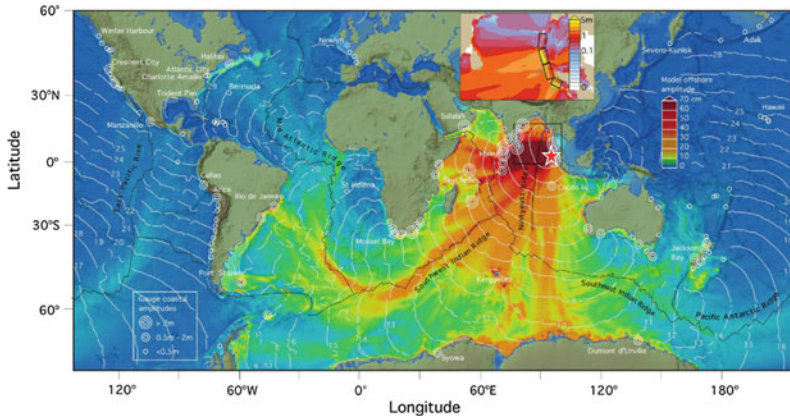


Fig. 6.12 Global chart showing energy propagation of the 2004 Sumatra tsunami calculated from MOST. *Filled colors* show maximum computed tsunami heights during 44h of wave propagation simulation. Contours show computed arrival time of tsunami waves. *Circles* denote the locations and amplitudes of tsunami waves in three range categories for selected tide-gauge stations. Inset shows fault geometry of the model source and close-up of the computed wave heights in the Bay of Bengal. Distribution of the slip among four subfaults (from south to north: 21, 13, 17, 2 m) provides best fit for satellite altimetry data and correlates well with seismic and geodetic data inversions (Reprinted from Titov et al. 2005 by permission of the publisher)

the earthquake of December 26, 2004, were concentrated, formed waves of large amplitude in the perpendicular, i.e., longitudinal, direction. The waves propagating in the meridional direction were of essentially smaller amplitude. This effect is not only manifest in simulations, but it also follows from analysis of records of mareographs and expedition data. Thus, for example, on the opposite coast of the Indian Ocean, 5000 km from the source, on the Somalia coast (East Africa) run-up heights from 5 up to 9 m have been observed (Synolakis et al. 2005). From numerical calculations of the distribution of maximum amplitudes (Fig. 6.12) it is seen that one of the “wave rays” ends precisely on this coast.

The main factor, determining the orientation of energy propagation in the remote zone, is now the topography of the bottom of the World Ocean (Fig. 6.13). Analysis of the Indonesian tsunami of December 26, 2004, reveals the important role of mid-oceanic ridges in channeling the tsunami energy. From comparison of Figs. 6.12 and 6.13 it is readily seen that the Southwest Indian Ridge, as well as the Mid-Atlantic Ridge served as waveguides for propagating the tsunami toward the Atlantic. The Pacific Antarctic Ridge and Southeast Indian Ridges, and, also, the East-Pacific Rise contributed to the penetration of waves into the Pacific Ocean. It is interesting that ridges cope well with the role of waveguides until their curvature does not exceed a critical value. Thus, for example, the sharp bend in the Mid-Atlantic Ridge at the parallel of 40° S contributed to the waveguide losing beams. As a result, waves of noticeable amplitude were observed at the Atlantic coast of South America.

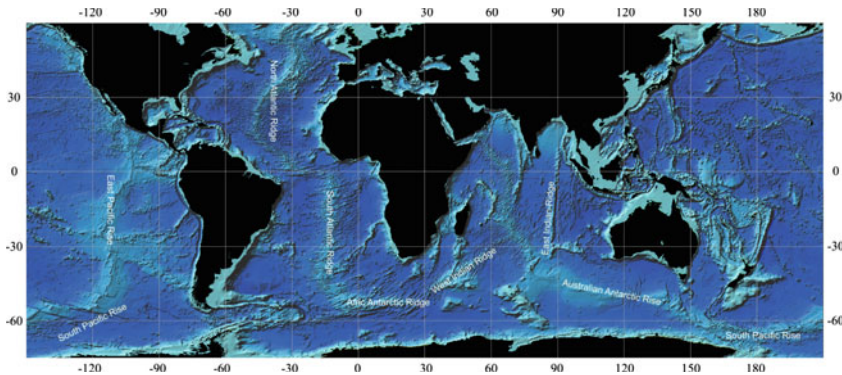


Fig. 6.13 Topography of World Ocean. Mid-oceanic ridges that essentially influenced propagation of the Indonesian tsunami of December 26, 2004

The numerical model pointed correctly to the significant amplitude (~ 1 m) in Rio de Janeiro. Regrettably, no other measurements were carried out at any points of the Atlantic coast of South America.

In the southern direction from the source, the waves propagated along the Ninety-East Ridge. In accordance with calculations they could have had a significant height on the Antarctic coast. However, it was practically impossible to check this fact, owing to the absence of mareograph stations. Two stations (one Japanese, “Syowa”, and the other French, “Dumont d’Urville”), located approximately 2000 km to the West and East, respectively, from the point of incidence of the main “beam”, registered moderate wave heights (of amplitude 60–70 cm).

In most cases of tsunami records, obtained in the eastern and central regions of the Indian Ocean (Fig. 6.11), only the first several waves exhibited the maximum amplitude. Further, the amplitude approximately exponentially decreased in time. The duration of anomalously large level oscillations amounted to 12 h. Numerical simulation shows that such a character of level oscillations at the coast corresponds to those cases, when waves of maximum amplitude, being focused by an extended source, traveled directly from the source to the observation point. The pronounced orientation of wave emission, seen well in Fig. 6.12, once more confirms the fact, that one of the most important factors determining tsunami propagation in the near zone is the shape of the source.

Tsunami records, obtained in the western part of the Indian Ocean and in other oceans, reveal a significant duration of tsunami “sounding”, while level oscillations of maximum amplitude were observed with an essential delay after the onset of the first wave. This is due to enhancement of the role of waves reflected from the coasts and from irregularities of the ocean bottom, and also to propagation along natural waveguides—submarine ridges. The relatively slow, but energy-saving waveguide propagation provides for a late onset of the largest waves. Numerical simulation has shown that a wave perturbation often consists of two (or more) clearly distinguishable packets. One of them has a relatively small amplitude and propagates

straightforwardly with a high velocity, “taking advantage of” deep areas of the ocean. The second packet has a greater amplitude, but propagates slower along underwater ridges (elevations).

It is interesting, that the tsunami penetrated the Pacific Ocean via two routes: directly from the Indian Ocean and through the southern part of the Atlantic Ocean, bypassing the Drake Passage between South America and Antarctica. Numerical simulation reveals the waves, that arrived in the Pacific Ocean from the West from the Indian Ocean, and those, that came from the East through the Atlantic, to have commensurable amplitudes. For all the Pacific coast, with the exception of southern Chile, the onset of waves arriving from the East occurs later.

To conclude the section we note that no destructions related to the tsunami of December 26, 2004 were reported outside the Indian Ocean. But experience in observations and simulations of the global propagation of tsunamis shows that the penetration of waves into all oceans is possible in principle. Such a danger can be withstood, if a global system of tsunami warning is created.

6.3 Tsunami Run-Up on the Coast

Of all problems relevant to tsunami dynamics, the description of wave transformation in the coastal belt, together with flooding of the coastal zone or uncovering of the ocean bottom, represents one of the most difficult tasks. This is, first of all, due to the problem being nonlinear and the boundary, i.e., the shoreline, being movable. The topic of tsunami run-ups on the coast is so vast that it could be the subject of a separate monograph. In this section we shall only briefly dwell upon some of the main results of and approaches to resolving the tsunami run-up problem and give references to key publications.

The well-known book by J. Stoker (1957) contains the classical formulation of the run-up problem. An extensive bibliography, reflecting development of the issue up to the end of the 1980s of the twentieth century, can be found in Voltsinger et al. (1989). A significant part of the monograph by E.N. Pelinovsky (1996) is devoted to analytic approaches to resolving the problem of a tsunami run-up. The most significant achievements in this field are also expounded in Carrier and Greenspan (1958), Keller et al. (1960), Shen and Meyer (1963), Sielecki and Wurtele (1970), Lyatkher and Militeev (1974), Spielvogel (1975), Hibberd and Peregrine (1979), Pedersen and Gjevik (1983), Kim et al. (1983), Kaistrenko et al. (1985a), Synolakis (1987), Synolakis et al. (1988), Golubtsova and Mazova (1989), Pelinovsky (1992, 1995), Pelinovsky et al. (1993), Tadepalli and Synolakis (1994), Liu et al. (1995), Pelinovsky (1995), Titov and Synolakis (1995), Liu et al. (2003), Carrier et al. (2003), Kanoglu (2004), Tinti (2005), Dotsenko (2005), Shermenewa and Shugan (2006), Kanoglu (2006), Madsen et al. (2008), Didenkulova (2007b, 2009a, b), Dobrokhotov and Tirozzi (2010), Bernatskiy and Nosov (2012). A large part of these references are based on approximation of the coastal topography by a flat escarp. However, the bottom profile in the coastal zone can evidently not always be represented by a linear

function. And, besides other features, the shape of the bottom profile also affects the run-up characteristics strongly. A special place, here, is occupied by the depth profile, that is proportional to the coordinate raised to the power $4/3$ and is presented in Cherkesov (1976), Tinti (2001), Didenkulova (2009a), and, also, by the profile proportional to the coordinate raised to the fourth power (Didenkulova 2010). Waves can propagate along such profiles without being reflected, which leads to their anomalous enhancement and, consequently, to an anomalous run-up onto the shore.

Similar “reflectionless” structures also exist in two-dimensional problems (Didenkulova 2011a, b). The most striking example, here, is a bay with a linear slope and parabolic cross section,—bays of similar shapes are quite often encountered in nature (Didenkulova 2011b). Thus, the anomalous tsunami run-up in the Pago Pago port during the 2009 tsunami on Samoa was primarily due to the specific “reflectionless” shape of the harbor (Didenkulova 2013).

Publications of the past two decades reveal significant progress in numerical simulation of tsunami interaction with the coast. Here, in calculating inundation of the shore use is made both of nonlinear shallow-water equations (in the case of long-period tsunamis, as a rule, of seismic origin and propagating short or moderate distances) and of Boussinesq equations (in the case of shorter wave tsunamis, as a rule, of landslide origin). Of the numerous models based on the nonlinear shallow-water equations the most well-known are TUNAMI (Imamura et al. 1995), ALASKA (Nicolosky et al. 2011), MOST (Wei et al. 2008; Tang et al. 2012) and GeoClaw (Berger and Leveque 1998). Of the models based on Boussinesq equations we note FUNWAVE (Shi et al. 2012; Grilli et al. 2013), COULWAVE (Park et al. 2013), BOSZ (Roeber and Cheung 2012) and GloBouss (Harbitz et al. 2014).

To verify numerical models analytic test problems have been developed, and special laboratory experiments have also been performed (Liu et al. 1991; Yeh et al. 1996). Known as the “Catalina benchmark” can be found on the site page http://isec.nace.org/workshop/2004_cornell/background.html. Another group of test problems is available at the following address (Mapping & Modeling Benchmarking Workshop, February 9–10, 2015, Portland, Oregon): http://coastal.usc.edu/currents_workshop/problems.html.

There exist different types of tsunami run-ups on a shore. They vary from gradual flooding (like during the tide) to the onslaught on the coast of a vertical wall of turbulent water—a bore. As a rule (in about 75 % of events), tsunami waves flood the shore without breaking (Mazova et al. 1983). Tsunami run-ups in the form of a wall are quite rare, and usually in the case of waves of significant amplitude.

The three following main types of wave run-ups onto the coast can be identified (Pelinovsky 1996):

- spilling breaker—crest of wave breaks, foam flows down its frontal slope, peculiar to gently sloping bottom;
- plunging breaker—crest of wave surpasses foot and curls down, peculiar to inclined bottom slopes;
- surging breaker—wave floods coast without breaking, peculiar to steep slopes.

We note that at different points one and the same tsunami may manifest both different run-up types and different run-up wave shapes (regular wave trains, single waves, N -waves, etc.). This variety of shapes explains the large number of works on tsunami wave run-ups of different shapes (see references at the beginning of this section). As an example we shall touch upon studies of the influence the shape of a wave hitting a shore has on its run-up characteristics (the maximum run-up height and velocity, the wave breaking parameter) performed in Didenkulova (2008) for a flat escarp and in Didenkulova et al. (2015) for narrow bays. The difference in shape was shown to be insignificant from the point of view of run-up characteristics in all the cases of symmetric pulses of bell-like shape (sinusoidal pulses, solitons, Lorentz pulses, and others). The asymmetry of the incident wave turned out to be essential. In particular, it was established that steepening of the wave front leads to significant enhancement of the height and velocity of a wave run-up on the shore (Didenkulova et al. 2007a). The last result was confirmed experimentally in the 309-m wave channel of the Hannover university (Didenkulova et al. 2015).

The most widespread mathematical model, applied in describing wave dynamics in the coastal zone, makes use of the nonlinear equations of long waves, (6.29)–(6.31), in which the Coriolis force is usually neglected. In many cases, for reasons of simplicity, bottom friction is also neglected, although this factor may actually influence the run-up value noticeably. The main ideas of the tsunami run-up process can be understood by considering a one-dimensional problem along the axis perpendicular to the shoreline. Most model studies are performed for a region, representing a slope connected with a smooth horizontal ocean bottom (Fig. 6.14).

In determining boundary conditions for practical tsunami calculations the so-called “vertical wall” approximation has become widespread. A boundary condition of this type provides for total reflection of the wave at a fixed isobath. Note that the vertical wall approximation is not a purely academic abstraction, it imitates quite a type of coast, encountered quite often—a rocky precipice, falling off to the water. In the notation, given in Fig. 6.14, the vertical wall corresponds to $\beta = 90^\circ$ or to $L = 0$.

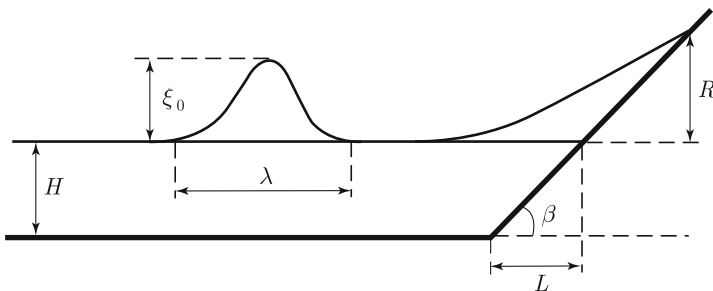


Fig. 6.14 Formulation of the problem of a tsunami run-up on the coast

From elementary theory of linear waves it is known, that, if a channel of fixed depth ends in a vertical wall, then the height of the run-up onto the wall is determined as twice the incident wave amplitude, $R_L = 2\xi_0$.

Actually, when approaching the coast, the tsunami amplitude may be commensurable with the depth. Therefore, to determine the run-up height one must, generally speaking, apply nonlinear theory. Omitting the details of resolving the nonlinear problem of long-wave theory, expounded in the book Pelinovsky (1996), we present the resulting analytical formula, that relates the run-up onto a vertical wall, R_N , and the wave amplitude far from the coast, ξ_0 ,

$$R_N = 4H \left(1 + \frac{\xi_0}{H} - \left(1 + \frac{\xi_0}{H} \right)^{1/2} \right), \quad (6.49)$$

where H is the basin depth. It is readily verified, that the relation $R_L = 2\xi_0$ is a partial case of formula (6.49) given the condition $\xi_0/H \ll 1$. Comparison of quantities R_L and R_N shows, that taking into account nonlinearity enhances the run-up amplitude insignificantly. As the nonlinearity (of quantity ξ_0/H) increases, the ratio R_N/R_L grows monotonously, but this growth is not without limit,

$$\lim_{\frac{\xi_0}{H} \rightarrow \infty} \left(\frac{R_N}{R_L} \right) = 2.$$

This means, the run-up amplitude, calculated with account of nonlinearity, cannot be superior to twice the amplitude corresponding to linear theory.

We further consider the one-dimensional problem of a long wave moving along a slope ($0 < \beta < \pi/2$). We write the nonlinear equations for shallow water, taking into account that the basin depth is a linear function of the horizontal coordinate, $H = H_0 - \alpha x$,

$$\frac{\partial U}{\partial t} + U \frac{\partial U}{\partial x} + g \frac{\partial \xi}{\partial x} = 0, \quad (6.50)$$

$$\frac{\partial \xi}{\partial t} + \frac{\partial}{\partial x} \left((\xi - \alpha x) U \right) = 0. \quad (6.51)$$

Consider the wave, arriving on the shelf, to be characterized by a height ξ_0 and period T . We introduce dimensionless variables (the asterisk “*” will be further dropped)

$$t^* = \frac{t}{T}, \quad x^* = \frac{x\alpha}{\xi_0}, \quad \xi^* = \frac{\xi}{\xi_0}, \quad U^* = \frac{U\alpha T}{\xi_0}.$$

In these variables the system (6.50)–(6.51) assumes the following form Kaistrenko et al. (1985a, b):

$$\frac{\partial U}{\partial t} + U \frac{\partial U}{\partial x} + \frac{1}{Br} \frac{\partial \xi}{\partial x} = 0, \quad (6.52)$$

$$\frac{\partial \xi}{\partial t} + \frac{\partial}{\partial x} [(\xi - x) U] = 0, \quad (6.53)$$

where $Br = \xi_0 / (g\alpha^2 T^2)$ is the only dimensionless parameter, which from a physical point of view represents a criterion for the breaking of a wave running up a plane slope. Note, that this criterion is not quite precise, since it does not take into account phase dispersion and bottom friction.

Numerous experimental studies have permitted to introduce the Iribarren number as a criterion for wave breaking (Battjes 1988),

$$Ir = \frac{\alpha \lambda^{1/2}}{\xi_0^{1/2}},$$

where λ is the deepwater wavelength. We consider the depth along the slope to increase indefinitely, therefore, for waves of any length there exists a region, where they do not “feel” the bottom. Expressing the wavelength via the period from the dispersion relation for gravitational waves in deepwater, $\lambda = gT^2 / (2\pi)$, we obtain, that the empirically introduced Iribarren parameter and the quantity Br are uniquely related to each other, $Ir^{-2} = 2\pi Br$. The existence of such a relationship testifies in favor of the correct choice of nonlinear long-wave model for describing the tsunami run-up on the shore. Transition from surging to plunging breaker (wave breaking) occurs when $Ir \approx 2$ ($Br \approx 0.04$).

An important step in resolving the run-up problem was the work (Carrier and Greenspan 1958), in which it was shown, that nonlinear long-wave equations can be reduced to a linear wave equation, which, unlike the initial system is resolved in semispace with a fixed boundary. We recall, that the initial system has an unknown movable boundary—the shoreline. This transformation was subsequently termed the Carrier–Greenspan transformation.

The approach based on the Carrier–Greenspan transformation has permitted to find a whole series of analytical solutions to the problem of tsunami run-up on a plane slope (Pelinovsky 1996).

One of the main results of the analysis of nonlinear run-up problems consists of the proof that run-up characteristics depend linearly on the wave amplitude far from the coast. This fact provides for the possibility of applying linear theory in calculating the run-up. A rigorous substantiation of such possibility can be found in Pelinovsky (1982), Kaistrenko et al. (1991).

Thus, for instance, in the case of the run-up of a monochromatic wave on a plane slope, resolution of the linear problem results in it being possible to construct the following simple approximation for the maximum run-up value:

$$R = \xi_0 \begin{cases} 2, & L < 0.05\lambda; \\ 2\pi \left(\frac{2L}{\lambda}\right)^{1/2}, & L > 0.05\lambda. \end{cases} \quad (6.54)$$

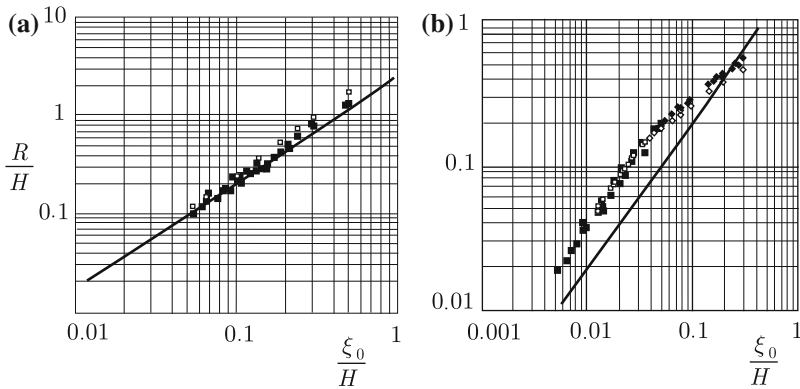


Fig. 6.15 Normalized maximum run-up of solitary waves on plane slope (**a** 1:1, **b** 1:19.85) versus normalized height of incident wave. *Squares*—nonbreaking data, rhombus—breaking data. *Full and empty symbols* correspond to laboratory and numerical experiments, respectively. *Solid line*—run-up height on vertical wall, calculated by formula (6.49) (Adapted from Titov and Synolakis 1995)

If the length of the slope is insignificant as compared with the length of the incident wave, then the run-up process will proceed like in the case of a vertical wall, i.e., the run-up height will turn out to be twice the amplitude of the incident wave. An increase in the slope length L (a decrease of the angle β) will lead to a certain enhancement of the run-up height.

Similar calculations were performed, also, for the run-up of an impulse wave. The maximum run-up in this case, also, is described by a formula identical to (6.54), but with a somewhat different numerical coefficient. It is interesting that oscillations of the shoreline on steep slopes repeat the form of the initial wave. Shoreline oscillations on a gentle slope are related to the form of the incident wave in a more complex manner. Thus, for instance, when a solitary wave (of positive sign) is incident upon a slope, shoreline oscillations turn out to alternate in sign.

The relation between the wave height far from the coast and its run-up height on a plane slope being linear is confirmed by results of laboratory and numerical experiments. Figure 6.15 presents such a relation, obtained for the run-up of solitary waves on steep (1:1) and gentle (1:19.85) slopes. The solid line in Fig. 6.15 shows the dependence corresponding to the run-up height on a vertical wall, calculated by formula (6.49). In the case of a run-up on a steep slope, the dependence of $R(\xi_0)$ is actually very close to (6.49). But in the case of the run-up of waves of large amplitude on a gentle slope deviation is seen of the dependence from (6.49) toward an increase in the run-up height. The bend in the dependence observed at $\xi_0/H \sim 0.03$ (Fig. 6.15b) corresponds to transition to run-ups involving wave breaking.

In Fig. 6.15a it is seen that the run-up on a steep slope is approximately twice the wave amplitude far from the coast, which complies with the theoretical result for the run-up on a vertical wall (6.49). In the case of a run-up on a gentle slope (Fig. 6.15b) the run-up height increases noticeably; here, it is 3–4 times higher than

the wave amplitude far from the coast. In any case, the energy losses, related to wave breaking, result in a reduction of the run-up height. In certain conditions the run-up height on a gentle slope, involving wave breaking, may even turn out to be smaller than the same quantity in the case of a vertical wall.

The data of numerical simulation, presented in Fig. 6.15, are in good accordance with the results of laboratory experiments. Details of the numerical algorithm are described in Titov and Synolakis (1995).

In conclusion of this section we shall dwell upon certain difficulties arising in numerical simulation of a tsunami run-up with account of the real relief of the coastal area. The *first difficulty* is related to the absence of or insufficiently detailed bathymetric and topographical data. For modeling tsunamis in the open ocean, where wavelengths are significant, of the order of 100 km, the existing global data, for example, GEBCO with a resolution of 30 arcseconds (~ 1 km) are quite sufficient. But for reliable numerical simulation of the tsunami dynamics in the coastal zone it is necessary to have data on the reliefs of the bottom and of the coastal area with a space resolution hundreds of times better (~ 10 m). This requirement is related not only to the significant reduction of wavelengths in shallow water. The quality of topographical data directly influences the precision in resolving the practical problem—determination of the run-up boundaries. Here, it must also be noted, that for resolving the run-up problem accurately it is also necessary to have at one's disposal information on tidal level oscillations.

The most reliable applicability criterion for one or another model of a tsunami run-up is based on practical tests. Large-scale experiments in basins of lengths exceeding a hundred meters, like the basin 309 m long of the Coastal Research Centre (FZK—Forschungszentrum Küste), Germany (Fernandez et al. 2014), the basin 205 m long of the Central Research Institute of Electric Power Industry) in Japan (Matsuyama et al. 2007), the basin 110 m long of the Oregon University in the USA (Linton et al. 2013; Riggs et al. 2014) and others, have recently become widespread.

After publication of Madsen et al. (2008), the authors of which showed that the shape of a real wave cannot be represented by a soliton, the philosophy of tsunami simulation in a laboratory started to undergo changes. At present the main accent in laboratory simulations is on the reproduction of real records of tsunamis (Rossetto et al. 2011; Chan and Liu 2012; Schimmels et al. 2014). Of course, laboratory experiments permit to judge the operational integrity of numerical models, but, nevertheless, most reliable tests are based on comparison of the results of simulation with data on real tsunamis. Here, we encounter the *second difficulty*, related to the existence and quality of results of in-situ measurements. To test a model detailed measurements of the run-up area are required, desirably supplemented with information on the water flow parameters on the coast. In recent years, the database of run-up parameters is regularly upgraded with high-precision measurements performed by international expeditions, for which the investigation of coastal areas hit by tsunamis is mandatory. Contributions to the resolution of this problem are also provided by high-quality satellite photographs, permitting to determine the run-up area. Until recently, the water flow velocity in a tsunami run-up on a shore was, as a rule, estimated on the basis of indirect data. In recent years such goals are more and more

often accomplished with the aid of video filming realized, for example, by cameras mounted on helicopters or other aircraft, by electronic surveillance or by amateur cameras (e.g., Fritz et al. 2006, 2012; Hayashi and Koshimura 2013).

The *third difficulty* is related to the fact, that strong tsunami waves are capable of changing the initial aspect of a coast, including the topography of the coastal belt (erosion, demolition of buildings, destruction of vegetation). Thus, subsequent waves will interact with a coast, the properties of which (topography, irregularities) were altered by the preceding wave. High-precision run-up simulation will inevitably encounter the necessity of taking these effects into account.

The *fourth difficulty* is due to a tsunami run-up on a shore often not being simply a flow of seawater. The water flow carries with it floating objects of different sizes (including vessels, vehicles, floating debris) and, also, boulders and suspended sediment particles. Significant damage to buildings and other engineering constructions in the coastal zone are often due to the presence of large floating objects and debris in the water flow. The hydrodynamic problem of describing such a flow is quite nontrivial, but at the same time extremely called for. Its solution is necessary for estimating the force exerted by a tsunami on coastal engineering constructions (e.g., Nistor et al. 2009; Ko et al. 2014; Riggs et al. 2014). Another quite important aspect consists of the transport of sediments and in analyzing the formation of tsunami deposits Sugawara et al. (2014). Note that understanding the laws of sediment transport and deposition is the key to the interpretation of paleotsunami deposits (see Sect. 7.2).

References

- Abe, K.: A dislocation model of the 1933 Sanriku earthquake consistent with tsunami waves. *J. Phys. Earth* **26**(4), 381–396 (1978)
- Abe, K.: Size of great earthquakes of 1837–1974 inferred from tsunami data. *J. Geophys. Res.* **84**, 1561–1568 (1979)
- Aida, I.: Numerical experiments for the tsunami propagation the 1964 Niigata tsunami and 1968 Tokachi-Oki tsunami. *Bull. Earthq. Res. Inst. Univ. Tokyo* **47**(4), 673–700 (1969)
- Aida, I.: Numerical computation of a tsunami based on a fault origin model of an earthquake. *J. Seism. Soc. Jpn.* **27**(2), 141–154 (1974)
- Androsov, A., Behrens, J., Danilov, S.: Tsunami Modelling with Unstructured Grids. Interaction between Tides and Tsunami Waves. *Computational Science and High Performance Computing IV. Notes on Numerical Fluid Mechanics and Multidisciplinary Design*, pp. 191–206. Springer, Berlin (2011)
- Battjes, J.A.: Surf-zone dynamics. *Ann. Rev. Fluid Mech.* **20**, 257–293 (1988)
- Berger, M.J., Leveque, R.J.: Adaptive mesh refinement using wave-propagation algorithms for hyperbolic systems. *SIAM J. Numer. Anal.* **35**, 2298–2316 (1998)
- Bernatskiy, A.V., Nosov, M.A.: The role of bottom friction in models of nonbreaking tsunami wave runup on the shore. *Izv. - Atmos. Ocean. Phys.* **48**(4), 427–431 (2012)
- Bolshakova, A., Inoue, S., Kolesov, S., Matsumoto, H., Nosov, M., Ohmachi, T.: Hydroacoustic effects in the 2003 Tokachi-oki tsunami source. *Russ. J. Earth. Sci.* **12**, ES2005 (2011). doi:10.2205/2011ES000509
- Briggs, M.J., Synolakis, C.E., Harkins, G.S., Green, D.R.: Laboratory experiments of tsunami runup on a circular island. In *Tsunamis: 1992–1994*, pp. 569–593. Birkhäuser Basel (1995)

- Burwell, D., Tolkova, E., Chawla, A.: Diffusion and dispersion characterization of a numerical tsunami model. *Ocean Model.* **19**, 10–30 (2007)
- Carrier, G.F., Greenspan, H.P.: Water waves of finite amplitude on a sloping beach. *J. Fluid Mech.* **4**, 97–109 (1958)
- Carrier, G.F., Wu, T.T., Yeh, H.: Tsunami runup and drawdown on a plane beach. *J. Fluid Mech.* **475**, 449–461 (2003)
- Chan, I.-C., Liu, P.L.-F.: On the runup of long waves on a plane beach. *J. Geophys. Res.* **117**, C08006 (2012)
- Cherkesov, L.V.: Hydrodynamics of Surface and Internal Waves. Naukova Dumka, Kiev (1976)
- Choi, B.H., Pelinovsky, E., Kim, K.O., Lee, J.S.: Simulation of the trans-oceanic tsunami propagation due to the 1883 Krakatau volcanic eruption. *Nat. Hazards Earth Syst. Sci.* **3**, 321–332 (2003)
- Choi, B.H., Kim, D.C., Pelinovsky, E., Woo, S.B.: Three-dimensional simulation of tsunami run-up around conical island. *Coast. Eng.* **54**(8), 618–629 (2007)
- Choi, B.-H., Pelinovsky, E., Kim, D.C., Didenkulova, I., Woo, S.-B.: Two- and three-dimensional computation of solitary wave runup on non-plane beach. *Nonlinear Process. Geophys.* **15**, 489–502 (2008)
- Chubarov, L.B., Yu.I., S., Gusiakov, V.K.: Numerical modeling of the 1973 Shikotan (Nemuro-Oki) tsunami. *Comput. Fluids* **12**(2), 123–132 (1984)
- Didenkulova, I.: New trends in the analytical theory of long sea wave runup. In: Quak, E., Somere, T. (eds.) *Applied Wave Mathematics: Selected Topics in Solids, Fluids, and Mathematical Methods*, pp. 265–296. Springer, Berlin (2009)
- Didenkulova, I.: Tsunami runup in narrow bays: the case of Samoa 2009 tsunami. *Nat. Hazards.* **65**(3), 1629–1636 (2013)
- Didenkulova, I., Pelinovsky, E.: Traveling water waves along a quartic bottom profile. *Proc. Est. Acad. Sci.* **59**(2), 166–171 (2010)
- Didenkulova, I., Pelinovsky, E.: Runup of tsunami waves in U-shaped bays. *Pure Appl. Geophys.* **168**(6–7), 1239–1249 (2011a)
- Didenkulova, I., Pelinovsky, E.: Nonlinear wave evolution and runup in an inclined channel of a parabolic cross-section. *Phys. Fluids* **23**(8) (2011b). Article No: 086602
- Didenkulova, I., Didenkulov, O., Pelinovsky, E.: A note on the uncertainty in tsunami shape for estimation of its run-up heights. *J. Ocean Eng. Mar. Energy* **1**, 199–205 (2015). doi:[10.1007/s40722-015-0017-3](https://doi.org/10.1007/s40722-015-0017-3)
- Didenkulova, I.I., Kurkin, A.A., Pelinovsky, E.N.: Run-up of solitary waves on slopes with different profiles. *Izv. RAN, Atmos. Ocean. Phys.* **43**(3), 419–425 (2007a)
- Didenkulova, I., Pelinovsky, E., Somere, T.: Run-up characteristics of tsunami waves of “unknown” shapes. *Pure Appl. Geophys.* **165**(11–12), 2249–2264 (2008)
- Didenkulova, I., Pelinovsky, E., Somere, T.: Long surface wave dynamics along a convex bottom. *J. Geophys. Res. Oceans.* **114** (2009). Article No: C07006
- Didenkulova, I., Pelinovsky, E., Somere, T., Zahibo, N.: In: Kundu, A. (ed.) *Tsunami and Nonlinear Waves*, pp. 175–190. Springer, Berlin (2007b)
- Dobrokhotov, S.Yu., Tirozzi, B.: Localized solutions of one-dimensional nonlinear system of shallow-water equations with velocity $c = \sqrt{x}$. *Usp. Mat. Nauk* **65**(1), 185–186 (2010)
- Dotsenko, S.F.: Run-up of a solitary tsunami wave on an sloping shore. *Morsk. Gidrofiz. Issled.* (4), 11–18 (2005)
- Fernandez, H., Sriram, V., Schimmels, S., Oumeraci, H.: Extreme wave generation using self correcting method - revisited. *Coast. Eng.* **93**, 15–31 (2014)
- Fine, I.V., Rabinovich, A.B., Bornhold, B.D., Thomson, R.E., Kulikov, E.A.: The grand banks landslide-generated tsunami of November 18, 1929: preliminary analysis and numerical modeling. *Mar. Geol.* **215**, 45–57 (2005)
- Fritz, H.M., Borrero, J.C., Synolakis, C.E., Yoo, J.: 2004 Indian Ocean tsunami flow velocity measurements from survivor videos. *Geophys. Res. Lett.* **33**(24), L24605 (2006)

- Fritz, H.M., Phillips, D.A., Okayasu, A., Shimozono, T., Liu, H., Mohammed, F., Skanavis, V., Synolakis, C.E., Takahashi, T.: The 2011 Japan tsunami current velocity measurements from survivor videos at Kesennuma Bay using LiDAR. *Geophys. Res. Lett.* **39**, L00G23 (2012)
- Fujii, Y., Satake, K.: Tsunami source of the 2004 Sumatra-Andaman earthquake inferred from tide gauge and satellite data. *Bull. Seismol. Soc. Am.* **97**(1A), S192–S207 (2007)
- Gonzalez F.I., Bernard S.N., Milbern H.B., et al.: The Pacific tsunami observation program (PacTOP). In: Proceedings of the IUGG/IOC, International Tsunami Symposium, pp. 3–19 (1987)
- Golubtsova, T.S., Mazova, R.Kh.: Run-Up of Alternating Waves on the Shore, in Oscillations and Waves in the Mechanics of Continuous Media, pp. 30–43. GPI, Gorky (1989)
- Gusakov, V.K., Chubarov, L.B.: Numerical simulation of the Shikotan (Nemuro-oki) tsunami of June 17, 1973 (in Russian). *Tsunami Evolution from the Source to the Coast Runup*, pp. 16–24. *Radio i svyaz*, Moscow (1982)
- Gusakov, V.K., Chubarov, L.B.: Numerical simulation of tsunami excitation and propagation in the coastal zone. *Earth Phys. (in Russian)* (1), 53–64 (1987)
- Grilli, S.T., Harris, J.C., Tajalibakhsh, T., Masterlark, T.L., Kyriakopoulos, C., Kirby, J.T., Shi, F.: Numerical simulation of the 2011 Tohoku tsunami based on a new transient FEM co-seismic source: comparison to far- and near-field observations. *Pure Appl. Geophys.* **170**(6–8), 1333–1359 (2013)
- Harbitz, C.B., Glimsdal, S., Løvholt, F., Kvelidsvik, V., Pedersen, G.K., Jensen, A.: Rockslide tsunamis in complex fjords: from an unstable rock slope at Åkerneset to tsunami risk in western Norway. *Coast. Eng.* **88**, 101–122 (2014)
- Harig, S., Chaeroni, C., Pranowo, W.S., Behrens, J.: Tsunami simulations on several scales: comparison of approaches with unstructured meshes and nested grids. *Ocean Dyn.* **58**, 429–440 (2008)
- Hayashi, S., Koshimura, S.: The 2011 Tohoku tsunami flow velocity estimation by the aerial video analysis and numerical modeling. *J. Disaster Res.* **8**(4), 561–572 (2013)
- Hibberd, S., Peregrine, D.H.: Surf and runup on a beach: a uniform bore. *J. Fluid Mech.* **95**, 323–345 (1979). Part 2
- Ilgamov M.P., Gilmanov P.N. Non-reflective Boundary Conditions, 240 pp. “Fizmatlit”, Moscow (2003) (in Russian)
- Imamura, F., Yalciner, A.C., Ozyurt, G.: Tsunami modelling manual (TUNAMI model). Revision due on APRIL, 58 pp. (2006)
- Imamura, F., Goto, C., Ogawa, Y., Shuto, N.: Numerical method of tsunami simulation with the leap-frog scheme. IUGG/IOC Time Project Manuals (May) (1995)
- Israeli, M., Orzag, S.A.: Approximation of radiation boundary conditions. *J. Comput. Physics.* **41**, 115–135 (1981)
- Jacques, V.M., Soloviev, S.L.: Remote registration of weak tsunami-type waves on the shelf of the Kuril islands. *DAN SSSR (in Russian)* **198**(4), 816–817 (1971)
- James, L.: *Waves in Fluids*. Cambridge University Press, Cambridge (1978)
- Kaistrenko, V.M., Pelinovsky, E.N., Simonov, K.V.: Wave runup and transformation in shallow water (in Russian). *Meteorol. Hydrol.* **10**, 68–75 (1985a)
- Kaistrenko, V.M., Pelinovskii, E.N., Simonov, K.V.: Run-up and transformation of tsunami waves in shallow water. *Meteorol. Hydrol.* **10**, 68–75 (1985b)
- Kaistrenko, V.M., Mazova, R.Kh., Pelinovsky, E.N., Simonov, K.V.: Analytical theory for tsunami run up on a smooth slope. *J. Tsunami Soc.* **9**(2), 115–127 (1991)
- Kanoglu, U.: Nonlinear evolution and runup-rundown of long waves over a sloping beach. *J. Fluid Mech.* **513**, 363–372 (2004)
- Kanoglu, U., Synolakis, C.: Initial value problem solution of nonlinear shallow water-wave equations. *Phys. Rev. Lett.* **97**, 148501 (2006)
- Kato, T., Terada, Y., Nishimura, H., Nagai, T., Koshimura, S.I.: Tsunami records due to the 2010 Chile earthquake observed by GPS buoys established along the Pacific coast of Japan. *Earth, Planets Space* **63**(6), e5–e8 (2011)
- Keller, H.B., Levine, D.A., Whitham, G.H.: Motion of a bore over sloping beach. *J. Fluid Mech.* **7**, 302–316 (1960)

- Kim, S.K., Liu, Ph.L-F, Liggett, J.A.: Boundary integral equation solutions for solitary wave generation, propagation and runup. *Coast. Eng.* **7**, 299–317 (1983)
- Ko, H.S., Cox, D.T., Riggs, H.R., Naito, C.J.: Hydraulic experiments on impact forces from tsunami-driven debris. *J. Waterway, Port Coast. Ocean Eng.* (2014)
- Kosloff, R., Kosloff, D.: Absorbing boundaries for the wave propagation problem. *J. Comput. Phys.* **63**, 363–376 (1986)
- Kowalik, Z., Knight, W., Logan, T., Whitmore, P.: The tsunami of 26 December, 2004: numerical modeling and energy considerations. *Pure Appl. Geophys.* **164**, 379–393 (2007)
- Kulikov, E.A., Gonzalez, F.I.: Reconstruction of the shape of a tsunami signal at the source by measurements of hydrostatic pressure oscillations using a remote bottom sensor (in Russian). *DAN RF* **344**(6), 814–818 (1995)
- Kulikov, E.A., Rabinovich, A.B., Thomson, R.E., Bornhold, B.D.: The landslide tsunami of November 3, 1994. Skagway Harbor. Alaska. *J. Geophys. Res.* **101**(C3), 6609–6615 (1996)
- Kulikov, E.A., Medvedev, P.P., Lappo, S.S.: Registration from outer space of the December 26, 2004, tsunami in the Indian Ocean (in Russian). *DAN RF* **401**(4), 537–542 (2005)
- Lamb, H.: *Hydrodynamics*. Cambridge University Press, Cambridge (1932)
- Landau, L.D., Lifshitz, E.M.: *Fluid Mechanics*, 2nd English edn. Pergamon Press, New York (1987)
- LeVeque, R.J., George, D.L., Berger, M.J.: Tsunami modelling with adaptively refined finite volume methods. *Acta Numerica.* **20**, 211–289 (2011)
- Linton, D., Gupta, R., Cox, D., van de Lindt, J., Oshnack, M.E., Clauson, M.: Evaluation of tsunami loads on wood-frame walls at full scale. *J. Struct. Eng.* **139**(8), 1318–1325 (2013)
- Liu, P.L.F., Synolakis, C.E., Yeh, H.H.: Report on the international workshop on long-wave run-up. *J. Fluid Mech.* **229**, 675–688 (1991)
- Liu, P.L.F., Cho, Y.S., Briggs, M.J., Kanoglu, U., Synolakis, C.E.: Runup of solitary waves on a circular island. *J. Fluid Mech.* **302**, 259–285 (1995)
- Liu P.L.F., Woo S.B., Cho Y.S.: Computer programs for tsunami propagation and inundation. Technical report, Cornell University, 104 pp. (1998)
- Liu, P.L.-F., Lynett, P., Synolakis, C.E.: Analytical solutions for forced long waves on a sloping beach. *J. Fluid Mech.* **478**, 101–109 (2003)
- Li, Y., Raichlen, F.: Non-breaking and breaking solitary wave run-up. *J. Fluid Mech.* **456**, 295–318 (2002)
- Løvholt, F., Pedersen, G., Glimsdal, S.: Coupling of dispersive tsunami propagation and shallow water coastal response. *Open Oceanogr. J.* **4**, 71–82 (2010)
- Lyatkher, V.M., Militeev, A.N.: Calculation of runup on slope for long gravitational waves (in Russian). *Oceanology* (1), 37–43 (1974)
- Lynett, P., Borrero, J., Liu, P.L.-F., Synolakis, C.E.: Field survey and numerical simulations: a review of the 1998 Papua New Guinea tsunami. *Pure Appl. Geophys.* **160**, 2119–2146 (2003)
- Ma, G., Shi, F., Kirby, J.T.: Shock-capturing non-hydrostatic model for fully dispersive surface wave processes. *Ocean Model.* **43–44**, 22–35 (2012)
- Madsen, P.A., Fuhrman, D.R., Schaffer, H.A.: On the solitary wave paradigm for tsunamis. *J. Geophys. Res.* **113**, C12012 (2008)
- Maeda, T., Furumura, T.: FDM simulation of seismic waves, ocean acoustic waves, and tsunamis based on tsunami-coupled equations of motion. *Pure Appl. Geophys.* **170**(1–2), 109–127 (2013)
- Marchuk, An.G, Chubarov, L.B., Shokin, Yu.I: Numerical Simulation of Tsunami Waves (in Russian). Nauka, Novosibirsk (1983)
- Matsuyama, M., Ikeno, M., Sakakiyama, T., Takeda, T.: A study of tsunami wave fission in an undistorted experiment. *Pure Appl. Geophys.* **164**(2–3), 617–631 (2007)
- Mazova, R.Kh., Pelinovsky, E.N., Soloviev, S.L.: Statistical data on the character of the runup of tsunami waves (in Russian). *Oceanology* **23**(6), 932–937 (1983)
- Milburn, H.B., Nakamura, A.I., González, F.I.: Real-time tsunami reporting from the deep ocean. In: Proceedings of the Oceans 96 MTS/IEEE Conference, 23–26 September 1996, Fort Lauderdale, FL, pp. 390–394 (1996)

- Mofjeld, H.O., Titov V.V., González, F.I., Newman, J.C.: Analytic theory of tsunami wave scattering in the open ocean with application to the North Pacific. NOAA Technical Memorandum OAR PMEL-116. PMEL, Seattle, Wash (2000)
- Murty, T.S.: Storm surges. Meteorological ocean tides. Department of Fisheries and Oceans, Bulletin 212, Ottawa (1984)
- Nakoulima, O., Zahibo, N., Pelinovsky, E., Talipova, T., Kurkin, A.: Solitary wave dynamics in shallow water above periodic bottom. *Chaos* **15**(3), 037107 (2005)
- Nekrasov, A.V.: On the reflection of tidal waves from the shelf zone (in Russian). *Oceanology* **13**(2), 210–215 (1973)
- Nicolisky, D.J., Suleimani, E.N., Hansen, R.A.: Validation and verification of a numerical model for tsunami propagation and runup. *Pure Appl. Geophys.* **168**(6–7), 1199–1222 (2011)
- Nistor, I., Palermo, D., Nouri, Y., Murty, T., Saatcioglu, M.: Tsunami-induced forces on structures. *Handbook of Coastal and Ocean Engineering*, pp. 261–286. World Scientific, Singapore (2009)
- Nosov, M.A., Kolesov, S.V.: Elastic oscillations of water column in the 2003 Tokachi-Oki tsunami source: in-situ measurements and 3-D numerical modelling. *Nat. Hazards Earth Syst. Sci.* **7**, 243–249 (2007)
- Nosov, M.A., Moshenceva, A.V., Kolesov, S.V.: Horizontal motions of water in the vicinity of a tsunami source. *Pure Appl. Geophys.* **170**(9–10), 1647–1660 (2013). doi:[10.1007/s00024-012-0605-2](https://doi.org/10.1007/s00024-012-0605-2)
- Okal, E.A., Piatanesi, A., Heinrich, P.: Tsunami detection by satellite altimetry. *J. Geophys. Res.* **104**, 599–615 (1999)
- Ohmachi, T., Tsukiyama, H., Matsumoto, H.: Simulation of tsunami induced by dynamic displacement of seabed due to seismic faulting. *Bull. Seismol. Soc. Am.* **91**(6), 1898–1909 (2001)
- Park, H., Cox, D.T., Lynett, P.J., Wiebe, D.M., Shin, S.: Tsunami inundation modeling in constructed environments: a physical and numerical comparison of free-surface elevation, velocity, and momentum flux. *Coast. Eng.* **79**, 9–21 (2013)
- Pedersen, G., Gjevik, B.: Run-up of solitary waves. *J. Fluid Mech.* **135**, 283–290 (1983)
- Pelinovsky, E.N.: *Nonlinear Dynamics of Tsunami Waves* (in Russian). Institute of Applied Physics, USSR AS, Gorky (1982)
- Pelinovsky, E.: Nonlinear hyperbolic equations and run-up of huge sea waves. *Appl. Anal.* **57**, 63–84 (1995)
- Pelinovsky, E.N.: *Hydrodynamics of Tsunami Waves* (in Russian). Institute of Applied Physics, RAS, Nizhnii Novgorod (1996)
- Pelinovsky, E., Mazova, R.: Exact analytical solutions of nonlinear problems of tsunami wave run-up on slopes with different profiles. *Nat. Hazards* **6**, 227–249 (1992)
- Pelinovsky, E.N., Stepanyants, Yu., Talipova, T.: Nonlinear dispersion model of sea waves in the coastal zone. *J. Korean Soc. Coast. Ocean Eng.* **5**(4), 307–317 (1993)
- Piatanesi, A., Tinti, S., Bortolucci, E.: Finite-element simulations of the 28 December 1908 Messina straits (Southern Italy) tsunami. *Phys. Chem. Earth (A)* **24**, 145–150 (1999)
- Popinet, S.: Adaptive modelling of long-distance wave propagation and fine-scale flooding during the Tohoku tsunami. *Nat. Hazards Earth Syst. Sci.* **12**, 1213–1227 (2012)
- Rabinovich, A.B., Eblé, M.C.: Deep-ocean measurements of tsunami waves. *Pure Appl. Geophys.* 1–32 (2015)
- Riggs, H.R., Cox, D.T., Naito, C.J., Kobayashi, M.H., Aghl, P.P., Ko, H.S., Khowitar, E.: Experimental and analytical study of water-driven debris impact forces on structures. *J. Offshore Mech. Arctic Eng.* **136**(4), 041603 (2014)
- Roeber, V., Cheung, K.F.: Boussinesq-type model for energetic breaking waves in fringing reef environments. *Coast. Eng.* **70**, 1–20 (2012)
- Rossetto, T., Allsop, W., Charvet, I., Robinson, D.I.: Physical modelling of tsunami using a new pneumatic wave generator. *Coast. Eng.* **58**(6), 517–527 (2011)
- Satake, K.: Effects of bathymetry on tsunami propagation: application of ray tracing to tsunamis. *PAGEOPH* **126**, 27–36 (1988)

- Schimmels, S., Sriram, V., Didenkulova, I., Fernandez, H.: On the generation of tsunami in a large scale wave flume. In: Lynett P.J. (ed.) Proceedings of 34th International Conference on Coastal Engineering, Seoul, Korea, pp. 1–10, 15–20 June 2014
- Sielecki, A., Wurtele, M.: The numerical integration of the nonlinear shallow water equations with sloping boundaries. *J. Comput. Phys.* **6**, 219–236 (1970)
- Shen, M.C., Meyer, R.E.: Climb of a bor on a beach. Part 3. Run-up. *J. Fluid Mech.* **16**, 113–125 (1963)
- Shermeneva, M.A., Shugan, I.V.: Calculating the wave runup on a low-sloping beach using a high-order Boussinesq model. *Tech. Phys. Lett.* **32**(1), 64–66 (2006)
- Shi, F., Kirby, J.T., Harris, J.C., Geiman, J.D., Grilli, S.T.: A high-order adaptive time-stepping TVD solver for boussinesq modeling of breaking waves and coastal inundation. *Ocean Model.* **43–44**, 36–51 (2012)
- Shokin, Yu.I., Babailov, V.V., Beisel, S.A., Chubarov, L.B., Eletsky, S.V., Fedotova, Z.I., Gussyakov, V.K.: Mathematical modeling in application to regional tsunami warning systems operations. Computational Science and High Performance Computing III. Notes on Numerical Fluid Mechanics and Multidisciplinary Design, pp. 52–68. Springer, Berlin (2008)
- Spielvogel, L.Q.: Single-wave runup on sloping beaches. *J. Fluid Mech.* **74**, 685–694 (1975)
- Stoker, J.J.: *Water Waves*. Interscience Publishers, New York (1957)
- Sugawara, D., Goto, K., Jaffe, B.E.: Numerical models of tsunami sediment transport-current understanding and future directions. *Mar. Geol.* **352**, 295–320 (2014)
- Synolakis, C.E.: The runup of solitary waves. *J. Fluid Mech.* **185**, 523–545 (1987)
- Synolakis, C.E., Deb, M.K., Skjelbreia, J.E.: The anomalous behavior of the run-up of cnoidal waves. *Phys. Fluids.* **31**(1), 3–5 (1988)
- Synolakis, C.E., Fritz, M.H., Borrero, C.J.: Far field surveys of the Indian Ocean tsunami: Sri Lanka, Maldives and Somalia. In: Papadopoulos, G.A. (ed.) 22nd International Tsunami Symposium, Chania, Crete island, Greece, pp. 57–64, 27–29 June, 2005
- Tadepalli, S., Synolakis, C.E.: The runup of N-waves on sloping beaches. *Proc. R. Soc. Lond. A.* **445**, 99–112 (1994)
- Tang, L., Titov, V.V., Bernard, E., Wei, Y., Chamberlin, C., Newman, J.C., Mofjeld, H., Arcas, D., Eble, M., Moore, C., Uslu, B., Pells, C., Spillane, M.C., Wright, L.M., Gica, E.: Direct energy estimation of the 2011 Japan tsunami using deep-ocean pressure measurements. *J. Geophys. Res.* **117**, C08008 (2012)
- Tinti, S., Bortolucci, E., Chiavettieri, C.: Tsunami excitation by submarine slides in shallow water approximation. *Pure Appl. Geophys.* **158**(4), 759–797 (2001)
- Tinti, S., Tonini, R.: Analytical evolution of tsunamis induced by near-shore earthquakes on a constant-slope ocean. *J. Fluid Mech.* **535**, 33–64 (2005)
- Titov, V.V., Synolakis, C.E.: Modelling of breaking and nonbreaking long wave evolution and runup using VTCS-2. *J. Waterways Ports Coast. Ocean Eng.* **121**(6), 308–316 (1995)
- Titov, V.V., Gonzalez, F.I., Mofjeld, H.O., Venturato, A.J.: NOAA time Seattle tsunami mapping project: procedures, data sources, and products. NOAA Technical Memorandum OAR PMEL-124, 21 pp. (2003)
- Titov, V.V., Gonzalez, F.I., Bernard, E.N., et al.: Real-time tsunami forecasting: challenges and solutions. *Nat. Hazards (Special Issue)* **35**(1), 41–58 (2005). U.S. National Tsunami Hazard Mitigation Program
- Voltsinger, N.E., Klevanny, K.A., Pelinovsky, E.N.: Longwave Dynamics of Coastal Zone (in Russian). Gidrometeoizdat, Leningrad (1989)
- Walters, R.A.: Design considerations for a finite element coastal ocean model. *Ocean Model.* **15**, 90–100 (2006)
- Watada, S., Kusumoto, S., Satake, K.: Traveltime delay and initial phase reversal of distant tsunamis coupled with the self-gravitating elastic earth. *J. Geophys. Res. Solid Earth* **119**, 4287–4310 (2014)

- Wei, Y., Bernard, E., Tang, L., Weiss, R., Titov, V., Moore, C., Spillane, M., Hopkins, M., Kanoglu, U.: Real-time experimental forecast of the Peruvian tsunami of August 2007 for U.S. coastlines. *Geophys. Res. Lett.* **35**, L04609 (2008)
- Yamazaki, Y., Kowalik, Z., Cheung, K.F.: Depth-integrated, non-hydrostatic model for wave breaking and run-up. *Int. J. Numer. Methods Fluids.* **61**, 473–497 (2009)
- Yeh, H., Liu, Ph., Briggs, M., Synolakis, C.: Propagation and amplification of tsunamis at coastal boundaries. *Lett. Nat.* **372**, 353–355 (1994)
- Yeh, H., Liu, Ph.L-F, Synolakis, C.: *Long-Wave Runup*. World Scientific, Singapore (1996) 403 pp
- Zaytsev, A.I., Chernov, A.G., Yalciner, A.C., Pelinovsky, E.N., Kurkin, A.A.: *MANUAL Tsunami Simulation/Visualization Code NAMI DANCE versions 4.9*, February 2010
- Zhang, Y.J., Baptista, A.M.: An efficient and robust tsunami model on unstructured grids. part i: inundation benchmarks. *Pure Appl. Geophys.* **165**, 2229–2248 (2008)

Chapter 7

Methods of Tsunami Wave Registration

Abstract The traditional method for tsunami wave registration by coastal mareographs is described. The technique is described for measuring tsunami waves in the open ocean with the aid of bottom pressure sensors. The advantages of this technique are discussed. The technique for studying and documenting effects of tsunami influence on the coast are briefly expounded. The significance of searching for and identifying paleotsunami sediments is discussed. The application is described of satellite altimeters for registering tsunamis in the open ocean. Data are presented on tsunami manifestations in the Earth's ionosphere.

Keywords Tsunami registration · Sea level · Tide gauge · Ocean bottom pressure gauge · DART · GPS buoy · Tsunami impact · Tsunami runoff · Tsunami inundation · Tsunami deposits · Erosion · Accumulation · Paleotsunami · Satellite altimetry · Phase dispersion · Ionosphere · Total electron content · Radiotomography · Ionospheric airglow

The first information on the potential generation of a tsunami comes from the World Seismic Network. Data on the time, epicenter coordinates, and energy (magnitude) of an underwater earthquake permit to estimate the location of the source, the probability for the tsunami to originate, and the time the wave will arrive at the coast. But tsunami waves are not related in a unique manner to a seismic event. A strong earthquake is sometimes accompanied by an insignificant tsunami, while, contrariwise, a weak earthquake in a number of cases causes the formation of catastrophic waves. For a more accurate estimation of the tsunami hazard, information is required on the actual development of the wave process with time. In the absence of such information, the existence of a great number of false alert signals and neglected tsunami events is practically inevitable.

Tsunami registration is performed by various methods, including traditional measurements of the sea level close to the coast (mareographs) (Lander et al. 1993; Merrifield et al. 2005), measurements with the aid of ocean bottom pressure sensors (Rabinovich and Eblé 2015), and GPS buoys (Kato et al. 2000, 2011) in the open ocean, measurements making use of coastal radar systems (Barrick 1979; Lipa et al. 2012), as well as methods, recently undergoing development, of distance measurements, which primarily involve satellite altimetry (Okal et al. 1999;

Kulikov et al. 2004) and interpretation of tsunamigenic ionosphere disturbances (Occhipinti et al. 2006; Kunitsyn et al. 2011). Investigation of tsunami manifestations on the coast is performed by in situ expeditions immediately after the event (post event field survey) (Borrero et al. 2006; Mori and Takahashi 2012). Some traces of the influence of tsunamis on the coast are conserved for many thousands of years. Searching for and analyzing such traces of prehistoric tsunamis, or paleotsunamis (Atwater 1987; Minoura and Nakaya 1991; Pinegina et al. 2013), permit to significantly supplement tsunami catalogs.

7.1 Coastal and Deepwater Measurements of Sea Level

The first instrumental registration of a tsunami was obtained by a coastal mareograph (tide gauge), a device intended for measuring low-frequency variations of the ocean level (primarily, of tides). The scheme of a traditional mareograph is presented in Fig. 7.1. Level measurements are carried out in a shaft connected with the ocean by a relatively thin pipe. Such a scheme permits to automatically filter out high-frequency level oscillations, related to wind waves.

Independently on how they work, modern coastal tide gauges (floating-type, hydrostatic, ultrasonic) are equipped with systems for transmitting and/or storing data. It goes without saying that precisely operative access to the information on sea level variations is of utmost importance for tsunami forecasting. Telemetric information on the sea level is received and processed in national tsunami warning centers in the real-time mode. Note that in the case of catastrophic tsunamis tide gauges may not only be damaged, but they may also be totally destroyed by the wave. In this connection, continuous transmission of data on the sea level becomes especially important. In the case of gauges that accumulate data, the destruction of a station may also involve a loss of information accumulated during a certain, even quite long, time interval.

Until recently, all ideas of the character of tsunami wave evolution in the open ocean were based exclusively on coastal measurements. The idea of “hydrophysical” tsunami forecasting based on advance wave registration far from the coast (in open ocean) by ocean bottom pressure gauges was put forward back in the 60–70s of the past century by Soloviev (1968), Jacques and Soloviev (1971). But broad practical implementation of this idea in such systems as DART was made possible by technological developments only at the beginning of the twenty-first century (Bernard and Meinig 2011), GITEWS (Münch et al. 2011), NEPTUNE (Thomson et al. 2011), EMSO (Favali et al. 2009), and DONET (Kaneda 2010; Matsumoto and Kaneda 2013).

The most well-known system used for measuring tsunami waves in the open ocean is DART (Deep-ocean Assessment and Reporting of Tsunamis). The system is based on deepwater pressure sensors, developed in one of the NOAA divisions—Pacific Marine Environmental Laboratory (PMEL). A DART station consists of an anchored surface buoy and a bottom platform; information is exchanged between them via an

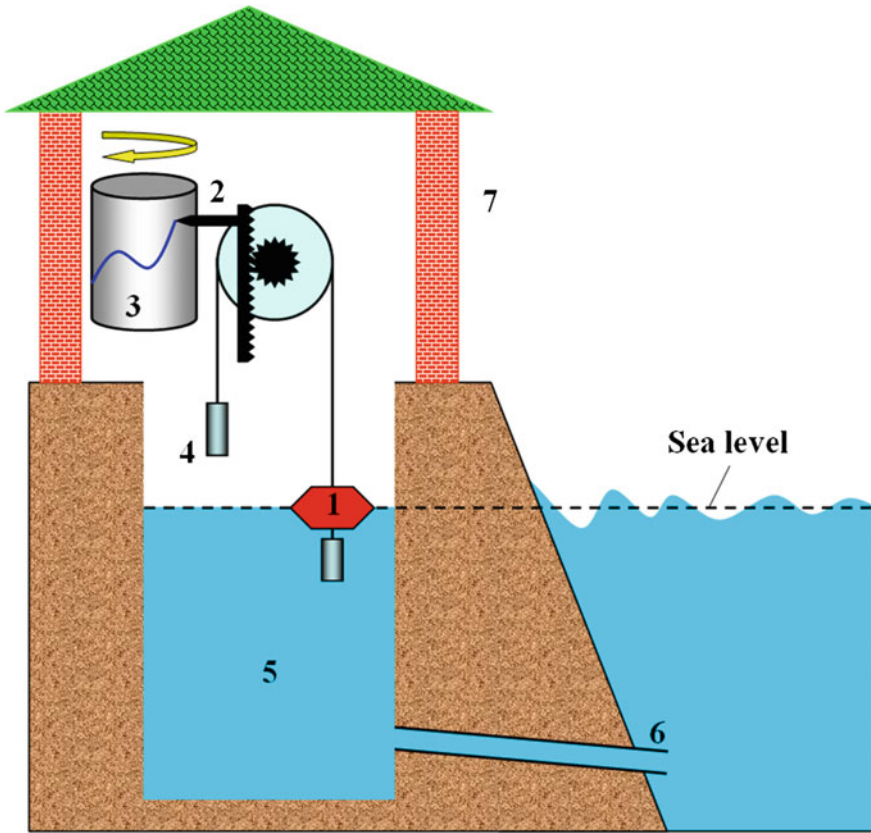


Fig. 7.1 Traditional tide gauge (mareograph) in a shaft: 1 float; 2 pen; 3 drum with chart strip; 4 counterweight; 5 shaft; 6 pipe connecting shaft with sea; 7 cabin housing the device

acoustic communication channel (Fig. 7.2). The sensor on the platform measures the pressure with an accuracy, corresponding to a 1 mm water column. The level of the natural longwave noise (without account of tides) in the deepwater part of the ocean is not high (its root-mean-square value is ~ 1 mm). This makes it possible to reliably single out tsunamis of heights of merely 1 cm, when the ocean depth at the site of the sensor varies between 1500 and 6000 m. The surface buoy is equipped with a satellite system for data transmission to the respective Tsunami Warning Centers for Hawaii and Alaska and, also to PMEL. At present, 62 DART stations are in operation. Information can be found at the freely accessible site <http://www.ndbc.noaa.gov/dart.shtml>.

The creation of an automatized system of level observation in the open ocean represents a promising way for providing reliable and timely tsunami warning. Moreover, deepwater level measurements are important for developing an understanding

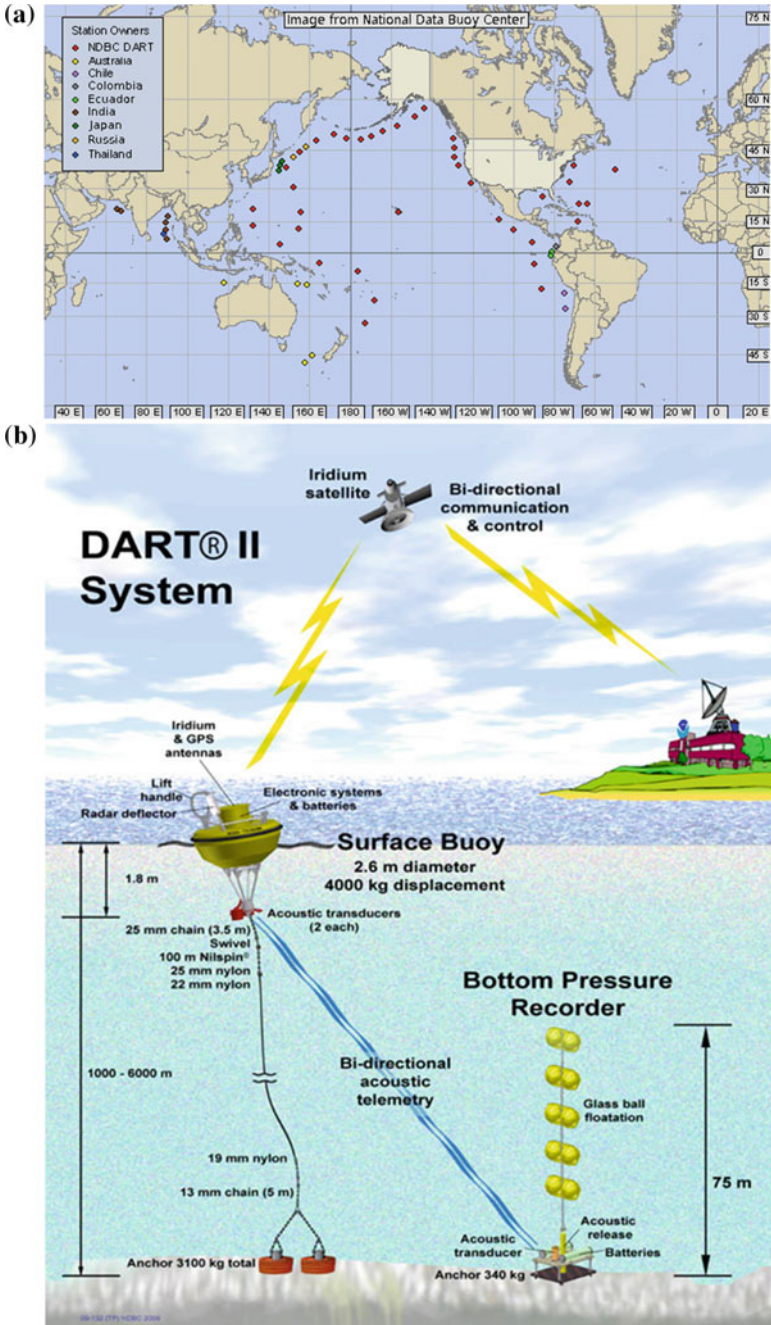


Fig. 7.2 Location of DART buoy stations, for registering tsunamis in the open ocean (as of June 2015) (a). Layout of station DART II (b). The figures is taken from <http://www.ndbc.noaa.gov/dart.shtml>

of the processes of wave excitation and propagation. Compared to coastal measurements, deepwater tsunami registration displays a whole number of important advantages (Titov et al. 2005). *First*, owing to the tsunami velocity depending on the ocean depth, the deepwater sensor registers a wave faster, than a coastal mareograph, located at the same distance from the source. *Second*, a tsunami wave approaching the coast is strongly distorted (for instance, owing to resonances in bays), and it “forgets” the properties of the source that generated it. Therefore, coastal mareographs are not sensitive to the true frequency spectrum of a tsunami. At the same time, a tsunami signal in the open ocean is not distorted or filtered and contains all the components of the original spectrum. *Third*, the amplitude–frequency characteristic (AFC) of bottom pressure sensors is totally flat within the range of tsunami waves, while the AFC, peculiar to many coastal mareographs, is complex and not constant. Most mareographs are, generally speaking, not intended for tsunami measurements, since they were created for observing relatively low-frequency tidal level oscillations. *Fourth*, the amplitude of a tsunami in the open ocean is small compared to the ocean depth; therefore, wave propagation is described with a very good accuracy by simple linear models. For this reason, the results of deepwater measurements can be applied effectively in resolving inverse problems (reconstruction of perturbation forms at sources, etc.). And, finally, *fifth*, one more important advantage of deepwater, as compared to coastal gauges, consists in their “invulnerability” to the destructive impact of catastrophic tsunami waves, which always occurs in the coastal shallow-water zone.

Level registration in the open ocean (at large depths) is a difficult technical task, which has been accomplished only in recent decades. Of the various numerous systems, quartz sensors provide the best measurement precision and stability.

The amplitude of variations of the bottom pressure p , which arise in the case of a monochromatic surface gravitational wave traveling in a basin of depth H , is known to be related to the amplitude ξ of this wave by the following classical formula (e.g. Lacombe 1965):

$$\frac{p}{\rho g \xi} = \frac{1}{\cosh(kH)}, \quad (7.1)$$

where k is the wavenumber related to the cyclic wave frequency ω by the dispersion relation $\omega^2 = gk \tanh(kH)$.

The quantity $p/\rho g \xi$ is presented in Fig. 7.3 versus the wave frequency (period) f . From the figure, it is seen that only sufficiently low-frequency/long-period ($T > 10$ min) waves are manifested in the bottom pressure variations practically without attenuation ($p/\rho g \xi \approx 1$). Short-period waves turn out to be either noticeably attenuated, or not to show up at all in bottom pressure variations. The cutoff frequency of this natural frequency filter is related to the ocean depth: $f_c \sim \sqrt{g/H}$ (see Sect. 4.2.1). Thus, the smaller the depth, at which the pressure gauge is established, the higher-frequency waves it is capable of registering. Note that direct measurements of the water surface position using GPS buoy systems (e.g., Kato et al. 2000, 2008, 2011) permit to reconstruct short-period sea level variations without distortion. However, this advantage, also, has its reverse side. Short-period level oscillations due, for instance, to wind waves give rise to significant noise that contaminates the useful

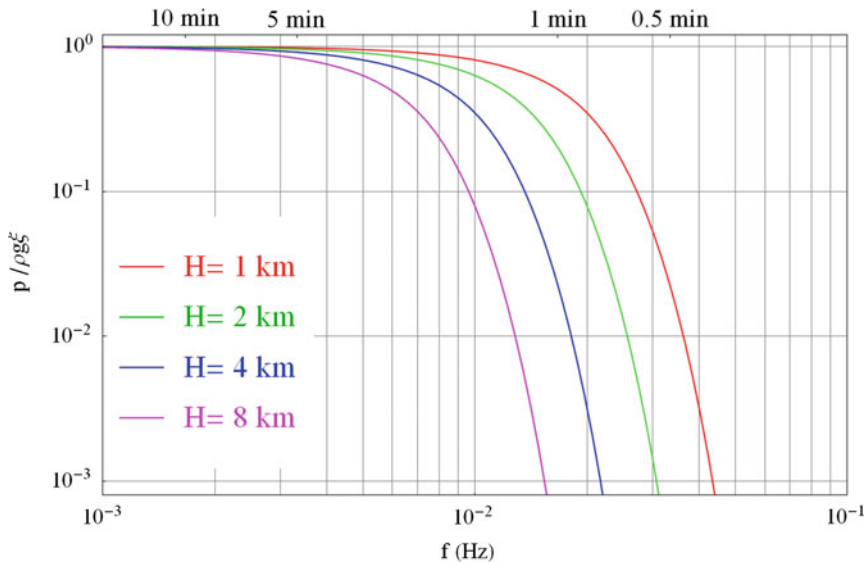


Fig. 7.3 Amplitude of bottom pressure variations versus frequency (period) of gravitational surface wave. The calculation is performed by formula (7.1) for different ocean depths (indicated in the figure)

signal, although the signal registered by a pressure gauge at the ocean bottom is initially free from short-period components related to surface gravitational waves. Such a pressure gauge, however, does not measure the position of the ocean surface directly: the surface position is reconstructed from the pressure taking advantage of existing theoretical ideas. An important advantage of the GPS buoy systems consists in that they measure the position of the ocean surface precisely.

Variations of pressure at the ocean bottom exhibit a broad frequency spectrum and are due to a whole complex of processes in the atmosphere, ocean, and lithosphere. Surface, internal, and elastic waves in the water column, as well as seismic surface waves and changes in the atmospheric pressure, all contribute to variations of the bottom pressure. The contribution of changes in the atmospheric pressure is readily taken into account, if observational data on this characteristic are available. The contribution of long internal waves to pressure variations is estimated by the quantity (the rigid lid case) $p_{int} = \delta\rho g A_{int}$, where A_{int} is the internal wave amplitude and $\delta\rho$ is the change in density at the pycnocline. A typical change in density for the ocean is $\delta\rho \sim 3 \text{ kg/m}^3$ (Gill 1982), therefore, the amplitude of pressure variations caused by internal waves even of significant amplitude $A_{int} = 10 \text{ m}$ will only be $p_{int} \approx 300 \text{ Pa}$ (3 cm of water).

The most significant contribution of noise to pressure variations is due to hydroacoustic and seismic waves (see Sect. 4.2), and, also, to tidal oscillations of the ocean level. The amplitude of tidal oscillations in open ocean ($\sim 1 \text{ m}$) is comparable to the amplitude of catastrophic tsunami waves. Manifestations of seismic and hydroa-

coustic waves in bottom pressure variations, especially in the near-source zone, are tens of times and more larger in amplitude than tsunami wave manifestations (see Sects. 4.2.2 and 4.2.3). Owing to the propagation velocities of seismic waves and tsunamis differing from each other, it can be easy to separate “seismic noise” and a tsunami signal in the distant zone, since they are separated in time. In the near-source zone, the tsunami signal is identified using a low-pass filter of cutoff frequency $f_c = 0.0718\sqrt{g/H}$ (the selection principle of the numerical coefficient in the formula is described in Sect. 4.2.1).

In comparing the results of numerical tsunami calculations with measurements, the necessity usually arises to remove the tidal component from the measured signal. This procedure has been termed “de-tiding.” Usually, harmonic analysis is applied for de-tiding. Application of this method implies the existence of quite a long row of observations of sea level variations at the gauge location (~ 1 month). From observations, one determines the harmonic constants, the knowledge of which permits to calculate the tidal behavior of the ocean level. Subtracting the tidal course of the level from the measured signal, we obtain the sought de-tided tsunami signal. Note that the application of simple high-pass filtration in de-tiding is far from yielding a satisfactory answer in all cases.

As an example of a record obtained by a deepwater DART station (21413), Fig. 7.4 presents a de-tided signal registered during the 2011 Tohoku-Oki tsunami. The signal is shown together with its spectrogram (Morelet transformation). The manifestations of seismic waves (the high-frequency splash) that reached the station first are seen

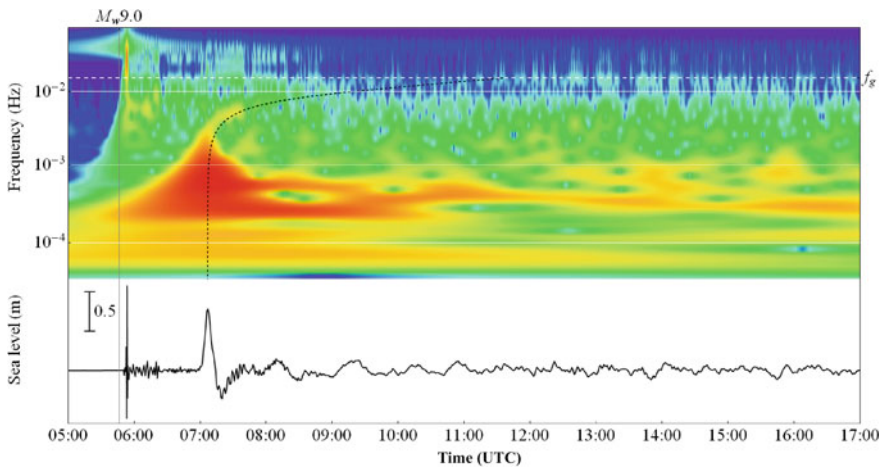


Fig. 7.4 Variations of sea level, registered by deepwater station DART21413 during the 2011 Tohoku-Oki tsunami (March 11), and spectrogram of signal. Recording lasted 12 hours. The time moment corresponding to the beginning of the earthquake of M_w 9.0 is indicated. The *white-dotted line* on the spectrogram shows the position of the critical frequency (f_g) of gravitational waves. The *black-dotted line* indicates the theoretical estimate for the arrival time of the signal, calculated by the formula: $t_{ar} = L/C_{gr}$

well from the record. The onset of the leading tsunami wave occurs significantly later—more than an hour after the arrival of seismic waves. The amplitude of the leading wave was of the order of 1 meter. The tsunami signal is characterized by quite a noticeable phase dispersion. The black-dotted line in the spectrogram indicates the calculated arrival time depending on the signal frequency: $t_{ar} = L/C_{gr}$, where L is the distance of the earthquake epicenter from the station DART21413 and C_{gr} is the group velocity of gravitational surface waves. The calculation is performed for $L = 1147$ km and for an ocean depth $H = 5776$ m (the average ocean depth along the propagation path). The theoretical estimate of the onset time is seen to be quite consistent with the observed picture.

7.2 The Investigation of Coasts After Tsunamis: Tsunami Deposits

Detailed investigation and documentation of results of the tsunami impact upon coasts is an important task that permits to study the nature of this phenomenon more thoroughly, to work out necessary recommendations for tsunami zoning, and to improve schemes for evacuation of the population. As a result of studies carried out in the close aftermath of the tsunami impact on a coast, it is possible to determine the height of the tsunami runup and the distance of the tsunami inundation, to estimate the water level at different segments of the coast and at different distances from the coastline, to reveal local peculiarities in tsunami parameters depending on the bathymetry of the coastal zone and on the coastal morphology. In a number of cases, the results of studies carried out after tsunamis permitted to correctly determine the number of tsunami waves and the velocity and direction of the tsunami runoff and runout.

All effects due to the onset of tsunamis on coasts can be divided into two groups: erosion and accumulative. On the whole, erosion effects are dominant in the accelerating flow zone, while accumulative effects are dominant in the quasistable or decelerating flow zone (Jaffe and Gelfenbaum 2007). In space, erosion of the relief and the most significant destruction of natural and civil objects occur closer to the coastline, while accumulation of the displaced material and deposits takes place at a certain distance from the coastline (Fig. 7.5). Studies performed in recent years reveal that both tsunami runoffs and tsunami runouts are capable of exerting erosion and accumulative effects on a shore (Choowong et al. 2008). Since a tsunami, as a rule, approaches the coast in the form of a series of waves, division of the coast into erosion and accumulative zones is, to a certain extent, somewhat arbitrary, as, for example, the erosion zone of the first wave may happen to be the accumulative zone of subsequent waves and vice versa. Therefore, in each concrete case one can only speak of the dominance of tsunamigenic erosion or accumulation at one or another segment of the coast (Kravchunovskaya et al. 2008; Pinegina et al. 2008).

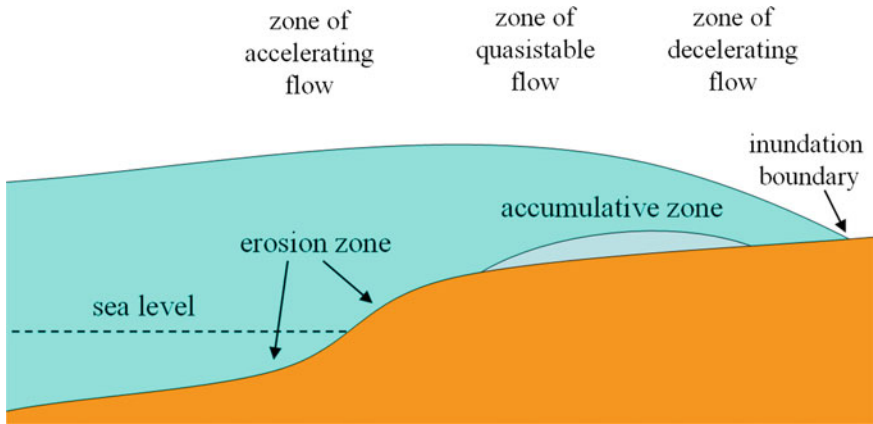


Fig. 7.5 Location of erosion and accumulative zones for tsunami runoff. Idealized scheme adapted from Jaffe and Gelfenbaum (2007)

In several cases, it turned out to be possible to measure the topographic profiles at one and the same segment of the coast before and after a tsunami (Pinegina et al. 2008; MacInnes et al. 2009a, b). These data permitted to estimate quantitatively the relationship between the volumes of eroded and accumulated material on the coast after the tsunami. The results of measurements, carried out on the Kuril islands before and after the tsunami of November 15, 2006, revealed the volume of material displaced as a result of erosion to exceed the volume of deposited material. When the tsunami height was less than 8 meters, the erosion volume was 5–15 times greater than the accumulative volume. When the tsunami height exceeded 15 meters, the erosion volume was 30–40 times greater than the accumulative volume (MacInnes et al. 2009a).

Investigation of the consequences of a whole series of historical tsunamis at different world sites revealed that tsunamis do not give rise to new forms (such as new beach ridges) of the coastal relief, but locally they can significantly erode the existent forms (Fig. 7.6). As a rule, strong erosion effects accompany strong tsunamis of heights >5 m with high flow velocities (Raszhigaeva et al. 2012). In such cases, tsunamis strip away from the surface the sod cover, erode beach ridges, river sandbars, terrace scarps, wash out niches along banks made up of sedimentary rock (Fig. 7.7). The width of the erosion zone depends, first of all, on the tsunami height and on the flow velocity. Thus, for example, the width of the erosion zone due to influence of the December 26, 2004 tsunami in the province of Aceh at the northern end of Sumatra amounted to 2–3 km, and farther, at a distance up to 5–10 km from the coastline, there existed an accumulative zone of material brought by the tsunami (Fig. 7.8).

Tsunamigenic sediments consist of the material that composes the beach and the shallow-water part of the coastal zone (Fig. 7.9). Tsunami deposits may contain silt, sand, pebbles, boulders, fragments of corals, blocks of unearthed and displaced turf and soil, trunks of trees, fragments of destroyed buildings, etc. Numerous surveys



Fig. 7.6 Coast of Matua island: **a** before tsunami of November 15, 2006 (photo by E. Vereschagin); **b** after the tsunami (photo by T. Pinegina)

have shown that in most cases the spreadout boundaries of tsunami sediments are close to the boundaries of maximum horizontal tsunami inundations (Bourgeois and Reinhart 1989; Dawson 1994; MacInnes et al. 2009b). Therefore, when the consequences of tsunamis on coasts are investigated, their deposits are used for determining inundation parameters.

The maximum height of the tsunami water column can reach any point between the maximum inundation line and the coastline. It can be measured by the dirt marks composed of the finest ground particles (silt, soil, sand), which are quite visible on smooth surfaces (for instance, on the walls of houses). The height at which one finds broken branches, torn off bark, or seaweed hanging from the branches of trees that survived a tsunami indicates the water column height. Thus, to study accumulative tsunami deposits is a reliable method for estimating tsunami runups and inundations in both historical and prehistorical (paleotsunamis) cases.

In spite of tsunamis occurring on Earth every year, strong and catastrophic tsunamis are quite rare phenomena, and in the case of most tsunami dangerous coasts, the catalog of these events is insufficiently representative to obtain statistical estimates. Therefore, by the end of the 80s, studies of paleotsunami deposits became important throughout the whole world.



Fig. 7.7 Erosion niches developed in sedimentary rock due to the Indonesian tsunami of December 26, 2004 on Sumatra island (photo by T. Pinegina)

The first studies of the deposits of paleotsunamis were carried out in Japan and the USA at the end of the 80s and the beginning of the 90s (Atwater 1987; Minoura and Nakaya 1991). During the subsequent period, similar work was performed on the western coast of Canada, in Chile, Australia, New Zealand and in a number of other countries—in most of the regions subject to tsunamis. In Russia, comprehensive work in this field was initiated by the middle of the 90s—on Sakhalin, Kamchatka, the Kuril islands—in the most tsunamihazardous regions of the Russian Far East (Pinegina et al. 1997a, b, 2000, 2003, 2012; Pinegina and Bourgeois 2001; Bourgeois et al. 2006; Raszhigaeva et al. 2012).

The main features distinguishing deposits of tsunamis from other genetic types include the following: (1) their confinement to a coastal belt beyond the zone of storm accessibility and to different hypsometric levels (approximately up to 30–40 m above the sea level); (2) they contain a beach and upper shoreface sediments; (3) the insignificant thickness of tsunami deposits (from several millimeters up to several tens of centimeters, rarely up to a meter); and (4) the periodicity in deposit formation (tens–hundreds of years). Numerous articles have been devoted to characterizing tsunami deposits and their peculiarities, for example, the following: Morton et al. (2007), Tuttle et al. (2004), Lakshmi et al. (2010), Fujiwara and Kamataki (2007), and Choowong et al. (2008).

The choice of sites for studying the tsunami deposits is based on a careful analysis of aerial photographs and space images as well as topographic maps. With their

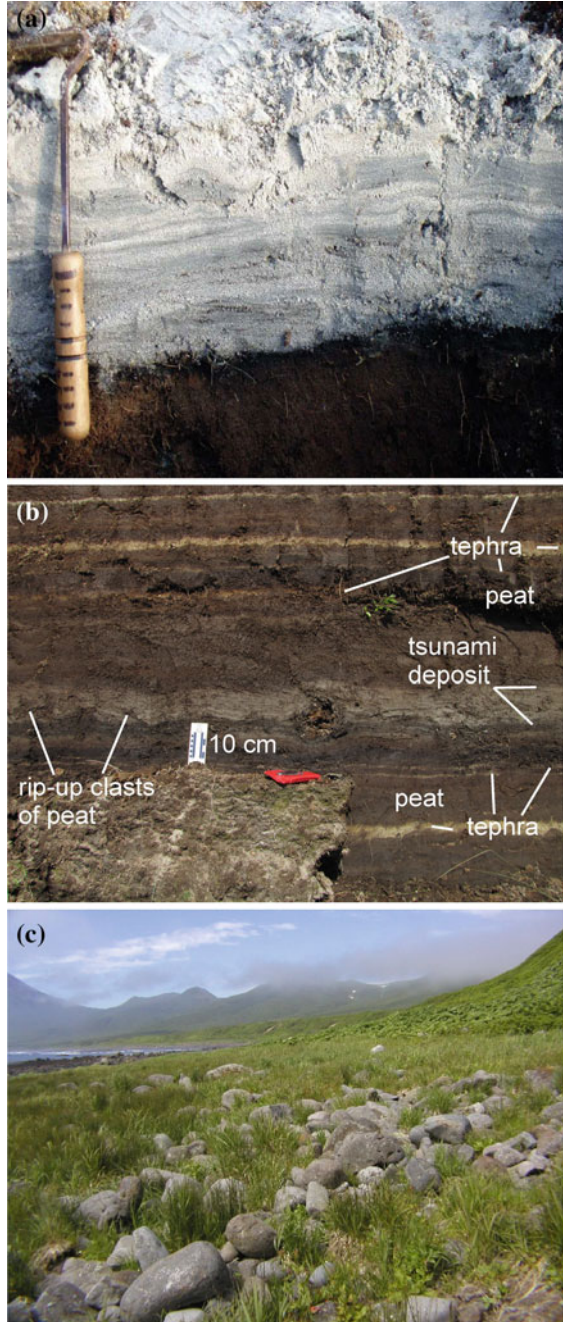


Fig. 7.8 Accumulative zone of deposits due to the tsunami of December 26, 2004 in the town of Banda-Aceh (photo by T. Pinegina)

aid, key sites on coasts are identified, where tsunamigenic deposits may have been preserved for a long period of time. These sites must not be within the zone of the influence of fluvial and slope processes; it is desirable for the coastal relief to exhibit different height levels and for the configuration of shores not to hinder the free penetration of tsunamis. Moreover, the descriptions are collected of historical tsunamis related to the contemplated site to be studied. The deposits of historical tsunamis serve as key deposits for the identification of even more ancient events. During field work, geodetic surveying is performed of topographic profiles from the coastline through the beach, beach ridges up to a distance exceeding the maximum tsunami inundations. Geological excavations are dug along the profiles and geological sections inside of them are described, and samples on mineralogical, radio-carbonic, diatomic, pollen, granulometric, and other analysis are collected.

In the Far East, in particular, on the Kamchatka, the investigation of tsunami deposits is closely related to the possibility of applying the method of tephrochronology. This method is based on studying and correlating identified horizons of volcanic ashes (tephras), each of which manifests a characteristic image, chemical and mineralogical composition, and is also spread over a large territory. In studies of tsunami deposits on the Kamchatka, the tephrochronological method is applied as the key method for correlating and dating deposits (Fig. 7.10).

Fig. 7.9 Different types of tsunami deposits: **a** fine sands deposited by the tsunami of 2004 on the Simelu island, Indonesia (photo by N. Raszhigaeva); **b** sandy loam with fragments of peat included, deposited by a prehistoric tsunami between 3000 and 3950 years ago at the Kamchatsky Bay, Kamchatka (photo by T. Pinegina); **c** boulders deposited by the tsunami of 2006 on the Kuril islands (photo by T. Pinegina)



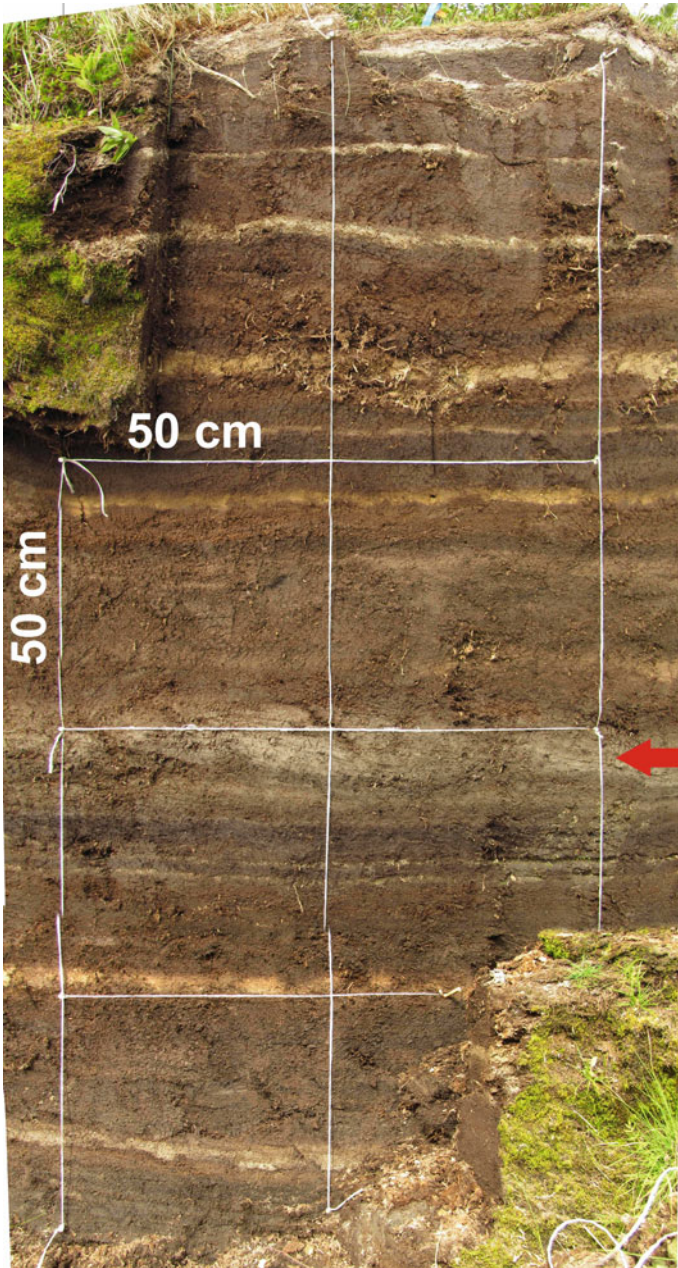


Fig. 7.10 Peat outcrop with strata of volcanic ashes (tephras) and tsunami deposits. The horizon is shown by the *red arrow* (photo by A. Kozhurin)

When the geological sections have been described, key geological sections and a geochronological (time) section are combined, on the basis of which it is possible to calculate the tsunami frequency on the coast. For the Kamchatka and Kuril coasts, tens of ancient tsunamis that occurred during the past 2–6 thousand of years were revealed (Bourgeois et al. 2006; Pinegina and Bourgeois 2001; Pinegina et al. 2013).

The data on tsunami frequencies at individual coastal sites are insufficient for estimation of the intensity of ancient tsunamis and of the sources of earthquakes that caused them. To resolve these issues, it is necessary to reconstruct the heights of tsunami runups and the zones of inundation, as well as the length of the coast, influenced by each of the tsunamis. This task is difficult and complex. For each of the sites investigated, it is necessary to reconstruct the ancient coastline and of the height of the relief at different moments of time during the Holocene. Only upon implementation of the above it will become possible to determine the necessary parameters of ancient tsunamis (Pinegina et al. 2012, 2013). Under conditions of rapid coastal uplifts and subsidence (which is typical for subduction and collision zones), the reconstruction of ancient coastal lines is especially important. In the case of most of the regions subject to tsunamis, investigation of their deposits provides the only possibility for extending the short historical catalogs of strong tsunamis and earthquakes back to thousands of years in the past.

7.3 Tsunami Detection in the Open Ocean by Satellite Altimetry

Revelation of the place and time a tsunami wave originates is based on seismic information obtained immediately after the earthquake. The absence of observational data on the tsunami parameters at the source leads to a low efficiency of the computational models, determining the arrival time and amplitude of a wave at each concrete point. As a result, the level of false tsunami warnings increases.

Thus, for example, during the Shikotan tsunami of October 4, 1994, which happened to be catastrophic for the Southern Kurils and the Hokkaido island, the international service sent a warning to the Hawaii islands about the possible approach of a tsunami several meters high. Significant financial means (up to 30 million US dollars) were applied in evacuating thousands of people, although the height of the tsunami turned out to be about half a meter. In these conditions, the application of remote satellite methods for registering tsunami waves would have permitted to obtain the lacking information at the very moment of the earthquake or immediately afterward.

Many thousands of human lives could have been saved during the tsunami of December 26, 2004, if the system for satellite registration of tsunami waves had already been functioning within the Indian Ocean.

Direct tsunami measurements, received by coastal level recorders, contain oscillations strongly distorting the initial record of a wave in the open ocean. The arrival

of a wave in shallow water and its reflection from the coast leads to enhancement of its amplitude, but the spectrum (shape) of the signal is distorted by the resonance properties of the shelf, bays, and straits. The best in quality records of tsunamis in the open ocean are provided by sensors of the bottom hydrostatic pressure (Kulikov and Gonzalez 1995). However, such systems are very expensive and they do not provide for total coverage of probable zones of tsunami wave origination. The rapid development of remote (satellite) methods opens up new possibilities for resolving problems of efficient tsunami forecasting.

At present, a cardinal way for resolving the problem of sea level investigation not only near but also at a significant distance from the coast with clear connection to a unique geodetic reference system consists in the application of satellite altimetry and, for example, high-precision radio altimetry measurements using the Earth's artificial satellites (EAS) GEOSAT, TOPEX/POSEIDON, ERS-1, 2, JASON-1, and ENVISAT. For this purpose, in the future, measurements can be made use of that were made by the Russian geodetic EAS "Musson-2" and other satellites with altimeters, designed in other countries. The accuracy, with which the data on the sea level are correlated to the common system of heights, is provided for by the receivers of one of the navigational systems, GLONASS, GPS, or DORIS, established on board the satellite. At present, the data of satellite altimetry are widely applied in investigations of mesoscale variations of flows, tides, etc.

Modern systems and means of satellite altimetry are successfully applied for studying properties of the oceanic lithosphere, determining the parameters of lunar-solar tides in the ocean. The existence of a correlation has been established between the level topography of the World Ocean and circulation of water masses and meteorological phenomena. Moreover, satellite altimetry has been shown and confirmed experimentally to serve as an effective means for studying deviations of the vertical slope, the ocean bottom relief, and the dynamics of the World Ocean surface.

Taking into account the prospects of applying satellite altimetry for resolving the above-indicated broad class of problems, intensive work was initiated during the period after 1980 for creating a new class of high-precision radio altimeters and EAS, to be equipped with them. From the middle of the 80s till the present day, seven EAS with high-precision radio altimeters on board were put into orbit. During this period, the precision in determining the orbit improved from 45 to 5 cm, while the measurement precision was improved from 1.5 m to 3–6 cm (ENVISAT-1), put into orbit in 2001 and 2002, provide for a root-mean-square measurement error within 2 cm.

Original satellite altimetry databases have been created and are regularly updated, and they are available for scientific purposes in the Distributed Archive of physical oceanography of the Jet Propulsion Laboratory of the California Institute of Technology (PODAAC) in the USA and the Center for satellite oceanographic data storage, control, and interpretation (AVISO) in Europe.

An integrated database for satellite altimetry (IDBSA) and a System for automated satellite altimetry data processing have also been created in the Geophysical Center of the Russian Academy of Sciences (GC RAS) with support of the RFBR. The database includes altimetry data from satellites GEOIC, GEOSAT,

TOPEX/POSEIDON, ERS 1, 2, GFO, and JASON for the period from 1985 to 2003. The System for automatized data processing, designed in the GC RAS, supports all data formats adopted in foreign centers and IDBSA.

The first attempts at applying satellite altimetry data in searching for tsunamis in the open ocean were evidently made in 1994–1999 (Okal et al. 1999). They analyzed satellite altimetry data, obtained in the experiments TOPEX/POSEIDON, related to several strongest tsunamigenic earthquakes: the Nicaragua tsunami of September 2, 1992, the Okushiri tsunami of July 12, 1993, the tsunami of June 2, 1994, on the island Java, and the Shikotan tsunami of October 4, 1994. Spectral analysis has only permitted to identify definitively the wave of the 1992 Nicaragua tsunami.

Tsunami researchers recently developed an improved procedure (Zaichenko et al. 2005) of satellite information processing, which comprised several stages for the registration of tsunami waves in the open ocean. At the first stage, the satellite cycle, corresponding to the tsunamigenic earthquake, was chosen. Then, all the routes of this cycle covering the Pacific Ocean were selected from the database of the RAS GC. The satellite circuits preceding the earthquake were further discarded. At the same time, the model, chosen for calculation of the arrival time of the waves, was applied to calculate the position of the wave front in the case of each tsunami source. Calculation of the arrival times was based on bathymetric data. Further, for each point of the satellite, route comparison was performed of the satellite time, counted from the earthquake origination moment, and the calculated time for the position of the wave front. This resulted in determination of the position of the intersection point of the satellite's route and the tsunami front.

The position of the wave front is to a certain extent conventional. Calculations are performed assuming the maximum of the wave propagation velocity to be $c = \sqrt{gH}$, where c is the wave propagation velocity, g is the acceleration of gravity, and H is the ocean depth. In reality, the wave velocity also depends on its length (see Sect. 6.1). The shorter the wavelength, the slower it propagates. Owing to this dispersion effect, the real front, as a rule, lags behind this theoretical estimate. The longer the propagation path, the stronger is the dispersion effect. The wave front can be distorted even stronger in shallow water. Nevertheless, the estimate of the tsunami wave front position, calculated by formula $c = \sqrt{gH}$, is quite accurate and its error does not exceed the size of the tsunami source ~ 50 – 100 km.

The evolution of a wave packet is due to the dependence of the group velocity on the frequency:

$$c_g = \frac{d\omega}{dk} = \frac{\omega}{2k} \left(1 + \frac{2kH}{\sinh(2kH)} \right), \quad (7.2)$$

where ω is the angular wave frequency, k is the wave number, and H is the ocean depth.

A detailed analysis of altimetry data has been performed in Zaichenko et al. (2004) for six strongest tsunamis: the Shikotan tsunami of 1994, the 1996 tsunami near the island Irian Jaya, the Okushiri tsunami of 1993, the 1998 tsunami near the coast of Papua New Guinea, and the tsunamis near Island Java (1994) and the coast of Peru (2001). In the first four cases, it turned out to be possible to reveal specific

perturbations of the ocean level, which appear in the records within the time range close to the moment, when the calculated tsunami front passes. Such perturbations were most strikingly revealed in the records obtained on July 17, 1998 (Papua New Guinea). In the last two cases, searches for traces of tsunamis in the records were not met with success.

Figures 7.11 and 7.12 present a map of the investigated region of the Pacific Ocean with isolines of tsunami arrival times and oceanic level profiles at the coast of Papua New Guinea, on which the perturbation, supposedly corresponding to the 1998 tsunami passage time, is indicated.

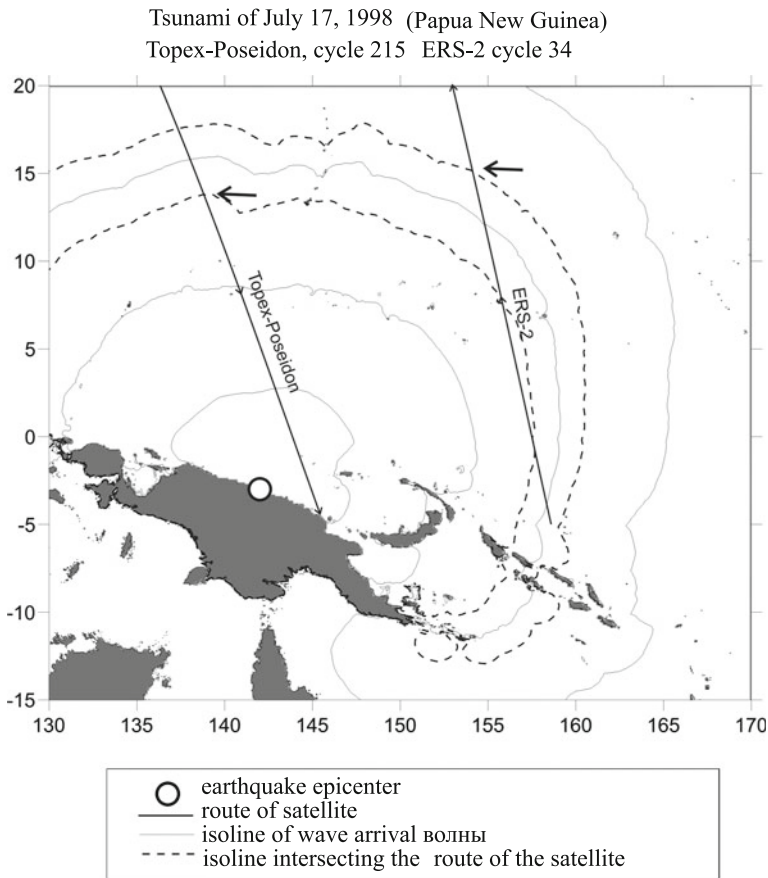


Fig. 7.11 Map of Pacific Ocean region adjacent to the island Papua New Guinea with isolines of arrival times of the 1998 tsunami (in 1 hour steps). Shown are the routes of the satellites Topex-Poseidon (circuit 215-18) and ERS-2 (circuit 34-304), which intersect the tsunami wave front. The crossing points of the routes and the respective isolines of the tsunami front arrival times (*dashed line*) are indicated by *arrows* (Adapted from Zaichenko et al. 2004)

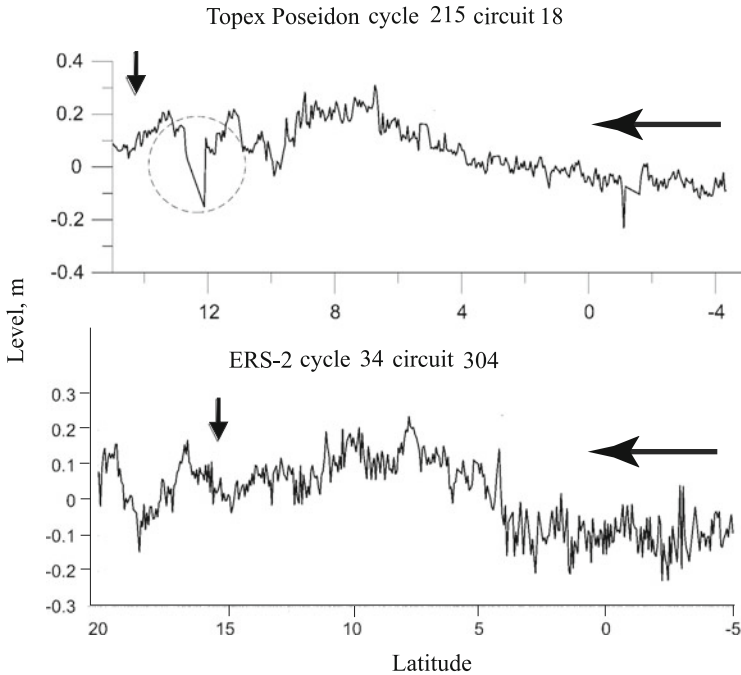


Fig. 7.12 Profiles of the ocean level with indication of the direction of wave motion (*horizontal arrows*) and the crossing point of the theoretical tsunami front and the route of the satellite (*vertical arrows*) (Adapted from Zaichenko et al. 2004)

Extremely interesting results were obtained from the analysis of radio altimetry observations of the catastrophic tsunami of December 26, 2004 in the Indian Ocean Kulikov et al. (2004). All available altimetry data from TOPEX/POSEIDON, ENVISAT, and JASON-1 were analyzed for the period immediately after the seismic shock. Individual routes revealed anomalous level variations, probably related to the passage of tsunami waves. The best-quality record JASON-1 (cycle 109, circuit 129) was chosen for further calculations.

Figure 7.13 presents the map of the north-eastern part of the Indian Ocean with epicenters of the main earthquake red star and the main aftershocks (circles). The isochrones, showing the calculated position of the tsunami front, are constructed with an interval of 0.5 an hour. The figure also shows the route of the satellite JASON-1 (cycle 109, circuit 129) and the respective profile of the ocean level, measured by the altimeter. In Fig. 7.14b, the profile is depicted in an enhanced scale. For comparison, the level profile, obtained 10 days before the tsunami (preceding cycle 108), is also plotted. The time it took the satellite to cross the Indian Ocean corresponds to the period between 2 h 51 min (12° of southern latitude) and 3 h 02 min (20° of northern latitude), i.e., approximately 2 hours after formation of the tsunami wave. The wave front is seen well at approximately 6° of southern latitude. The maximum wave amplitude amounts to 80 cm.

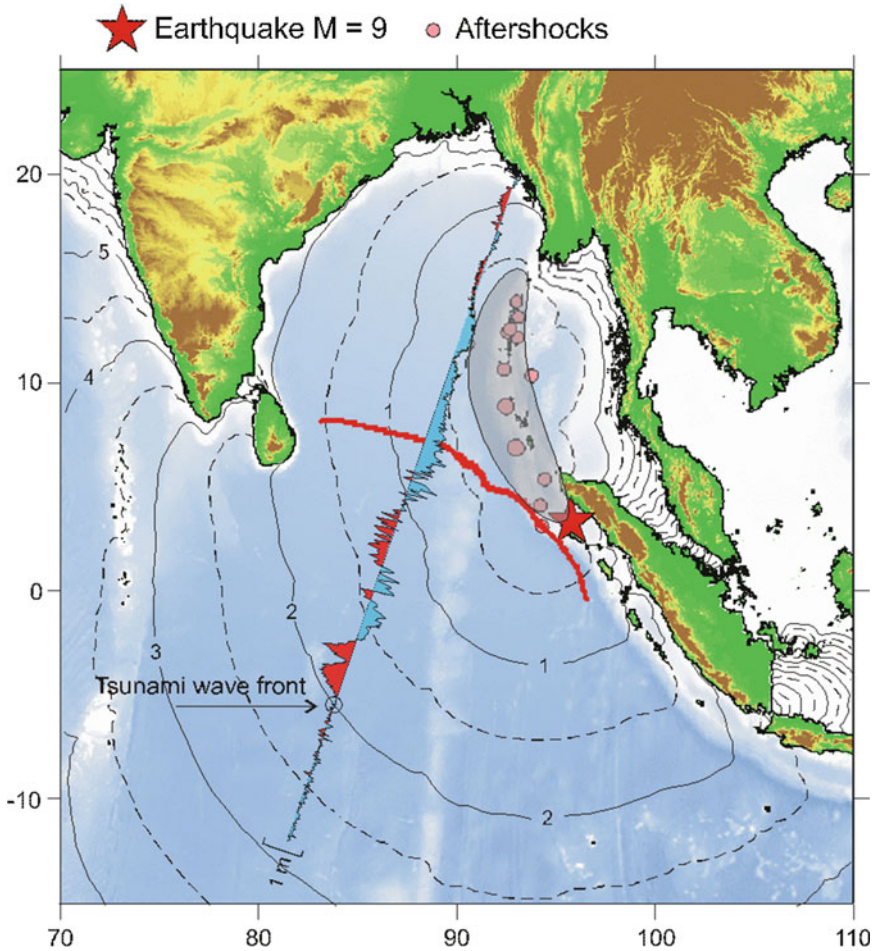


Fig. 7.13 Map of north-eastern part of the Indian Ocean with isochrones, showing the calculated front position of the tsunami of December 24, 2004 (with an interval of 0.5 an hour), epicenter of the main earthquake (*red star*) epicenters of main aftershocks (*circles*) Route of JASON-1 satellite (circuit 109-129). The profile of the ocean level determined from altimetry data is shown along the route (Courtesy of E.A. Kulikov)

From Fig. 7.13, the intersection angle of the satellite's route and the wave front is seen to be approximately 45° . Therefore, the real horizontal scales of ocean level variations must be (for geometrical reasons) divided by 1.4. The main wave length in the record of an altimeter amounts to about 700 km, which corresponds to 500 km for the length of a real tsunami wave. On the basis of the average wave velocity

in the open ocean, equal to ~ 200 m/s, it is possible to calculate the main tsunami period $T \approx 40$ min. Attention should be drawn to manifestations of higher-frequency oscillations of the level being observed noticeably more to the North, i.e., closer to the source. This actually reflects linear tsunami wave dispersion, when short-period waves exhibit propagation velocities inferior to those of long-period components.

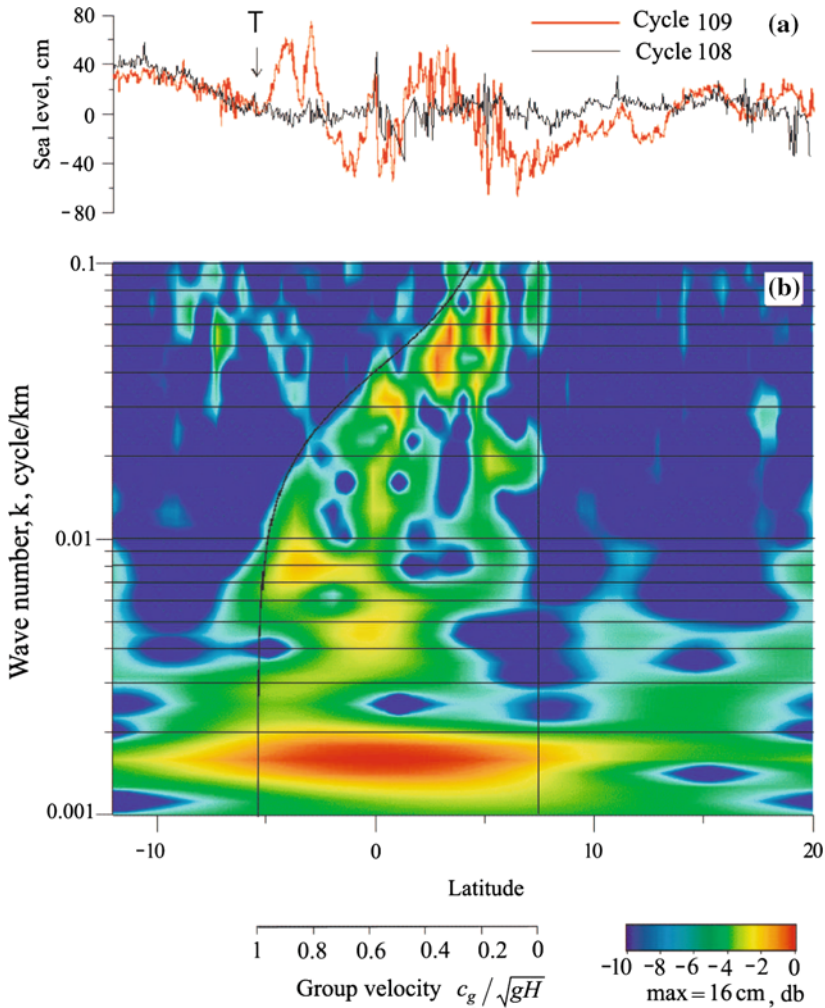


Fig. 7.14 **a** Altimetry sea level taken along track 129 of the Jason-1 satellite for Cycle 109 and along the same track 10 days earlier for Cycle 108; and **b** wavelet analysis of the sea level profile in **(a)**. The theoretical curve, calculated in accordance with the linear dispersion law for surface gravitational waves, shows the calculated ‘onset’ moments of the respective spectral components. Letter “T” indicates the tsunami wavefront (Courtesy of E.A. Kulikov)

To analyze the effect of linear tsunami wave dispersion, the dependence was calculated of the spectral amplitude of the signal on time and the wave number (wavelet diagram). The result of calculations is presented in Fig. 7.14b. The wave front is clearly seen to be related to the onset moment of the low-frequency components ($k < 0.05 \text{ km}^{-1}$). High-frequency components appear to the North of the front. The dispersion curve $c_g(k)$, corresponding to formula (7.2), is also shown in the figure. It was calculated taking into account the intersection angle between the satellite's route and the front. Good accordance is observed between "onsets" of the signal spectral components and the theoretical curve.

The revealed effect of tsunami wave dispersion demonstrates the restrictions of the longwave approximation, widely applied in numerical models of tsunami wave propagation. Owing to the "lag" of the high-frequency components in the wave spectrum, the tsunami amplitude decreases more rapidly than in the "shallow-water" model. This error is especially noticeable in calculations of the wave field at significant distances from the source. In Kulikov and Gonzalez (1995), it was shown that the effect of linear dispersion can actually totally distort the form of the tsunami signal in the open ocean. In this case, the main energy is concentrated in the region of periods around 30–50 min, and at a distance of about 1000 km from the source, the distortion is not so significant.

The results described above, in principle, demonstrate the possibility of timely registration of a dangerous tsunami wave in the open ocean with the aid of modern systems, permitting to observe the ocean from outer space. Such methods of effective tsunami forecasting will obviously develop in the direction of creating a technology for continuous monitoring of the ocean surface both with the aid of sensors of the open ocean level, equipped with telemetric connection to the processing centers, and making use of satellite altimetry measurements.

Note that the ocean bottom pressure gauges (see Sect. 7.1) used for measuring the level of the open ocean possesses an essential advantage as compared to the satellite altimeter. The point is that the frequency range of tsunami waves is practically free of irrelevant signals, while the corresponding range of wavelengths is quite noisy (for example, owing to ocean mesoscale eddies). Therefore, a tsunami wave can be readily singled out in the record of ocean level variations in time, but not in space. A sole "instantaneous shot" of the ocean level along the track is insufficient for reliable identification of a tsunami wave—it will just be invisible against the background of other processes. But, by comparing the data, obtained from two or more satellites traveling along the same track with a certain time delay between them, it is possible to single out a tsunami wave against a noisy background. Anyhow, such an approach will require significant enhancement of the number of satellites, equipped with altimeters.

7.4 Tsunami Wave Manifestations in the Ionosphere

The upper layers of the Earth's atmosphere, including the ionosphere, happen to be quite sensitive to vertical movements of the ocean or land surface, which involve sufficiently large areas. Such movements may be seismic oscillations of the Earth's surface or perturbations of the ocean surface that occur at the tsunami source or that are caused by the wave propagation. The ionosphere sensitivity to perturbations of the ocean or land surface can be explained as follows. Vertical displacements generate acoustic-gravitational waves (AGW) that penetrate upper layers of the atmosphere, where the collisions of neutral and charged particles initiate motion of the ionospheric plasma. The energy flux density of elastic waves caused by perturbation of the ocean or land surface is determined by the formula $q = c\rho u^2$, where c is the velocity of sound in the atmosphere, $\rho(z)$ is the atmospheric density at height z , and u is the mass velocity of air particles. The density of Earth's atmosphere drops exponentially as the height increases. Consequently, an increase in height should be accompanied by a multiple increase in the wave perturbation amplitude.

The ionosphere is understood to be the upper part of the atmosphere, where the concentration of ions and electrons is high. Several layers can be distinguished in the Earth's ionosphere, which actually have no clearly identifiable boundaries. Maximum ionization is observed in the upper layer (F). This layer can be split into layers F1 and F2 with ionization maxima at heights of 160–200 and 220–320 km, respectively. At nighttime, layer F ascends up to heights of 300–400 km. Layer E is located at heights of 90–150 km. Layer D is below 90 km. It is important to note that the concentration of electrons in the ionosphere layers depends essentially on solar activity, on solar wind, on the actual season, as well as the time of day or night and on other factors. Characteristics of the ionosphere also exhibit a strong latitudinal dependence. In this connection, the interpretation of tsunami and earthquake manifestations in the ionosphere represents a non-trivial problem.

The ionospheric response, caused by a tsunami wave, was first analyzed in a number of theoretical studies in the past century (Hines 1972; Najita et al. 1974; Peltier and Hines 1976). The first experimental work, which confirmed the theory, appeared only three decades later (Artru et al. 2005). Using the dense Japanese Global Positioning System (GPS) network GEONET, the authors of this work succeeded in identifying the Total Electron Content (TEC) disturbance, caused by tsunami waves due to the $M_w = 8.2$ earthquake in Peru on June 23, 2001. Before long, after the pioneering work (Artru et al. 2005), a whole series of publications appeared on ionospheric manifestations of the catastrophic tsunami that occurred in 2004 in the Indian Ocean (e.g., Liu et al. 2006a, b; DasGupta et al. 2006). The first attempt at a reconstruction of TEC disturbances associated with tsunamis applying the method of numerical simulation was made in Occhipinti et al. (2006). The result obtained in this work, and, also, in subsequent investigations (e.g., Mai and Kiang 2009; Occhipinti et al. 2008; Makela et al. 2011; Kunitsyn and Vorontsov 2014) confirmed the existence of a clear relationship between tsunami waves and ionospheric disturbances. In recent years, the interest in ionospheric tsunami manifestations has risen significantly. Without

claiming to present a complete list, we shall indicate some more publications in this field (Hickey et al. 2010; Occhipinti et al. 2011; Kunitsyn et al. 2011; Rozhnoi et al. 2012, 2014a, b).

The existing Global Navigation Satellite systems (GPS, GLONASS, Galileo and others) with a network of land-based receivers make it possible to probe the ionosphere in different directions. With the aid of tomographic methods, it is possible from the results of probing to reconstruct the spatial structure of the concentration of electrons in the ionosphere. For this purpose, the measured phases are usually used of radiosignals of two working frequencies (for GPS satellites: 1575.42 MHz and 1227.60 MHz) propagating from a satellite to a land-based receiver. The obtained data represent the phase paths of radiosignals measured in wavelengths. Knowledge of the phase paths permits to calculate the total electron content (TEC) along the ray connecting the transmitter and the receiver.

From a mathematical standpoint, a radiotomography problem reduces to resolution of a set of integral equations. Each equation is an integral along the propagation path of the signal between the receiver and the transmitter on the satellite. Details of this method can be found in the monograph (Kunitsyn and Tereshchenko 2003).

Let us examine certain results of ionosphere probing during the 2011 Tohoku-Oki earthquake and tsunami, presented in Kunitsyn et al. (2011). The Japanese network of land-based stations includes about 1200 GPS receivers, each of which simultaneously receives signals from 10 satellites. Thus, the number of aforementioned integral equations in the set amounts to $\sim 10^4$. For simplification, a two-dimensional, instead of three-dimensional, tomographic problem was resolved (in the thin-layer approximation). As a result, TEC maps were obtained with time intervals of 2 min and horizontal spatial resolution of about 20 km for the region of Japan (125–155°E, 25–50°N). From the TEC maps, a sharp increase in TEC was revealed that occurred immediately after the earthquake (after 6 min) in a region with a radius of the order of 50 km. The disturbance center was located at approximately 200 km east of the earthquake epicenter (which corresponds to the position of maximum bottom deformations (see Fig. 4.21)—comment by authors). After about 20 minutes from the beginning of the earthquake, the maps clearly show concentric circles that represent the ionospheric perturbation propagating from the region, where the acoustic pulse enters the ionosphere (see Fig. 7.15). An analysis of the acoustic-gravitational waves generated in the atmosphere after the 2011 Tohoku-Oki earthquake was performed in Kherani et al. (2012) on the basis of three-dimensional simulation and a detailed dynamic reconstruction of the ocean surface. The results of calculations are in good agreement with the data of radiotomographic reconstructions presented in Kunitsyn et al. (2011).

The sharp TEC enhancement observed after the earthquake is evidence of a rapid and significant uplift of the ocean surface and, consequently, of tsunamigenicity of the seismic event. It is important to note that information on the sharp TEC enhancement was received 10 min after the beginning of the earthquake, i.e., such information can, at least in principle, be used for issuing tsunami warnings.

Another interesting result, concerning ionospheric manifestations of the 2011 Tohoku-Oki tsunami, was obtained for the region of the Hawaiian Islands, where the

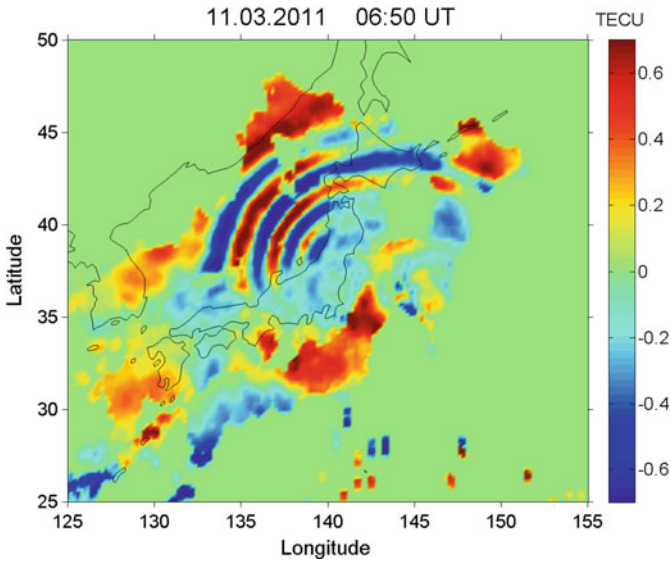


Fig. 7.15 Radiotomographic reconstruction of the ionospheric perturbation (acoustic-gravity waves) generated by the 2011 Tohoku-Oki earthquake. The scale of TECU variations ($1 \text{ TECU} = 10^{16} \text{ electron/m}^2$) is shown on the right (Courtesy of V.E. Kunitsyn)

tsunami wave arrived approximately 7 hours after the earthquake. According to data provided by the DART51407 station (the station closest to the Hawaiian Islands), the amplitude of the leading tsunami wave amounts to 15 cm. Observations of the ionosphere were performed by intensity surveys of the red airglow (630.0nm) of ionospheric plasma (Makela et al. 2011). The height of the assumed peak in the airglow intensity was 250 km.

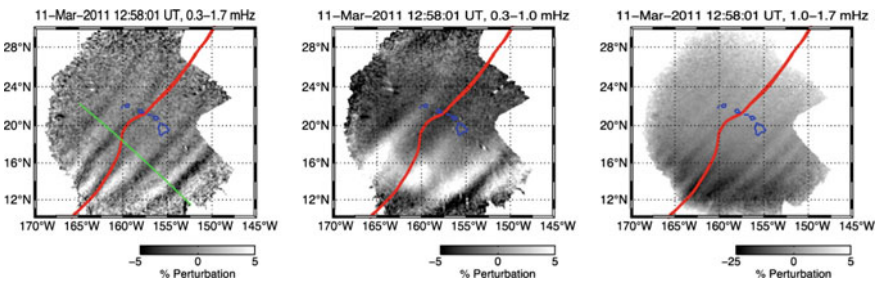


Fig. 7.16 The ionospheric airglow response over Hawaii to the 2011 Tohoku-Oki tsunami. Example of 630.0nm images processed using length-8 FIR filters with passbands of (left) 0.3-1.7 mHz, (middle) 0.3-1.0mHz to highlight the 26.2 min period waves, and (right) 1.0-1.7mHz to highlight the 14.2 min period waves. The red line in each image indicates the tsunami location at the time of the image (Reprinted from Makela et al. 2011 by permission of the publisher)

The picture of the ionospheric response (see Fig. 7.16) clearly shows that it represents a series of waves, and some of them are significantly ahead (by an hour) of the tsunami front. In attempts to explain the nature of the waves propagating more rapidly than the tsunami front, the authors of Makela et al. (2011) put forward the following three hypotheses: “(a) an infrasonic wave generated at the earthquake source propagating in the ionosphere faster than the ocean tsunami wave front, (b) a plasma diffusion oscillation related to the sea level disturbances of the tsunami wave front, or (c) the initial tsunami wave generated by pre-rupture processes.” On the basis of the data of numerical simulation (Occhipinti et al. 2011), the authors of the publication (Makela et al. 2011) finally considered the third hypothesis to be correct. The results of simulations performed by a Russian group (Kunitsyn and Vorontsov 2014) rather testify in favor of the second hypothesis. Apparently, it is still too early to make a final conclusion concerning the physical nature of an “ionospheric precursor.” In any case, however, the existence of an “ionospheric precursor” opens up one more possibility for the early revelation of a tsunami.

Methods of radiotomography and of observation of the airglow of ionospheric plasma, which are mainly relevant to the upper ionosphere, are not the only possible ways of registering ionospheric disturbances. In certain conditions, low-frequency and very-low-frequency radio signals (the range of 10–40 kHz), propagating from the emitter to the receiver within the layer in between the Earth’s surface and the lower ionosphere, are also capable of identifying perturbations in the plasma density and of transmitting this information to the antenna of the receiving device. Application of this technique permitted, in particular, to observe ionospheric manifestations of tsunami waves caused by the 2006 Central Kuril Island earthquake, the 2010 Chile earthquake, and the 2011 Tohoku-Oki earthquake (Rozhnoi et al. 2012, 2014a, b).

At present, the effect of tsunami manifestations in the ionosphere is very important as a scientific fact that was, first, predicted theoretically, and, then, registered in natural conditions by several independent methods. Whether this effect is promising from the point of view of its application in systems of tsunami warning will be clarified in the nearest future.

References

- Artru, J., Ducic, V., Kanamori, H., Lognonne, P., Murakami, M.: Ionospheric detection of gravity waves induced by tsunamis. *Geophys. J. Int.* **160**, 840–848 (2005)
- Atwater, B.F.: Evidence for Great Holocene earthquakes along the outer coast of Washington state. *Science* **236**, 942–944 (1987)
- Barrick, D.E.: A coastal radar system for tsunami warning. *Remote Sens. Env.* **8**(4), 353–358 (1979)
- Bernard, E., Meinig, C.: History and future of deep-ocean tsunami measurements. In: *Proceedings of Oceans’ 11 MTS/IEEE, Kona, IEEE, Piscataway, NJ*, 19–22 September 2011, No 6106894, 7 pp. (2011)
- Borrero, J.C., Synolakis, C.E., Fritz, H.: Northern Sumatra field survey after the December 2004 great Sumatra earthquake and Indian Ocean tsunami. *Earthq. Spectra* **22**(S3), 93–104 (2006)

- Bourgeois, J., Reinhart, M.A.: Onshore erosion and deposition by the 1960 tsunami at Rio Lingue estuary, south-central Chile. *Eos*, vol. 70, p. L1331 (Transactions, American Geophysical Union) (1989)
- Bourgeois, J., Pingina, T.K., Ponomareva, V.V., Zaretskaia, N.E.: Holocene tsunamis in the south-western Bering Sea, Russian Far East, and their tectonic implications. *GSA Bull.* **118**(3–4), 449–463 (2006)
- Chooiwong, M., Murakishi, N., Hisada, K., et al.: Erosion and deposition by the 2004 Indian Ocean tsunami in Phuket and Phang-Nga Provinces. Thailand. *J. Coast. Res.* **23**, 1270–1276 (2008)
- DasGupta, A., Das, A., Hui, D., Bandyopadhyay, K.K., Sivaraman, M.R.: Ionospheric perturbations observed by the GPS following the December 26th, 2004 Sumatra-Andaman earthquake. *Earth Planets Space* **58**, 167–172 (2006)
- Dawson, A.G.: Geomorphological effects of tsunami run-up and backwash. *Geomorphology* **10**(1–4), 83–94 (1994)
- Favali, P., Beranzoli, L.: EMSO: European multidisciplinary seafloor observatory. *Nucl. Instrum. Methods Phys. Res. Sect. A: Accel. Spectrom. Detect. Assoc. Equip.* **602**(1), 21–27 (2009)
- Fujiwara, O., Kamataki, T.: Identification of tsunami deposits considering the tsunami waveform: An example of subaqueous tsunami deposits in Holocene shallow bay on southern Boso Peninsula. Central Japan. *Sediment. Geol.* No **200**, 295–311 (2007)
- Gill, A.E.: *Atmosphere-Ocean Dynamics*, 662 pp. Academic Press, New York (1982)
- Hickey, M.P., Schubert, G., Walterscheid, R.L.: Atmospheric airglow fluctuations due to a tsunami-driven gravity wave disturbance. *J. Geophys. Res.* **115**, A06308 (2010)
- Hines, C.O.: Gravity waves in the atmosphere. *Nature* **239**, 73–78 (1972)
- Jacques, V.M., Soloviev, S.L.: Remote registration of weak tsunami-type waves on the shelf of the Kuril islands. *DAN SSSR (in Russian)* **198**(4), 816–817 (1971)
- Jaffe, B.E., Gelfenbaum, G.: A simple model for calculating tsunami flow speed from tsunami deposits. *Sediment. Geol.* **200**, 347–361 (2007)
- Kaneda, Y.: The advanced ocean floor real time monitoring system for mega thrust earthquakes and tsunamis-application of DONET and DONET2 data to seismological research and disaster mitigation. *Proc. Oceans Conf.* (2010). doi:[10.1109/OCEANS.2010.5664309](https://doi.org/10.1109/OCEANS.2010.5664309)
- Kato, T., Terada, Y., Kinoshita, M., Kakimoto, H., Isshiki, H., Matsuishi, M., Tanno, T.: Real-time observation of tsunami by RTK-GPS. *Earth Planets Space* **52**(10), 841–845 (2000)
- Kato, T., Terada, Y., Nagai, T., Shimizu, K., Tomida, T., Koshimura, S.: Development of a new tsunami monitoring system using a GPS buoy. *Proceedings of International Symposium on GPS/GNSS 2008*, 846–845 (2008)
- Kato, T., Terada, Y., Nishimura, H., Nagai, T., Koshimura, S.I.: Tsunami records due to the 2010 Chile earthquake observed by GPS buoys established along the Pacific coast of Japan. *Earth Planets Space* **63**(6), e5–e8 (2011)
- Kravchunovskaya, E.A., Pingina, T.K., Bourgeois, J., MacInnes, B.T.: Geological and geomorphological effects of 15.11.2006 tsunami on the Central Kuriles. *Geophysical monitoring and the problems of seismic safety of the Russian Far East*. vol. 1, pp. 180–183. GS RAS, Petropavlovsk-Kamchatsky (2008)
- Kulikov, E.A., Medvedev, P.P., Lappo, S.S.: Registration from outer space of the December 26, 2004, tsunami in the Indian Ocean (in Russian). *DAN RF* **401**(4), 537–542 (2005)
- Kulikov, E.A., Gonzalez, F.I.: Reconstruction of the shape of a tsunami signal at the source by measurements of hydrostatic pressure oscillations using a remote bottom sensor (in Russian). *DAN RF* **344**(6), 814–818 (1995)
- Kunitsyn, V.E., Nesterov, I.A., Shalimov, S.L.: Japan megathrust earthquake on March 11, 2011: GPS-TEC evidence for ionospheric disturbances. *JETP Lett.* **94**(8), 616–620 (2011)
- Kherani, E.A., Lognonne, P., Hébert, H., Rolland, L., Astafyeva, E., Occhipinti, G., De Paula, E.R.: Modelling of the total electronic content and magnetic field anomalies generated by the 2011 Tohoku-Oki tsunami and associated acoustic-gravity waves. *Geophys. J. Int.* **191**(3), 1049–1066 (2012)

- Kunitsyn, V.E.: Modeling the ionospheric propagation of acoustic gravity waves from the Tohoku tsunami of 2011. *Mosc. Univ. Phys. Bull.* **69**(3), 263–269 (2014)
- Kunitsyn, V.E., Tereshchenko, E.D.: *Ionospheric Tomography*. Springer Science & Business Media, New York (2003)
- Lacombe, H.: *Cours d’océanographie physique: Théories de la circulation générale. Houles et vagues*. Gauthier-Villars, Paris (1965)
- Lakshmi, V., Srinivasan, P., Murthy, S., Trivedi, D., Nair, R.: Granularity and textural analysis as a proxy for extreme wave events in southeast coast of India. *J. Earth Syst. Sci. IAS* **119**(3), 297–305 (2010)
- Lander, J.F., Lockridge, P.A., Kozuch, M.J.: Tsunamis affecting the west coast of the United States, 1806–1992 (No. 29). US Department of Commerce, National Oceanic and Atmospheric Administration, National Environmental Satellite, Data, and Information Service, National Geophysical Data Center, 242 pp. (1993)
- Lipa, B., Isaacson, J., Nyden, B., Barrick, D.: Tsunami arrival detection with high frequency (HF) radar. *Remote Sens.* **4**(5), 1448–1461 (2012)
- Liu, J.Y., Tsai, Y.B., Chen, S.W., Lee, C.P., Chen, Y.C., Yen, H.Y., Chang, W.Y., Liu, C.: Giant ionospheric disturbances excited by the M9.3 Sumatra earthquake of 26 December 2004. *Geophys. Res. Lett.* **33**, L021103 (2006a)
- Liu, J.-Y., Tsai, Y.-B., Ma, K.-F., Chen, Y.-I., Tsai, H.-F., Lin, C.-H., Kamogawa, M., Lee, C.-P.: Ionospheric GPS total electron content (TEC) disturbances triggered by the 26 December 2004 Indian Ocean tsunami. *J. Geophys. Res.* **111**, A05303 (2006b)
- MacInnes, B.T., Bourgeois, J., Pinegina, T.K., Kravchunovskaya, E.A.: Before and after: geomorphic change from the 15 November 2006 Kuril Island tsunami. *Geology* **37**(11), 995–998 (2009a)
- MacInnes, B.T., Pinegina, T.K., Bourgeois, J., Razhegava, N.G., Kaistrenko, V.M., Kravchunovskaya, E.A.: Field survey and geological effects of the 15 November 2006 Kuril tsunami in the middle Kuril Islands. *Pure Appl. Geophys.* **166**, 9–36 (2009b)
- Mai, C.-L., Kiang, J.-F.: Modeling of ionospheric perturbation by 2004 Sumatra tsunami. *Radio Sci.* **44**, RS3011 (2009)
- Makela, J., Lognonne, P., Hébert, H., Gehrels, T., Rolland, L., Allgeyer, S., Kherani, A., Occhipinti, G., Astafyeva, E., Coisson, P., Loevenbruck, A., Clévéde, E., Kelley, M.C., Lamouroux, J.: Imaging and modeling the ionospheric airglow response over Hawaii to the tsunami generated by the Tohoku earthquake of 11 March 2011. *Geophys. Res. Lett.* **38**, L00G02 (2011)
- Matsumoto, H., Kaneda, Y.: Some features of bottom pressure records at the 2011 Tohoku earthquake—Interpretation of the far-field DONET data. In: *Proceedings of 11th SEGJ International Symposium, Yokohama, Japan*, p. 493 (2013). doi:[10.1190/segj112013-124](https://doi.org/10.1190/segj112013-124)
- Merrifield, M.A., Firing, Y.L., Aarup, T., Agricole, W., Brundrit, G., Chang Seng, D., Turetsky, N.: Tide gauge observations of the Indian Ocean tsunami, December 26, 2004. *Geophys. Res. Lett.* **32**(9) (2005)
- Minoura, K., Nakaya, S.: Traces of tsunami preserved in inter-tidal lacustrine and marsh deposits: some examples from northeast Japan. *J. Geol.* **99**, 265–287 (1991)
- Mori, N., Takahashi, T.: The 2011 Tohoku earthquake tsunami joint survey group: nationwide post event survey and analysis of the 2011 Tohoku earthquake tsunami. *Coast. Eng. J.* **54**(01), 1250001 (2012)
- Morton, R.A., Gelfenbaum, G., Jaffe, B.E.: Physical criteria for distinguishing sandy Tsunami and storm deposits using modern examples. *Sediment. Geol.* **200**, 184–207 (2007)
- Münch, U., Rudloff, A., Lauterjung, J.: Postface “The GITEWS project—results, summary and outlook”. *Nat. Hazards Earth Syst. Sci.* **11**, 765–769 (2011). doi:[10.5194/nhess-11-765-2011](https://doi.org/10.5194/nhess-11-765-2011)
- Najita, K., Weaver, P., Yuen, P.: A tsunami warning system using an ionospheric technique. *Proc. IEEE* **62**(5), 563–577 (1974)
- Occhipinti, G., Coisson, P., Makela, J.J., Allgeyer, S., Kherani, A., Hébert, H., Lognonné, P.: Three-dimensional numerical modeling of tsunami-related internal gravity waves in the Hawaiian atmosphere. *Earth Planets Space* **63**(7), 847–851 (2011)

- Occhipinti, G., Kherani, E.A., Lognonné, P.: Geomagnetic dependence of ionospheric disturbances induced by tsunamigenic internal gravity waves. *Geophys. J. Int.* **173**, 753–765 (2008)
- Occhipinti, G., Lognonné, P., Kherani, E.A., Hébert, H.: Three-dimensional waveform modeling of ionospheric signature induced by the 2004 Sumatra tsunami. *Geophys. Res. Lett.* **33**(20), L20104 (2006)
- Okal, E.A., Piatanesi, A., Heinrich, P.: Tsunami detection by satellite altimetry. *J. Geophys. Res.* **104**, 599–615 (1999)
- Peltier, W.R., Hines, C.O.: On the possible detection of tsunamis by a monitoring of the ionosphere. *J. Geophys. Res.* **81**, 1995–2000 (1976)
- Pinegina, T.K., Melekestsev, I.V., Braitseva, O.A., et al.: Traces of prehistoric tsunamis on the eastern coast of Kamchatka (in Russian). *Priroda* **4**, 102–106 (1997a)
- Pinegina, T.K., Melekestsev, I.V., Bazanova, L.I., Braitseva, O.A., Storcheus, A.V.: East Kamchatka paleotsunami traces (in Russian). *Priroda* **6**, 102–106 (1997b)
- Pinegina, T.K., Bazanova, L.I., Melekestsev, I.V., et al.: Prehistoric tsunamis on the coast of Kronotsky Bay, Kamchatka, Russia (preliminary communication) (in Russian). *Volcanol. Seismol.* (2), 66–74 (2000)
- Pinegina, T.K., Bourgeois, J.: Historical and paleo-tsunami deposits on Kamchatka, Russia: long-term chronologies and long-distance correlations. *Nat. Hazards Earth Syst. Sci.* **1**(4), 177–185 (2001)
- Pinegina, T., Bourgeois, J., Bazanova, L., Melekestsev, I., Braitseva, O.A.: Millennial-scale record of Holocene tsunamis on the Kronotskiy Bay coast, Kamchatka, Russia. *Quat. Res.* **59**, 36–47 (2003)
- Pinegina, T.K., Bourgeois, J., Razzhigaeva, N.G., Levin, B.V., Kaistrenko, V.M., Kravchunovskaya, E.A., MacInnes, B.T.: 2006 Nov. 15 tsunami on the Central Kuriles and the recurrence of the similar events in the past (from paleoseismological data). *Geophysical monitoring and the problems of seismic safety of the Russian Far East*, vol. 1, pp. 200–204. GS RAS, Petropavlovsk-Kamchatsky (2008)
- Pinegina, T.K., Kozhurin, A.I., Ponomareva, V.V.: Seismic and tsunami hazard assessment for Ust-kamchatsk settlement, Kamchatka, based On Paleoseismological Data (in Russian). *Bulletin of Kamchatka Regional Association “Educational-Scientific Center”*. *Earth Sci.* **19**(1), 138–159 (2012)
- Pinegina, T.K., Bourgeois, J., Kravchunovskaya, E.A., Lander, A.V., Arcos, M.E.M., Pedoja, K., MacInnes, B.T.: A nexus of plate interaction: segmented vertical movement of Kamchatsky Peninsula (Kamchatka) based on Holocene aggradational marine terraces. *Geol. Soc. Am. Bull.* **125**(9/10), 1554–1568 (2013). doi:[10.1130/B30793.1](https://doi.org/10.1130/B30793.1)
- Rabinovich, A.B., Eblé, M.C.: Deep-ocean measurements of tsunami waves. *Pure Appl. Geophys.* 1–32 (2015)
- Razzhigaeva, N.G., Ganzey, L.A., Grebennikova, T.A., Kharlamov, A.A., Kaistrenko, V.M., Arslanov, KhA, Gorbunov, A.O.: Paleotsunami manifestation in the Lesser Kuril arc in the Holocene (in Russian). *Rus. J. Pac. Geol.* **31**(6), 48–56 (2012)
- Rozhnoi, A., Shalimov, S., Solovieva, M., Levin, B., Hayakawa, M., Walker, S.: Tsunami-induced phase and amplitude perturbations of subionospheric VLF signals. *J. Geophys. Res.* **117**, A09313 (2012)
- Rozhnoi, A., Shalimov, S., Solovieva, M., Levin, B., Shevchenko, G., Hayakawa, M., Hobara, Y., Walker, S.N., Fedun, V.: Detection of tsunami-driven phase and amplitude perturbations of subionospheric VLF signals following the 2010 Chile earthquake. *J. Geophys. Res.* **119**, 5012–5019 (2014a)
- Rozhnoi, A., Solovieva, M., Hayakawa, M., Yamaguchi, H., Hobara, Y., Levin, B., Fedun, V.: Tsunami-driven ionospheric perturbations associated with the 2011 Tohoku earthquake as detected by subionospheric VLF signals. *Geomat. Nat. Hazards Risk* **5**(4), 285–292 (2014b)
- Soloviev, S.L.: The tsunami problem and its significance for the Kamchatka and the Kuril islands (in Russian). In: *The Tsunami Problem*, pp. 7–50. Nauka (1968)

- Titov V.V., Gonzalez F.I., Bernard E.N., et al.: Real-time tsunami forecasting: challenges and solutions. *Nat. Hazards*, 35(1), Special Issue, pp. 41–58. U.S. National Tsunami Hazard Mitigation Program (2005)
- Thomson, R., Fine, I., Rabinovich, A., et al.: Observation of the 2009 Samoa tsunami by the NEPTUNE-Canada cabled observatory: test data for an operational regional tsunami forecast model // *Geophys. Res. Lett.* **38**, L11701 (2011). doi:[10.1029/2011GL04](https://doi.org/10.1029/2011GL04)
- Tuttle, M.P., Ruffman, A., Anderson, T., Jeter, H.: Distinguishing tsunami from storm deposits in Eastern North America: The 1929 Grand Banks tsunami versus the 1991 Halloween storm. *Seismol. Res. Lett.* **75**(1), 117–131 (2004)
- Zaichenko, M.Yu., Kulikov, E.A., Levin, B.W., Medvedev, P.P.: Examples of tsunami registration in the open ocean based on data from a satellite altimeter (1993–2001). Tsunami Laboratory. Yanus-K, Moscow, Preprint IORAH (in Russian) (2004)
- Zaichenko, M.Yu., Kulikov, E.A., Levin, B.W., Medvedev, P.P.: On the possibility of tsunami registration in the open ocean by data from a satellite altimeter (in Russian). *Oceanology* **45**(2), 222–229 (2005)